THE JOURNAL
OF
CHEMICAL PHYSICS

VOLUME 17, NUMBER 12 DECEMBER, 1949

Rates of Ionic Reactions in Aqueous Solutions

A. R. OLSON AND T. R. SIMONSON
Department of Chemistry, University of California, Berkeley, California
(Received October 26, 1948)

The effect of the addition of "inert" salts on ionic reaction rates is discussed. For reactions between ions of the same charge sign, the effect is caused almost exclusively by the concentration and character of salt ions of charge sign opposite to that of the reactants. The rate is not dependent upon the ionic strength of the solutions. In reactions between ions of opposite charge sign, both salt ions may affect the rate, but the effect of one type may be dominant. The effects are quantitatively interpretable in terms of an ion association constant and specific rate constants for the associated and non-associated reactants. The further introduction of activity coefficients is not necessary. The reactions upon which the Livingston Diagram is based have been explored from this viewpoint and found to be in quantitative accord.

THE rate of reaction between bromopentammine cobaltic ion, $Co(NH_3)_5Br^{++}$, and mercuric ion in dilute aqueous solution was investigated by Brønsted and Livingston.[1] Their results are shown graphically in Fig. 1. The dashed line shows the theoretical change in specific rate with ionic strength as calculated from the Brønsted theory of salt effects,[2] $k=k_0(f_Af_B/f_X)$, combined with the Debye-Hückel limiting law for the activity coefficients of ions in aqueous solutions. Apparently, the only hydrogen ions in the solution came from an unspecified amount of nitric acid added to the stock solution of mercuric nitrate to prevent hydrolysis. This might account for the rapid drop in the specific rate at low ionic strengths, since the smaller the amount of such stock solution added to the reaction mixture, the smaller would be the concentration of hydrogen ions, and the greater would be the degree of hydrolysis. We have therefore reinvestigated this reaction, taking advantage of the improved precision made possible by the use of a quartz spectrophotometer and the very high extinction coefficient of the bromo-cobaltammine in the ultra-violet. The large absorption of nitrate ion in this region made it desirable to employ the perchlorate compounds.

Bromopentammine cobaltic bromide was prepared by the method of Jörgensen.[3] Mercuric perchlorate solution was prepared by permitting perchloric acid to react with an excess of freshly precipitated mercuric oxide. The centrifuged and filtered solution was analyzed for mercury by titration with thiocyanate[4] which had been standardized against redistilled mercury. The perchloric acid content of the solution was determined by titration with sodium hydroxide after complexing the mercuric ion with a large excess of sodium bromide. Methyl red indicator was used. The final stock solution was approximately $0.1M$ in mercuric perchlorate and $0.004M$ in perchloric acid. Sodium perchlorate solution was prepared by the neutralization of standardized perchloric acid with analytical reagent grade sodium carbonate, boiling off carbon dioxide, and diluting to a known volume. Lanthanum perchlorate solution was prepared by permitting standardized perchloric acid to react with an excess of pure lanthanum oxide which had been ignited and weighed. After a few hours stirring, the excess oxide was filtered off, washed, and ignited. The weight of oxide used checked with the amount of perchloric acid added within a few tenths of a percent.

The large difference between the extinction coefficients for the two cobaltammine compounds in the ultraviolet region, and the use of a modern spectrophotometer permit precise rate determinations at very low reactant concentrations. Absorption spectra of the cobaltammines involved in this reaction and one to be discussed later are shown in Fig. 2. A Beckman quartz

[1] J. N. Brønsted and R. Livingston, J. Am. Chem. Soc. **49**, 435 (1927).
[2] J. N. Brønsted, Zeits f. physik. Chemie **102**, 169 (1922); **115**, 337 (1925).
[3] S. M. Jörgensen, Zeits. f. anorg. allgem. Chemie **17**, 455 (1898).
[4] I. M. Kolthoff and E. B. Sandell, *Quantitative Inorganic Analysis* (The Macmillan Company, New York, 1943), pp. 480 and 575.

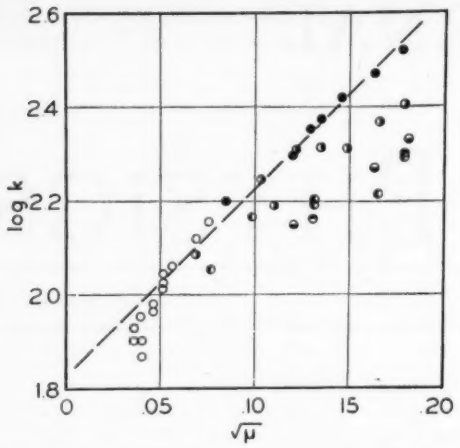

FIG. 1. Data of Brønsted and Livingston (see reference 1) for the reaction $Co(NH_3)_5Br^{++}+Hg^{++}$. ○ no added salt, ● HNO_3 added, ◑ KNO_3 added, ◐ $Ba(NO_3)_2$ added, ◓ $Sr(NO_3)_2$ added, ◒ $La(NO_3)_3$ added. Dashed line: Debye-Hückel limiting slope from Brønsted equation as drawn by Brønsted and Livingston.

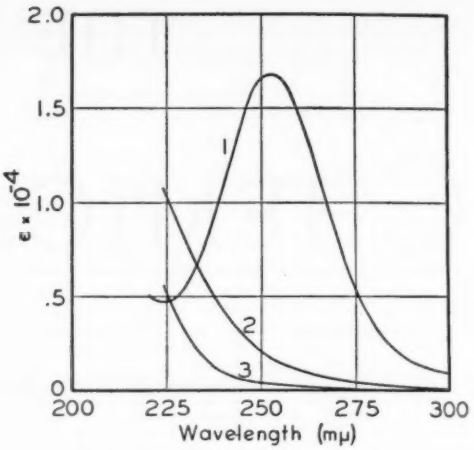

FIG. 2. Ultraviolet absorption spectra of cobaltammines. 1: $Co(NH_3)_5Br^{++}$, 2: $Co(NH_3)_5OH^{++}$, 3: $Co(NH_3)_5H_2O^{+++}$.

spectrophotometer was used for all rate measurements. A small thermostat chamber was constructed to replace the usual cell compartment assembly for 10-cm cells. It consisted of a brass box with fused silica windows in the optical path. Making the box longer (toward the operator) than the usual compartment provided space for a stirrer and a thermoregulator. A grid of copper tubing on the bottom of the box permitted the circulation of a coolant. Insulation was provided by a layer of sheet cork surrounding the thermostat.

Solutions of the cobaltammine and mercuric perchlorate were separately brought to temperature (15.0°C in all these experiments) in the arms of a *Y*-shaped mixing vessel in a separate thermostat. After rapid mixing, the final solution was transferred to a 10-cm absorption cell which had also been brought to temperature, the cell holder was placed in the spectrophotometer, and measurements begun.

In our experiments the concentration of the cobaltammine was so small compared to that of mercuric ion that the change in ionic strength as well as the change in mercuric ion concentration was less than five percent during the course of the reaction in the most extreme case. For those runs in which the mercuric ion concentration changed appreciably during reaction, bimolecular specific rates have been calculated from the average mercuric ion concentration.

In the first series of experiments, shown in Fig. 3, the rate of the reaction was determined at various concentrations of mercuric perchlorate, keeping the initial concentration of cobaltammine constant ($5.00\times10^{-6}M$). The only perchloric acid present came from the mercury stock solution. Figure 4 shows the strictly first-order character of the rate of disappearance of bromocobaltammine in a typical experiment. The curve resulting from this series parallels rather closely the Brønsted and Livingston[1] data, again showing the rapid drop in specific rate at low ionic strengths.

When the series was repeated using enough added acid to make the total perchloric acid concentration $0.001M$, the rapid drop in the specific rate at low mercuric ion concentrations was avoided. This does not mean that hydrolysis of mercuric ion has been eliminated. It means merely that the hydrogen ion concentration is large enough so that the degree of hydrolysis of mercuric ion does not change greatly as the mercuric ion concentration is changed. In fact from the work of Garrett and Hirschler[5] and the free energy data for the mercuric compounds, an appreciable fraction of the mercury may be present as $HgOH^+$. The measured reaction therefore is complex, but this complexity does not vitiate the conclusions to which we are led below. The observations measure the change in the concentration of the bromopentammine cobaltic ion. The relative concen-

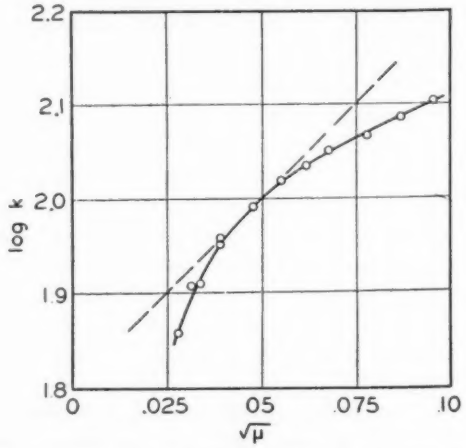

FIG. 3. The reaction $Co(NH_3)_5Br^{++}+Hg^{++}$. Cobaltammine concentration $5.0\times10^{-6}M$, varying amounts of $Hg(ClO_4)_2$. Dashed line: Debye-Hückel limiting slope from Brønsted equation.

[5] A. B. Garrett and A. E. Hirschler, J. Am. Chem. Soc. **60**, 305 (1938).

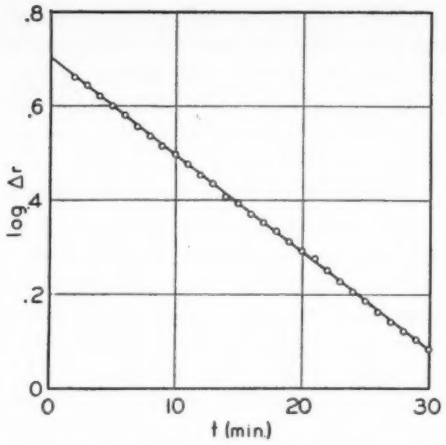

FIG. 4. A typical run showing first-order disappearance of bromocobaltammine in the reaction $Co(NH_3)_5Br^{++}+Hg^{++}$. Δr is the difference of two optical densities measured a constant time interval apart (Guggenheim method). Wave-length 253 mμ.

trations of mercuric ion and its hydrolysis products may be and probably are complex functions not only of the hydrogen ion concentration, but also of the "inert" salt concentration. In the presence of a great excess of mercuric ion, as in our experiments, the only important reaction product of mercury is $HgBr^+$.[6] The kinetic data for this series at constant total acidity are shown in Table I and in Fig. 5.

In Table II are shown the results of a series of runs in solutions 0.001*M* in perchloric acid to which sodium perchlorate or lanthanum perchlorate was added to vary the ionic strength, all other components of the solutions being kept constant. These data are plotted in Fig. 6. In those runs containing the highest salt concentrations the rates are almost twice as great as the rate in the reference solution. The ionic strengths of the lanthanum perchlorate solutions are almost double those of the corresponding sodium perchlorate solutions. It is obvious that the rate for the addition of sodium perchlorate is identical with that for the addition of lanthanum perchlorate at the same perchlorate ion concentration in spite of ionic strength differences. The functional dependence of the rate of this reaction is on the concentration of negative ions, and not on the ionic strength as such.

We arrive at the same conclusion by examining the data of Brønsted and Livingston[1] for this reaction. Table III includes all the data they presented which permit such a comparison.

The substitution of the bromine in bromoacetate ion by thiosulfate ion was studied by von Kiss and Vass.[7] These investigators added salts of various types to the reactants to change the ionic strength. For convenience we have reproduced in Table IV that portion of their data taken at 25°C which involved the addition of sodium nitrate or sodium sulfate, and we have plotted the results in the usual way in Fig. 7. Data for three runs by the present authors in which potassium nitrate, potassium sulfate, or potassium cobalticyanide was added as "inert salt," also shown in Fig. 7, are given in Table V. If we compare sets of runs where in one case sodium nitrate has been added and in the other sodium sulfate has been added as the "inert salt," we see that even up to half-normal the rate is about the same at equal sodium ion concentrations, even though the ionic strength is very different. This is shown in Fig. 8, where we have plotted log*k* *versus* the square root of the sodium ion concentration. A similar treatment of their experiments involving the addition of magnesium salts (the only additional group where such a comparison may be made), while more closely conforming to a

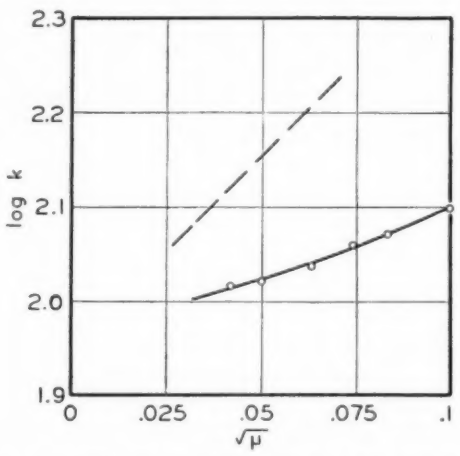

FIG. 5. The reaction $Co(NH_3)_5Br^{++}+Hg^{++}$. Cobaltammine concentration $5.0\times10^{-6}M$, $HClO_4$ concentration $1.00\times10^{-3}M$, varying amounts of $Hg(ClO_4)_2$. Dashed line: Debye-Hückel limiting slope from Brønsted equation.

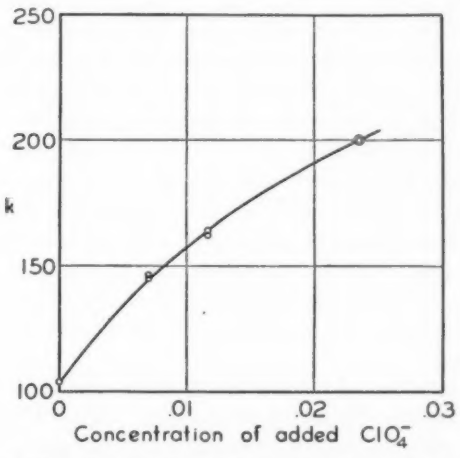

FIG. 6. The effect of the addition of sodium and lanthanum perchlorate to the reaction $Co(NH_3)_5Br^{++}+Hg^{++}$. Concentrations: cobaltammine, $5.0\times10^{-6}M$; $Hg(ClO_4)_2$, $2.50\times10^{-4}M$; $HClO_4$, $1.0\times10^{-3}M$. In each pair of points one is sodium and one lanthanum perchlorate.

[6] L. G. Sillén, Svensk Kem. Tid. **58**, 52 (1946). L. G Sillén and G. Infeldt, Svensk Kem. Tid. **58**, 61 (1946).

[7] A. von Kiss and P. Vass, Zeits. f. anorg. allgem. Chemie **217**, 305 (1934).

TABLE I. Rate data for the reaction $Co(NH_3)_5Br^{++}+Hg^{++}$.

Cobaltammine $5.0\times10^{-6}M$ Total $HClO_4$ $1.00\times10^{-3}M$		$T=15.0°C$
$10^4\times[Hg(ClO_4)_2]$	k	$10^3\mu$
2.50	103.8	1.75
4.98	105.1	2.49
9.97	109.1	3.99
14.93	114.8	5.48
19.90	117.8	6.97
29.89	125.6	9.96

TABLE II. Rate data for the reaction $Co(NH_3)_5Br^{++}+Hg^{++}$.

Concentrations: Cobaltammine $5.0\times10^{-6}M$, $Hg(ClO_4)_2$ $2.50\times10^{-4}M$, $HClO_4$ $1.00\times10^{-3}M$

$10^3\times[NaClO_4]$	$10^3\times[La(ClO_4)_3]$	$10^3\times$[added (ClO_4^-)]	k	$T=15.0°C$ $10^3\mu$
0	0	0	103.8	1.75
7.06		7.06	145.0	8.81
	2.35	7.06	146.7	15.85
11.70		11.70	162.2	13.45
	3.90	11.70	164.2	25.15
23.56		23.56	200.4	25.31
	7.85	23.55	200.4	48.85

concentration than an ionic strength comparison, is somewhat less striking from a quantitative viewpoint than the one discussed above.

The saponification of nitrourethane ion by hydroxide ion, $NO_2{=}N{-}COOC_2H_5^-+OH^-=N_2O+CO_3^{--}+C_2H_5OH$, was studied by Brønsted and Delbanco.[8] The first four entries of Table VI, taken from their paper (with the column for ionic strength added by us), show the effect on the rate of adding various potassium salts, all at the same concentration of potassium ion. It is seen that under these conditions the rate is nearly constant, independent of the type of negative ion and of the ionic strength, provided that the change in ionic strength is due to a change in the character and concentration of the added negative ion. The remaining entries of Table VI show further that the rate is influenced very markedly by the character of the added positive ion, even though the ionic strength remains the same. Brønsted and Delbanco noted this effect of positive ion character, and stated that it was in agreement with Brønsted's "principle of specific interaction of ions."[9] The inescapable conclusion from this work is that the rate of this reaction depends on the concentration and character of positive ions, and that it is independent of ionic strength, in complete accord with the preceding examples.

The reaction of bromopentammine cobaltic ion with hydroxide ion, $Co(NH_3)_5Br^{++}+OH^-=Co(NH_3)_5OH^{++}+Br^-$, was studied by Brønsted and Livingston.[1] Their data, though perhaps as good as could be got by visual colorimetric methods, are not very consistent. We have therefore re-examined the rates for this reaction, again using the ultraviolet absorption region which permitted us to work with very low reactant concentrations. The absorption spectra involved are shown in Fig. 2. The first series of experiments was performed by varying the initial hydroxide ion concentration, keeping the initial cobaltammine concentration constant at $5.0\times10^{-6}M$. No salts were added. Our data for this series are shown in Table VII and by the filled circles in Fig. 9. For comparison we have included all the Brønsted and Livingston data up to an ionic strength of 0.01. The dashed line shows the limiting slope predicted by the Brønsted theory, employing the Debye-Hückel limiting law for calculating activity coefficients. The line is drawn as it was placed by Brønsted and Livingston. The experiments at the bottom of Table VII, in which the concentration of cobaltammine was increased twenty-fold, indicate that within the experimental limits, the specific rate is independent of the cobaltammine concentration in this concentration region.

These experiments were performed in much the same way as were those in connection with the cobaltammine-mercuric ion reaction described above. The principal difference was the necessity for the exclusion of carbon dioxide. All stock solutions were prepared with carbon

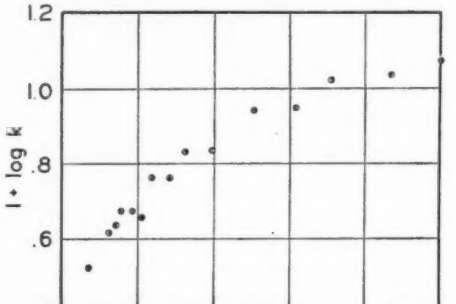

FIG. 7. The effect of the addition of salts to the reaction $BrCH_2COO^-+S_2O_3^{--}$. Data of von Kiss and Vass (reactants $0.00125M$): ● no added salt, ◑ $NaNO_3$ added, ◐ Na_2SO_4 added. Data of present authors (reactants $0.001M$): ⊖ KNO_3 added, ⊕ K_2SO_4 added, ⊗ $K_3Co(CN)_6$ added.

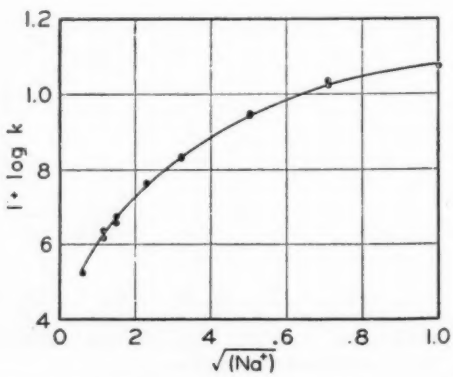

FIG. 8. The data of Fig. 7 replotted against square root of positive ion concentration.

[8] J. N. Brønsted and A. Delbanco, Zeits. f. anorg. allgem. Chemie 144, 248 (1925).
[9] J. N. Brønsted, J. Am. Chem. Soc. 44, 877 (1922).

TABLE III. Rate data for the reaction $Co(NH_3)_5Br^{++}+Hg^{++}$.

(Brønsted and Livingston)

$C_{Co}=4.00\times10^{-4}M$, $T=15°C$; $C_{Hg}=2.78\times10^{-4}M$ (except No. 25 where it is $5.56\times10^{-4}M$)

Run	Salt	C_{salt}	k	μ
21	KNO_3	0.0025	122	0.0047
29	$Ba(NO_3)_2$	0.00125	113	0.0059
23	KNO_3	0.0100	155	0.0122
31	$Ba(NO_3)_2$	0.0050	160	0.0174
32	$Ba(NO_3)_2$	0.0050	156	0.0174
25	KNO_3	0.0150	207	0.0182
39	$La(NO_3)_3$	0.00512	215	0.0329
26	KNO_3	0.0200	205	0.0222
34	$Ba(NO_3)_2$	0.0100	196	0.0322
36	$Sr(NO_3)_2$	0.0100	200	0.0322

TABLE IV. Rate data for the reaction $BrCH_2COO^-+S_2O_3^{--}$.

(von Kiss and Vass)

Equimolar reactants, $0.00125M$; $T=25°C$

Normality of added salt	$NaNO_3$ added k	μ	Na_2SO_4 added k	μ
0.01	0.412	0.015	0.432	0.020
0.05	0.580	0.055	0.577	0.080
0.10	0.678	0.105	0.682	0.155
0.25	0.875	0.255	0.886	0.380
0.50	1.05	0.505	1.10	0.755
1.00	1.18	1.005	1.40	1.505

dioxide free water and kept in bottles provided with guard tubes. Vessels used in solution preparation were swept out with purified air, and a stream of this air was introduced into each flask during dilution to the low concentrations employed.

The effect on the rate due to the addition of sodium bromide or of sodium sulfate is shown in Fig. 10 and in Table VIII.

In commenting upon the Brønsted and Livingston data for this reaction, Brønsted stated:[10] "The effect seems to be more uniform when in the solution of the various salt types (KCl, $BaCl_2$, etc.) equivalent concentrations instead of ionic strengths are compared." If the added "inert" salt is restricted to a chloride, or perhaps to one with a univalent negative ion, the above statement is adequate. However, if we include salts of higher negative charge types we see that it is the concentration and character of the negative ion that exerts the dominant effect on the rate. If the two reactants had equal but opposite charges, it appears probable to us that both salt ions might exert noticeable effects.

The reactions discussed above comprise the group upon which the Livingston Diagram[11] is based. This diagram, shown in Fig. 11, has been widely reproduced in support of the Brønsted theory of ionic reaction rates combined with the Debye-Hückel activity coefficient calculation. We have omitted discussing two of the reactions of the diagram. Reaction 4, the alkaline hydrolysis of ethyl acetate[12] is not a reaction between two ions, and is not relevant to our present work. Reaction 5, the decomposition of hydrogen peroxide by hydrogen bromide was studied by Livingston.[13] The points shown in the diagram for this reaction include no data for any run in which the ionic strength was changed by the addition of "inert" salts. The analogous reaction involving hydrogen iodide was investigated by Liebhafsky and Mohammad.[14] In this case the measured rate is the sum of two reactions. For that part of the total reaction involving hydrogen and iodide ions, these authors found no salt effect over a range of ionic strengths from 0.05 to 0.5 in solutions in which the ionic strength was varied by the addition of sodium or barium perchlorate. Until these results are reconciled, it does not seem advisable to us to consider either of these reactions in testing a theory of salt effects. Livingston used the results of La Mer[15] for Reaction 2, the bromoacetate-thiosulfate reaction. However, since La Mer, in general, did not add "inert" salts to his reactants, we found the data of von Kiss and Vass[7] of more interest to us.

In the other reactions of the diagram, wherever precise experimental data have been available, we have been able to show that the specific reaction rates, to as low concentration ranges as are accessible to experiment, show a functional dependence on the concentration of

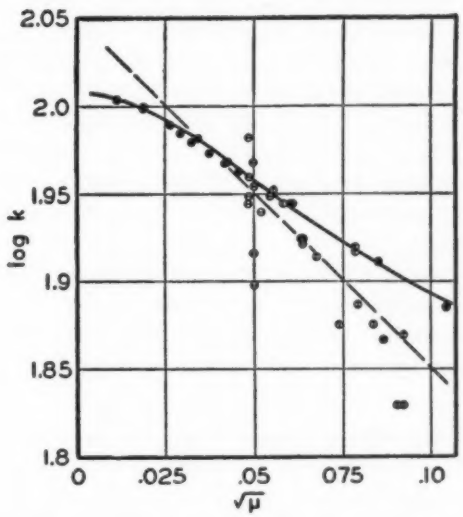

FIG. 9. The reaction $Co(NH_3)_5Br^{++}+OH^-$. Filled circles are data of present authors, cobaltammine concentration $5.0\times10^{-6}M$, sodium hydroxide concentration varied, no added salts. Data of Brønsted and Livingston: ⊖ no added salts, ⊙ $BaCl_2$ added, ⊕ NaCl added. Dashed line: Debye-Hückel limiting slope from Brønsted equation as drawn by Brønsted and Livingston. Curve is calculated from equation in text.

[10] J. N. Brønsted, *Contemporary Developments in Chemistry* (Columbia University Press, New York, 1927).
[11] R. Livingston, J. Chem. Education **7**, 2887 (1930).
[12] S. Arrhenius, Zeits. f. physik. Chemie **1**, 111 (1887).
[13] R. Livingston, J. Am. Chem. Soc. **48**, 53 (1926).
[14] H. A. Liebhafsky and A. Mohammad, J. Am. Chem. Soc. **55**, 3977 (1933); J. Phys. Chem. **38**, 857 (1934).
[15] V. K. La Mer, J. Am. Chem. Soc. **51**, 3341 (1929); *ibid.* 3678.

TABLE V. Rate data for the reaction $BrCH_2COO^- + S_2O_3^{--}$.

Equimolar reactants, 0.00100M Salt	C_{salt}=0.02N k	T=25.0°C μ
KNO_3	0.472	0.0240
K_2SO_4	0.472	0.0340
$K_3Co(CN)_6$	0.462	0.0440

TABLE VI. Saponification of nitrourethane ion by hydroxide ion.

(Brønsted and Delbanco)

C_{N^-}=0.00581 Salt	C_{OH^-}=0.0250 Total equivalent concentration	C_{salt}=0.07N k	T=20°C μ
None	0.0308	0.196	0.0308
KCl	0.1008	0.242	0.101
K_2SO_4	0.1008	0.243	0.136
$K_3Co(CN)_6$	0.1008	0.247	0.171
$Pt(NH_3)_4Cl_2$	0.1008	0.306	0.136
$Co(NH_3)_6Cl_3$	0.1008	0.586	0.171

some particular ion and not upon the ionic strength. This seems to imply that if we retain the Brønsted theory of reaction rates, we must abandon the Debye-Hückel theory either in its limiting or in its more extended forms for calculating activity coefficients of ions; for in these theories, activity coefficients, and therefore Brønsted's "kinetic activity factor," $f_A f_B / f_X$, are functionally dependent on ionic strength. The experimental rates, however, show a quite different functional dependence, as has been shown above. We must emphasize that the Brønsted-Debye combined theory is not being criticized here on the basis of small deviations from quantitative predictions. We are trying to point out that a different kind of comparison gives a much more successful method of correlating the results of kinetic experiments.

With complete freedom of choice of both mathematical form and complexity, a large number of empirical equations could be used to fit the foregoing rate data. Influenced by some other work now in progress in this laboratory, we decided to try the form

$$k = k_a\left[\frac{1}{1+K(X)} + k'\frac{K(X)}{1+K(X)}\right].$$

That we were successful in fitting the data can be seen from the solid lines in the various diagrams which were calculated from equations of this form. At high salt concentrations or for some reactions involving higher ionic charges, $K(X)$ was replaced by $K(X)+K'(X)^2$, in order to get an agreement to about one percent. In this equation k is the specific rate at some concentration of salts and reactants, k_a the specific rate at some low concentration of these substances, and k' and K are adjustable constants. (X) represents the concentration of a particular ion contributed either by added salts or by the reactants or by both.

Thus for the reaction of bromopentammine cobaltic ion with hydroxide ion, without added salts, the experimental specific rates are expressed by

$$k = 101.7\left[\frac{1}{1+158.8(X)} + 0.6198\frac{158.8(X)}{1+158.8(X)}\right]$$

with an average deviation of 0.4 percent. Here (X) is the concentration of hydroxide ion in moles per liter. The value 101.7 is the calculated bimolecular specific rate at this cobaltammine concentration ($5.0\times10^{-6}M$) and zero hydroxide concentration. As mentioned above, another series of experiments at a cobaltammine concentration twenty-fold greater than this indicated no significant change in the specific rate at any hydroxide concentration in this range. We therefore may be justified in assuming that k_a will not change appreciably from its value, 101.7, as we decrease the cobaltammine concen-

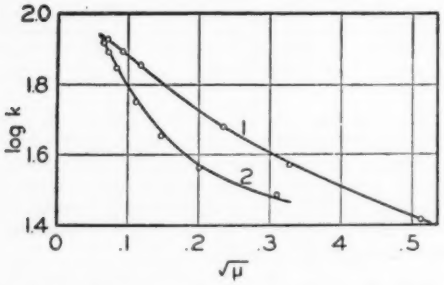

FIG. 10. The addition of salts to the reaction $Co(NH_3)_5Br^{++} + OH^-$. Cobaltammine concentration, $5.0\times10^{-6}M$; hydroxide ion concentration $3.46\times10^{-3}M$. Curve 1, NaBr added; curve 2, Na_2SO_4 added.

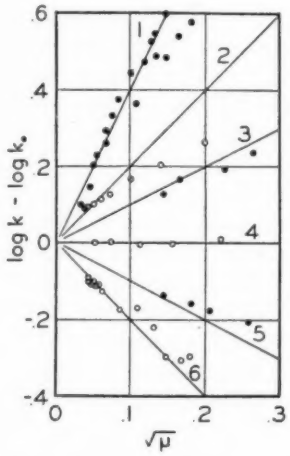

FIG. 11. The Livingston Diagram (see reference 11).

1. $Co(NH_3)_5Br^{++} + Hg^{++} + H_2O \rightarrow Co(NH_3)_5H_2O^{+++}$. Reference 1
2. $BrCH_2COO^- + S_2O_3^{--} \rightarrow S_2O_3CH_2COO^{--} + Br^-$. Reference 15
3. $NO_2{=}N{-}COOC_2H_5^- + OH^- \rightarrow N_2O + CO_3^{--} + C_2H_5OH$. Reference 8
4. $CH_3COOC_2H_5 + OH^- \rightarrow CH_3COO^- + C_2H_5OH$. Reference 12
5. $H_2O_2 + H^+ + Br^- \rightarrow H_2O + Br_2$. Reference 13
6. $Co(NH_3)_5Br^{++} + OH^- \rightarrow Co(NH_3)_5OH^{++} + Br^-$. Reference 1

TABLE VII. Rate data for the reaction $Co(NH_3)_5Br^{++}+OH^-$.

(No added salts) $10^4\times$(cobaltammine)	$10^4\times$(NaOH)	k	$T=15.0°C$ $(\mu)^{\frac{1}{2}}$
5.0	1.202	101.0	0.0116
	3.460	99.8	0.0190
	3.460	99.7	0.0190
	6.91	97.5	0.0266
	8.55	96.4	0.0295
	10.37	95.4	0.0325
	10.88	95.9	0.0332
	13.92	94.0	0.0375
	17.41	92.7	0.0419
	18.05	92.9	0.0427
	20.89	91.6	0.0459
	36.35	88.0	0.0604
	72.6	81.4	0.0853
	109.0	76.7	0.1045
98.6	18.05	92.4	0.0458
	36.35	87.3	0.0627
	72.6	81.3	0.0870

TABLE VIII. Rate data for the reaction $Co(NH_3)_5Br^{++}+OH^-$.

(Cobaltammine) $=5.0\times10^{-4}M$ (NaOH) $=3.46\times10^{-3}M$ (NaBr)	(Na_2SO_4)	k	$T=15.0°C$ $(\mu)^{\frac{1}{2}}$
$0.001557M$		85.0	0.0709
0.00520		78.2	0.0932
0.01033		71.5	0.1175
0.0520		47.9	0.236
0.1038		37.4	0.328
0.2600		26.0	0.513
	$0.000308M$	82.9	0.0664
	0.000621	78.2	0.0731
	0.001233	70.1	0.0847
	0.003080	56.2	0.1128
	0.00621	45.0	0.1487
	0.01240	36.5	0.2018
	0.03102	30.6	0.3110

tration to zero. At infinite dilution then,

$$k=k_0\left[\frac{1}{1+158.8(X)}+0.6198\frac{158.8(X)}{1+158.8(X)}\right].$$

Comparing this expression with Brønsted's equation, we find that if the Brønsted equation is valid,

$$\frac{f_A f_B}{f_X}=\frac{1}{1+158.8(X)}+0.6198\frac{158.8(X)}{1+158.8(X)}$$

for this particular reaction.

The form of this expression is suggestive of an alternative interpretation. Thus, instead of considering an average effect on all of the reactant particles of a given charge type, we might consider a more intimate picture in which we divide each of the reactants into two groups. In the one group would be those particles which have the same specific reaction rate, k_0, as they would have at infinite dilution. This fraction is designated by $1/[1+K(X)]$. In the other group would be those reactant particles that are so closely associated with other particles, usually salt ions of opposite charge sign, that the electric force between the reactants is distinctly altered; i.e., they would have the specific rate constant $k'k_0$. This fraction is designated by $K(X)/[1+K(X)]$. Since such association would always result in a decrease of the absolute value of the electric force between reactant ions, k' must be less than one for a reaction between ions of opposite sign, and greater than unity for reactions between ions of the same sign. This consideration alone gives the qualitative effect of salts on the rates of ionic reactions. Quantitative agreement with experiments may be got by assigning numerical values to k' and K.

Dipole Moment and Restricted Rotation in Some Chlorinated Hydrocarbons*

RICHARD A. ORIANI AND CHARLES P. SMYTH
Frick Chemical Laboratory, Princeton University, Princeton, New Jersey
(Received December 15, 1948)

Measurements of the variation of gas phase dipole moment with temperature of six chlorinated hydrocarbons are described. 1,2-dichloropropane, and, to a very small extent, 2,3-dichloropropene and 1,1,2-trichloroethane display a dependence of dipole moment on temperature. 1,4-dichlorobutane and the two isomers of 1,3-dichloropropene have dipole moments constant over the temperature range investigated. The results are analyzed both by adopting simple parametric functions to represent the potential hindering intramolecular rotation, and by computations of intramolecular energies.

RESTRICTED internal rotation can be studied in many ways, such as by electron diffraction,[1,2] infra-red and Raman spectra,[3] thermochemical measurements linked with statistical thermodynamical calculations,[4] and by the temperature variation of the dipole moments.[5] Of these, the latter is the most direct when applicable, since the observed phenomenon is an unambiguous function of the internal rotation. Because only relatively few vapor measurements of moment as a function of temperature exist in the literature,[6–13] it was thought worth while to investigate some of the chlorinated ethanes, as well as some dichlorinated methyl- and methylene-substituted ethanes. A preliminary note on our experimental results has already been published.[14]

EXPERIMENTAL

The heterodyne beat apparatus used to measure the dielectric constants of the vapors has been described elsewhere.[15] The pressure of the vapor in the dielectric cell is increased by using air pressure to force liquid up one leg of a U-tube into a heated region in which it vaporizes. Similarly, to decrease the pressure of the vapor, the air pressure is decreased on the other side of the liquid in the U-tube. The slope of the capacitance-pressure curve was determined, using some six pressures, or the two-point method was used and several determinations made and the average taken.

All the compounds were purified by careful distillation over a suitable desiccant through a four-foot packed column, and fractions boiling over 0.1° range or less were used in the measurements. The 1,1,2-trichloroethane and 1,4-dichlorobutane were obtained from Eastman Kodak; the 2,3-dichloropropene was received from Columbia Organic Chemicals Company, the 1,2-dichloropropane, from the Paragon Testing Laboratories, and the two isomers of 1,3-dichloropropene, from Halogen Chemicals Company. The dielectric cell was calibrated with the vapors of chlorobenzene, ethyl bromide, and nitrobenzene. Molar refractions were computed from refractive indices and densities of the liquids in the literature; these were measured when literature values were lacking.

RESULTS

Table I presents the molar refractions, and the polarizations and dipole moments *versus* temperatures for the six compounds examined. The dipole moments, μ, were computed from the polarizations, P, by the well-known relationship, $\mu=0.01281\times10^{-18}[(P-R_D)T]^{\frac{1}{2}}$, where R_D is the molar refraction for the D sodium line and T is the absolute temperature. The moment-temperature relationships for 1,1,2-trichloroethane, 1,2-dichloropropane, and 2,3-dichloropropene are shown graphically in the A-curves of Fig. 1, in which are also shown for comparison the data of Zahn[8] for 1,2-dichloroethane, the other data for this substance in the literature[9,13] being in essential agreement with these. In Table II are gathered together the vapor dipole moment measurements for the halogenated ethanes, propanes, propenes, and butane that might be expected to display a variation of dipole moment with temperature and also two similar compounds containing bromine. The table also includes values calculated by the equation of Smyth and Walls[16,17] for the dipole moment that would be observed if completely free intramolecular

* This work was carried out with the support of the ONR.
[1] P. Debye, J. Chem. Phys. **9**, 55 (1941).
[2] J. Y. Beach and K. J. Palmer, J. Chem. Phys. **6**, 639 (1938).
[3] G. Herzberg, *Infrared and Raman Spectra of Polyatomic Molecules* (D. Van Nostrand Company, New York, 1945).
[4] E. B. Wilson, Jr., Chem. Revs. **27**, 17 (1940); K. S. Pitzer, J. Chem. Phys. **14**, 239 (1946); Conn, Kistiakowsky, and Smith, J. Am. Chem. Soc. **61**, 1868 (1939).
[5] Smyth, Dornte, and Wilson, Jr., J. Am. Chem. Soc. **53**, 4242 (1931); L. Meyer, Zeits. f. physik. Chemie **8B**, 27 (1930).
[6] Ghosh, Mahanti, and Sen Gupta, Zeits. f. Physik **54**, 711 (1929).
[7] Sänger, Zeits. f. Physik **32**, 21 (1931).
[8] C. T. Zahn, Phys. Rev. **40**, 291 (1932); **38**, 521 (1931).
[9] E. W. Greene and J. W. Williams, Phys. Rev. **42**, 119 (1932).
[10] C. P. Smyth and K. B. McAlpine, J. Am. Chem. Soc. **57**, 979 (1935).
[11] R. H. Wiswall and C. P. Smyth, J. Chem. Phys. **9**, 356 (1941).
[12] Maryott, Hobbs, and Gross, J. Am. Chem. Soc. **63**, 659 (1941).
[13] Watanabe, Mizushima, and Morino, Sc. Pap. Inst. Phys. and Chem. Res. No. 1090 **39**, 401 (1942).
[14] R. A. Oriani and C. P. Smyth, J. Chem. Phys. **16**, 930 (1948).
[15] R. H. Wiswall, Jr. and C. P. Smyth, J. Am. Chem. Soc. **64**, 2212 (1942).
[16] H. Eyring, Phys. Rev. **39**, 746 (1932).
[17] C. P. Smyth and W. S. Walls, J. Am. Chem. Soc. **54**, 2261 (1932).

rotation existed. The values used for the group moments in these calculations were 1.85×10^{-18} for $-CH_2Cl$ in 1,2-dichloroethane, 1,1,2-trichloroethane, and 1,2-dichloropropane,[17] 1.57×10^{-18} for $-CHCl_2$[18] in 1,1,2-trichloroethane and 1,1,2,2-tetrachloroethane, and 1.85×10^{-18} for $-CH_2Br$. Values calculated for the restricting potential energy V_0 as discussed subsequently are given in the last column. The ± percent given after each value is the average deviation from the mean of the values calculated at different temperatures over the range indicated and is not an estimate of absolute accuracy.

DISCUSSION OF RESULTS

We shall employ two general approaches in the treatment of the data. Firstly, we shall attempt to find a relatively simple mathematical function that will roughly express the net interaction between the rotating groups, and from which the observed dipole moment and its variation with temperature can be deduced. Secondly, we shall attempt to calculate from first principles a curve of potential energy of interaction between the groups as a function of azimuthal configuration, which can then be used either to establish qualitatively the reasonableness of the observed phenomena, or to compute the temperature variation of the dipole moment.

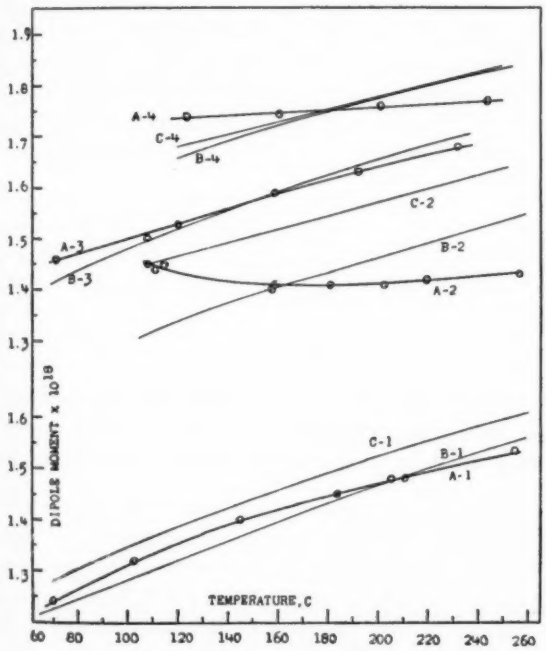

FIG. 1. Temperature dependence of dipole moments of chlorinated hydrocarbons.

A: Experimental curves.
B: Curves calculated from one-parameter analysis.
C: Curves calculated by special functions.
Molecules:
1. 1,2-dichloroethane.
2. 1,1,2-trichloroethane.
3. 1,2-dichloropropane.
4. 2,3-dichloropropene.

[18] C. P. Smyth and K. B. McAlpine, J. Chem. Phys. 1, 193 (1933).

TABLE I. Polarizations, molar refractions, and dipole moments.

Compound	T, °K	P, cc	$\mu(\times10^{18})$
1,1,2-trichloroethane	381.0	59.4	1.45
(R_D=25.85)	384.4	58.9	1.44
	388.2	59.0	1.45
	431.2	53.6	1.40
	431.8	54.0	1.41
	454.7	52.5	1.41
	476.2	51.4	1.41
	493.2	55.7	1.42
	530.4	49.5	1.43
1,2-dichloropropane	344.7	63.1	1.46
(R_D=25.60)	381.7	61.4	1.50
	393.8	61.8	1.53
	432.2	61.0	1.59
	465.6	60.3	1.63
	505.7	59.6	1.68
2,3-dichloropropene	397.0	72.1	1.74
(R_D=25.49)	434.0	68.2	1.74
	474.7	65.2	1.76
	517.9	62.4	1.77
1,3-dichloropropene	397.2	74.8	1.79
104° isomer	399.2	74.6	1.79
(R_D=25.4)	478.3	65.5	1.78
112° isomer	395.2	76.0	1.81
(R_D=25.5)	449.7	70.5	1.82
	502.7	65.0	1.81
1,4-dichlorobutane	432.9	99.6	2.22
(R_D=30.27)	468.7	94.8	2.23
	506.7	88.5	2.21

For a 1,2-disubstituted ethane, one can write[19] for the instantaneous dipole moment,

$$\mu^2(\phi)=A+B\cos\phi, \tag{1}$$

where

$$A=m_1^2+m_2^2-2m_1m_2\cos\theta_1\cos\theta_2,$$

and

$$B=2m_1m_2\sin\theta_1\sin\theta_2.$$

In these expressions, m_1 and m_2 are the group moments of the polar substituents on the two carbons assumed constant irrespective of internal configuration; these are located at angles θ_1 and θ_2 to the direction of the C−C bond. ϕ is the azimuthal angle between the two group dipoles, zero at the *cis*- and 180° at the *trans*-position. From Eq. (1) it follows that the dipole moment measured for an assembly of molecules is

$$\mu=[A+B\langle\cos\phi\rangle_{Av}]^{\frac{1}{2}}, \tag{2}$$

where $\langle\cos\phi\rangle_{Av}$, the mean of $\cos\phi$ averaged over all the molecules, is given by

$$\langle\cos\phi\rangle_{Av}=\frac{\int_0^{2\pi}\cos\phi\exp[-V(\phi)/RT]d\phi}{\int_0^{2\pi}\exp[-V(\phi)/RT]d\phi}. \tag{3}$$

[19] J. Y. Beach and D. P. Stevenson, J. Chem. Phys. 6, 635 (1938).

TABLE II. Temperature variation of dipole moment and restricting potential energy.

	t, °C	μobs	μ_f*	V_0 (cal./mole)
ClH_2C-CH_2Cl[8]	32–271°	1.12–1.54	2.46	3215 ± 2.9 percent
BrH_2C-CH_2Cl[9]	66–163°	1.09–1.28	2.46	3900 ± 1.5 percent
BrH_2C-CH_2Br[8]	66–163°	0.94–1.10	2.46	5090 ± 1.6 percent
Cl_2HC-CH_2Cl	105–258°	1.43	2.36	2820 ± 10.5 percent
$Cl_2HC-CHCl_2$[10]	128–163°	1.36	2.10	
$ClH_2C-CHClCH_3$	71–235°	1.46–1.68	2.46	2500 ± 2.2 percent
$ClH_2C-CCl=CH_2$	125–245°	1.74–1.77	2.46	2075 ± 7.7 percent
$ClH_2C-CH_2-CH_2Cl$	101–201°	2.07	2.36	
$ClH_2C-(CH_2)_2-CH_2Cl$	160–235°	2.22	2.60	

* Calculated for completely free internal rotation.

Here, $V(\phi)$ represents the functional relationship that exists between the intramolecular potential energy and azimuthal angle ϕ, T is the temperature, and R the gas constant. With $V(\phi)=(V_0/2)(1+\cos\phi)$ as assumed in former papers on this subject,[19,20–23] Beach and Stevenson have shown that Eq. (3) can be evaluated analytically as a ratio of Bessel functions with imaginary argument:

$$\langle\cos\phi\rangle_{Av}=\frac{iJ_1(iV_0/2RT)}{J_0(iV_0/2RT)}. \quad (4)$$

The value of the parameter V_0 can thus be calculated by means of Eqs. (2) and (4) from an experimental value of the dipole moment at one temperature. This has been done for the substituted ethanes and propanes that show variation of dipole moment with temperature. If the one-parameter potential function assumed is an adequate representation of the actual energy relationship, the parameter for any one molecule should be independent of temperature and deviation from constancy may be taken as a measure of the inadequacy of the assumed potential function. In Table II the last column gives the mean values of V_0 obtained from the moment values at several temperatures, as well as the deviation from constancy expressed as a percentage. The effect of using a larger group moment is to raise the calculated V_0. Thus, adopting a group moment of 2.03×10^{-18} for $-CH_2Cl$, Beach and Stevenson[19] computed a V_0 of 4000 cal./mole for 1,2-dichloroethane.

It is evident from the small percentage variations in V_0 that the simple potential function empirically represents the facts for the disubstituted ethanes and 1,2-dichloropropane. The potential barrier in the 1,2-dihaloethanes increases regularly as bromine replaces chlorine, in qualitative agreement with the expected effect of the larger bulk of the bromine atom. Figure 1B shows the curves for dipole moment against temperature calculated by means of Eqs. (2) and (4), using the mean values of V_0 tabulated in Table II for the chlorinated hydrocarbons. The agreement between the experimental curves and those calculated is not bad for the 1,2-dichloroethane and 1,2-dichloropropane. In the case of 1,2-dichloroethane, the agreement is about the same if a two-parameter function

$$V(\phi)=V_1\cos\phi+V_2\cos2\phi \quad (5)$$

is used, and the effects of the moments of inertia are included as done by Altar[24] (see curve C-1 of Fig. 1), a procedure now recognized[4] as leading to error.

Since such a function as that in Eq. (5) has clearly the incorrect symmetry in the second term for representing the interactions among the hydrogens on one carbon and the chlorine on the other, Gwinn and Pitzer[25] have adopted the form

$$V(\phi)=(V_1/2)(1-\cos\phi)+(V_3/2)(1-\cos3\phi), \quad (6)$$

from which they successfully calculate the heat capacity, entropy and dipole moment of 1,2-dichloroethane, using a partition function which is the weighted sum of the partition functions for molecules in the *trans* and in the skew configurations.

The V_0 values from the one-parameter analysis give a satisfactory qualitative explanation for the observed magnitudes and temperature dependence of the dipole moments of 1,2-dichloroethane and 1,2-dichloropropane. However, the simple one-parameter function is not successful in the cases of 2,3-dichloropropene and 1,1,2-trichloroethane as is evident from Fig. 1. The case of 2,3-dichloropropene is complicated by the presence of the double bond whose effect is difficult to evaluate. One group moment is lowered by resonance among structures,

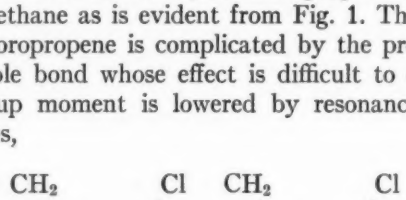

If we regard this effect as approximately independent of the azimuthal configuration of the $-CH_2Cl$ group, we may take as the constant group moment of the $CH_2=\underset{|}{C}-Cl$ the gas value of vinyl chloride, 1.44×10^{-18}, instead of the 1.85 used in the calculation of V_0 listed in Table II. This lower value of the group moment gives $V_0=725$ cal./mole ± 7 percent for 2,3-dichloropropene, which gives as low a degree of self-consistency as the former calculation. Hence, it is not an improper choice of group moment that produces the poor result, though it may well be the assumption of its constancy with azimuthal angle. In an attempt to find a potential function of the type in Eq. (6) that yields a calculated $\mu-T$ curve in better agreement with the experimental

[20] S. Mizushima and K. Higasi, Proc. Imp. Acad. **8**, 482 (1932).
[21] J. Y. Beach and K. J. Palmer, J. Chem. Phys. **6**, 640 (1938); J. Y. Beach and A. Turkevich, J. Am. Chem. Soc. **61**, 306 (1939).
[22] G. L. Lewis and C. P. Smyth, J. Chem. Phys. **7**, 1085 (1939).
[23] K. S. Pitzer and W. D. Gwinn, J. Chem. Phys. **10**, 428 (1942).
[24] W. Altar, J. Chem. Phys. **3**, 460 (1935).
[25] W. D. Gwinn and K. S. Pitzer, J. Chem. Phys. **16**, 303 (1948).

TABLE III. Interaction energies (kcal./mole) for 1,1,2-trichloroethane.

Interactions	$\phi=0°$	30°	60°	90°	120°	150°	180°
Dipole-dipole	2.64	2.60	2.43	1.83	1.15	0.55	0.34
Exchange repulsions	16.09	17.42	19.19	17.53	15.78	16.16	16.70
van der Waals	−2.47	−2.97	−3.46	−2.60	−1.44	−0.85	−0.69
Induction	−0.71	−0.85	−1.00	−0.74	−0.42	−0.24	−0.20
Sum	15.55	16.20	17.16	16.02	15.07	15.62	16.15

results we have tried several sets of values of the parameters V_1 and V_3, and have obtained the best results with values of 2000 and 200 cal./mole respectively. The calculated $\mu-T$ curve, using the potential function $V(\phi)=(2000/2)(1+\cos\phi)+(200/2)(1+\cos3\phi)$, is shown in Fig. 1 (curve *C*-4), and it is evident that the agreement achieved is only slightly better than that obtained with the one-parameter function. This calculation was performed with the aid of charts in an article by W. J. Taylor,[26] written in connection with another problem, but making use of similar functions.

The one-parameter analysis fits 1,1,2-trichloroethane even less well, since it leads to a monotonic rise of dipole moment with temperature whereas the experimental curve shows a flat minimum, amounting to but a slight departure from constancy, so slight as possibly to be due to an abnormal experimental error, not evidenced but shortly to be checked. Figure 1 (curve *C*-2) shows a $\mu-T$ curve computed from Eqs. (2) and (3), and $V(\phi)=(2080/2)(1+\cos\phi)+(1260/2)(1+\cos3\phi)$, the curves being made to match at 110°C. Taylor's charts were used to evaluate the integrals. It is clear that the results are as poor as with the one-parameter function. Several other attempts were made to adjust the parameters in functions of the type of Eq. (6), as well as the type $V(\phi)=(V_1/2)(1+\cos\phi)+(V_3/2)(1-\cos3\phi)$, but not with good results. For example, evaluating graphically the integrals with $V(\phi)=(1100/2)(1+\cos\phi)+(2100/2)(1-\cos3\phi)$ at $T=383.2°K$, and using $m(CH_2Cl)=1.85$ and $m(CHCl_2)=1.57$, one obtains $\mu=1.89$, rather than the experimental value 1.45. This $V(\phi)$ was employed because it is an approximate algebraic expression of the potential energy *vs.* ϕ curve computed by intramolecular interactions as described below.

The moment variation of 1,1,2-trichloroethane is so slight that it might well be considered with those of the molecules in Table IV. The potential energy curve calculated by Turkevich and Beach[27] and found consistent with their electron diffraction results has been recalculated with the addition of the attractive energy due to the inductive effects of the permanent dipoles upon the polarizable atoms and the attractive energy due to dispersion interaction. The calculated interaction energies in Table III give a curve similar in general form to that of Turkevich and Beach.

[26] W. J. Taylor, J. Chem. Phys. **16**, 257 (1948).
[27] A. Turkevich and J. Y. Beach, J. Am. Chem. Soc. **61**, 3127 (1939).

TABLE IV. Molecules with temperature independent dipole moments.

	Temp. range, °C	Dipole moment $\times10^{18}$
1,1,2,2-tetrachloroethane*	128–163	1.36
1,3-dichloropropane*	101–201	2.07
1,4-dichlorobutane	160–235	2.22
1,3-dichloropropene		
104° isomer	124–205	1.79
112° isomer	122–230	1.81

* See reference 10.

Quantitative calculations with these energies and also with a second set of values obtained by choosing 0.15 as the ratio of coulombic to exchange energy instead of 0.20 as in the first set of values fail to reproduce the moment values satisfactorily. Qualitatively, it appears that the explanation of the absence of any considerable variation of moment with temperature is similar to that offered previously[10] in the case of 1,1,2,2-tetrachloroethane, namely, the inability of the molecules to pass in considerable numbers from potential minima corresponding to moderate moment values over high barriers to positions of higher energy and higher moment.

Molecules with Temperature Independent Dipole Moments

Table IV lists the molecules whose dipole moments might be expected to be temperature sensitive but which are found to be constant over the temperature range investigated. The reason for expecting a variation of moment with temperature is that for each molecule there is hindered rotation between two groups, each of which carries an unbalanced dipole. In general, if the experimental temperature range were great enough, a variation of dipole moment would be evident for each of the five molecules in the table. The only exception to this is the *trans*-isomer of 1,3-dichloropropene, as will be explained below. From a consideration of the interactions among the chlorines in 1,1,2,2-tetrachloroethane, Smyth and McAlpine[10] have shown why it is reasonable to expect only a small increase in the dipole moment for this molecule in the short temperature range available.

The case of the isomers of 1,3-dichloropropene is interesting in that the measured vapor dipole moments do not serve to identify the isomers as the *cis*- or *trans*-stereoisomers. From a study of the Stuart models of these molecules one can see qualitatively why the two measured dipole moments should be so similar. In the *trans*

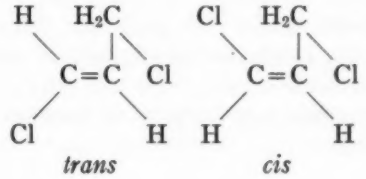

isomer the C−C axis of rotation is parallel to the fixed C−Cl vector. Hence one would expect a net dipole moment practically independent of temperature, whether or not the hindrance to the internal rotation be large, small, or varying strongly with azimuthal angle. If the value 1.44 is assigned to the moment of the C−Cl dipole adjacent to the double bond and 1.85 to the other C−Cl moment with an angle of 110° between the directions of the two dipole axes, a resultant moment 1.92 is calculated for the molecule. The discrepancy between this calculated value and the observed, 1.79 or 1.81, is less than the possible error resulting from uncertainties in the bond moment values. In the *cis*-molecule, a very large potential energy should exist in the position $\phi=0°$ ($\phi=0°$ when the two chlorines are in closest proximity), a minimum energy at 180°, and two shallow minima not far from 80–90° and 270–280°. The positions of maximum moment, which are virtually excluded because of their high potential energies, lie not far from $\phi=0°$, while the minimum moment, about 1.2×10^{-18}, should occur at $\phi=180°$. The moment value corresponding to the two shallow minima is calculated to be about 2.5, if one neglects mutual inductive effects, which would lower the resultant moment somewhat. To push a considerable number of molecules to positions in the neighborhood of $\phi=0°$ would require a temperature above that usable in the present measurements, while the variation in energy between the angles 80° and 280° is so small that a moderate change of temperature does not greatly alter the moment distribution. The absence of measurable moment variation in the rather limited temperature range obtainable is, therefore, not surprising, and the observed moment value, 1.79 or 1.81, is of the magnitude to be expected.

A factor which has not been considered in the discussion of the three unsaturated molecules is the possible introduction of some double bond character into the single carbon-carbon bond by resonance contributions arising from the presence of the double bond. Such double bond character would tend to introduce new potential barriers restricting rotation or alter the heights and locations of the barriers arising from steric and electrostatic effects. This would generally tend to reduce the variation of moment with temperature over the limited range experimentally attainable. In the *cis*-1,2-dichloropropene molecule, the near approach of the two chlorines for values of ϕ not far from zero would tend to stabilize the resonating structure with a positive chlorine and thus reduce the high moment of this configuration. Induction between the two adjacent C−Cl dipoles would also lower the moment of this configuration. Insofar as these positions were occupied to an appreciable extent, these two effects would tend further to reduce any increase of moment with rising temperature.

1,3-dichloropropane and 1,4-dichlorobutane have respectively two and three degrees of internal restricted rotation. If there were completely free internal rotation about each of the bonds, we would expect the significantly larger moments given μ_f in Table II. In view of the uncertainty in the assignment of group moments in these molecules, no great significance should be attached to the numerical discrepancy between the moment for free rotation μ_f and the experimental values. However, in going from the two-carbon to the three-carbon molecules having terminal polar groups, the discrepancy $\mu_f-\mu_{obs}$ decreases considerably. This is due to the decrease in polar group interaction caused by their greater average separation.[17,28] In the 1,4-dichlorobutane we would expect much less interaction between the terminal C−Cl groups, since here they are separated by two methylene groups. Were there no other type of interaction then we would look for $\mu_f-\mu_{obs}=0$ in the butane. Another interaction is that which occurs between the methylene groups in long paraffin chains. Taylor[26] has shown that, if one accepts the planar *trans*-configuration of three successive carbons in a paraffin chain as the most stable, as shown by x-ray analysis on crystalline normal paraffins, the existence of the restricted rotation at each C−C bond causes a greater contribution to the average configuration from the extended forms than would occur if there were completely free rotation. In 1,3-dichloropropane, this paraffin-like interaction may make itself felt and give greater prominence to the zig-zag configuration, for which the two C−Cl moments are on the same side of the chain. In 1,4-dichlorobutane, the paraffin-like interaction may well be the predominant one, but here the extended zig-zag configuration brings the C−Cl moments more into opposition. Consequently, the consideration of the paraffinic interactions alone would lead one to expect a larger $\mu_f-\mu_{obs}$ for the 4-carbon compound than for the 1,3-dichloropropane.

It will be noted that no quantitative account has been taken of variation of inductive effect with azimuthal angle. When change in azimuthal angle brings two C−Cl dipoles close together, their moments are lowered by mutual induction. Even when the two dipoles are far apart, the angle made by the axis of the resultant moment of the C−Cl dipole and its environment with the adjacent C−C bond is actually somewhat different from the assumed 110° and may change a little with change in azimuthal angle. The more important effect of lowering of moment by mutual induction cannot be calculated with accuracy. The effect would be partially compensated by the use of a somewhat lower moment value, which would incorrectly average the effect over the whole 360° variation of the azimuthal angle, but would give lower calculated potential barriers and moment variations, more nearly as observed.

[28] C. P. Smyth and W. S. Walls, J. Chem. Phys. **1**, 200 (1933).

Reduced Temperatures for the Liquid State. General Equations for the Orthobaric Densities as Functions of the Reduced Temperature

ARTHUR F. SCOTT AND ROBERT DILLON*
Department of Chemistry, Reed College, Portland, Oregon
(Received January 28, 1949)

The reduced temperature θ proposed by Bauer, Magat, and Surdin for the liquid state is presented and their work is reviewed. Attention is directed to the fact that a number of empirical power law equations that represent the variation of a property of a liquid as a function of the van der Waals reduced temperature are directly transformable into analogous functions of θ. General equations are derived for the variation of the orthobaric liquid and vapor densities as function of the reduced temperature.

IN developing the concept of corresponding states for liquids it has been customary to employ as the temperature scale the familiar reduced temperature $T_r=T/T_c$. A number of years ago, however, Bauer, Magat, and Surdin[1] defined a new reduced temperature for liquids and undertook to show "that the use of this new variable simplifies the study of the static properties of liquids in the same way as the reduced variables of van der Waals do for gases." The reduced temperature of Bauer, Magat, and Surdin is defined:

$$\theta=(T-T_f)/(T_c-T_f), \tag{1}$$

where T is the Kelvin temperature; T_c, the critical temperature; and T_f, the melting point temperature, or more correctly, the triple point temperature. As can be seen the reduced temperature θ assumes all values between 0 and 1, as the temperature of the liquid varies from T_f to T_c. According to an abstract, another group of investigators, Sibaiya and Rao,[2] have also hit upon the idea of the reduced temperature θ and are reported to have described it as a "new reduced temperature."

Bauer, Magat, and Surdin based the validity of their reduced temperature θ on a limited number of empirical tests which they carried out as follows. For a given property of a liquid P, values of the ratio P_t/P_f (P_t, value of property P at temperature T; P_f, value of property at triple point temperature) for a number of different liquids were plotted against θ-values corresponding to temperature T. In a graph constructed in this way for molecular volumes the plotted points for 17 different liquids were shown to fall closely on a common curve for which the authors established the following empirical two-constant formula:

$$V_t/(V_f-1)=3.36[1-(1-\theta)^{1/10}]. \tag{2}$$

(Two liquids, H_2 and H_2O, were found to be represented by a curve similar to, but slightly lower than, the main curve in the graph.) Combining their relationship with the Eötvös law for surface tension, Bauer, Magat, and Surdin derived an expression for the variation of surface tension with θ which they showed graphically to hold for the so-called normal liquids. In a plot of values of the ratio of compressibilities β/β_f for 10 different liquids against corresponding θ-values it was found that the plotted points fall on a common curve for which an empirical equation was also established. An analogous test of the specific heat was made with data for only 5 liquids. In the case of this property the curves for mono- and diatomic liquids have the same general shape, but the difference between C_v values, for the same θ is about 2 calories, as it is for perfect gases. Bauer, Magat, and Surdin sought to extend their method to the dynamical properties, viscosity and heat conduction, but found that the points for each liquid formed a separate curve rather than a common one.

The primary purpose of this note is to call attention to the fact that simple functions involving the reduced temperature T/T_c can be transformed readily into functions involving the reduced temperature θ. We shall consider here only one case. The variation of many properties of liquids have been found to be representable by an expression of the form

$$P=P_0(1-T/T_c)^n, \tag{3}$$

where the power index n is a general constant dependent only on the property being represented; and P_0 is a constant characteristic of each substance. Now at the triple point temperature T_f Eq. (3) becomes

$$P_f=P_0(1-T_f/T_c)^n. \tag{4}$$

Dividing (3) by (4) we get

$$P/P_f=[(T_c-T)/(T_c-T_f)]^n. \tag{5}$$

Since

$$T_c-T_f=(T_c-T)+(T-T_f), \tag{6}$$

the right-hand term of (5) can be rearranged as follows

$$P/P_f=[(T_c-T_f)/(T_c-T_f) -(T-T_f)/(T_c-T_f)]^n=(1-\theta)^n. \tag{7}$$

Empirical power law expressions of the type shown in Eq. (3) are known for the following properties of liquids:

* Present address: Graduate School, Northwestern University.
[1] Bauer, Magat, and Surdin, "A discussion on structure and molecular forces in pure liquids," Trans. Faraday Soc. (September 1936), p. 81.
[2] L. Sibaiya and M. R. Rao, Curr. Sci. 8, 359 (1939).

orthobaric densities,[3] surface tension,[4] compressibility,[5] internal latent heat,[6] total latent heat,[6] and viscosity.[7] In the expression for a given property the power-index is found to differ little in value from liquid to liquid, and is generally regarded as a constant. These expressions for the different properties of liquids, therefore, can all be transformed directly into expressions of the type of Eq. (7) in which, for a given property, the ratio P/P_t for all liquids is represented by a single general function of θ.

In passing it may be noted that it should be possible to invent other reduced temperature scales, analogous to the θ-scale, for functions of the type shown in Eq. (3). Obviously, however, no such scale for liquids would have the same general significance or usefulness as the θ-scale of Bauer, Magat, and Surdin.

It will be of interest to indicate the derivations for two expressions representing the variation of the orthobaric liquid and vapor densities in terms of the reduced temperature θ. The starting point of the derivation is the Verschaffelt equation

$$(D-d)=D_0[1-(T/T_c)]^n \tag{8}$$

where D is the density of the liquid and d, the density of the vapor in equilibrium with the liquid, at temperature T; D_0 is a constant, and T_c is again the critical temperature. This empirical equation has had a rather curious history. It was originally proposed by Verschaffelt[3] who set $n=\frac{1}{3}$, and had in place of the constant D_0, the term mD_c (m=a general constant, and D_c=the density of the substance at the critical temperature). Goldhammer,[3] from a rather extensive test of Verschaffelt's relationship, concluded that, while $n=\frac{1}{3}$, the other constant m was a variable which varied slightly from substance to substance. Sugden[3] derived the expression (8) from van der Waals' relationship between surface tension, and MacLeod's relationship between surface tension and $(D-d)$. Sugden's derivation made $n=\frac{3}{10}$. Without any reference to Sugden's work Ferguson and Miller[8] derived, by the same route, Sugden's equation with $n=\frac{3}{10}$; for their purposes, in place of D_0, they wrote $4D_c$. Recently, Guggenheim,[9] from considerations relating to the principle of corresponding states derived Eq. (8) with $n=\frac{1}{3}$ and $D_0=7/2D_c$. Apparently Guggenheim was unfamiliar with the previous history of this relationship, for he refers to his equation as "new" and one which, on certain occasions, "in view of its extreme simplicity and surprisingly high accuracy has much to recommend it."

A decision as to the correct value of the exponent n is complicated by Sugden's manner of treating the equation. Having accepted $\frac{3}{10}$ as the correct value of the exponent Sugden adjusted the value of T_c in order to get the best representation of the experimental data by his equation. In the case of "unassociated" liquids the differences between the experimental and adjusted T_c values were quite small, the maximum difference not exceeding 5°C. In the case of associated liquids the differences were of the order of 15°C. For the time being the present writers are inclined to accept $\frac{3}{10}$ as the best value of the power index and also to recommend Sugden's scheme of using the adjusted T_c values where these can be established conveniently. It is recognized, of course, that a thorough study of the Verschaffelt equation is desirable and that this might lead to a modification of the views expressed above.

Equation (8) can be transformed, as shown above, into the expression

$$(D-d)/(D_f-d_f)=(1-\theta)^n, \tag{9}$$

where D_f and d_f are the densities of the liquid and vapor, respectively, at the triple point. Since for most liquids d_f would be negligible relative to the density of the liquid at the triple point D_f, the denominator of the left-hand member of the expression can be written simply as D_f. If we may assume a constant value for the index n for all liquids, we have the striking result that the variation of the difference between the orthobaric densities with temperature is represented by a simple general function of θ in which D_f is the only constant characteristic of a particular liquid.

When D/D_f and d/D_f values of a substance are plotted as abscissae against corresponding θ-values as ordinates, the resulting graph resembles the familiar plots of orthobaric densities given in textbooks to illustrate the law of rectilinear diameters. In a plot of this kind the mean density is given quite accurately by a linear relationship which is derivable from the familiar approximate equation of Cailletet and Mathias:

$$\tfrac{1}{2}(D/D_f+d/D_f)=d_m/D_f=0.5-K\theta. \tag{10}$$

But plots of D/D_f and d/D_f values for different substances against θ-values do not yield one common curve because of small differences in values of the constant K in (10). The nature of the differences in K can be seen from the fact that at the critical temperature $\theta=1$, and d_m becomes D_c, giving for the constant K

$$K=0.5-D_c/D_f. \tag{11}$$

Values of the term D_c/D_f for representative liquids fall within the narrow range, 0.31 to 0.38. The constant K will, therefore, have a value 0.12–0.19, depending on the liquid.

[3] J. E. Verschaffelt, Communication of Leiden, No. XXVIII (1896); S. Sugden, J. Chem. Soc. 1780 (1927); D. A. Goldhammer, Zeits. f. physik. Chemie **71**, 577 (1910).

[4] A. Ferguson, Phil. Mag. **31**, 37 (1916); A. Ferguson and S. J. Kennedy, Trans. Faraday Soc. **32**, 1474 (1936).

[5] Unpublished studies with James G. Wendel.

[6] For discussion of these functions see article by W. J. Jones and S. T. Bowden, Phil. Mag. **37**, 480 (1946).

[7] The power-law function for viscosity takes the form $(\eta-\eta_c)=(\eta_0-\eta_c)(1-T/T_c)^n$; W. J. Jones and S. T. Bowden, Phil. Mag. **36**, 705 (1945); see also reference 6.

[8] A. Ferguson and J. T. Miller, Proc. Phys. Soc. London **46**, 140 (1934).

[9] E. A. Guggenheim, J. Chem. Phys. **13**, 253 (1945).

If we combine Eqs. (9) and (10), by adding and subtracting, we get

$$D/D_f=\tfrac{1}{2}[1-2K\theta+(1-\theta)^n], \quad (12)$$

and

$$d/D_f=\tfrac{1}{2}[1-2K\theta-(1-\theta)^n]. \quad (13)$$

It appears, therefore, that D/D_f for all liquids is represented by the same function of the reduced temperature θ with only the single constant K being characteristic of the liquid, assuming, as was discussed above, that the exponent n is identical for all liquids. The same is true for the vapor density ratio d/D_f. If values of $D/D_f+K\theta$ and $d/D_f-K\theta$ are plotted as abscissae against corresponding θ-values, the plotted points should fall on a symmetrical curve represented by $0.5[1\pm(1-\theta)^n]$. This fact suggests the possibility of a graphical method for establishing the value of K.

An approximate expression for the characteristic constant K in terms of characteristic properties T_c and T_f of the liquids can be derived by the following argument. Assuming again that the density of the vapor of a liquid is negligible at the triple point, Eq. (8) can be written in the form

$$D_f/D_0=[(T_c-T_f)/T_c]^n. \quad (14)$$

Now, in his work with Eq. (8), ($n=\frac{3}{10}$), Sugden found the following relationship to hold for all the liquids included in his study

$$D_c=0.27D_0. \quad (15)$$

Assuming this to be a general relationship we can obtain from (15), (14), and (11) the following expression for the constant K:

$$K=0.5-0.27[T_c/(T_c-T_f)]^n \quad (16)$$

which relates K to the limits involved in the definition of θ.

Since Eqs. (12) and (13) were derived from the Verschaffelt equation and the law of rectilinear diameters, with the temperature expressed as the reduced temperature θ, it might be expected that similar equations would already have been deduced with temperatures expressed in the form of van der Waals' reduced temperatures. So far as the writers are aware this has been done only by Ferguson and Miller.[8] They derived an expression for D/D_c as a universal function of T/T_c and pointed out that a relation for d/D_c could be obtained in a similar manner. The equation of Ferguson and Miller can be transformed into a function of θ identical in form to our Eq. (12). The values of the constant factors in the two expressions are not susceptible to a simple comparison. It is significant, however, that Ferguson and Miller, using $n=\frac{3}{10}$, found their equation to represent satisfactorily the density data for thirty organic liquids. Only in the case of alcohols did the value of $\frac{3}{10}$ for the power index n seem unsuitable. It was with this class of liquids, it will be recalled, that Sugden found a significant adjustment of T_c to be necessary.

Equations similar to our Eqs. (12) and (13) have been presented recently by Guggenheim.[9] Starting on the assumption that the principle of corresponding states would lead one to expect D/D_c and d/D_c to be universal functions of T/T_c, Guggenheim developed empirical expressions to represent the experimental data for argon. His empirical formulas, Guggenheim points out, portray fairly well the experimental data of the other inert gases and also oxygen and nitrogen, but do not fit particularly well the data of carbon monoxide and methane. Although Guggenheim's formula is quite similar in form to that of Ferguson and Miller, he makes no reference to the work of these investigators. Both of Guggenheim's expressions can be transformed into functions of θ identical in form to Eqs. (12) and (13) but with $n=\frac{1}{3}$. The limited evidence which Guggenheim adduces in support of his value of n does not, in our opinion, outweigh the evidence assembled by both Sugden, and Ferguson and Miller in support of the value of $\frac{3}{10}$ for that exponent.

The results presented in this article increase considerably the number of those properties of liquids whose variation with temperature can each be represented by a general function of the reduced temperature θ, and so lend further support to the view, "There is only one simple liquid." An examination of the further implications of these results and also of the transformability of the functions from the van der Waals' scale of reduced temperature to the θ-scale will be taken up in a subsequent note.

Effects of Perturbations on Phosphorescence: Luminescence of Metal Organic Complexes

PHILIP YUSTER* AND S. I. WEISSMAN
Department of Chemistry, Washington University, Saint Louis, Missouri

(Received February 16, 1949)

Fluorescence and phosphorescence spectra, phosphorescence lifetimes, and relative ratios of intensities of fluorescence to phosphorescence of the dibenzoylmethane derivatives of the trivalent ions of Al, Sc, Y, La, Gd, and Lu have been measured. The lifetimes and intensity ratios of the various compounds differ widely, while the spectra are very similar. For instance, although the Lu and Gd compounds have practically indistinguishable phosphorescent spectra, the lifetimes of their phosphorescences differ by a factor of fifty. The results are interpreted in terms of Lewis's triplet theory of the phosphorescent state and spin-orbit perturbation of the levels. The largest effect is produced by the paramagnetic gadolinium ion. The effects produced by the non-magnetic ions depend on their nuclear charge and on their electronic structure.

THE existence of metastable excited states in many organic molecules is revealed by the long-lived luminescences which they exhibit under suitable conditions. Lewis and co-workers[1] suggested that these excited states differ in multiplicity from the ground states and that prohibition of transitions between states of different multiplicity is responsible for the observed metastability. For one substance, the acid form of fluorescein, the molecules in the metastable state are paramagnetic and the observed magnetism is compatible with a triplet configuration.[2] For other molecules Lewis and Kasha[3] showed that the energy of the metastable level corresponds reasonably well with the energy estimated for the lowest lying triplet state.

In the compounds investigated by Lewis and Kasha the transition probabilities from metastable to ground state were estimated from lifetimes of the luminescence of the substances dissolved in rigid media at low temperatures. These transition probabilities ranged from about 10^5 sec.$^{-1}$ for certain ketones to 1 sec.$^{-1}$ for fluorescein. In the work heretofore published no reasons for the variations in transition probabilities were given, but subsequent work by McClure[4] and Kasha[5] on lifetimes in a series of halogen-substituted naphthalenes has indicated that spin-orbit interaction is involved.

TABLE I. Mean lifetimes of phosphorescence in EPA and alcohol.

Compound	Z of metal ion	τ (seconds) in alcohol	τ (seconds) in EPA
Al	13	0.70 ±0.05	0.50±0.05
Sc	21	0.39 ±0.05	0.30±0.05
Y	39	0.24 ±0.05	0.24±0.05
Lu	71	0.10 ±0.03	0.12±0.03
La	57	0.06 ±0.01	0.09±0.01
Gd	64	0.002±0.0005	

If the absence of spin-orbit interaction, each level may be described by a wave function which is the product of an orbital function and a spin function of unique multiplicity. Since the integrals which determine transition probabilities vanish for pairs of functions of different multiplicity, the "intercombination" prohibition is exact only when spin-orbit interaction does not exist. It is possible to approximate the actual wave function of a level as a sum of wave functions, subject to the limitation that the sum transform properly under the symmetry group of the system. The various components of such a sum are not, in general, of the same multiplicity. The level is usually classified according to the multiplicity of the principle constitutent in this sum although certain transition probabilities may be determined entirely by the minor constituents.[6]

The admixture of wave functions of multiplicity different from the "multiplicity" assigned to a level, and the consequent apparent violation of the intercombination prohibition increases with increasing magnitude of the spin-orbit interaction. Thus the triplet-singlet transition $^3P_1 \rightarrow {}^1S_0$ in atomic Mg where the spin-orbit interaction is about 30 cm^{-1} has a transition probability of 2.5×10^2 sec.$^{-1}$ while the corresponding transition in atomic Hg with a spin-orbit interaction of about 3000 cm^{-1} has a transition probability of 10^7 sec.$^{-1}$. The magnitude of the spin-orbit interaction is determined by the way in which the spin dependent part of the energy varies with position of the electrons. The interaction in atoms depends on the nuclear charge, Z. At positions close to the nucleus there is a high electric field with a consequent high magnetic field in the reference system of a moving electron, whereas at positions distant from the nucleus this effect is small. The perturbation may be described as the interaction of the magnetic moment of a spinning electron with the non-uniform magnetic field associated with the motion of

* E. I. du Pont de Nemours and Company Fellow (1948–1949).

[1] Lewis, Lipkin, and Magel, J. Am. Chem. Soc. **63**, 3005 (1941); G. N. Lewis and M. Kasha, *ibid.* **66**, 2100 (1944); G. N. Lewis and M. Kasha, *ibid.* **67**, 994 (1945).

[2] G. N. Lewis and M. Calvin, J. Am. Chem. Soc. **67**, 1232 (1945).

[3] G. N. Lewis and M. Kasha, J. Am. Chem. Soc. **66**, 2100 (1944).

[4] D. S. McClure, J. Chem. Phys. (to be published).

[5] M. Kasha (University of California, Berkeley) (to be published).

[6] This topic is fully covered in treatises on spectroscopy such as E. U. Condon and G. Shortley, *Theory of Atomic Spectra* (The Cambridge University Press, New York, 1935).

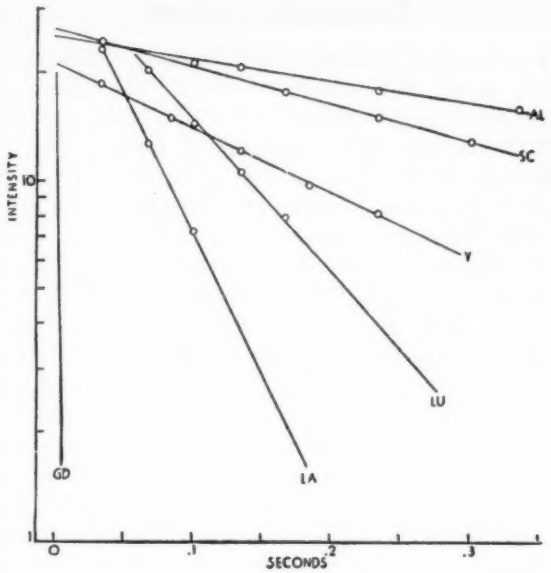

FIG. 1. Logarithmic decay curves of phosphorescence of dibenzoylmethane derivatives.

the electron through the electric field of the nucleus and other electrons. In general, any non-uniform magnetic field introduces a spin-orbit term into the Hamiltonian, i.e., a term which makes the spin energy dependent on the position of the electron.

In this paper we shall describe the effects of introduction of perturbations on the luminescence of an organic molecule. A series of trivalent metal complexes of dibenzoylmethane possess similar luminescence spectra but have widely varying phosphorescence lifetimes. The ratio of fluorescence intensity to phosphorescence intensity also varies greatly from compound to compound in the series. The above differences we shall attribute to interactions between the optical electrons of the molecules and the fields of the metal ions.

EXPERIMENTAL OBSERVATIONS

The series which we have studied consists of the dibenzoylmethane derivatives of the trivalent ions of Al, Sc, Y, La, Gd, and Lu. These compounds are characterized by a chelated structure with three dibenzoylmethide ions surrounding the central metal ion. The six oxygen atoms are presumably at the corners of an octahedron.[7] In all of these compounds the first excited state of the trivalent metal ion lies considerably higher than the levels responsible for the luminescence of the metal organic complex. Dilute solutions of the compounds in glasses of either ethyl alcohol or EPA[8] at liquid air temperatures when exposed to ultraviolet radiation (3200–4000A) give similar light emission. This luminescence varies in color from green in the Gd compound to blue in the Al compound. In all cases, however, the after-glow is green but varies in lifetime—the lifetimes of the Al, Sc, Y, Lu, La, and Gd compounds decrease in the order as written. The fluorescence of these solutions is blue and the difference in color of the luminescence is due to varying ratios of fluorescence to phosphorescence. We have studied both phosphorescence lifetimes and the ratio of phosphorescence to fluorescence intensity in these compounds. The quantum yield of luminescence in all cases is high; a comparison with fluorescein indicates the quantum yield to be close to unity. Hence, the differences in lifetime which we shall describe cannot be produced by quenching. Compounds whose phosphorescence lifetime differs by a factor of several hundred have almost identical luminescence yields.

[7] W. T. Astbury, Proc. Roy. Soc. (London) **112**, 448 (1928).

[8] A mixture of ether, alcohol, and isopentane described by Lewis and co-workers, J. Am. Chem. Soc. **64**, 2801 (1942).

Phosphorescence Lifetime Measurements

For our measurements of lifetime we used a modified Becquerel phosphoroscope which consisted of two disks mounted on a common shaft which could be rotated at either 45 r.p.m. or 1800 r.p.m. depending upon the speed of the motor attached. The first disk had cut in it a 120° sector of an annulus while the second disk had cut in it a 1° sector of an annulus. The angle between the openings on the two disks could be changed so that the time elapsed between cutting off the exciting light and

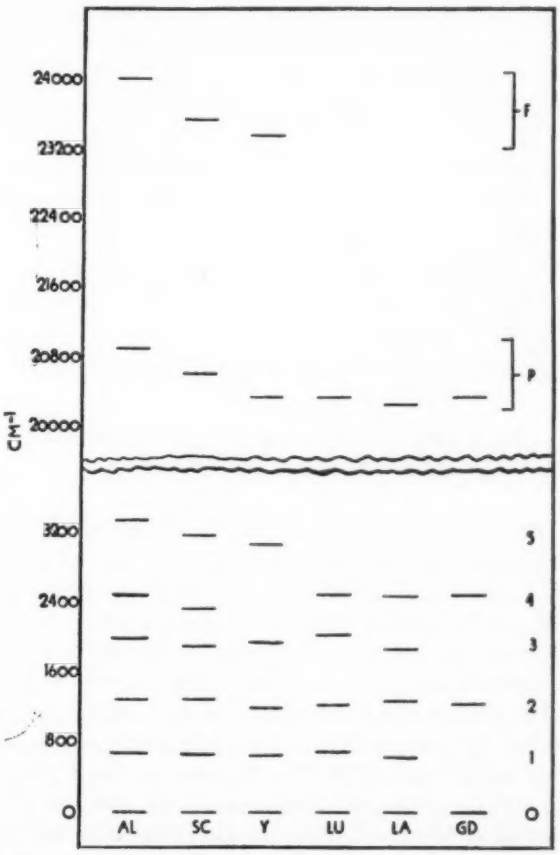

FIG. 2. Energy levels of dibenzoylmethane derivatives listed according to decreasing lifetime from left to right.

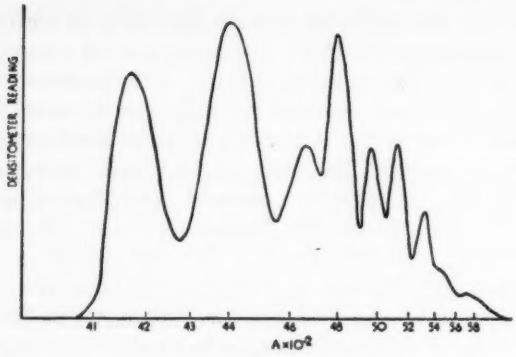

FIG. 3. Densitometer tracing of combined fluorescence and phosphorescence of Al derivative.

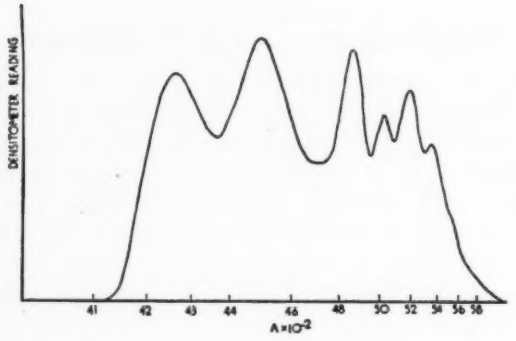

FIG. 4. Densitometer tracing of combined fluorescence and phosphorescence of Sc derivative.

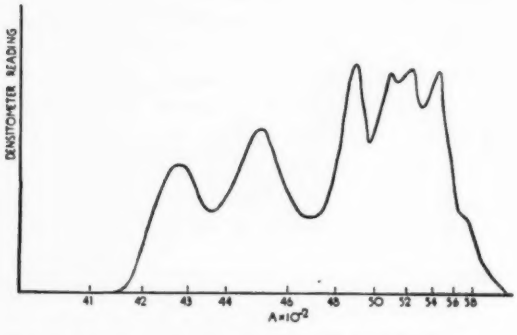

FIG. 5. Densitometer tracing of combined fluorescence and phosphorescence of Y derivative.

observation of phosphorescence could be varied. For measuring the intensity of phosphorescence of 1-P-22 RCA photo-multiplier tube was used in conjunction with a galvanometer. In order to obtain a steady reading of the galvanometer a condenser and resistance of time constant of about 10 sec. were included in the circuit.

The phosphorescence lifetime of each of the samples studied was measured at liquid air temperatures in both ethyl alcohol and EPA. The lifetimes of the Al, Sc, Y, Lu, and La compounds were measured with the wheel rotating at 45 r.p.m., while the Gd compound measurement was taken at 1800 r.p.m. The results of these measurements are shown in Table I and Fig. 1.

Luminescence Spectra

Two kinds of spectrograms were taken—phosphorescence alone and phosphorescence and fluorescence combined. The procedure used to obtain the combined phosphorescence and fluorescence spectra was the following: Light from a high pressure mercury arc (G.E. A-H-6) was focused on the sample contained in a 12 mm Pyrex tube immersed in liquid N_2 in a clear Pyrex Dewar. The visible light was removed from the exciting beam by a Corning 5860 filter and the luminescence from the sample was photographed on a Steinheil 3-prism spectrograph. In all the tracings shown Eastman 103-F spectrographic plates were used. In order to obtain phosphorescence spectra alone a suitable phosphoroscope was included in the above apparatus in such a way that the spectrograph was exposed only to afterglow. In Figs. 3 through 11 are given the densitometer tracings of the spectra of phosphorescence and in some cases the spectra of phosphorescence and fluorescence of these compounds dissolved in EPA. The spectra were also taken in alcohol but differ little from those reproduced in the figures. Liquid nitrogen was used as coolant for all these photographs to eliminate interference from absorption in the visible due to oxygen.

Intensity Measurements

The determination of the relative fluorescence to phosphorescence intensity ratios for the various compounds was made in the following way: First, a measurement was made of the sum of the fluorescence and phosphorescence intensities during illumination, and then, an estimate of the phosphorescence intensity alone during illumination was made by a suitable extrapola-

FIG. 6. Densitometer tracing of phosphorescence of Al derivative.

tion of the intensity of phosphorescence determined at a known time after cessation of illumination.

The detailed procedure follows: For these intensity measurements the phosphoroscope was modified slightly. One of the disks now had a 320° sector of an annulus cut in it, and the second disk had, the same as before, a 1° sector of an annulus cut in it. The apparatus was changed in this manner to allow the sample to be exposed to the exciting light as long as possible and to allow the phosphorescence to decay as little as possible so that steady-state conditions are reached. The disks were arranged so that a measurement was taken with the exciting light on and the wheel turning at 45 r.p.m. This measurement included both phosphorescence and fluorescence. In order to eliminate all exciting light a Corning 5860 filter was used on the exciting light and a

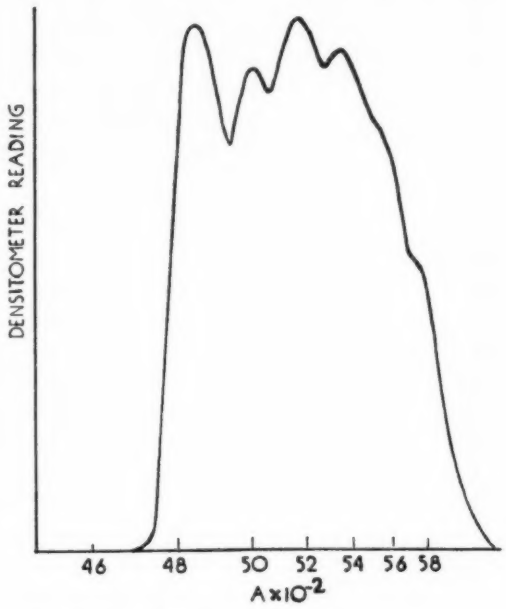

FIG. 7. Densitometer tracing of phosphorescence of Sc derivative.

flat filter of dibenzoylmethane dissolved in alcohol was placed between the luminescing sample and the photo-multiplier tube. The next measurement was made on the phosphorescence at some known time from zero. The lifetime of the phosphorescence had already been determined and the intensity of phosphorescence at zero time was estimated by extrapolation. This value is subtracted from the first reading and the ratio of these two is the quantity R listed in Table II.

The R values listed in Table II are not absolute values of the ratio of fluorescence to phosphorescence intensity. However, under the assumptions listed below, these R values differ from the absolute values only by some undetermined constant factor. This constant arises because the photo-multiplier tube does not have the same response to the phosphorescence spectra as it does to the fluorescence spectra.

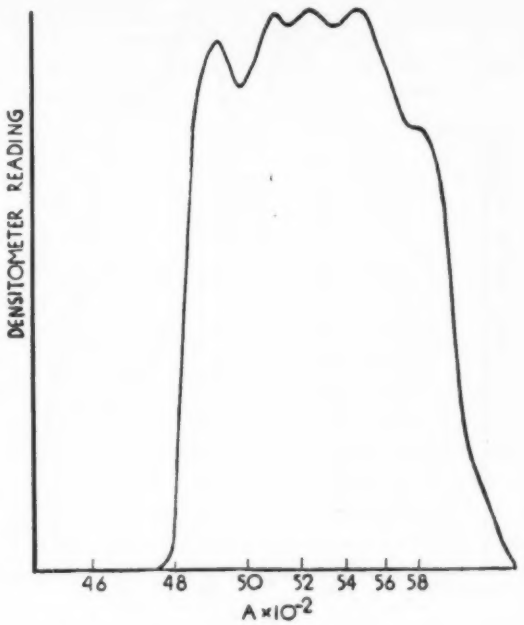

FIG. 8. Densitometer tracing of phosphorescence of Y derivative.

(1) The only appreciable non-radiative process taking place at this low temperature is the transition from the fluorescent to phosphorescent state (transitions from the phosphorescent to fluorescent state do not take place since no fluorescence spectra are observed in the afterglow).

(2) The measuring photo-multiplier tube responds approximately the same to all the phosphorescences and the same to all the fluorescences of this series (their spectra are very much alike).

(3) Steady-state conditions are attained.

A simple calculation using these assumptions leads to the result:

$$R_1/R_2 = k_2/k_1,$$

where R_1 and R_2 are the values listed in Table II for compounds 1 and 2 respectively and k_1 and k_2 are the radiationless transition probabilities from the F to P state in compounds 1 and 2, respectively.

DISCUSSION

The energy level diagrams obtained from fluorescence and phosphorescence spectra and shown in Fig. 2 are quite similar. The spacing of the low lying levels (presumably due to vibrations) is approximately the same in all cases while there are small shifts in the phosphorescent levels. The positions of these phosphorescent levels are given in Table III and it can be seen that the shift in going from the Al compound to the La compound is about 700 cm^{-1}. There is little correspondence between the lifetime of phosphorescence and position of the phosphorescent level. This can be seen from the lifetimes of the Y, Lu, and Gd compounds whose phosphorescent levels lie at the same position and whose lifetimes vary greatly.

The position of the phosphorescent level (in this series) seems to be determined only by the size of the

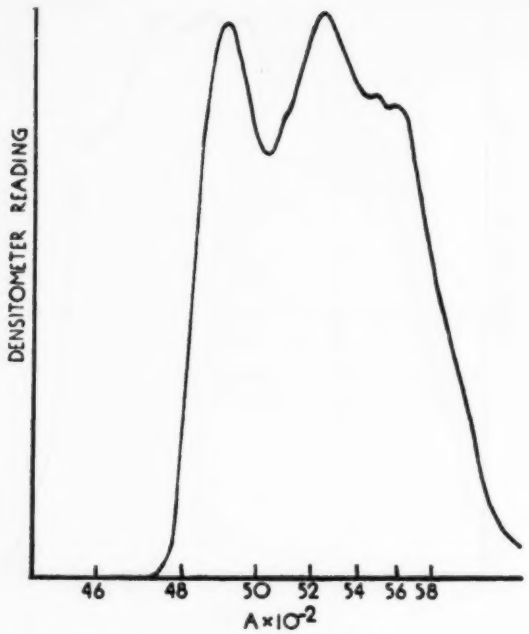

FIG. 9. Densitometer tracing of phosphorescence of Lu derivative.

metal ion involved and not by its atomic number, Z. Because of the lanthanide contraction, although Z changes by 32 in going from Y to Lu, the size of the ion is constant and the position of the phosphorescent level in these two cases is the same. On the other hand, the lifetime of phosphorescence shows drastic changes in going from the Al compound to the Gd compound. The great change in lifetime in going from the La compound to the Gd compound may be attributed in great part to a perturbation due to the inhomogeneous field of the paramagnetic Gd ion, while the change in lifetime in the remainder of the series may be attributed to perturbations due to spin-orbit interactions described previously. In all cases, even in the Gd case, the perturbation need not be large to account for the lifetime.

If we suppose that the fluorescent state has a lifetime of about 5×10^{-9} sec. (absorption corresponding to transitions between ground and fluorescent levels are very strong) even in the Gd compound with a lifetime of 2×10^{-3} sec. a "contamination"[9] of a triplet phosphorescent level by only a few tenths of a percent of the singlet fluorescent level is sufficient to produce the observed transition probability. The perturbation required is only about 10 cm^{-1}, and crude considerations show that an electron approaching within 0.8A or 0.9A of a Gd ion will have such an interaction energy.

For the compounds with the non-magnetic ions of Al, Sc, Y, Lu, and La, spin-orbit interactions of only a few tenths of a wave number are required to account for the transition probabilities. From Table I it is evident that the phosphorescence lifetime does not depend solely on a simple parameter such as the size of the central ion or on its Z. For instance in the Lu and Y compounds the sizes, as judged by ionic radii, are almost identical, and the lifetimes are quite different. On the other hand, the lifetimes of the La and Lu compounds indicate that the phosphorescence lifetime is not a function of Z alone since the lifetime of the La compound is less than that of the Lu compound.

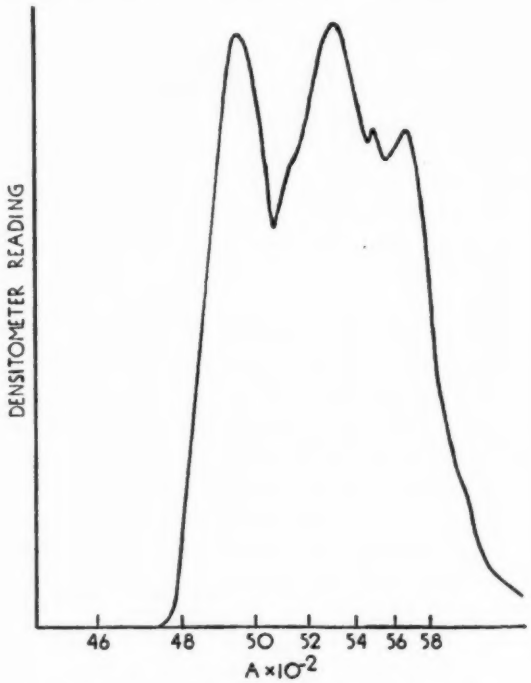

FIG. 10. Densitometer tracing of phosphorescence of La derivative.

The effectiveness of Z of the perturbing ion depends to a great extent on how close the optical electrons get to the nucleus, and so one would expect this perturbation to be a function of Z and other parameters which describe the structure of the ion. Apparently, the Lu ion with its completed $4f$ shell can be penetrated less easily by the electrons involved in phosphorescence than the La ion with an empty $4f$ shell. Another example of the fact that the electronic configuration of the metal ion is important was observed by a qualitative measurement of the relative lifetimes of the Ga and Sc compounds. Although the Ga compound, with its completed $3d$ shell, has a greater Z, it has a longer lifetime than that of the Sc compound. Comparisons of dibenzoylmethane salts within series with like electronic configurations, e.g., (1) Ga, In, (2) Ca, Sr, Ba, (3)

[9] The "contamination" here described is a type of resonance which has been excluded from most chemical thinking. This is a resonance between configurations having different numbers of unpaired electrons. Even in the extreme case of the Gd compound, this resonance, which is of great importance for the luminescence phenomena, can effect the energy of the states by 0.03 kcal per mole at most. However, the rates of certain reactions may be determined by the "contamination" of singlet states by triplet and for such cases study of the phosphorescent states of the molecules involved may lead to valuable chemical information.

TABLE II. Ratio of intensity, R, of fluorescence to phosphorescence.

Compound	R in alcohol	R in EPA
Sc	5.2 ±1.0	6.5 +1.0
Y	0.98±0.20	2.3 ±0.06
Lu	0.48±0.10	0.86±0.20
La	0.36±0.10	0.43±0.10
Gd	0.00 (no observable fluorescence)	0.00

TABLE III. Position of phosphorescent and fluorescent levels (normal state is taken as zero).

Compound	Phosphorescent level cm^{-1}	Fluorescent level cm^{-1}
Al	20,900±50	23,950±50
Sc	20,600±50	23,500±50
Y	20,350±50	23,350±50
Lu	20,350±50	
La	20,250±50	
Gd	20,350±50	

Li, Na, K reveal within each series decreasing lifetimes with increasing Z.

The ratio of the intensity of phosphorescence to fluorescence gives information regarding the radiationless transition probability from the fluorescent state to the phosphorescent state. Since we have ascribed the changes in phosphorescence lifetime to perturbations due to spin-orbit interactions, we expect a decrease in phosphorescence lifetime to be accompanied by an increase in the ratio of the yield of phosphorescence to fluorescence. However, the increase in the latter cannot be compared in a simple way with the decrease in lifetime of the phosphorescence since two different processes, one a radiation process, the other a radiationless process are involved.

Figure 2 shows the energy levels required for description of the luminescence of the compounds. The spectra indicate that the relative transition probabilities from the phosphorescent state to the various vibrational levels of the ground state change as one goes down the series from the Al compound to the Gd compound. In the Al compound fluorescence results from transitions from the F level to the levels 0, 2, 4 while phosphorescence results from transitions from the P level to these same levels 0, 2, 4 as well as from transitions with almost equal intensities to the levels 1, 3, 5. The ratio of intensity of the phosphorescence arising from transitions to the levels 0, 2, 4 to the intensity from transitions to the levels 1, 3, 5 increases with decreasing lifetime of the phosphorescence, until in the Gd compound the latter are not observed. It is difficult to make comparisons between neighboring members of the series since the change is small, but the effect is very evident when two extreme members are chosen.

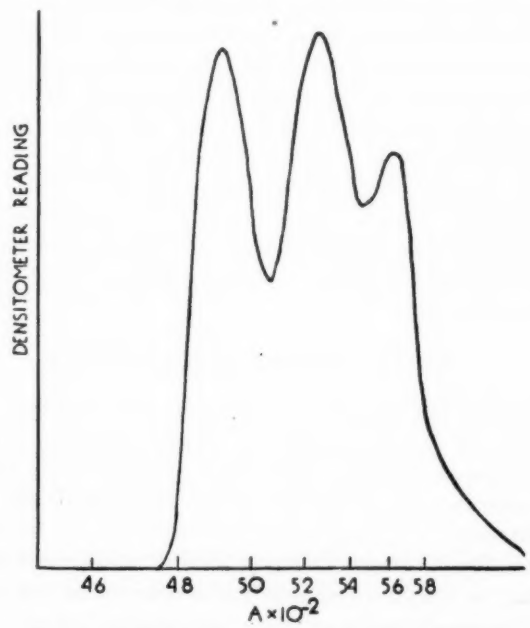

FIG. 11. Densitometer tracing of phosphorescence of Gd derivative.

We have attributed the observed changes in transition probability between phosphorescent and normal state to admixture of singlet wave functions into the phosphorescent level. Which of the singlet wave functions is the principle contributor is as yet unknown. The experimental observation of the similarity in pattern of the fluorescence spectrum of the aluminum compound and the phosphorescence spectrum of the gadolinium compound suggests that this contributor is the fluorescent level wave function. Theoretically this might be expected since the fluorescent level is the closest lying "singlet" level to the phosphorescent level.

We anticipate further information concerning this suggestion from as yet uncompleted measurements of the polarization of the luminescene spectra. The phosphorescence of fluorescein is almost completely unpolarized, while the fluorescence is highly polarized.[1] This result has been intuitively explained by the statement that the electronic spin of the unpaired electrons in the phosphorescent state is but weakly coupled to the molecular axes. A more complete statement, justifiable by group theoretical arguments, is that in molecules of sufficiently low symmetry the three close lying levels of the phosphorescent state yield mutually perpendicular directions of polarization in undergoing transitions to the normal state. If a particular one of these levels is contaminated by admixture of singlet wave function, the phosphorescence arises almost entirely from this level and should be polarized.

The most striking change in all the compounds was accomplished by the introduction of the paramagnetic Gd ion. We had hoped to study the effect of magnetic moment of the central ion on the phosphorescent lifetime by introduction of other paramagnetic ions but found this to be impracticable for reasons we now describe. The most suitable ions available appeared to be those of the other rare earths. With the exception

of Ce^{+++} and Yb^{+++}, all the other rare earth ions possess levels lower than the phosphorescence level of the dibenzoylmethane complex and yield, because of excitation into these levels by a process already described,[10] compounds which exhibit no visible luminescence or sharp line luminescence characteristic of the rare earth ion. For the former ions, Ce^{+++} and Yb^{+++}, our preparative methods failed to produce the Ce^{+++} compound apparently due to an oxidation to Ce^{++++}, while the Yb^{+++} compound, although easily prepared, failed to luminesce. The first excited state of Yb^{+++} involves removal of an electron from the shielded $(4f)^{12}$ configuration to $5d$ or $6s$ or $6p$. The change in the potential energy surfaces of the states of the molecule produced by this mode of excitation may be sufficient to lead to quenching by internal conversion to a high vibrational level of the ground state.[11]

[10] S. I. Weissman, J. Chem. Phys. **10**, 214 (1942).

[11] Franck and Livingston, J. Chem. Phys. **9**, 184 (1941). E. Teller, J. Phys. Chem. **41**, 109 (1937).

THE JOURNAL OF CHEMICAL PHYSICS VOLUME 17, NUMBER 12 DECEMBER, 1949

The General Kinetics of Co-Polymerization and an Extension of the Viscosity Method to Determine Velocity Constants

C. H. BAMFORD AND M. J. S. DEWAR
Courtaulds Ltd., Research Laboratories, Maidenhead, Berkshire, England

(Received February 21, 1949)

Completely general kinetic expressions have been developed for the co-polymerization of n monomers, assuming that the reactivities of the radicals depend only on their terminal groups. Allowance has been made for chain transfer and the fact that thermal and photo-chemical initiation may proceed via diradicals. The equations are of the same form as those developed previously for a simple polymerization. The latter appear as a special case in which $n=1$.

It is pointed out that the method previously developed for determining the velocity constants in simple polymerizations can be used without modification in the study of co-polymerizations. In this way 12 of the 14 velocity constants in a binary co-polymerization can be determined absolutely, and a relation between the remaining two obtained.

WE have recently described a method for determining the absolute velocity constants in simple vinyl polymerizations.[1] This method, which has been justified by work in these laboratories,[1,2] has several advantages; in particular the rate of chain starting need not be measured independently, the velocity constant for the transfer reaction with the monomer can be determined directly, and the measurements can be made at very low conversions. It seemed desirable to see how much information could be obtained by extending this method to co-polymerization. The viscosity method should be particularly convenient, since the low conversions would eliminate inconvenience arising from changes in reactant composition.

As was the case of simple polymerization, a more exact kinetic scheme is required than the one in current use. Not only must chain transfer be included, but also the fact that the initial centers in thermal or photo-polymerizations may be diradicals. The importance of these factors in the polymerization of single monomers was established by Bamford and Dewar.[1]

We have found it possible to derive simple expressions for the co-polymerization of n monomers at small conversions, which provide the most complete account of the reaction kinetics at present available. The method is essentially that used by Walling and Briggs[3] to derive the co-polymer composition for mixtures of n monomers. However, previous workers have not given general expressions for molecular weights etc., of the co-polymer, possibly because they did not fully realize the similarity between the equations for polymerization and co-polymerization. As already indicated, even the calculations for binary mixtures involved unjustifiable simplifications.

KINETIC SCHEME AND NOTATION

The kinetic scheme is an elaboration of that described in Part I[1] for simple polymerizations. As in the simple case there will in general be two types of radical present; double radicals formed by photo-chemical or thermal initiation, and single radicals formed by catalytic initiation or transfer. We make the usual assumption that the reactivity of a radical is determined solely by its terminal monomer unit. The entities present, and

[1] Bamford and Dewar, Proc. Roy. Soc. London, **192**, 309 (1948); This paper is called Part I in the text.

[2] Bamford and Dewar, (methyl methacrylate) Proc. Roy. Soc. London, **197**, 356 (1949); Axford (p-methoxystyrene) ibid., p. 374; Dixon-Lewis (vinyl acetate) ibid. **198**, 510 (1949).

[3] Walling and Briggs, J. Am. Chem. Soc. **67**, 1774 (1945).

the relevant notation are as follows:

M_r monomer r ($r=1, 2, \cdots, n$).
X_r any radical center ending in M_r.
D_{2rs} diradical ending in M_r and M_s.
D_{1r} single radical ending in M_r, and formed by the death of one end of a D_2 radical.
R_r single radical ending in M_r produced by transfer.

$$[M]=\sum_r[M_r],\quad [X]=\sum_r[X_r],\quad [R]=\sum_r[R_r],$$

$$[D_2]=\sum_r\sum_s[D_{2rs}],\quad [D_1]=\sum_r[D_{1r}],$$

$$\phi_r=[M_r]/[M],\quad \theta_r=[X_r]/[X].$$

Velocity constants for initiation, propagation, transfer, and termination are denoted as in Part I[1] by k_1, k_2, k_3, k_4 respectively. Two additional suffixes are necessary, however, to specify the reactants. In the propagation and transfer reactions, the second suffix denotes the radical, and the third the monomer. Thus k_{2rs} is the propagation constant for the reaction

$$X_r+M_s\rightarrow X_s. \tag{1}$$

The velocity constant for the thermal initiation

$$M_r+M_s\rightarrow D_{2rs}\quad (\text{or } X_r+X_s) \tag{2}$$

would similarly be k_{1rs}, and no distinction would be drawn between k_{1rs} and k_{1sr}. It is convenient, however, to divide this constant into two equal parts k_{1rs}' and k_{1sr}'. Thus for reaction (2) we have

$$\begin{aligned}-d[M_r]/dt&=-d[M_s]/dt=d[D_{2rs}]/dt\\&=k_{1rs}[M_r][M_s]=k_{1rs}'[M_r][M_s]\\&\quad+k_{1sr}'[M_s][M_r]=2k_{1rs}'[M_r][M_s].\end{aligned} \tag{3}$$

The termination constant k_{4rs} is also split into equal parts k_{4rs}' and k_{4sr}'. Likewise D_{2rs} is divided into equal parts D_{2rs}' and D_{2sr}'.

In deriving the stationary state equations it is convenient to assume that the chains are long, so that the initiation and termination reactions can be neglected. It is also assumed that the degree of polymerization is large, so that transfer is slow compared to propagation and that termination occurs exclusively by disproportionation (see reference 2). The stationary state equations may now be written down. They are

$$-[X_r]\sum_s k_{2rs}[M_s]+[M_r]\sum_s k_{2sr}[X_s]=0 \qquad (r=1, 2, \cdots, n). \tag{4}$$

Dividing (4) throughout by $\sum_r[M_r]\sum_s[M_s]$ we obtain

$$-\theta_r\sum_s k_{2rs}\phi_s+\phi_r\sum_s k_{2sr}\theta_s=0 \quad (s=1, 2, \cdots, n). \tag{5}$$

This system of homogeneous linear equations has a non-zero solution, for it is evident that

$$\Delta\equiv det\left|\, k_{2rs}\phi_s-\delta_{rs}\sum_t k_{2rt}\phi_t\,\right|=0 \tag{6}$$

since the sum of the elements of any row is zero. Let D_r be the determinant obtained by striking out the first row and r^{th} column of Δ, and let Δ_r be defined by

$$D_r=(-1)^{n-r+1}\Delta_r, \tag{7}$$

so that Δ_r is always positive. The solution of (5) is

$$\theta_r=\mu\Delta_r=\Delta_r/\sum_s\Delta_s, \tag{8}$$

where μ is a constant. The stationary state equations for $[D_2]$, $[D_1]$, $[R]$ and $[X]$ may now be written down for a thermal polymerization. They are

$$\begin{aligned}d[D_2]/dt=&\sum_r\sum_s k_{1rs}'[M_r][M_s]\\&-\sum_r\sum_s\sum_t k_{3rt}[D_{2rs}'][M_t]\\&-\sum_r\sum_s\sum_t k_{3st}[D_{2rs}'][M_t]\\&-\sum_r\sum_s\sum_t k_{4rt}'[D_{2rs}'][X_t]\\&-\sum_r\sum_s\sum_t k_{4st}'[D_{2rs}'][X_t]=0,\end{aligned} \tag{9}$$

$$\begin{aligned}d[D_1]/dt=&\sum_r\sum_s\sum_t k_{3rt}[D_{2rs}'][M_t]\\&+\sum_r\sum_s\sum_t k_{3st}[D_{2rs}'][M_t]\\&+\sum_r\sum_s\sum_t k_{4rt}'[D_{2rs}'][X_t]\\&+\sum_r\sum_s\sum_t k_{4st}'[D_{2rs}'][X_t]\\&-\sum_r\sum_s k_{3rs}[D_{1r}][M_s]\\&-\sum_r\sum_s k_{4rs}'[D_{1r}][X_s]=0,\end{aligned} \tag{10}$$

$$\begin{aligned}d[R]/dt=&\sum_r\sum_s\sum_t k_{3rt}[D_{2rs}'][M_t]\\&+\sum_r\sum_s\sum_t k_{3st}[D_{2rs}'][M_t]\\&+\sum_r\sum_s k_{3rs}[D_{1r}][M_s]\\&-\sum_r\sum_s k_{4rs}'[R_r][X_s]=0,\end{aligned} \tag{11}$$

$$\begin{aligned}d[X]/dt=&\sum_r\sum_s k_{1rs}'[M_r][M_s]\\&-\sum_r\sum_s k_{4rs}'[X_r][X_s]=0.\end{aligned} \tag{12}$$

Also, from the definition of θ_r,

$$[D_{2rs}]=\theta_r\theta_s[D_2],\quad [D_{1r}]=\theta_r[D_1],\quad [R_r]=\theta_r[R]. \tag{13}$$

We define λ_1, λ_2, λ_3, λ_4 by the equations

$$\lambda_1=\sum_r\sum_s k_{1rs}'\phi_r\phi_s,\quad \lambda_2=\sum_r\sum_s k_{2rs}\theta_r\phi_s,$$

$$\lambda_3=\sum_r\sum_s k_{3rs}\theta_r\phi_s,\quad \lambda_4=\sum_r\sum_s k_{4rs}'\theta_r\theta_s. \tag{14}$$

Equations (9)–(12) now become

$$\lambda_1[M]^2-2\lambda_3[D_2]-2\lambda_4[D_2][X]=0, \quad (15)$$

$$2\lambda_3[D_2][M]+2\lambda_4[D_2][X]-\lambda_3[D_1][M]-\lambda_4[D_1][X]=0, \quad (16)$$

$$2\lambda_3[D_2][M]+\lambda_3[D_1][M]-\lambda_4[R][X]=0, \quad (17)$$

$$\lambda_1[M]^2=\lambda_4[X]^2. \quad (18)$$

From Eqs. (15)–(18) it follows that

$$\left.\begin{aligned}
[X]&=(\lambda_1/\lambda_4)^{\frac{1}{2}}[M],\\
[D_2]&=\lambda_1[M]/[4\{\lambda_3+(\lambda_1\lambda_4)^{\frac{1}{2}}\}],\\
[D_1]&=2[D_2],\\
[R]&=4\lambda_3(\lambda_1\lambda_4)^{-\frac{1}{2}}[D_2]=4\beta[D_2],\\
\beta&=k_3(k_1k_4)^{-\frac{1}{2}},\\
\bar{P}_1&=\lambda_2/\{\lambda_3+(\lambda_1\lambda_4)^{\frac{1}{2}}\},\\
\bar{P}_2&=2\bar{P}_1,\\
d[P_1]/dt&=\lambda_3(\lambda_1/\lambda_4)^{\frac{1}{2}}[M]^2=\beta\lambda_1[M]^2,\\
d[P_2]/dt&=\tfrac{1}{2}\lambda_1[M]^2,\\
-d[M]/dt&=\lambda_2(\lambda_1/\lambda_4)^{\frac{1}{2}}[M]^2,
\end{aligned}\right\} \quad (19)$$

where $\bar{P}_1$, $\bar{P}_2$ are the mean degrees of polymerization of transfer and initial polymer respectively, and β is the number of times chain transfer occurs in a kinetic chain. These equations are identical in form with those of a simple polymerization,[1] the velocity constants in the latter being replaced by the corresponding λ's.

In a photo-chemical polymerization, the rate of chain starting is proportional to the light intensity for a given composition, and may then be written in the form

$$\lambda_1[M]^2(1+AI)\equiv\lambda_1\xi^2[M]^2. \quad (20)$$

Equations (19) then hold for photo-polymerizations with λ_1 replaced by $\lambda_1\xi^2$.

We may also assume that the co-polymer obeys the Houwink viscosity law, $[\eta]=K\bar{P}^a$. This is a reasonable assumption since individual polymers appear to obey the law with exponents close to $\frac{2}{3}$. The following results may now be obtained* by applying the method of Part I.[1]

$$\left.\begin{aligned}
\bar{P}&=[2\lambda_2(\lambda_1\lambda_4)^{-\frac{1}{2}}/(2\beta+\xi)],\\
-d[M]/dt&=\lambda_2\xi[M]^2(\lambda_1/\lambda_4)^{\frac{1}{2}},\\
\frac{d\eta}{dt}&=K[M]^2\left\{\frac{\lambda_1^{\frac{1}{2}(1-\alpha)}\lambda_2^{1+\alpha}}{\lambda_4^{\frac{1}{2}(1+\alpha)}}\right\}\\
&\qquad\times\frac{\xi[\beta+(1+\tfrac{1}{2}\alpha)\xi]}{(\beta+\xi)^{1+\alpha}},
\end{aligned}\right\} \quad (21)$$

where η is the ideal specific viscosity.[4] These expressions are naturally identical with those given previously for simple polymerizations,[1] and corresponding equations may be written down for the photo-chemical after- and pre-effects.

For numerical work involving Eqs. (21), it is first necessary to calculate the λ's from Eq. (14). It is easily seen, however, that Eqs. (21) are unchanged if θ_r is replaced by Δ_r in calculating the λ's, and for this purpose it is therefore unnecessary to use the full expression in Eq. (8).

To complete the kinetic treatment we give two additional results. The rate of consumption of monomer M_r is given by

$$-d[M_r]/dt=\sum_s k_{2sr}[X_s][M_r]=\phi_r[M]^2(\lambda_1/\lambda_4)^{\frac{1}{2}}\sum_s k_{2sr}\theta_s, \quad (22)$$

and the average length of a sequence of M_r units in the polymer, $\bar{n}_r$, is given by

$$\bar{n}_r=c/(c-k_{2rr}\phi_r), \quad (23)$$

where

$$c=\sum_s\{k_{2rs}\phi_s+k_{3rs}\phi_s+(\lambda_1/\lambda_4)^{\frac{1}{2}}k_{4rs}'\theta_s\}.$$

POLYMERIZATION IN SOLVENTS

The velocity constant for reaction between x_r and solvent S will be denoted by k_{5r}. A quantity λ_5 is defined by

$$\lambda_5=\sum_r k_{5r}\theta_r. \quad (24)$$

As before, we obtain the equations

$$\bar{P}_1=\frac{\lambda_2[M]}{\lambda_3[M]+\sqrt{(\lambda_1\lambda_4)}[M]+\lambda_5[S]},$$

$$\bar{P}_2=2\bar{P}_1,$$

$$[R]=2[D_1](\lambda_3[M]+\lambda_5[S])/\sqrt{(\lambda_1\lambda_4)}[M],$$

$$d[P_1]/d[P_2]=[R]/2[D_1].$$

Hence

$$\bar{P}=2\lambda_2[M]/\{2\lambda_3[M]+\sqrt{(\lambda_1\lambda_4)}[M]+2\lambda_5[S]\},$$

i.e.,

$$\frac{1}{\bar{P}}=\frac{1}{\bar{P}_0}+\frac{\lambda_5}{\lambda_2}\frac{[S]}{[M]}. \quad (25)$$

Equation (25) is identical in form with that derived by Mayo[5] for polymerization of a single monomer in a solvent.

* This involves the additional assumption that the molecular weight distribution is similar to that for a single polymer. It can be shown that this is so if Eq. (4) holds.

[4] Ideal specific viscosity is defined by $\eta=c[\eta]$, where c is the concentration of the polymer. The determination of η from the observed specific viscosity is discussed in Part I.

[5] Mayo, J. Am. Chem. Soc. 65, 2324 (1943).

SPECIAL CASES

(1) $n=1$. Here $\theta=\phi=1$ and $\lambda_r=k_r(r=1, 2, 3, 4)$. Equations (21) thus reduce to those given in Part I[1] for a simple polymerization.

(2) $n=2$.

$$\left.\begin{aligned}
&\Delta_1=k_{221}\phi_1, \quad \Delta_2=k_{212}\phi_2,\\
&\lambda_1=k_{111}\phi_1^2+k_{112}\phi_1\phi_2+k_{122}\phi_2^2,\\
&\lambda_2=k_{211}k_{221}\phi_1^2+2k_{212}k_{221}\phi_1\phi_2+k_{222}k_{212}\phi_2^2,\\
&\lambda_3=k_{311}k_{221}\phi_1^2+(k_{312}k_{221}+k_{321}k_{212})\phi_1\phi_2\\
&\qquad\qquad +k_{322}k_{212}\phi_2^2,\\
&\lambda_4=k_{411}k_{221}^2\phi_1^2+k_{412}k_{221}k_{212}\phi_1\phi_2+k_{422}k_{212}^2\phi_2^2.
\end{aligned}\right\} \quad (26)$$

From Eq. (22)

$$\frac{d[M_1]}{d[M_2]}=\frac{[M_1]}{[M_2]}\frac{k_{211}\Delta_1+k_{221}\Delta_2}{k_{212}\Delta_1+k_{222}\Delta_2}$$

$$=\frac{k_{221}[M_1]}{k_{212}[M_2]}\left\{\frac{k_{211}[M_1]+k_{212}[M_2]}{k_{221}[M_1]+k_{222}[M_2]}\right\}, \quad (27)$$

which is a well-known result first obtained by Mayo and Lewis.[6]

(3) $n=3$. In this case only the values of Δ_r will be given. These are sufficient to enable the composition of the co-polymer to be calculated immediately.

$$\Delta_1=k_{221}k_{231}\phi_1^2+k_{221}k_{232}\phi_1\phi_2+k_{231}k_{223}\phi_1\phi_3,$$

$$\Delta_2=k_{232}k_{212}\phi_2^2+k_{232}k_{213}\phi_2\phi_3+k_{212}k_{231}\phi_2\phi_1,$$

$$\Delta_3=k_{213}k_{223}\phi_3^2+k_{213}k_{221}\phi_3\phi_1+k_{223}k_{212}\phi_3\phi_2,$$

and

$$\frac{d\log[M_1]}{k_{211}\Delta_1+k_{221}\Delta_2+k_{231}\Delta_3}=\frac{d\log[M_2]}{k_{212}\Delta_1+k_{222}\Delta_2+k_{232}\Delta_3}$$

$$=\frac{d\log[M_3]}{k_{213}\Delta_1+k_{223}\Delta_2+k_{233}\Delta_3}. \quad (28)$$

This equation is identical with that obtained by Walling and Briggs.[3]

DISCUSSION

It was pointed out above that there is a formal identity between the equations representing the polymerization of a single monomer, and those for the co-polymerization of n monomers. Since the λ's will be constant for a constant temperature, and constant composition of reactants, a mixture of n monomers will behave kinetically as a single monomer with velocity constants λ_1, λ_2, λ_3, λ_4, provided that measurements are carried out at very small conversions, so that the composition of the reactant mixture is not changed. The methods described previously[1,7] fulfil this condition, and can therefore be taken over in toto to determine the λ's in a co-polymerization, and also the quantities K, α which determine the molecular weight-viscosity relation.

With the assumption made previously that the reactivity of a radical depends only on its terminal monomer unit, it is clear that constants of the form $k_{rss}(r=1, 2, 3, 4)$ can be identified with velocity constants of the single monomers, and constants of the form $k_{rst}(s\neq t)$ with those for co-polymerization of pairs of monomers. To determine absolute velocity constants, including the crossed constants, all that is necessary therefore is to study single monomers, and pairs of monomers. The general equations developed above can then be used to predict the behavior of more complicated mixtures. We therefore consider specially the case of two monomers.

There are in all 14 velocity constants, of which 8 can be determined by measurements on the single monomers. From a study of the co-polymerization of one mixture four further relations—the λ's—are obtained as indicated above. The study of other compositions gives only one further relation. Thus it is impossible to determine all 14 constants absolutely. Inspection of the equations shows that k_{112}, k_{212}, k_{221}, k_{412} can be evaluated separately, but the quantity $k_{312}k_{221}+k_{321}k_{212}$ cannot be resolved, and hence the crossed transfer constants cannot be isolated.

The following further points of interest emerge:

(1) It is well known that small amounts of an easily polymerizable monomer act as a retarder when added to a monomer which is less reactive (e.g., styrene added to vinyl acetate). This behavior can easily be interpreted in terms of Eqs. (21) and (26). Measurements in these laboratories suggest that the termination constants for radicals of different reactivity do not differ widely; consequently at a given rate of chain starting the stationary concentration of radicals will not be appreciably affected by small additions of one monomer to another. The over-all rate will then be proportional to λ_2, and it is evident from Eq. (26) that λ_2 will be small when k_{221} and ϕ_2 are both small.

(2) By carrying out solvent polymerization with different monomer ratios it would be possible to study the variation of K and α with the composition of the co-polymer. This could provide some basis for the theoretical treatment of the viscosity of polymer solutions.

(3) A knowledge of the variation of A (Eq. (20)) with composition would provide information as to the nature of the primary photo-chemical process.

(4) It would not be necessary to know the constants for the individual monomers in studying the co-polymerization of a pair provided that the co-polymerization were carried out for at least four different compositions.

Investigations along these lines are now in progress.

[6] Mayo and Lewis, J. Am. Chem. Soc. **66**, 1594 (1944).

[7] Bamford and Dewar, Proc. Roy. Soc. London **192**, 329 (1948).

Refractive Indices and Dielectric Constants of Liquids and Gases under Pressure

JOSEPH S. ROSEN
University of Kansas City, Kansas City, Missouri

(Received February 23, 1949)

Several interpolation formulas are given which reproduce refractive index and dielectric constant data for liquids and gases at high pressures. These formulas involve functions of the refractive indices and dielectric constants which appear in the formulas of Lorentz-Lorenz, Clausius-Mosotti, Gladstone and Dale, the empirical Eykman formula, etc. One formula shows the reciprocals of these functions to be linear in the specific volumes at various pressures. Another interpolation formula, involving the reciprocals of the same functions, contains a logarithmic term which is similar to that appearing in the Tait equation for compressibilities of liquids. The parameters involved in the Tait equations for compressibilities and in the analogous interpolation formula for refractive indices and dielectric constants are discussed.

The article also shows that the Tait equation which has been so successfully adapted to compressibility data of liquids can also be applied to gases.

INTRODUCTION

In a recent article[1] it was shown that the compressions[2] of alcohol, water and their mixtures calculated from the refraction formulas of Lorentz-Lorenz and of Gladstone and Dale are a linear function of the observed compressions of the solution. A logarithmic equation is given which reproduces with great precision the refractive indices of alcohol, water, and their mixtures under pressure; the logarithmic term is the same as that in the Tait equation for compressibilities, and the part of the equation containing the refractive indices involves the same functions of n_P which appear in the formulas of Gladstone and Dale, Lorentz-Lorenz, etc.

It is the purpose of this paper to show that the results of the above article can be extended to existing data of both refractive indices and dielectric constants of liquids as well as to gases at high pressures.

Of the important formulas for the refractive index or dielectric constant of a substance which give a specific refractive or specific polarization "constant," all have the form $f(v_P)v_P=\mathrm{C}$, where $f(v_P)$ is a function of the refractive index n_P or the dielectric constant ϵ_P, v_P is the specific volume and C the "constant." Where the formula is applied to solutions on which the pressure is varied, the expression

$$1-[f(v_0)/f(v_P)]=k_P' \qquad (1)$$

would equal the observed compression, k_P, if C remained constant. Characteristic functions are the Lorentz-Lorenz expression $(n^2-1)/(n^2+2)$, Gladstone and Dale's $(n-1)$, the Newton expression (n^2-1) and the empirical function of Eykman $(n^2-1)/(n+.4)$. In all of these expressions n_P^2 may be replaced by ϵ_P to obtained the corresponding formula involving dielectric constants.

It has generally been found that with none of these functions $f(v_P)$ can the observed compressions, k_P, of the solutions be computed from Eq. (1) with any great accuracy;[1,3,4] but Eq. (1) has frequently been used as a criterion in selecting the most suitable formula $f(v_P)v_P=C$ applicable to a particular substance. It will, however, be shown here that the compressions, k_P', computed from Eq. (1), may be taken as a linear function of the observed compressions k_P. Accordingly, we may write

$$k_P'=m'k_P+b', \qquad (2)$$

where m' and b' are constants for a given substance. A more useful equation which is equivalent to (2) is obtained if we replace k_P by $(v_0-v_P)/v_0$ and k_P' by the left member in Eq. (1). We obtain the expression

$$1/f(v_P)=mv_P+b, \qquad (3)$$

where m and b are constants independent of the pressure. Equation (3) will be shown to hold for existing data at high pressures both for the refractive indices and dielectric constants of liquids and gases. The forms of the function $f(v_P)$ in Eq. (3) may be those of theoretical significance already mentioned as well as others which have no theoretical foundations, such as for example, $f(v_P)=v_P$, etc. Though a number of these forms have been examined, only the Clausius-Mosotti and Lorentz-Lorenz functions, because of their theoretical interest, will be considered.

The equation, proposed by Tait for water,

$$dk_P/dp=C/(B+P),$$

has been shown in recent years,[1,5] notably by Gibson,

[1] J. S. Rosen, J. Opt. Soc. Am. **37**, 932 (1947).

[2] The symbols used in this article are the following: n_P, ϵ_P and v_P are the refractive index, dielectric constant and specific volume, respectively, at pressure P. The subscript 0 indicates atmospheric pressure ($P=0$). The bulk compression, k_P, is $-(v_P-v_0)/v_0$. Where the symbol v_P occurs in the function $f(v_P)$ it will designate ϵ_P or n_P^2, and $f(v_P)$ will refer to the same function of ϵ_P or n_P^2.

[3] W. C. Röntgen and L. Zehnder, Ann. d. Physik **44**, 49 (1891); G. Quincke, *ibid.* **44**, 774 (1891).

[4] R. E. Gibson and J. F. Kincaid, J. Am. Chem. Soc. **60**, 511 (1938).

[5] Harned and Owen, *The Physical Chemistry of Electrolytic Solutions* (Reinhold Publishing Corporation, New York, 1943), p. 270; P. W. Bridgman, Rev. Mod. Phys. **18**, 17 (1946); H. Carl, Zeits. f. physik. Chemie **101**, 238 (1922).

to represent successfully the compressibilities of liquids. This equation involves two parameters[6] C and B both independent of the pressure; B is a function of the temperature, concentration (in mixtures),[1] and the properties of the solution; while C is approximately independent of the temperature. It will be shown in this article that Tait's equation can also be applied to gases. In the integrated form this equation is

$$v_{P'}-v_P=v_0C\ln\{(P+B)/(P'+B)\}, \qquad (4)$$

where the initial pressure, usually one atmosphere, is P'.

From Eq. (3), we have

$$\frac{1}{f(\nu_{P'})}-\frac{1}{f(\nu_P)}=m(v_{P'}-v_P).$$

If we substitute (4) into this equation, we obtain

$$\frac{1}{f(\nu_{P'})}-\frac{1}{f(\nu_P)}=A\log\left(\frac{P+B}{P'+B}\right) \qquad (5)$$

where A and B are constants for a given substance. If initially the pressure is the atmospheric pressure, and if the pressure range is large, it is most convenient to set P' equal to zero. A better adjustment of the data may be obtained by replacing $(P'+B)$ by a third parameter, but in general this is not justified either by the accuracy of the data or the additional computation involved.

In this article we will justify Eqs. (3) and (5) as interpolation formulas for the considerable body of refractive index and dielectric constant measurements at high pressures for both liquids and gases. The Clausius-Mosotti and Lorentz-Lorenz functions will be adjusted by the method of least squares to these equations, but for Eq. (5) we will also study the form $f(\nu_P)=\nu_P$.

THE INTERPOLATION FORMULAS

The literature on the subject of refractive indices and dielectric constants at high pressures contains some precedence for Eq. (3) and (5). Danforth,[7] in a much quoted paper on the dielectric constants at high pressure for some ten organic liquids, finds that the reciprocal of the Clausius-Mosotti expression $\rho_P/f(\epsilon_P)$ when plotted against the density ρ_P gives a straight line for most liquids. This is evidently similar to Eq. (3), with $1/f(\epsilon_P)=(\epsilon_P+2)/(\epsilon_P-1)$. Owen and Brinkley,[8] on theoretical grounds, derive the Eq. (5) with $f(\nu_P)=\epsilon_P$ and $P'=1$, and adapt the equation to data on dielectric constants at high pressure, and to the refractive indices of one non-polar liquid (benzene). Keyes and Kirkwood[9] find an expression similar to Eq. (3) to hold for their dielectric constant measurements on carbon dioxide and ammonia for various temperatures and pressures.

We shall have occasion later in this article to comment further on the work in these papers.

Older formulas on the refractive indices of binary mixtures at atmospheric pressure are reminiscent of the equations evolved above. The formulas of Pulfrich and Hubbard[10] resemble closely Eq. (1). Since, however, at atmospheric pressure the compressions of the mixture cannot enter, the right member of Eq. (1) is replaced by an analogous term which involves the ratio of the actual volume of the mixture and its volume calculated by a simple rule of mixtures. The interpretation of such a

TABLE I. The constants m and b of the equation $1/f_P=m\nu_P+b$, where $1/f_P=(\epsilon_P+2)/(\epsilon_P-1)$, evaluated by the method of least squares from dielectric constant data for liquids at high pressures. In the last two columns are shown the average and maximum percent difference between the observed and computed values of the dielectric constants. The pressures and volumes are in the units of the original data.

Liquid	t°C	P_{max}*	m	b	$(\%)_{av}$	$(\%)_{max}$
			Data of Danforth**			
Ethyl ether	30	12000	1.17659	0.31125	1.21	2.74
Ethyl ether	75	12000	1.42582	0.06676	1.16	2.52
Pentane	30	12000	2.63595	0.36305	0.06	0.33
Ethyl alcohol	30	12000	0.12407	0.97643	0.38	1.08
Ethyl alcohol	0	12000	0.09448	0.99580	0.57	1.38
Hexyl alcohol	30	4000	0.23520	0.96426	0.59	0.83
Hexyl alcohol	75	8000	0.38421	0.90341	0.58	0.92
Bromobenzene	30	4000	1.01806	1.01761	0.15	0.35
Bromobenzene	75	8000	1.16001	0.94717	0.08	0.23
Chlorobenzene	30	4000	0.91212	0.77397	0.27	0.43
Chlorobenzene	75	8000	0.96532	0.76365	0.17	0.33
Carbon bisulfide	30	12000	3.03747	0.38371	0.48	1.03
Carbon bisulfide	75	12000	3.15413	0.31914	0.21	0.38
Eugenol	30	3000	0.48120	0.87206	0.39	0.79
Glycerine	30	12000	0.16428	0.94074	0.41	0.93
Glycerine	0	8000	0.13400	0.95619	0.20	0.38
i-Butyl alcohol	0	12000	0.12782	0.99198	0.42	0.86
i-Butyl alcohol	30	12000	0.17220	0.96906	0.36	0.67
			Data of Chang[a]			
Carbon bisulfide	75	12000	3.31543	0.19076	0.23	0.37
Carbon bisulfide	30	12000	3.27849	0.22453	0.41	1.77
i-Amyl alcohol	22.4	12000	0.26914	0.89999	1.85	2.19
Ethyl ether	30	12000	1.10326	0.35194	1.04	2.93
Ethyl ether	75	12000	1.34818	0.11343	0.62	2.93
Toluene	30	9500	2.43974	0.34378	0.13	0.31
			Data of Kyropoulos[b]			
Carbon bisulfide	20	3000	3.35849	0.16093	0.08	0.16
Ethyl alcohol	20	3000	0.10254	0.99178	0.25	0.37
Methyl alcohol	20	3000	0.08320	0.98660	0.14	0.21
Water	20	3000	0.04890	0.98860	0.08	0.31
Acetone	20	3000	0.14357	0.96469	0.27	0.48
Ethyl ether	20	3000	1.29268	0.08743	0.53	0.90

* The pressures of Chang and Kyropoulos are in kg/cm²; those of Danforth's are in atmospheres.
** See reference 7.
[a] Z. T. Chang, Chinese J. Phys. **1**, (No. 2), 1 (1935).
[b] S. Kyropoulos, Zeits. f. Physik **40**, 507 (1926).

[6] When the true compressibility dk/dP at atmospheric pressure is known only one parameter B is necessary. This is especially important when adjusting data to the equation by the method of least squares. See reference 1.
[7] W. E. Danforth, Jr., Phys. Rev. **38**, 1224 (1931).
[8] B. B. Owen and S. R. Brinkley, Jr., Phys. Rev. **64**, 32 (1943).
[9] F. G. Keyes and J. G. Kirkwood, Phys. Rev. **36**, 754 (1930); *ibid.* **36**, 1570 (1930).
[10] *International Critical Tables*, Vol. VII, p. 65. The formulas for the indexes of refraction for binary mixtures are discussed here and a bibliography is given.

TABLE II. The constants m and b of the equation $1/f_P = mv_P + b$ evaluated by the method of least squares from dielectric constant data at high pressures for gases and from refractive indices for liquids and gases. The average and maximum percent deviations between the observed and calculated values of ϵ_P (or n_P) are given in the last columns. The pressures and volumes are in the units of the original data.

Substance	t°C	P_{max}	m	b	$(\%)_{av}$	$(\%)_{max}$
Dielectric Constants of Gases*						
		$1/f_P=(\epsilon+2)/(\epsilon-1)$				
Carbon dioxide (liquid)	0	200[a]	128.733	−0.03195	0.06	0.12
Carbon dioxide	35	100	132.4435	−0.7808	0.54	3.02
Carbon dioxide	100	151	133.7713	−0.7962	0.04	0.24
Ammonia	100	55	23.9453	−0.2956	0.03	0.10
Ammonia	175	100	27.5442	−0.2266	0.06	0.15
Refractive Indices of Gases and Liquids						
		$1/f_P=(n_P^2+2)/(n_P^2-1)$				
Carbon dioxide[b]	32	122[e]	3294.03	0.0363	0.13	0.31
Nitrogen[c]	25	2053	5092.274	−0.1734	0.09	0.29
Ethylene[d]	100	2269	2082.868	−0.0413	0.19	0.64
Benzene**	25	868[f]	2.68806	0.33320	0.002	0.003
Water†	25	1500[g]	4.17917	0.66864	0.010	0.013
Alcohol†	25	1500[g]	3.30631	0.31927	0.020	0.025

* See reference 9.
[a] In all of Keyes and Kirkwood's data the pressures are in atmospheres and the volumes are in liters/mol. The lower pressure limit is in all cases above atmospheric pressure.
[b] Michels and Hammers, Physica **4**, 1002 (1937). $\lambda = 5876$A.
[c] Michels, Lebesque, and De Groot, Physica **13**, 337 (1947). $\lambda = 5876$A.
[d] Michels, Botzen, and De Groot, Physica **13**, 343 (1947). $\lambda = 5876$A.
** See reference 4.
† See reference 1.
[e] In all of Michels' data the pressures are in atmospheres and the densities are given in Amagat units; the volumes used in calculating the constants above are the reciprocals of these densities. The lower pressure limit is (except for Nitrogen) the atmospheric pressure.
[f] Pressure in bars. $\lambda = 589\ m\mu$.
[g] Pressure in atmospheres. $\lambda = 579\ m\mu$.

term as a compression would be consistent with Tammann's hypothesis that the introduction of a dissolved substance has the same effect upon a solvent as compressing the pure liquid under external pressure.

In Tables I and II the constants m and b of Eq. (3) are given for liquids and gases whose dielectric constants and indexes of refraction have been measured under pressure by various investigators. These constants were determined by the method of least squares by minimizing the sums of the squares of the difference of the observed and computed values of the function $1/f_P$ (the line of regression of $1/f_P$ on v_P).

As has already been noted, Danforth[7] plotted the reciprocals of the Clausius-Mosotti expression against the densities, i.e.,

$$\rho_P/f(\epsilon_P) = b''\rho_P + m'', \qquad (6)$$

where ρ_P is the reciprocal of the specific volume v_P and $1/f_P=(\epsilon+2)/(\epsilon-1)$. We prefer the arrangement of Eq. (3) which can more readily be related to the logarithmic form of Eq. (5). Theoretically, Eqs. (3) and (6) are the same, but it must be noted that in practice, because of the change of variables, the least-square method of fitting the best line of Eq. (3) does not give the same line as in fitting Eq. (6). (The line of regression of $1/f_P$ on v_P is not the same as the line of regression of ρ_P/f_P on $1/v_P$). It can be shown that if instead of assuming observations of equal weights in fitting the line of Eq. (3), we ascribe to the observations the weights $1/v_P^2$ we will obtain the line of Eq. (6). Conversely, with the weights v_P^2 the least-square line of Eq. (6) will be the line of Eq. (3).

In practice, the two lines of regression (3) and (6) give essentially the same results for a number of cases tried. Thus, for carbon bisulfide at 75°C (data of Danforth) and for ammonia at 100°C the two line of Eqs. (3) and (6) give values for ϵ_P whose average and maximum percent deviation from the observed dielectric constants are practically the same.

Danforth observed that the reciprocal of the Clausius-Mosotti function ρ_P/f_P is linear in the density in the case of all polar substances except ethyl ether and the two more simple non-polar substances carbon bisulfide and pentane. This conclusion is not altogether admissible from the results shown in Table I. Ethyl ether does consistently show the greatest deviations from linearity in the data of Chang and Kyropoulos as well as in the work of Danforth. However, the least-square line for pentane is associated with the smallest deviations shown in Table I, while at 75°C carbon bisulfide (Danforth and Chang) fits comparatively well, and at 30°C the results for carbon bisulfide are better than those for ethyl alcohol (0°C), which according to Danforth behaves normally. Evidently, Danforth drew his conclusions on the exceptional behavior of these substances by relying on graphical representation to estimate linearity.

TABLE III. Two least square formulas $1/f_P = mv_P + b$ for the refractive indices of a gas* for which the range of the function $1/f_P=(n_P^2+2)/(n_P^2-1)$ is extensive. The equation $1/f_P$ $3294.03v_P+0.0363$ was obtained by minimizing the sum of the squares of the difference of the observed from the computed value of the function $1/f_P$. The better fitting equation $1/f_P=3330.76v_P$ $+0.1108$ was obtained by minimizing the sum of the squares of the percent difference between the observed and computed values of the refractive indices of the gas. The last two columns show the percent difference between the observed refractive indices and those computed from these equations.

Pressure, atmos.	n_{4358}	v_P**	$1/f_P$ obs'd.	Percent deviation of n	
21.35	1.0097	0.047015	154.9250	0.002	0.010
49.24	1.0278	0.016316	55.2198	−0.057	−0.039
56.25	1.0345	0.013101	43.2000	0.025	0.042
63.35	1.0438	0.010337	34.5121	−0.012	0.004
67.41	1.0512	0.008827	29.5660	−0.021	−0.009
72.35	1.0676	0.006691	22.4638	−0.018	−0.019
77.92	1.1482	0.003103	10.4232	0.208	0.030
86.45	1.1642	0.002802	9.4421	0.235	0.002
96.74	1.1735	0.002655	8.9554	0.263	−0.003
106.46	1.1794	0.002569	9.6730	0.278	−0.010
121.60	1.1864	0.002476	8.3612	0.312	−0.007
			Average percent deviaion of n	0.130	0.016

Maximum percent deviation of n, 0.312, 0.042.

* Carbon Dioxide at 32.075°C. Data of Michels and Hamers, Physica **4**, 1002 (1937).
** The volumes shown are the reciprocals of the densities originally given in Amagat units.

TABLE IV. The parameters A and B of the Tait equation $A \log_{10}(1+P/B)$ fitted by the method of least squares to the functions $1/f_0-1/f_P$*, $1/\epsilon_0-1/\epsilon_P$ and the compressions v_0-v_P. The three sets of parameters are given for each substance in the foregoing order. The last two columns give the average and maximum percent deviations between the observed and calculated values of ϵ_P. The pressures and volumes are in the units of the original data.

Substance	t°C	ϵ_0	P_{max}	A	B‡	$(\%)_{av}$	$(\%)_{max}$
Pentane**	30	1.82	12000[a]	0.9113	359	0.096	0.285
				0.09106	625	0.154	0.334
				0.3449	354	0.113	0.511
Glycerine**	0	49.9	8000	0.02315	3807	0.051	0.098
				0.07472	3826	0.063	0.163
				0.1464	2845	0.134	0.190
Carbon bisulfide**	30	2.61	12000	0.5054	610	0.186	0.544
				0.08231	848	0.281	0.671
				0.2005	1129	0.074	0.211
Bromobenzene**	75	4.87	8000	0.1732	936	0.121	0.242
				0.03989	1049	0.124	0.268
				0.1520	983	0.108	0.238
Acetone[b]	20	21.50	3000[b]	0.03911	795	0.085	0.176
				0.01196	799	0.087	0.177
				0.3202	1085	0.077	0.229
Carbon tetrachloride[b]	18	2.246	1000[b]	0.8403	1144	0.009	0.020
				0.1033	1376	0.010	0.023
				—	934[c]	—	—
Ammonia†	100	1.0940[d]	55	28.789	−14.12[e]	0.163	0.314
				—	—[f]	—	—
				1.2085	−14.05[e]	0.675	1.167
Benzene††	45	1.4851[g]	1188[h]	0.699133	859	0.003	0.005
				0.082786	1030	0.002	0.004
				0.253355	829[c]	—	—

* $1/f_P=(\epsilon_P+2)/(\epsilon_P-1)$. $1/f_0$ is the value of the function at either the atmospheric or the initial pressure.
‡ B is in the same units as the pressure.
** See reference 7.
[a] Atmospheres. All of Danforth's pressures are in this unit.
[b] The data of Kyropoulos. His pressures are in kg/cm².
[c] The value of Gibson.
† See reference 9.
†† See reference 4.
[d] The value at 20 atmos., the lower pressure limit.
[e] The function fitted here is that of Eq. (5) where v_0 and $1/f_0$ are replaced by their values at $P'=20$ atmos., the initial pressure.
[f] The function $1/\epsilon_0-1/\epsilon_P$ cannot, in this case, be represented by a Tait equation.
[g] The index of refraction ($\lambda=589$ $m\mu$). ϵ_P is replaced by n_P^2 in the equations.
[h] Pressure in bars.

WEIGHTED FORMULAS FOR GASES

In the last two columns of Tables I and II are shown the average and the maximum percent difference between the observed and computed value of the dielectric constant or refractive index ($100\Delta n/n$).[11] This is the criterion used for the closeness of fit of the interpolation formula of Eq. (3), though in fitting this line by the method of least squares, we minimized the sum of the squares of $\Delta(1/f_P)$, the difference of the observed and the computed values of the function $1/f_P$. Obviously, this is not the proper function to minimize to give us the most favorable deviations of n_P (or ϵ_P). Generally, this inconsistency is not serious and it has the advantage of lessening the computational work involved in applying the method of least squares. The parameters m and b shown in Tables I and II were all found by fitting Eq. (3) in this way. However, where the range of the function $1/f_P$ is extensive (e.g., in the case of a gas, see Table III), the simplification of minimizing the sums of the squares of the residuals of $1/f_P$ tends to pile up at the higher pressures large percent differences between the observed and computed values of n_P (or ϵ_P). This is apparent from the second to last column of Table III, where the data for the refractive indices of carbon dioxide are given as an illustrative example. The distribution of percentages in this column resulted from fitting Eq. (3) in the usual way. The last column, however, shows a better distribution of the percent difference between the observed and computed values of n_P; in fact, an over-all improvement in fitting the observed values of n_P to Eq. (3) has been affected.

To obtain the distribution of percentages indicated in the last column of Table III, we fit the observed data to Eq. (3) in another manner. Instead of minimizing $\sum\{\Delta(1/f)\}^2$ we minimize $(\sum\Delta n/n)^2$, i.e., the sum of the squares of the percent difference between the observed

[11] Δn (or $\Delta\epsilon$) will denote the absolute value of the difference between the observed and computed value of n_P (or ϵ_P). The Δ will have the same significance when used with the function $1/f_P$.

and computed values of n_P. We assume below that the function $1/f_P$ involves the indices of refraction n_P, but obviously the same procedure will apply where the dielectric constants are considered.

If we write the approximate relation

$$\Delta n=\Delta(1/f)/(1/f)',$$

where $(1/f)'=d(1/f)/dn$; then

$$\sum(\Delta n/n)^2=\sum\{\Delta(1/f)/n(1/f)'\}^2$$

is the new function we must minimize. This is equivalent to ascribing to the function $1/f_P$ a weight w_P, which is for each observation given by

$$w=\{1/n(1/f)'\}^2.$$

The published results of most of the investigators whose data we have used do not include enough information to permit a precise comparison with the deviations from our interpolation formula. Danforth, from whom the bulk of our data for very high pressures is taken, gives no estimate of the uncertainties in his measurements. However, with few exceptions, the Eq. (3) will represent his data within a few units in the last significant figure in ϵ. A reasonable estimate of the experimental error of Gibson's measurements of the indices of refraction of benzene is perhaps 0.01 percent, and it may be seen that our interpolation formula reproduces his results well within this experimental error. Keyes and Kirkwood's experimental error for carbon dioxide is about 0.2 percent (and presumably, though they do not indicate this, it may be assumed to be the same for ammonia). Table II shows that we have fitted their data within this experimental error except in the case of carbon dioxide at 35°C. But Keyes and Kirkwood point out that they consider Amagat's compressibility data, which they used, unreliable above 60 atmospheres; and here, too, is where our interpolation formula fails. Except in this case and that of the gases discussed below there are no visible trends in the residuals from the interpolation formula for the substances in Tables I and II.

The situation, however, for the refractive index measurements of Michels *et al.* for carbon dioxide, nitrogen, and ethylene shown in Table II is somewhat different. The average deviations indicated for these gases in Table II are considerably in excess of the general accuracy claimed for their measurements. Furthermore, in the second last column of Table III, where the deviations are enumerated in detail for carbon dioxide, a systematic trend may be observed at higher pressures. However, the last column, which gives the deviations for the weighted formula, shows that this trend has been obliterated. The average percent deviation of n indicated in this column (0.016 percent) is in accord with the accuracy which Michels usually claims, but the maximum percent deviation in n (0.042 percent) may be too high. Considering the difficulties recorded by the investigators because the measurements pass through the region of the critical point, this abnormal deviation may reflect only this experimental situation.

It may reasonably be claimed that the interpolation formula (3) represents the data for liquids, and that the same weighted formula reproduces the results for gases within the experimental error.

SIGNIFICANCE OF THE PARAMETER B

Owen and Brinkely[8] conclude that the parameter B in the equation

$$1/\epsilon_0-1/\epsilon_P=A\ \log(1+P/B) \qquad (7)$$

has the same value as in the analogous Tait equation for the compressions of the liquid, i.e., the same value of B may be determined independently from either the dielectric constants or the densities. Their evidence for this conclusion is, aside from considerations of electrostatic theory and Tammann's hypothesis, that Eq. (7) accurately reproduces the variations of the dielectric constant with pressure for some liquids with values for B obtained by Gibson[12] from compressibility data. Since, however, it has been shown in this article that it is possible to replace $1/\epsilon$ in Eq. (7) by other functions, and especially the function $1/f=(\epsilon+2)/(\epsilon-1)$, it seemed necessary to investigate more rigorously the nature of the parameter B when it is determined from compressibility as well as dielectric constant data over the *same* range of pressures and with $1/f_P$ as both $(\epsilon_P+2)/(\epsilon_P-1)$ and $1/\epsilon_P$.

Another factor prompts a reconsideration of the significance of the parameter B in these equations. The value of B in the Tait equation is not critical, and as the equation has another disposable constant it is understandable that widely varying values of B in (7) may yet enable the equation to express the isothermal variations of the dielectric constant of liquids with pressure. It is, therefore, not surprising to see values of B, determined from compressibility data to pressures of approximately 1000 atmospheres,[13] successfully used by Owen and Brinkely in Eq. (7) to represent dielectric constant data to as high as 12,000 atmospheres. This assumes what is only approximately true, that the parameter B in Tait's equation is independent of the external pressure on the solution. But B is not quite constant for a given liquid but depends on the pressure range of the data.[14] For this reason all values of B

[12] Gibson's values of B are summarized by Harned and Owen. See reference 5.

[13] Gibson's values of B were determined from compressibility data in this range. These were applied by Owen and Brinkely to Danforth's data whose maximum pressure range is 12,000 atmos. and to Kyropoulos's data to 3000 kg/cm².

[14] Besides the relevance of this observation here it should also have some bearing in speculation (see reference 4) on the theoretical significance of the parameter B in Tait's equation. This should not only take into consideration the dependence of B on the pressure range but should also consider the manner in which the curve was fitted to the data.

presented here for comparison have been determined from the same pressure range.

In Table IV are given the parameters A and B of $A \log_{10}(1+P/B)$ fitted by the method of least squares to the functions $1/f_0-1/f_P$, $1/\epsilon_0-1/\epsilon_P$ and to the compressions v_0-v_P. For each substance in the table three sets of the two parameters A and B are given corresponding to the functions given in the above order; the pressure range for these three functions is, for any particular substance, the same.[15]

Generally, it will be observed, the function $1/f_0-1/f_P$ fits the data somewhat better than $1/\epsilon_0-1/\epsilon_P$, but the values of the parameter B corresponding to these two functions sometimes differ considerably. When ϵ_P is large (e.g., glycerine and acetone), it may easily be shown by expansion in series that the function $1/f_P$ is approximately linear in $1/\epsilon_P$ so that $1/f_0-1/f_P$ is proportional to $1/\epsilon_0-1/\epsilon_P$, in which case the parameters B in the logarithmic form of these functions necessarily have nearly the same value (but this value of B is not necessarily the same value of B obtained from the compressibility data).

On the other hand, where the values of ϵ_P are small (as in pentane) the B in the logarithmic representation of the function $1/\epsilon_0-1/\epsilon_P$ does not, if pentane is typical of this class, have even nearly the value of B obtained by fitting the dielectric constant data to the function $1/f_P=(\epsilon_P+2)/(\epsilon_P-1)$.

For ammonia where the values of ϵ_P are only somewhat larger than one, and for other gases that were tried (where B is negative), the function $1/\epsilon_0-1/\epsilon_P$ gives, when plotted against the pressure, a curve that is concave upward, so that it is not possible to represent the function $1/\epsilon_0-1/\epsilon_P$ by a Tait equation. However, the function $1/f_P=(\epsilon_P+2)/(\epsilon_P-1)$, as may be seen from Table IV, when adjusted to the data gives a value of B which agrees well with the value of B obtained from the compressibility data.

In conclusion it might be said that the results of Table IV lend some plausibility to the thesis that the parameters B of the logarithmic representation of the function $1/f_0-1/f_P$ (and sometimes the function $1/\epsilon_0-1/\epsilon_P$) is the same as the B determined by the Tait equation for v_0-v_P. However, it is evident that more reliable data would be required before this proposition could be established conclusively; for it must be kept in mind that the parameter B is extremely sensitive to very small variations in the data from which it is determined and that small deviations in the measurements affect the value of B enormously.

THE TAIT EQUATION FOR GASES

As we have shown in Table IV, it has been possible to adjust $v_{P'}-v_P$ and $1/f_{P'}-1/f_P$ for ammonia at 100°C to the Tait function

$$A \log\{(P+B)/(P'+B)\},$$

where $v_{P'}=1.385$ and $1/f_{P'}=32.915$, the values corresponding to the initial pressure $P'=20$ atmos. It has already been pointed out that it is not possible to use the function $1/\epsilon_0-1/\epsilon_P$ for gases; and that B, unlike that for liquids, is negative.

It may be observed that though the pressure range is relatively small (20–55 atmos.), the compressibility data of ammonia are not reproduced by the Tait equation as well as it is for liquids over greater ranges of pressure. That this is not because the data are inherently less accurate may be indicated by the fact that the ammonia densities used are the measurements of Beattie and Lawrence,[16] who also represented them by an equation of state (over the range 17–58 atmos.) but with somewhat better results. Their maximum percent deviation between the observed and calculated volumes was about 0.8 percent as compared to the 1.17 percent (and 0.68 percent average) shown in Table IV.

It is, however, quite noteworthy that the Tait equation, which can so well be adapted to compressibility data for liquids (and some solids), can also be used with gases.[17] The somewhat inferior results obtained for gases emphasize what has already been pointed out—that the parameter B is not independent of the external pressure, and this dependence is particularly greater for gases as is demonstrated by the results obtained for ammonia and by other gases that were examined.

[15] The compressibility data used are those given by the investigator. It must be pointed out that though Danforth's work was done in Bridgman's laboratory the densities he used do not always agree with Bridgman's published data. Thus, Bridgman's compressibility data for glycerine would give a much higher value for B than that shown in Table IV, but this value of B, too, would be of dubious value since the glycerine Bridgman used is admittedly contaminated with water. P. W. Bridgman, Proc. Am. Acad. Sci. **67**, 11 (1932).

[16] J. A. Beattie and C. K. Lawrence, J. Am. Chem. Soc. **52**, 6 (1930).

[17] It might be of some interest to point out that v_0-v_P is only the simplest function of the volumes that can be represented by the Tait equation. As in the case of the dielectric constants and refractive indices, other functions of v_P may be used, e.g., the Lorentz-Lorenz function $1/f(kv_P)=(1+2kv_P)/(1-kv_P)$ where k is a constant for which $1-kv_P>0$.

A Quantum-Mechanical Theory of Light Absorption of Organic Dyes and Similar Compounds*

HANS KUHN
Institute of Physical Chemistry of the University of Basel, Basel, Switzerland
(Received February 21, 1949)

The most important organic compounds which absorb visible light can be classified into three groups typified: (a) by symmetrical polymethines, (b) by porphyrines, (c) by polyenes.

Recently it was shown that the position of the absorption maxima of *symmetrical polymethines and related compounds* (symmetrical cyanine and oxanole dyes; Michler's hydrol blue and derivatives; malachite green and other triphenyl methane dyes; etc.) can be calculated by adopting a model of the dye molecule which is analogous to the free-electron gas model used in particular by Sommerfeld to describe the condition of metals. The π-electrons of the polymethine chain are considered as a one-dimensional free-electron gas which extends itself along the length of the chain.

In the normal state the stablest energy states of the electron gas each contain two electrons in accordance with Pauli's exclusion principle. The remaining states are empty. The existence of the first absorption band is a consequence of the jump of a π-electron from the highest energy level occupied in the normal state to the lowest empty level.

For the wave-length of the maximum of the first absorption band of this group of dyes, the relationship obtains that

$$\lambda_1=(8mc/h)(L^2/[N+1]),$$

where L is the length of the polymethine zig-zag chain, N, the number of π-electrons, m, the mass of the electron, c, the velocity of light, h, Planck's universal constant. Good agreement with experimental results for λ_1 is obtained by the use of this equation.

The problem of *porphyrine and phthalocyanine* compounds can also be dealt with on the basis of a free-electron gas model. We treat the π-electrons of the porphyrine ring as electrons which are confined to move in a closed ring-shaped path in a field of constant potential energy.

In the case of *polyenes and related compounds* (Carotenes, unsymmetrical cyanines and oxanoles, merocyanines, azo- and stilbene dyes, etc.) a description by means of a free-electron gas model is no longer permissible. The electron gas in this case suffers a disturbance from its condition in the case of the first and second groups of dyes, and, to allow for this, the π-electrons are considered placed in a one-dimensional potential having a sine curve periodicity. The wave-length λ_1 is expressed by

$$\lambda_1=\left[\frac{V_0}{hc}\left(1-\frac{1}{N}\right)+\frac{h}{8mc}\frac{N+1}{L^2}\right]^{-1},$$

where V_0 is the amplitude of the sine-shaped potential along the chain.

This relation is confirmed by the experimental data. It also gives an explanation for the markedly different manner (compared with the symmetrical polymethines) in which the position of the absorption bands of polyenes and related compounds depends on the chain length.

The results of the classical color theory of Witt are capable of a simple explanation when considered in the light of the electron gas model.

THE problem of setting up a quantitative theory for the light absorption of organic molecules has been attempted only in a few instances. The most important results are those of Sklar[1] and Förster[2] who found quantitatively the absorption bands of some unsaturated hydrocarbons (benzene, anthracene, phenanthrene, butadiene, fulvene, and azulene). Their calculations were based on the two well-known quantum-mechanical approximations of the bond orbital and molecular orbital methods. Later these methods were applied to polymethine dyes.[3] It turns out, however, that the calculated values of the wave-lengths of the absorption maxima of these compounds are about four times larger than the experimentally determined ones. This would mean that according to these calculations the dyes would absorb in the infra-red and not in the visible spectrum. So far then, these methods, when applied to dyes, do not seem to give satisfactory results.

Recently, by using the concept of the free-electron gas, as used in particular by Sommerfeld[4] for metals,[5] the author has shown[6,7] that this can lead to a satisfactory interpretation of the color of the symmetrical polymethine dyes.[8] The model based on the electron gas was then refined[9] and will now be shown to be capable of being extended to give a quantitative theory of light absorption of the most important groups of colored organic compounds typified by the symmetrical polymethines, porphyrines, and polyenes.

* Translated from the German by Alexander Silberberg.

[1] A. L. Sklar, J. Chem. Phys. **5**, 669 (1937).

[2] Th. Förster, Zeits. f. Elektrochemie **45**, 548 (1939); Zeits. f. physik. Chemie (B) **41**, 287 (1938).

[3] K. F. Herzfeld, J. Chem. Phys. **10**, 508 (1942); A. L. Sklar, J. Chem. Phys. **10**, 521 (1942); K. F. Herzfeld and A. L. Sklar, Rev. Mod. Phys. **14**, 294 (1942).

[4] A. Sommerfeld and H. Bethe, *Handbuch der Physik* (1933), Vol. 24, second edition.

[5] The density of the π-electrons in aromatic compounds and the diamagnetic anisotropy of such molecules has been treated on the basis of free-electron gas models by: (a) O. Schmidt, Zeits. f. physik. Chemie (B) **39**, 59 (1938); **42**, 83 (1939); **44**, 185, 194 (1939); **47**, 1 (1940). (b) L. Pauling, J. Chem. Phys. **4**, 673 (1936). (c) K. Lonsdale, Proc. Roy. Soc. **159**, 149 (1937).

[6] H. Kuhn, Helv. Chim. Acta **31**, 1441 (1948), lecture at the chemistry colloquium at the University of Basel on January 22, 1948.

[7] H. Kuhn, J. Chem. Phys. **16**, 840 (1948).

[8] Very recently J. R. Platt, J. Chem. Phys. **17**, 484 (1949), has used a free-electron gas model for treating the absorption of polyacenes, and W. T. Simpson, J. Chem. Phys. **16**, 1124 (1948), has treated polymethines in a similar way as it has been done earlier by H. Kuhn (references 6 and 7). N. S. Bayliss, J. Chem. Phys. **16**, 287 (1948), has treated the absorption of polyenes on the basis of a free-electron gas model. However, as we shall see in Section C-3, the use of such a model is not permissible in this case.

[9] H. Kuhn, Chimia **2**, 11 (1948). For an extension of the treatment to molecules with branched π-electron gas see H. Kuhn, Helv. Chim. Acta **32**, nr. 7 (1949) (in print).

A. SYMMETRICAL POLYMETHINE DYES AND SIMILAR COMPOUNDS

1. Qualitative Description of the Electron Gas Model

We consider as a particularly simple example the symmetrical polymethine dye Ia, Ib. The cation, which is responsible for the color, is considered to be resonating between two limiting structures, Ia and Ib, each of which makes the same contribution to the normal state of the cation.

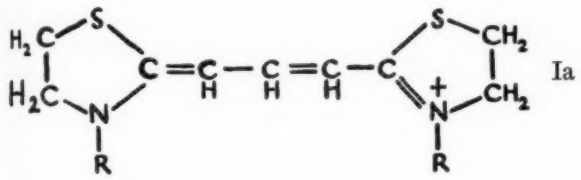

Ia

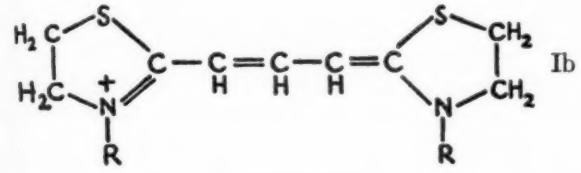

Ib

Each structure results from the other when the single and double bonds of the polymethine chain change over. This picture shows that we are not dealing with a conjugated chain of double and single bonds, but with a chain of equal bonds, whose nature is intermediate between double and single bond. Their character compares with the C—C bonds in benzene.

A qualitative quantum-mechanical picture of this bond condition is illustrated in Fig. 1. The atoms constituting the polymethine chain lie with their centers in a plane and are joined by σ-bonds. Each carbon atom of the chain and the two nitrogen atoms at the ends are the center of three such σ-bonds as indicated by the lines in Fig. 1(a).

To form the σ-bonds each carbon atom and each of the two terminal nitrogen atoms uses three of its valency electrons. The fourth valency electrons of the carbon atoms in the chain and the remaining electrons in the outer shells of the two nitrogen atoms find themselves in the electrostatic field of the molecular skeleton. These electrons (π-electrons) are attracted by the positively charged carbon and nitrogen atoms, but are repelled by the electrons forming the σ-bonds. Due to the influence of the above electrostatic attractions and repulsions, the π-electrons form an "electron gas" which in the shape of a charged cloud stretches along the polymethine chain both above and below the plane xy of the molecule.

If such a molecule absorbs visible light, it means that the light vector concerned interacts with the easily displaceable π-electrons of the electron gas, which is thereby brought into a state of excitation.

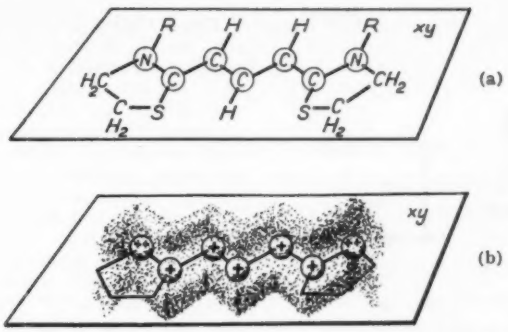

FIG. 1. Cation of the cyanine dye Ia, Ib. (a) Molecular skeleton. (b) The π-electron gas extends along the polymethine chain above and below plane xy in the form of a charged cloud. Light absorption is caused by the electrical vector of the incident light acting on the easily displaceable π-electrons.

2. Quantitative Treatment

The Bohr relationship between the wave-length λ of an absorption maximum and the excitation energy ΔE of the corresponding excited state (i.e., the difference in energy between the particular excited state considered and the normal state) is

$$\lambda = hc/\Delta E, \qquad (1)$$

where h is Planck's constant, and c is the velocity of light. This relation permits us to predict the absorption spectrum (i.e., the position of possible absorption maxima) from the excitation energies of the possible excited states of the π-electrons.

In order to find the energy of the possible excited states of the electron gas, a few simplifying assumptions have to be made. Firstly, we restrict the π-electrons so that they can only move in the direction of the chain, i.e., only along the zig-zag line of the polymethine chain. Secondly, we assume that the potential energy of an electron remains constant as it moves along the chain, and that it rises sharply to infinity as it comes to the ends of the chain. That means that we replace the π-electrons of the polymethine chain by electrons moving in a one-dimensional box of length L, where L is the length of the polymethine zig-zag chain (Fig. 2).[a]

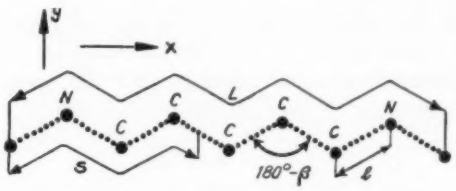

FIG. 2. According to the model the π-electrons can only move along and in the direction of the polymethine zig-zag chain of length L. The potential energy along the length L is considered constant.

[a] The potential energy along the chain does not actually rise sharply to infinity at the ends of the resonating portion. It shows a more or less steep increase at these points, depending on the nature of the groups in the neighborhood of the terminal nitrogen atoms. For most of the cases dealt with here these groups are simple saturated structures, and we can assume that L is measured by the length of the polymethine zig-zag chain between the nitrogen atoms plus one bond distance to either side (see Fig. 2).

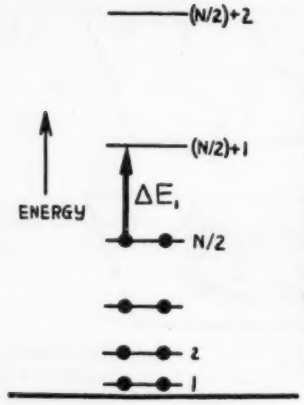

FIG. 3. Cation of the cyanine dye Ia, Ib. Energy levels in which a π-electron of the electron gas can remain. In the normal state the $N/2$ stablest levels are filled by two electrons each, as required by the Pauli exclusion principle. The remaining levels are empty. (N is the number of π-electrons in the gas).

The existence of the first (by far the strongest) absorption band is a result of the jump of an electron from the highest occupied level, No. $N/2$, to level No. ($[N/2]+1$).

With these assumptions it is easy to set up and solve the Schrödinger equation for the π-electrons, and the energy values which a particular electron can assume are simply calculated).[b] Figure 3 shows the energy levels of some of the lowest quantum states.

According to the Pauli exclusion principle, not more than two of the electrons of the π-electron gas can coexist in the same quantum state, and thus be at the same energy level. In the normal state all the lowest levels will then be filled, with two electrons each, to a certain height, depending upon the number of electrons available. All higher levels in this normal state will be empty. If N is the number of π-electrons making up the gas (in the case of the dye Ia, Ib, N is 8), then for the normal state the $N/2$ lowest levels contain two electrons each; the other levels are empty (see Fig. 3, the electrons are represented by dots).

The existence of the first absorption band, which is practically the only important one, is associated with the jump of one electron from the highest occupied level, No. $N/2$, to the lowest free level, No. ($[N/2]+1$). For the energy difference, ΔE_1, between level No. $N/2$ and the next highest one we obtain, on account of the assumptions made, the relation

$$\Delta E_1=(h^2/8mL^2)(N+1), \tag{2}$$

where m is the mass of the electron, L (see above) is the length of the polymethine chain measured along zig-zag line of the chain links. By substituting (2) in (1) we immediately obtain an expression for the wave-length of the maximum of the first absorption band

$$\lambda_1=\frac{hc}{\Delta E_1}=\frac{8mc}{h}\frac{L^2}{N+1}. \tag{3}$$

The intensity of the absorption band, which is measured by the oscillator strength, f, is also easily calculated on the basis of this model.

For the special case of a polymethine chain where every bond in the chain has a *trans*-configuration (like the chain represented in Figs. 1 and 2) the oscillator strength is given by

$$f_1=\frac{8}{3\pi^2}\cos^2(\beta/2)\cdot\frac{N^2(N+2)^2}{(N+1)^3}, \tag{4}$$

where $180°-\beta$ is the valency angle between successive chain links. If the polymethine chain does not exhibit *trans*-configuration at every bond, but if at some, or even all links, the *cis*-structure prevails, the oscillator strength (which on our model is easily calculated for all configurations) must always be less than according to (4).

The manner in which Eq. (4) can be derived will now be briefly indicated. From general quantum theory the transition probability, with which an electron under the influence of light passes from a lower quantum state A to a higher state B, is easily calculated and obviously determines the oscillator strength $f_{A\to B}$ corresponding to this transition. Hence,

$$f_{A\to B}=\frac{8m\pi^2}{3h^2}\Delta E_{A\to B}(|X_{A\to B}|^2+|Y_{A\to B}|^2+|Z_{A\to B}|^2), \tag{4.1}$$

where

$$X_{A\to B}=\int\psi_A\psi_B^* x\,d\tau, \tag{4.2}$$

$$Y_{A\to B}=\int\psi_A\psi_B^* y\,d\tau, \tag{4.3}$$

$$Z_{A\to B}=\int\psi_A\psi_B^* z\,d\tau. \tag{4.4}$$

In the above $\Delta E_{A\to B}$ is the energy difference of the two states and $\psi_A(x,y,z)$ and $\psi_B(x,y,z)$ are the wave functions of the electron in state A and B, respectively, when the molecule is fixed relative to an xyz coordinate system. The symbol $d\tau$ is used to represent the volume element $dxdydz$ in space, and the integrals are to be taken over the whole space.

Here we are concerned with the transition of a π-electron of the polymethine chain from quantum state No. $N/2$ to state No. ($[N/2]+1$). The energy difference $\Delta E_{A\to B}$ in this case equals ΔE_1 as given by Eq. (2), and the wave functions of the electron in the two states, according to our one-dimensional electron-gas model, are:

$$\psi_{N/2}=(2/L)^{\frac{1}{2}}\sin((\pi s/L)N/2), \tag{4.5}$$

$$\psi_{N/2+1}=(2/L)^{\frac{1}{2}}\sin((\pi s/L)([N/2]+1)), \tag{4.6}$$

where the variable s is the distance between a point on the zig-zag chain L and one of its ends when measured along the zig-zag path of the chain (see Fig. 2). The xyz coordinate system is now so placed relative to the molecule that the origin is at one end of the chain and that the x axis coincides with the direction of the chain as shown in Fig. 2. Consequently,

$$x=s\cos(\beta/2). \tag{4.7}$$

Formula (4.2) suitably applied to these conditions transforms to

$$X_{N/2\to N/2+1}=\int_{s=0}^{L}\psi_{N/2}\psi_{N/2+1}x\,ds. \tag{4.8}$$

Substituting Eqs. (4.5), (4.6), and (4.7) in (4.8) and integrating we obtain

$$X_{N/2\to N/2+1}=-(2L/\pi^2)\left(\cos\frac{\beta}{2}\right)(N(N+2)/(N+1)^2). \tag{4.9}$$

Similar calculations applied to formulas (4.3) and (4.4) show that in this case $Y_{N/2\to N/2+1}$ and $Z_{N/2\to N/2+1}$ are zero.

Introducing these results in Eq. (4.1) gives the following result for $f_{N/2\to N/2+1}$

$$f_{N/2\to N/2+1}=\frac{4}{3\pi^2}(\cos^2\beta/2)\frac{N^2(N+2)^2}{(N+1)^3} \tag{4.10}$$

As there are two electrons in the quantum state No. $N/2$, both of which can carry out this transition, the total oscillator strength

[b] For details see reference 6.

f_1 assigned to the first absorption band must be double the value of $f_{N/2\to N/2+1}$ in Eq. (4.10), i.e., the value of f_1 is as in Eq. (4).

The value of $f_{A\to B}$ as given by Eq. (4.1) corresponds to a random orientation of the dye molecules relative to the incident light which may be polarized or unpolarized. Different are the conditions in the case when all the dye molecules are orientated parallel to one another and when the electric vector of the incident light is parallel to, say, the x direction of the coordinate system mentioned in connection with Eq. (4.1). The oscillator strength of the transition would then be

$$f_{x,A\to B}=(8m\pi^2/h^2)\Delta E_{A\to B}|X_{A\to B}|^2. \tag{4.11}$$

Similarly,

$$f_{y,A\to B}=(8m\pi^2/h^2)\Delta E_{A\to B}|Y_{A\to B}|^2, \tag{4.12}$$

$$f_{z,A\to B}=(8m\pi^2/h^2)\Delta E_{A\to B}|Z_{A\to B}|^2. \tag{4.13}$$

In the case of a polymethine chain with an all-*trans*-configuration, we have from Eq. (4.9) etc., that $X_{N/2\to N/2+1}\neq 0$; $Y_{N/2\to N/2+1}=Z_{N/2\to N/2+1}=0$. Hence, it follows from Eqs. (4.11), (4.12), and (4.13) that $f_{x,N/2\to N/2+1}\neq 0$; $f_{y,N/2\to N/2+1}=f_{z,N/2\to N/2+1}=0$. This expresses the fact that under these circumstances only the component of the incident light in the direction of the chain interacts with the molecule and hence light whose electric vector is parallel to the chain axes of the molecules will be most strongly absorbed while light whose electric vector is perpendicular to these axes will not be absorbed at all.[c]

Beyond the first absorption band we expect further though weaker bands at shorter wave-lengths which are caused by a π-electron jumping, say, from energy level No. $([N/2]-1)$ to level No. $([N/2]+1)$, or to No. $([N/2]+2)$ etc., or, say, from level No. $N/2$ to level No. $([N/2]+2)$, or to No. $([N/2]+3)$ etc.

From our model it follows that these transitions in part have polarization or components of polarization perpendicular to that of the first absorption band, and that the intensity of these bands will differ largely as we go from one *cis-trans*-isomer to the other.

3. Comparison with Experiment

All the factors entering Eqs. (3) and (4) can easily be determined in an actual case: h, c, and m are universal constants; L, the length of the polymethine chain is found from the known bond distances; and N, the number of π-electrons of the electron gas, results directly from the structural formula.

In the case of the dye Ia, Ib we find for L from Fig. 2,

$$L=8l, \tag{5}$$

where l is the bond length of the chain elements. (l equals 1.39×10^{-8} cm, which according to Pauling[10] is the bond length of a C—C bond, with bond number 1.5, as is found in benzene.) Further, as already mentioned, $N=8$. Each carbon atom in the chain yields its fourth valency electron, and the two nitrogen atoms at the ends together give three. Finally $(180°-\beta)=124°$, which is the C—C=C valency angle.

Using these values, as well as the usual ones of h, c, and m, in Eqs. (3) and (4), we obtain,

$$\left.\begin{aligned}\lambda_1&=4530\text{A}\\ f_1&=1.86\end{aligned}\right\}\text{theoretical.}$$

[c] Similar conclusions have been derived on the basis of the molecular and bond orbital methods. See Mulliken, reference 20.

[10] L. Pauling, *The Nature of the Chemical Bond* (Cornell University Press, Ithaca, New York, 1945), second edition.

For this dye Brooker[11] obtained the values,[d]

$$\left.\begin{aligned}\lambda_1&=4450\text{A}\\ f_1&=1.2\end{aligned}\right\}\text{experimental,}$$

which are in good agreement with the calculated ones. The experimentally found value for f_1 is smaller than that calculated for the all-*trans*-configuration shown in Fig. 1. It will be remembered that in connection with Eq. (4) we pointed out that such a *trans*-configuration yields the highest value of f_1 as against any configuration having some *cis*-links. The lower value thus shows that the dye which was used in the experiment probably was a *cis-trans*-isomer mixture.

As a further example we take the symmetrical carbocyanine dyes whose cations have the equivalent limiting structures

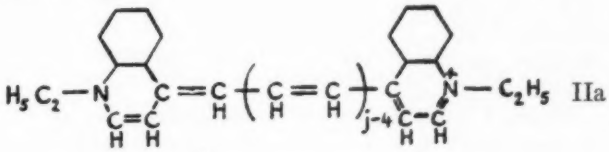

IIa

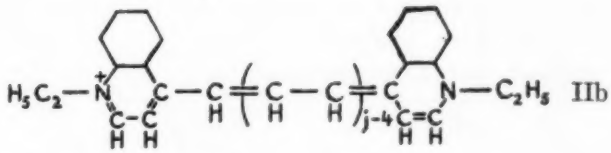

IIb

As in the case of the dye Ia, Ib we have a polymethine chain wherein each C—C bond can be considered to be of bond number 1.5 as in the benzene nucleus.

As a generalization of Eq. (5) we find the following expression for L, the length of the polymethine chain (see Fig. 2),

$$L=(2j+2)l, \tag{6}$$

where j is the number of double bonds counted along the chain in either of the limiting structures. Further,

$$N=2j+2. \tag{7}$$

[11] L. G. S. Brooker, Rev. Mod. Phys. 14, 275 (1942); R. E. Burk and O. Grummitt, *Advances in Nuclear and Theoretical Organic Chemistry* (Interscience Publishers, Inc., New York, 1945), Chapter 4; Brooker, Sprague, Smyth, and Lewis, J. Am. Chem. Soc. 63, 1116 (1940); Brooker, Keyes, and Williams, J. Am. Chem. Soc. 64, 199 (1942).

[d] The result given for the wave-length of the absorption maximum refers to the dye Ia, Ib; the corresponding value of the absorption intensity could not be found in the literature, and the result for f_1 reported refers to a dye which differs from Ia, Ib only in that the two thiazoline nuclei

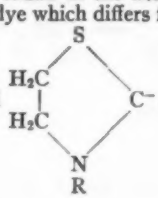

are replaced by two

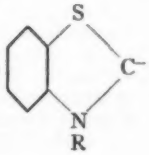

nuclei.

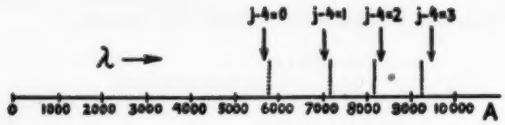

FIG. 4. Cation of the dye IIa, IIb. Position of the maximum of the first absorption band in the cases, $j-4=0, 1, 2, 3$. Dotted lines: Experimentally found position (according to Brooker). Arrows: Calculated from Eq. (8).

From Eqs. (6), (7), and (3) we obtain

$$\lambda_1 = 637\frac{(2j+2)^2}{2j+3} \quad \text{(angstrom)}. \tag{8}$$

In Fig. 4 the dotted lines show the absorption maxima found experimentally by Brooker[11] for the cases $(j-4)=0$, 1, 2, and 3. The values for the absorption maxima calculated from (8) are shown by arrows. In all cases excellent agreement between theory and experiment is found.

Figure 5 gives the experimental absorption curve in the case $(j-4)=1$. Arrow No. 1 shows the position of the band maximum on the basis of the electron gas model. Arrows No. 2, 2′, and 3 give the positions of the maximum calculated on the basis of the bond orbital and molecular orbital methods, respectively, by using the equations of Herzfeld and Sklar.[e]

Besides the cyanines a further number of dye types are known where the electron gas model can be considered to yield relatively sound results, and where good agreement with experiment is found. We will select the following dyes as examples.[f]

Oxanole dyes:

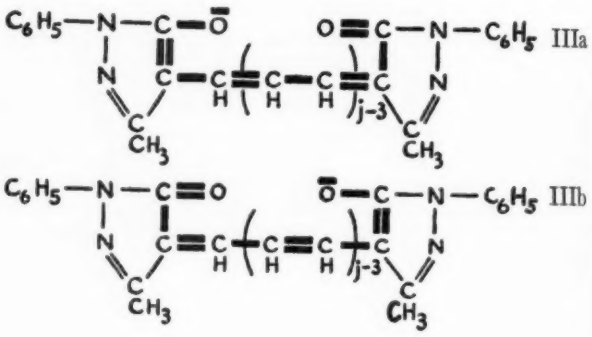

Michler's hydrol blue and derivatives:

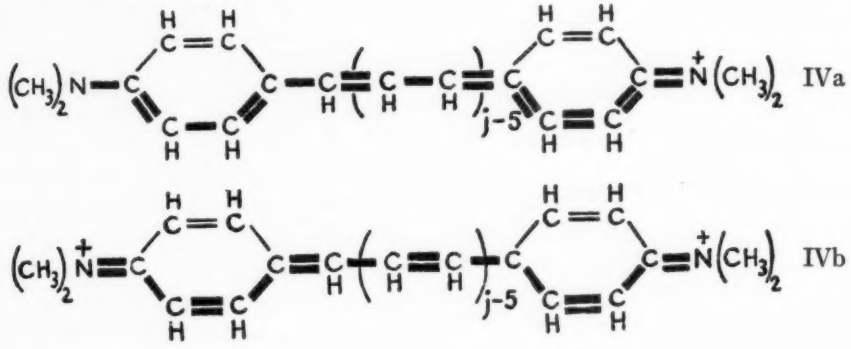

Cyanine dyes:

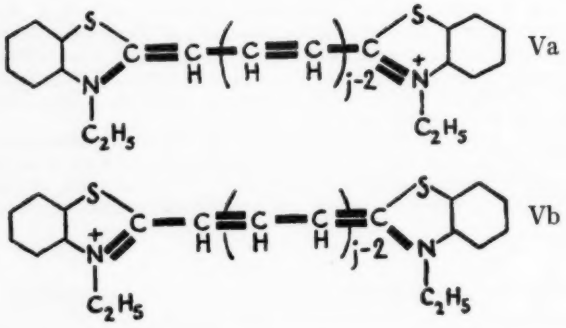

[e] K. F. Herzfeld and A. L. Sklar, Rev. Mod. Phys. **14**, 294 (1942), Eq. (8) or (10), Eq. (7). For the exchange energy (which enters the equation based on the bond orbital method) we have used the values $\alpha=36$ kcal./mole (arrow No. 2) and $\alpha=49$ kcal./mole (arrow No. 2′). The former is based on the experimentally found resonance energies of a number of aromatic hydrocarbons (compare, e.g., Eyring, Walter, and Kimball, *Quantum Chemistry* (John Wiley and Sons, Inc., New York, 1944), p. 256), the latter is based on the absorption spectra of aromatic hydrocarbons (compare, e.g., Förster, reference 2). For the overlap energy (which enters the equation based on the molecular orbital method) the value $\beta=20$ kcal./mole (arrow No. 3) was found from resonance energies using the same source as above.

The values of these parameters deduced by introducing the experimental value of λ_1 of the dye considered in Herzfeld and Sklar's equations are as follows: $\alpha=210$ kcal./mole; $\beta=81$ kcal./mole.

[f] In order to get satisfactory agreement with experiment it is necessary in some of these and in other cases to make allowance for the influence of neighboring substituting groups (compare reference a). In the case of dye Va, Vb, for example, due to the easily polarized benzene nuclei at both ends of the polymethine chain, the potential energy of the π-electrons increases less rapidly at the ends of the chain than when these benzene nuclei are absent. We take this into account by increasing the length L by a constant amount $(\frac{2}{3})l$ over its value given by Eq. (6) in the absence of these nuclei. We then write $L=(2j+2+\frac{2}{3})l$. More generally, $L=(2j+2+\alpha)l$ and thus,

$$\lambda_1 = 637[(2j+2+\alpha)^2/(2j+3)] \text{(angstrom)},$$

where α is a constant for each series of symmetrical polymethines, depending upon the nature of neighboring substituting groups. α turns out to be within the limits -1 and $+1$ for most series. (Cf. also reference 6, p. 1451 ff.).

Malachite green:

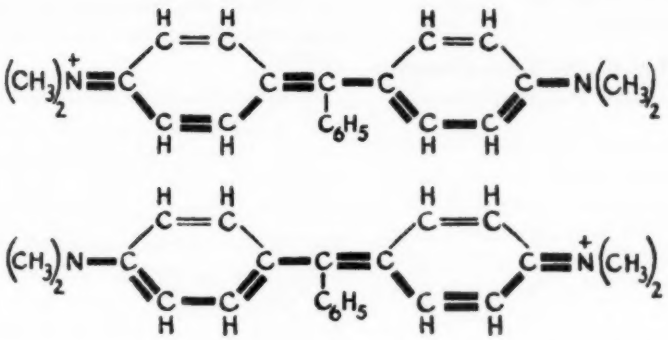

VIa

VIb

In each case, the molecule is shown as two equivalent limiting structures, labeled a and b, which are formed, one from the other, when the single and double bonds interchange. The resonating portion is indicated by heavy lines. It must be mentioned that in the cases of dyes IV and VI the resonating portion is actually extended over both sides of the benzene nuclei: there is thus a branched π-electron gas. The simplified treatment as an unbranched gas, that is by neglecting the π-electrons of the double bonds indicated by thin lines, leads in such cases to similar results as are obtained by a more refined treatment[9] based on a branched electron gas model.

We mentioned in Section 2 that a medium which contains dye molecules orientated parallel to one another should in the region of the first band absorb light whose electric vector is parallel to the axes of the molecules more strongly than light whose electric vector is perpendicular to the chain axes. This is actually the case as has been shown by Land and West.[12] These authors have prepared molecular dispersions of cyanine and other dyes in polyvinyl alcohol foils and have orientated the axes of the dye molecules by stretching the foils in a certain direction. They found that the absorption of light whose electric vector was parallel to the direction of strain was by far stronger than the absorption of light whose electric vector was perpendicular to this direction.

Observations of the *fluorescence* of polymethine dyes orientated in polyvinyl alcohol lead to conclusions similar to those deduced from the above-mentioned measurements of the dichroism of such dispersions. This has been shown by experiments on a number of dyes which were kindly supplied by Dr. J. D. Kendall (Ilford Ltd., London) and by the CIBA A. G. Basel. It has been found that a foil of cyanine dye molecules (orientated in polyvinyl alcohol as mentioned above) when illuminated with unpolarized ultraviolet light in most cases gives out a strong fluorescence. This fluorescent light is almost completely polarized in such a way that its electric vector is parallel to the direction of strain, i.e., parallel to the axes of the chains of the dye molecules.

This can be readily understood if we consider that the wavelength region of the fluorescent light is in the neighborhood of the first absorption band of the dye investigated (though shifted somewhat toward longer wave-lengths) so that it is on hand to presume that the fluorescence band is simply the reverse electronic transition corresponding to the absorption band. The fluorescence band would then be the result of a jump of an electron from level No. $([N/2]+1)$ back to level No. $N/2$. It is thus not surprising when the polarization of the fluorescence and absorption bands are the same as the experiments mentioned show.

[12] E. H. Land and C. D. West, *Alexander's Colloid Chemistry*, Reinhold, New York, 1946, Vol. VI, p. 160.

B. PORPHYRINES AND SIMILAR COMPOUNDS

In the case of the porphyrines and the phthalocyanines we find conditions similar to those in the cases so far considered. These molecules also may be shown as resonating between two equivalent limiting structures,

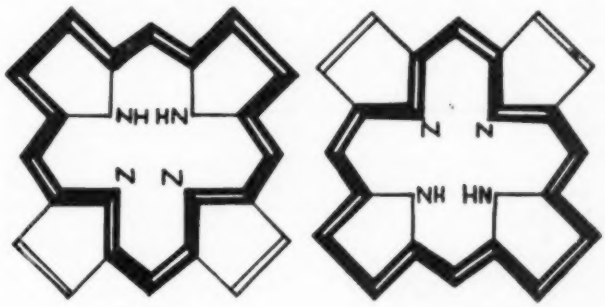

VIIa VIIb

by an interchange of the alternating single and double bonds indicated by the heavy lines. These bonds in character between single and double bonds form the closed ring system shown.

For a quantitative treatment we again make the simplifying assumption that the π-electrons can move only in the direction of the closed chain, and that the potential energy is constant along its whole length. This model leads to an explanation of the color of the blood porphyrines.[g]

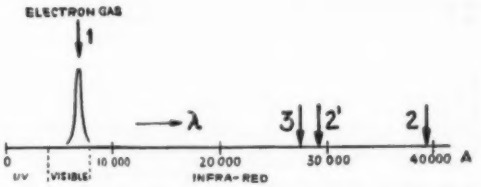

FIG. 5. Cation of the dye IIa, IIb in the case when $j-4=1$. The drawn-out curve is the experimentally found absorption curve. The arrows indicate the positions of the absorption maximum calculated on the basis of the various methods: Arrow No. 1: Electron gas model (according to Eq. (3) or (8)). Arrows No. 2 and 2': bond orbital method. Arrow No. 3: molecular orbital method.

[g] The mean position of the absorption bands of the porphyrines in the visible spectrum can be interpreted, although their complexity cannot be explained, on the basis of the simple model

C. UNSYMMETRICAL POLYMETHINE DYES, POLYENES, AND RELATED COMPOUNDS

1. More Detailed Discussion of the Free-Electron Gas Model for Symmetrical Polymethines

For the quantitative discussion of the light absorption by symmetrical polymethines, a model was set up on the assumption that the potential energy V of a π-electron is constant along the chain and rises sharply to infinity at the ends (Fig. 7(b)). In the following we will discuss how far we were justified in making this simplification.

We will lead a π-electron along the polymethine chain, e.g., along the zig-zag line indicated in Fig. 6 for the case $j=3$. Its potential energy will vary as shown in Fig. 7(a), i.e., it will alternately decrease and increase as the electron approaches and moves away from the positively charged carbon and nitrogen atoms. At the ends of the polymethine chain the potential energy rises rapidly and forms a barrier to an outward moving electron.

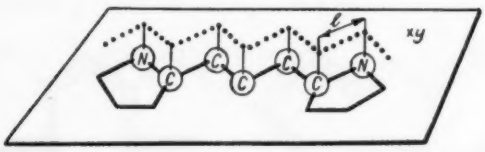

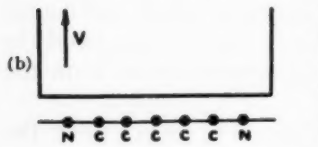

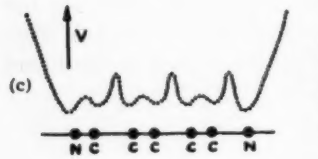

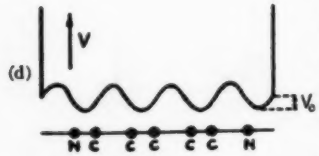

FIGS. 6 and 7a–d. Symmetrical and unsymmetrical polymethines. We follow a π-electron as it moves along the dotted line in Fig. 6, i.e., as it moves along the chain of what can be a symmetrical or unsymmetrical polymethine.

If the chain is that of a *symmetrical* polymethine, the potential energy, V, will alternatively increase and decrease along the chain as indicated in Fig. 7(a). For the quantitative treatment of the optical behavior we consider this curve replaced by the lines of Fig. 7(b) (V constant along the chain, and rising to infinity at the ends).

If the chain is that of an *unsymmetrical* polymethine (where the bond distances are alternatively longer and shorter), V will vary along the chain as shown in Fig. 7(c). In the quantitative treatment of the optical behavior we think this curve replaced by the curve indicated by the lines of Fig. 7(d). (V has a sine curve variation of amplitude V_0 along the chain, and rises sharply to infinity at the ends).

Note coincidence of the crests and troughs of the sine curve with the longer and shorter bonds, respectively.

A quantum-mechanical treatment of an electron in such a periodically varying potential[h] has been worked out by Morse.[13] He showed that here the levels group themselves into bands. Each band contains $(2j+2)$ levels. For the case considered in Fig. 8(a) $j=3$, and the number of levels in each band is 8. (Only the 8 levels of the first band and the lowest two levels of the second are shown in Fig. 8(a).) The grouping of levels into bands is characteristic of a periodically varying potential, and will not be found when the potential is constant (Fig. 8(b)).

The normal state of the π-electron gas corresponds to the arrangement in Fig. 8(a) where the first energy band is half-filled with the electrons. The first absorption band, as well as further bands, are associated with electron jumps from the highest occupied levels to the next and higher levels. In the case of the symmetrical polymethines, which we are considering, this would mean jumps between levels in the central region of the first energy band. The distances between levels situated in the region of the middle of an energy band are very nearly the same as the distances between energy levels in the case of a free-electron gas. Hence we were justified in assuming the simplified model of a free-electron gas when dealing with the light absorption of the symmetrical polymethine dyes.[i]

2. Qualitative Discussion of the Quantum-Mechanical Aspect of Unsymmetrical Polymethine Dyes

Somewhat more complicated conditions are found in the case of unsymmetrical polymethines and related

discussed. This can be done with a model which in particular takes into account the π-electrons associated with those double bonds in VIIa, VIIb not indicated heavily, and which further allows for the fact that the H atoms in the center of the ring system are actually equally shared by the four N atoms. For a detailed discussion of this see a paper to be published shortly in Helv. Chim. Acta.

[h] The potential along the chain is of course not strictly periodical, because it was not entirely correct to assume that the bonds along the resonating portion of a symmetrical polymethine have all the same double bond character (bond number 1.5) and that consequently all C—C bond distances along the chain are equal. According to a suggestion by L. Pauling (Proc. Nat. Acad. Sci. **25**, 577 (1939); H. Gilman, *Organic Chemistry* (John Wiley and Sons, Inc., New York, 1938), Chapter 22), we have to consider besides the two equivalent resonating structures with the positive charge on either of the two terminal nitrogen atoms, intermediate structures with the positive charge on some other one of the atoms of the resonating portion. The effect of these intermediate structures is to change somewhat the double bond character and consequently the bond distance of each chain bond, depending on the position of the bond in the chain. Here we shall neglect the influence of these intermediate structures on the bond distances, but it should be pointed out that they should be considered in a more precise treatment.

[13] P. M. Morse, Phys. Rev. **35**, 1310 (1930).

[i] The same applies in the case of radical-like colored compounds such as Wurster's red, Tschitschibabin hydrocarbon, quinhydrone, the colored reduction product of π,π' dipyridyl, and similar substances. Here too the levels of the first energy band are only partly filled in the normal state and the model of the free-electron gas can be considered to describe the light absorption of these compounds. Values obtained (see reference 9) by this method are indeed also in good agreement with experiment.

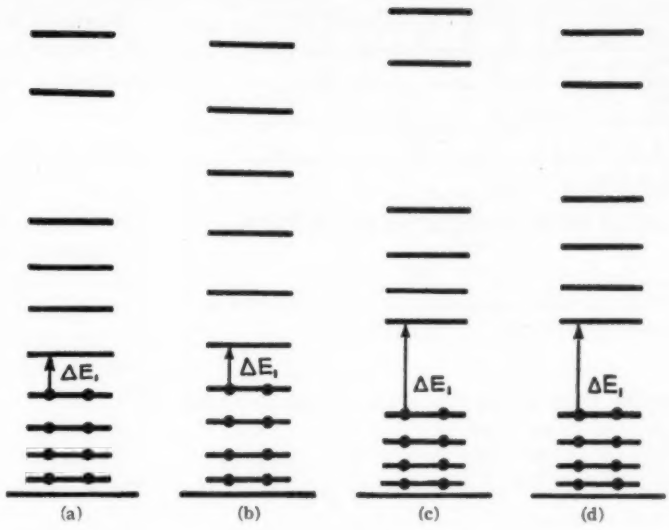

FIG. 8(a), (b), (c), (d). Energy levels of an electron in the potential fields shown in Fig. 7(a) to (d). (Fig. 8(a) corresponds to Fig. 7(a), Fig. 8(b) to Fig. 7(b), etc.). Representation is schematic with distances between higher levels shown reduced.

compounds. Let us, for example, consider the dye with the cation:

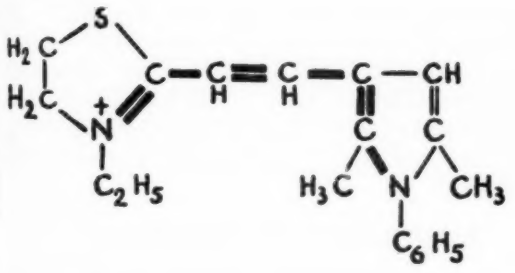

VIIIa

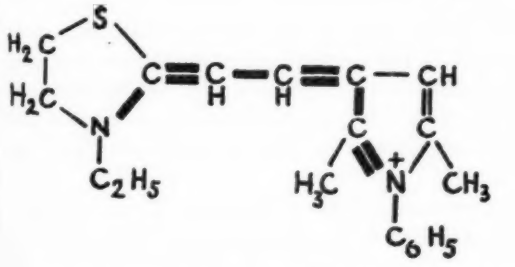

VIIIb

As was the case for the cations of symmetrical polymethines it is possible to write two limiting structures VIIIa and VIIIb which arise from a changing over of double and single bonds in the chain. Unlike the case of the symmetrical compounds, however, we now find that the two limiting structures are not equal in energy, and they will not make equal contributions to the normal state. For example VIII, Brooker[11] found that structure VIIIa contributes more than VIIIb.

In view of this we can no longer expect that as in the case of symmetrical polymethines the chain should consist of like C—C bonds of bond number 1.5. What we find are alternating somewhat longer and somewhat shorter bonds with predominating single and double bond character, respectively. The longer and shorter bonds are there where the single and double bonds are written in the structure which contributes more to the normal state.

We shall see that this alternation of longer and shorter C to C distances brings about a disturbance in the behavior of the π-electron gas along the chain. If we lead a π-electron along the chain in the manner discussed in Section 1 in connection with Fig. 6, we will find that for the unsymmetrical polymethine the potential energy varies not as in Fig. 7(a) but as in Fig. 7(c), i.e., the periodic variation is complete only after passing two carbon atoms as against one when the polymethine is symmetrical.

This difference in length of the period of the potential along the chain, distinguishing the cases of a symmetrical and an unsymmetrical polymethine, causes each of the energy bands found for the symmetrical compound to divide into two separate energy bands for the corresponding unsymmetrical compound. (See Fig. 8(c)).

In the normal state of the unsymmetrical polymethine the first energy band formed, as above, is now completely filled with the available π-electrons, and all the other bands are empty, as illustrated by Fig. 8(c). The first absorption band results, as always, when an electron jumps from the highest occupied to the next free level, i.e., in this case from the highest level of the first energy band to the lowest level of the second energy band. This distance, however, is larger than the distance between the corresponding levels in the case of a free-electron gas (Fig. 8(b)). Hence, we are no longer able to use the free-electron gas as the basis of our approximation.

3. Quantitative Treatment

As seen above, the π-electrons are actually in a potential field whose periodicity is as shown by Fig. 7(c). It is permissible, however, as an approximation, to assume a one-dimensional potential field which has a sine wave variation along the chain, as indicated in Fig. 7(d). The maxima of this sine curve correspond to the middles of the longer C—C bonds; the minima, to the middles of

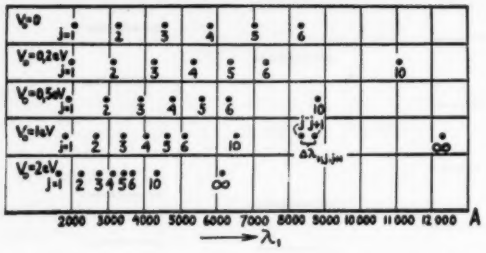

FIG. 9. Dependence of λ_1 on V_0 for various values of j, according to Eq. (11). Note that the increment $\Delta\lambda_{1;j,j+1}$ decreases the more rapidly with increasing values of j, the larger V_0 is.

the shorter. At both ends of the chain the potential energy is assumed to rise to infinity as in the case of the free-electron gas model (Fig. 7(b)). The small effect that this approximation has on the position of the energy levels is shown schematically for the two cases Fig. 7(c) and Fig. 7(d) in Figs. 8(c) and 8(d), respectively. Using the procedure of Morse[13] we obtain, in good approximation,

$$\Delta E_1=\frac{h^2}{8mL^2}(N+1)+V_0\left(1-\frac{1}{N}\right), \tag{9}$$

where ΔE_1 is the energy difference between the highest energy level of the first energy band and the lowest level of the second energy band. L is (as before) the length of the polymethine chain measured along the zig-zag line of the chain links, N is the number of π-electrons, V_0 is the amplitude of the sine curve used to approximate the variations of the potential energy. V_0 is a measure of the asymmetry of the dye, i.e., of the relative contributions of the two limiting structures. If we put V_0 equal to zero corresponding to the case of a symmetrical polymethine, we find, as would be expected, that Eq. (9) reduces to Eq. (2).

If we substitute (9) in (1) we obtain for the wavelength of the first absorption band[9]

$$\lambda_1=\frac{1}{(V_0/hc)(1-1/N)+(h/8mc)([N+1]/L^2)}. \tag{10}$$

Further, if we substitute for L and N from (6) and (7), respectively, and introduce the values of the constants h, c, and m, Eq. (10) transforms to

$$\lambda_1=\frac{1.23\times10^4}{19.3[(2j+3)/(2j+2)^2]+V_0[1-1/(2j+2)]}, \tag{11}$$

where λ_1 is in angstrom units, V_0 is in electron volts.

Figure 9 illustrates the dependence according to Eq. (11) of λ_1 on j for various values of V_0. In the case of dyes typified by the *symmetrical* polymethines ($V_0=0$), we see that the first absorption band is displaced toward higher wave-lengths by a certain amount $\Delta\lambda_{1;j,j+1}$ as we move up step by step (increasing j) in a particular series. $\Delta\lambda_{1;j,j+1}$ can in practice be considered constant for these series. In the case of dyes typified by the *unsymmetrical* polymethines, the amount $\Delta\lambda_{1;j,j+1}$ *decreases* as we move up a homologous series, i.e., increase j. The larger V_0 (i.e., the larger the contribution of the one limiting structure relative to the other), the more marked is the rate with which $\Delta\lambda_{1;j,j+1}$ decreases.

The first absorption band of a dye typified by the unsymmetrical polymethines will thus *always be found at a shorter wave-length* than the band of the corresponding symmetrical compound of the same length of chain. The displacement toward shorter wave-lengths will be the bigger the more the one limiting structure outweighs the other.

4. Comparison with Experiment

The expected displacement toward shorter wavelengths in going from a dye of the symmetrical polymethine type to the corresponding unsymmetrical compound has already been observed by Schwarzenbach[14] and Brooker[11] for a large number of examples. We shall limit ourselves to a discussion of a few selected cases.

Unsymmetrical Cyanines, Oxanoles, Merocyanines, and Anhydro Bases of Symmetrical Cyanines

As a first example let us again consider the unsymmetrical cyanine VIIIa and VIIIb. This can be regarded as a hybrid of the two dyes

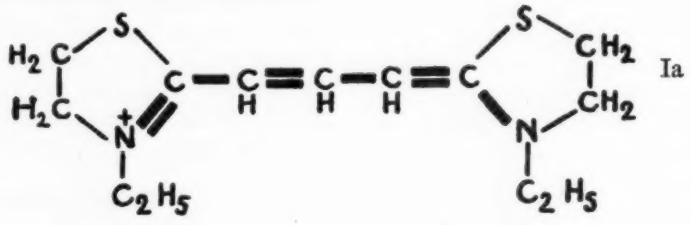

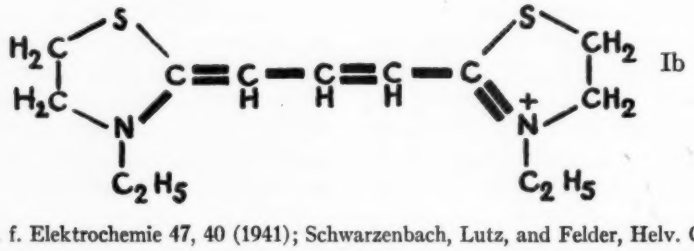

[14] G. Schwarzenbach, Zeits. f. Elektrochemie 47, 40 (1941); Schwarzenbach, Lutz, and Felder, Helv. Chim. Acta 27, 576 (1944).

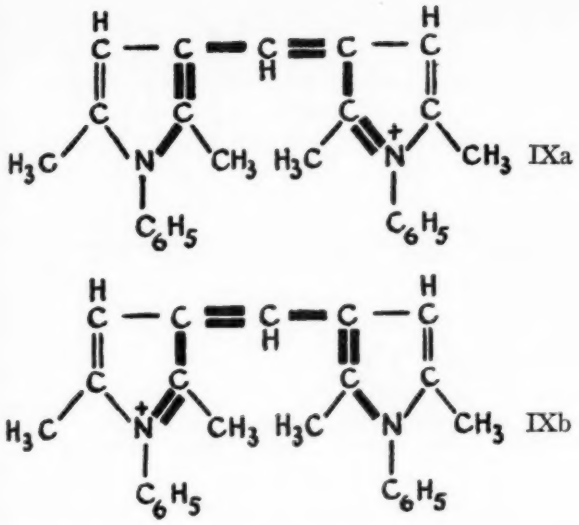

IXa

IXb

For the two symmetrical dyes ($V_0=0$) we obtain from Eqs. (8) or (11) a theoretical result, $\lambda_{1,\,theor}=4530$A. In good agreement with this we have, according to Brooker[11] the experimental value $\lambda_{1,\,exp}=4450$A for the dye Ia, Ib; and $\lambda_{1,\,exp}=4490$A for the dye IXa, IXb. For the unsymmetrical dye VIIIa, VIIIb, on the other hand, we find[11] $\lambda_{1,\,exp}=4170$A, which as expected constitutes a considerable displacement toward shorter wave-lengths. To assess quantitatively the asymmetry of our dye VIIIa, VIIIb we introduce the experimentally found wave-length λ_1 into Eq. (11) and thus find that the amplitude $V_0=0.26$ ev.

As a further example, we consider the dye

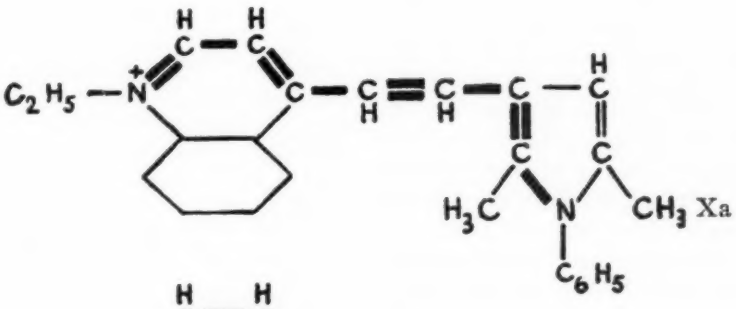

Xa

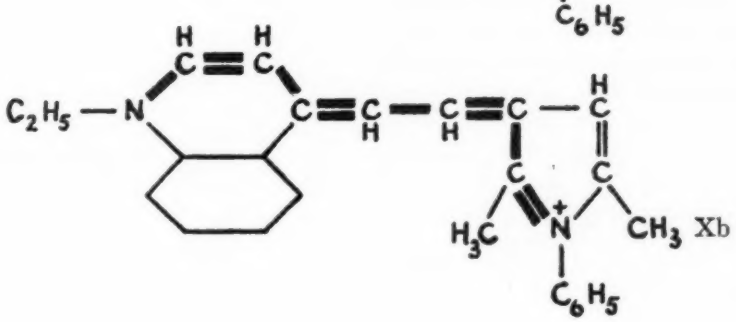

Xb

which is the hybrid of the dyes

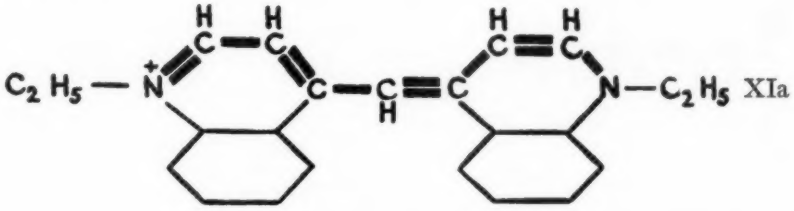

XIa

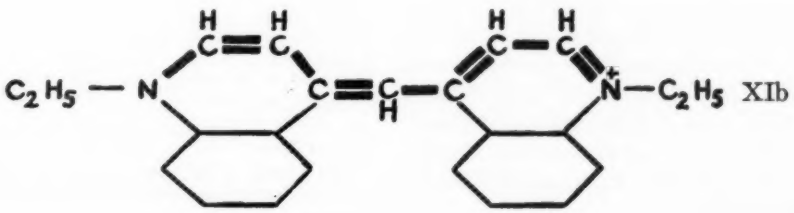

XIb

and

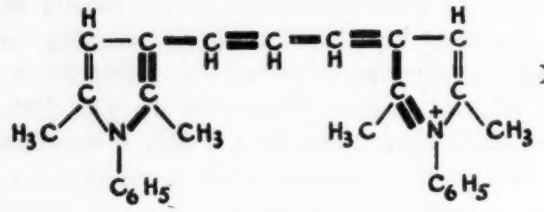

XIIa

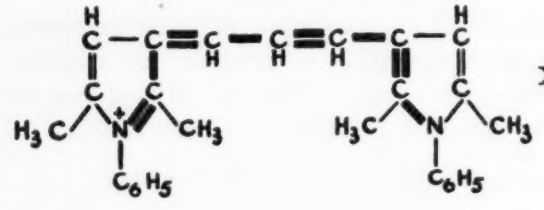

XIIb

For the two symmetrical dyes we obtain from Eq. (8) the value $\lambda_{1,\,theor}=5790$A. This is in satisfactory agreement with the experimental results $\lambda_{1,\,exp}=5910$A (dye XIa, XIb), and $\lambda_{1,\,exp}=5750$A (dye XIIa, XIIb). For the unsymmetrical cyanine Xa, Xb the largely differing value $\lambda_{1,\,exp}=5020$A is found.[11] Using this result to determine V_0 from Eq. (11), we find $V_0=0.37$ ev, i.e., a value larger than that for the dye VIIIa, VIIIb considered above. From this follows, as has already been found by Brooker,[11] that in the normal state Xa outweighs Xb by more than VIIIa outweighs VIIIb.

Similar relationships were found by Brooker[11] to exist for a large number of further cyanines and merocyanines. Of particular interest is the behavior of the merocyanines of the general structure XIIIa, XIIIb:

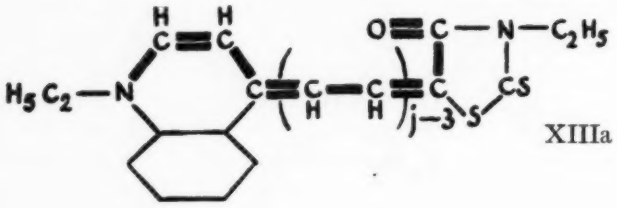

XIIIa

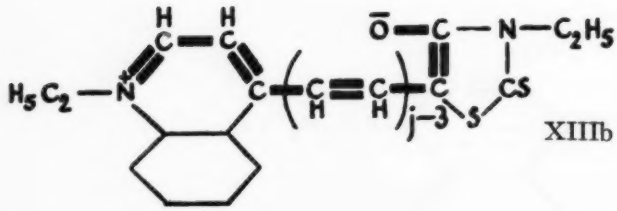

XIIIb

In these compounds it is found that the maximum of the absorption band occurs there in the spectrum, where it would be expected on the assumption of a symmetrical structure, and is thus not displaced to shorter wavelengths as in the other cases. This shows[11] that the two limiting structures XIIIa and XIIIb take equal shares and that the polymethine chain as in the case of symmetrical cyanines is made up of like C—C bonds of bond number 1.5 (see reference *h*).

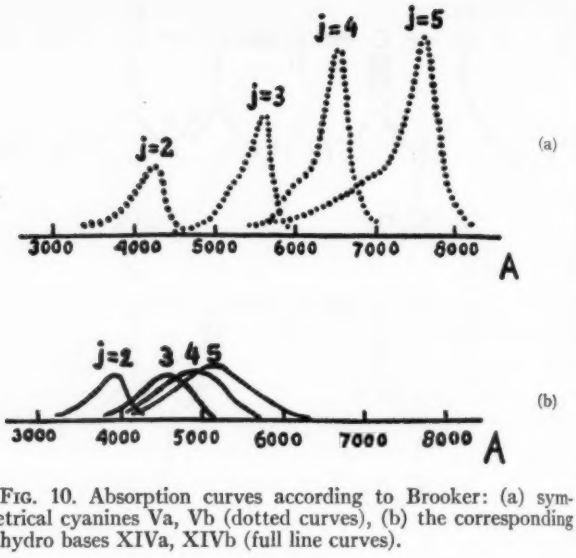

FIG. 10. Absorption curves according to Brooker: (a) symmetrical cyanines Va, Vb (dotted curves), (b) the corresponding anhydro bases XIVa, XIVb (full line curves).

Free Cyanine Bases

It is interesting to compare the exceptional case of the merocyanines XIIIa and XIIIb with the case of the anhydro bases of the symmetrical cyanines; for example, the compounds of general structure XIVa, XIVb:

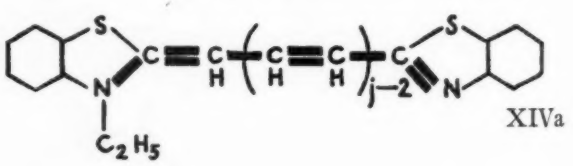

XIVa

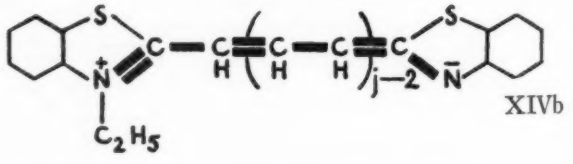

XIVb

The limiting structure XIVa (corresponding to XIIIa) clearly contributes much more to the normal state than the dipolar structure XIVb (corresponding to XIIIb).[i] We thus expect a very pronounced decrease in the dis-

TABLE I.

Polyene	j'	λ_1(A) exper.	λ_1(A) calculated from Eq. (14) for $V_0=2.00$ ev
Butadiene	2	2170	2330
Hexatriene	3	2600	2820
Octatetraene	4	3020	3200
Axerophtene	5	3460	3500
Anhydro Vitamin A	6	3690	3750
β-Carotene	11	4510	4510
Dehydro-β-Carotene	12	4750	4610
Dehydrolycopene	15	5040	4860

[i] In changing over from structure XIVa to structure XIVb energy must be expended in the separation of the opposing electric charges.

placement $\Delta\lambda_{1;j,j+1}$ as the polymethine chain grows longer, i.e., as we increase j.

The experimentally determined[11] absorption peaks of the bases XIVa, XIVb are shown for the case when $j=2$, 3, 4, and 5 in Fig. 10(b). For the sake of comparison peaks (taken from Brooker[11]) of the corresponding symmetrical cyanines Va, Vb are shown in Fig. 10(a). The relative position of the maxima of these curves are as expected. By introducing the observed λ_1-values of the maxima of the absorption curves of the anhydro bases in Eq. (10), we obtain approximately 1 ev for the amplitude V_0 of the potential energy along the chain.[k]

Polyenes

Still more marked than in the case of the anhydro bases of the symmetrical cyanines, is the predominance of the reference structure XVa

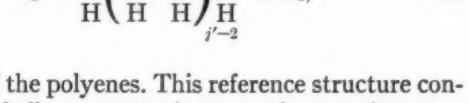

XVa

in the case of the polyenes. This reference structure contributes decidedly more to the normal state than any limiting structure that arises from an interchange of single and double bonds such as, e.g.,

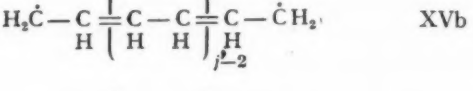

XVb

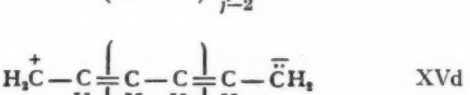

XVc

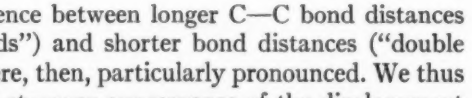

XVd

The difference between longer C—C bond distances ("single bonds") and shorter bond distances ("double bonds") is here, then, particularly pronounced. We thus expect a still stronger convergence of the displacement $\Delta\lambda_{1;j',j'+1}$ with increasing j' than in the case of the anhydro bases of the cyanines.

In Table I, column 3, we have collected[l] the experimentally determined maxima[m] of the first absorption bands of a number of polyenes with j'-values from 2 to 15. (j' is the number of conjugated double bonds). These results show the expected relationship. They deviate more than any of the other examples dealt with in this section from the results that would be expected on the basis of a free-electron gas model. In the case of dehydrolycopene ($j'=15$), for example, calculating λ_1 from Eq. (3) which assumes a free π-electron gas we obtain 20300A, while the experimental result, $\lambda_1=5040$A, is four times smaller. To consider the π-electron gas of a polyene as a free-electron gas for a quantitative treatment as has recently been attempted by Bayliss[8] would thus not seem permissible.

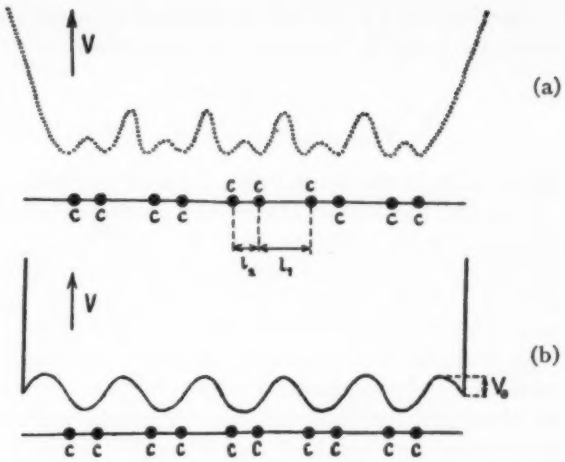

FIG. 11. Potential energy fields of the polyenes. The potential energy of a π-electron as it moves along the zig-zag chain of the polyene is shown in (a). For the quantitative treatment, the curve (a) is considered replaced by the sine curve (b) of the same periodicity.

As in the preceding cases we consider the π-electrons placed in a one-dimensional potential field with a sine wave variation. If we designate the C—C bond distance of the "single bond" with l_1, and the "double bond" distance with l_2, we find, according to Fig. 11, the following expression for L.[n]

$$L=(j'+\tfrac{1}{2})(l_1+l_2). \tag{12}$$

From measurements by Schomaker and Pauling[15] on butadiene, it follows that $l_1=1.46\times10^{-8}$ cm, $l_2=1.35\times10^{-8}$ cm. Further, we have for the number of π-electrons,

$$N=2j'. \tag{13}$$

[k] In the quantitative treatment we have taken into account the disturbing effect of the two benzene nuclei situated at the end of the polymethine chain, as had to be done in the case of the corresponding symmetrical cyanine Va, Vb (cf., reference f).

[l] The results are for solutions in hexane. They are taken from the following: J. R. Platt and H. B. Klevens, Rev. Mod. Phys. **16**, 182 (1944); P. Karrer and E. Jucker, *Carotinoide* (Verlag. Birkhäuser, Basel, 1948). The result for Axerophten (the hydrocarbon of fundamental importance in Vitamin A) is taken from P. Karrer and J. Benz, Helv. Chim. Acta. **31**, 1048 (1948), and is for a solution in ethanol. The result for anhydro-Vitamin A was very kindly communicated to me by Dr. M. Kofler of Firma Hoffman LaRoche Basel.

[m] The first absorption band of the polyenes possesses as a rule three neighboring peaks. These, however, have to be attributed to the same electron jump. The result given for λ_1 in such a case refers to the centroid of the total band. In the instances of the polyenes, here investigated, the wave-length of this centroid coincides with the wave-length of the center one of the three peaks.

[n] As previously discussed the points where the potential can be assumed to be infinite are taken one bond distance to either side of the terminal C-atoms of the conjugated chain system.

[15] V. Schomaker and L. Pauling, J. Am. Chem. Soc. **61**, 1769 (1939).

Substituting (12) and (13) in (10) and using the above values for l_1 and l_2, we obtain the expression

$$\lambda_1=\frac{1.23\times10^4}{18.8(2j'+1)^{-1}+V_0(1-(2j')^{-1})}, \qquad (14)$$

where λ_1, is in angstrom units, V_0 is in electron volts.

If we put V_0 equal to 2.00 ev, i.e., a value double that proposed for the anhydro bases XIVa, XIVb, we can calculate λ_1 for various values of j'. The results are given in Table I, column 4, and are in satisfactory agreement with the experimental values.

All the same, we can see from the manner in which the calculated and experimental values compare, that V_0 is not absolutely constant, but that it decreases slightly as we increase the length of the chain, i.e., increase j'.[o] This tends to show that in the case of a polyene containing a large number of conjugated double bonds, the C—C "double bonds" are less double bond in character, and the "single bonds" correspondingly more double bond in character than those of, say, butadiene. We thus agree with Lennard-Jones,[16] Pauling and Sherman,[17] Coulson,[18] Penney,[19] and Mulliken,[20] who also point out that the character of the two kinds of bonds in polyenes becomes more and more alike as the number of conjugated double bonds is increased.

The particular case of the light absorption of the polyenes has been subject to a number of theoretical considerations by various authors. The best results are those of W. Kuhn.[21] His model replaces the polyene chain by a series of coupled linear oscillators. Each oscillator corresponds to a double bond of the conjugated system. For the wave-length λ_1 of the first absorption maximum he finds the expression:

$$\lambda_1=\frac{a}{[1-b\cos(\pi/[j'+1])]^{\frac{1}{2}}}, \qquad (15)$$

where a and b are constants. The values of the two parameters a and b have to be found from the positions of the absorption maxima of *two* representatives of the polyene series. Let us, according to W. Kuhn, put $a=1.57\times10^3$A, $b=0.922$. We obtain from Eq. (15) results for λ_1, which agree with the experimentally observed values about as well as those obtained from Eq. (14) when the *single* experimentally to be determined parameter, V_0, is made equal to 2.00 ev.

The model used by W. Kuhn is in part the same as the one used by Lewis and Calvin[22] whose quantitative treatment, however, was based on assumptions which do not seem justified. Other authors have used the bond orbital and the molecular orbital methods.[23] These have led to quite satisfactory expressions for the intensity of the absorption band of the polyenes, but the results for the positions of these bands do not agree with experiment.

5. The Classical Color Theory of Witt on the Basis of the Electron Gas Model

According to the theory of Witt[24] as extended by Dilthey and Wizinger,[25] a dye molecule will, in general, have these three parts:

1. A system containing aromatic nuclei, or a chain of conjugated double bonds: the *chromophor*.

2. An electron-donating group like CH_3—, HO—, H_2N—, CH_3O—, R_2N—; the *auxochrom*.

3. An electron-accepting group like —CN, —NO, —NO_2: the *antiauxochrom*.

As typical examples we will consider the following stilbene derivatives:

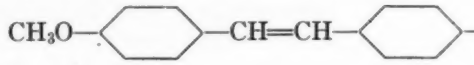

(colorless), XVI

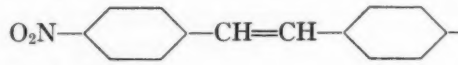

(pale yellow), XVII

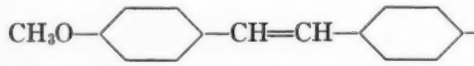

(yellow), XVIII

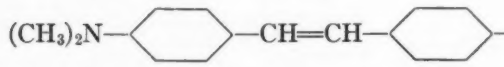

(red). XIX

[o] If in each case we calculate V_0 from Eq. (14) using the observed value of λ_1, we obtain $V_0=2.55$ ev, 2.26 ev, 2.06 ev, 1.92 ev, 1.89 ev for $j=2$, 4, 6, 12, 15, respectively.

[16] J. E. Lennard-Jones, Proc. Roy. Soc. London (A) **158**, 280 (1937).
[17] L. Pauling and J. Sherman, J. Chem. Phys. **1**, 679 (1933).
[18] C. A. Coulson, Proc. Roy. Soc. London (A) **169**, 413 (1939); J. Chem. Phys. **7**, 1069 (1939).
[19] W. S. Penney, Proc. Roy. Soc. London (A) **158**, 306 (1937).
[20] R. S. Mulliken, J. Chem. Phys. **7**, 364, 570 (1939).
[21] W. Kuhn, Helv. Chim. Acta **31**, 1780 (1948).
[22] G. N. Lewis and M. Calvin, Chem. Rev. **25**, 237 (1939); G. E. K. Branch and M. Calvin, *The Theory of Organic Chemistry* (Prentice-Hall, Inc., New York, 1941), p. 165.
[23] E. Hückel, Zeits. f. Physik **70**, 204 (1931); **76**, 628 (1932); Zeits. f. Elektrochemie **43**, 752 (1937); R. S. Mulliken, J. Chem. Phys. **7**, 364, 570 (1939); Rev. Mod. Phys. **14**, 265 (1942); Th. Förster, Zeits. f. physik. Chemie (B) **47**, 245 (1940).
[24] O. N. Witt, Ber. d. D. chem. Ges. **9**, 522 (1876); **21**, 321 (1888).
[25] W. Dilthey and R. Wizinger, J. prakt. Chem. (2) **118**, 321 (1928); R. Wizinger, J. prakt. Chem. **157**, 1940 (1941).

The first two compounds, of which the first has no antiauxochrom, and the second no auxochrom, are colorless and pale yellow, respectively. Only the other two compounds, which possess all three of the above parts, have strong yellow and red color, respectively.[25]

These things can be explained on the basis of the electron gas model in the following manner.[p]

In the case of the colorless compound XVI we have a polyene-like system because here too the reference structure XVIa

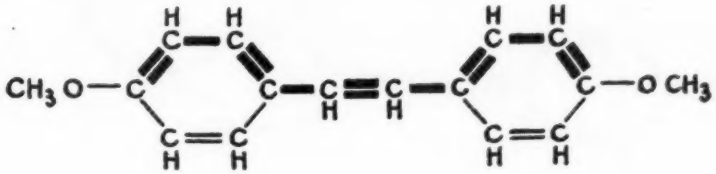

XVIa

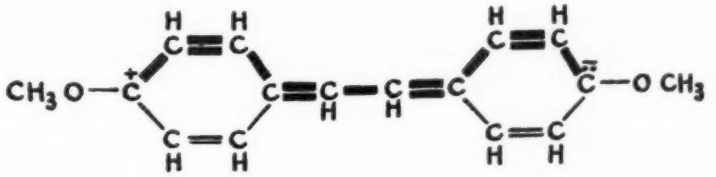

XVIb

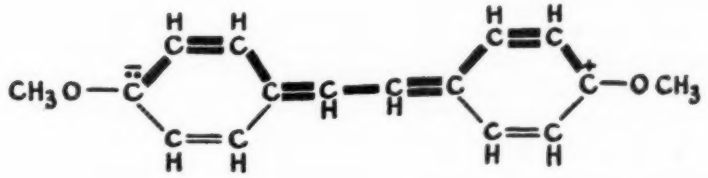

XVIc

contributes more to the normal state than such limiting structures as XVIb, XVIc formed by a changing over of double and single bonds. The first absorption band of this compound will then be expected approximately, where that of the corresponding polyene with five conjugated double bonds is to be found, i.e., at about 3500A in the ultraviolet. Hence, it is understandable that this compound should be colorless.

Also in the case of the pale yellow compound XVII do we have a polyene-like system. Here, however, we have a chain of seven conjugated double bonds.

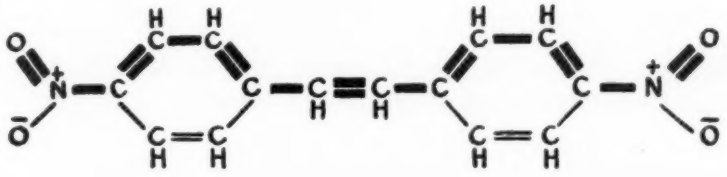

XVIIa

From Table I we can see that the first absorption band is to be expected near 3900A, i.e., just within the visible part of the spectrum and the pale yellow color is explained.

In case of the colored compound XVIII the reference structure XVIIIa is of comparable importance to the dipolar structure XVIIIb which arises from the reference structure by the double and single bonds in the chain changing over. The stability of the limiting structure XVIIIb arises from the fact that the electron donating methoxyl group (the auxochrom) is positively charged, while the electron-accepting nitro group (the antiauxochrom) is negatively charged. This condition is similar to that of the merocyanines XIIIa, XIIIb, and the other polymethine dyes. Thus, the presence of both auxochrom and antiauxochrom changes the otherwise polyene-like chromophor system into a cyanine-like system. This brings about a shift of the absorption band to longer wave-lengths as has already been discussed. The observed strong color of the compound XVIII is thus very understandable.

[p] The fact that dye molecules can as a rule be represented as resonating between two or more valency structures of comparable importance has already been recognized by B. Eistert and F. Arndt [see B. Eistert, Angew. Chem. **49**, 33 (1936), Ber. d. D. Chem. Ges. **69**, 2395 (1936), Tautomerie und Mesomerie (Enke, Stuttgart, 1938)] and independently by C. R. Bury, J. Am. Chem. Soc. **57**, 2115 (1935). An investigation of the empirical connection between resonance and color is in particular due to G. Schwarzenbach (reference 14). For qualitative theories of the cause of light absorption by dyes, see Pauling (reference h), Lewis and Calvin (reference 22).

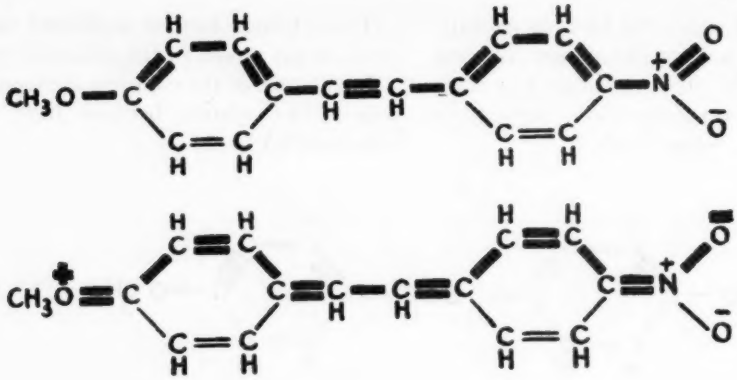

XVIIIa

XVIIIb

The maximum shift that an auxochrom-antiauxochrom combination can cause would be achieved when the dipolar structure and the reference structure contribute each just 50 percent to the normal state.

This can be brought about by a suitable combination of the electron-donating property of the auxochrom and the electron-accepting tendency of the antiauxochrom, and is just realized in the case of the merocyanines XIIIa, XIIIb. In the case of the stilbene dye XVIII, however, the reference structure XVIIIa is markedly more predominant than the dipolar structure XVIIIb, as the absorption band is still found at far shorter wavelengths than would be expected on the basis of the free-electron gas model.

In the compound XIX the dipolar structure contributes relatively more than that of the dye XVIII just discussed. The dye XIX arises from XVIII when the auxochrom —OCH_3 is replaced by the stronger electron donator —NH_2, which thus enhances the importance of the dipolar structure. It would then be expected that the absorption band of XIX will lie at longer wave-lengths than that of XVIII. This is also the case, as is shown by their red and yellow colors, respectively.

We have seen that a one-dimensional electron gas model leads to a quantitative explanation of the color of simple dye molecules. The success of the model in giving qualitative information about complex cases allows us to hope that a more general theory will be established on this basis which very likely would also be able to explain the color of inorganic complexes such as Prussian blue and molybdenum blue.

Acknowledgments: The author is grateful to Alexander Silberberg for his help in the preparation of the manuscript, to Professor Werner Kuhn for his interest in this work, and to the Ciba-Stiftung and Jacques-Brodbeck-Sandreuter-Stiftung for a grant.

THE JOURNAL OF CHEMICAL PHYSICS VOLUME 17, NUMBER 12 DECEMBER, 1949

The Kinetics of Heterogeneous Atom and Radical Reactions. I. The Recombination of Hydrogen Atoms on Surfaces

K. E. SHULER* AND K. J. LAIDLER
Department of Chemistry, The Catholic University of America, Washington, D. C.
(Received February 28, 1949)

The data on the kinetics of the recombination of hydrogen atoms on various types of surfaces are analyzed in the light of the theory of absolute reaction rates. Expressions are derived for the recombination coefficient and the first-order rate constant, enabling these quantities to be calculated on the basis of postulated mechanisms. It is shown that the experimental activation energies are consistent with estimates using either Hirschfelder's rule or an expression utilizing the experimental "desorption temperature." For the reaction on dry oxides and dry glass good agreement is found assuming that reaction occurs between a gas-phase hydrogen atom and an adsorbed hydrogen atom, the adsorption being of the van der Waals type at low temperatures and chemisorption at higher ones. The mechanism of surface poisoning by water vapor is shown to be not due to the necessity for desorbing the water molecule: in the high temperature region it is due to an increase in activation energy, the mechanism being S−OH+H→S−O+H_2; in the low temperature region to a decrease in the number of active centers, the reaction being between a gaseous atom and a van der Waals adsorbed hydrogen atom above the water layer.

INTRODUCTION

THERE have now accumulated sufficient data on heterogeneous atomic and free radical recombinations to permit an analysis of the kinetics and a discussion of possible reaction mechanisms. The work up to 1941 has been reviewed by L. von Müffling,[1] and an important investigation since then has been carried

* Present address: Applied Physics Laboratory, The Johns Hopkins University, Silver Spring, Maryland.

[1] L. von Müffling, in G. M. Schwab's *Handbuch der Katalyse* (Verlag Julius Springer, Berlin, 1943), Vol. VI, p. 94.

out by W. V. Smith.[2] Most of the data are on hydrogen atom recombination, and this work will be considered in the present paper; many of the conclusions arrived at are, however, applicable to recombinations of other types of atoms and radicals.

KINETIC MECHANISMS

All atom and radical recombinations on surfaces, whether poisoned or not, have been found to be of the first order over a wide range of temperatures, and it is necessary to consider what mechanisms will account for this. One that might be postulated is surface adsorption of the atoms (a first-order process), followed by migration and recombination on the wall; this is, however, excluded by M. C. Johnson's observation[3] that hydrogen atoms may be packed tightly on a glass surface without recombination. An alternative mechanism, and by far the most probable one, is reaction between a surface-adsorbed atom and a gaseous atom. The observed first-order kinetics then require the fraction of surface covered by atoms to be independent of the atomic concentration in the gas phase, i.e., the surface must be fully covered. That this condition actually obtains in atomic adsorption has been shown directly by I. Langmuir.[4] In a theoretical discussion of surface processes one of us[5] has developed the kinetic laws applicable to both of the above mechanisms, and has shown on the basis of energy considerations why the second will almost invariably occur to the exclusion of the first.

THE RECOMBINATION COEFFICIENT

The fact that the order is the first implies that each gaseous atom arriving at the surface and reacting with an adsorbed atom has a certain constant reaction probability, which is independent of the pressure. One can therefore define a recombination coefficient γ, equal to the ratio of atoms striking the surface and reacting to the total number striking the surface; this coefficient is equivalent to the *Haftungskoefficient* defined by F. A. Paneth and K. F. Herzfeld.[6] The relationship between γ and the first-order rate constant k is readily obtained for a static system as follows. Consider a system of volume V cc containing n atoms reacting at a surface of S sq. cm. By the definition of k the number reacting per second is given by

$$-dn/dt = kn \text{ atom sec.}^{-1}, \tag{1}$$

while the number of atoms striking a surface of S cm² per second is given according to kinetic theory by

$$Z = (n\bar{v}/V4)S, \tag{2}$$

[2] W. V. Smith, J. Chem. Phys. **11**, 110 (1943); thesis, Harvard University (1941).
[3] M. C. Johnson, Trans. Faraday Soc. **28**, 162 (1932).
[4] I. Langmuir, J. Chem. Soc. 511 (1940).
[5] K. J. Laidler, J. Phys. Chem. **53**, 712 (1949).
[6] F. A. Paneth and K. F. Herzfeld, Zeits. f. Elektrochemie **37**, 577 (1931).

TABLE I. Experimental and estimated activation energies for atom recombinations.

Atom	Surface	T_d (°K)	$-\Delta H_{ads.}$ (kcal.)	Activation energy (kcal.) Experimental	Eq. (14)	Eq. (16)
H	Clean glass	500[a]	10–11[b]	0.9[e]	1	0.6
H	Metals	1500[d]	50–60[b]	2.5–3[e]	3	2.5–3.3
N	Nickel	1200–1350[f]	55[f]	2.5–3[f]	2.4–2.7	3

[a] M. C. Johnson, Trans. Faraday Soc. **28**, 162 (1932).
[b] See reference 1.
[c] A. L. Robinson and I. Amdur, J. Am. Chem. Soc. **55**, 2615 (1933).
[d] See reference 4.
[e] O. I. Leipunsky, Acta physicochimica, U.R.S.S. **5**, 271 (1936).
[f] N. Buben and A. Schechter, Acta physicochimica, U.R.S.S. **10**, 371 (1939).

where $\bar{v}$ is the mean atomic velocity. The recombination coefficient is the ratio of these quantities, i.e.,

$$\gamma = (4kV/\bar{v}S). \tag{3}$$

Usually the experiment is carried out in a cylindrical tube, so that $V = \pi r^2 L$ and $S = 2\pi rL$ where r is the radius and L is the length; in this case*

$$\gamma = (2kr)/\bar{v}. \tag{4}$$

This equation is identical with that derived by Paneth and Herzfeld[6] for the case of a flow experiment involving an inert transport gas. It will be shown in the Appendix that this equation is also valid for a flow system where the transport of the atoms in a reaction tube is by diffusion alone. The experimental data quoted in this paper pertain to a system of this nature.

Expressions for k and γ will now be obtained using the theory of absolute reaction rates,[7] and will be applied to the data in subsequent sections. The rate of a first-order surface reaction has been shown[8] to be

$$v_1 = C_g C_s (kT/h)(f^{\#}/F_g f_s) e^{-E/RT}, \tag{5}$$

where C_g is the concentration of gaseous atoms, C_s the number per sq. cm of surface species with which reaction occurs, k is the Boltzmann constant, h is Planck's constant, $f^{\#}$ the partition function for the activated complex, f_s the partition function of the surface reactant and F_g that per unit volume of the reacting gas; E is the energy of activation of the process. This rate is related to the rate constants k and k' by $v_1 = kC_gV/S = k'C_g$, whence

$$k' = C_s (kT/h)(f^{\#}/F_g f_s) e^{-E/RT}. \tag{6}$$

With the usual assumption that $f^{\#}/f_s = 1$ for an immobile layer, and evaluating the partition function F_g

* It may be noted that the appearance of r in this equation is due to the fact that k as ordinarily defined for a surface reaction (see Eq. (1)) is not a true constant but is inversely proportional to r; the true heterogeneous first-order rate constant is $k' = kV/S$; γ on the other hand is a true constant.

[7] H. Eyring, J. Chem. Phys. **3**, 107 (1935); see Glasstone, Laidler, and Eyring, *The Theory of Rate Processes* (McGraw-Hill Book Company, Inc., New York, 1941).
[8] Laidler, Glasstone, and Eyring, J. Chem. Phys. **8**, 659, 667 (1940).

for the gaseous atoms of mass m, Eq. (6) becomes

$$k'=C_s\frac{h^2}{(2\pi m)^{\frac{1}{2}}(kT)^{\frac{1}{2}}b_g}e^{-E/RT}, \tag{7}$$

where b_g represents the rotational and vibrational factors in the partition function of the gaseous reactants (unity in the case of atoms).

The recombination coefficient γ has been evaluated by Laidler[5] using absolute rate theory, making use of the fact that the number of collisions on a surface is equivalent to the rate of adsorption to give a mobile layer when there is no activation energy for adsorption, namely,

$$\gamma=\frac{v_1\text{ (immobile)}}{v_1\text{ (mobile)}} \tag{8}$$

$$\gamma=\frac{C_gC_s(kT/h)(f^{\ddagger}/F_gf_s)\exp(-E/RT)}{C_g(kT/h)(F^{\ddagger}/F_g)}, \tag{9}$$

where $F^{\ddagger}$ is the partition function for the activated complex in the mobile layer. Evaluation of the partition functions gives

$$\gamma=\frac{C_sh^2}{2\pi mkTb_g}e^{-E/RT}. \tag{10}$$

Expressions (7) and (10) for k' and γ may be seen to be consistent with Eq. (4) when it is noted that $\bar{v}=(8kT/\pi m)^{\frac{1}{2}}$.

THE ENERGY OF ACTIVATION

Equations (7) and (10) permit an absolute calculation of the first-order rate constant and the recombination coefficient provided that C_s and E are known. An approximate estimate of C_s can usually be obtained, but the energy of activation presents a little more difficulty. Two useful procedures are available. According to Hirschfelder[9] the activation energy of an exothermic process $A+BC\rightarrow AB+C$ is given to a rough approximation by

$$E=0.055D_{BC}, \tag{11}$$

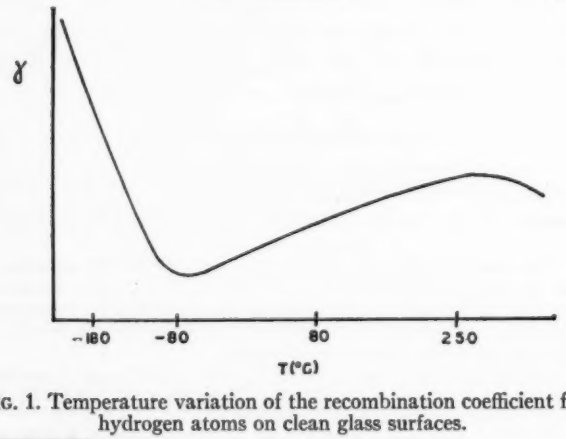

FIG. 1. Temperature variation of the recombination coefficient for hydrogen atoms on clean glass surfaces.

[9] J. O. Hirschfelder, J. Chem. Phys. **9**, 645 (1941).

where D_{BC} is the energy of dissociation of BC; if the reaction is endothermic the energy of activation is

$$E=0.055D_{AB}+\Delta H, \tag{12}$$

where $-\Delta H$ is the heat of reaction. This semi-empirical equation can be applied to a heterogeneous atom recombination proceeding by the mechanism

$$SA+A\rightarrow S+A_2,$$

where S is the surface and A the atom; these processes are generally exothermic so that the activation energy is

$$E=0.055D_{SA}. \tag{13}$$

D_{SA} is equal to the heat of adsorption $-\Delta H_{\text{ads.}}$ of the atom on the surface, so that

$$E=-0.055\Delta H_{\text{ads.}}; \tag{14}$$

the activation energy for the recombination can therefore be estimated if the heat of adsorption of the atoms is known. It may be noted that this procedure is only applicable to reaction at clean surfaces; if surfaces are contaminated, e.g., with water, the treatment must be modified in the manner to be considered later.

The activation energy can also be estimated from the "desorption temperature," T_d, at which desorption of the atoms becomes appreciable. If Eq. (10), with b_g equal to unity for atomic recombination, is differentiated with respect to T and set equal to zero the result is

$$E/RT_m=1, \tag{15}$$

where T_m is the temperature at which γ will be a maximum. It has been noted[10] that T_m is approximately equal to T_d, so that Eq. (15) becomes

$$E=RT_d. \tag{16}$$

That these two methods of estimating E give good agreement with experimental values when these are known is shown by the figures in Table I.

THE RECOMBINATION ON DRY OXIDES

Absolute rate constants and recombination coefficients will now be calculated for several types of surfaces. The case of dry oxides will be considered first, as these are the easiest to treat. The oxides may be assumed to resemble glass as far as their surface properties are concerned, and $\Delta H_{\text{ads.}}$ may therefore be taken as -11 kcal (see Table I). It has been found[3,4] that the number of hydrogen atoms adsorbed per sq. cm of glass is about 1.35×10^{15}, and on the mechanism assumed these adsorbed atoms react directly with gaseous atoms; C_s is therefore taken as 1.35×10^{15} cm^{-2}. Calculation of γ at 300°K on the basis of these values, using Eqs. (10) and (14), gives 5×10^{-2}, in excellent agreement with Smith's values[2] ranging from 3×10^{-2} to

[10] N. Buben and A. Schechter, Acta physicochimica, U.R.S.S. **10**, 371 (1939).

TABLE II. Calculated values of γ and k' for clean glass surfaces.

T(°K)	γ	k' (cm sec.$^{-1}$)
90	0.46	6.8×10^{4}
180	0.22	1.1×10^{4}
200	2.2×10^{-2}	1.1×10^{3}
300	3.1×10^{-2}	1.9×10^{3}
400	3.3×10^{-2}	2.4×10^{3}
550	3.2×10^{-2}	2.8×10^{3}

6×10^{-2} for the oxides investigated ($ZnO\cdot Cr_2O_3$, Al_2O_3, K_2CO_3, K_2SiO_3, Na_3PO_4).

THE RECOMBINATION ON CLEAN GLASS SURFACES

Hydrogen atoms recombine very rapidly on clean glass surfaces[11,12] and it is consequently difficult to make accurate quantitative rate measurements. At liquid air temperatures[11] the recombination coefficient is close to unity, but at higher temperatures the value becomes smaller.[13] In the region from −79°C to 99°C the recombination coefficient increases in accordance with an activation energy of about 0.9 kcal.[14] As the temperature approaches the desorption temperature, which is at about 250°C,[3] the coefficient reaches a maximum and then decreases, the order increasing at the same time from unity to two. This effect is due to the depletion of the layer of hydrogen atoms (so that C_s varies with the pressure of hydrogen atoms), and has also been noted for the recombination of methyl radicals on glass[15] and of nitrogen atoms on nickel.[10] The temperature dependence of γ is shown schematically in Fig. 1, the curve being based on the data summarized above.

In the temperature region from −180°C to −80°C the curve can be fitted by Eq. (10) taking $C_s=1.35\times10^{15}$ and $E=0$; in the region from −80° to 250° it can be fitted with $C_s=1.35\times10^{15}$ and $E=0.9$ kcal. The calculated recombination coefficients and rate constants so obtained are shown in Table II. These values are of the right order. Roberts[16] states that γ for glass at liquid air temperatures should be somewhat less than unity. The values of γ between 200° and 500°K agree with that found by Smith[2] for dry oxides and are also in agreement with the observation of Steiner and Wicke[17] that γ on clean glass is several order of magnitudes higher than on water vapor poisoned glass surfaces (see Table IV).

[11] K. F. Bonhoeffer, Zeits. f. physik. Chemie **113**, 199 (1924).
[12] H. Senftleben and O. Riechemeier, Physik. Zeits. **30**, 745 (1929).
[13] P. Harteck and E. Roeder, Zeits. f. physik. Chemie **178**, 396 (1937).
[14] A. L. Robinson and I. Amdur, J. Am. Chem. Soc. **55**, 2615 (1933).
[15] F. Paneth and W. Lautsch, Ber. **B64**, 2708 (1931); Paneth, Hofeditz, and Wunsch, J. Chem. Soc. 372 (1935).
[16] J. K. Roberts, *Some Problems in Adsorption* (The Cambridge University Press, New York, 1939).
[17] W. Steiner and E. Wicke, Zeits. f. physik. Chemie, Bodenstein Band, 817 (1931).

TABLE III. Recombination coefficients on water-vapor poisoned glass surfaces.

T(°K)	Recombination coefficient $\gamma\times10^{5}$
93	4.45
193	2.04
288	2.01
453	6.8
573	16.0
723	53.0
863	89.0

In order to explain these results, including the fact that the reaction is of the first order over most of the temperature range, it is proposed that the surface is fully covered by hydrogen atoms, which react with gas-phase hydrogen atoms;

(1) $S-H+H\rightarrow S+H_2$
(2) $S+H\rightarrow S-H$.

This is consistent with Langmuir's result[4] that hydrogen atoms are adsorbed on clean glass down to liquid air temperatures, with a packing of about 1.35×10^{15} atoms per cm^2 (the value used by us above); moreover Johnson[3] found that desorption only sets in between 200° and 300°C. To explain the fact that the activation energy of the reaction is zero at low temperatures and 0.9 kcal. at higher ones it is suggested that the hydrogen atoms are van der Waals adsorbed to the glass in the low temperature region and chemisorbed at the higher temperatures. Thus R. A. Beebe and his co-workers[18] have shown that in certain cases the heat of adsorption increases with increasing temperature. Support for the mechanism proposed is provided by the fact that, as shown in Table I, the estimated activation energies for the high temperature region are in satisfactory agreement with the experimental values.

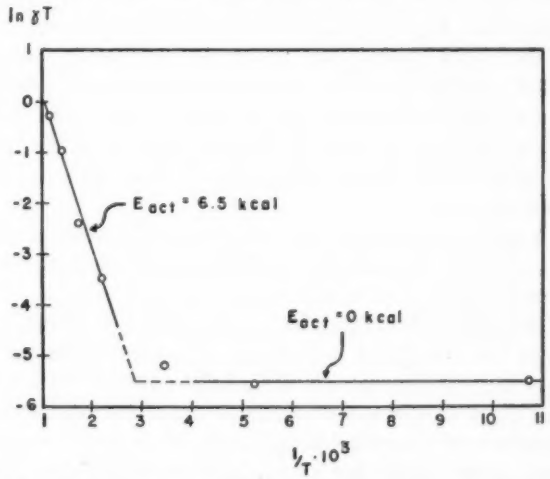

FIG. 2. Plot of $\ln\gamma T$ *vs.* $1/T$ for the hydrogen atom recombination on glass surfaces poisoned by water vapor.

[18] R. A. Beebe, in G. M. Schwab's *Handbuch der Katalyse* (Verlag Julius Springer, Berlin, 1943), Vol. IV, p. 473 (see e.g., Table 3, p. 494).

TABLE IV. Recombination coefficients and rate constants for atom recombination on H_2O-poisoned glass.

T(°K)	$\gamma(\times 10^5)$ Calc.	$\gamma(\times 10^5)$ Obs.	k'(cm sec.$^{-1}$) Calc.	k'(cm sec.$^{-1}$) Obs.
453	5.1	6.8	3.91	(1.96)*
573	18.0	16.0	16.2	
723	47.0	53.0	46.4	
863	81.0	89.0	86.9	

* This value refers to a surface poisoned by syrupy phosphoric acid (I. Amdur, J. Am. Chem. Soc. 60, 2347 (1938)).

THE RECOMBINATION ON WATER VAPOR POISONED GLASS SURFACES

The well-known poisoning effect of water on glass surfaces[19] could be due to two factors, (1) a decrease in the number of active centers, and (2) an increase in activation energy. An increase in activation energy could in turn be due to two causes: (2a) a tighter binding of the adsorbed hydrogen atoms on the poisoned surface as compared with the clean surface, and (2b) the necessity for desorption of the poison in order for the reaction to proceed on the bare surface.

That the poisoning is not due to cause (2b) may readily be shown. The rate of a poisoned first-order reaction occurring only on the bare surface is given by[8]

$$v_1=\frac{C_gC_s}{C_{gp}}\frac{kT}{h}\frac{F_{gp}f^{\ddagger}}{F_gf_{ap}}e^{-(E+E_p)/RT} \qquad (17)$$

where E_p is the heat of adsorption of the poison and the subscript gp applies to the poison in the gas phase. The rate is therefore inversely proportional to the partial pressure of the poison in the gas phase, and the same applies to the recombination coefficient; it has, however, been shown by von Wartenberg and Schultze,[20] and by Smith,[2] that the water vapor pressure has no influence on the rate. An additional argument against this explanation stems from the activation energy calculated from Eq. (17) according to the method outlined below. This calculation gives an activation energy $E+E_p$ of 3 kcal. which means that the heat of adsorption of the water vapor on the glass would have to be 3 kcal. or less. In fact, it is much greater in the temperature range where adsorption of H_2O on glass has been observed.

A decision between the two remaining possibilities, i.e., (1) and (2a), can be made by considering the temperature dependence of the rate in more detail. It is evident from Eq. (10) that a plot of $\ln\gamma T$ *versus* $1/T$ gives the energy of activation, the assumption being that the reaction occurs on a fully covered surface so that C_s is temperature independent; the equations are therefore only applicable up to the desorption temperature. Some values for γ obtained by Smith[2] are given in Table III, and a plot of $\ln\gamma T$ against $1/T$ is shown in Fig. 2. The activation energy is seen to be zero in the range from about -180°C to 0°C, and is 6.5 kcal. from 100°C to 600°C; in the intermediate region from 0°C to 100°C the activation energy varies with the temperature. The high and low temperature mechanisms will now be considered separately.

High Temperature Mechanism

The behavior in the high temperature region can be analyzed more easily, and will therefore be considered first. The value of 6.5 kcal. for the activation energy, as compared with 0.9 kcal. on clean surfaces, indicates that the poisoning is not due to a decrease in the number of reaction sites but to the additional energy required to form hydrogen molecules by reaction between a gas phase hydrogen atom and a hydrogen atom attached to the surface. This is confirmed by the fact that calculated values of γ and k', employing the activation energy of 6.5 kcal. and 10^{15} for C_s, are in good agreement with the experimental values; the results are shown in Table IV. This value for C_s is the same as that for unpoisoned surfaces. The poisoning is thus shown to be due to cause (2a). The observed value of k' is that of Amdur's[21] mechanism C, involving first-order wall recombination. Since it has been shown by Smith[2] and by Poole[22] that the recombination coefficient for hydrogen atoms is the same on a phosphoric acid poisoned surface as for one poisoned by water, one can assume the same mechanism in both cases, and it is therefore valid to compare our results with those of Amdur. This mechanism will now be discussed.

It has been shown by van Itterbeck and Vereycken[23] that water in the molecular form is not adsorbed on glass at above 180°C; the poisoning agent in Smith's experiments must therefore be the hydroxyl radicals formed from the water vapor in the discharge employed by him. The simplest and most plausible recombination mechanism is therefore

$$(3)\quad S-OH+H\rightarrow S-O+H_2$$
$$(4)\quad S-O+H\rightarrow S-OH$$

where S represents a site on the clean glass surface. The dissociation energy of the free hydroxyl radical is 100 kcal., and the dissociation energy of the first OH bond in water is 118 kcal.;[24] the dissociation energy of the OH radical adsorbed on the surface may be expected to fall within that range. On the basis of the lower value reaction (3) is exothermic, and using Hirschfelder's rough procedure the activation energy would be $\sim$5.5 kcal.; the upper value on the other hand, would require an endothermic reaction, and Hirschfelder's rule gives $E=\sim$20.7 kcal. The experimental value of 6.5 kcal. is clearly of the right order to be consistent with the

[19] R. W. Wood, Proc. Roy. Soc. 97, 455 (1920).
[20] H. von Wartenberg and G. R. Schultze, Zeits. f. physik. Chemie B6, 261 (1929).
[21] I. Amdur, J. Am. Chem. Soc. 60, 2347 (1938).
[22] H. G. Poole, Proc. Roy. Soc. A163, 404 (1937).
[23] A. van Itterbeck and W. Vereycken, Zeits. f. physik. Chemie B48, 131 (1941).
[24] R. J. Dwyer and O. Oldenburg, J. Chem. Phys. 12, 351 (1944).

mechanism, and might be taken to suggest that the OH dissociation energy of the adsorbed radicals is ~104 kcal.

Low Temperature Mechanism

The activation energy in the low temperature region has been shown to be close to zero, and this implies that the poisoning mechanism involves a reduction in the number of active sites per sq. cm. Using Eq. (10) it is possible to calculate the value of C_s which will make the calculated values of γ agree with the experimental ones: the result is 1.4×10^{11} cm^{-2}, a reduction by a factor of 10^4 of the value for a normal active surface. This conclusion is in agreement with other results obtained for hydrogen at low temperatures; thus in an analysis of results of J. K. Roberts[25] on the adsorption of hydrogen on tungsten between 79°K and 295°K, Laidler, Glasstone, and Eyring[8] concluded that the data required C_s to be $\sim10^{10}$.

At low temperatures water is known to be strongly van der Waals adsorbed on glass, and is probably in the molecular form. The reaction of the gaseous hydrogen atoms cannot be with chemically-bound hydrogen (as the activation energy is zero), but must be with hydrogen atoms van der Waals adsorbed above the water layer. The mechanism proposed can be written as

$$(5)\quad S\cdots H_2O\cdots H + H \rightarrow S\cdots H_2O + H_2$$
$$(6)\quad S\cdots H_2O + H \rightarrow S\cdots H_2O\cdots H,$$

where the dotted lines indicate van der Waals adsorption. It may be mentioned that van der Waals adsorption of hydrogen atoms on a film of adsorbed water has also been postulated by Roberts[25] to explain some of his data.

Note added in proof.—Since the present paper was submitted we have seen a translation of an article by V. V. Voievodsky and G. K. Lavroskaiia, Doklady Akad. Nauk. U.S.S.R. **63**, 151 (1948). (See Chem. Abstracts **43**, 1635.) These authors do not discuss any specific recombination or poisoning mechanisms, but their experimental values are consistent with those discussed above.

ACKNOWLEDGMENT

The authors wish to express their thanks to Professors H. M. Hulburt and W. J. Moore for valuable discussions on several points in this paper, and to Dr. W. V. Smith for the loan of a copy of his thesis.

APPENDIX

The Recombination Coefficient for a Flow System

Since the data of Smith[2] used in this paper were obtained by means of a flow system, it is necessary to show that Eq. (4) for the recombination coefficient in a static system is identical with that derived for a flow system.

In Smith's experiments the hydrogen atoms produced in the discharge tube and pumped through it were allowed to diffuse into a side arm closed on one end and joined perpendicular to the discharge tube on the other. The recombination of the atoms takes place on the walls of this side arm during their diffusion along this side arm.

[25] J. K. Roberts, Proc. Roy. Soc. **A152**, 445 (1935).

Let n = number of atoms per cc,
Let x = distance along side arm from discharge tube,
Let D = diffusion coefficient,
Let F = drift velocity of atoms along side arm,
Let γ = coefficient of recombination,
Let V = volume per unit length of side arm,
Let S = surface per unit length of side arm,
Let ϑ = mean atomic speed,
Let k = first order rate constant for recombination,
Let r = radius of side arm.

The subscript 0 indicates the junction of the side arm with the discharge tube. It will be assumed that the atomic concentration is constant over the cross section of the side arm so that $n=n(x)$, and $F\neq F(r)$. Smith[2] has shown that these assumptions are valid under his experimental conditions.

The following equations then hold:

Number of atoms lost to wall per cm per sec.
= gradient of flow through tube

$$(n\vartheta/4)S\gamma = -V(\partial/\partial x)(nF), \tag{18}$$

and the diffusion equation

$$nF = -D(\partial n/\partial x). \tag{19}$$

Combination of (18) and (19) gives

$$\partial^2 n/\partial x^2 = n\vartheta S\gamma/4VD. \tag{20}$$

the solution of which is

$$n = A\exp[(\vartheta S\gamma/4VD)^{\frac{1}{2}}x] + B\exp-[(\vartheta S\gamma/4VD)^{\frac{1}{2}}x]. \tag{21}$$

For a tube of finite length neither A nor B is equal to zero. The term with the positive exponent, which increases with increasing x, can be considered as representing the stream of atoms reflected from the closed end of the tube, and the term with the negative exponent, which decreases with increasing x, can be considered as representing the incoming stream of atoms from the discharge tube. If the side arm through which the atoms move is long enough so that the atoms will make many collisions with the walls before reaching the end of the tube, most of the atoms will have recombined to molecules, and the stream of atoms reflected from the closed end of the tube will be negligible compared to the incoming stream of atoms. Since the experimental conditions are such that $2r\gg\lambda$, where λ is the mean free path of the atoms, one is in the region of Poiseuille rather than Knudsen flow, and the backward reflection of atoms from the walls of the tube can be neglected. Equation (21) then reduces to

$$n = n_0\exp-[(\vartheta S\gamma/4VD)^{\frac{1}{2}}x] \tag{22}$$

under the boundary conditions $n=n_0$ when $x=0$. Therefore n is expressible as

$$n = n_0e^{-\beta x} \tag{23}$$

where $\beta=(\vartheta S\gamma/4VD)^{\frac{1}{2}}$. Substituting (23) into (19) one obtains

$$F = D\beta. \tag{24}$$

It will be noted that not only is $F\neq F(r)$, but also $F\neq F(x)$. The first-order rate constant k is given by the relation

$$n = n_0e^{-kt}. \tag{25}$$

Replacing the time t by its equivalent $t=x/F$ and expressing F by Eq. (24) gives

$$n = n_0e^{-kx/D\beta}. \tag{26}$$

Combination of (26) and (23) gives

$$\beta^2 = k/D. \tag{27}$$

Introducing the explicit expression for β and solving for γ,

$$\gamma = 4kV/\vartheta S. \tag{28}$$

Since $V=\pi r^2$ and $S=2\pi r$, Eq. (28) reduces to

$$\gamma = 2kr/\vartheta, \tag{29}$$

which is identical with Eq. (4) derived earlier.

On the Theory of the π-Electron System in Porphines

WILLIAM T. SIMPSON
Department of Chemistry and Chemical Engineering, University of Washington, Seattle 5, Washington

(Received February 28, 1949)

The failure of certain LCAO molecular orbital calculations of the spectrum of porphine is attributed to the incorrect assumption of complete "aromaticity." A division of the π-electron system into non-interacting parts is supported by the fact that the dynamical properties of the divided system, as calculated by the free-electron model, are in approximate agreement with experiment. A proof of the equivalency of the LCAO method (with overlap neglected) and an approximation to the free-electron method is indicated for certain dynamical systems.

INTRODUCTION

THE electronic spectra of porphines, dihydroporphines (chlorins), and tetrahydroporphines (bacteriochlorophylls) are complex. Factors which make a theoretical treatment difficult include the presence of tautomerism, possible ring strain, heteroatoms, and the large number of unsaturation electrons. Nevertheless it seems desirable at this time to discuss porphine spectra, because porphines are in the first rank in biological importance.

A few general remarks will be made about π-electron calculations. The simplest procedures from the standpoint of computation involve the greatest use of prior experimental data. A factor of particular importance in this respect will be called aromaticity. By this is meant the characteristic: having equal bond lengths. Unrefined theoretical procedures sometimes lead to a qualitatively correct prediction of the extent to which a substance approaches aromaticity. Thus a preliminary assumption of full aromaticity for butadiene gives, in LCAO approximation, bond orders which suggest that the original assumption was erroneous.

Another less direct but more widely applicable means exists for the theoretical prediction of aromaticity. Under the assumption of equal resonance and Coulomb integrals one may calculate a property of a substance such as the position of its electronic absorption bands. Dramatic disagreement between the calculation and observation may then be taken as a probable indication that the assumption (tantamount to the assumption of full aromaticity) was incorrect. By means of such an argument Mulliken investigated the aromaticity of pyrrole and concluded that the nitrogen electron pair may be incompletely conjugated.[1,a]

A combination of theory and experiment will be used below in an attempt to assess the aromaticity of porphines.

THE AROMATICITY OF PORPHINE

The representation discussed by Rabinowitch[2] (Fig. 1) and the picture of the molecule generated by the molecular orbital point of view are very different. It is well known that the former implies an isolation of two double bonds: on the contrary, the molecular orbital point of view suggests that the mesomerically implied isolation of two double bonds is a fiction of the representation. The latter view was adopted here as a trial hypothesis.

An LCAO set of orbitals (which constituted a basis for irreducible representations of the supposed symmetry group of the molecule, D_{4h}) and their energies were accordingly obtained. Heteroatoms were considered as being carbons, and all resonance integrals between adjacent carbons were considered to be equal, as were all Coulomb integrals. The calculations were next repeated in such a way as substantially to incorporate the slight modification of the LCAO method introduced earlier.[3] That is, the Coulomb integral was changed according to the number of adjacent nuclei.[b] Finally the effect of variation in the Coulomb integrals with the number of next-to adjacent nuclei was considered. When the calculations were calibrated, with 205 mμ equal to the calculated "color" of benzene,[c] a prediction of an intense band in the region 1100 to 1600 mμ invariably arose.

It was thought that an intense band in the infra-red might have been overlooked. The spectrum in CCl_4 of α-, β-, γ-, δ-tetraphenylporphine (Fig. 1, with phenyls on the four carbons which join the pyrrole rings), a substance whose visible bands are quite similar to the bands of the parent compound, was investigated. The concentration employed was such as to have given an overwhelming absorption peak, but in a search (using a Beckman Model 1R2 infra-red spectrophotometer) from 1000 to 3000 mμ, no intense electronic transition was detected.

[1] R. S. Mulliken, J. Chem. Phys. **7**, 339 (1939).

[a] The effect of including overlap in the calculation is greatly to reinforce the conclusion that the nitrogen electron pair is incompletely conjugated. There remains the possibility, however, that the LCAO method is at fault. For instance, the free-electron method predicts a benzene-like spectrum for homocyclic conjugation.

[2] E. Rabinowitch, Rev. Mod. Phys. **16**, 226 (1944).

[3] W. T. Simpson, J. Chem. Phys. **16**, 1124 (1948).

[b] Employment of this modification is formally a departure from the assumption of full aromaticity, but still the nitrogens are regarded as being like carbons.

[c] It would be more accurate to employ singlet-triplet centers of gravity, but the present lack of knowledge of the values of triplet-singlet transition energies is a hindrance.

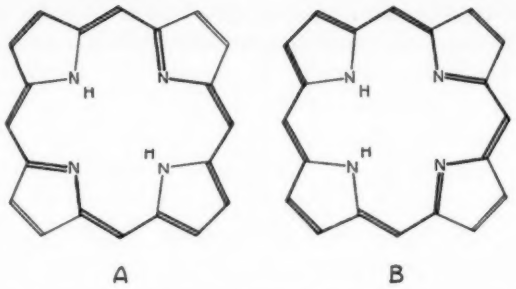

A B

FIG. 1. Tautomers of porphine. Two Kekule-like mesomeric forms correspond to each tautomer.

A possible conclusion is that porphine is not fully aromatic. While other results to be presented below support this conclusion, still it is well to list some of the factors which might vitiate it.

The usual insufficiencies of an LCAO molecular orbital treatment are ordinarily overcome by the empirical procedure of calibrating the method with the spectrum of a known compound. The consideration of a 24-electron problem such as porphine may have placed too great a burden on the calibration procedure. In addition, interactions between product wave functions of the same symmetry were not taken into account.[d]

NATURE OF THE DEPARTURE FROM AROMATICITY

Even if the preceding conclusion is accepted, it remains to be shown that a particular alternative, the representation indicated in Fig. 1 is correct. Certain features of the spectra of porphines and related compounds do, in fact, support such a representation.

One implication contained in the Kekule-like mesomeric forms of either of the two tautomers shown in Fig. 1 is that hydrogenation of one, or even of two double bonds, should not result in a significant change in the positions of the absorption bands. Huennekens,[4] working with α-, β-, γ-, δ-tetraphenylporphines and chlorins, has found various examples which are in accord with this implication. In the case of the free base, for example, the intense band of the porphine at 430 mμ (called the Soret band) shifts by only 2 or 3 mμ when the substance is converted into a chlorin.

A second deduction from the mesomeric forms relates to the electron pairs on the pyrrole-like nitrogens. The substitution of a central metal ion that can act as an acid toward these electron pairs would be expected to change the spectrum considerably; molecular orbitals having a node at the center would be unaffected, while orbitals for which there is antisymmetry with respect to inversion would be stabilized. For instance, in the fully aromatic representation discussed in the previous section the symmetries of the orbitals which give rise to the predicted infra-red band are (neglecting the horizontal plane) $A_1 \rightarrow E$; hence the spectrum should shift toward shorter wave-lengths.

In actual fact, the substitution of Ni^{++}, a central metal "acid"[e] for Zn^{++}, a central metal "base" gives a shift that is hypsochromic, but slight (~25 mμ). This comparison of Ni and Zn salts was made by Corwin and Erdman[5] for the compound Mesoheme IX dimethyl ester, a substituted porphine which is essentially a simple porphine from the standpoint of the π-electron system.

If the pyrrole electron pairs are in comparatively weak interaction with the main chromophoric system, as implied in Fig. 1, then the relatively small Ni−Zn spectral shift is understandable. The evidence having to do with hydrogenation is better, but the two arguments reinforce one another. Each argument supports the more general conclusion of the preceding section that porphine is not fully aromatic.

The object of the remainder of this paper is to investigate the representation shown in Fig. 1 by a further means: to obtain the absorption spectrum which it implies. A "model substance" consisting of an 18-membered benzenoidal ring, strain free, was chosen. In regard to the neglect of hetero-atoms, the question of the trigonal electron pairs on the pyridine-like nitrogens arises. The virtual identity of the spectra of porphine dihydrochlorides and the disodium salts[6] indicates that the presence of the trigonal electron pairs is not a perturbing factor.

CALCULATION OF THE TRANSITION ENERGY

There is very little difference between the LCAO method in its simplest form and the free electron model.[7,8] A solution according to the latter, but with the use of difference equations[8] instead of the Schrödinger equation, yields a secular equation; and if the continuous closed curve around which the electrons are supposed to move is divided into a lattice of 18 points the secular equation becomes identical in form to the LCAO secular equation for the problem. The solutions give the same energy level spacing as the LCAO method with overlap neglected.[f]

[d] The writer wishes to acknowledge a private communication from Professor C. A. Coulson which served to call his attention to this possibility.

[4] F. M. Huennekens, Ph.D. thesis, University of California (1948).

[e] According to Pauling and Coryell, Proc. Nat. Acad. Sci. **22**, 159 (1936), sp_2d hybridization is appropriate. In consequence there remains an empty $4p_z$ Ni^{++} orbital in a position to interact with the π-orbitals of the porphine.

[5] A. H. Corwin and J. G. Erdman, J. Am. Chem. Soc. **68**, 2473 (1946).

[6] J. G. Erdman and A. H. Corwin, J. Am. Chem. Soc. **68**, 1885 (1946).

[7] N. S. Bayliss, J. Chem. Phys. **16**, 287 (1948); H. Kuhn, Helv. Chim. Acta **31**, 1441 (1948); J. R. Platt, J. Chem. Phys. **17**, 484 (1949).

[8] L. C. Pauling and E. B. Wilson, *Introduction to Quantum Mechanics* (McGraw-Hill Book Company, Inc., New York, 1935), p. 202.

[f] The relation between the methods leads to the speculation that with respect to the most energetic electrons the LCAO method may owe its applicability to its resemblance to the free electron model.

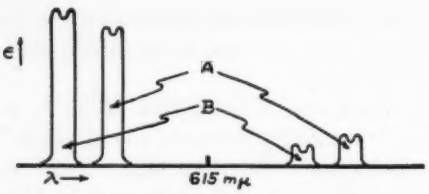

FIG. 2. Band system calculated for A and B tautomers of porphines. The displacement of the A bands relative to the B is arbitrary.

The free electron model was employed to obtain the orbital energies of the hypothetical 18-membered ring compound. The equation for the energy of a particle on a circle was used, where it is understood that the circle need only be a simple closed curve in order for the energy equation:

$$W=n^2h^2/8\pi^2mr^2$$

to hold. (A typographical error in reference 3 led to the omission of the exponent on π.) The calculation was calibrated with the "color" of benzene. Thus

$$1/205\ \text{m}\mu=\text{constant}\ (2^2-1^2)/r_B^2$$

where r_B is the effective benzene radius, and the parenthesis encloses the difference of the squares of the appropriate quantum numbers. If a is an effective interatomic distance:

$$2r_B=6a/\pi,$$

and for porphines

$$2r_P=18a/\pi.$$

Thus for the porphine absorption peak λ_P:

$$\lambda_P/205\ \text{m}\mu=18^2(2^2-1^2)/6^2(5^2-4^2);$$
$$\lambda_P=615\ \text{m}\mu.$$

THE SELECTION RULES

The quantum numbers of the highest filled level are ±4, and of the lowest unfilled level, ±5; hence the transition is fourfold degenerate. Some understanding of how the degeneracy splits up can be obtained even from the free electron calculation. To this end, the wave functions (not normalized) involved in the transition are listed. The most energetic electrons are labeled one to four, and interchanges are neglected. For the ground state,

$$\varphi_0=\cdots e^{+4i\theta}\ (1)\quad e^{+4i\theta}\ (2)\quad e^{-4i\theta}\ (3)\quad e^{-4i\theta}\ (4).$$

The zero subscript refers to the sum of the quantum numbers and may be regarded as a resultant angular momentum.

For the excited state:

$$\varphi_{+1}=\cdots e^{+4i\theta}\ (1)\quad e^{+5i\theta}\ (2)\quad e^{-4i\theta}\ (3)\quad e^{-4i\theta}\ (4),$$
$$\varphi_{-1}=\cdots e^{+4i\theta}\ (1)\quad e^{+4i\theta}\ (2)\quad e^{-4i\theta}\ (3)\quad e^{-5i\theta}\ (4),$$
$$\varphi_{+0}=\cdots e^{+4i\theta}\ (1)\quad e^{+4i\theta}\ (2)\quad e^{-4i\theta}\ (3)\quad e^{+5i\theta}\ (4),$$
$$\varphi_{-0}=\cdots e^{+4i\theta}\ (1)\quad e^{-5i\theta}\ (2)\quad e^{-4i\theta}\ (3)\quad e^{-4i\theta}\ (4).$$

The transition moment is $\int\varphi^*q\varphi d\tau$; thus for the transition $\varphi_0\rightarrow\varphi_{+1}$ and for light plane polarized in the x direction (and assuming the simple closed curve is actually a circle), the integral is:

$$r_P/4\pi\int_0^{2\pi}e^{-4i\theta}(e^{i\theta}+e^{-i\theta})e^{+5i\theta}d\theta\neq0.$$

A consideration of the four transition moments shows that the allowed bands correspond to changes of the quantum number of ±1; while the remaining transitions, corresponding to a change of ±9, are forbidden. Moreover Hund's rule, that for a given multiplicity the lowest states have the greatest angular momentum, puts the forbidden pair of transitions at longer wave-lengths.[8]

THE CHARACTER OF THE ABSORPTION SPECTRUM

The changes in the spectrum calculated for the model substance which are to be expected for the free base of porphine may now be considered. Various effects are illustrated schematically in Fig. 2.

The center of gravity of the bands is at 615 mμ. The contributions of each tautomer are unknown (and would be determined by a Boltzmann factor). The long wave-length bands are represented as being weak, corresponding to their quasi-forbidden character. Each band is represented as having a double maximum, in order to indicate that it still corresponds to a doubly degenerate transition, and that this degeneracy will split under the influence of the field of the nuclei. The forbidden band corresponding to the A tautomer is represented as having a higher $\epsilon_{\max}$ than for the B band, because the tautomer is a more nearly circular system (the selection rules were obtained for a particle on a circle). The A allowed band is represented as correspondingly less intense.

If the dihydrochloride is formed from the free base, giving a molecule with one hydrogen on each nitrogen but only C_{2v} symmetry, the Boltzmann factor then favors the A form, because of repulsion between the formal charges; therefore, the B bands should virtually disappear, and the spectrum assume a simplified appearance.

If the free base is hydrogenated once or even twice, the center of gravity of the bands should remain constant, but the forbidden bands should gain in intensity. Unless the tautomerism in porphine is slow, there will be greater circular symmetry than is indicated by an individual tautomer. (If the tautomeric shift occurred many times during the lifetime of the electronic excited state, the lack of circular symmetry implied by a tautomeric form would be meaningless; but Erdman and Corwin[6] have given evidence that this rapid shift does not occur.) For the tetrahydro compound, however, one or the

[8] A perturbation theoretical analysis which employed free electron wave functions confirmed the prediction of Hund's rule for the singlet states but gave a degeneracy for the triplets. The functions were antisymmetrized to the exchanges of the most energetic four electrons.

other of the tautomers is "frozen," and the selection rules for the particle on a circle particularly inapplicable.

COMPARISON WITH EXPERIMENT

The band maxima determined by Erdman and Corwin[6] for a simple porphine, etioporphine II, and its dihydrochloride occur grouped about centers of gravity of 477 and 495 mμ, respectively:

Free base	λ	622	595	572	532	498	397
	$\epsilon\times10^{-4}$	0.480	0.195	0.621	0.850	1.37	15.7,
Dihydrochloride	λ	598		555		415	
	$\epsilon\times10^{-4}$	0.680		1.54		18.1.	

The predictions of the last section fit the observed data about as well as might be expected, considering the many approximations.

The hydrogenated porphines exhibit the behavior attributed to them in the previous section, in that the center of gravity of their bands remains about the same, but the ϵ_{max} of the long wave-length bands increase. The center of gravity for a bacteriochlorophyll that was studied by French[9] is 549 mμ. From the standpoint of the transition energy, a bacteriochlorophyll is most similar to the model substance, so that the approximate agreement of the calculated 615 mμ is gratifying.

ACKNOWLEDGMENT

The writer wishes to thank Dr. Frank M. Huennekens for calling his attention to the problem and for many stimulating discussions. He likewise extends thanks to Professors H. J. Dauben, Jr., and P. Rothemund for samples of porphines. Finally he would like to acknowledge a debt to the publications on benzene of Drs. A. L. Sklar and M. Goeppert-Mayer.

[9] C. S. French, J. Gen. Physiol. 21, 71 (1937).

THE JOURNAL OF CHEMICAL PHYSICS VOLUME 17, NUMBER 12 DECEMBER, 1949

A Kinetic Study of the Thermoluminescence of Lithium Fluoride

CHARLES A. BOYD
*Department of Chemistry, University of Wisconsin, Madison, Wisconsin**

(Received March 14, 1949)

The isothermal decay of the thermoluminescence of single crystals of lithium fluoride activated by x-rays has been determined at various temperatures. The results are interpreted in terms of a simple reaction rate mechanism based on a picture of the thermoluminescent process similar to that of Johnson. The analysis of the isothermal decay studies is in agreement with the results of "glow curve" experiments on similar lithium fluoride samples where the intensity of luminescence is measured as the temperature of the crystal is heated at a constant rate.

Two principal types of electron traps in lithium fluoride are found to have trapping energies of 19,800 cal./mole and 45,300 cal./mole respectively.

INTRODUCTION

THIS paper describes an investigation of the thermoluminescence of single crystals of lithium fluoride activated by exposure to x-rays at room temperature. Studies have been made of the variation of luminescent intensity with time when the crystal is held at constant temperature and also when it is heated at a constant rate. The experimental data are analyzed from the standpoint of a simple reaction rate mechanism, and a method is developed for experimentally determining the energy of electron traps from the isothermal decay of the luminescent intensity.

It is found that in the lithium fluoride crystals investigated there are two principal types of electron traps having trapping energies of 19,800 cal./mole and 45,300 cal./mole respectively. A third type of trap of intermediate energy is indicated, but it is of secondary importance.

* Supported by the research committee of the Graduate School from funds supplied by the Wisconsin Alumni Research Foundation.

Johnson[1] has used the band theory of solids to develop a picture which qualitatively explains thermoluminescence in terms of the trapping of electrons which have been excited to the conduction band by the external radiation. These are subsequently released from the traps by energy transfer as the temperature of the crystal is raised. This type of model has been used by investigators for quantitative interpretation of their experimental results[2] in studies of the various phosphors.

The physical interpretation of electron traps has been discussed by several authors.[3] They are usually associated with some type of distortion of the regular crystal lattice.

The earlier investigations of thermoluminescence

[1] R. P. Johnson, J. Opt. Soc. Am. 29, 387 (1939).

[2] G. Fonda and F. Seitz, *Preparation and Characteristics of Solid Luminescent Materials* (John Wiley and Sons, Inc., New York, 1948); also, H. W. Leverenz, Science 109, 183 (1949).

[3] N. F. Mott and R. W. Gurney, *Electronic Processes in Ionic Crystals* (Oxford University Press, New York, 1940); I. Tamm, Zeits. f. Physik 76, 849 (1932); L. Landau, Physik. Zeits. Sowjetunion 3, 664 (1933); J. J. Markham and F. Seitz, Phys. Rev. 74, 1014 (1948).

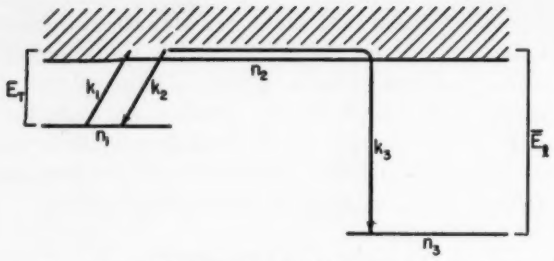

FIG. 1. Simplified energy level diagram illustrating the thermoluminescent process.

have been carried out along two major lines. One type of experiment is concerned with the functional form of the decay of the thermoluminescence with time when the crystal is held at an elevated temperature. Different analytical expressions have been derived to describe this decay based upon different assumptions. For example, Randall and Wilkins[4] have shown that if the electrons which are released from the traps recombine directly with the parent ions the intensity of luminescence should decrease with time according to a first order expression of the type

$$I=I_0\exp(-at). \tag{1}$$

The treatment of Randall and Wilkins has been extended by Garlick[2] to include the possibility of recapture of the released electrons by other empty electron traps. He has assumed first, that the number of electrons in the conduction band is small compared to the number trapped, and second that the capture cross section of empty traps for electrons is the same as that of the empty luminescent centers. This leads to the following time dependence of the luminescence:

$$I^{-\frac{1}{2}}=[(N)/[n_0^2 s\exp(-E/RT)]]^{\frac{1}{2}} +[(s/N)\exp(-E/RT)]^{\frac{1}{2}}t \tag{2}$$

where N is the total number of traps, n_0 is the initial number of trapped electrons, s is the frequency factor for the release of electrons from the traps, T is the absolute temperature, and E is the energy of the traps. At any fixed temperature this equation is of general form

$$I^{-\frac{1}{2}}=a+bt \tag{3}$$

which corresponds to the so-called "second-order" decay.

In practice the luminescent decays of most phosphors do not follow any simple functional form but are usually empirically fitted by some type of power law

$$I=I_0t^{-n} \tag{4}$$

where n varies between 0.1 and 2.

However, in the present work the thermoluminescent decay of lithium fluoride has been resolved into two major components, each of which corresponds to a single type of trap decaying according to the second order decay law. By choosing the proper temperature for the decay one or the other component can be made predominate, and its trapping energy can be determined.

The second type of experiment used in studies of thermoluminescence is concerned with the so-called "glow curves" first reported by Urbach.[5] In this type of experiment the crystal is first irradiated and then heated so as to raise its temperature at a constant rate. The intensity of the luminescence is found to go through maxima which can be related to the various types of traps contributing to the luminescent process. Since the intensity decay of the industrial phosphors is usually complex this second type of experiment has found more general use. The thermoluminescent decay of lithium fluoride is of a sufficiently simple nature to permit analysis of both types of experiments from the standpoint of the second order decay law, Eq. (3).

This type of analysis when applied to the experimental data obtained for lithium fluoride crystals indicates that two major types of traps contribute to the thermoluminescence. These have trapping energies of 19,800 cal./mole and 45,300 cal./mole respectively. The same type of analysis is also applied to the results of "glow curve" experiments made with similar lithium fluoride crystals and it is found that the trapping energy for the higher energy traps as determined from the glow curve is in good agreement with that determined from isothermal decay. The lower trapping energy cannot be evaluated from the glow curve because of the composite nature of the decay in this region.

DEVELOPMENT OF EQUATIONS

When a crystal such as lithium fluoride is irradiated with x-rays, some of the electrons originally associated with ions in the crystal are excited to the conduction band where they are free to wander through the lattice. These excited electrons may encounter lattice imperfections such as negative ion vacancies or impurities where they are attracted and bound or "trapped" at ordinary temperatures.

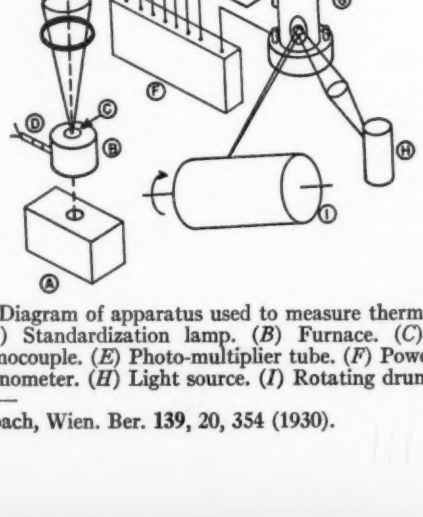

FIG. 2. Diagram of apparatus used to measure thermoluminescence. (*A*) Standardization lamp. (*B*) Furnace. (*C*) Sample. (*D*) Thermocouple. (*E*) Photo-multiplier tube. (*F*) Power supply. (*G*) Galvanometer. (*H*) Light source. (*I*) Rotating drum camera.

[4] J. T. Randall and M. F. Wilkins, Proc. Roy. Soc. **184**, 366 (1945).

[5] F. Urbach, Wien. Ber. **139**, 20, 354 (1930).

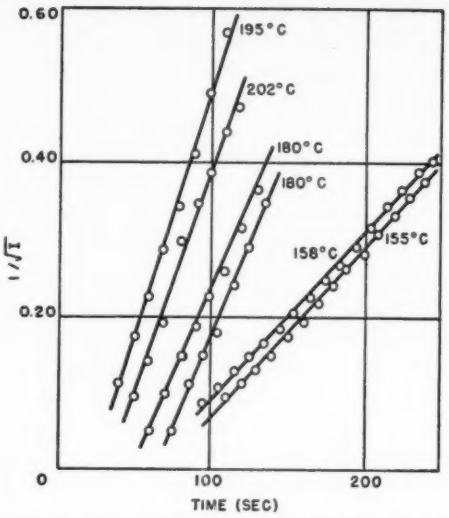

FIG. 3. Thermoluminescent decay of lithium fluoride at various temperatures.

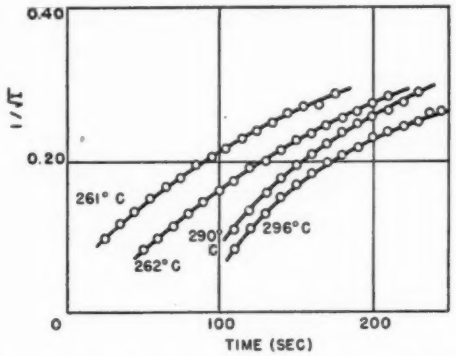

FIG. 4. Thermoluminescent decay of lithium fluoride at various temperatures.

As the temperature of the crystal is raised the probability is increased that a trapped electron will be released to the conduction band again by energy transfer. A released electron will remain in the conduction band until it encounters another trapping center and is retrapped or until it encounters and recombines with one of the ions which originally yielded electrons under the influence of the x-rays.

This second type of recombination results in the release of energy in the form of a quantum of light giving rise to the observed luminescence. A kinetic treatment of this process can be considered by referring to Fig. 1. n_1 represents the number of trapped electrons; n_2, the number of electrons in the conduction band; and n_3, the number of ionized ions with which electrons can recombine giving up quanta of light of average energy $\bar{E}_l = hc/\lambda$. Since the luminescence for lithium fluoride is predominantly blue, $\bar{E}_l$ in this case will be of the order of 60,000 to 70,000 cal./mole.

In Fig. 1, the energy which a trapped electron must acquire in order to be excited back to the conduction band is represented by E_t.

If the crystal remains electrically neutral

$$n_1+n_2=n_3. \tag{5}$$

The situation as represented by Fig. 1 is analogous to the model used by Eyring in the development of the theory of absolute reaction rates for chemical reactions. Electrons which are trapped correspond to the initial state of the reaction; excitation to the conduction band corresponds to the formation of the activated complex; and electrons which have recombined with the parent ions correspond to the final state.

Following Eyring's development, we will assume that at a given temperature equilibrium exists between n_1 and n_2, the molecule in the initial and in the activated states. This assumption of equilibrium becomes valid when n_2 is small compared to n_1. Thus, if

$$K=n_2/n_1 \tag{6}$$

and

$$-dn_3/dt=k_3n_2n_3 \tag{7}$$

it follows from a simple kinetic treatment that

$$(1/n_3)-(1/n_3^0)=\left(\frac{K}{K+1}\right)k_3t. \tag{8}$$

However, the intensity of thermoluminescence, I, is given by

$$I=\bar{E}_l(-dn_3/dt). \tag{9}$$

Where $\bar{E}_l$ is the average energy involved in transition 3 and is not a sharp value because of the fact that the transition does not occur between sharp levels.

Combining Eqs. (6), (8), and (9) gives the intensity as a function of time as

$$I=\frac{\bar{E}_lk_3[K/(K+1)]}{[k_3[K/(K+1)]t+1/n_3^0]^2}. \tag{10}$$

The variation of K with temperature is given by

$$K=K_0\exp(-E_t/RT). \tag{11}$$

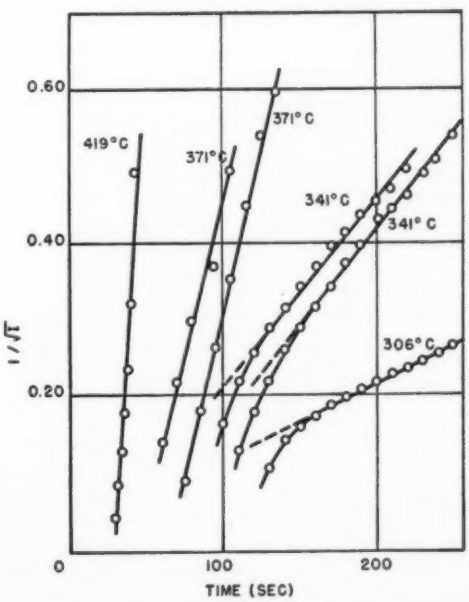

FIG. 5. Thermoluminescent decay of lithium fluoride at various temperatures.

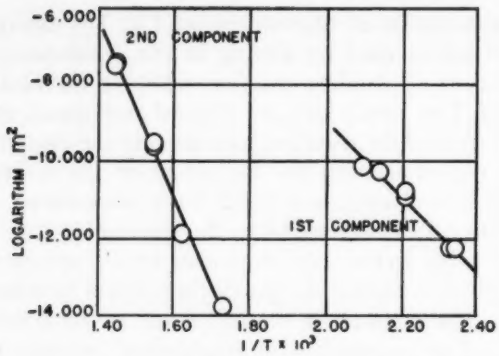

FIG. 6. Plot of ln m² against $1/T$ for the two major components observed in the thermoluminescence of lithium fluoride. E for first component = 19,800 cal./mole. E for second component = 45,300 cal/mole.

Further, it will be noticed that K will be small compared to one and consequently

$$[K/(K+1)] \cong K. \tag{12}$$

Substituting Eqs. (11) and (12) into Eq. (5) and rearranging gives

$$I^{-\frac{1}{2}} = [(k_3/\bar{E}_l)K_0 \exp(-E_t/RT)]^{\frac{1}{2}} t + (1/n_3^0)[\bar{E}_l k_3 K_0 \exp(-E_t/RT)]^{-\frac{1}{2}} \tag{13}$$

which is essentially the same equation as that derived by Garlick.

According to Eq. (13), plots of $I^{-\frac{1}{2}}$ against t at a constant temperature should give a straight line having a slope given by

$$m_T = [(k_3/\bar{E}_l)K_0 \exp(-E_t/RT)]^{\frac{1}{2}}. \tag{14}$$

Determination of m_T at various temperatures makes it possible to evaluate E_t since from Eq. (14)

$$\ln(m_T^2) = -(E_t/R)(1/T) + (k_3/\bar{E}_l)K_0 \tag{15}$$

and a plot of $\ln(m_T^2)$ against $1/T$ should give a line of slope, $-E_t/R$.

EXPERIMENTAL DETERMINATION OF INTENSITY DECAY CURVES AT CONSTANT TEMPERATURE

Equations (13) and (15) were tested experimentally by observing the intensity decay of the thermoluminescence of lithium fluoride at various temperatures. The samples used in these experiments were in the form of plates one centimeter square and approximately two millimeters thick. These were cleaved from larger single crystals obtained from the Harshaw Chemical Company. The plates were exposed on both faces to 35-kilovolt x-rays from a tube equipped with a copper target and an aluminum window. The exposure time for each face was two minutes and was carried out at room temperature.

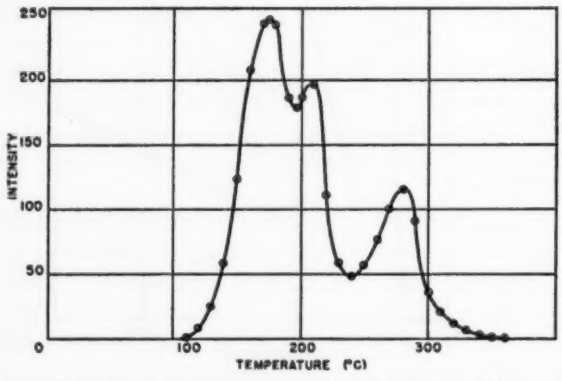

FIG. 7. Intensity temperature curve for lithium fluoride crystal. Rate of heating = 1.25°C/sec.

The apparatus used to measure the thermoluminescence is shown diagrammatically in Fig. 2. The irradiated sample was placed in a shallow Wood's metal bath on the face of the furnace. The light emitted was focused upon a photo-multiplier tube connected to a galvanometer, the deflection of which was recorded photographically on a drum camera rotating at a known speed.

Since the proportionality constant $\bar{E}_l$ appears in the expression for the slope, Eq. (14), it was necessary to standardize the recording circuit to the same relative value for all of the constant temperature decay studies. This was accomplished by means of the standardization lamp shown.

The spectral distribution of the luminescence was not determined in these experiments. However, it was visually examined and found to be of a light blue color. No apparent change in spectral distribution occurred during the course of the intensity decay.

The decay of the thermoluminescence of lithium fluoride with time is shown in Figs. 3, 4, and 5 for various temperatures. The decay is plotted in the form of $I^{-\frac{1}{2}}$ against time as indicated by Eq. (15).

For the temperature range between 150°C and 200°C the data follow straight lines as required by the equations. However, between 260°C and 290°C the data show pronounced curvature. At 304°C and 340°C the curvature appears in the initial portion of the decay but with additional time the data again become linear. At 370°C and at 420°C there is no further evidence of curvature.

This behavior can be explained on the basis of two luminescent processes one of which has a low trapping energy and the other, a higher trapping energy. At the lower temperatures only the low energy process contributes to the luminescence. As the temperature of the decay is increased the low energy process occurs more rapidly until at the high temperatures the high energy process is the only one which is left to give a measurable decay after the initial warm up period of the crystal.

In between these two temperature regions of low and high activation decay there is a region in which both processes contribute to the luminescence and thus the data cannot be represented by a simple $I^{-\frac{1}{2}}$ function.

According to Eq. (15) it is possible to determine the trapping energy from the plots of $I^{-\frac{1}{2}}$ against time at various temperatures. It has been shown that a plot of the logarithms of the squares of the slopes should also result in a straight line, the slope of which is $-E/R$.

Such plots were made for the two groups of straight lines obtained and shown in Fig. 6. The trapping energies corresponding to the two groups of lines are determined to be 19,800 cal./mole and 45,300 cal./mole from these plots.

GLOW CURVE EXPERIMENTS WITH IRRADIATED LITHIUM FLUORIDE

A second type of phenomena associated with thermoluminescence is the so-called "glow curves" of Randall and Wilkins which were first used by Urbach in studies on some of the alkali halides.

In this type of experiment the irradiated crystal is heated at a constant rate and the intensity of luminescence is observed to go through maxima which are related to the trapping energies contributing to the thermoluminescence. To describe this process, I is given by

$$I=-\bar{E}_t dn_3/dt \tag{16}$$

and the time variable is replaced by the temperature giving

$$I=-\bar{E}_t r dn_3/dT \tag{17}$$

where r is the rate of heating of the crystal.

Integration of Eq. (12) gives

$$\int_T^\infty I dT=\bar{E}_t r n_3. \tag{18}$$

Using this expression for n_3 in the kinetic treatment, and again introducing the temperature dependence of K gives

$$I^1=[(kK_0)/(\bar{E}_t r^2)]^1 \exp[-E_t/(2RT)] \int_T^\infty I dT. \tag{19}$$

The condition at the maximum can be described by setting the derivative of Eq. (19) equal to zero. This resulting expression can then be solved for E_t giving

$$E_t=2RT_m^2 I_m\left[\int_{T_m}^\infty I dT\right]^{-1} \tag{20}$$

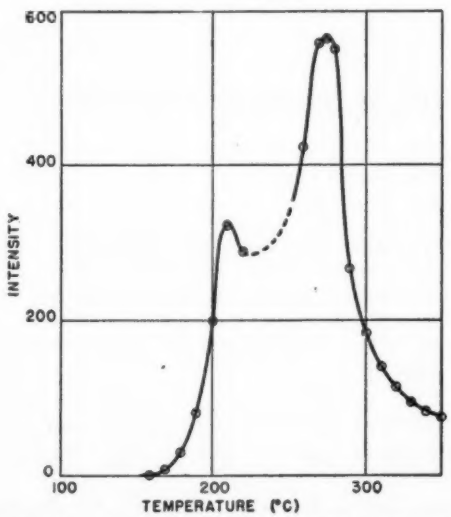

FIG. 8. Intensity temperature curve for lithium fluoride crystal annealed at 150°C after x-ray exposure.

TABLE I.

Rate of heating (°C/sec.)	T_{max} (°K)	I_{max}	$\int_{T_m}^\infty I dT$	E_t (cal./mole)
1.25	551	116	3040	45,800
1.26	534	116	3248	40,300
0.25	525	6.0	136	48,000
				Average 43,700

where the subscript m indicates the quantity at the intensity maximum.

Equation (20) indicates that we may evaluate E_t directly from the glow curve if $I_m T_m$ and $\int_{T_m}^\infty I dT$ can be determined.

Glow curves were obtained for the irradiated lithium fluoride crystals using the same apparatus, the temperature of the Woods metal both being measured at specified time intervals. These data allow one to plot the intensity as a function of temperature and a typical curve is shown in Fig. 7. It will be seen that there are two major peaks corresponding to the two major trapping energies observed in the previous experiments. In addition there is a small secondary peak which is too small to be detected by the constant temperature decay method.

The peak which occurs at the higher temperature is sufficiently isolated so that its corresponding trapping energy can be determined by using Eq. (20). The following table summarizes the results of measurements on several similar curves:

It should be noted in Table I that the value of E is relatively independent of the rate of heating used in the determination of the glow curve. This, of course, is in line with Eq. (20) which does not include the rate of heating.

The average value of 43,700 cal./mole for the second peak is in good agreement with the value of 45,300 cal./mole determined for the higher trapping energy by the constant temperature decay method.

MISCELLANEOUS EXPERIMENTS

1. Effect of Annealing

Crystals of lithium fluoride were exposed to x-rays in the manner described above and then placed in an oven

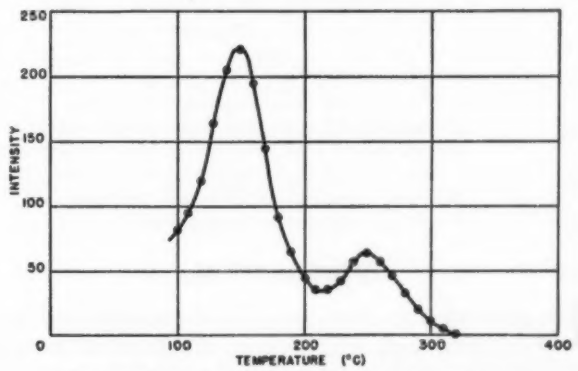

FIG. 9. Intensity temperature curve for lithium fluoride fused and ground.

held at 150°C for a period of five minutes. From a consideration of Fig. 6 it will be seen that the low energy traps are unstable at this temperature whereas the higher energy traps are still stable. Consequently, one might expect to be able to selectively empty the low energy traps and, if the retrapping concept of the simple model is correct, to increase the number in the higher energy traps. An intensity-temperature curve for a crystal treated in this manner is shown in Fig. 8, plotted on the same relative intensity scale as Fig. 7. The peak ordinarily occurring at 150°C corresponding to low energy trapping has been removed. However, the secondary peak and the high energy peak are still present. It will be noticed that the intensity of the high energy peak is increased by this treatment which can be interpreted to mean that more electrons are in the higher energy traps. These additional electrons can be accounted for on the basis of the simple model used in this paper by assuming that some of the electrons which were removed from the low energy traps were recaptured by the traps which were still stable.

2. Effect of Fusion

Experiments were run to determine the effect of fusion upon the characteristic glow curve of lithium fluoride. Some of the same crystalline material used in the above experiment was fused in a platinum crucible and cooled rapidly by pouring out on a clean platinum plate. The solid button was then ground in an agate mortar. Copper foil squares, one centimeter on a side were coated on one side with glyptol and a layer of the ground sample was pressed on top of this. These samples were then exposed to x-rays and glow curves were run in the manner described above. A typical curve is shown in Fig. 9. It will be seen that the two major peaks corresponding to the two major trapping energies are both present in about the same relation as for the single crystal samples. However, there is no evidence of the smaller secondary peak which appears for the single crystals on the high temperature side of the first peak. This suggests that this secondary peak is due to the presence of a volatile impurity such as one of the components of air in the original samples. The fusion and quick chilling removed the volatile component without noticeably affecting the other types of traps.

CONCLUSIONS

The kinetic equations derived from the simple reaction rate mechanism are adequate to describe the thermoluminescence of lithium fluoride as a function of time and temperature. Two major types of traps and one secondary type of trap have been found in lithium fluoride by constant temperature decay studies and by glow curve experiments. In the case where the trapping energy could be determined by both methods the values so obtained were in substantial agreement.

The observed effect of annealing at a temperature where the low energy trap alone is unstable can also be explained on the basis of the simplified model.

Fusion of the crystal and subsequent quick chilling of the melt removes the secondary traps but does not affect the two major traps. This indicates that the secondary traps may be due to volatile impurities, possibly one of the components of air.

Further experiments on the cause of these traps and on the general effects of impurities in the thermoluminescent process in alkali halides will be reported in a subsequent paper.

The author would like to acknowledge gratefully the advice and counsel of Professor Farrington Daniels during the course of this work. He would also like to acknowledge the assistance of Mr. Donald Saunders in taking the experimental data. He wishes to thank Professor Joseph Hirschfelder for helpful comments during the preparation of the manuscript.

THE JOURNAL OF CHEMICAL PHYSICS VOLUME 17, NUMBER 12 DECEMBER, 1949

Electrochemical Thermodynamics and Kinetics of Hydrogen Overvoltage

PIERRE VAN RYSSELBERGHE
Department of Chemistry, University of Oregon, Eugene, Oregon
(Received March 15, 1949)

The problem of hydrogen overvoltage is attacked by a method making systematic use of chemical and electrochemical potentials. More precise formulas are thereby obtained than in previous theories and a more definite interpretation of the transfer coefficient of Erdey-Grúz and Volmer is arrived at. The Tafel empirical equation is discussed and the existence, in some cases, of several Tafel regions is considered. Activation free energies, energies, and entropies for the discharge process are calculated and the mechanism involving formation of atomic hydrogen is shown to be entirely plausible.

INTRODUCTION

IN spite of the large amount of experimental and theoretical work which has accumulated in the field of hydrogen overvoltage, confusion and disagreement are still prevailing, as is characteristically shown by the papers presented at the General Discussion on Electrode Processes held by the Faraday Society.[1] Very

[1] Faraday Society Discussion, I (1947). See the papers on hydrogen overvoltage in Part II, pp. 50–126, and their discussion, pp. 127–141.

complete references to the literature of the subject are available in this most interesting series of papers and only the essential ones will be given in the present communication. The general approach to the kinetics of electrode processes is presented in convenient form by Glasstone, Laidler, and Eyring.[2] They give in their discussion a prominent place to their own theory of hydrogen overvoltage, which is one of the several theories considering the hydrogen ion discharge as the rate determining step. The opposite group of theories, of which the rather recent one by Hickling and Salt[3] is a good representative, considers the combination of hydrogen atoms as the rate determining step. Attempts at reconciling the two points of view by assigning them to the two extreme cases of low and high overvoltages instead of regarding them as mutually exclusive have met with difficulties.[4]

Another major difficulty is that pointed out by Frumkin[5] concerning the transfer coefficient α which is found empirically to be very often close to 0.5, a value which has so far received no theoretical explanation. The original proof that $\alpha=0.5$ given by Erdey-Grúz and Volmer[6] is actually no proof at all since these authors introduced the same transfer coefficient for the two opposite processes of discharge and ionization. The sum of the two coefficients being one, it follows then that obviously each one is equal to 0.5. In a later paper, however, Erdey-Grúz and Wick[7] introduced two transfer coefficients α and β not necessarily equal to each other.

These various difficulties have led us to a re-examination of the fundamental theory of overvoltage. In so doing we have found it particularly convenient and clear systematically to use chemical and electrochemical potentials and we believe that in this manner we have avoided certain pitfalls and errors of other treatments. As a result we have arrived, among several other improvements, at a concrete interpretation of the transfer coefficient.

ELECTRODE REACTIONS

Regardless of whether the hydrogen ion is still hydrated or not when it is being neutralized by an electron, we shall write the discharge process as

$$H^+ + \epsilon^- \rightarrow H, \qquad (1)$$

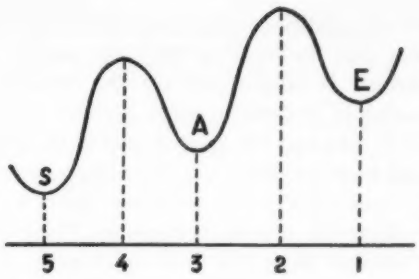

FIG. 1. Structure of double layer in neighborhood of electrode. S=solution, A=adsorbed layer, E=electrode.

which is eventually followed by the combination of two hydrogen atoms to molecular hydrogen

$$H + H \rightarrow H_2. \qquad (2)$$

Let us assume, for the time being, that these are the only steps of the mechanism. In a steady state corresponding to a constant overvoltage for a given current density the actual rates of these two processes must necessarily be equal although their specific rates may be different. Without having to decide in advance, by intuitive choice or otherwise, which of the two steps has the lower specific rate, the calculation of either one of the two rates which proves feasible will give the rate of the over-all process.

It seems clear, on the basis of previous theories, in particular those of the Erdey-Grúz-Volmer type, that the rate of step (1) is more amenable to calculation than that of step (2). Actually, other reactions can be expected to occur simultaneously with (1) and (2). Besides reaction (1) we may expect two more electron-consuming reactions if we assume that the only possible metallic hydride is MH. These two reactions are

$$H^+ + M + \epsilon^- \rightarrow MH \qquad (3)$$

$$H^+ + MH + \epsilon^- \rightarrow M + H_2. \qquad (4)$$

In the metallic phase we shall then have, besides reaction (2) above,

$$H + M \rightarrow MH \qquad (5)$$

$$H + MH \rightarrow M + H_2 \qquad (6)$$

$$MH + MH \rightarrow 2M + H_2. \qquad (7)$$

Finally, if we assume that M and MH are neither soluble nor volatile, we have the transfer reactions for H and H_2:

$$H\ (\text{metal}) \rightarrow H\ (\text{solution}) \qquad (8)$$

$$H\ (\text{metal}) \rightarrow H\ (\text{gas}) \qquad (9)$$

$$H_2\ (\text{metal}) \rightarrow H_2\ (\text{solution}) \qquad (10)$$

$$H_2\ (\text{metal}) \rightarrow H_2\ (\text{gas}). \qquad (11)$$

Our list is similar to that of Gatty and Spooner[8]

[2] Glasstone, Laidler, and Eyring, *The Theory of Rate Process* (McGraw-Hill Book Company, Inc., New York, 1941).

[3] A. Hickling and F. W. Salt, Trans. Faraday Soc. **38**, 474 (1942).

[4] See the remarks by A. Hickling, Faraday Soc. Discussion, I (1947), pp. 127 and 140.

[5] A. Frumkin, Faraday Soc. Discussion, I, 60 (1947).

[6] T. Erdey-Grúz and M. Volmer, Zeits. f. physik. Chemie **150**, 203 (1930). In a recent paper N. D. Sokolov (Doklady Akad. Nauk S.S.S.R. **61**, 87 (1948); Chem. Abs. **43**, 48 A (1948)) gives a theoretical calculation leading to the value 0.48 of the transfer coefficient.

[7] T. Erdey-Grúz and H. Wick, Zeits. f. physik. Chemie **162**, 53 (1932). See, for instance, the discussion by J. A. V. Butler in *Electrocapillarity: The Chemistry and Physics of Electrodes and Other Charged Surfaces* (Methuen and Company, Ltd., London, 1940), pp. 124–158, in particular p. 141.

[8] O. Gatty and E. C. R. Spooner, *The Electrode Potential Behaviour of Corroding Metals in Aqueous Solutions* (Clarendon Press, Oxford, 1938).

except for the additional reactions resulting from their assumption that the hydride MH_2 also exists.

The current is determined by the consumption of electrons and is, therefore, given by the total rate of reactions (1), (3), and (4). In each one of these reactions the forward rate depends on the production of activated hydrogen ions in a state enabling them to capture electrons from the metallic electrode. These activated ions are formed from the free hydrogen ions in the solution by a process which is the same for the three reactions. In other words, there is only one forward rate. The reverse rates, however, will be different as will be shown below.

When a steady state is established, the properties of the metallic surface do not change any more with time and enough hydrogen has been produced to saturate the surface and maintain equilibria between H, M, MH and H_2. We shall first leave out of consideration the overvoltages corresponding to very low current densities such as those studied by Bowden and Grew.[9] We shall assume that, at all overvoltages except the latter, for a given metal and a given electrolyte composition, all steady states characterized by a constant overvoltage for a constant current density correspond to the same composition of the metallic surface. This assumption brings a great deal of clarity into the whole problem of overvoltage.

DESCRIPTION OF THE DOUBLE LAYER IN THE NEIGHBORHOOD OF THE CATHODE—NOTATIONS

We shall use essentially the same configuration of the double layer as that of Kimball, Glasstone, and Glassner[10] sketched on Fig. 1. The curve represents qualitatively the values of the standard chemical potentials of the different forms of hydrogen ions and hydrogen atoms:

Position 1 corresponds to the metallic surface. Discharged hydrogen atoms under the three forms of atomic hydrogen, molecular hydrogen, and metallic hydride are located in this position.

Position 2 corresponds to activated hydrogen ions ready and able to become neutralized by the electrons which are in position 1.

Position 3 corresponds to adsorbed hydrogen ions in equilibrium with the free hydrogen ions in the solution.

Position 4 corresponds to activated hydrogen ions being adsorbed or desorbed.

Position 5 corresponds to free hydrogen ions in solution. All positions beyond 5 to the left are equivalent to 5 if ohmic RI corrections are made.

In 5, 4, and 3 the ions are probably solvated. In 2 they may still be solvated or the passage from 3 to 2 may involve separation from the solvent.

[9] F. P. Bowden and K. E. W. Grew, Faraday Soc. Discussion, I, 86 (1947).

[10] Kimball, Glasstone, and Glassner, J. Chem. Phys. **9**, 91 (1941).

The electric potentials in positions 1 to 5 are designated by ψ_1 to ψ_5. The potential difference $\psi_5-\psi_1$ between solution and electrode referred to a constant electrode (one of the calomel electrodes for instance) represents the cathodic potential under which electrolysis is taking place. If we call $\psi_5^r-\psi_1^r$ the reversible Nernst potential of a hydrogen electrode corresponding to the hydrogen ion activity of the solution, assumed to remain constant during electrolysis, the overvoltage is the difference

$$\omega=\psi_5-\psi_1-(\psi_5^r-\psi_1^r). \tag{12}$$

To simplify the writing of the mathematical formulas we shall represent by s_1, s_2, $\cdots$ the ratios ψ_1F/RT, ψ_2F/RT, $\cdots$ in which F is the Faraday, R the molar gas constant and T the absolute temperature. Similarly, we shall represent by m_1, m_2, $\cdots$ the chemical potentials μ_1, μ_2, $\cdots$ divided by RT and by $\bar{m}_1$, $\bar{m}_2$, $\cdots$ the electrochemical potentials $\bar{\mu}_1=\mu_1+\psi_1F$, $\cdots$ divided by RT. The ratio $\omega F/RT$ will be represented by v.

ADSORPTION EQUILIBRIUM BETWEEN POSITIONS 5 AND 3

During the existence of the steady state corresponding to electrolysis under the overvoltage ω and the current density I, the outer portion 5—4—3 of the double layer will certainly be of constant composition as long as the hydrogen ion activity of the solution remains constant and no concentration polarization occurs. This will be assumed to be the case in the whole treatment. We therefore can write the condition of electrochemical equilibrium for the hydrogen ion in positions 5 and 3:

$$\bar{\mu}_5=\bar{\mu}_3 \quad \text{or} \quad \mu_5+\psi_5F=\mu_3+\psi_3F. \tag{13}$$

The difference $\psi_3-\psi_5$ is the electrokinetic potential ζ and we thus have:

$$\zeta=(\mu_5-\mu_3)/F. \tag{14}$$

The relationship between the surface concentration C_3 of hydrogen ion in the layer 3 and the bulk activity a_5 could be derived from the chemical potentials

$$\mu_5=\mu_5^0+RT\ln a_5 \tag{15}$$

and

$$\mu_3=\mu_3^0+RT\ln C_3^z, \tag{16}$$

in which the μ^0's are standard chemical potentials of the hydrogen ion and z is an exponent greater than one, as in a Freundlich isotherm equation. Combination of (13), (14), (15) and (16) gives:

$$C_3^z=\exp(m_5^0-m_3^0)\cdot a_5\cdot\exp(-\zeta F/RT) \tag{17}$$

in which $\exp(m_5^0-m_3^0)$ is an equilibrium constant. Expression (17) is more complicated than that assumed by Frumkin,[11] even when z is taken equal to one.

[11] A. Frumkin, Zeits. f. physik. Chemie **160**, 116 (1932); **164**, 121 (1933); see Butler, reference 1, p. 132.

Equation (17) will, however, not be needed in our treatment.

KINETICS OF THE DISCHARGE PROCESS

The successive steps by which a hydrogen ion passes from the state of free ion in the bulk of the solution to that of neutral hydrogen atom on the surface of the electrode are the following:

$$H^+(5)\rightarrow H^+(4)\rightarrow H^+(3)\rightarrow H^+(2)\rightarrow H(1)-e^-(1) \quad (18)$$

in which states 4 and 2 are activated states. The net velocity of passage from 3 to 1 is the difference between the velocity of discharge from 3 to 1 and the velocity of ionization from 1 to 3. We have, according to the absolute rate theory,

$$v_{3-2}=(kT/h)C_{H^+2} \quad (19)$$

in which k is the Boltzmann constant, h the Planck constant and C_{H^+2} the concentration of the activated hydrogen ion in position 2 in equivalents/cm². Since there is equilibrium between H^+ in 2 and H^+ in 3 or 5 we may write, assuming an activity coefficient of 1 for the activated H^+ in 2,

$$v_{3-2}=(kT/h)\cdot a_5\cdot\exp(m_5^0-m_2^0)\cdot\exp(s_5-s_2) \quad (20)$$

in which m_5^0 and m_2^0 are the ratios over RT of the standard chemical potentials in 5 and 2. If we introduce the reversible hydrogen electrode potential corresponding to the activity a_5 we have

$$a_5=\exp(s_1^r-s_5^r). \quad (21)$$

Combining this exponent $s_1^r-s_5^r$ with the s_5-s_2 of Eq. (20) and introducing the overvoltage $\omega=vRT/F$ we have

$$s_5-s_2-(s_5^r-s_1^r)=s_5-s_1-(s_5^r-s_1^r)+s_1-s_2=v+s_1-s_2 \quad (22)$$

and hence

$$v_{3-2}=(kT/h)\cdot\exp(m_5^0-m_2^0)\cdot\exp(s_1-s_2+v). \quad (23)$$

We note that this expression does not include any concentration or activity factor. Any dependence of v_{3-2} on the H^+ activity would come through s_1-s_2. The specific rate of discharge can easily be obtained by dividing Eq. (20) by $C_5=a_5/f_5$ in which f_5 is the activity coefficient of H^+ in solution and another expression for this same specific rate can be deduced from (23), the precise form of the factor depending on electric potentials being thus obtained directly.[12]

For the reverse process in reaction (1) we have

$$v_{1-2}'=(kT/h)C_{H^+2}' \quad (24)$$

in which the concentration C_{H^+2}' is in equilibrium with H^+ in 1 or with $H(1)-e(1)$. We thus have

$$v_{1-2}'=(kT/h)\cdot\exp(m_1-\bar{m}_{e1}-\bar{m}_2^0) \quad (25)$$

in which m_1 is the ratio over RT of the chemical potential of H in 1, $\bar{m}_{e1}$ is the ratio over RT of the electrochemical potential of the electron in 1 and $\bar{m}_2^0$ is $m_2^0+s_2$. We also have

$$v_{1-2}'=(kT/h)\cdot\exp(m_1-m_{e1}-m_2^0)\cdot\exp(s_1-s_2). \quad (26)$$

For the reverse process in reaction (3) we have

$$v_{1-2}''=(kT/h)C_{MH^+2}' \quad (27)$$

in which the concentration C_{MH^+2}' of a complex MH^+, whose H^+ is in 2, is in equilibrium with MH^+ in 1 or with $MH(1)-e(1)$. We thus have

$$v_{1-2}''=(kT/h)\cdot\exp(m_{MH}-\bar{m}_{e1}-\bar{m}_{MH^+0}) \quad (28)$$

or also

$$v_{1-2}''=(kT/h)\cdot\exp(m_{MH}-m_{e1}-m_{MH^+0})\cdot\exp(s_1-s_2). \quad (29)$$

For the reverse process in reaction (4) we have

$$v_{1-2}'''=(kT/h)C'_{MH_2^+2} \quad (30)$$

in which the concentration $C'_{MH_2^+2}$ of a complex MH_2^+, whose H^+ is in 2, is in equilibrium with MH_2^+ in 1 or with $M(1)+H_2(1)-e(1)$. We thus have

$$v_{1-2}'''=(kT/h)\cdot\exp(m_M+m_{H_2}-\bar{m}_{e1}-\bar{m}_{MH_2^+0}) \quad (31)$$

or also

$$v_{1-2}'''=(kT/h)\cdot\exp(m_M+m_{H_2}-m_{e1}-m_{MH_2^+0})\cdot\exp(s_1-s_2). \quad (32)$$

Since the composition of the electrode surface is the same at all overvoltages we see that, in (26), (29), and (32), only the factor $\exp(s_1-s_2)$ is variable and the total reverse rate v_{1-2} is of the form

$$v_{1-2}=(kT/h)\cdot A\cdot\exp(s_1-s_2) \quad (33)$$

in which A can be determined by the equilibrium condition $v_{3-2}=v_{1-2}$ which holds when $v=0$. From (23) and (33) we easily find

$$A=\exp(m_5^0-m_2^0). \quad (34)$$

The net velocity of discharge is $v_{3-2}-v_{1-2}$ and the current density is thus

$$I=vF=(kTF/h)\cdot\exp(m_5^0-m_2^0)\cdot\exp(s_1-s_2)[\exp(v)-1]. \quad (35)$$

We thus obtain the very interesting result that the effective discharge potential is not ω but $\omega+\psi_1-\psi_2$, while the effective potential for the opposite process of ionization is $\psi_1-\psi_2$. If we write

$$I_0=(kTF/h)\cdot\exp(m_5^0-m_2^0), \quad (36)$$

we have

$$I=I_0\cdot\exp(s_1-s_2)\cdot[\exp(v)-1]. \quad (37)$$

[12] See the discussion of this point in Glasstone, Laidler, and Eyring (reference 2, p. 584) and in Kimball, Glasstone, and Glassner (reference 10).

One will easily verify that even at overvoltages as low as 0.1 volt the value of e^v is about 50.

APPEARANCE OF THE TAFEL EQUATION AND INTRODUCTION OF THE TRANSFER COEFFICIENT OF ERDEY-GRÚZ AND VOLMER

Let us consider a range of values of v for which the ionization process is negligible, i.e., for which e^v is much greater than 1. Equation (37) then reduces to

$$I=I_0\cdot\exp(s_1-s_2+v). \tag{38}$$

Let us examine the implications of the assumption that, in some cases at least, s_1-s_2 will be a linear function of v such that

$$s_1-s_2+v=\alpha v \tag{39}$$

in which α is a constant. Formula (38) becomes

$$I=I_0\cdot\exp(\alpha v) \tag{40}$$

which gives an equation of the form of Tafel's empirical equation

$$\omega=vRT/F=(RT/\alpha F)\ln(I/I_0). \tag{41}$$

We see that α is the transfer coefficient of Erdey-Grúz and Volmer. In more familiar form

$$\omega=b\log I+a \tag{42}$$

in which

$$b=2.3(RT/\alpha F)\quad\text{and}\quad a=-2.3(RT/\alpha F)\log I_0 \tag{43}$$

The foregoing reasoning gives to α a precise meaning. The effective discharge potential is

$$\begin{aligned}\alpha v&=s_1-s_2+[s_5-s_1-(s_5^r-s_1^r)]\\&=s_5-s_2-(s_5^r-s_1^r).\end{aligned} \tag{44}$$

One may assume $s_5=s_5^r$, the overvoltage and the reversible potential being then referred to the same reference electrode. We thus see that the effective discharge potential can in general be regarded as equal to $s_1^r-s_2$. Since s_1^r is constant for a given hydrogen ion activity the effective discharge potential differs by a constant term from the potential at the activation peak 2 of Fig. 1. For the rather common case $\alpha=0.5$ we have $s_1-s_2=-0.5v$. If the effective discharge potential is $(RT/F)\alpha v$ the effective potential for the opposite process is $(RT/F)(\alpha-1)v$. The difference between these two potentials is $(RT/F)v$. The quantity $1-\alpha$ is the β of Erdey-Grúz and Wick[7] and we have $\alpha+\beta=1$, a feature of our treatment which coincides with assumptions made in the majority of the other treatments. (See, however, the discussion by Audubert.[13])

An important feature of the domain of validity of Tafel's equation is that the relationship between overvoltage and current density is independent of the hydrogen ion activity of the solution. It has already been found above (Eq. (35)) that the current does not depend explicitly on the H^+ ion activity of the solution. Validity of the Tafel equation in a range of I and ω values would imply that α is independent of H^+ ion activity, while departure from the Tafel behavior could be assigned to the dependence of α on pH or to a more complicated dependence of s_1-s_2+v on v such as

$$s_1-s_2+v=\alpha v+\gamma v^2+\cdots. \tag{45}$$

LOW AND HIGH OVERVOLTAGES—EXISTENCE OF SEVERAL TAFEL REGIONS

Experimental confirmation of the Tafel equation has been obtained for many electrode materials and many different compositions of solutions. The summary of Bowden and Agar[14] has been reproduced and discussed by many authors.[15,2,7] Observations made by Bowden and collaborators[9,14] show that in general the Tafel equation for hydrogen overvoltage holds well between current densities of 10^{-2} to 10^{-7} amp./cm^2. In 0.2 Normal H_2SO_4 electrolyzed with a mercury cathode the transfer coefficient was found to be 0.52 and the extrapolated I_0 defined by formula (40) was found to be 6×10^{-12} amp./cm^2. Bowden and Grew[9] found that, for the same solution and metal, at current densities from 10^{-6} to 10^{-9} or even 10^{-10} amp./cm^2 the overvoltage also follows a Tafel equation with a transfer coefficient of 0.45, the extrapolated I_0 being now 4×10^{-11} amp./cm^2. On the basis of formulas (36) and (40) we see that the different I_0 values of the two Tafel regions characterized by $\alpha=0.52$ and $\alpha=0.45$ correspond to different values of $m_5^0-m_2^0$. In other words, changes in α necessarily imply changes in the chemical activation free energy. One can easily calculate that the difference in the chemical potential μ_2^0 between the two Tafel regions is about 1.1 kilocalorie, the value for the lower current densities being the higher. If one examines other overvoltage data one notices that it is sometimes possible as an approximation to distinguish several Tafel regions corresponding to successive linear segments of what is actually a continuous curve. The region corresponding to $\alpha=0.5$ is often an extended one but it will cover a different range of current densities for different metals and different electrolyte compositions. As the current density increases the plots of overvoltage against the logarithm of the current density tend to flatten out, the overvoltage becoming very nearly constant. The values of α are then in the neighborhood of 1 and can even become greater than 1, provided no concentration polarization occurs. A value of α larger than 1 would indicate a reversal of sign for s_1-s_2 as is shown by formula (39). For α exactly one $s_1-s_2=0$. Values of α which decrease upon increase of current density after the $\alpha=0.5$ region indicate concentration polarization.

[13] R. Audubert, Faraday Soc. Discussion, I, 72 (1947).

[14] F. P. Bowden and J. N. Agar, Ann. Rep. on Progress Chem. (Chem. Soc. London) **35**, 90 (1938).

[15] H. J. Creighton, *Principles and Application of Electrochemistry* (John Wiley and Sons, Inc., New York, 1943), see Vol. I, p. 253.

It appears as a whole that previous theories of overvoltage have been oversimplified and that α varies continuously with a simultaneous variation of the chemical potential μ_2^0. As an approximation one may, in some cases at least, consider α as constant over more or less considerable ranges of current density, μ_2^0 being then also constant. In the theory presented here the variation of the current density is due to the combination of effects described by formula (35) in which only the universal constants and m_5^0 are truly constant.

VERY SMALL OVERVOLTAGES

At very small overvoltages, such that $e^v=1+v$, the experimental data available point towards the proportionality of I with v. Formula (35) gives us then, if we still admit the linear relation (39), with a value of α different from that in the Tafel region,

$$I=(kTF/h)\cdot\exp(m_5^0-m_2^0)\cdot[v+(\alpha-1)v^2]. \quad (46)$$

Since v^2 would then be negligible in comparison with v the theory developed here is in agreement with experimental observations.

ACTIVATION FREE ENERGY, ENERGY AND ENTROPY OF THE DISCHARGE PROCESS

The quantity $m_5^0-m_2^0$ is obtained by extrapolation of any portion of the $\omega-\ln I$ plot corresponding to a constant value of α, for instance for the various cases of the tabulation of Bowden and Agar.[14]

For instance, with 0.2 Normal H_2SO_4 and a mercury cathode in the middle Tafel region for which $\alpha=0.52$, we have, as standard free energy change,

$$\Delta F^{\ddagger}=RT(m_2^0-m_5^0)=\mu_2^0-\mu_5^0=40 \text{ kilocalories}. \quad (47)$$

Such a value is not surprising since the activated state 2 of the hydrogen ion is to be regarded as being at least at the same free energy level as the product of the reduction in its adsorbed state on the electrode.

Our Eq. (21) implies

$$\tfrac{1}{2}\mu_{H_21}^0-\mu_5^0+\tfrac{1}{2}RT\ln p_{H_2}=0 \quad (48)$$

in which p_{H_2} is the pressure of H_2 in a gaseous phase in equilibrium with the H_2 adsorbed on the electrode. Adsorbed atomic hydrogen has a chemical potential which can be written

$$\mu_{H1}=\mu_{H1}^0+RT\ln p_H \quad (49)$$

such that[16]

$$\mu_{H1}^0-\tfrac{1}{2}\mu_{H_21}^0=48.3 \text{ kilocalories} \quad (50)$$

the pressure p_H being that of an atomic hydrogen phase in equilibrium with the H adsorbed on the electrode. Combination of (48), (49) and (50) gives

$$\mu_{H1}=48.3+\mu_5^0+RT\ln(p_H/p_{H_2}^{\frac{1}{2}}). \quad (51)$$

The difference $\mu_{H1}-\mu_5^0$ can be as large as 40 kilocalories which leads to a plausible value of the $p_H/_{H_2}p^{\frac{1}{2}}$ ratio. With 0.2 Normal H_2SO_4 and bright platinum we would have 32 kilocalories instead of 40 for the difference $\mu_2^0-\mu_5^0$. The corresponding energies of activation are 18 kilocalories for mercury and 9.5 to 11.5 (or 10.5 as an average) kilocalories for bright platinum[2] making the products of standard entropies of activation with temperature -22 and -21.5 kilocalories respectively.

These calculations, which can easily be extended to many other cases, seem to be in general agreement with a discharge process to atomic hydrogen in spite of opinions by some authors that energies of activation like 18 or even 10.5 kilocalories are too large for a mechanism involving simple addition of an electron to a hydrogen ion or proton and of opinions by other authors that these same values are too small for a mechanism of neutralization to atomic hydrogen. The values of the free energy of activation are of the right order of magnitude for the latter mechanism. The entropies of activation appear very large in absolute value but they indicate that the activated state 2 represents a much more organized state of the hydrogen ions than their standard state in solution.

The very valuable review of the hydrogen overvoltage problem by Bockris[17] came to our attention after the completion of the present manuscript. His discussion of the various theories does not require any modification in the foregoing treatment. The only point on which we wish to comment is the pH dependence of the overvoltage-current density relationship which is observed in some cases. Our treatment would account for such a dependence through a variation of the chemical portion of the activation free energy $\mu_2^0-\mu_5^0$, a possible dependence of α on pH or also by introducing, at the starting point (Eq. (20)), an activity coefficient for the activated hydrogen ion in position 2.

In connection with Bockris' brief reference to the effect of dissolved oxygen on hydrogen overvoltage, it might be well to mention the detailed experimental investigation of Piontelli and Poli.[18] In this same connection the extensive literature on the polarographic reduction of oxygen and of hydrogen ion is of direct significance.

The reason for undertaking the foregoing theoretical study of hydrogen overvoltage arose in connection with some aspects of a research project entitled "Polarographic Study of Corrosion Phenomena" being carried out under a contract between the University of Oregon and the Office of Naval Research. To the latter organization and to Dr. Paul Delahay, Research Associate on the ONR program, with whom the contents of this paper were thoroughly discussed, the writer expresses his gratitude. He is also indebted to Dr. Samuel Glasstone for the loan of unpublished material on electrode processes and overvoltage.

[16] W. M. Latimer, *The Oxidation States of the Elements and their Potentials in Aqueous Solutions* (Prentice-Hall, Inc., New York, 1938), p. 29.

[17] J. O'M. Bockris, Chem. Rev. **43**, 525 (1948).

[18] R. Piontelli and G. Poli, Atti reale accad. Italia. Mem. classe sci. fis. mat. e nat. **13**, 903 (1942).

The Infra-Red Spectrum and Molecular Configuration of Hydrogen Persulfide*

M. KENT WILSON** AND RICHARD M. BADGER
Gates and Crellin Laboratories of Chemistry, California Institute of Technology, Pasadena, California
(Received March 25, 1949)

The infra-red spectrum of hydrogen persulfide has been investigated in the region 1.5 to 15μ, and vibrational assignments have been made. The perpendicular band at 2μ has been studied under high resolution and a value for one of the rotational constants has been obtained. The data strongly support a chain structure for hydrogen persulfide and probably exclude *cis*- or *trans*-planar structures, but give no very definite information regarding the azimuthal angle.

1. INTRODUCTION

ALTHOUGH the structure of hydrogen peroxide has been the object of much experimental work and speculation,[1] comparatively little attention has been paid to its sulfur analog, hydrogen persulfide. Stevenson and Beach[2] investigated the persulfide by means of electron diffraction and reported the $S-S$ distance to be 2.05±0.02A. Since this distance corresponds closely to the single-bond distance for sulfur, 2.08A,[3] they concluded that the persulfide molecule had the chain structure with the hydrogens attached to different sulfur atoms. It is reasonable to expect that the structures of hydrogen persulfide and hydrogen peroxide should be similar and that the former molecule should have at least the symmetry C_2, which is reasonably well established for hydrogen peroxide by the spectroscopic observations of Zumwalt and Giguère,[4] but the angles between the two planes including the heavy atoms and a hydrogen atom may well be somewhat different in the two molecules.

The only previously existing spectroscopic data on hydrogen persulfide are three Raman shifts of 510, 882, and 2513 cm^{-1}, respectively, obtained on the liquid by Fehér and Baudler.[5] The present work is concerned with an investigation of the infra-red vibration spectrum of this substance and the rotational structure of the first overtone of the $S-H$ stretching vibration at 2μ in an attempt to obtain further information regarding the molecular structure.

2. EXPERIMENTAL PROCEDURE

Materials and Methods

The hydrogen persulfide used in this investigation was prepared by the procedure detailed by Butler and Maass.[6] Briefly this method consists of dropping a sodium polysulfide solution into cold, concentrated hydrochloric acid and fractionally distilling under vacuum the mixture of hydrogen polysulfides formed. The colorless redistilled hydrogen persulfide was used immediately for the spectroscopic investigations. Two separate preparations were made and no spectroscopic difference was noted.

Hydrogen persulfide decomposes rapidly in the presence of alkali. To minimize this decomposition, the Pyrex cells were first cleaned in boiling concentrated nitric acid and thoroughly dried. The sodium chloride windows with Koroseal gaskets were then clamped in place, the cell evacuated, and filled with dry hydrogen chloride gas. The hydrogen chloride gas was allowed to remain in the cell for 10–15 minutes before the cell was again evacuated and the hydrogen persulfide introduced.

At 25°C the vapor pressure of hydrogen persulfide is 109 mm.[5] With this vapor pressure a path length of 50 cm was found to be adequate.

Prism Instrument

The vibration spectrum was traced from 1.5 to 15μ with a Beckman IR-2 spectrophotometer which has a resolution of about 3 cm^{-1} at 9μ. The wave-length drive and slit control of our instrument are coupled in such a fashion that the intensity of the background is reasonably constant through the region 4–13μ, though a noticeable dip occurs in the vicinity of 9.3μ. A Brown recorder was used to give a continuous plot of intensity *versus* wave-length.

Grating Instrument

The 2μ-band of hydrogen persulfide was also investigated under high dispersion with an automatic recording one-meter grating vacuum spectrograph which has recently been described by Badger, Zumwalt, and Giguère.[7] The spectra were taken in the first order of a replica grating with 7500 lines per inch, using a lead sulfide cell as the photo-sensitive element and a slit width of 0.05 mm, corresponding to 0.85 cm^{-1}.

* Contribution No. 1264 from the Gates and Crellin Laboratories of Chemistry.

** Present address: Mallinckrodt Laboratory, Harvard University, Cambridge, Massachusetts.

[1] G. Herzberg, *Infrared and Raman Spectra of Polyatomic Molecules* (D. Van Nostrand Company, Inc., New York, 1945), p. 301.

[2] D. P. Stevenson and J. Y. Beach, J. Am. Chem. Soc. **60**, 2872 (1938).

[3] L. Pauling, *The Nature of the Chemical Bond* (Cornell University Press, Ithaca, New York, 1942).

[4] L. R. Zumwalt and P. A. Giguère, J. Chem. Phys. **9**, 458 (1941).

[5] F. Fehér and M. Baudler, Zeits. f. Elektrochemie **47**, 844 (1941).

[6] K. H. Butler and O. Maass, J. Am. Chem. Soc. **52**, 2184 (1930).

[7] Badger, Zumwalt, and Giguère, Rev. Sci. Inst. **19**, 861 (1948).

The instrument was calibrated by observing first and higher orders of visible and near-infra-red argon lines from a sodium vapor lamp containing argon at low pressure. The wave-lengths of these standards were corrected to vacuum. In the case of lines having a sharp maximum it is believed that our wave-length and frequency determinations are accurate to 1 part in 25,000.

3. EXPERIMENTAL RESULTS AND INTERPRETATION

Vibrational Structure

Traces of the prismatic spectrum from 1 to 12μ and of the overtone band at 2μ under high dispersion are shown in Figs. 1 and 2, respectively. The frequencies of the band centers are given in Table I together with the previous Raman data on the liquid and probable assignments. The assignments were made on the assumption of a chain structure, which, as will be shown, is compatible with the observations. Structures resembling formaldehyde or chloramine appear to be excluded by the data.

If hydrogen persulfide has the chain structure with point group symmetry C_2, the six normal modes in probable order of decreasing frequency may be described as unsymmetrical and symmetrical $S-H$ vibrations, $\nu_5(b)$ and $\nu_1(a)$; symmetrical and unsymmetrical bending motions, $\nu_2(a)$ and $\nu_6(b)$; an $S-S$ valence vibration $\nu_3(a)$; and a torsional oscillation, $\nu_4(a)$. In principle ν_5 and ν_6 may both give rise to hybrid bands unless the molecule has higher symmetry than C_2. The relative intensities of the "parallel" and "perpendicular" components of the hybrid fundamental of ν_5 should be quite sensitive to the azimuthal angle, but the fundamental of ν_6 should in any case be expected to have predominantly "parallel" character. The remaining fundamentals must give rise to bands of pure "perpendicular" type. Owing to the relatively large mass of the central atoms, the C_2 model is very nearly a symmetrical rotator for any value of the azimuthal angle, and one might anticipate difficulty in distinguishing bands in which the change in electric moment is parallel to major or intermediate axes of inertia. For a planar *trans*-structure, ν_1 should be inactive, and ν_5 active, but for smaller azimuthal angles it is at present not possible to predict their relative activities.

TABLE I.

Infra-red bands (vapor) ν(cm^{-1})	Relative intensity* (a)	Raman shifts[5] (liquid) ν(cm^{-1})	Assignment
—	—	510	$\nu_3(a)$
—	—	882	$\nu_2(a)$
886 {875	0.035	—	$\nu_6(b)$
886 {897	0.043		
—	—	2513	$\nu_1(a)$
2577	0.015	—	predominantly $\nu_5(b)$
3065	0.002	—	$\nu_3+\nu_5(B)$
3400	0.002	—	$\nu_5+\nu_6(A)$ or $\nu_2+\nu_5(B)$
5007.2	0.003	—	$\nu_1+\nu_5(B)$ and possibly $2\nu_1(A)$

* The figure given is the apparent absorption coefficient at the maximum of the band defined by the equation $a=(1/pl)\log T_0/T$ and measured under conditions such that the absorption was between 15 and 50 percent. The equivalent path, pl, is expressed in cm atmos. at 0°C.

In the neighborhood of the $S-H$ fundamentals only one absorption region was observed with center at 2577 cm^{-1}, which might include both ν_1 and ν_5. Though no structure was resolvable with the low dispersion employed, the narrowness of the band suggests, however, that it is predominantly of parallel type and should be ascribed chiefly to $\nu_5(b)$. The Raman shift of 2513 cm^{-1} in the liquid is presumably $\nu_1(a)$. In the vapor this frequency is probably appreciably greater and not greatly different from ν_5. The second harmonic $S-H$ band appears to have a strong "parallel" type component, as is discussed below, and consequently must be attributed at least in considerable part to $\nu_1+\nu_5(B)$. It may contain traces of $2\nu_1(A)$ or of absorp-

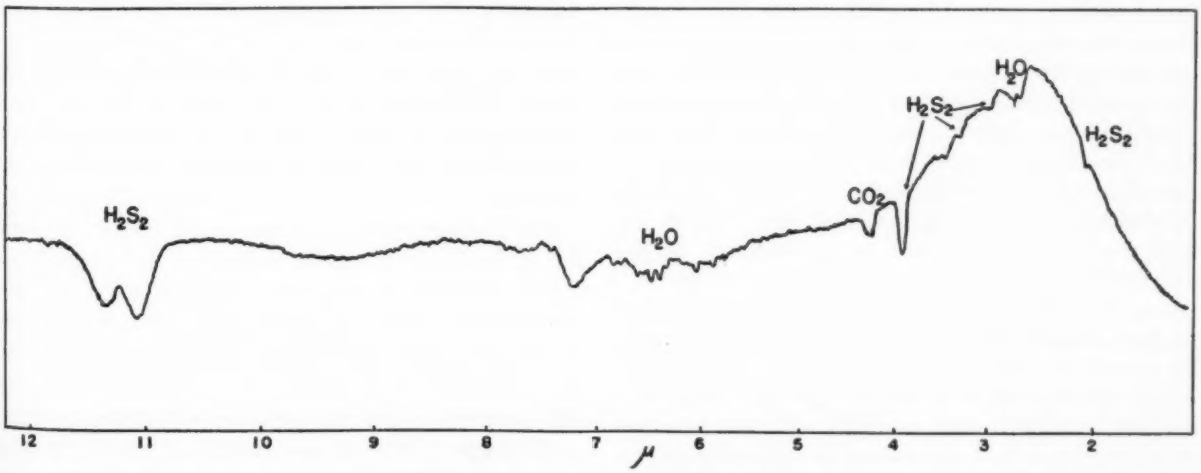

FIG. 1. Prismatic spectrum of hydrogen persulfide; equivalent path length=6.2 cm (S.T.P.); temp.=25°C. The minima at about 7.2μ and 3.3μ are "ghost" bands due to the contamination of a window in the spectrograph.

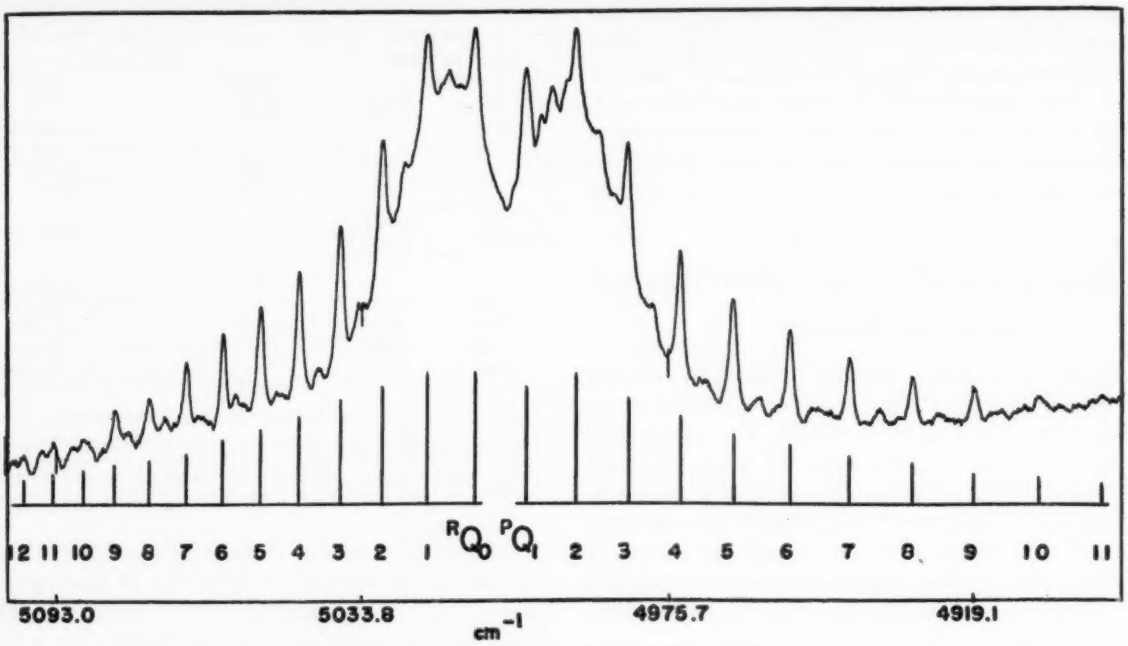

FIG. 2. Rotational structure of the hydrogen persulfide band at 2μ; equivalent path length = 12.4 cm (S.T.P.).

tion from the first excited level of ν_4. We regard it as unlikely that $2\nu_5(A)$ will appear with significant intensity. In the spectra of the non-linear triatomic molecules there is a conspicuous absence of harmonics or combination bands in which the unsymmetrical frequency ν_3 would occur in an even multiple.

The frequency of the $S-H$ fundamental differs no more from the frequencies in H_2S than should be expected from the difference in reduced masses. This indicates that the $S-H$ distance is not greatly different in the two molecules and is possibly some evidence for the chain structure of the polysulfide.

In the region $5-15\mu$ only one band of appreciable intensity was found. This moderately strong band at 886 cm^{-1} has a frequency less than that of ν_2 in H_2S by a factor slightly greater than the square root of two. It is rather definitely of the parallel type, and the separation of the maxima in P and R branches is that which would be predicted from the calculated moments of inertia which will be discussed below. With the limited resolution employed the failure to observe a Q-branch is not unexpected since it should be relatively weak because of the large ratio of major to minor moments of inertia and should be "washed out" by the noticeable band convergence. The resolution was adequate to distinguish a perpendicular type structure, had such been present with appreciable intensity. We can, with assurance assign this band to $\nu_6(b)$, the unsymmetrical bending vibration of the chain structure. The Raman shift at 882 cm^{-1} is probably $\nu_2(a)$, but the very near equality of ν_6 and ν_2 is somewhat surprising and indicates very little interaction between the two $H-S-S$ bendings.

The frequency of the 11μ-band, its structure, and the absence of other bands of appreciable intensity in the region $5-15\mu$ are very good evidence for the chain structure of hydrogen persulfide. A formaldehyde structure would have three bending frequencies, presumably all on the short wave side of 15μ, and all should be expected to have reasonable intensity in the infra-red. Only one of these fundamentals $\nu_2(a_1)$, would have parallel structure, and its frequency might be expected to lie close to that of ν_2 in H_2S. In a model of the chloramine type even the analogous vibration would give rise to hybrid bands, and the previous remark regarding frequency would be applicable.

The weak bands at 3065 cm^{-1} and 3400 cm^{-1} may reasonably be assigned to combinations of a $S-H$ valence vibration with the $S-S$ valence frequency, $\nu_3(a)$, and with one of the bending frequencies, respectively. The Raman shift in the liquid at 510 cm^{-1} must certainly be ascribed to the $S-S$ vibration, and the frequency in the vapor is probably not significantly different.

The fundamental of the twisting frequency, $\nu_4(a)$ should be expected to lie well below the limit of the region available to rock salt optics. A search for this fundamental would be worth while since its intensity would give some information regarding the angle between the $H-S-S$ planes. Its presence in the infra-red spectrum would exclude the possibility of a planar, *cis*-structure for hydrogen persulfide, which possibly cannot be completely ruled out by our present observations.

Structure of the Overtone Band at 2μ

Although the absorption region at 5007.2 cm^{-1} shows rather strong and well-resolved ^{P}Q- and ^{R}Q-branches the distribution of intensity is not that to be expected in a band of pure perpendicular type. The strong concentration of absorption in the unresolved background immediately to both sides of the band center indicates the presence of a fairly strong parallel type component which can result only from $\nu_1+\nu_5(B)$. We believe that the most probable explanation of this band is that it is a truly hybrid structure similar to the third harmonic band of hydrogen peroxide[4] and is due almost entirely to the transition just mentioned. Some weak maxima lying between the intense ^{P}Q- and ^{R}Q-branches may conceivably be due to a weak and nearly coincident $2\nu_1(A)$, or to absorption from the first excited level of ν_4. If this explanation is correct the planar *cis*-structure for hydrogen persulfide is of course excluded because of the hybrid structure of the band. Furthermore, the relatively greater intensity of the perpendicular component of the band as compared with both overtone hydrogen peroxide bands[4,8] suggests that the azimuthal angle may be slightly larger in the persulfide than in the peroxide. It is of particular interest that the persulfide absorption shows no indication of the doubling found in both overtone bands of the OH frequency in hydrogen peroxide, and attributed by Zumwalt and Giguère to a double minimum in the torsional potential.

The frequencies of the principal maxima of the 2μ-band are given in Table II, together with rotational constants for the upper and lower states. In Table III are given approximate moments of inertia and rotational constants calculated for C_2 models for hydrogen persulfide with several azimuthal angles.

The moment of inertia about the axis of symmetry is given by the expression:

$$I_s=2m_Hp^2+2m_Sa^2/4 \qquad (1)$$

and the remaining moments of inertia by the expression:

$$I_{1,2}=2m_H[(n-m)^2+p^2\sin^2(\varphi+\alpha)]+2m_S[m^2+(a^2/4)\sin^2\varphi] \qquad (2)$$

when φ is given the two complementary values given by the relation below. Quantities entering into these equations are defined as follows:

$$n=b\sin\beta\cos\theta$$
$$m=m_Hn/(m_H+m_S)$$
$$p^2=[(a/2)+b\cos\beta]^2+(b\sin\beta\sin\theta)^2$$
$$\alpha=\tan^{-1}[(b\sin\beta\sin\theta)/(b\cos\beta+a/2)]$$
$$\varphi=-\tfrac{1}{2}\tan^{-1}[\sin2\alpha/(\cos2\alpha+m_Sa^2/4m_Hp^2)]$$

where a is the $S-S$ distance, b the $S-H$ distance, β the angle between the $S-H$ bond and the projection of the $S-S$ bond, 2θ the azimuthal angle, or angle between $H-S-S$ planes, and m_H and m_S are the masses of the hydrogen and sulfur atoms.

[8] P. A. Giguère (to be published).

TABLE II. Principal maxima in the hydrogen persulfide band at 5007.1 cm^{-1}.

K	$^{P}Q(K)$ (cm^{-1})	$^{R}Q(K)$ (cm^{-1})	$\frac{^{R}Q(K)-{}^{P}Q(K)}{4K}$	$\frac{^{R}Q(K-1)-{}^{P}Q(K+1)}{4K}$
0		5012.0		
1	5002.3	21.0	4.67	4.80
2	4992.8	29.5	4.59	4.73
3	83.2	37.6	4.53	4.60
4	73.4	45.6	4.51	4.64
5	63.4	52.9	4.48	4.64
6	52.8	60.3	4.48	4.63
7	41.8	67.3	4.48	4.65
8	30.1	74.6	4.51	4.64
9	18.7	81.1	4.51	4.66
10	06.8	87.1	4.51	4.62
11	4896.2	93.0	4.47	
12		99.4		

Rotational Constants

$(A'-B')=4.50\ cm^{-1}$
$(A''-B'')=4.64\ cm^{-1}$

In making the calculations, a was given the electron diffraction value, 2.05A. For reasons given above the $H-S$ distance was taken to be 1.334A and the $H-S-S$ angle was assumed to be 92° 16′, the apex angle in H_2S.

The small moment of inertia varies roughly as the square of the $S-H$ distance, which is not known exactly. It is very insensitive to the $S-S$ distance, the $H-S-S$ angle and to the azimuthal angle. A change of 0.01A in the $S-H$ distance produces a greater effect than a change of 180° in the azimuthal angle. Consequently it is evident that no very definite conclusion regarding the azimuthal angle can be drawn from the rotational spacing of the 2μ-band. Though the agreement is best for an azimuthal angle of about 90° it must be regarded as satisfactory for any angle.

The general appearance of the band is compatible with the angle mentioned. None of the ^{P}Q- or ^{R}Q-branches are missing near the band center nor do they show evidence of splitting, and the minimum at the center may be attributed largely to the presence of the parallel type band component rather than to asymmetry. The hydrogen persulfide molecule becomes a symmetrical top when the azimuthal angle is very close to 90° but it is not very unsymmetrical even for the two extremes of this angle. The angle could consequently deviate rather greatly from 90° without having a significant effect upon the appearance of the band.

TABLE III. Moments of inertia and rotational constants for hydrogen persulfide model.

Azimuthal angles (2θ)	Moments of inertia ($g\ cm^2\times10^{40}$)			Rotational constants (cm^{-1})	
	I_1	I_s	I_2	B	$(A-B)$
0°	5.76	115	121	0.24	4.62
60°	5.75	116	120	0.24	4.63
140°	5.72	120	116	0.24	4.65
180°	5.72	121	115	0.24	4.65

It should be noted, however, that the rotational constant shows that the $S-S-H$ angles must be near to 90° unless the $S-H$ distance is abnormally long. This fact offers very strong support for the chain structure, since such angles are rather improbable for any other structure.

4. CONCLUSION

As has been shown, the character of the hydrogen persulfide spectrum offers very strong support for a chain structure of the molecule, but gives no very direct information regarding the azimuthal angle, though the apparent hybrid character of the 2μ-overtone band makes the *cis*-planar model quite improbable. The significant differences between the overtone $S-H$ band and the O—H overtones of hydrogen peroxide are probably related to differences in the angle in these two molecules. It is hoped that a study of the fundamental of ν_4, the twisting vibration, may be made in the near future. The presence of this band in the infra-red spectrum would definitely exclude the *cis*-planar form. If the molecule has neither planar form the double minimum in the torsional potential would probably give rise to a detectable doubling of this band which would possibly permit an estimate to be made of the azimuthal angle.

THE JOURNAL OF CHEMICAL PHYSICS VOLUME 17, NUMBER 12 DECEMBER, 1949

The Vibrational Spectra of Molecules and Complex Ions in Crystals. II. Benzene*†

ROBERT D. MAIR** AND DONALD F. HORNIG
Metcalf Research Laboratory, Brown University, Providence, Rhode Island

(Received March 28, 1949)

The infra-red spectrum of crystalline benzene has been studied at −12°C, −65°C and −170°C as well as the liquid at 28°C. The lines are extremely sharp, the mean line width for fundamentals being 7 cm^{-1} in the crystal. In three cases, it is less than the spectral slit width. All out-of-plane degenerate modes are split by about 10 cm^{-1}. Selection rules are obeyed and agree with the reported x-ray structure. All ungerade fundamentals are observed directly, some for the first time. Fifty-two combination bands are observed. The frequency assignments of Ingold *et al.* are confirmed except for the B_{2u} species. Evidence is cited for re-assigning ν_{14} from 1648 cm^{-1} to 1310 cm^{-1} and ν_{15} from 1110 cm^{-1} to 1150 cm^{-1}. Ingold's isotopic data does not conflict with this change. Combination frequencies involving torsional lattice modes are apparently observed at −170°C.

I. INTRODUCTION

THE study of the infra-red and Raman spectra of crystals is a potentially powerful but as yet little used tool in the determination of molecular and crystal structure. In the first paper in this series[1] it was shown that in the harmonic approximation the spectrum of the crystalline solid (Raman or infra-red) should consist of only a relatively small number of extremely sharp lines, and that in this approximation the simple selection rules suggested by Halford[2] are correct. It was further pointed out that, particularly in the case of molecular crystals, this state of affairs should be most nearly approached at low temperatures.

The utility of the crystal in studying molecular vibrations arises, as has been pointed out by Halford,[2] from the fact that the crystalline field produces a new set of selection rules which are, in general, less strict than for the vapor. Some of the previously forbidden vibrations may become allowed, but their frequencies will be shifted very little, if at all. In addition, the fact that the lines are usually very sharp, particularly at low temperatures, may be of considerable importance in dealing with a spectrum as complicated as that of benzene. The polarization properties of the lines may supply further information.

The determination of the normal vibrations of the benzene molecule has been the subject of a long series of investigations.[3]

The most successful attack has been the comprehensive study by Ingold and co-workers,[4] utilizing the infra-red and Raman spectra of benzene and five deutero-benzenes, together with the Redlich-Teller frequency product rule. Their frequency assignments appear to be largely correct.

Several attempts have been made to calculate the benzene frequencies from an assumed potential function.[5–8] In particular, Miller and Crawford have calcu-

* The work reported here was supported in part by the ONR under Contract N6ori-88, Task 1.

† Based on a thesis submitted by Robert D. Mair in partial fulfillment of the requirements for the degree of Doctor of Philosophy at Brown University.

** Present address: Hercules Experiment Station, Hercules Powder Company, Wilmington, Delaware.

[1] D. F. Hornig, J. Chem. Phys. **16**, 1063 (1948). Hereafter called I.

[2] R. S. Halford, J. Chem. Phys. **14**, 8 (1946).

[3] See G. Herzberg, *Infra-Red and Raman Spectra of Polyatomic Molecules* (D. Van Nostrand Company, Inc., New York, 1945), p. 362.

[4] C. K. Ingold *et al.*, Parts I–VIII, J. Chem. Soc., 912–987 (1936); Part IX, *ibid.*, 1210 (1936); Part X, *ibid.*, 1728 (1937); Parts XI–XXI, *ibid.*, 222–333 (1946). Hereafter designated simply by the part number.

[5] E. B. Wilson, Jr., Phys. Rev. **45**, 706 (1934).

[6] K. W. F. Kohlrausch, Zeits. f. physik. Chemie **308**, 305 (1935).

[7] R. C. Lord and D. H. Andrews, J. Phys. Chem. **41**, 149 (1937).

[8] W. G. Penney and J. Duchesne, Bull. Soc. Roy. Sci., Liege **11**, 514 (1939).

lated the frequencies of the out-of-plane vibrations with considerable success[9] and have recently given a similar treatment of the in-plane vibrations.[10]

In the present investigation the spectrum of crystalline benzene has been studied between −12°C and −170°C. The spectrum of the liquid was also studied to provide auxiliary information useful in the interpretation of the solid spectra, since in the liquid all selection rules are relaxed. Halford and Schaeffer[11] had previously obtained the infra-red spectrum of solid benzene in the vicinity of its melting point, but with low resolving power. It was felt desirable to redetermine this spectrum with better resolution, particularly at low temperatures. This has been done, revealing a characteristic sharpness of bands and a wealth of detail, both of which have proved very useful in interpreting the data. The spectrum of the liquid, obtained under the same conditions, reveals more structure than was observed either by Ingold *et al.*[12] or by Halford and Schaeffer. It may be noted that it agrees in every detail with the spectrogram reported by the U. S. Naval Research Laboratories.[13]

Interpretation of these spectra has yielded information of several sorts. In particular, except for ν_{14} and ν_{15}, it has confirmed the assignments given by Ingold *et al.*[14] for the nine frequencies forbidden in the spectrum of the free molecule. Six of these have been observed directly and the others are upheld by combination bands. Secondly, it has demonstrated the chief features predicted in I for crystalline spectra. Selection rules appear to be strictly obeyed, for both internal and lattice modes as well as their combinations, and temperature effects, such as a general sharpening of lines at low temperatures, are plainly shown.

II. CRYSTALLINE BENZENE

It was shown in I that the symmetry properties of active fundamentals can be completely described by the factor group of the space group which is isomorphous with the crystallographic point group. It was shown further that selection rules could be obtained from the local symmetry of the molecule in the crystal, the site group of Halford. These same statements are approximately correct for combinations and overtones.

The x-ray structure of benzene has been determined most completely by Cox[15] who found the space group V_h^{15} with 4 molecules per unit cell. From the tables published by either Niggli[16] or Halford,[2] the site symmetry of the benzene molecules is then C_i. The thirty modes of vibration should therefore result in 30 distinct frequencies as compared to twenty under D_{6h}, although the splitting due to removal of the degeneracies may not be resolved. The three rotations of the free molecule correspond to three torsional oscillations in the crystal whereas the three translations remain translations of the crystal.

The fifteen internal modes deriving from the *gerade* representations of D_{6h} plus the three torsional lattice modes belong to the species A_g of C_i. The fifteen deriving from the *ungerade* representations of D_{6h} belong to the species A_u of C_i. All A_g modes are allowed in the Raman spectrum and all A_u modes are allowed in the infra-red spectrum. All combinations are allowed, A_gA_g and A_uA_u in the Raman spectrum, and A_uA_g in the infra-red spectrum. It is apparent that in crystalline benzene the mutual exclusion rule should apply rigorously. These selection rules apply without distinction to lattice as well as internal modes of vibration.

III. EXPERIMENTAL METHODS AND TECHNIQUES

The spectrometer used was a Perkin-Elmer Model 12B in which the single beam optical system had been replaced by a double-beam arrangement. By means of rotating sector mirrors, radiation from the source was sent into the monochromator alternately over one or the other of two optically identical paths. As used here, the instrument produced a point-by-point record of the transmission of the sample and the blank alternately. (These were placed one in each beam.) In addition, the instrument recorded the zero or base line after each transmission point. This very effectively eliminated errors due to drift, which is especially important in low temperature work where the base line may drift appreciably and irregularly. The records were reduced to superimposed base line, sample and blank curves by drawing smooth envelopes through the three sets of points.

Water and carbon dioxide were effectively eliminated by blowing dry nitrogen through the spectrometer housing. The strongest water band in the 6μ-region showed a maximum absorption of less than 30 percent and, in fact, only the stronger lines of this band could be detected.

The amount of stray radiation reaching the thermocouple was found to be appreciable only in the region near the cut-off of each prism. It was reduced by a factor ten by employing a scattering filter of the type described by McGovern and Friedel.[17] The filter used had a transmission of 4 percent at 2μ, 45 percent at 4μ, 75 percent at 6μ, and 85 percent at 7μ.

[9] F. A. Miller and B. L. Crawford, Jr., J. Chem. Phys. **14**, 282 (1946).

[10] B. L. Crawford, Jr. and F. A. Miller, J. Chem. Phys. **17**, 249 (1949).

[11] R. S. Halford and O. A. Schaeffer, J. Chem. Phys. **14**, 141 (1946).

[12] See reference 4, Part IV.

[13] A. P. I. Research Project, 44, Spectrogram No. 307, contributed by the U. S. Naval Research Laboratory, Washington, D. C.

[14] See reference 4, Part XXI.

[15] E. G. Cox, Proc. Roy. Soc. **135A**, 491 (1932).

[16] P. Niggli, *Geometrische Kristallographie des Diskontinuums* (Gebruder Borntraeger, Leipzig, 1919), Table IV, pp. 404–411.

[17] J. J. McGovern and R. A. Friedel, J. Opt. Soc. Am. **37**, 660 (1947).

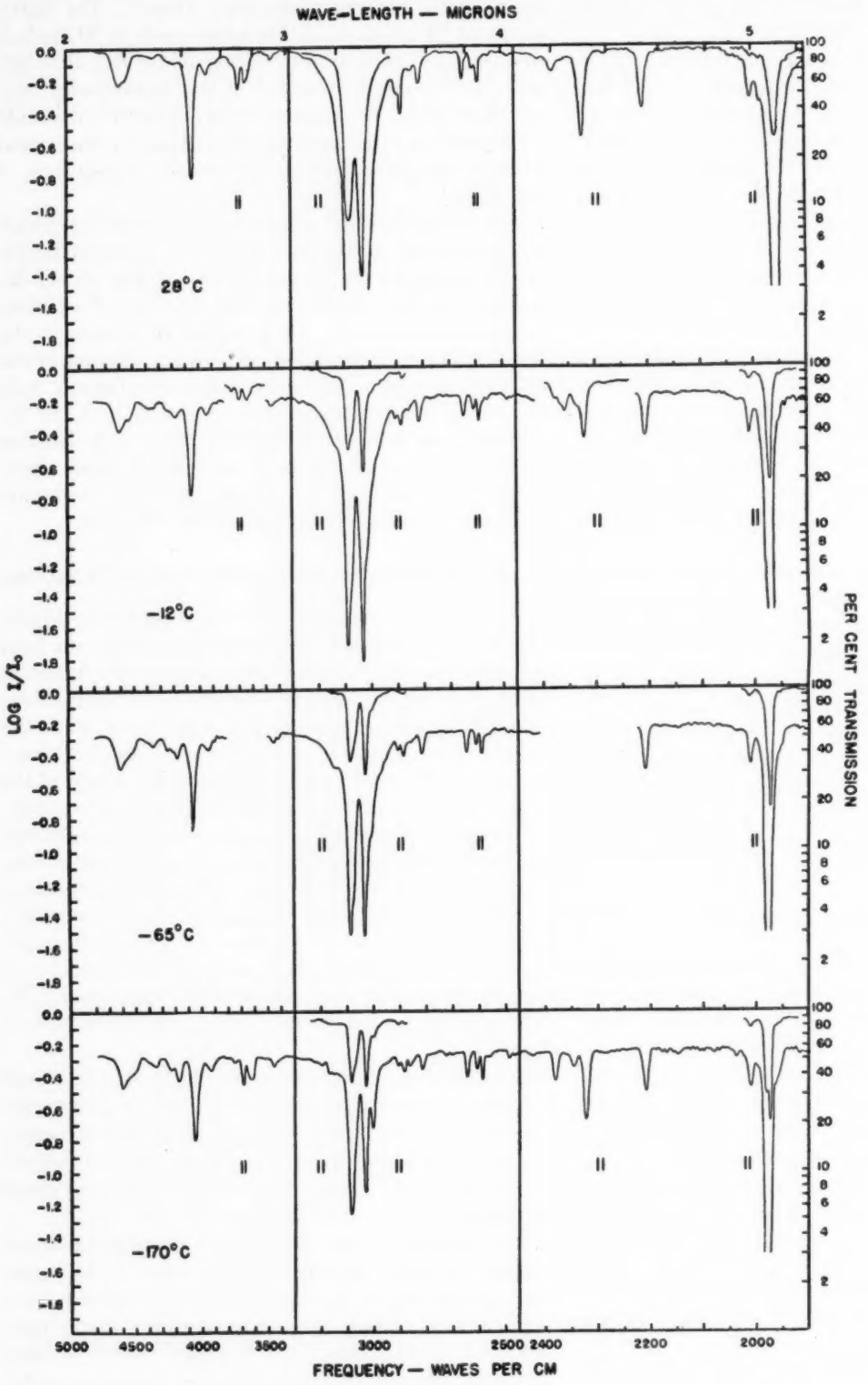

FIG. 1a. The infra-red spectrum of liquid and crystalline benzene between 5000 cm^{-1} and 1900 cm^{-1}. Spectral slit widths used in each region are indicated.

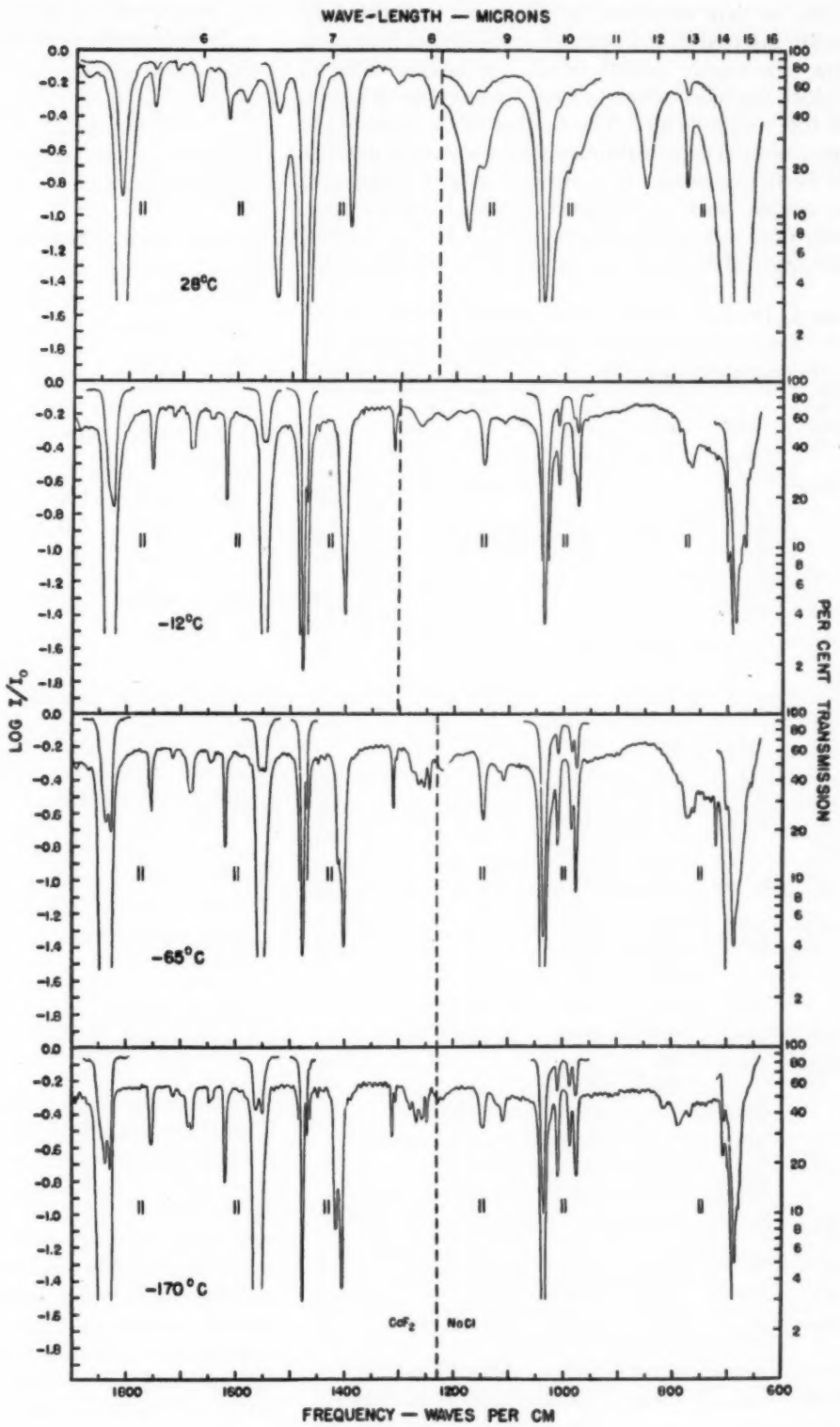

FIG. 1b. The infra-red spectrum of liquid and crystalline benzene between 1900 cm^{-1} and 650 cm^{-1}. Spectral slit widths used in each region are indicated.

The absorption cell was of the transmission type similar to that described by Wagner[18] and could be directly inserted in the beam. It consisted of four main parts—the copper cooling block, the coolant reservoir to which the block was attached, the enveloping jacket, and the sample holder. The cooling block consisted of a piece of solid copper through which a rectangular hole had been machined. Two annular copper plugs kept the sample holder positioned in the block between them. One was soldered permanently in the opening while the other could be removed to introduce the sample holder. A thermocouple junction was soldered directly to the side of the block.

The sample holders were made from single crystal sheet silver chloride. This material has been described by Kremers.[19] Sample holders were constructed by placing a mica or silver chloride spacer between two rectangles of silver chloride, one 3 mm, the other 0.25 mm thick. The two pieces of silver chloride were then sealed around all sides with an electrically heated platinum wire loop, except for a minute opening left at one end for introducing the sample. When the sample holder had been filled, this opening was also sealed. The spacers used were either 50 microns or 250 microns thick.

Previous attempts to use potassium bromide were unsuccessful due to air bubbles being drawn in, and

TABLE I. The infra-red frequencies of liquid and solid benzene.

Observed frequencies and intensities 28°C	−12°C	−65°C	−170°C	Assignment	D_{6h} species	Calc. freq. Liq.	Solid
~675 *s*	685 *s*	687 *s*	687 *s*	ν_{11}	A_{2u}	...	...
...	700 *ww*	702 *ww*	707 *ww*	...	...	...	...
776 *mw*	...	...	...	$\nu_9-\nu_{16}$	A_{2u}	773	759 769
...	769 *mw*	770 *mw*	769 788 *mw* 816	ν_{11}+torsional lattice modes		...	768 785 811
852 *m*	...	...	...	ν_{10}	E_{1g}	849[a]	854 864
975	975 982 *mw*	975 984 *mw*	975 987 *mw*	ν_{17}	E_{2u}	...	...
995	...	...	...	ν_5 or ν_1	B_{2g}, A_{1g}	...	...
~1013	1010 *mw*	1010 *mw*	1009 *mw*	ν_{12}	B_{1u}	...	...
1038 *s*	1036 *s*	1036 *s*	1035 *s*	ν_{18}	E_{1u}	...	...
...	1109 1117 *ww*	1109 1117 *ww*	1109 ~1120 *w*	$\nu_{16}+\nu_4$	E_{1u}	1108	1108 1118
1150	1147 *mw*	1147 *mw*	1147 *mw*	ν_{15}	B_{2u}	...	...
1179 *s*	...	...	...	ν_9	E_{2g}	1178[a]	...
...	1215 *ww*	1220 *ww*	1220 *ww*	$3\nu_{16}$	A_{2u}	1215	1215 1245
1246 *mw*	1245 1260 *mw*	1245 1255 1265 *mw* 1275	1249 1258 1267 *mw* 1279	$\nu_{16}+\nu_{10}$	E_{1u}	1255	1259 1269 1269 1279
...	1305	1305	1306	$\nu_{14}(C^{13}C_5^{12}H_6)$	B_{2u}	...	...
1310 *w*	1311 *w*	1311 *w*	1312 *w*	ν_{14}	B_{2u}	...	...
1394 *ms*	1401 *ms*	1402 ~1412 *ms*	1405 1416 *ms*	$\nu_{18}+\nu_5$	E_{1u}	1400	1400 1410
...	1470 *w*	1470 *w*	1470 *w*	$\nu_{19}(C^{13}C_5^{12}H_6)$	...	...	...
1478 *s*	1478 *s*	1478 *s*	1478 *s*	ν_{19}	E_{1u}	...	...
1528 *ms*	1544 1551 *ms*	1547 1555 *ms*	1551 1563 *ms*	$\nu_{11}+\nu_{10}$	E_{1u}	1524	1551
1587 ~1605 *mw*	...	...	...	ν_8 in res. with $\nu_1+\nu_6$	E_{2g} E_{2g}	1596[b] 1597	... ...
1618 *mw*	1618 *mw*	1618 *mw*	1618 *mw*	$\nu_{12}+\nu_6$	E_{1u}	1616	1615
1647 ?	1644 *ww*	1644 *ww*	1645 *ww*	$\nu_{18}+\nu_6$	E_{1u}	1644	1642
1671 *mw*	1679 1684 *mw*	1680 1685 *mw*	1680 1687 *mw*	$\nu_{17}+\nu_4$	E_{1u}	1678	1678 1690
1713 *ww*	1715 *ww*	1714 *ww*	1714 *ww*	$\nu_{12}+\nu_4$	A_{2u}	1713	1713
1754 *mw*	1754 *mw*	1754 *mw*	1754 *mw*	$\nu_{15}+\nu_6$	E_{1u}	1756	1753
1815 *s*	1825 ~1835 *s*	1828 1836 *s*	1829 1839 *s* ~1850	$\nu_{17}+\nu_{10}$	E_{1u}	1824	1829 1839 1841 1851

TABLE I. *Continued.*

Observed frequencies and intensities 28°C	−12°C	−65°C	−170°C	Assignment	D_{6h} species	Calc. freq. Liq.	Solid
1877 *ww*	1886 *ww*	1891 *ww*	1893 *ww*	$\nu_{18}+\nu_{10}$	A_{2u}	1886	1901
1959 *s*	1971 *s*	1973 ~1980 *s*	1974 1986 *s*	$\nu_{17}+\nu_5$	E_{1u}	1970	1970 1982
1987 *ww*	...	...	...	$\nu_{12}+\nu_{17}$	E_{1g}	1985	...
2003 *w*	2008 *w*	2012 *w*	2011 *w*	$\nu_{16}+\nu_5$ or $\nu_{12}+\nu_8$	A_{2u} A_{2u}	2001 2005	2011 2005
2208 *mw*	2206 *mw*	2210 *mw*	2210 *mw*	$\nu_{18}+\nu_9$	E_{1u}	2216	2210
2324 *mw*	2322 *mw*	...	2323 *mw*	$\nu_{15}+\nu_9$	E_{1u}	2328	2325
...	...	...	2347 *ww*	$\nu_{19}+\nu_{10}$	A_{2u}	2327	2342
2381 *ww*	2380 *ww*	...	2382 *ww*	$\nu_{18}+\nu_3$	E_{1u}	2378	2376
2591 2612 *ww*	2591 2610 *ww*	2588 2610 *ww*	2588 2608 *ww*	$\nu_{12}+\nu_8$[c]	E_{1u}	2597 2615	2597 2615
2648 *ww*	2648 *ww*	2647 *ww*	2647 *ww*	$\nu_{19}+\nu_5$	E_{1u}	2656	2652
2815 *ww*	2817 *ww*	2817 *ww*	2816 *ww*	$\nu_{19}+\nu_3$	E_{1u}	2818	2818
2845 *ww*	...?	...?	2862 *ww*	...	...	...	...
2883 *w*	2884 *ww*	2884 *ww*	2883 *ww*	...	...	...	...
2903 *ww*	2907 *ww*	2907 *ww*	2907 *ww*	$\nu_{14}+\nu_8$	E_{1u}	2906	2906
...	~2980 ?	~2990 ?	3000 *w*	...	...	...	...
3030 3080 *s*	3033 3087 *ms*	3030 3086 *ms*	3030 3085 *ms*	ν_{20} in res. with $\nu_{19}+\nu_8$	E_{1u} E_{1u}	3063 3074	3063 3074
...	~3070	~3070	~3070	ν_{13}	B_{1u}	...	...
...	~3140	3150 *ww*	3160 *ww*	...	...	...	...
3445 *ww*	3455 *ww*	3450 *ww*	3455 *ww*	$\nu_{16}+\nu_7$	A_{2u}	3452	3455
3645 3695 *w*	3640 3695 *w*	... ...	3630 3688 *w*	ν_{20}[d]$+\nu_8$	E_{1u} E_{1u}	3642 3696	3642 3696
3940 *ww*	3940 *ww*	3940 *ww*	3935 *ww*	$\nu_{20}+\nu_{10}$	A_{2u}	3912	3917
4050 *m*	4063 *m*	4063 *m*	4057 *m*	several possibilities	...	...	...
4200 *ww*	4180 *ww*	4177 *ww*	4177 *ww*	$\nu_{15}+\nu_7$	E_{1u}	4197	4187
...	~4240	4250 *ww*	4235 *ww*	$\nu_{13}+\nu_9$	E_{1u}	4248	4243
4350 *ww*	4360 *ww*	4360 *ww*	4355 *ww*	$\nu_{14}+\nu_7$	E_{1u}	4357	4352
~4560 4600 *m*	4605 *m*	4605 *m*	4605 *m*	several possibilities	...	...	...

[a] Observed in Raman spectrum.
[b] Calculated from Raman doublet.
[c] Including resonance with $\nu_1+\nu_8$.
[d] Includes resonance with $\nu_{19}+\nu_8$.

[18] E. L. Wagner, thesis, Brown University, Providence, Rhode Island (1948).

[19] H. C. Kremers, J. Opt. Soc. Am. **37**, 337 (1947).

cracking of the sample holder when it was cooled. In the silver chloride sample holders, the 3-mm layer provided both rigidity and heat conduction from the center of the film. The 0.25-mm layer, on the other hand, was flexible and yielded to atmospheric pressure when the volume decreased as the benzene solidified. This prevented the formation of vacuum pockets within the sample and was a major factor in minimizing scattering from the film.

The 0.25-mm silver chloride was found to cause pronounced interference bands throughout the sodium chloride and potassium bromide prism regions. The computed spacing of the interference peaks was $\Delta\nu=9.7$ cm^{-1}. The observed value varied from 9.5 to 10 cm^{-1}. For the thick plate $\Delta\nu=0.8$ cm^{-1} and the bands could not be detected. The interference bands were suppressed by rolling the silver chloride with a 35-mm glass tube on a glass plate so as to form shallow corrugations on the top surface. Thus a non-uniform thickness was obtained while the bottom surface remained essentially plane.

The temperatures attained by benzene films in this absorption cell were somewhat above those of the cooling block. This was demonstrated by embedding a thermocouple in a rectangle of 3-mm silver chloride of the same size as the sample holder, and measuring its temperature while the block was cooled. With the cooling block at −15°C, −78°C and −195°C, equilibrium temperatures of the silver chloride plate were −12°C, −65°C, and −170°C. These probably correspond quite well to the film temperatures during absorption measurements.

The benzene was purified by the method of Kraus and Fuoss.[20] It was subjected to four successive fractional crystallizations, the resulting material freezing completely at the constant temperature of 5.51±0.01°C. When care was taken to exclude moisture, it solidified to an ice-like mass composed of large single crystals. The benzene was stored over sodium-lead alloy in an all-glass still protected from atmospheric moisture.

The sample holder was filled by standing it vertically, with inlet downward, in a small bulb attached to a reservoir of dry, air-free benzene, thoroughly evacuating bulb and sample holder, condensing benzene vapor from the reservoir until the bottom of the holder was immersed in liquid, and then slowly admitting atmospheric pressure to the bulb. This last step forced liquid benzene through the tiny inlet, completely filling the space between the silver chloride plates. The sample holder was then removed from the bulb and the inlet sealed quickly with the hot platinum wire. If any benzene evaporated during this operation, so that an air bubble appeared in the film, the inlet was reopened and the sample holder refilled.

The behavior on freezing varied somewhat from film to film. If the sample holder had not been tightly sealed, or if it contained a small air bubble or even a considerable amount of dissolved air, a cavity formed in the middle section of the film on solidification. If cooling was too rapid the supercooled benzene froze instantly to a translucent film which scattered incident radiation severely. All samples used for absorption measurements were observed, however, to crystallize slowly over a period of several seconds to a transparent continuous film. The 50μ-thickness, in particular, showed only slight visible indications of solidification and caused practically no scattering, as the experimental curves of Section IV indicate. The 250μ-films, on the other hand, scattered 40 to 50 percent of the incident radiation. As would be expected, the scattering increased as the temperature was lowered, and was slightly less at long than at short wave-lengths.

It seems possible that essentially non-scattering films of any thickness could be obtained by long periods of annealing at a temperature close to the melting point. For example, when a translucent 250μ-film was held at a temperature of 3 to 4°C for a period of two hours, a transparent spot appeared in the center and gradually enlarged toward the edges of the film, while the scattering decreased from 90 percent to 50 percent. It was observed that while a film was being cooled to low temperatures, scattering increased least when the cooling rate was very slow.

A careful analysis of errors arising in reading band centers, in calibration, in changing prisms and from

TABLE II. Fundamental benzene frequencies.

Active in D_{6h} model				Inactive in D_{6h} model			
Number and species	Frequencies This research Liquid	Solid	Ingold *et al.*	Number and species	Frequencies This research Liquid	Solid	Ingold *et al.*
$\nu_{11}(A_{2u})$	675*	687*	671§	$\nu_{12}(B_{1u})$	1010**	1010*	1010§§
$\nu_{18}(E_{1u})$	1038*	1036*	1037§	$\nu_{13}(B_{1u})$	3071†	3069†	3060§§
$\nu_{19}(E_{1u})$	1478*	1478*	1485§	$\nu_{14}(B_{2u})$	1310*	1312*	1648§§
$\nu_{20}(E_{1u})$	3063†	3063†	3073† 3080§§	$\nu_{15}(B_{2u})$	1150*	1147*	1110§§
$\nu_1(A_{1g})$	992§	990††	991.6§	$\nu_{16}(E_{2u})$	405**	405** 415**	405§§
$\nu_2(A_{1g})$	3062§	3060††	3061.9§	$\nu_{17}(E_{2u})$	975*	975* 987*	970§§
$\nu_6(E_{2g})$	606§	606**	605.6§	$\nu_3(A_{2g})$	1340**	1340**	1326§§
$\nu_7(E_{2g})$	3047§	3040††	3046.8§	$\nu_4(B_{2g})$	703§§	703**	703§§
$\nu_8(E_{2g})$	1596§§	1596**	1596§§	$\nu_5(B_{2g})$	995**	995**	985§§
$\nu_9(E_{2g})$	1178§	1174††	1178.0§				
$\nu_{10}(E_{1g})$	849§	854** 864**	848.9§				

* Observed, this research.
** Inferred, this research.
§ Observed, Ingold *et al.*
§§ Inferred, Ingold *et al.* Many of these values were confirmed by combinations observed here. See Table I.
† Assigned from Leberknight (see reference 23). 3073 cm^{-1} value is for benzene vapor.
†† Observed, Sirkar (see reference 21) Epstein and Steiner (see reference 22).

[20] C. A. Kraus and R. M. Fuoss, J. Am. Chem. Soc. **55**, 21 (1933).

[21] S. C. Sirkar, Ind. J. Phys. **10**, 109 (1936); **10**, 189 (1936).

[22] H. Epstein and W. Steiner, Nature **133**, 910 (1934); Zeits. f. physik. Chemie **26B**, 131 (1934).

[23] C. E. Leberknight, Phys. Rev. **43**, 967 (1933).

calibration drifts indicates that frequency assignments are good to within ± 10 cm^{-1} at 3μ and ± 0.6 cm^{-1} at 8μ with the calcium fluoride prism, and to within ± 2.4 cm^{-1} at 8μ and ± 0.4 cm^{-1} at 15μ with the sodium chloride prism. The reproducibility should be somewhat better since calibration errors are not involved.

IV. EXPERIMENTAL RESULTS

The absorption spectra of liquid benzene at room temperature, and of crystalline benzene at $-12°$C, $-65°$C and $-170°$C, in the wave-length region from 2μ to 15.6μ are presented in Figs. 1a and 1b. No scattering corrections have been made on these experimental curves, and the noise level has not been smoothed out. Table I lists the frequencies of the line centers as well as our assignments of the lines. The latter will be discussed in Sections VI and VII.

The data presented have been obtained with a calcium fluoride and a sodium chloride prism. The spectrum of the 15μ-region was obtained as well with a potassium bromide prism. Since it was identical with that obtained with the sodium chloride prism except for the effects of lower resolving power, it has not been reproduced here.

The spectra were obtained for a film thickness of approximately 250μ over the whole wave-length range, and of approximately 50μ in the vicinity of intense bands. The same thin film was used throughout the investigation, while three thick films were necessary. The complete solid spectra at $-170°$C and $-65°$C, and the spectrum from 2μ to 8μ at $-12°$C were determined from one such film. The remainder of the $-12°$C spectrum was obtained from another, and the liquid spectrum from a third. Although spacers of the same thickness were used for all three, it should be borne in mind that because of the low dimensional stability of the thin silver chloride sheet, the thicknesses of the three films were probably only approximately equal.

During the absorption runs at $-65°$C and $-12°$C the cell became contaminated with carbon dioxide gas and a trace of isopropyl alcohol. This invalidated portions of the spectra in the vicinity of 3750 cm^{-1} and 2350 cm^{-1}. These portions were redetermined later on the same film used to complete the $-12°$C spectrum, but at this temperature only.

Although the sample holders were constructed so as to suppress interference effects, series of very weak bands, regularly spaced at ~ 10 cm^{-1} apart, which must be residual interference bands, still occur throughout the spectra. Because of this, little significance can be attached to extremely weak bands of about the same intensity.

The spectrum of the liquid indicates that the benzene used in this research was of high spectroscopic purity. It is identical in every detail with that obtained by the U. S. Naval Research Laboratory, Washington, D. C.,[13] for a NBS Standard 99.95 ± 0.02 mole percent specimen except that the spectrum reported here is more completely resolved in some regions.

A striking feature of the solid spectra is the extreme sharpness of many of the bands, particularly of those assigned to the fundamental frequencies. Excluding the band system at about 3060 cm^{-1} which involves two fundamentals plus a combination and the 685 cm^{-1} band which is broadened for another reason, the seven remaining fundamentals at 1478, 1312, 1147, 1036, 1010, 987, and 975 cm^{-1} have half-widths varying from 3.0 to 11 cm^{-1} with an average of 7 cm^{-1}. This contrasts with widths of 13, 15, and 16 cm^{-1} for the three corresponding bands in the liquid spectrum which are not overlapped by Raman-active fundamentals. The narrowness of these bands may be emphasized by remarking that the 1312 cm^{-1} band at all three temperatures, and the 1478 and 1010 cm^{-1} bands at the lowest temperature, are no wider than the spectral slit width. Their half-widths are 3, 5, and 5.5 cm^{-1}, respectively. These are among the narrowest infra-red bands ever reported.

A possible source of error in these measurements is the effect of reflection and scattering. They both depend upon the refractive index and the extinction coefficient at any wave-length. In the vicinity of a strong absorption band both quantities vary widely and may give rise to spurious peaks or shoulders, particularly on the high frequency side of the peak.[24] In the case of benzene the possible magnitude of reflection effects is negligible, but the presence of considerable scattering makes errors from this source possible, particularly in the 250μ-films. However, the thin film was essentially non-scattering, so that such effects should appear much more prominently in the thick film. Examination of Figs. 1a and 1b indicates that there are no significant scattering effects in the spectra presented here.

Comparison of the spectra at room temperature and at $-12°$C reveals all the changes generally observed to accompany transition from the liquid to the solid state. Most striking is the disappearance of two moderately strong bands at 850 cm^{-1} and 1180 cm^{-1} and a weaker band at 1585 cm^{-1}, as well as components at 995 cm^{-1} and 1605 cm^{-1}. There is also a general pronounced sharpening of the remaining bands, disclosing in a number of cases a composite structure. In addition, frequency shifts of more than 5 cm^{-1} are observed for nine bands, the largest being from 1527 cm^{-1} to 1547 cm^{-1}. For all but the band at 776 cm^{-1}, these shifts are to higher frequencies.

A number of temperature effects are observed within the three solid spectra. One such is the improved characterization of band structure at lower temperatures. Single lines are more sharply defined, and the components of composite bands more clearly resolved. In fact, the double nature of the strong band at 1975 cm^{-1} is revealed only at the lowest temperature. Apparent

[24] W. C. Price and K. S. Tetlow, J. Chem. Phys. 16, 1157 (1948).

changes in the integrated intensities of some of the strong bands are observed. Those at higher frequencies have essentially constant intensities, but the intensities of the three strong lower frequency fundamentals at 1478 cm^{-1}, 1036 cm^{-1}, and 687 cm^{-1} decrease with temperature in the respective ratios 100:82:64, 100:85:63, and 100:92:63. The combination band at about 1400 cm^{-1} maintains a constant intensity, however.

The band at 1110 cm^{-1} exhibits an unusual effect. As the temperature of the film is lowered, the intensity of this band increases manyfold. This is accompanied by a decrease in intensity of the neighboring band at 1147 cm^{-1}, which is identified as one of the B_{2u} fundamentals. The behavior appears to be due to an interesting case of Fermi resonance. It is discussed in Section VII.

Frequency changes are generally slight, being of about the order of the reproducibility, although in the case, for example, of the band at 1547 cm^{-1}, there is evidence of a real trend to slightly higher frequencies as temperature is decreased.

V. ASSIGNMENTS

Our assignments for the fundamental vibration frequencies are given in Table II, along with those obtained by Ingold *et al.* They have been obtained from a number of sources and represent what we believe to be the best choices available. Their origin is indicated in the table. They are classified according to their D_{6h} species, since this proves convenient in referring to the work of other investigators and in comparison with the free molecule. Wilson's number system[5] for the benzene fundamentals is used.

These assignments, with but two exceptions, agree with those of Ingold *et al.* to better than 1 percent. The other two, ν_{14} and ν_{15} of the species B_{2u}, were observed directly in the present investigation and differ from their earlier assignments by 20 percent and 3.2 percent, respectively. Since the evidence for these assignments is independent of that of Ingold *et al.*, based on the Redlich-Teller product rule, it will be discussed in some detail.

VI. THE ACTIVE D_{6h} FUNDAMENTALS

A. The A_{2u} and E_{1u} Fundamentals, ν_{11}, ν_{18} and ν_{19}

Apart from shifts due to change of phase, the frequencies observed here agree closely with those obtained by Ingold *et al.* There is no indication of splitting of the degenerate E_{1u} mode, ν_{18}, in the solid. The very sharp but weak line at 1470 cm^{-1}, on the shoulder of ν_{19}, may possibly result from splitting of ν_{19} along with a crystal orientation effect but both the magnitude of the frequency shift and the intensity suggest strongly that it is due to $C^{13}C_5^{12}H_6$ which constitutes 6.6 percent of the sample.

B. The E_{1u} Fundamental, ν_{20}

The best data available for the assignment of this mode are the high resolution studies of gaseous, liquid, and solid benzene in the 3μ-region made by Leberknight.[24] In the vapor he found two strong perpendicular bands whose Q-branches lay at 3100 and 3046 cm^{-1} as well as a weak maximum at 3074 cm^{-1}. In the liquid and solid he observed three strong components at 3091, 3071, and 3036 cm^{-1}. In both cases the lowest frequency was most intense. In addition a weak component appeared in the solid at 3055 cm^{-1}.

Ingold *et al.* interpreted the corresponding doublet in their vapor spectrum as due to Fermi resonance between ν_{20} and $\nu_{19}+\nu_8$. This interpretation is probably valid. In the vapor three components may result from resonance between ν_{20}, $\nu_{19}+\nu_8$ and $\nu_{19}+\nu_1+\nu_6$, all at about the doublet mean of 3073 cm^{-1}.†† In the liquid and solid, both strong branches drop by about 10 cm^{-1} and the mean is at 3063 cm^{-1}. The middle member at 3071 cm^{-1} in the liquid, and 3069 cm^{-1} in the solid, may be assigned to the B_{1u} fundamental, ν_{13}, which is allowed in these spectra. It had been estimated by Ingold *et al.* to lie at 3060 cm^{-1}. The bands in Fig. 1a agree with Leberknight's spectra except for the lower resolution.

The resonating doublet just described appears to enter into a combination with the Raman active fundamental ν_6 to produce the doublet observed in both liquid and solid at 3645 and 3695 cm^{-1}. Ingold attributed this doublet to $\nu_{20}+\nu_6$ and $\nu_{13}+\nu_6$, but the present explanation seems preferable.

C. The A_{1g}, E_{2g}, and E_{1g} Fundamentals, ν_1, ν_2, ν_6, ν_7, ν_8, ν_9, ν_{10}

None of these Raman active fundamentals have been observed in the solid. On the other hand, ν_9 and ν_{10} are both observed in the liquid, as is the doublet due to Fermi resonance between ν_8 and $\nu_1+\nu_6$ first explained by Wilson.[25] This appearance of Raman frequencies in the liquid spectrum and their complete absence from the spectrum of the crystal has been pointed out by Halford and Schaeffer[11] as a striking demonstration that the selection rules for the crystal are strictly obeyed.

The behavior of the combination bands which involve the fundamental $\nu_{10}(E_{1g})$ in the infra-red spectrum of the crystal is very interesting. They indicate strongly that in the solid state this fundamental is split into two components, separated by 10 cm^{-1} and whose frequencies lie about 5 and 15 cm^{-1} higher than those of the liquid. For instance, the strong band at 1528 cm^{-1} in the liquid can be assigned only to the combination $\nu_{11}+\nu_{10}$. In the solid it becomes a doublet at 1544,

†† The rather large splitting, 54 cm^{-1}, and the extent to which intensity is partitioned suggests a rather close coincidence of levels. Since the lower branch is more intense, ν_{20} may be slightly lower than the assigned frequency.

[25] E. B. Wilson, Jr., Phys. Rev. **46**, 146 (1934).

1551 cm^{-1} (at −12°C), 1547, 1555 cm^{-1} (at −65°C) and 1551, 1563 cm^{-1} (at −170°C). Even with the higher ν_{11} value observed in the crystal it is necessary, in order to get reasonable agreement between calculated and observed values, to split ν_{10} and raise the frequency of its components. The suggested shift of ν_{10} is the minimum which can be tolerated.

The strong band at about 1830 cm^{-1}, and the much weaker one at about 1250 cm^{-1}, both support this splitting convincingly. They are due to the combinations $\nu_{17}+\nu_{10}$ and $\nu_{16}+\nu_{10}$, respectively, involving the pair of degenerate E_{2u} fundamentals. The latter plainly exhibits four components and the shoulders on the former suggest more than two. They require the frequencies previously chosen for ν_{10}. They will be considered in greater detail in the discussion of ν_{16} and ν_{17}.

On the other hand, the evidence from three very weak combination bands, all of species A_{2u}, is less definite. $\nu_{20}+\nu_{10}$, at 3940 cm^{-1}, shows only one component, but in this region the resolution was inadequate to resolve two components 8 cm^{-1} apart. $\nu_{19}+\nu_{10}$ was observed at 2347 cm^{-1} in the solid at −170°C. It also shows but one maximum although, again, the resolution may have been inadequate. $\nu_{18}+\nu_{10}$ is observed in both liquid and solid, and although structure appears to be exhibited at −170°C, the band is too weak to reach definite conclusions.

The conclusions reached about the behavior of ν_{10} in the crystal await direct confirmation in the Raman spectrum. That some splitting and frequency shift takes place seems inescapable.

VII. INACTIVE FUNDAMENTALS

A. The E_{2u} Fundamentals, ν_{16} and ν_{17}

The value of about 405 cm^{-1} for ν_{16} in the liquid and in the vapor is by now firmly established. Although it was not found in this research, Plyler[26] has recently observed it at 403 cm^{-1} in the infra-red spectrum of liquid benzene. It has also been obtained from the Raman spectrum of the liquid,[27] from partially deuterated benzene,[4] from the ultraviolet absorption spectrum[28] and from the fluorescence spectrum.[29] The last two have shown this frequency to be degenerate, and since all other degenerate vibrations are known, it is positively assigned to the E_{2u} class.

Ingold's assignment of ν_{17} to about 970 cm^{-1} was based on two independent values of the frequency product $\nu_{16}\times\nu_{17}$, together with the frequency of ν_{16}. It is certainly firm. We have observed ν_{17} directly in both the liquid and solid spectra. The 985 cm^{-1} shoulder found by Ingold *et al.* in the liquid has been resolved into two definite lines, one of which, at 975 cm^{-1}, can only be ν_{17}. In the crystal it appears plainly and the splitting of this degenerate fundamental is striking, a second component appearing at a frequency 12 cm^{-1} higher.

The strong combination line, $\nu_{17}+\nu_5$ (ν_5 is the nondegenerate B_{2g} mode), at about 1970 cm^{-1}, mirrors almost exactly the behavior of the fundamental. Although single in the liquid, the splitting is resolved at −170°C in the crystal, the two peaks being separated by 11 cm^{-1}. As in the fundamental, the higher frequency branch appears less intense.

The strong combination, $\nu_{17}+\nu_{10}$, which we have previously mentioned, is also fruitful. Using the observed ν_{17}-frequencies and the postulated ν_{10}-frequencies, components are predicted at 1829, 1839, 1841, and 1851 cm^{-1}. The observed structure with sharp peaks at 1829 and 1839 cm^{-1} and a shoulder at approximately 1845 cm^{-1} (−170°C) agrees well with this prediction.

Still another weaker combination band, $\nu_{17}+\nu_4$, involving the other inactive B_{2g} mode, is split at all three temperatures. At −170°C the splitting is 7 cm^{-1}.

Let us now consider ν_{16} further. Like ν_{17} it is associated in three bands with the fundamentals ν_5, ν_{10}, and ν_4. The behavior of the two sets is so similar that a splitting and upward shift of one branch of ν_{16} is obvious. The moderately strong combination, $\nu_{16}+\nu_5$, at 1410 cm^{-1} is fully resolved at −170°C and the splitting is 10 cm^{-1}. As with ν_{17}, the high frequency branch is definitely the weaker. We must accordingly conclude that in the crystal the two components of ν_{16} lie at 405 and 415 cm^{-1}.

We have previously mentioned the weaker combination $\nu_{16}+\nu_{10}$. Using the postulated splitting, we predict components at 1259, 1269, 1269, and 1279 cm^{-1}. In fact, all four components are resolved. The resemblance between the outlines of this band and the corresponding $\nu_{17}+\nu_{10}$ is marked, although the resolution is somewhat better in this region.

In the case of the third band, $\nu_{16}+\nu_4$ (species E_{1u}), a shoulder is almost resolved at −170°C. It is at a frequency 7 cm^{-1} higher than the peak. This band is quite unusual in that as the temperature is *lowered*, its intensity shows a remarkable *increase*, accompanied by a decrease in the intensity of the neighboring fundamental, $\nu_{15}(B_{2u})$. This interesting effect, attributed to Fermi resonance, is considered further under ν_{15}.

These fundamentals are also observed in the very weak combinations $\nu_{16}+\nu_7$, $\nu_{17}+\nu_7$, $\nu_{16}+\nu_8$ and $\nu_{17}+\nu_8$. None of these are resolved, however.

B. The B_{1u} Fundamentals, ν_{12} and ν_{13}

The carbon bending frequency, ν_{12}, has been firmly established at about 1010 cm^{-1}. It is observed here for the first time as a sharp line at 1010 cm^{-1} in the solid at all three temperatures. We have assigned the hydrogen stretching frequency, ν_{13}, to the middle component of the 3.25μ-band in Leberknight's data.[24] In this research it is present as a shoulder only.

[26] E. K. Plyler, J. Chem. Phys. **16**, 1008 (1948).
[27] R. C. Lord and D. H. Andrews, J. Chem. Phys. **41**, 149 (1938).
[28] H. Sponer *et al.*, J. Chem. Phys. **7**, 207 (1939).
[29] See reference 4, Part XXI.

C. The A_{2g} Fundamental, ν_3

Ingold *et al.* placed this vibration firmly in the vicinity of 1330 cm^{-1} by means of the frequency product rule. They then assigned it to the extremely weak Raman line at 1326 cm^{-1} observed only by Grassmann and Weiler.[30] In support they cite the Raman frequency 2925 cm^{-1} which they ascribe to $\nu_3+\nu_8$, and a "rather prominent" infra-red band at 2356 cm^{-1}, which they assign to $\nu_{18}+\nu_3$. This investigation shows that the 2356 cm^{-1} band has three components, a prominent one at 2323 cm^{-1}, a weaker one at 2380 cm^{-1} and a very weak third already mentioned in connection with ν_{10}. The first must involve ν_{15}, as will be shown, but the second is probably the $\nu_{18}+\nu_3$ combination. Figure 1a also shows a weak but definite band at 2816 cm^{-1} which may be attributed to $\nu_{19}+\nu_3$.

Both of these infra-red combinations as well as the Raman combination cited by Ingold indicate a fundamental frequency of about 1340 cm^{-1}, and if the Raman value for the fundamental proved spurious, this higher value would be preferred.

D. The B_{2g} Fundamentals, ν_4 and ν_5

Ingold *et al.* have placed these two puckering vibrations in the vicinity of 700 and 990 cm^{-1}, respectively, using two independent values of the frequency product $\nu_4\times\nu_5$. They then assigned ν_5 to a shoulder which they had observed in the infra-red spectrum of liquid benzene. The shoulder observed by Ingold has been resolved into two distinct bands at 975 cm^{-1} and 995 cm^{-1}. The first we have assigned to ν_{17} and the other, since it is present in the liquid spectrum alone, must be either ν_5 or ν_1. This value is also obtained from the two strong combination bands, $\nu_{16}+\nu_5$ and $\nu_{17}+\nu_5$ which were discussed previously. These bands might also involve ν_1, but this seems unlikely because of the parallelism between them and the combination bands involving ν_4. Moreover, if ν_1 were involved these would be the only combination bands observed in which the D_{6h} selection rules were violated. No other combination lines involving ν_5 are observed in the infra-red spectrum except that $\nu_{12}+\nu_5$, which is predicted at 2005 cm^{-1}, is one of two possibilities for the line observed at 2011 cm^{-1} and $\nu_{13}+\nu_5$ is a possible candidate for the band at 4060 cm^{-1}.

ν_4 has not been observed directly, but Ingold's value of the fundamental frequency is supported by three combination bands, $\nu_{16}+\nu_4$ which is a weak temperature-dependent band at 1110 cm^{-1}, $\nu_{17}+\nu_4$ which is the weak band at 1680 cm^{-1} and $\nu_{12}+\nu_4$ which is an extremely weak but definite band at 1715 cm^{-1}. All have been discussed previously. On the other hand, it appears to us that the Raman line at 2294 cm^{-1} which Ingold *et al.* have used to support this same assignment is in fact $2\nu_{15}$.

[30] P. Grassmann and J. Weiler, Zeits. f. Physik **86**, 321 (1933).

E. The B_{2u} Fundamentals, ν_{14} and ν_{15}

One of the most striking results of the study of the benzene crystal is that it appears likely that the B_{2u} carbon stretching frequency, ν_{14}, occurs at 1311 cm^{-1}, a frequency almost 200 cm^{-1} lower than the lowest value that has been obtained theoretically, and 338 cm^{-1} lower than that obtained by Ingold *et al.*[31]

Ingold *et al.* have pointed out, however, that since ν_{14} should have very nearly the same frequency in all of the isotopic benzenes, the frequency product ratios give practically no information regarding it. On the other hand, their deductions regarding the hydrogen frequency, ν_{15}, are certainly sound.

Ingold *et al.* indicated a frequency of 1110 cm^{-1} for ν_{15}. In the infra-red spectrum of the crystal, where ν_{15} is allowed, one is struck by the presence of the weak but fairly sharp line at 1147 cm^{-1} at all three temperatures. It has no possible interpretation as a combination frequency, so its assignment to ν_{15} is clearly indicated. In the liquid spectrum, it is present as a band just resolved at 1152 cm^{-1} on the shoulder of an adjacent moderately strong Raman-active frequency.

There is strong support for this assignment among the combination bands. A weak but sharp line at 1754 cm^{-1} in all four spectra can have no interpretation other than $\nu_{15}+\nu_6$ with a calculated value of 1753 cm^{-1}. Similarly, the fairly prominent band at 2323 cm^{-1} in both the liquid and the crystal must be attributed to $\nu_{15}+\nu_9$. In addition, the Raman line at 2294 cm^{-1}, already mentioned, agrees well with the interpretation $2\nu_{15}$ although in this case the alternative $\nu_4+\nu_8$ is also a possibility.

It is also satisfying that the Raman line and infra-red vapor band used by Ingold *et al.* in arriving at the 1110 cm^{-1} value for ν_{15} can be simply interpreted. The former, at 2128 cm^{-1}, fits the combination $\nu_{15}+\nu_{17}$ (calculated 2125 cm^{-1}). A higher resolution study of benzene vapor[32] has shown that the band observed by Ingold at 2288 cm^{-1} has components at 2220 and 2340 cm^{-1}, the latter having a pronounced shoulder at about 2400 cm^{-1}. These all correspond to lines in the liquid and solid spectra; in particular, that at 2340 cm^{-1} corresponds to the 2323 cm^{-1} band $\nu_{15}+\nu_9$. It is interesting to note that the other ν_{15} combination appears at 1770 cm^{-1} in this vapor spectrum compared with 1754 cm^{-1} in the liquid and solid. These data indicate that ν_{15} has a somewhat higher frequency in the vapor, tentatively estimated to be about 1160 cm^{-1}.

The band which does in fact occur in the vicinity of 1110 cm^{-1} (which we have assigned to $\nu_{16}+\nu_4$) shows a peculiar temperature dependence. As the temperature is lowered its intensity shows a manyfold increase, accompanied by a steady decrease in the intensity of ν_{15}. Whereas a variety of factors can explain a decrease in intensity in the spectrum of the solid, only one, Fermi

[31] See reference 4, Part XXI.

[32] A.P.I. Research Project 44, Spectrogram No. 122, contributed by the Texas Company, Beacon, New York.

resonance, can account for such an increase. The difference in symmetry species of fundamental and combination, B_{2u} and E_{1u}, offers no fundamental difficulty since in the benzene crystal, vibrations, strictly speaking, belong only to the two representations, A_g and A_u of the point group C_i. On the other hand, it is surprising to find appreciable interaction when it is not allowed by the gas symmetry. The intensity change may be explained in this way if the separation between the two levels decreases somewhat as the temperature is lowered and intensity is increasingly "borrowed" from the fundamental by the combination. In this regard, it is noteworthy that the sum of the two intensities is very nearly constant.

In order to preserve Ingold's frequency products, the suggested change in ν_{15} would fix ν_{14} in the vicinity of 1600 cm^{-1}. Its assignment to the weak but extremely sharp line at 1618 cm^{-1} is a possibility since it is generally observed that fundamentals are particularly sharp in crystalline spectra. Only one line in the entire spectrum is narrower than the 1618 cm^{-1} line. There is, however, an alternative assignment to this line, namely, the combination $\nu_{12}+\nu_6$ which is allowed in the vapor spectrum, and has been observed by Ingold *et al.*, Halford and Schaeffer and others. This would appear to make the fundamental assignment unlikely except for a discrepancy in the gas spectra in that the spectrum of the vapor obtained by the Texas Company[32] with the highest resolution yet used on benzene vapor, and a sample of exceptional purity, does not show the 1617 cm^{-1} band. In the same spectrum, nevertheless, the weak band at 779 cm^{-1} shows a peak absorption of about 15 percent as compared to less than 5 percent found by Ingold, *et al.* It is perhaps revealing that the sample pressure used in this instance was 24.1 mm, compared to 40 mm employed by Ingold, *et al.* and 48 mm by Halford and Schaeffer. This suggests that the line in the gas may be due to benzene adsorbed on the cell windows so that this assignment for ν_{14} is at least tenable. However, it has practically no support from combination frequencies. The very weak line at 2610 cm^{-1} which has already been assigned to $\nu_{12}+\nu_8$ might be assigned to $\nu_{14}+\nu_1$, but in that case it would be the only combination observed which is not allowed in the vapor spectrum.

However, if this assignment is accepted for ν_{14}, there is no reasonable assignment for the very sharp line which appears at 1311 cm^{-1}. Its extreme sharpness suggests that it may be a fundamental. It fits the forbidden combination $\nu_4+\nu_6(E_{1g})$ very well, but if it were indeed this forbidden transition it would be the more surprising since not only would it be the only such case observed but, in fact, the only combination observed which is not allowed in the vapor. We suggest that it is the fundamental, ν_{14}.

A variety of evidence supports this assignment. Ingold, *et al.* have observed Raman lines which they consider of anomalous intensity for combination frequencies at 2618 cm^{-1} in C_6H_6, 2590 cm^{-1} in C_6H_5D, 2583 cm^{-1} in 1,4-$C_6H_4D_2$ and 2571 cm^{-1} in C_6D_6. They have also found a weak Raman line at 2581 cm^{-1} in 1,2,4,5-$C_6H_2D_4$.[33]

It seems likely that these are all first overtones of ν_{14} (and ν_{14}-like vibrations of the less symmetrical benzenes). They also observe a Raman fundamental at 1292 cm^{-1} in C_6H_5D which they assign to the B_1 species of C_{2v}. This species includes B_{2u} of D_{6h}. Similarly, their infra-red curves for C_6H_5D show a shoulder at about 1295 cm^{-1}.

Using these frequencies we can recalculate some of the product ratios used by Ingold. For example, using one-half the Raman frequencies for ν_{14} in the isotopic benzenes we obtain:

$$\frac{\prod B_{2u}(C_6H_6)}{\prod B_{2u}(C_6D_6)}=\frac{1310\times1150}{1285\times825}$$

$$=1.421 \text{ (harmonic value } 1.414).$$

$$\frac{\prod B_{2u}\cdot E_{1u}(C_6H_6)}{\prod B_{3u}(1,4\text{-}C_6H_4D_2)}=\frac{1310\times1150\times1037\times1478\times3080}{1292\times1106\times814\times1413\times3079}$$

$$=1.405 \text{ (harmonic value } 1.396).$$

We have used Ingold's frequencies in these products except for ν_{14} and ν_{15}. It is apparent that the agreement is good. This is not surprising since the ratios are almost independent of the choice of ν_{14}, although it is interesting that the new choice of ν_{14} apparently compensates the shift in ν_{15} adequately.

The strongest support in our own data lies in the sharp but extremely weak peak at 1305 cm^{-1} which can be ascribed to the ν_{14}-like vibration of $C^{13}C_5^{12}H_6$. ν_{14} is one of the three fundamentals in these spectra in which this isotope shift might be observed and the shift is just that expected. The combination band at 2907 cm^{-1}, to which no other binary combination can be assigned, may result from $\nu_{14}+\nu_8$ (calculated, 2908). Finally, the line at 4355 cm^{-1} can be assigned to $\nu_{14}+\nu_7$ (calculated 4359 cm^{-1}) and in this case, too, no other binary combination will fit. This assignment obviously demands further examination, but the evidence for 1310 cm^{-1} seems stronger than for any frequency previously proposed.

VIII. COMBINATION BANDS

Most of the bands arising from binary combinations have been discussed in preceding sections. Details of others are given in Table I. A number, however, deserve further consideration.

The sharp band appearing in the liquid at 776 cm^{-1} and present as an apparently real component of the vapor spectrum at 779 cm^{-1} has been attributed by Ingold *et al.* to the difference band $\nu_9-\nu_{16}$ (A_{2u}, calculated 773 cm^{-1}). The corresponding band system appear-

[33] Personal communication.

ing in the solid cannot possibly be explained by the difference frequency alone. The intensities of the difference band at −12°C, −65°C, and −170°C would have to be in the ratio 100:57:3 while the bands in Fig. 1b show little, if any, total intensity change. It should be noted, however, that the shape of the band does change markedly with temperature. Another explanation for this absorption region may be suggested in the case of the crystal, namely, a combination between ν_{11} and certain torsional lattice modes which have been observed in the Raman spectrum of solid benzene.[22,34] If the $\nu_9-\nu_{16}$ assignment is valid for liquid and vapor, the solid band must result from a superposition of the two effects.

If the $\nu_9-\nu_{16}$ assignment is correct for this reasonably strong band, it seems surprising that the corresponding summation band does not appear at all at about 1583 cm^{-1}. There is certainly no trace of it in the solid spectra. The validity of this assignment could readily be tested by measuring the temperature dependence of its intensity in the liquid. The expected intensity increases by 51.2 percent in going from 6°C to 75°C.

Several lines can be interpreted only as ternary combinations. Such possible combinations are very numerous and may be responsible for some of the very weak bands which we have assigned otherwise. Because of the large number of possibilities no assignment has been attempted for these lines.

Gross and Vuks[34] and Sirkar[22] have investigated the Raman spectrum of crystalline benzene in the vicinity of the exciting line. The former, using single crystals of unspecified orientation, found intense Raman lines at 63 and 108 cm^{-1} when the specimen was at 2°C to 3°C. The latter, using translucent, multicrystalline masses, found three intense lines at 81, 98, and 124 cm^{-1} with the specimen at liquid air temperature. He also found that the frequencies are strongly temperature dependent.

According to I, three lattice modes of the crystal, corresponding to in-phase libration of all benzene molecules about the three Cartesian axes, may be active in the Raman spectrum. It seems likely that the observed frequencies are those modes.[35] In that case it is possible that Gross and Vuks failed to observe the third component because of the orientation of their crystal. These modes may combine with any infra-red active modes. If we assign the three observed components at −170°C, as combinations with ν_{11}, the lattice frequencies are approximately 82 cm^{-1}, 101 cm^{-1} and 128 cm^{-1}. The agreement with the Raman data taken at the same temperature is surprisingly good.

[34] E. Gross and M. Vuks, Nature **135**, 100 (1935); J. de phys. et rad., series 7, **7**, 113 (1936).

[35] A. Kastler and A. Rousset, Phys. Rev. **71**, 455 (1947).

At the two higher temperatures, it appears that, in accordance with the Raman data, the lattice frequencies become lower. The simultaneous increase in the intensity of the superimposed difference band makes a detailed analysis impossible. That ν_{11} couples with lattice modes is made more probable by the fact, also, that the line width is more than twice as great as for any other fundamental. Furthermore, the line is not symmetrical and it appears to have considerable structure.

IX. ORIENTATION EFFECTS

It is possible to obtain still further information by considering the effect of crystal orientation in unpolarized light, or better, in polarized light. According to the x-ray structure of Cox,[15] the plane of the benzene molecule is approximately parallel to the *b*-axis of the crystal and approximately bisects the angle between the *a* and *c* axes. The three axes are all orthogonal and the *a* and *c* axes are nearly equal.

On this basis we can predict that the dipole moment vector of all out-of-plane vibrations (A_{2u} and E_{2u} modes) will lie in the *ac* plane. Hence they should be observed with infra-red radiation polarized in the *ac* plane but not if the electric vector is parallel to the *b*-axis of the crystal. In the case of unpolarized light no orientation effects may be expected.

In the case of non-degenerate in-plane modes (B_{1u} and B_{2u} modes), we can only say that the dipole moment change lies in a plane containing the *b*-axis. Using light polarized perpendicular to and along the *b*-axis would allow the determination of the direction of the dipole moment change when these modes are made allowed in the crystal.

In the case of the E_{1u} modes, which may be split by the crystalline field, we expect that one of the components will be polarized along the *b*-axis and one perpendicular to it. Hence they can be plainly distinguished in polarized light. Further than that, one of the components should not be observed in unpolarized light directed along the *b*-axis of the crystal. This last is the only such effect we might have observed. Except for ν_{19} we found no indication of splitting of these modes, and in the case of ν_{19} the sharp peak on its low frequency side appears to be due to isotopic carbon. The absence of any observable splitting of these modes leads to two possible conclusions: either the films were highly oriented with the *b*-axis perpendicular to the surface and one component was completely suppressed, or the splitting of the E_{1u} modes does not exceed 2 or 3 cm^{-1}. The same reasoning applies to E_{1u} combinations involving the Raman active E_{2g} fundamentals. Since no splitting of any of these lines was observed, we are left with the same alternative conclusions.

Formulas and Numerical Tables for Overlap Integrals*

R. S. MULLIKEN, C. A. RIEKE,† D. ORLOFF, AND H. ORLOFF††
Departments of Physics and Mathematics, University of Chicago, Chicago, Illinois

(Received April 27, 1949)

Explicit formulas and numerical tables for the overlap integral S between AO's (atomic orbitals) of two overlapping atoms a and b are given. These cover all the most important combinations of AO pairs involving ns, $np\sigma$, and $np\pi$ AO's. They are based on approximate AO's of the Slater type, each containing two parameters μ [equal to $Z/(n-\delta)$], and $n-\delta$, where $n-\delta$ is an effective principal quantum number. The S formulas are given as functions of two parameters p and t, where $p=\frac{1}{2}(\mu_a+\mu_b)R/a_H$, R being the interatomic distance, and $t=(\mu_a-\mu_b)/(\mu_a+\mu_b)$. Master tables of computed values of S are given over wide ranges of p and t values corresponding to actual molecules, and also including the case $p=0$ (intra-atomic overlap integrals). In addition, tables of computed S values are given for several cases involving 2-quantum s, p hybrid AO's.

Hybrid S values for any desired type of hybrid can be obtained very easily from the tables as simple linear combinations of non-hybrid S values. It is shown how S values corresponding to orthogonalized Slater AO's and approximate S values for SCF (self-consistent-field) AO's can also be obtained as linear combinations of the Slater-AO S values. S values for carbon-carbon $2p\sigma$- and $2p\pi$-bonds using SCF carbon AO's have been computed (see Table in Section Vb); they correspond to stronger overlap than for Slater AO's. Non-localized MO group-orbital S values are also discussed, and are illustrated by an application to H_2O. The use of the tables to obtain dipole moments for electronic transitions in certain cases is also mentioned. The use of the tables to obtain S values for various specific atom-pairs and bond-types, and resulting conclusions, will be discussed in another paper.

I. INTRODUCTION

As is well known, the quantity known as the overlap integral is of considerable importance in the theory of molecular structure. Although the existing literature[1] contains a number of formulas and some numerical values for overlap integrals, it was thought worth while to carry through the much more systematic and comprehensive study whose results are presented below.

The overlap integral S for a pair of overlapping AO's (atomic orbitals) χ_a and χ_b of a pair of atoms a and b is defined for any value of the internuclear distance R by

$$S(\chi_a, \chi_b; R)=\int \chi_a^* \chi_b d\tau. \quad (1)$$

In the present paper we give formulas for S for all *AO pairs* involving ns, $np\sigma$, and $np\pi$ AO's for $n=1, 2, 3,$ and 5 using Slater AO's. We also give numerical tables for the most important of these cases, applicable to a wide variety of *atom pairs* over a wide range of R. In addition, we show how the tables, though based on Slater AO's, may be used to obtain S values for central-field AO's, as well as for hybrid AO's. Explicit tables of hybrid S values are also given for $n=2$.

In a subsequent paper, tables and figures for a variety of selected atom-pairs will be presented, together with some comments on their significance for the theory of chemical binding.

II. THE CHOICE OF ATOMIC ORBITAL FORMS

In order to evaluate overlap integrals, it is necessary first to specify the forms of the AO's. As a background, and also to obtain certain needed formulas, we first give a brief review of useful approximate AO forms. We are primarily concerned with *central-field* orbitals, classified under the familiar designations ns, np, nd, nf, $\cdots$ corresponding to $l=0, 1, 2, 3, \cdots$, with $n \gtrless l+1$. However, since the application of our computations is to atom-pairs in which each atom is under the influence of the cylindrically-symmetrical field of its partner, we need a sub-classification according to values of the diatomic quantum number λ ($\lambda=|m_l|$). This gives the AO types ns, $np\sigma$, $nd\sigma$, $\cdots(\lambda=0)$; $np\pi$, $nd\pi$, $\cdots(\lambda=1)$; and so on.

Let us consider an electron belonging to either of a pair of atoms a and b, using spherical polar coordinates about either center, as in Fig. 1. Intentionally, we take

* This work was assisted by the ONR under Task Order IX of Contract N6ori-20 with the University of Chicago.

† Present address: Physics Department, Purdue University, Lafayette, Indiana.

†† The work was begun before the war with computations on a considerable variety of individual atom-pairs (see abstract by R. S. Mulliken and C. A. Rieke, Rev. Mod. Phys. **14**, 259 (1942)). Recently, with the indispensable assistance of Mr. Tracy J. Kinyon in making the numerical computations, it was extended to the comprehensive effort reported here.

[1] (a) W. Heitler and F. London, Zeits. f. Physik **44**, 455 (1927), for homopolar $S(1s, 1s)$; (b) J. H. Bartlett, Jr., Phys. Rev. **37**, 507 (1931), for homopolar $S(2p\sigma, 2p\sigma)$ and $S(2p\pi, 2p\pi)$ and a table of values of the integrals A (see Eq. (15) below); (c) J. H. Bartlett, Jr. and W. H. Furry, Phys. Rev. **38**, 1615 (1931); **39** 210 (1932), especially table of values of homopolar $S(2s, 2s)$, $S(2s, 2p\sigma)$, $S(2p\sigma, 2p\sigma)$, $S(2p\pi, 2p\pi)$: Table VII, p. 222; (d) N. Rosen, Phys. Rev. **38**, 255 (1931) for formulas and extensive tables of values of the integrals A and B (see Eqs. (15), (16) below); (e) Kotani, Amemiya, and Simose, Proc. Phys. Math. Soc. Japan **20**, 1 (1938); **22**, 1 (1940). These authors give equations for S for all AO combinations with $n=1$ and 2, and (1940, p. 13) numerical tables for $S(1s, 2s)$ and $S(1s, 2p\sigma)$ for various t values. They also (1938, pp. 24–30, corrections 1940, pp. 17–18) give very complete and useful numerical tables for the integrals A and B. (f) C. A. Coulson, Proc. Camb. Phil. Soc. **38**, 210 (1941). Coulson gives very extensive formulas but no numerical tables, for integrals which differ from S only by multiplicative factors. These correspond to S for all combinations of ns, $np\sigma$, and $np\pi$ AO's with $n=1-3$ (and a few more), both for $t\neq 0$ (in our notation) and for $t=0$. (g) Several of the S formulas and a few numerical values are also given elsewhere.

the positive direction of the z axis for each atom to be directed toward the other atom, since this ensures a positive sign for S in all ordinary cases. Every central-field AO of atom a is of the form

$$\chi_a{}^{nl\lambda}=R_{nl}(r_a)Y_{l,\lambda}(\theta_a,\phi). \tag{2}$$

In normalized form, the Y's for the cases considered in this paper are:

$$\left.\begin{aligned} Y_{ns}&=(1/4\pi)^{\frac{1}{2}};\\ Y_{np\sigma}&=(3/4\pi)^{\frac{1}{2}}\cos\theta_a;\\ Y_{np\pi}&=(3/4\pi)^{\frac{1}{2}}\sin\theta_a\{\cos\phi \text{ or } \sin\phi\}. \end{aligned}\right\} \tag{3}$$

Corresponding expressions hold for atom b.

When there is only one electron (hydrogenic AO's), R_{nl} takes the well-known form

$$R_{nl}(r)=\left(\sum_{k=l}^{n-1}c_{nlk}r^k\right)e^{-Zr/na_{\mathrm{H}}}, \tag{4}$$

where Z is the nuclear charge, and a_{H} (0.529A) is the 1-quantum Bohr radius. The coefficients in Eq. (4) are those of the associated Laguerre polynomials, and the R_{nl}'s for each l form an orthogonal set.

When there is more than one electron, the best R_{nl}'s are of the SCF (self-consistent-field) type obtainable by the method of Hartree and Fock. These are not given by analytical expressions, and are usually presented in the form of numerical tables. Moreover, these SCF R_{nl}'s as tabulated are not always all orthogonal; however, it is always possible to find an equivalent set of equally good SCF R_{nl}'s which *are* orthogonal.[2] For practical computations, as Slater has shown,[3] the SCF R_{nl}'s may be approximated passably well by a finite series similar to that of Eq. (4) but with a different exponential factor in each term:

$$R_{nl}(r)=\sum_{k=l}^{n-1}d_kr^ke^{-\mu_kr/a_{\mathrm{H}}}, \tag{5}$$

where the d_k's and μ_k's depend on n, l, and on the particular atom and electronic state. A considerably better series is obtained if the exponential factor in the term for which $k=n-1$ is replaced by a sum of two or three exponential terms, as follows:[3]

$$R_{nl}(r)=\sum_{\substack{k=l\\(\neq n-1)}}^{n-2}d_kr^ke^{-\mu_kr/a_{\mathrm{H}}}+r^{n-1}\sum_i d_ie^{-\mu_ir/a_{\mathrm{H}}}. \tag{6}$$

For atoms containing $1s$, $2s$, and $2p$ electrons, the best approximate R_{nl}'s of the type of Eq. (5), so far as we know, are those obtained by Morse, Young, and Haurwitz, and Duncanson and Coulson.[4] These were obtained for several states of several atoms by minimizing the total energy of a complete antisymmetrized wave function built of AO's having R_{nl}'s of the type given by Eq. (5), subject also to the condition that the $2s$ AO is kept orthogonal to the $1s$. These AO's were also chosen in such a way that the virial theorem for the mean total kinetic and potential energies is satisfied.

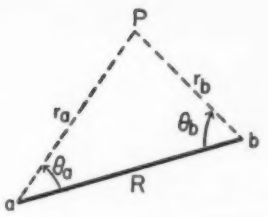

FIG. 1. Polar coordinates for an electron at P in an AO of atom a or b. In addition (not shown), $\phi=\phi_a=\phi_b$.

The well-known Slater AO's[5] are obtained by approximating the series of Eq. (5) by the single term $N_{nl}r^{n-1}e^{-\mu r/a_{\mathrm{H}}}$ (or by a modification of this, $N_{nl}r^{n-1-\delta}e^{-\mu r/a_{\mathrm{H}}}$). The values of μ and δ are specified by Slater for any AO of any atom by a simple recipe. This gives μ-values surprisingly close,[4b] for 2-quantum AO's, to those obtained for the r^{n-1} term by minimizing the total energy. Unlike most of the forms given by Eqs. (2)–(5), Slater's AO's have no radial nodes. This, however, does not much impair their ability to represent the *outer parts* of AO's, hence they should be especially useful for the computation of overlap integrals. Following is a summary of Slater's recipe as applied to s and p AO's in normalized form:

$$\left.\begin{aligned} R_{nl}(r)&=N_{nl}r^{n-1-\delta}e^{-\mu r/a_{\mathrm{H}}};\\ \delta&=0 \text{ for } n=1 \text{ to } 3;\ 0.3 \text{ for } 4s,\ 4p;\\ &\qquad 1 \text{ for } 5s,\ 5p;\\ \mu_{ns}&=\mu_{np}=Z_{a,n}/(n-\delta),\\ 1/N_{nl}{}^2&=\int_0^\infty r^{2n-2\delta}e^{-2\mu_{nl}r/a_{\mathrm{H}}}dr, \end{aligned}\right\} \tag{7}$$

with Z values dependent on the atom a and on n. For convenience of later reference, Slater μ-values for the *valence-shell* ns and np AO's of several atoms and ions are given in Table I. Inner-electron AO's if present are assigned larger Z values.[3]

As a consequence of their nodeless character, Slater AO's of equal l and different n (e.g., $1s$ and $2s$) are very far from being orthogonal, but they can easily be orthogonalized if desired. This process restores the missing nodes, giving AO's of the form of Eq. (5), and surprisingly close to the best possible of this form.[6] As an example, if χ_{1s} and χ_{2s} refer to Slater AO's, and $\chi_{2s}{}^{\mathrm{or}}$

[2] See, e.g., C. C. J. Roothaan, forthcoming paper.

[3] J. C. Slater, Phys. Rev. **42**, 33 (1932).

[4] (a) Morse, Young, and Haurwitz, Phys. Rev. **48**, 948 (1935); (b) extended and partially corrected by W. E. Duncanson and C. A. Coulson, Proc. Roy. Soc. Edinburgh **62A**, 37 (1944).

[5] J. C. Slater, Phys. Rev. **36**, 57 (1930); C. Zener, Phys. Rev. **36**, 51 (1930).

[6] W. E. Moffitt and C. A. Coulson, Phil. Mag. [7], **38**, 634 (1937). These authors also give instructive contour diagrams of carbon atom $2te$, $2tr$, and $2di$ hybrid AO's, using orthogonalized Slater $2s$ AO's.

TABLE I. Slater μ-values[a] for valence-shell ns, np AO's.

H	1.00	C^-	1.45	O^-	2.10	Na	0.733	S	1.817
Li	0.65	C	1.625	O	2.275	Mg	0.95	Cl	2.033
Be	0.975	C^+	1.80	O^+	2.45	Al	1.167	Br	2.054
B^-	1.125	N	1.95	F	2.60	Si	1.383	I	1.90
B	1.30	N^+	2.125			P	1.60		

[a] For 1s inner-shell AO's, $\mu=Z-0.3$ in all cases, where Z is the actual nuclear charge.

refers to the orthogonalized Slater 2s AO, we have

$$\left.\begin{aligned}\chi_{2s}^{\text{or}}&=(\chi_{2s}-Q\chi_{1s})/(1-Q^2)^{\frac{1}{2}}\\ Q\equiv S(1s_a,\,2s_a)&\equiv\int\chi_{2s_a}\chi_{1s_a}d\tau.\end{aligned}\right\}\qquad(8)$$

Although Q is often fairly large (for example, 0.220 if atom a is carbon), the process of orthogonalization has little effect on the computed values of overlap integrals (see Section V).

In addition to overlap integrals for pure central-field AO's, those for hybrid AO's are obviously of great interest for molecular problems. Hybrid AO's, although they can be constructed as linear combinations of central-field AO's, are not themselves central-field AO's. Hybrid overlap integrals can be obtained as simple linear combinations of Slater-AO S's (see Section V), so that no laborious new computations are required. For purposes of computing S's, approximate hybrid AO's built from Slater AO's without orthogonalization should according to our previous reasoning give satisfactory results.

The hybrid AO's which can be formed from s and p AO's are all of σ-type, that is, have cylindrical symmetry. Let χ be a normalized hybrid σ AO of the form

$$\chi=\alpha\chi_{ns}\pm(1-\alpha^2)^{\frac{1}{2}}\chi_{np\sigma},\qquad(9)$$

where $0\leqslant\alpha\leqslant1$, and χ_{ns} and $\chi_{np\sigma}$ are as defined by Eqs. (2)–(3) and Fig. 1, with R_{nl} given by Eqs. (7) for the case of hybrid Slater AO's. In the following, the abbreviations *te*, *tr*, and *di* (tetrahedral, trigonal, and digonal) will be used for hybrids with $\alpha^2=\frac{1}{4}$, $\frac{1}{3}$, and $\frac{1}{2}$ respectively and with the plus sign in Eq. (9). A further, complementary, set of hybrid AO's *te'*, *tr'*, and *di'* is obtained by using the minus sign in Eq. (9). The hybrids *te*, *tr*, *di* of an atom give *large overlap* (large S) with corresponding or similar AO's of a second atom, while *te'*, *tr'*, and *di'* give *small overlap*.

III. NOMENCLATURE AND PARAMETERS FOR OVERLAP INTEGRALS

In discussing and tabulating overlap integrals, a careful choice of nomenclature will prove to be important. In order to characterize an overlap integral fully, we need to specify (a) the two AO's involved; (b) the two atoms involved, and which AO belongs to each atom; (c) the value of R. Two suitable types of general symbols for this purpose, also a symbol for an internal overlap or non-orthogonality integral, are indicated by the following examples. Simplified symbols can be used in special cases.

$$\left.\begin{aligned}&\text{(a) Atom-pair at any distance } R:\\ &\quad\text{general AO's and atoms: } S(n_ax,\,n_by;\,R)\\ &\quad\text{specific AO's, general atoms:}\\ &\quad\quad S(1s_a,\,2p\sigma_b;\,R)\text{ or }S(1s,\,2p\sigma;\,R)\\ &\quad\text{specific AO's and atoms:}\\ &\quad\quad S(2p\pi_{\text{C}},\,3p\pi_{\text{Si}};\,1.75\text{A})\\ &\text{(b) Atom-pair involved in specified bond at equilibrium distance:}\\ &\quad S(2s,\,2p\sigma;\,\text{C}=\text{C});\,S(2te,\,3p\sigma;\,\text{C}-\text{Cl});\\ &\quad S(1s,\,2s;\,\text{H}-\text{Li});\,S(2p\pi,\,2p\pi,\,\text{O}^+\equiv\text{C})\\ &\text{(c) Single atom } a\text{ (internal overlap integral):}\\ &\quad S(1s_a,\,2s_a).\end{aligned}\right\}\qquad(10)$$

In the atom-pair symbols above, it is intended to be understood that the *first AO symbol always goes with the first atom, the second with the second*. However, it is not essential here to follow any fixed rule as to which AO (or atom) symbol shall be written first. Nevertheless, in another type of notation which will be required below, it *does* become essential to adopt certain fixed conventions in this matter, and it will diminish the possibilities of error if we follow the same conventions also in using the types of notation given above. These conventions are: the AO of smaller n is to be written first, or if both n's are equal, the AO belonging to the atom of larger Z is to be written first. These rules were followed in the examples given above.

We turn now to the matter of coordinates and parameters to be used in the evaluation of the S's. The computation is best effected after transforming from polar coordinates of the two atoms (see Fig. 1) to spheroidal coordinates ξ, η, ϕ given by:

$$\xi=(r_a+r_b)/R;\quad\eta=(r_a-r_b)/R;\quad\phi=\phi_a=\phi_b.\qquad(11)$$

The coordinate ξ ranges from 1 to ∞, η from -1 to $+1$.

For any given AO pair, we shall wish to obtain S values for various pairs of atoms, each for various interatomic distances R. To accomplish this, the best procedure is first to set up for each AO pair a single master formula expressed in terms of suitable parameters depending on the μ's of the two AO's and on R, and from this to compute and tabulate numerical values of S as a function of the chosen parameters. For this purpose, the two parameters p and t defined as follows are found to be appropriate for the case of Slater AO's (see Eqs. (7) and Table I).

$$\left.\begin{aligned}p&\equiv\tfrac{1}{2}(\mu_a+\mu_b)R/a_{\text{H}},\\ t&\equiv(\mu_a-\mu_b)/(\mu_a+\mu_b).\end{aligned}\right\}\qquad(12)$$

To find S for a given Slater-AO pair, atom pair and R value, one then first computes p and t for the particular case, then looks up the value of S in the master table for the given AO pair. Methods of obtaining S values for other types of AO's will be described in Section V.

Since in connection with the master tables we replace atom designations by parameters p and t, it is now necessary to introduce a type of S symbol different from those given in (10), and indicated by the following examples:

(a) Atom pair characterized by parameters p, t:
General form: $S(n_a x, n_b y; p, t)$;
Specific form: $S(2s_a, 3p\sigma_b; p, t)$,
or more briefly, but with the same meaning,
$S(2s, 3p\sigma; p, t)$.
(b) Single atom (internal overlap integral):
General form: $S(n_a x, n_a' y)$
Specific form: $S(1s, 2s; \mathrm{O}, t)$. (13)

The signs of the coordinate η in Eqs. (11) and of the parameter t in Eqs. (12) obviously depend on the assignment of the labels a and b to the two atoms in any atom pair. In order to make the master formulas and tables unambiguous with respect to the signs of η and t, it is therefore necessary to adopt suitable conventions to fix this assignment. The following two (necessarily arbitrary) conventions will be used in this paper:

(1) *In case the two AO's have unequal n, the atom whose AO has smaller n will always be identified with atom a, and its AO will always be written first in the symbol for S,* for example $S(2s_a, 3p\sigma_b; p, t)$ or more briefly $S(2s, 3p\sigma; p, t)$; but *never* $S(3p\sigma_a, 2s_b; p, t)$ or $S(3p\sigma, 2s; p, t)$. As another example, we may write $S(2p\sigma, 3s)$, but never $S(3s, 2p\sigma)$. Further examples are $S(2s, 3s)$ and $S(2p\sigma, 3p\sigma)$. In general formulations, symbols such as $S(n_a s, n_b p\sigma)$ or $S(n_a p\sigma, n_b s)$ will be used, always with the implication that $n_a < n_b$. It will be noticed that for the present case of two AO's with unequal n, both positive and negative t values are possible, depending on the sign of $\mu_a - \mu_b$. For example (see Table I),

$$t(2p\sigma_{\mathrm{F}}, 3s_{\mathrm{Mg}}) = (2.60-0.95)/(2.60+0.95) > 0,$$

but

$$t(2p\sigma_{\mathrm{Be}}, 3s_P) = (1.30-1.60)/(1.30+1.60) < 0.$$

Also, but only by accident, $t=0$ is possible. The relative practical importance of the positive and negative ranges of t varies according to what AO pair-type one considers.

(2) *In case the two AO's have equal n, the atom with larger μ will always be identified with atom a, and its AO will always be written first in the symbol for S; if the μ's are equal, either atom may be called a.* For example, $S(ns_a, np\sigma_b)$ or briefly $S(ns, np\sigma)$; $S(np\sigma_a, ns_b)$ or briefly $S(np\sigma, ns)$; and $S(2p\pi_a, 2p\pi_b)$ or briefly $S(2p\pi, 2p\pi)$, all imply $Z_a \geqslant Z_b$. Hence, according to Eqs. (12), convention (2) here restricts t to the range $t \geqslant 0$. The integrals $S(ns_a, np\sigma_b)$ and $S(np\sigma_a, ns_b)$—see Eqs. (14) below, taking $n_a = n_b$—require a little special comment because of their somewhat confusing similarity.[7] For $t > 0$, the two integrals are different and have different values, but for $t = 0$ they become identical. For instance, $S(2p\sigma_{\mathrm{O}}, 2s_{\mathrm{C}})$ and $S(2s_{\mathrm{O}}, 2p\sigma_{\mathrm{C}})$, which are examples of the two cases written in accordance with convention (2), have different values; but $S(2p\sigma_{\mathrm{C}}, 2s_{\mathrm{C}})$ and $S(2s_{\mathrm{C}}, 2p\sigma_{\mathrm{C}})$ are identical.

IV. MASTER FORMULAS AND COMPUTATION METHODS FOR MASTER TABLES OF SLATER-AO OVERLAP INTEGRALS

With the foregoing conventions, the S master formulas fall into five basic types. Using Eqs. (1)–(3), (7), (11)–(12), letting

$$m = n - \delta,$$

and integrating over ϕ, these five types take the forms:

$$S(n_a s, n_b s; p, t) = \tfrac{1}{2} N_a N_b (\tfrac{1}{2}R)^{m_a+m_b+1} \int_1^\infty \int_{-1}^1 (\xi+\eta)^{m_a-1}(\xi-\eta)^{m_b-1}(\xi^2-\eta^2) e^{-p(\xi+\eta t)} d\eta d\xi,$$

$$S(n_a s, n_b p\sigma; p, t) = (\tfrac{1}{2}\sqrt{3}) N_a N_b (\tfrac{1}{2}R)^{m_a+m_b+1} \int_1^\infty \int_{-1}^1 (\xi+\eta)^{m_a-1}(\xi-\eta)^{m_b-2}(-\xi\eta+1)(\xi^2-\eta^2) e^{-p(\xi+\eta t)} d\eta d\xi,$$

$$S(n_a p\sigma, n_b s; p, t) = (\tfrac{1}{2}\sqrt{3}) N_a N_b (\tfrac{1}{2}R)^{m_a+m_b+1} \int_1^\infty \int_{-1}^1 (\xi+\eta)^{m_a-2}(\xi-\eta)^{m_b-1}(-\xi\eta-1)(\xi^2-\eta^2) e^{-p(\xi+\eta t)} d\eta d\xi, \quad (14)$$

$$S(n_a p\sigma, n_b p\sigma; p, t) = (3/2) N_a N_b (\tfrac{1}{2}R)^{m_a+m_b+1} \int_1^\infty \int_{-1}^1 (\xi+\eta)^{m_a-2}(\xi-\eta)^{m_b-2}(\xi^2\eta^2-1)(\xi^2-\eta^2) e^{-p(\xi+\eta t)} d\eta d\xi,$$

$$S(n_a p\pi, n_b p\pi; p, t) = (3/4) N_a N_b (\tfrac{1}{2}R)^{m_a+m_b+1} \int_1^\infty \int_{-1}^1 (\xi+\eta)^{m_a-2}(\xi-\eta)^{m_b-2}(\xi^2-1)(1-\eta^2)(\xi^2-\eta^2) e^{-p(\xi+\eta t)} d\eta d\xi.$$

[7] Without convention (2), $S(ns_a, np\sigma_b)$ would be defined for positive, zero, and negative values of t ($Z_a > Z_b$, $Z_a = Z_b$, $Z_a < Z_b$; see Eqs. (12)). The same would be true of $S(np\sigma_a, ns_b)$. The two integrals would then differ only in the manner in which the labels a and b are associated with the AO forms ns and $np\sigma$. Now as will be seen from Eqs. (11), (12), an exchange of the labels a and b merely changes the definitions of η and t in such a way that the positive domains of η and t for the one labeling (say η', t') become the corresponding negative domains for the other (say η'', t''). Consequently, if in Eqs. (14) for $S(ns, np\sigma)$ and $S(np\sigma, ns)$ we write η', t' in the one equation and η'', t'' in the other, and then make the substitution $\eta'' = -\eta'$, $t'' = -t'$, the two equations

The integrals over ξ and η in Eqs. (14) may be evaluated by making use of the following mathematical relations:[1]

$$A_k(p)\equiv\int_1^\infty \xi^k e^{-p\xi}d\xi = e^{-p}\sum_{\mu=1}^{k+1}[k!/p^\mu(k-\mu+1)!] \tag{15}$$

$$\left.\begin{aligned} B_k(pt)&\equiv\int_{-1}^{1}\eta^k e^{-pt\eta}d\eta \\ &=-e^{-pt}\sum_{\mu=1}^{k+1}[k!/(pt)^\mu(k-\mu+1)!]-e^{pt}\sum_{\mu=1}^{k+1}[(-1)^{k-\mu}k!/(pt)^\mu(k-\mu+1)!];\end{aligned}\right\} \tag{16}$$

but $B_k(0)=2/(k+1)$ for k even; $=0$ for k odd. The factors N in Eqs. (14) (see N_{nl} in Eqs. (7)) may be evaluated by means of:

$$C(k,q)\equiv\int_0^\infty \lambda^k e^{-q\lambda}d\lambda = k!/q^{k+1}. \tag{17}$$

The numerical computation of the overlap integrals is comparatively simple if the A_k's and B_k's are first computed for appropriate values of the parameters p and t; here the simplest procedure (rather than using Eqs. (15), (16) directly) is to obtain the higher k A's and B's from those with lower k by using certain *recursion formulas*.[1d, 1e] We first note that any particular S involves the integral of a polynomial in ξ and η. Then it is plain that each value of S is the product of a factor times a linear combination of A_k's and B_k's all computed at the same values of p and t.

For the computation of the master tables given below, the necessary A_k's and B_k's were first computed[8] for the desired values of p and t, and then combined in accordance with the following Eqs. (18)–(50) to give the S values.[9] These formulas were obtained by the use of Eqs. (15)–(17) in connection with Eqs. (14) and (7). It will be noted that a separate formula is given in each case for $t=0$, for reasons that will be understood on looking at Eqs. (16). Certain additional special formulas will now be described.

Although in general the computation of the A's and B's followed by the use of Eqs. (18)–(50) is the most expeditious procedure, an alternative set of formulas very considerably simplifies the computation in the important special case of two identical atoms ($n_a=n_b$, $t=0$), if one is interested *only* in this case. This case includes not only integrals of the type $S(nx, nx; p, 0)$, but also such integrals as $S(ns, np\sigma; p, 0)$ or $S(np\sigma, ns; p, 0)$; these are particularly important in the computation of hybrid-AO S values (see Section V). The simplified formulas were obtained by substituting for the A's in the $t=0$ formulas in Eqs. (18)–(50), using Eq. (15). Although we did not use them in computing the master tables, they are given below as Eqs. (51)–(63) for the convenience of readers who may wish to make their own computations for additional p values.[9]

One further set of special formulas is required, for the internal overlap integrals $S(n_a x, n_b y; \mathrm{O}, t)$,—see (10) and (13). This type of integral occurs if one orthogonalizes Slater AO's, and also if one wishes to compute SCF S's from Slater S's (see Section V). The necessary formulas are given below as Eqs. (64)–(73).

MASTER FORMULAS FOR SLATER-AO OVERLAP INTEGRALS

$$\begin{aligned} &t=0: \\ &\quad S(1s,1s)=(6)^{-1}p^3[3A_2-A_0] \\ &t>0: \\ &\quad S(1s,1s)=(4)^{-1}p^3(1-t^2)^{+3/2}[A_2B_0-A_0B_2] \end{aligned} \tag{18}$$

become identical except for the sign of t in the exponential, and completely identical for $t=0$. Hence $S(ns, np\sigma)$ for positive t would be equal to $S(np\sigma, ns)$ for negative t, and *vice versa*, if negative t here were not excluded by convention (2); and for $t=0$, $S(ns, np\sigma)\equiv S(np\sigma, ns)$.

[8] Most of this labor could have been avoided by the use of the A and B tables of references 1d or especially 1e. Actually, however, independent computations were made. Afterward, checks were made of some of our A and B values against those in the tables of reference 1e, and excellent agreement was found.

[9] Coulson (reference 1f) also gives formulas corresponding to the majority of the S integrals listed here. However, his formulas for $t\neq 0$ are in terms of μ_a, μ_b, and R, in a form not adapted to the present computation and tabulation. His formulas for $t=0$ are identical with our Eqs. (51)–(63) except that they are not normalized like ours to give S values directly.

$t=0$:
$$S(1s, 2s)=(12)^{-1}(3)^{-\frac{1}{2}}p^4[3A_3-A_1]$$
$t\neq 0$:
$$S(1s, 2s)=(8)^{-1}(3)^{-\frac{1}{2}}p^4(1+t)^{3/2}(1-t)^{5/2}[A_3B_0-A_2B_1-A_1B_2+A_0B_3] \tag{19}$$

$t=0$:
$$S(1s, 2p\sigma)=(12)^{-1}p^4[3A_2-A_0]$$
$t\neq 0$:
$$S(1s, 2p\sigma)=(8)^{-1}p^4(1+t)^{3/2}(1-t)^{5/2}[-A_3B_1+A_2B_0+A_1B_3-A_0B_2] \tag{20}$$

$t=0$:
$$S(1s, 3s)=(60)^{-1}(10)^{-\frac{1}{2}}p^5[5A_4-A_0]$$
$t\neq 0$:
$$S(1s, 3s)=(24)^{-1}(10)^{-\frac{1}{2}}p^5(1+t)^{3/2}(1-t)^{7/2}[A_4B_0-2A_3B_1+2A_1B_3-A_0B_4] \tag{21}$$

$t=0$:
$$S(1s, 3p\sigma)=(15)^{-1}(30)^{-\frac{1}{2}}p^5[5A_3-2A_1]$$
$t\neq 0$:
$$S(1s, 3p\sigma)=(8)^{-1}(30)^{-\frac{1}{2}}p^5(1+t)^{3/2}(1-t)^{7/2}[A_3(B_0+B_2)-A_1(B_2+B_4)-B_1(A_2+A_4)+B_3(A_0+A_2)] \tag{22}$$

$t=0$:
$$S(1s, 5s)=(720)^{-1}(35)^{-\frac{1}{2}}p^6[15A_5+10A_3-9A_1]$$
$t\neq 0$:
$$S(1s, 5s)=(96)^{-1}(35)^{-\frac{1}{2}}p^6(1+t)^{3/2}(1-t)^{9/2}[A_5B_0-3A_4B_1+2A_3B_2+2A_2B_3-3A_1B_4+A_0B_5] \tag{23}$$

$t=0$:
$$S(1s, 5p\sigma)=(240)^{-1}(105)^{-\frac{1}{2}}p^6[25A_4-6A_2-3A_0]$$
$t\neq 0$:
$$S(1s, 5p\sigma)=(32)^{-1}(105)^{-\frac{1}{2}}p^6(1+t)^{3/2}(1-t)^{9/2}[A_4(B_0+2B_2)+A_1(2B_3+B_5)-B_1(2A_3+A_5)-B_4(A_0+2A_2)] \tag{24}$$

$t=0$:
$$S(2s, 2s)=(360)^{-1}p^5[15A_4-10A_2+3A_0]$$
$t>0$:
$$S(2s, 2s)=(48)^{-1}p^5(1-t^2)^{5/2}[A_4B_0-2A_2B_2+A_0B_4] \tag{25}$$

$t=0$:
$$S(2s, 2p\sigma)=(60)^{-1}(3)^{-\frac{1}{2}}p^5[5A_3-A_1]$$
$t\neq 0$:
$$S(2s, 2p\sigma)=(16)^{-1}(3)^{-\frac{1}{2}}p^5(1-t^2)^{5/2}[A_3(B_0-B_2)+A_1(B_4-B_2)+B_1(A_2-A_4)+B_3(A_2-A_0)] \tag{26}$$
$S(2p\sigma, 2s)$: same as $S(2s, 2p\sigma)$ except each $B_k(t)$ replaced by $B_k(-t)$

$t=0$:
$$S(2s, 3s)=(360)^{-1}(30)^{-\frac{1}{2}}p^6[15A_5-10A_3+3A_1]$$
$t\neq 0$:
$$S(2s, 3s)=(48)^{-1}(30)^{-\frac{1}{2}}p^6(1+t)^{5/2}(1-t)^{7/2}[A_5B_0-A_4B_1-2A_3B_2+2A_2B_3+A_1B_4-A_0B_5] \tag{27}$$

$t=0$:
$$S(2s, 3p\sigma)=(360)^{-1}(10)^{-\frac{1}{2}}p^6[15A_4-10A_2+3A_0]$$
$t\neq 0$:
$$S(2s, 3p\sigma)=(48)^{-1}(10)^{-\frac{1}{2}}p^6(1+t)^{5/2}(1-t)^{7/2}[-A_5B_1+A_4B_0+2A_3B_3-2A_2B_2-A_1B_5+A_0B_4] \tag{28}$$

$t=0$:
$$S(2s, 5s)=(10{,}080)^{-1}(105)^{-\frac{1}{2}}p^7[105A_6-35A_4-21A_2+15A_0]$$
$t\neq 0$:
$$S(2s, 5s)=(192)^{-1}(105)^{-\frac{1}{2}}p^7(1+t)^{5/2}(1-t)^{9/2}[A_6B_0-2A_5B_1-A_4B_2+4A_3B_3-A_2B_4-2A_1B_5+A_0B_6] \tag{29}$$

$t=0$:
$$S(2s, 5p\sigma)=(2520)^{-1}(35)^{-\frac{1}{2}}p^7[35A_5-28A_3+9A_1]$$
$t\neq 0$:
$$S(2s, 5p\sigma)=(192)^{-1}(35)^{-\frac{1}{2}}p^7(1+t)^{5/2}(1-t)^{9/2}[-A_6B_1+A_5(B_0+B_2)+A_4(2B_3-B_1)-2A_3(B_2+B_4)+A_2(2B_3-B_5)+A_1(B_4+B_6)-A_0B_5] \tag{30}$$

$t=0$:
$$S(2p\sigma, 2p\sigma)=(120)^{-1}p^5[5A_4-18A_2+5A_0]$$
$t>0$:
$$S(2p\sigma, 2p\sigma)=(16)^{-1}p^5(1-t^2)^{5/2}[B_2(A_0+A_4)-A_2(B_0+B_4)] \tag{31}$$

$t=0$:
$$S(2p\sigma, 3s)=(360)^{-1}(10)^{-\frac{1}{2}}p^6[5A_4+6A_2-3A_0]$$
$t\neq 0$:
$$S(2p\sigma, 3s)=(48)^{-1}(10)^{-\frac{1}{2}}p^6(1+t)^{5/2}(1-t)^{7/2}[A_4(B_0-2B_2)+A_1(2B_3-B_5)+B_1(A_5-2A_3)+B_4(2A_2-A_0)] \tag{32}$$

$t=0$:
$$S(2p\sigma, 3p\sigma)=(120)^{-1}(30)^{-\frac{1}{2}}p^6[5A_5-18A_3+5A_1]$$
$t\neq 0$:
$$S(2p\sigma, 3p\sigma)=(16)^{-1}(30)^{-\frac{1}{2}}p^6(1+t)^{5/2}(1-t)^{7/2}[A_2(B_1+B_5)-A_3(B_0+B_4)-B_3(A_0+A_4)+B_2(A_1+A_5)] \tag{33}$$

$t=0$:
$$S(2p\sigma, 5s)=(630)^{-1}(35)^{-\frac{1}{2}}p^7[7A_3-3A_1]$$
$t\neq 0$:
$$S(2p\sigma, 5s)=(192)^{-1}(35)^{-\frac{1}{2}}p^7(1+t)^{5/2}(1-t)^{9/2}[A_6B_1+A_5(B_0-3B_2)+A_4(2B_3-3B_1)+2A_3(B_2+B_4)+A_2(2B_3-3B_5)+A_1(B_6-3B_4)+A_0B_5] \tag{34}$$

$t=0$:
$$S(2p\sigma, 5p\sigma)=(3360)^{-1}(105)^{-\frac{1}{2}}p^7[35A_6-105A_4-15A_2+21A_0]$$
$t\neq 0$:
$$S(2p\sigma, 5p\sigma)=(64)^{-1}(105)^{-\frac{1}{2}}p^7(1+t)^{5/2}(1-t)^{9/2}[A_6B_2-A_4B_0+2A_3(B_1+B_5)-2B_3(A_1+A_5)+B_4A_0-B_6A_2] \tag{35}$$

$t=0$:
$$S(3s, 3s)=(25{,}200)^{-1}p^7[35A_6-35A_4+21A_2-5A_0]$$
$t>0$:
$$S(3s, 3s)=(1440)^{-1}p^7(1-t^2)^{7/2}[A_6B_0-3A_4B_2+3A_2B_4-A_0B_6] \tag{36}$$

$t=0$:
$$S(3s, 3p\sigma)=(12{,}600)^{-1}(3)^{-\frac{1}{2}}p^7[35A_5-14A_3+3A_1]$$
$t\neq 0$:
$$S(3s, 3p\sigma)=(480)^{-1}(3)^{-\frac{1}{2}}p^7(1-t^2)^{7/2}[-A_6B_1+A_5(B_0-B_2)+A_4(B_1+2B_3)+2A_3(B_4-B_2)-A_2(2B_3+B_5)+A_1(B_4-B_6)+A_0B_5] \tag{37}$$
$S(3p\sigma, 3s)$: same as $S(3s, 3p\sigma)$ except each $B_k(t)$ replaced by $B_k(-t)$.

$t=0$:
$$S(3s, 5s)=(50{,}400)^{-1}(14)^{-\frac{1}{2}}p^8[35A_7-35A_5+21A_3-5A_1]$$
$t\neq 0$:
$$S(3s, 5s)=(2880)^{-1}(14)^{-\frac{1}{2}}p^8(1+t)^{7/2}(1-t)^{9/2}[A_7B_0-A_6B_1-3A_5B_2+3A_4B_3+3A_3B_4-3A_2B_5-A_1B_6+A_0B_7] \tag{38}$$

$t=0$:
$$S(3s, 5p\sigma)=(16{,}800)^{-1}(42)^{-\frac{1}{2}}p^8[35A_6-35A_4+21A_2-5A_0]$$
$t\neq 0$:
$$S(3s, 5p\sigma)=(960)^{-1}(42)^{-\frac{1}{2}}p^8(1+t)^{7/2}(1-t)^{9/2}[-A_7B_1+A_6B_0+3A_5B_3-3A_4B_2-3A_3B_5+3A_2B_4+A_1B_7-A_0B_6] \tag{39}$$

$t=0$:
$$S(3p\sigma, 3p\sigma)=(25{,}200)^{-1}p^7[35A_6-147A_4+85A_2-21A_0]$$
$t>0$:
$$S(3p\sigma, 3p\sigma)=(480)^{-1}p^7(1-t^2)^{7/2}[A_6B_2-A_4(B_0+2B_4)+A_2(B_6+2B_2)-A_0B_4] \tag{40}$$

$t=0$:
$$S(3p\sigma, 5s)=(50{,}400)^{-1}(42)^{-\frac{1}{2}}p^8[35A_6+49A_4-51A_2+15A_0]$$
$t\neq 0$:
$$S(3p\sigma, 5s)=(960)^{-1}(42)^{-\frac{1}{2}}p^8(1+t)^{7/2}(1-t)^{9/2}[A_7B_1+A_6(B_0-2B_2)-A_5(B_3+2B_1)+A_4(4B_4-B_2)+A_3(4B_3-B_5)-A_2(2B_6+B_4)+A_1(B_7-2B_5)+A_0B_6] \tag{41}$$

$t=0$:
$$S(3p\sigma, 5p\sigma)=(50{,}400)^{-1}(14)^{-\frac{1}{2}}p^8[35A_7-147A_5+85A_3-21A_1]$$

$t\neq 0$: (42)

$$S(3p\sigma, 5p\sigma)=(960)^{-1}(14)^{-\frac{1}{2}}\rho^8(1+t)^{7/2}(1-t)^{9/2}[A_7B_2-A_6B_3-A_5(B_0+2B_4)+A_4(B_1+2B_5)+A_3(2B_2+B_6)-A_2(2B_3+B_7)-A_1B_4+A_0B_5] \quad (31)$$

$t=0$:

$$S(5s, 5s)=(12{,}700{,}800)^{-1}\rho^9[315A_8-420A_6+378A_4-180A_2+35A_0] \quad (43)$$

$t>0$:

$$S(5s, 5s)=(80{,}640)^{-1}\rho^9(1-t^2)^{9/2}[A_8B_0-4A_6B_2+6A_4B_4-4A_2B_6+A_0B_8] \quad (32)$$

$t=0$:

$$S(5s, 5p\sigma)=(2{,}116{,}800)^{-1}(3)^{-\frac{1}{2}}\rho^9[105A_7-63A_5+27A_3-5A_1]$$

$t\neq 0$:

$$S(5s, 5p\sigma)=(26{,}880)^{-1}(3)^{-\frac{1}{2}}\rho^9(1-t^2)^{9/2}[-A_8B_1+A_7(B_0-B_2)+A_6(B_1+3B_3)+3A_5(B_4-B_2)-3A_4(B_3+B_5)+3A_3(B_4-B_6)+A_2(3B_5+B_7)+A_1(B_8-B_6)-A_0B_7] \quad (44)$$

$S(5p\sigma, 5s)$: same as $S(5s, 5p\sigma)$ except each $B_k(t)$ replaced by $B_k(-t)$. (33)

$t=0$:

$$S(5p\sigma, 5p\sigma)=(4{,}233{,}600)^{-1}\rho^9[105A_8-504A_6+450A_4-224A_2+45A_0] \quad (34)$$

$t>0$:

$$S(5p_\sigma, 5p\sigma)=(26{,}880)^{-1}\rho^9(1-t^2)^{9/2}[A_8B_2-A_6(B_0+3B_4)+3A_4(B_2+B_6)-A_2(B_8+3B_4)+A_0B_6] \quad (45)$$

$t=0$:

$$S(2p\pi, 2p\pi)=(120)^{-1}\rho^5[5A_4-6A_2+A_0] \quad (35)$$

$t>0$:

$$S(2p\pi, 2p\pi)=(32)^{-1}\rho^5(1-t^2)^{5/2}[A_4(B_0-B_2)+A_2(B_4-B_0)+A_0(B_2-B_4)] \quad (46)$$

$t=0$:

$$S(2p\pi, 3p\pi)=(120)^{-1}(30)^{-\frac{1}{2}}\rho^6[5A_5-6A_3+A_1]$$

$t\neq 0$:

$$S(2p\pi, 3p\pi)=(32)^{-1}(30)^{-\frac{1}{2}}\rho^6(1+t)^{5/2}(1-t)^{7/2}[A_5(B_0-B_2)+A_4(B_3-B_1)+A_3(B_4-B_0)+A_2(B_1-B_5)+A_1(B_2-B_4)+A_0(B_5-B_3)] \quad (36)$$

$t=0$:

$$S(2p\pi, 5p\pi)=(3360)^{-1}(105)^{-\frac{1}{2}}\rho^7[35A_6-35A_4-3A_2+3A_0]$$

$t\neq 0$:

$$S(2p\pi, 5p\pi)=(128)^{-1}(105)^{-\frac{1}{2}}\rho^7(1+t)^{5/2}(1-t)^{9/2}[A_6(B_0-B_2)+2A_5(B_3-B_1)+A_4(B_2-B_0)+2A_3(B_1-B_5)+A_2(B_6-B_4)+2A_1(B_5-B_3)+A_0(B_4-B_6)] \quad (37)$$

$t=0$:

$$S(3p\pi, 3p\pi)=(25{,}200)^{-1}\rho^7[35A_6-49A_4+17A_2-3A_0]$$

$t>0$:

$$S(3p\pi, 3p\pi)=(960)^{-1}\rho^7(1-t^2)^{7/2}[A_6(B_0-B_2)+A_4(2B_4-B_0-B_2)+A_2(2B_2-B_4-B_6)+A_0(B_6-B_4)] \quad (38)$$

$t=0$:

$$S(3p\pi, 5p\pi)=(50{,}400)^{-1}(14)^{-\frac{1}{2}}\rho^8[35A_7-49A_5+17A_3-3A_1]$$

$t\neq 0$:

$$S(3p\pi, 5p\pi)=(1920)^{-1}(14)^{-\frac{1}{2}}\rho^8(1+t)^{7/2}(1-t)^{9/2}[A_7(B_0-B_2)+A_6(B_3-B_1)+A_5(2B_4-B_2-B_0)+A_4(B_1+B_3-2B_5)+A_3(2B_2-B_4-B_6)+A_2(B_5-2B_3+B_7)+A_1(B_6-B_4)+A_0(B_5-B_7)] \quad (49a)$$

$t=0$:

$$S(5p\pi, 5p\pi)=(4{,}233{,}600)^{-1}\rho^9[105A_8-168A_6+90A_4-32A_2+5A_0]$$

$t>0$:

$$S(5p\pi, 5p\pi)=(53{,}760)^{-1}\rho^9(1-t^2)^{9/2}[A_8(B_0-B_2)+A_6(3B_4-2B_2-B_0)+3A_4(B_2-B_6)+A_2(B_8+2B_6-3B_4)+A_0(B_6-B_8)] \quad (50)$$

SPECIAL FORMULAS FOR SLATER-AO OVERLAP INTEGRALS FOR $t=0$

$$S(1s, 1s)=e^{-\rho}[1+\rho+(1/3)\rho^2] \quad (51)$$

$$S(2s, 2s)=e^{-\rho}[1+\rho+(4/9)\rho^2+(1/9)\rho^3+(1/45)\rho^4] \quad (52)$$

$$S(3s, 3s)=e^{-\rho}[1+\rho+(7/15)\rho^2+(2/15)\rho^3+(2/75)\rho^4+(1/225)\rho^5+(1/1575)\rho^6] \quad (53)$$

$$S(5s,5s)=e^{-p}[1+p+(10/21)p^2+(1/7)p^3+(16/525)p^4+(8/1575)p^5+(8/11{,}025)p^6 +(1/11{,}025)p^7+(1/99{,}225)p^8] \quad (54)$$

$$S(2p\sigma,2p\sigma)=e^{-p}[-1-p-(1/5)p^2+(2/15)p^3+(1/15)p^4] \quad (55)$$

$$S(3p\sigma,3p\sigma)=e^{-p}[-1-p-(9/25)p^2-(2/75)p^3+(34/1575)p^4+(13/1575)p^5+(1/525)p^6] \quad (56)$$

$$S(5p\sigma,5p\sigma)=e^{-p}[-1-p-(29/70)p^2-(17/210)p^3-(1/735)p^4+(1/294)p^5+(67/66{,}150)p^6 +(13/66{,}150)p^7+(1/33{,}075)p^8] \quad (57)$$

$$S(2s,2p\sigma)=S(2p\sigma,2s)=(\sqrt{3}/6)e^{-p}[p+p^2+(7/15)p^3+(2/15)p^4] \quad (58)$$

$$S(3s,3p\sigma)=S(3p\sigma,3s)=(\sqrt{3}/9)e^{-p}[p+p^2+(12/25)p^3+(11/75)p^4+(17/525)p^5+(1/175)p^6] \quad (59)$$

$$S(5s,5p\sigma)=S(5p\sigma,5s)=(\sqrt{3}/12)e^{-p}[p+p^2+(17/35)p^3+(16/105)p^4+(128/3675)p^5 +(23/3675)p^6+(31/33{,}075)p^7+(4/33{,}075)p^8] \quad (60)$$

$$S(2p\pi,2p\pi)=e^{-p}[1+p+(2/5)p^2+(1/15)p^3] \quad (61)$$

$$S(3p\pi,3p\pi)=e^{-p}[1+p+(34/75)p^2+(3/25)p^3+(31/1575)p^4+(1/525)p^5] \quad (62)$$

$$S(5p\pi,5p\pi)=e^{-p}[1+p+(33/70)p^2+(29/210)p^3+(41/1470)p^4+(1/245)p^5+(29/66{,}150)p^6+(1/33{,}075)p^7] \quad (63)$$

SPECIAL FORMULAS FOR SLATER-AO OVERLAP INTEGRALS FOR $p=0$

$$S(1s,1s)=(1-t^2)^{3/2} \quad (64)$$

$$S(1s,2s)=[(3/4)(1+t)^3(1-t)^5]^{\frac{1}{2}} \quad (65)$$

$$S(1s,3s)=[(2/5)(1+t)^3(1-t)^7]^{\frac{1}{2}} \quad (66)$$

$$S(1s,5s)=[(5/28)(1+t)^3(1-t)^9]^{\frac{1}{2}} \quad (67)$$

$$S(2s,2s)=-S(2p\sigma,2p\sigma)=S(2p\pi,2p\pi)=(1-t^2)^{5/2} \quad (68)$$

$$S(2s,3s)=-S(2p\sigma,3p\sigma)=S(2p\pi,3p\pi)=[(5/6)(1+t)^5(1-t)^7]^{\frac{1}{2}} \quad (69)$$

$$S(2s,5s)=-S(2p\sigma,5p\sigma)=S(2p\pi,5p\pi)=[(15/28)(1+t)^5(1-t)^9]^{\frac{1}{2}} \quad (70)$$

$$S(3s,3s)=-S(3p\sigma,3p\sigma)=S(3p\pi,3p\pi)=(1-t^2)^{7/2} \quad (71)$$

$$S(3s,5s)=-S(3p\sigma,5p\sigma)=S(3p\pi,5p\pi)=[(7/8)(1+t)^7(1-t)^9]^{\frac{1}{2}} \quad (72)$$

$$S(5s,5s)=-S(5p\sigma,5p\sigma)=S(5p\pi,5p\pi)=(1-t^2)^{9/2} \quad (73)$$

V. USE OF THE TABLES TO OBTAIN NON-SLATER OVERLAP INTEGRALS

Although the master formulas above and the master tables below are for Slater-AO overlap integrals, they can also be used in a relatively simple way to obtain S's for orthogonalized Slater AO's, for SCF AO's, for hybrid AO's, and in other ways. This follows from the definition of S in Eq. (1) and the fact that other types of AO's can be written as linear combinations of Slater AO's.

Va. Orthogonalized-Slater-AO Overlap Integrals

As a simple example for the case of orthogonalized Slater AO's, we have for $S^{or}(2s,2s)$ from Eqs. (1) and (8), using the atom-pair notation of (10):

$$S^{or}(2s_a,2s_b;R)=[S(2s_a,2s_b;R)-2QS(1s_a,2s_b;R) +Q^2S(1s_a,1s_b;R)]/(1-Q^2), \quad (74)$$

where $Q\equiv S(1s_a,2s_a)$. Using the parameter notation of (13), Eq. (74) becomes

$$S^{or}(2s,2s;p,t)=[S(2s,2s;p,t)-2QS(1s,2s;p,t) +Q^2S(1s,1s;p,t)]/(1-Q^2), \quad (75)$$

with $Q=S(1s,2s;0,t)$. It will be noted that the computation of S's corresponding to orthogonalized AO's involves the knowledge of internal Slater S's, like $S(1s_a,2s_a)$, and of other Slater S's involving inner-shell AO's, like $S(1s_a,2s_b)$ and $S(1s_a,1s_b)$ in Eq. (74). These, however, differ from like-designated outer-shell S's only in the particular ranges of p and t values needed. For internal S's we have $p=0$, but $t\neq 0$,—see Eqs. (64)–(73).

In the master tables, an effort has been made to include such ranges of p and t that orthogonalized-AO S's can be computed if desired. However, we believe that these are not likely to be important for the range

TABLE II. Comparison of Slater-AO with orthogonalized Slater-AO S's.

Integral	Slater AO's	Orthogonalized Slater AO's
$S(1s_H, 2s_C; 1.06A)$	0.575	0.572
$S(1s_H, 2s_{Li}; 1.60A)$	0.423	0.415
$S(2s_C, 2s_C; 1.20A)$	0.507	0.503
$S(2s_C, 2p\sigma_C; 1.20A)$	0.470	0.480

of R values (medium and large R) that occur for molecular problems. This conclusion is based on the sample cases in Table II, where it will be noted that the two sets of S values differ little, in spite of the rather considerable magnitude (0.220) of the integral $S(1s_C, 2s_C)$,—Q of Eq. (74),—which is involved in three of the cases. A wider variety of cases might of course sometimes disclose larger differences, but it seems unlikely that these would ever become important.

Vb. SCF-AO Overlap Integrals

We have made no extensive study of SCF-AO S's, but it is obvious from Eqs. (1) and (5) or (6) that these are approximately expressible as linear combinations of Slater S's similar to Eq. (75), although usually containing a number of terms. As an example, and for its own intrinsic interest, we have, however, computed $S^{SCF}(2p\pi_C, 2p\pi_C; R)$ and $S^{SCF}(2p\sigma_C, 2p\sigma_C; R)$. This was done after fitting the following normalized formula to the SCF $2p$ AO as given by Jucys in tabular numerical form[10] for the state $1s)^2 2s)^2 2p)^2$, ^1D:

$$\chi^{SCF}(2p_C) \approx 0.260\chi(2p; 2.694) + 0.518\chi(2p; 1.416) + 0.309\chi(2p; 0.898). \quad (76)$$

The formula applies equally to $2p\sigma$ or $2p\pi$. Each of the symbols $\chi(2p; \mu)$ denotes a $2p$ (σ or π) normalized Slater AO with R_{2p} of the form $N_\mu r e^{-\mu r/a_H}$ (see Eqs. (7)). A three-term formula (see Eq. (6)) was found necessary here to obtain a reasonably good fit to the numerical values of Jucys.

When Eq. (76), used for either $2p\sigma$ or $2p\pi$, is combined with Eq. (1), one obtains an expression for $S^{SCF}(2p\sigma_C, 2p\sigma_C; R)$ or $S^{SCF}(2p\pi_C, 2p\pi_C; R)$ as a linear combination of six terms involving Slater-AO S's. For a given R, all of these have different p values; three of them have $t=0$, the rest, other t values >0. Referring to the master tables for the necessary Slater S's, we obtained the $S^{SCF}(R)$ values given in Table III. The Table also includes comparisons with the corresponding simple Slater-AO quantities.

The foregoing example shows that good SCF AO's may give quite different S values than Slater AO's,

[10] A. Jucys, Proc. Roy. Soc. **173A**, 59 (1939); accurate SCF method including exchange. Jucys' $2p$ AO's are appreciably different for the states ^3P, ^1D, and ^1S, of which we have selected the ^1D, where the AO form approximates the average of those for the three cases. We should have preferred the presumably somewhat different SCF $2p$ AO for $2s2p^3$, but Jucys did not compute this.

TABLE III. Comparison of SCF and Slater S's for carbon-carbon $2p$ bonds.

R (A)	p (for Slater AO)	$S(2p\sigma_C, 2p\sigma_C; R)$ SCF	Slater	$S(2p\pi_C, 2p\pi_C; R)$ SCF	Slater
0.00	0.00	−1.00	−1.00	1.00	1.00
0.50	1.54	−0.53	−0.46	0.82	0.80
1.00	3.07	0.02	0.18	0.53	0.45
1.20	3.68	0.14	0.29	0.43	0.34
1.35	4.15	0.19	0.33	0.36	0.265
1.39	4.27	0.21	0.33	0.34	0.25
1.54	4.73	0.24	0.33	0.29	0.19
2.00	6.14	0.25	0.24	0.16	0.08
2.41	7.40	0.21	0.14	0.10	0.035
2.78	8.55	0.16	0.08	0.06	0.016
4.00	12.3	0.05	0.01	0.01	0.001

especially at large R values.[11] When one examines the forms of SCF AO's as given by Hartree and other authors in numerical tables for such atoms as carbon and oxygen, it is seen that they differ characteristically from those of Slater and hydrogenic AO's in their more gradual decrease at large R values, especially for p AO's.[11a] This typical difference makes understandable the results set forth in Table III. For the computation of S values (and of other interatomic integrals used in molecular calculations) these results evidently raise much more serious questions than does the matter of orthogonalization. In particular, they suggest that non-neighbor interactions in polyatomic molecules may be relatively large. It might then seem that we ought to proceed to compute SCF S values for suitable parameter-ranges for the more important AO pairs. However, second thought brings to mind the fact that the best AO's for *atoms in molecules* must be very considerably different than in free atoms, even though we are not very well informed as to the exact nature of these differences and as to their variety in different molecular states. Still, for the case of AO's used in molecular states with stable binding, we would probably

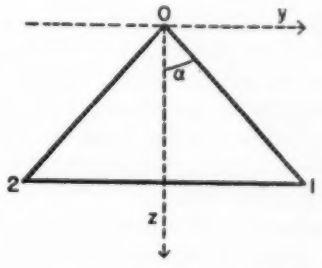

FIG. 2. Axes and notation for H_2O.

[11] Our conclusions given above as to the smallness of the effect on S of orthogonalization (which introduces inner nodes into Slater's radially nodeless AO's) suggests that the inner nodes in SCF AO's might be dropped without much error for the computation of S values. That is, it might be adequate to retain only the outermost loop as Slater does; *provided*, however, this is represented by a sum of two or more exponential terms as in Eq. (76), instead of by a single Slater function.

[11a] *Note added in proof.* In subsequent work in this laboratory, Dr. H. Shull has found that in the case of $2s$ AO's there is little difference between SCF and Slater AO's except for small R values where the SCF AO has an inner loop. Hence S values computed using Slater *ns* AO's are nearly the same as using SCF *ns* AO's.

expect the free-atom AO's to be so modified as to correspond to *increased* rather than decreased overlap; and this increase should be relative to SCF AO's, and therefore all the more so relative to Slater AO's. Obviously the matter deserves further study. Obviously also, the exact values of Slater S's should not be taken too seriously.

Vc. Hybrid-AO Overlap Integrals

The computation of S values for hybrid AO's is a rather satisfying matter, since it is very easy to obtain these from Slater S's, and since the results are very striking. As discussed at the end of Section II, only σ-hybrid AO's can be formed from s and p AO's. The notation (see (10), (13)) and conventions of Section II for Slater-AO S's can be used without change for hybrid-Slater-AO S's.

In general, for a σ-bond between two atoms a and b, formed by AO's with respective hybridization coefficients α_a and α_b (see Eq. (9)), Eqs. (1) and (9) give

$$\begin{aligned}S^{hy}(n_a x, n_b y; p, t)=&\alpha_a\alpha_b S(n_a s, n_b s; p, t)\\&+\sigma_b\alpha_a(1-\alpha_b^2)^{\frac{1}{2}}S(n_a s, n_b p\sigma; p, t)\\&+\sigma_a\alpha_b(1-\alpha_a^2)^{\frac{1}{2}}S(n_a p\sigma, n_b s; p, t)\\&+\sigma_a\sigma_b(1-\alpha_a^2)^{\frac{1}{2}}(1-\alpha_b^2)^{\frac{1}{2}}S(n_a p\sigma, n_b p\sigma; p, t),\end{aligned}\quad(77)$$

where σ_a and σ_b denote the signs before $(1-\alpha^2)^{\frac{1}{2}}$ in Eq. (9), and the parameter-pair p, t have the same values in all the integrals. For a homopolar bond this reduces to

$$\begin{aligned}S^{hy}(nx, nx; p, 0)=&\alpha^2 S(ns, ns; p, 0)\\&\pm 2\alpha(1-\alpha^2)^{\frac{1}{2}}S(ns, np\sigma; p, 0)\\&+(1-\alpha^2)S(np\sigma, np\sigma; p, 0).\end{aligned}\quad(78)$$

For a bond between a $1s$ hydrogen atom AO and a hybrid σ-AO of another atom b, it becomes

$$\begin{aligned}S^{hy}(1s_H, n_b y; p, t)=&\alpha_b S(1s_H, ns_b; p, t)\\&\pm(1-\alpha_b^2)^{\frac{1}{2}}S(1s_H, np\sigma_b; p, t).\end{aligned}\quad(79)$$

In order to obtain numerical values of S for any given hybrid case, it is necessary only to specify α_a and α_b, then to look up the appropriate Slater-AO S values in the master tables, and finally to form linear combinations in accordance with Eqs. (77)–(79). If desired, S values corresponding to hybrid orthogonalized Slater AO's,[6] or to hybrid SCF AO's, can similarly be obtained by using Eqs. (77)–(79) in connection with orthogonalized or SCF pure-AO S values.

Since S values for any desired pair of Slater-AO hybrids can readily be obtained using Eqs. (77)–(79) and the master tables, no extensive hybrid tables will be given here. Nevertheless, two sets of Slater-AO hybrid S tables (Tables XXIV–XXVIII) have been computed explicitly in order to aid the reader in appreciating quantitatively the rather remarkable effects of hybridization on S values. Further examples of hybrid S values for specific molecules, and a discussion, will be given in a following paper.[11b]

[11b] For a preliminary report, see J. Chem. Phys. **17**, 510 (1949).

Vd. Group Overlap Integrals

A further simple application of the present tables is to the computation of overlap integrals in which one or both atoms are replaced by groups of atoms. S's of this sort frequently occur when one is working with non-localized MO's (molecular orbitals) in LCAO approximation. The non-localized MO structure of H_2O furnishes a convenient example. Neglecting s, p hybridization, the electron configuration may be written:

$$\begin{aligned}(1s_O)^2(2s_O)^2(a2py_O+b[1s_1-1s_2])^2(c2pz_O\\+d[1s_1+1s_2])^2(2px_O)^2.\end{aligned}\quad(80)$$

Here the two bonding MO's have been written out in LCAO form (see Fig. 2 for notation). In connection with these MO's, the overlap integrals

$$\left.\begin{aligned}S(y_O, s-s)\equiv&\int 2py_O[(1s_1-1s_2)/(2-2S_{1s_1 1s_2})^{\frac{1}{2}}]d\tau\\S(z_O, s+s)\equiv&\int 2pz_O[(1s_1+1s_2)/(2+2S_{1s_1 1s_2})^{\frac{1}{2}}]d\tau\end{aligned}\right\}\quad(81)$$

are of interest. The internal H—H group normalization factors $(2\pm 2S_{1s,1s})^{\frac{1}{2}}$ are obtained using the $S(1s, 1s)$ master table. The remaining integrals are easily evaluated by writing $2py_O$ or $2pz_O$ as a linear combination of a $2p\sigma$ and a $2p\pi$ function, relative to the axis of *either* the O—H_1 or the O—H_2 bond. Thus

$$\begin{aligned}2py_O=&(\sin\alpha)(2p\sigma_1)+(\cos\alpha)(2p\pi_1)\\=&-(\sin\alpha)(2p\sigma_2)-(\cos\alpha)(2p\pi_2),\\2pz_O=&(\cos\alpha)(2p\sigma_1)+(\sin\alpha)(2p\pi_1)\\=&(\cos\alpha)(2p\sigma_2)+(\sin\alpha)(2p\pi_2).\end{aligned}$$

On substituting into the expressions for $S(y_O, s-s)$ and $S(z_O, s+s)$ above, and noting that $\int 2p\pi_i 1s_i d\tau=0$, we obtain

$$\left.\begin{aligned}S(y_O, s-s)=&\sqrt{2}\sin\alpha[1-S(1s_H, 1s_H; R_{12})]^{-\frac{1}{2}}\\&\times S(1s, 2p\sigma; H-O),\\S(z_O, s+s)=&\sqrt{2}\cos\alpha[1+S(1s_H, 1s_H; R_{12})]^{-\frac{1}{2}}\\&\times S(1s, 2p\sigma; H-O).\end{aligned}\right\}(82)$$

Here the notation of (10), (13) has been used in a convenient way for the S's.

Equations (82) illustrate how the computation or even the mere formulation of group overlap integrals affords added insight into the bonding characteristics of non-localized MO's. If 2α in H_2O were 90°, Eqs. (82) would give

$$S(y_O, s-s)\approx S(z_O, s+s)\approx S(1s, 2p\sigma; H-O),$$

the same integral that would occur using localized MO's or using the valence-bond AO method. Actually, the experimental $2\alpha=105°$ makes $S(y_O, s-s)$ distinctly larger and $S(z_O, s+s)$ distinctly smaller than this; the factors $(1\mp S_{1s,1s})^{\frac{1}{2}}$ enhance this effect considerably. To the extent that S values can be taken as measures

of bonding strengths (see following paper), this indicates that the $y_O+(1s-1s)$ MO is more strongly bonding in H_2O than the $z_O+(1s+1s)$; also that the binding (i.e., ionization) energies of the two MO's are in the same order.

The discussion could be further elaborated by a consideration of s, p hybridization, which is undoubtedly of some importance here. For reasons of symmetry, this can affect only the $[z_O+(1s+1s)]$ MO in the non-localized MO treatment; the result must be that the $2s_O$ AO in (80) acquires some MO bonding properties and the bonding character of $[z_O+(1s+1s)]$ is further weakened; but with an over-all gain in bonding. $S(z_O, s+s)$ in Eqs. (81) now is replaced by a linear combination including $S(2s_O, s+s)$, the final S being easily computed as a function of the extent of hybridization if this were known.

Group overlap integrals can be used to obtain insight into bond strengths in many molecular problems, for example in the study of hyperconjugation. This subject will not be developed here, however, since the object of the present paper is to give methods rather than to discuss applications.

Ve. Transition Moment Integrals

Certain transition moment integrals for electronic transitions in homopolar diatomic molecules can be obtained very simply from overlap integrals,[12] for example:

$$Q_{\pi\sigma'} \equiv \int \chi_{np\pi_x} \times \chi_{np\sigma'} d\tau = \tfrac{1}{2} RS(np\pi, np\pi; p, 0). \quad (83)$$

ACKNOWLEDGMENT

We are very greatly indebted to Mr. Tracy J. Kinyon for his cooperation in the preparation of the tables. Mr. Kinyon carried through the arduous task of making all the extensive numerical computations for the tables in Sections VI and VII.

VI. MASTER TABLES FOR SLATER-AO OVERLAP INTEGRALS**

TABLE IV.

$S(1s, 1s)$

p	$t=0.0$	$t=0.1$	$t=0.2$	$t=0.3$	$t=0.4$	$t=0.5$	$t=0.6$	$t=0.7$	$t=0.8$
0.0	1.000	0.985	0.941	0.868	0.770	0.650	0.512	0.364	0.216
0.5	0.960	0.946	0.905	0.837	0.744	0.630	0.499	0.357	0.213
1.0	0.858	0.847	0.812	0.756	0.678	0.580	0.465	0.337	0.205
1.2	0.807	0.797	0.766	0.715	0.644	0.554	0.447	0.327	0.200
1.3	0.780								
1.4	0.753	0.744	0.717	0.671	0.608	0.526	0.428	0.316	0.196
1.5	0.725								
1.6	0.697	0.689	0.666	0.626	0.570	0.498	0.409	0.305	0.191
1.7	0.669								
1.8	0.641	0.635	0.615	0.581	0.533	0.469	0.388	0.293	0.185
1.9	0.614								
2.0	0.586	0.581	0.565	0.536	0.495	0.439	0.368	0.281	0.180
2.1	0.560								
2.2	0.533	0.529	0.515	0.493	0.458	0.410	0.348	0.269	0.175
2.3	0.508								
2.4	0.483	0.479	0.469	0.451	0.423	0.382	0.328	0.256	0.169
2.5	0.458								
2.6	0.435	0.432	0.425	0.411	0.388	0.355	0.308	0.244	0.164
2.7	0.412								
2.8	0.390	0.388	0.383	0.373	0.356	0.329	0.289	0.233	0.158
2.9	0.369								
3.0	0.349	0.348	0.344	0.338	0.325	0.304	0.271	0.221	0.153
3.2	0.310	0.310	0.309	0.305	0.297	0.281	0.254	0.210	0.148

$S(1s, 1s)$

p	$t=0.0$	$t=0.1$	$t=0.2$	$t=0.3$	$t=0.4$	$t=0.5$	$t=0.6$	$t=0.7$	$t=0.8$
3.4	0.275	0.276	0.276	0.274	0.270	0.259	0.237	0.200	0.143
3.5	0.259								
3.6	0.244	0.244	0.246	0.247	0.245	0.238	0.221	0.189	0.138
3.8	0.215	0.216	0.218	0.221	0.222	0.219	0.206	0.180	0.133
4.0	0.189	0.190	0.194	0.198	0.201	0.201	0.192	0.170	0.128
4.2	0.166	0.167	0.171	0.176	0.182	0.184	0.179	0.161	0.123
4.4	0.146	0.147	0.151	0.157	0.164	0.168	0.166	0.152	0.119
4.5	0.136								
4.6	0.127	0.129	0.133	0.140	0.148	0.154	0.155	0.144	0.114
5.0	0.097	0.098	0.103	0.110	0.120	0.129	0.134	0.129	0.106
5.5	0.068	0.069	0.074	0.082	0.091	0.102	0.111	0.112	0.097
6.0	0.047	0.049	0.053	0.060	0.070	0.081	0.092	0.097	0.088
6.5	0.032	0.034	0.037	0.044	0.053	0.064	0.076	0.084	0.080
7.0	0.022	0.023	0.026	0.032	0.040	0.050	0.063	0.073	0.072
7.5	0.015	0.016	0.018	0.023	0.030	0.040	0.052	0.063	0.066
8.0	0.010	0.011	0.013	0.017	0.023	0.031	0.043	0.054	0.059
9.0	0.005	0.005	0.006	0.009	0.013	0.019	0.029	0.040	0.049
10.0	0.002	0.002	0.003	0.004	0.007	0.012	0.019	0.030	0.040
12.0	0.000	0.000	0.001	0.001	0.002	0.004	0.009	0.017	0.027
15.0	0.000	0.000	0.000	0.000	0.000	0.001	0.003	0.007	0.015
20.0	0.000	0.000	0.000	0.000	0.000	0.000	0.000	0.002	0.005

TABLE V.

$S(1s, 2s)$

p	$t=-0.5$	$t=-0.4$	$t=-0.3$	$t=-0.2$	$t=-0.1$	$t=0.0$	$t=0.1$	$t=0.2$	$t=0.3$	$t=0.4$	$t=0.5$	$t=0.6$	$t=0.7$	$t=0.8$	$t=0.9$
0.0	0.844	0.933	0.977	0.978	0.938	0.866	0.768	0.652	0.526	0.400	0.281	0.177	0.095	0.037	0.007
0.5	0.829	0.916	0.959	0.960	0.923	0.854	0.760	0.647	0.525	0.401	0.284	0.180	0.097	0.039	0.007
1.0	0.787	0.866	0.906	0.907	0.875	0.814	0.730	0.628	0.516	0.400	0.288	0.186	0.102	0.042	0.008
1.5	0.722	0.790	0.823	0.825	0.799	0.749	0.679	0.593	0.496	0.393	0.290	0.192	0.109	0.046	0.009
2.0	0.644	0.697	0.722	0.723	0.702	0.664	0.610	0.542	0.463	0.376	0.285	0.195	0.114	0.050	0.011
2.2	0.611	0.657	0.679	0.679	0.661	0.627	0.579	0.519	0.447	0.367	0.282	0.196	0.116	0.051	0.011
2.4	0.577	0.617	0.635	0.635	0.619	0.589	0.547	0.494	0.430	0.357	0.277	0.195	0.117	0.053	0.012
2.6	0.543	0.578	0.592	0.591	0.576	0.550	0.514	0.468	0.411	0.345	0.272	0.194	0.119	0.054	0.012
2.8	0.510	0.539	0.550	0.547	0.534	0.512	0.481	0.441	0.392	0.333	0.265	0.192	0.119	0.055	0.013
3.0	0.478	0.501	0.508	0.505	0.493	0.474	0.448	0.414	0.372	0.320	0.258	0.190	0.120	0.057	0.013
3.2	0.446	0.464	0.468	0.464	0.453	0.437	0.416	0.388	0.352	0.306	0.251	0.187	0.120	0.058	0.014
3.4	0.416	0.428	0.430	0.425	0.415	0.402	0.384	0.361	0.331	0.292	0.243	0.184	0.120	0.058	0.014
3.6	0.386	0.395	0.394	0.388	0.379	0.368	0.354	0.336	0.311	0.278	0.234	0.180	0.119	0.059	0.014

[12] R. S. Mulliken, J. Chem. Phys. **8**, 238 (1940), footnote 14. (In this footnote, Eq. (12) should read Eq. (15).)

** See Section III, especially Eqs. (12), (13), for definitions and conventions.

TABLE V.—(*Con't*)

$S(1s, 2s)$

p	$t=-0.5$	$t=-0.4$	$t=-0.3$	$t=-0.2$	$t=-0.1$	$t=0.0$	$t=0.1$	$t=0.2$	$t=0.3$	$t=0.4$	$t=0.5$	$t=0.6$	$t=0.7$	$t=0.8$	$t=0.9$
3.8						0.335	0.325	0.311	0.291	0.263	0.225	0.176	0.119	0.060	0.015
4.0	0.332	0.333	0.327	0.320	0.312	0.305	0.297	0.287	0.272	0.249	0.216	0.172	0.118	0.060	0.015
4.2						0.276	0.271	0.264	0.253	0.235	0.207	0.167	0.116	0.061	0.016
4.4						0.250	0.246	0.242	0.235	0.221	0.198	0.162	0.115	0.061	0.016
4.5	0.272	0.265	0.256	0.247	0.241										
4.6						0.225	0.223	0.221	0.217	0.208	0.189	0.157	0.113	0.061	0.016
5.0	0.221	0.209	0.197	0.188	0.183	0.181	0.182	0.184	0.185	0.182	0.170	0.147	0.109	0.062	0.017
5.5						0.136	0.139	0.144	0.149	0.152	0.149	0.134	0.104	0.061	0.018
6.0	0.143	0.127	0.114	0.105	0.101	0.101	0.105	0.111	0.119	0.126	0.128	0.120	0.098	0.060	0.018
6.5						0.074	0.078	0.085	0.094	0.104	0.110	0.108	0.092	0.059	0.019
7.0	0.091	0.075	0.063	0.056	0.053	0.054	0.058	0.065	0.074	0.085	0.093	0.096	0.086	0.058	0.019
7.5						0.039	0.042	0.048	0.058	0.068	0.079	0.085	0.079	0.056	0.020
8.0	0.057	0.044	0.034	0.029	0.027	0.027	0.030	0.036	0.044	0.055	0.066	0.075	0.073	0.054	0.020
9.0						0.014	0.016	0.020	0.026	0.035	0.046	0.057	0.061	0.050	0.020
10.0						0.007	0.008	0.010	0.015	0.022	0.032	0.043	0.051	0.046	0.020
12.0						0.001	0.002	0.003	0.005	0.008	0.014	0.023	0.034	0.037	0.020
15.0						0.000	0.000	0.000	0.001	0.002	0.004	0.009	0.017	0.025	0.019
20.0						0.000	0.000	0.000	0.000	0.000	0.000	0.002	0.005	0.013	0.015

TABLE VI.

$S(1s, 2p\sigma)$

p	$t=-0.5$	$t=-0.4$	$t=-0.3$	$t=-0.2$	$t=-0.1$	$t=0.0$	$t=0.1$	$t=0.2$	$t=0.3$	$t=0.4$	$t=0.5$	$t=0.6$	$t=0.7$	$t=0.8$
0.0	0.000	0.000	0.000	0.000	0.000	0.000	0.000	0.000	0.000	0.000	0.000	0.000	0.000	0.000
0.5	0.117	0.155	0.189	0.216	0.234	0.240	0.235	0.218	0.191	0.157	0.119	0.080	0.046	0.022
1.0	0.208	0.276	0.336	0.385	0.417	0.429	0.421	0.394	0.348	0.288	0.220	0.151	0.087	0.038
1.5	0.264	0.348	0.423	0.484	0.525	0.544	0.538	0.507	0.454	0.381	0.296	0.206	0.121	0.054
2.0	0.287	0.375	0.454	0.518	0.564	0.586	0.585	0.558	0.506	0.433	0.344	0.245	0.148	0.067
2.2	0.289	0.375	0.453	0.517	0.563	0.587	0.587	0.563	0.515	0.444	0.355	0.256	0.156	0.071
2.4	0.287	0.371	0.447	0.509	0.554	0.579	0.582	0.561	0.517	0.449	0.363	0.264	0.164	0.076
2.6	0.282	0.363	0.435	0.495	0.540	0.565	0.570	0.553	0.513	0.450	0.368	0.271	0.170	0.079
2.8	0.275	0.352	0.420	0.477	0.520	0.546	0.553	0.540	0.505	0.447	0.369	0.275	0.175	0.083
3.0	0.266	0.338	0.402	0.456	0.497	0.523	0.532	0.522	0.492	0.441	0.368	0.278	0.179	0.086
3.2	0.255	0.323	0.382	0.432	0.471	0.497	0.508	0.502	0.477	0.431	0.364	0.279	0.182	0.089
3.4	0.244	0.306	0.361	0.407	0.443	0.468	0.481	0.479	0.459	0.419	0.359	0.278	0.184	0.091
3.6	0.232	0.289	0.338	0.380	0.414	0.439	0.453	0.454	0.439	0.406	0.351	0.276	0.186	0.093
3.8						0.409	0.424	0.428	0.418	0.390	0.342	0.273	0.186	0.095
4.0	0.207	0.253	0.293	0.327	0.356	0.379	0.394	0.401	0.396	0.374	0.332	0.269	0.186	0.097
4.2						0.349	0.365	0.374	0.373	0.357	0.321	0.264	0.186	0.098
4.4						0.320	0.337	0.348	0.350	0.339	0.310	0.258	0.185	0.099
4.5	0.176	0.210	0.239	0.264	0.286									
4.6						0.293	0.309	0.322	0.328	0.321	0.298	0.252	0.183	0.100
5.0	0.147	0.171	0.190	0.208	0.225	0.241	0.258	0.273	0.284	0.286	0.272	0.238	0.179	0.101
5.5						0.186	0.202	0.219	0.234	0.243	0.241	0.219	0.172	0.102
6.0	0.099	0.108	0.115	0.122	0.130	0.141	0.155	0.172	0.189	0.204	0.210	0.199	0.163	0.101
6.5						0.105	0.118	0.133	0.151	0.169	0.181	0.179	0.154	0.100
7.0	0.064	0.066	0.066	0.068	0.071	0.078	0.088	0.102	0.120	0.139	0.155	0.160	0.144	0.098
7.5						0.057	0.065	0.077	0.094	0.113	0.132	0.142	0.134	0.095
8.0	0.041	0.039	0.037	0.036	0.037	0.041	0.048	0.058	0.073	0.092	0.111	0.126	0.124	0.092
9.0						0.021	0.025	0.032	0.043	0.059	0.078	0.097	0.104	0.086
10.0						0.010	0.013	0.017	0.025	0.037	0.054	0.073	0.087	0.078
12.0						0.002	0.003	0.005	0.008	0.014	0.025	0.040	0.058	0.063
15.0						0.000	0.000	0.001	0.001	0.003	0.007	0.015	0.030	0.044
20.0						0.000	0.000	0.000	0.000	0.000	0.001	0.003	0.009	0.022

TABLE VII.

$S(1s, 3s)$

p	$t=-0.4$	$t=-0.3$	$t=-0.2$	$t=-0.1$	$t=0.0$	$t=0.1$	$t=0.2$	$t=0.3$	$t=0.4$
0.0	0.954	0.928	0.857	0.754	0.632	0.505	0.381	0.269	0.175
0.5	0.945	0.920	0.851	0.751	0.632	0.507	0.384	0.273	0.179
1.0	0.915	0.893	0.832	0.739	0.628	0.510	0.393	0.284	0.190
1.5	0.864	0.847	0.792	0.713	0.615	0.508	0.399	0.295	0.203
2.0	0.794	0.780	0.736	0.670	0.588	0.495	0.399	0.304	0.215
2.5	0.712	0.701	0.665	0.612	0.546	0.470	0.389	0.306	0.224
3.0	0.623	0.612	0.584	0.544	0.494	0.436	0.370	0.299	0.227
3.2	0.587	0.575	0.551	0.515	0.471	0.419	0.360	0.295	0.226
3.4	0.551	0.539	0.516	0.486	0.447	0.402	0.347	0.289	0.225
3.6	0.516	0.504	0.483	0.456	0.423	0.383	0.334	0.283	0.223
3.8	0.481	0.469	0.450	0.426	0.398	0.364	0.320	0.275	0.220
4.0	0.448	0.435	0.418	0.397	0.373	0.344	0.309	0.267	0.217
4.2	0.416	0.403	0.386	0.369	0.348	0.324	0.295	0.257	0.212

$S(1s, 3s)$

p	$t=-0.4$	$t=-0.3$	$t=-0.2$	$t=-0.1$	$t=0.0$	$t=0.1$	$t=0.2$	$t=0.3$	$t=0.4$
4.4	0.385	0.371	0.356	0.341	0.324	0.305	0.280	0.248	0.207
4.6	0.355	0.341	0.327	0.314	0.301	0.285	0.265	0.238	0.202
4.8	0.327	0.312	0.300	0.288	0.279	0.266	0.249	0.227	0.195
5.0	0.301	0.287	0.274	0.265	0.256	0.248	0.235	0.217	0.190
5.5	0.242	0.227	0.216	0.210	0.206	0.204	0.200	0.190	0.173
6.0	0.193	0.178	0.168	0.164	0.163	0.165	0.166	0.164	0.155
6.5	0.152	0.137	0.129	0.126	0.127	0.132	0.137	0.140	0.137
7.0	0.119	0.105	0.098	0.096	0.098	0.104	0.111	0.117	0.120
7.5	0.092	0.080	0.073	0.072	0.074	0.080	0.089	0.098	0.104
8.0	0.071	0.060	0.054	0.053	0.056	0.062	0.070	0.080	0.089
9.0	0.042	0.033	0.029	0.028	0.030	0.035	0.043	0.053	0.064
10.0	0.024	0.018	0.015	0.015	0.016	0.020	0.025	0.034	0.044

TABLE VIII.

$S(1s, 3p\sigma)$

ρ	$t=-0.4$	$t=-0.3$	$t=-0.2$	$t=-0.1$	$t=0.0$	$t=0.1$	$t=0.2$	$t=0.3$	$t=0.4$
0.0	0.000	0.000	0.000	0.000	0.000	0.000	0.000	0.000	0.000
0.5	0.162	0.183	0.194	0.192	0.179	0.158	0.130	0.100	0.071
1.0	0.302	0.343	0.363	0.362	0.340	0.302	0.251	0.195	0.139
1.5	0.404	0.461	0.490	0.491	0.466	0.418	0.353	0.278	0.202
2.0	0.464	0.529	0.565	0.571	0.547	0.497	0.427	0.343	0.255
2.5	0.483	0.550	0.590	0.601	0.582	0.538	0.470	0.387	0.294
3.0	0.470	0.534	0.574	0.589	0.578	0.543	0.485	0.408	0.320
3.2	0.458	0.520	0.559	0.575	0.567	0.536	0.483	0.411	0.326
3.4	0.444	0.502	0.541	0.558	0.553	0.526	0.478	0.412	0.330
3.6	0.427	0.482	0.519	0.536	0.535	0.512	0.470	0.409	0.332
3.8	0.408	0.460	0.495	0.513	0.514	0.496	0.459	0.404	0.332
4.0	0.388	0.436	0.469	0.487	0.490	0.477	0.446	0.397	0.330
4.2	0.367	0.411	0.442	0.460	0.466	0.457	0.431	0.388	0.327
4.4	0.346	0.386	0.415	0.433	0.440	0.435	0.415	0.377	0.323
4.6	0.325	0.360	0.387	0.405	0.414	0.412	0.397	0.366	0.317
4.8	0.303	0.335	0.360	0.377	0.387	0.388	0.378	0.352	0.309
5.0	0.283	0.311	0.333	0.350	0.361	0.365	0.359	0.339	0.302
5.5	0.234	0.254	0.270	0.285	0.297	0.307	0.310	0.302	0.279
6.0	0.190	0.203	0.215	0.227	0.240	0.253	0.262	0.264	0.253
6.5	0.153	0.160	0.168	0.178	0.190	0.204	0.218	0.227	0.225
7.0	0.121	0.125	0.129	0.137	0.148	0.162	0.178	0.192	0.198
7.5	0.096	0.096	0.098	0.104	0.114	0.127	0.144	0.161	0.173
8.0	0.074	0.073	0.074	0.078	0.086	0.099	0.115	0.133	0.149
9.0	0.044	0.041	0.040	0.042	0.048	0.057	0.071	0.088	0.107
10.0	0.026	0.023	0.021	0.022	0.026	0.032	0.042	0.057	0.075

TABLE IX.

$S(1s, 5s)$

ρ	$t=-0.4$	$t=-0.3$	$t=-0.2$	$t=-0.1$	$t=0.0$	$t=0.1$	$t=0.2$	$t=0.3$	$t=0.4$
0.0	0.893	0.806	0.687	0.554	0.423	0.303	0.204	0.126	0.070
0.5	0.888	0.803	0.687	0.556	0.426	0.308	0.208	0.129	0.073
1.0	0.873	0.795	0.685	0.560	0.435	0.313	0.219	0.139	0.080
1.5	0.846	0.776	0.676	0.562	0.444	0.333	0.234	0.153	0.091
2.0	0.805	0.745	0.658	0.557	0.450	0.346	0.251	0.169	0.104
2.5	0.749	0.699	0.627	0.540	0.448	0.354	0.265	0.185	0.118
3.0	0.682	0.642	0.583	0.513	0.435	0.354	0.273	0.198	0.131
3.2	0.653	0.616	0.562	0.498	0.427	0.351	0.275	0.202	0.135
3.4	0.624	0.589	0.540	0.482	0.417	0.347	0.275	0.205	0.140
3.6	0.593	0.561	0.517	0.465	0.406	0.342	0.275	0.207	0.143
3.8	0.562	0.533	0.493	0.447	0.394	0.335	0.273	0.209	0.147
4.0	0.531	0.504	0.468	0.427	0.380	0.327	0.270	0.209	0.149
4.5	0.454	0.432	0.405	0.376	0.341	0.303	0.257	0.208	0.154
5.0	0.384	0.363	0.343	0.323	0.300	0.273	0.240	0.200	0.154
5.5	0.319	0.300	0.285	0.272	0.258	0.242	0.219	0.190	0.152
6.0	0.261	0.244	0.232	0.224	0.218	0.209	0.196	0.176	0.147
6.5	0.213	0.197	0.187	0.183	0.181	0.179	0.173	0.161	0.140
7.0	0.170	0.155	0.147	0.145	0.147	0.149	0.149	0.144	0.130
7.5	0.135	0.121	0.115	0.114	0.117	0.123	0.127	0.127	0.120
8.0	0.106	0.094	0.089	0.089	0.093	0.100	0.107	0.111	0.109
9.0	0.065	0.055	0.051	0.052	0.056	0.063	0.073	0.082	0.087
10.0	0.039	0.031	0.028	0.029	0.032	0.039	0.048	0.058	0.067

TABLE X.

$S(1s, 5p\sigma)$

ρ	$t=-0.4$	$t=-0.3$	$t=-0.2$	$t=-0.1$	$t=0.0$	$t=0.1$	$t=0.2$	$t=0.3$	$t=0.4$
0.0	0.000	0.000	0.000	0.000	0.000	0.000	0.000	0.000	0.000
0.5	0.153	0.161	0.157	0.143	0.121	0.096	0.071	0.047	0.029
1.0	0.293	0.310	0.304	0.278	0.238	0.190	0.141	0.096	0.059
1.5	0.409	0.435	0.429	0.397	0.344	0.279	0.210	0.146	0.091
2.0	0.493	0.526	0.524	0.490	0.431	0.355	0.273	0.194	0.124
2.5	0.540	0.580	0.581	0.550	0.493	0.414	0.326	0.238	0.157
3.0	0.553	0.596	0.603	0.579	0.526	0.453	0.366	0.274	0.186
3.2	0.550	0.593	0.603	0.581	0.532	0.462	0.377	0.286	0.197
3.4	0.543	0.586	0.597	0.578	0.534	0.467	0.385	0.296	0.207
3.6	0.532	0.574	0.587	0.572	0.531	0.470	0.392	0.304	0.215
3.8	0.518	0.559	0.573	0.561	0.526	0.469	0.395	0.311	0.223
4.0	0.501	0.541	0.556	0.548	0.516	0.465	0.396	0.316	0.230
4.5	0.453	0.488	0.504	0.502	0.482	0.445	0.390	0.321	0.242
5.0	0.396	0.426	0.442	0.445	0.436	0.412	0.372	0.316	0.247
5.5	0.339	0.363	0.377	0.384	0.383	0.371	0.345	0.303	0.246
6.0	0.285	0.302	0.315	0.324	0.328	0.326	0.313	0.285	0.240
6.5	0.237	0.248	0.258	0.268	0.277	0.282	0.279	0.263	0.230
7.0	0.192	0.199	0.206	0.216	0.227	0.237	0.242	0.237	0.216
7.5	0.155	0.158	0.163	0.172	0.184	0.197	0.208	0.211	0.200
8.0	0.123	0.124	0.127	0.135	0.147	0.161	0.175	0.185	0.182
9.0	0.076	0.074	0.074	0.080	0.090	0.104	0.121	0.137	0.147
10.0	0.046	0.042	0.042	0.045	0.052	0.064	0.079	0.098	0.114

TABLE XI.

$S(2s, 2s)$

ρ	$t=0.0$	$t=0.1$	$t=0.2$	$t=0.3$	$t=0.4$	$t=0.5$	$t=0.6$
0.0	1.000	0.975	0.903	0.790	0.647	0.487	0.328
0.5	0.986	0.962	0.892	0.782	0.642	0.486	0.328
1.0	0.948	0.926	0.862	0.760	0.629	0.481	0.329
1.5	0.890	0.871	0.815	0.725	0.608	0.472	0.329
2.0	0.815	0.799	0.753	0.678	0.578	0.458	0.327
2.5	0.729	0.717	0.679	0.622	0.540	0.438	0.322
3.0	0.637	0.629	0.603	0.559	0.496	0.413	0.312
3.2	0.600	0.593	0.571	0.533	0.477	0.402	0.308
3.4	0.563	0.557	0.539	0.507	0.457	0.389	0.302
3.6	0.527	0.522	0.507	0.480	0.438	0.377	0.296
3.8	0.491	0.487	0.476	0.454	0.417	0.364	0.290
4.0	0.456	0.454	0.445	0.427	0.397	0.350	0.283
4.2	0.423	0.421	0.415	0.402	0.377	0.336	0.276
4.4	0.390	0.389	0.386	0.376	0.357	0.323	0.268
4.6	0.360	0.359	0.358	0.352	0.337	0.309	0.260
4.8	0.330	0.331	0.331	0.328	0.318	0.295	0.252
5.0	0.302	0.307	0.305	0.305	0.299	0.281	0.244
5.5	0.240	0.242	0.247	0.252	0.255	0.248	0.223
6.0	0.188	0.190	0.197	0.206	0.215	0.216	0.203
6.5	0.145	0.148	0.155	0.167	0.179	0.187	0.182
7.0	0.111	0.113	0.121	0.133	0.148	0.160	0.163
7.5	0.083	0.086	0.093	0.106	0.121	0.136	0.145
8.0	0.062	0.064	0.071	0.083	0.099	0.116	0.128
8.5	0.046	0.048	0.054	0.065	0.080	0.097	0.112
9.0	0.034	0.035	0.041	0.050	0.064	0.082	0.098
9.5	0.024	0.026	0.030	0.039	0.051	0.068	0.086
10.0	0.018	0.019	0.023	0.030	0.041	0.057	0.075
10.5	0.013	0.014	0.017	0.023	0.032	0.047	0.065
11.0	0.009	0.010	0.012	0.017	0.026	0.039	0.056
11.5	0.006	0.007	0.009	0.013	0.020	0.032	0.048
12.0	0.004	0.005	0.007	0.010	0.016	0.026	0.041
12.5	0.003	0.004	0.005	0.007	0.012	0.021	0.036
13.0	0.002	0.002	0.003	0.006	0.010	0.017	0.030
13.5	0.002	0.002	0.002	0.004	0.008	0.014	0.026
14.0	0.001	0.001	0.002	0.003	0.006	0.012	0.022

TABLE XII.

	$S(2p\sigma, 2s)$						$S(2s, 2p\sigma)$						
p	$t=0.6$	$t=0.5$	$t=0.4$	$t=0.3$	$t=0.2$	$t=0.1$	$t=0.0$	$t=0.1$	$t=0.2$	$t=0.3$	$t=0.4$	$t=0.5$	$t=0.6$
0.0	0.000	0.000	0.000	0.000	0.000	0.000	0.000	0.000	0.000	0.000	0.000	0.000	0.000
0.5	−0.008	0.002	0.020	0.047	0.079	0.112	0.143	0.167	0.180	0.180	0.166	0.139	0.103
1.0	−0.010	0.011	0.047	0.098	0.158	0.220	0.276	0.319	0.343	0.342	0.315	0.265	0.198
1.5	−0.005	0.028	0.081	0.151	0.231	0.313	0.386	0.443	0.473	0.472	0.437	0.369	0.278
2.0	0.006	0.049	0.114	0.197	0.289	0.381	0.464	0.526	0.561	0.560	0.521	0.446	0.340
2.5	0.019	0.070	0.143	0.218	0.327	0.420	0.504	0.567	0.603	0.602	0.569	0.493	0.383
3.0	0.033	0.089	0.163	0.251	0.342	0.431	0.509	0.570	0.606	0.612	0.582	0.513	0.407
3.2	0.037	0.096	0.169	0.254	0.342	0.427	0.503	0.562	0.598	0.606	0.580	0.515	0.412
3.4	0.042	0.099	0.173	0.255	0.339	0.421	0.492	0.549	0.586	0.596	0.573	0.513	0.415
3.6	0.046	0.103	0.175	0.254	0.335	0.411	0.479	0.534	0.570	0.582	0.563	0.509	0.416
3.8	0.049	0.106	0.176	0.252	0.327	0.399	0.463	0.515	0.551	0.565	0.550	0.502	0.415
4.0	0.052	0.109	0.176	0.247	0.318	0.385	0.444	0.494	0.529	0.545	0.535	0.492	0.412
4.2	0.055	0.110	0.174	0.241	0.307	0.369	0.425	0.471	0.505	0.523	0.518	0.481	0.407
4.4	0.057	0.111	0.172	0.234	0.295	0.351	0.402	0.446	0.480	0.500	0.499	0.469	0.401
4.6	0.059	0.111	0.168	0.226	0.281	0.333	0.380	0.421	0.455	0.476	0.479	0.454	0.394
4.8	0.060	0.110	0.164	0.217	0.267	0.314	0.357	0.396	0.428	0.451	0.458	0.439	0.386
5.0	0.061	0.109	0.159	0.208	0.253	0.295	0.334	0.370	0.402	0.426	0.436	0.423	0.377
5.5	0.062	0.104	0.145	0.182	0.216	0.248	0.278	0.308	0.337	0.364	0.382	0.382	0.351
6.0	0.061	0.096	0.129	0.157	0.181	0.203	0.226	0.250	0.277	0.305	0.328	0.339	0.324
6.5	0.058	0.088	0.112	0.132	0.148	0.163	0.180	0.200	0.224	0.251	0.278	0.297	0.295
7.0	0.055	0.079	0.096	0.109	0.119	0.129	0.141	0.157	0.178	0.205	0.233	0.258	0.266
7.5	0.051	0.070	0.082	0.089	0.095	0.101	0.109	0.122	0.140	0.165	0.193	0.222	0.238
8.0	0.047	0.061	0.068	0.072	0.074	0.077	0.083	0.093	0.109	0.131	0.159	0.189	0.212
8.5	0.043	0.053	0.057	0.057	0.057	0.059	0.063	0.070	0.084	0.103	0.130	0.160	0.187
9.0	0.039	0.045	0.047	0.045	0.044	0.044	0.046	0.053	0.064	0.081	0.105	0.135	0.165
9.5	0.035	0.038	0.038	0.036	0.033	0.033	0.034	0.039	0.048	0.063	0.085	0.113	0.144
10.0	0.031	0.033	0.031	0.028	0.025	0.024	0.025	0.029	0.036	0.048	0.068	0.095	0.126
10.5							0.018	0.021	0.027	0.037	0.054	0.079	0.109
11.0	0.024	0.023	0.020	0.016	0.014	0.013	0.013	0.015	0.020	0.028	0.043	0.065	0.095
11.5							0.009	0.011	0.015	0.022	0.034	0.054	0.082
12.0	0.018	0.016	0.012	0.010	0.008	0.007	0.007	0.008	0.011	0.016	0.027	0.044	0.070
12.5							0.005	0.006	0.008	0.012	0.021	0.036	0.060
13.0							0.003	0.004	0.006	0.009	0.016	0.030	0.052
13.5							0.002	0.003	0.004	0.007	0.013	0.024	0.044
14.0							0.002	0.002	0.003	0.005	0.010	0.020	0.038

TABLE XIII.

	$S(2s, 3s)$												
p	$t=-0.6$	$t=-0.5$	$t=-0.4$	$t=-0.3$	$t=-0.2$	$t=-0.1$	$t=0.0$	$t=0.1$	$t=0.2$	$t=0.3$	$t=0.4$	$t=0.5$	$t=0.6$
0.0	0.479	0.667	0.826	0.937	0.989	0.979	0.913	0.801	0.659	0.505	0.354	0.222	0.120
0.5	0.477	0.663	0.820	0.929	0.979	0.970	0.905	0.796	0.657	0.505	0.356	0.225	0.122
1.0	0.473	0.651	0.801	0.904	0.952	0.943	0.884	0.782	0.650	0.505	0.361	0.231	0.127
1.5	0.466	0.634	0.771	0.865	0.909	0.902	0.849	0.758	0.638	0.504	0.367	0.240	0.136
2.0	0.457	0.611	0.733	0.815	0.853	0.847	0.803	0.725	0.620	0.499	0.372	0.250	0.146
2.5	0.445	0.582	0.688	0.756	0.789	0.785	0.747	0.682	0.594	0.488	0.373	0.258	0.156
3.0	0.430	0.549	0.637	0.692	0.716	0.712	0.684	0.632	0.560	0.472	0.371	0.265	0.165
3.5	0.411	0.512	0.582	0.623	0.639	0.636	0.614	0.575	0.519	0.448	0.362	0.268	0.173
4.0	0.390	0.472	0.524	0.552	0.562	0.557	0.541	0.514	0.473	0.418	0.349	0.267	0.178
4.5	0.365	0.429	0.466	0.483	0.485	0.481	0.469	0.451	0.423	0.384	0.329	0.261	0.181
5.0	0.339	0.387	0.408	0.415	0.413	0.407	0.395	0.389	0.372	0.347	0.307	0.252	0.182
5.5	0.312	0.344	0.354	0.352	0.346	0.339	0.334	0.329	0.322	0.308	0.282	0.239	0.180
6.0	0.285	0.304	0.303	0.295	0.285	0.278	0.275	0.275	0.275	0.270	0.255	0.225	0.175
6.5	0.259	0.266	0.258	0.245	0.233	0.226	0.225	0.227	0.232	0.234	0.229	0.209	0.170
7.0	0.232	0.230	0.216	0.200	0.187	0.180	0.179	0.184	0.191	0.199	0.201	0.191	0.162
7.5	0.207	0.198	0.180	0.162	0.149	0.142	0.142	0.147	0.157	0.168	0.176	0.173	0.153
8.0	0.184	0.169	0.148	0.130	0.117	0.111	0.111	0.117	0.127	0.140	0.152	0.156	0.144
9.0	0.143	0.121	0.099	0.082	0.071	0.065	0.066	0.071	0.081	0.095	0.111	0.123	0.124
10.0	0.110	0.085	0.065	0.050	0.041	0.037	0.037	0.042	0.050	0.062	0.079	0.095	0.104

TABLE XIV.

$S(2s, 3p\sigma)$

p	$t=-0.6$	$t=-0.5$	$t=-0.4$	$t=-0.3$	$t=-0.2$	$t=-0.1$	$t=0.0$	$t=0.1$	$t=0.2$	$t=0.3$	$t=0.4$	$t=0.5$	$t=0.6$
0.0	0.000	0.000	0.000	0.000	0.000	0.000	0.000	0.000	0.000	0.000	0.000	0.000	0.000
0.5	0.001	0.020	0.048	0.081	0.113	0.140	0.156	0.160	0.150	0.130	0.101	0.070	0.041
1.0	0.004	0.042	0.096	0.158	0.219	0.269	0.300	0.307	0.290	0.251	0.198	0.138	0.082
1.5	0.013	0.067	0.143	0.229	0.312	0.380	0.422	0.433	0.410	0.358	0.285	0.201	0.122
2.0	0.027	0.095	0.187	0.289	0.386	0.465	0.515	0.529	0.505	0.445	0.359	0.258	0.159
2.5	0.044	0.122	0.224	0.334	0.438	0.522	0.576	0.593	0.570	0.509	0.416	0.306	0.193
3.0	0.060	0.146	0.252	0.363	0.466	0.550	0.605	0.624	0.605	0.548	0.457	0.343	0.222
3.5	0.076	0.164	0.267	0.374	0.470	0.549	0.603	0.625	0.612	0.563	0.480	0.369	0.246
4.0	0.088	0.175	0.273	0.370	0.456	0.527	0.577	0.601	0.596	0.558	0.486	0.384	0.264
4.5	0.098	0.180	0.268	0.352	0.427	0.488	0.533	0.558	0.561	0.535	0.478	0.390	0.277
5.0	0.102	0.178	0.255	0.326	0.387	0.438	0.478	0.505	0.514	0.500	0.459	0.385	0.283
5.5	0.104	0.172	0.236	0.293	0.342	0.383	0.418	0.444	0.459	0.457	0.430	0.373	0.285
6.0	0.103	0.162	0.214	0.258	0.295	0.328	0.356	0.382	0.401	0.409	0.397	0.356	0.282
6.5	0.101	9.150	0.191	0.224	0.251	0.275	0.299	0.323	0.346	0.361	0.361	0.335	0.276
7.0	0.095	0.135	0.166	0.189	0.207	0.225	0.245	0.267	0.291	0.311	0.321	0.309	0.265
7.5	0.089	0.121	0.143	0.158	0.170	0.182	0.198	0.218	0.242	0.266	0.283	0.283	0.252
8.0	0.083	0.107	0.122	0.130	0.137	0.145	0.157	0.175	0.198	0.224	0.247	0.257	0.238
9.0	0.069	0.081	0.085	0.085	0.086	0.088	0.096	0.109	0.129	0.154	0.183	0.205	0.207
10.0	0.055	0.059	0.059	0.054	0.051	0.052	0.056	0.065	0.080	0.103	0.131	0.159	0.175

TABLE XV.

$S(2p\sigma, 2p\sigma)$

p	$t=0.0$	$t=0.1$	$t=0.2$	$t=0.3$	$t=0.4$	$t=0.5$	$t=0.6$
0.0	−1.000	−0.975	−0.903	−0.790	−0.647	−0.487	−0.328
0.5	−0.927	−0.906	−0.840	−0.738	−0.607	−0.461	−0.312
1.0	−0.736	−0.720	−0.673	−0.599	−0.502	−0.389	−0.271
1.5	−0.483	−0.475	−0.452	−0.416	−0.360	−0.292	−0.214
2.0	−0.226	−0.226	−0.226	−0.222	−0.211	−0.188	−0.150
2.5	0.005	−0.007	−0.029	−0.053	−0.076	−0.092	−0.092
3.0	0.159	0.148	0.121	0.079	0.032	−0.011	−0.040
3.2	0.208	0.196	0.167	0.120	0.067	0.016	−0.022
3.4	0.248	0.237	0.204	0.155	0.097	0.040	−0.005
3.6	0.279	0.268	0.235	0.184	0.123	0.061	0.010
3.8	0.303	0.291	0.258	0.207	0.144	0.079	0.023
4.0	0.319	0.308	0.275	0.224	0.161	0.094	0.035
4.2	0.328	0.318	0.286	0.237	0.175	0.107	0.045
4.4	0.332	0.322	0.293	0.245	0.185	0.117	0.054
4.6	0.332	0.322	0.294	0.250	0.191	0.126	0.062
4.8	0.327	0.318	0.293	0.251	0.196	0.132	0.068
5.0	0.319	0.311	0.288	0.249	0.197	0.136	0.074
5.5	0.289	0.282	0.266	0.236	0.193	0.141	0.083

$S(2p\sigma, 2p\sigma)$

p	$t=0.0$	$t=0.1$	$t=0.2$	$t=0.3$	$t=0.4$	$t=0.5$	$t=0.6$
6.0	0.250	0.247	0.235	0.214	0.181	0.138	0.087
6.5	0.210	0.208	0.201	0.187	0.164	0.131	0.087
7.0	0.171	0.171	0.167	0.160	0.145	0.120	0.085
7.5	0.137	0.137	0.137	0.134	0.126	0.109	0.081
8.0	0.107	0.108	0.109	0.110	0.107	0.096	0.075
8.5	0.083	0.084	0.086	0.089	0.090	0.085	0.069
9.0	0.063	0.064	0.067	0.071	0.075	0.073	0.063
9.5	0.047	0.048	0.052	0.057	0.061	0.063	0.057
10.0	0.035	0.036	0.039	0.045	0.050	0.054	0.051
10.5	0.026	0.027	0.030	0.035	0.041	0.045	0.045
11.0	0.019	0.020	0.021	0.027	0.033	0.038	0.040
11.5	0.013	0.014	0.017	0.021	0.026	0.032	0.035
12.0	0.010	0.010	0.012	0.016	0.021	0.027	0.031
12.5	0.007	0.007	0.009	0.012	0.017	0.022	0.027
13.0	0.005	0.005	0.007	0.009	0.013	0.018	0.023
13.5	0.003	0.004	0.005	0.007	0.010	0.015	0.020
14.0	0.002	0.003	0.003	0.005	0.008	0.012	0.017

TABLE XVI.

$S(2p\sigma, 3s)$

p	$t=-0.6$	$t=-0.5$	$t=-0.4$	$t=-0.3$	$t=-0.2$	$t=-0.1$	$t=0.0$	$t=0.1$	$t=0.2$	$t=0.3$	$t=0.4$	$t=0.5$	$t=0.6$
0.0	0.000	0.000	0.000	0.000	0.000	0.000	0.000	0.000	0.000	0.000	0.000	0.000	0.000
0.5	0.110	0.134	0.142	0.135	0.114	0.085	0.054	0.025	0.002	−0.013	−0.019	−0.018	−0.013
1.0	0.214	0.261	0.278	0.265	0.227	0.173	0.114	0.058	0.013	−0.017	−0.032	−0.032	−0.024
1.5	0.307	0.374	0.399	0.383	0.333	0.261	0.179	0.102	0.034	−0.009	−0.034	−0.039	−0.031
2.0	0.385	0.466	0.497	0.480	0.424	0.340	0.245	0.152	0.071	+0.011	−0.025	−0.038	−0.034
2.5	0.445	0.534	0.569	0.551	0.492	0.405	0.303	0.201	0.111	0.039	−0.008	−0.030	−0.033
3.0	0.486	0.576	0.609	0.591	0.533	0.447	0.346	0.243	0.148	0.069	+0.013	−0.019	−0.028
3.5	0.509	0.594	0.622	0.603	0.547	0.466	0.371	0.272	0.179	0.097	0.035	−0.005	−0.021
4.0	0.515	0.590	0.611	0.589	0.535	0.462	0.376	0.287	0.199	0.120	0.055	+0.010	−0.014
4.5	0.508	0.569	0.580	0.555	0.505	0.439	0.365	0.287	0.208	0.135	0.061	0.023	−0.005
5.0	0.490	0.536	0.537	0.508	0.461	0.404	0.341	0.275	0.208	0.143	0.083	0.034	+0.002
5.5	0.465	0.495	0.485	0.453	0.409	0.360	0.308	0.255	0.199	0.144	0.090	0.043	0.009
6.0	0.434	0.449	0.430	0.395	0.354	0.314	0.271	0.230	0.185	0.139	0.093	0.050	0.015
6.5	0.402	0.403	0.376	0.339	0.301	0.266	0.233	0.201	0.167	0.131	0.093	0.054	0.020
7.0	0.366	0.354	0.322	0.284	0.250	0.220	0.194	0.171	0.147	0.120	0.089	0.055	0.024
7.5	0.331	0.310	0.273	0.236	0.204	0.180	0.160	0.143	0.126	0.107	0.083	0.055	0.027
8.0	0.297	0.268	0.229	0.193	0.165	0.144	0.129	0.118	0.107	0.094	0.076	0.054	0.028
9.0	0.235	0.197	0.157	0.125	0.103	0.089	0.081	0.076	0.073	0.069	0.061	0.048	0.029
10.0	0.182	0.140	0.104	0.078	0.062	0.053	0.048	0.047	0.047	0.048	0.047	0.040	0.028

TABLE XVII.

	$S(2p\sigma, 3p\sigma)$												
p	$t=-0.6$	$t=-0.5$	$t=-0.4$	$t=-0.3$	$t=-0.2$	$t=-0.1$	$t=0.0$	$t=0.1$	$t=0.2$	$t=0.3$	$t=0.4$	$t=0.5$	$t=0.6$
0.0	−0.479	−0.667	−0.826	−0.937	−0.989	−0.979	−0.913	−0.801	−0.659	−0.505	−0.354	−0.222	−0.120
0.5	−0.462	−0.640	−0.790	−0.894	−0.942	−0.934	−0.872	−0.768	−0.636	−0.490	−0.347	−0.220	−0.120
1.0	−0.414	−0.564	−0.687	−0.771	−0.811	−0.805	−0.757	−0.674	−0.567	−0.446	−0.323	−0.211	−0.118
1.5	−0.343	−0.453	−0.537	−0.593	−0.618	−0.615	−0.585	−0.531	−0.460	−0.375	−0.284	−0.194	−0.114
2.0	−0.261	−0.324	−0.365	−0.389	−0.398	−0.396	−0.384	−0.362	−0.330	−0.285	−0.230	−0.168	−0.107
2.5	−0.177	−0.194	−0.195	−0.187	−0.180	−0.178	−0.181	−0.188	−0.192	−0.187	−0.169	−0.136	−0.094
3.0	−0.097	−0.076	−0.042	−0.010	+0.010	+0.013	−0.002	−0.029	−0.062	−0.089	−0.104	−0.101	−0.080
3.5	−0.028	+0.022	+0.081	+0.130	0.159	0.163	+0.142	+0.102	+0.050	−0.002	−0.043	−0.064	−0.063
4.0	+0.027	0.099	0.172	0.230	0.264	0.268	0.245	0.198	0.136	+0.070	+0.012	−0.029	−0.045
4.5	0.070	0.153	0.232	0.292	0.326	0.330	0.307	0.260	0.196	0.124	0.056	+0.003	−0.027
5.0	0.101	0.187	0.264	0.321	0.351	0.355	0.334	0.291	0.231	0.161	0.090	0.029	−0.011
5.5	0.122	0.205	0.275	0.324	0.350	0.353	0.335	0.298	0.246	0.182	0.113	0.050	+0.004
6.0	0.134	0.210	0.270	0.310	0.330	0.331	0.317	0.287	0.244	0.189	0.127	0.066	0.016
6.5	0.139	0.206	0.256	0.286	0.299	0.299	0.288	0.265	0.232	0.187	0.133	0.077	0.026
7.0	0.138	0.194	0.232	0.253	0.261	0.259	0.251	0.235	0.211	0.177	0.133	0.082	0.034
7.5	0.134	0.179	0.207	0.220	0.222	0.220	0.213	0.203	0.186	0.162	0.128	0.085	0.040
8.0	0.127	0.162	0.181	0.186	0.185	0.182	0.177	0.171	0.161	0.145	0.120	0.084	0.044
9.0	0.109	0.127	0.131	0.128	0.122	0.118	0.115	0.115	0.114	0.110	0.099	0.078	0.047
10.0	0.089	0.095	0.091	0.083	0.076	0.072	0.071	0.072	0.075	0.078	0.076	0.067	0.046

TABLE XVIII.

p	$S(3s, 3s)$ $t=0.0$	$S(3p\sigma, 3p\sigma)$ $t=0.0$	$S(3s, 3p\sigma)$ $t=0.0$	p	$S(3s, 3s)$ $t=0.0$	$S(3p\sigma, 3p\sigma)$ $t=0.0$	$S(3s, 3p\sigma)$ $t=0.0$
0.0	1.000	−1.000	0.000	6.4	0.328	0.377	0.371
0.5	0.992	−0.965	0.096	6.6	0.306	0.368	0.352
1.0	0.968	−0.866	0.189	6.8	0.285	0.358	0.333
1.5	0.932	−0.715	0.276	7.0	0.264	0.346	0.314
2.0	0.885	−0.531	0.354	7.2	0.245	0.333	0.295
2.5	0.832	−0.333	0.419	7.4	0.227	0.319	0.277
3.0	0.772	−0.140	0.468	7.6	0.209	0.304	0.259
3.5	0.708	0.031	0.499	7.8	0.193	0.288	0.241
4.0	0.641	0.171	0.511	8.0	0.177	0.273	0.225
4.5	0.572	0.273	0.504	8.5	0.141	0.233	0.185
5.0	0.504	0.342	0.483	9.0	0.114	0.195	0.151
5.2	0.477	0.359	0.470	9.5	0.089	0.161	0.121
5.4	0.451	0.372	0.457	10.0	0.070	0.130	0.096
5.6	0.425	0.380	0.441	10.5	0.054	0.104	0.076
5.8	0.400	0.385	0.425	11.0	0.041	0.082	0.059
6.0	0.375	0.385	0.407	11.5	0.031	0.064	0.045
6.2	0.351	0.382	0.389	12.0	0.024	0.050	0.034

TABLE XIX.

p	$S(5s, 5s)$ $t=0.0$	$S(5p\sigma, 5p\sigma)$ $t=0.0$	$S(5s, 5p\sigma)$ $t=0.0$	p	$S(5s, 5s)$ $t=0.0$	$S(5p\sigma, 5p\sigma)$ $t=0.0$	$S(5s, 5p\sigma)$ $t=0.0$
0.0	1.000	−1.000	0.000	7.0	0.417	0.413	0.445
0.5	0.994	−0.979	0.072	7.5	0.367	0.418	0.411
1.0	0.977	−0.917	0.142	8.0	0.320	0.407	0.374
1.5	0.950	−0.819	0.210	8.5	0.276	0.384	0.334
2.0	0.915	−0.693	0.273	9.0	0.235	0.354	0.294
2.5	0.874	−0.547	0.331	9.5	0.198	0.318	0.255
3.0	0.828	−0.390	0.383	10.0	0.166	0.281	0.218
3.5	0.780	−0.231	0.427	10.5	0.137	0.244	0.185
4.0	0.730	−0.079	0.462	11.0	0.113	0.208	0.154
4.5	0.679	0.059	0.486	11.5	0.091	0.175	0.127
5.0	0.627	0.177	0.499	12.0	0.074	0.145	0.104
5.5	0.574	0.272	0.501	12.5	0.059	0.119	0.084
6.0	0.521	0.343	0.491	13.0	0.047	0.097	0.067
6.5	0.468	0.389	0.472				

TABLE XX.

	$S(2p\pi, 2p\pi)$						
p	$t=0.0$	$t=0.1$	$t=0.2$	$t=0.3$	$t=0.4$	$t=0.5$	$t=0.6$
0.0	1.000	0.975	0.903	0.790	0.647	0.487	0.328
0.5	0.976	0.951	0.882	0.772	0.633	0.478	0.323
1.0	0.907	0.887	0.823	0.723	0.596	0.453	0.308
1.5	0.809	0.790	0.737	0.652	0.542	0.416	0.287
2.0	0.695	0.680	0.638	0.568	0.477	0.372	0.261
2.5	0.578	0.567	0.535	0.481	0.410	0.325	0.233
3.0	0.468	0.460	0.437	0.398	0.345	0.279	0.205
3.2	0.427	0.420	0.401	0.367	0.320	0.262	0.194
3.4	0.389	0.383	0.366	0.337	0.297	0.245	0.183
3.6	0.352	0.348	0.334	0.309	0.274	0.228	0.173
3.8	0.318	0.315	0.303	0.283	0.253	0.213	0.163
4.0	0.287	0.284	0.275	0.258	0.232	0.198	0.153
4.2	0.258	0.255	0.248	0.234	0.213	0.183	0.144
4.4	0.231	0.229	0.224	0.213	0.195	0.170	0.135
4.6	0.207	0.205	0.201	0.193	0.179	0.157	0.127
4.8	0.184	0.183	0.181	0.174	0.163	0.145	0.119
5.0	0.164	0.163	0.162	0.157	0.149	0.134	0.111
5.2	0.146						
5.4	0.129						
5.5	0.121	0.122	0.122	0.121	0.117	0.109	0.094
5.6	0.114						
5.8	0.101						
6.0	0.089	0.089	0.091	0.092	0.092	0.089	0.079
6.2	0.078						
6.4	0.069						
6.5	0.064	0.065	0.067	0.069	0.072	0.071	0.066
7.0	0.046	0.047	0.049	0.052	0.055	0.057	0.055
7.5	0.033	0.033	0.036	0.039	0.043	0.046	0.046
8.0	0.023	0.024	0.026	0.029	0.033	0.037	0.038
9.0	0.011	0.012	0.013	0.016	0.019	0.023	0.026
10.0	0.005	0.006	0.007	0.008	0.011	0.013	0.018

TABLE XXI.

	$S(2p\pi, 2p\pi)$												
p	$t=-0.6$	$t=-0.5$	$t=-0.4$	$t=-0.3$	$t=-0.2$	$t=-0.1$	$t=0.0$	$t=0.1$	$t=0.2$	$t=0.3$	$t=0.4$	$t=0.5$	$t=0.6$
0.0	0.479	0.667	0.826	0.937	0.989	0.979	0.913	0.801	0.659	0.505	0.354	0.222	0.120
0.5	0.473	0.658	0.814	0.923	0.973	0.963	0.899	0.786	0.652	0.500	0.352	0.221	0.120
1.0	0.456	0.632	0.779	0.881	0.928	0.920	0.860	0.758	0.628	0.485	0.344	0.219	0.119
1.5	0.431	0.591	0.724	0.816	0.858	0.851	0.798	0.708	0.591	0.461	0.331	0.213	0.118
2.0	0.399	0.541	0.656	0.735	0.771	0.765	0.720	0.643	0.542	0.429	0.313	0.206	0.117
2.5	0.363	0.484	0.581	0.645	0.676	0.672	0.633	0.569	0.486	0.390	0.290	0.195	0.114
3.0	0.325	0.426	0.503	0.554	0.575	0.571	0.542	0.492	0.426	0.348	0.264	0.182	0.109
3.5	0.287	0.369	0.428	0.466	0.480	0.477	0.454	0.416	0.366	0.303	0.237	0.168	0.104
4.0	0.251	0.315	0.359	0.384	0.394	0.389	0.373	0.345	0.308	0.262	0.209	0.153	0.097
4.5	0.218	0.266	0.297	0.313	0.316	0.312	0.301	0.282	0.255	0.222	0.182	0.137	0.090
5.0	0.187	0.222	0.241	0.250	0.251	0.246	0.238	0.225	0.208	0.185	0.157	0.122	0.083
5.2					0.228	0.223	0.216	0.205	0.191	0.172			
5.4					0.206	0.202	0.195	0.187	0.175	0.159			
5.5	0.160	0.184	0.195	0.198	0.196	0.192	0.186	0.178	0.167	0.153	0.133	0.107	0.076
5.6					0.186	0.182	0.176	0.169	0.160	0.147			
5.8					0.168	0.164	0.159	0.153	0.146	0.135			
6.0	0.136	0.151	0.156	0.155	0.151	0.147	0.143	0.139	0.133	0.125	0.112	0.093	0 069
6.5	0.115	0.123	0.124	0.120	0.115	0.112	0.109	0.107	0.104	0.101	0.093	0.081	0.062
7.0	0.097	0.100	0.097	0.092	0.087	0.084	0.082	0.081	0.081	0.080	0.077	0.069	0.055
7.5	0.082	0.081	0.076	0.070	0.065	0.062	0.061	0.061	0.062	0.064	0.063	0.059	0.049
8.0	0.068	0.065	0.059	0.053	0.049	0.046	0.045	0.046	0.048	0.050	0.052	0.050	0.043
9.0	0.048	0.042	0.036	0.030	0.026	0.024	0.024	0.025	0.027	0.030	0.034	0.035	0.033
10.0	0.033	0.027	0.021	0.017	0.014	0.012	0.012	0.013	0.015	0.018	0.022	0.025	0.025

TABLE XXII.

	$S(2p\pi, 5p\pi)$			$S(2p\pi, 5p\pi)$	
p	$t=0.0$	$t=0.1$	p	$t=0.0$	$t=0.1$
0.5	0.726	0.58	7.5	0.093	0.090
1.0	0.707	0.563	8.0	0.072	0.071
1.5	0.677	0.543	8.5	0.055	0.055
2.0	0.635	0.515	9.0	0.041	0.042
2.5	0.584	0.482	9.5	0.030	0.032
3.0	0.526	0.438	10.0	0.023	0.024
3.5	0.464	0.393	10.5	0.017	0.018
4.0	0.401	0.345	11.0	0.012	0.014
4.5	0.341	0.298	11.5	0.009	0.010
5.0	0.284	0.253	12.0	0.007	0.008
5.5	0.234	0.212	12.5	0.005	0.006
6.0	0.189	0.174	13.0	0.003	0.004
6.5	0.151	0.142	13.5	0.002	0.003
7.0	0.119	0.114	14.0	0.002	0.003

TABLE XXIII.

p	$S(3p\pi, 3p\pi)$ $t=0.0$	$S(5p\pi, 5p\pi)$ $t=0.0$	p	$S(3p\pi, 3p\pi)$ $t=0.0$	$S(5p\pi, 5p\pi)$ $t=0.0$
0.0	1.000	1.000	6.4	0.184	0.338
0.5	0.988	0.993	6.6	0.167	0.317
1.0	0.955	0.972	6.8	0.152	0.297
1.5	0.901	0.938	7.0	0.137	0.277
2.0	0.832	0.893	7.2	0.124	0.259
2.5	0.752	0.839	7.4	0.112	0.241
3.0	0.666	0.778	7.6	0.101	0.224
3.5	0.578	0.712	7.8	0.091	0.208
4.0	0.493	0.644	8.0	0.081	0.193
4.5	0.413	0.575	8.5	0.062	0.159
5.0	0.341	0.508	9.0	0.046	0.130
5.2	0.314		9.5	0.035	0.105
5.4	0.289		10.0	0.026	0.084
5.5		0.443	10.5		0.067
5.6	0.265		11.0		0.053
5.8	0.243		11.5		0.042
6.0	0.222	0.383	12.0		0.033
6.2	0.202	0.360	12.5		0.025

VII. TABLES OF SELECTED HYBRID SLATER-AO OVERLAP INTEGRALS***

TABLE XXIV.

	$S(1s, 2di\sigma)$									$S(1s, 2di\sigma)$							
p	$t=-0.5$	$t=-0.4$	$t=-0.3$	$t=-0.2$	$t=-0.1$	$t=0.0$	$t=0.1$	$t=0.2$	p	$t=-0.5$	$t=-0.4$	$t=-0.3$	$t=-0.2$	$t=-0.1$	$t=0.0$	$t=0.1$	$t=0.2$
0.0						0.612	0.543	0.461	4.0	0.381	0.414	0.439	0.457	0.472	0.483	0.489	0.486
0.5	0.669	0.757	0.812	0.832	0.818	0.773	0.704	0.611	4.2						0.442	0.450	0.451
1.0	0.704	0.807	0.878	0.914	0.913	0.879	0.814	0.723	4.4						0.403	0.412	0.417
1.5	0.697	0.804	0.881	0.925	0.936	0.914	0.860	0.778	4.5	0.317	0.336	0.350	0.362	0.372			
2.0	0.658	0.758	0.831	0.877	0.895	0.884	0.845	0.778	4.6						0.366	0.377	0.384
2.2	0.636	0.730	0.800	0.846	0.865	0.858	0.825	0.765	5.0	0.260	0.269	0.274	0.280	0.288	0.299	0.311	0.323
2.4	0.611	0.699	0.765	0.809	0.829	0.826	0.798	0.746	5.5						0.228	0.241	0.256
2.6	0.583	0.665	0.727	0.768	0.789	0.789	0.767	0.722	6.0	0.171	0.166	0.162	0.160	0.163	0.171	0.184	0.200
2.8	0.555	0.630	0.686	0.725	0.746	0.748	0.731	0.694	6.5						0.127	0.138	0.155
3.0	0.526	0.593	0.644	0.680	0.700	0.705	0.693	0.662	7.0	0.110	0.100	0.092	0.088	0.088	0.093	0.103	0.118
3.2	0.496	0.556	0.601	0.634	0.654	0.660	0.653	0.629	7.5						0.067	0.076	0.089
3.4	0.466	0.519	0.559	0.588	0.607	0.615	0.612	0.594	8.0	0.070	0.058	0.050	0.046	0.045	0.048	0.055	0.067
3.6	0.437	0.483	0.518	0.543	0.561	0.570	0.570	0.558	9.0						0.024	0.029	0.037
3.8						0.526	0.529	0.522	10.0						0.012	0.014	0.020

TABLE XXV.

	$S(1s, 2tr\sigma)$									$S(1s, 2tr\sigma)$							
p	$t=-0.5$	$t=-0.4$	$t=-0.3$	$t=-0.2$	$t=-0.1$	$t=0.0$	$t=0.1$	$t=0.2$	p	$t=-0.5$	$t=-0.4$	$t=-0.3$	$t=-0.2$	$t=-0.1$	$t=0.0$	$t=0.1$	$t=0.2$
0.0						0.500	0.443	0.376	4.0	0.360	0.399	0.428	0.452	0.471	0.485	0.493	0.493
0.5	0.574	0.655	0.708	0.731	0.727	0.689	0.631	0.551	4.2						0.444	0.455	0.458
1.0	0.624	0.725	0.797	0.838	0.845	0.821	0.765	0.684	4.4						0.405	0.417	0.424
1.5	0.633	0.740	0.821	0.871	0.890	0.876	0.831	0.756	4.5	0.301	0.325	0.343	0.358	0.372			
2.0	0.606	0.708	0.788	0.840	0.866	0.862	0.830	0.769	4.6						0.369	0.381	0.391
2.2	0.588	0.686	0.762	0.814	0.841	0.841	0.814	0.759	5.0	0.247	0.260	0.270	0.278	0.289	0.302	0.316	0.329
2.4	0.567	0.659	0.732	0.782	0.810	0.813	0.791	0.743	5.5						0.231	0.245	0.262
2.6	0.544	0.630	0.697	0.746	0.773	0.779	0.762	0.722	6.0	0.163	0.162	0.160	0.160	0.165	0.174	0.187	0.205
2.8	0.519	0.598	0.661	0.706	0.733	0.741	0.729	0.696	6.5						0.129	0.141	0.158
3.0	0.493	0.565	0.622	0.664	0.690	0.701	0.693	0.666	7.0	0.105	0.097	0.091	0.088	0.089	0.094	0.105	0.121
3.2	0.466	0.531	0.583	0.621	0.646	0.658	0.655	0.634	7.5						0.068	0.077	0.091
3.4	0.439	0.497	0.543	0.577	0.601	0.614	0.615	0.599	8.0	0.067	0.057	0.050	0.046	0.046	0.049	0.056	0.068
3.6	0.412	0.463	0.504	0.534	0.557	0.571	0.574	0.564	9.0						0.025	0.029	0.038
3.8						0.527	0.534	0.529	10.0						0.012	0.015	0.020

*** See Section III, especially Eqs. (12), (13), for definitions and conventions, and Eqs. (9), (78), (79) for the hybrid S formulas.

TABLE XXVI.

$S(1s, 2l\epsilon\sigma)$

p	$t=-0.5$	$t=-0.4$	$t=-0.3$	$t=-0.2$	$t=-0.1$	$t=0.0$	$t=0.1$	$t=0.2$
0.0						0.433	0.384	0.326
0.5	0.516	0.592	0.643	0.667	0.664	0.635	0.584	0.512
1.0	0.574	0.672	0.744	0.787	0.798	0.779	0.730	0.655
1.5	0.590	0.696	0.778	0.832	0.854	0.845	0.805	0.736
2.0	0.570	0.673	0.754	0.810	0.839	0.840	0.811	0.754
2.2	0.555	0.654	0.732	0.787	0.818	0.822	0.798	0.747
2.4	0.537	0.630	0.705	0.758	0.789	0.796	0.777	0.733
2.6	0.516	0.603	0.673	0.724	0.755	0.765	0.751	0.713
2.8	0.493	0.574	0.639	0.687	0.718	0.729	0.720	0.688
3.0	0.469	0.543	0.603	0.647	0.677	0.690	0.685	0.660
3.2	0.444	0.511	0.565	0.606	0.634	0.649	0.648	0.628
3.4	0.419	0.479	0.527	0.565	0.591	0.606	0.609	0.595
3.6	0.394	0.447	0.490	0.523	0.548	0.564	0.569	0.561
3.8						0.522	0.530	0.526

$S(1s, 2l\epsilon\sigma)$

p	$t=-0.5$	$t=-0.4$	$t=-0.3$	$t=-0.2$	$t=-0.1$	$t=0.0$	$t=0.1$	$t=0.2$
4.0	0.345	0.385	0.417	0.443	0.464	0.480	0.490	0.491
4.2						0.440	0.452	0.456
4.4						0.402	0.415	0.422
4.5	0.288	0.314	0.335	0.352	0.368			
4.6						0.366	0.380	0.390
5.0	0.238	0.252	0.264	0.274	0.286	0.300	0.314	0.329
5.5						0.229	0.244	0.261
6.0	0.157	0.157	0.157	0.158	0.163	0.173	0.187	0.205
6.5						0.128	0.141	0.158
7.0	0.101	0.094	0.089	0.087	0.088	0.094	0.105	0.121
7.5						0.068	0.077	0.091
8.0	0.064	0.056	0.049	0.046	0.046	0.049	0.056	0.068
9.0						0.025	0.029	0.038
10.0						0.012	0.015	0.020

TABLE XXVII.

$S[1s, 2(\alpha=\frac{1}{2})]$

p	$t=-0.5$	$t=-0.4$	$t=-0.3$	$t=-0.2$	$t=-0.1$	$t=0.0$	$t=0.1$	$t=0.2$
0.0						0.289	0.256	0.217
0.5	0.386	0.451	0.498	0.524	0.528	0.511	0.475	0.421
1.0	0.459	0.549	0.619	0.665	0.684	0.676	0.641	0.581
1.5	0.490	0.591	0.673	0.731	0.762	0.762	0.733	0.676
2.0	0.485	0.586	0.668	0.730	0.766	0.774	0.755	0.707
2.2	0.476	0.573	0.653	0.714	0.751	0.762	0.747	0.704
2.4	0.462	0.556	0.633	0.691	0.729	0.742	0.731	0.694
2.6	0.447	0.535	0.608	0.664	0.701	0.716	0.709	0.677
2.8	0.429	0.511	0.580	0.633	0.668	0.685	0.682	0.656
3.0	0.410	0.486	0.549	0.598	0.633	0.651	0.651	0.631
3.2	0.389	0.459	0.517	0.562	0.595	0.614	0.617	0.602
3.4	0.369	0.431	0.483	0.525	0.556	0.575	0.581	0.572
3.6	0.347	0.404	0.450	0.488	0.517	0.536	0.545	0.540
3.8						0.497	0.507	0.507

$S[1s, 2(\alpha=\frac{1}{2})]$

p	$t=-0.5$	$t=-0.4$	$t=-0.3$	$t=-0.2$	$t=-0.1$	$t=0.0$	$t=0.1$	$t=0.2$
4.0	0.306	0.349	0.385	0.415	0.440	0.459	0.471	0.471
4.2						0.421	0.435	0.440
4.4						0.385	0.400	0.449
4.5	0.256	0.286	0.311	0.331	0.350			
4.6						0.351	0.366	0.378
5.0	0.212	0.231	0.245	0.259	0.273	0.288	0.304	0.319
5.5						0.221	0.237	0.254
6.0	0.141	0.144	0.146	0.150	0.156	0.167	9.181	0.199
6.5						0.124	0.137	0.154
7.0	0.091	0.087	0.084	0.082	0.085	0.091	0.102	0.118
7.5						0.066	0.075	0.089
8.0	0.058	0.051	0.046	0.044	0.044	0.048	0.055	0.067
9.0						0.024	0.029	0.037
10.0						0.012	0.014	0.020

TABLE XXVIII.

p	$S(2di\sigma, 2di\sigma)$ $t=0.0$	$S(2tr\sigma, 2tr\sigma)$ $t=0.0$	$S(2t\epsilon\sigma, 2t\epsilon\sigma)$ $t=0.0$	$S[2(\alpha=\frac{1}{2}), 2(\alpha=\frac{1}{2})]$ $t=0.0$
0.0	0.000	−0.333	−0.500	−0.778
0.5	0.172	−0.155	−0.325	−0.625
1.0	0.382	+0.086	−0.076	−0.375
1.5	0.590	0.339	+0.195	−0.087
2.0	0.758	0.558	0.436	+0.181
2.5	0.871	0.721	0.622	0.402
3.0	0.907	0.798	0.719	0.532
3.2	0.907	0.813	0.742	0.568
3.4	0.898	0.818	0.753	0.593
3.6	0.882	0.813	0.756	0.608
3.8	0.860	0.802	0.750	0.614
4.0	0.832	0.783	0.738	0.613
4.2	0.801	0.761	0.720	0.606
4.4	0.765	0.733	0.696	0.592

p	$S(2di\sigma, 2di\sigma)$ $t=0.0$	$S(2tr\sigma, 2tr\sigma)$ $t=0.0$	$S(2t\epsilon\sigma, 2t\epsilon\sigma)$ $t=0.0$	$S[2(\alpha=\frac{1}{2}), 2(\alpha=\frac{1}{2})]$ $t=0.0$
4.6	0.725	0.699	0.668	0.573
4.8	0.685	0.664	0.637	0.552
5.0	0.645	0.628	0.604	0.527
5.5	0.542	0.534	0.517	0.458
6.0	0.445	0.443	0.430	0.385
6.5	0.358	0.358	0.350	0.316
7.0	0.282	0.284	0.278	0.253
7.5	0.219	0.222	0.218	0.199
8.0	0.168	0.170	0.168	0.154
8.5	0.127	0.129	0.128	0.118
9.0	0.095	0.097	0.096	0.089
9.5	0.070	0.072	0.071	0.066
10.0	0.051	0.053	0.052	0.049

Measurements of Normal Burning Velocities and Flame Temperatures of Bunsen Flames*

J. W. ANDERSEN† AND R. S. FEIN‡
Department of Chemistry and Naval Research Laboratory, University of Wisconsin, Madison, Wisconsin
(Received April 1, 1949)

Stroboscopically illuminated particle tracks are used to accurately measure normal burning velocities of laminar flames. The precision of the measurements is increased by the use of a constant-velocity profile nozzle which gives a straight-sided Bunsen cone. Normal burning velocity data are presented for 3.7 to 5.3 percent propane-air mixtures. The value for the stoichiometric flame was determined to be 44.8 cm/sec.

From stroboscopic and streak photographs of particle tracks it is possible to obtain the maximum flame temperature and temperature distribution in the flame front. Measurements from the two types of photographs are combined with the equation of continuity and the equation of state to obtain the flame temperature. The flame temperature for a stoichiometric propane-air flame was determined to be 2220°K. An extension of this method is used to obtain an approximation of the temperature distribution in the flame front.

TABLE OF NOMENCLATURE

u = velocity of gas.
b = distance between streamlines measured parallel to the flame front.
A = cross-sectional area of the stream tube.
r = radius from axis of flame to stream line.
α = angle between flame front and the vertical.
β = angle between flame front and emergent streamline on the hot side of the flame.
ρ = density of gas.
M = mean molecular weight of gas.
M_i = molecular weight of ith component of gas.
n_i = number of moles of ith component of gas.
V = molar volume of gas.
R = gas constant.
P = total pressure.
T = absolute temperature.
Subscript 1 refers to initial gas.
Subscript 2 refers to exit gas.
Subscript n refers to velocity component normal to flame front.

PART I. NORMAL BURNING VELOCITIES FROM STROBOSCOPICALLY ILLUMINATED PARTICLE TRACKS

Introduction

SEVERAL different experimental procedures have been proposed for the determination of the normal burning velocities of Bunsen flames. All of these methods involve the measurement of flame areas or cone angles. These quantities are difficult to define accurately because of the thickness of the flame front and the curvature of the flame. Additional errors are introduced by the pre-heating of the unburned gas at the top of the cone; the quenching of the burning gas at the base of the flame; and divergence of the streamlines in the unburned gas. The stroboscopically illuminated particle method of Lewis and von Elbe[1] allows measurements to be made at any point in the flame, thus eliminating most of the above mentioned uncertainties. Therefore, in this work, a modified version of their procedure is used. The straight tube is replaced with a constant-velocity profile nozzle producing a straight-sided flame cone.

The normal burning velocity of a laminar flame is defined as the rate of flame propagation normal to the surface of combustion and relative to the cold gas. Figure 1 illustrates the application of the above definition to a Bunsen type flame.

To obtain the necessary data for the determination of u_{n1} particles of magnesium oxide are introduced into the base of the burner tube. When the particles appear in the flame, they are illuminated by a periodically intermittent sheet of light in the plane of the diameter. A photograph of the particles at right angles to the beam of light records the tracks. From the length of the particle tracks and the time interval of illumination the filament velocity may be calculated.

Thus, measurements of normal burning velocity may be made at any point along the Bunsen cone. This property is constant in the central portion of the side of the cone, where pre-heating at the tip and quenching at the base have negligible effect.

Apparatus

The equipment used in this study is illustrated in Fig. 2. Heavy construction was utilized to give maximum rigidity. To eliminate the effects of vibrations, the motor driven stroboscopic disk is mounted independently of the burner housing. As a further precaution, the entire burner housing is mounted on soft rubber.

The burner tube is 54 inches long, 2.00 inches in diameter, and topped by a copper nozzle made by an electroforming process.[2] This nozzle has a smooth internal surface, a wall thickness at the top of 0.040 inch, and an exit diameter of 0.500 inch. Magnesium oxide particles are introduced at the bottom of the burner from a particle-feeding chamber containing steel wool pads at top and bottom. A charge of particles is placed between these pads; the lower pad serves to support

* This work was carried out under Contract NOrd 9938 between the Navy Bureau of Ordnance and the University of Wisconsin.
† Present address: Monsanto Chemical Company, Dayton, Ohio.
†† Present address: The Texas Company, Beacon, New York.
[1] B. Lewis and G. von Elbe, J. Chem. Phys. **11**, 75 (1943).
[2] J. W. Andersen, Rev. Sci. Inst. **19**, 822 (1948).

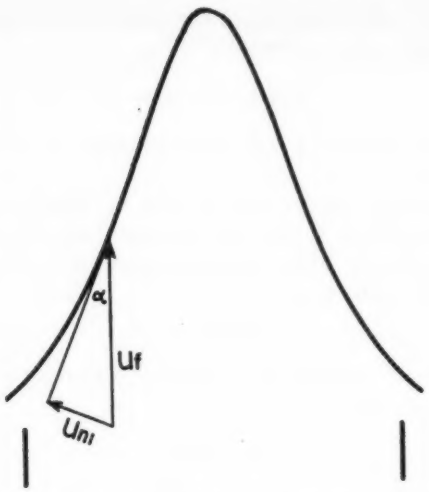

FIG. 1. Definition of normal burning velocity. u_f = filament velocity, u_{n1} = normal burning velocity = $u_f \sin\alpha$.

the charge, and the upper breaks up agglomerates. By diverting the gas flow through the feeder, particles are obtained in the flame. Their presence is detected by the yellow light produced by the small amount of sodium in the particles.

A standard type high peak, long-duration flash bulb provides illumination which is rendered intermittent by a sectored wheel driven by a synchronous motor. This light passes through a pair of slits arranged so that the thickness of the sheet of light along the plane of the diameter of the burner tube never exceeds 0.02 inch.

Photographs are taken on 4×5 inch film, and an extension bellows on the camera provides images on the negative with up to a threefold magnification. For convenience in making measurements, the negatives are enlarged tenfold. Because small quantities of sodium in the particles produce strong *D*-lines in the flame, orthochromatic film is used to avoid masking of the particle tracks. Increased emulsion speeds are obtained by heating the film to 70°C just prior to exposure. To obtain definition of particle tracks, it is necessary to keep the background on the negative low by use of short exposures.

Gas mixtures are provided by a critical velocity orifice metering system.[3] This system accurately meters three separate gas streams and then mixes them.

Particles

The size range of particles delivered by the particle feeder was determined by catching samples on a microscope slide at the top of the burner tube. This test was run on samples of magnesium oxide supplied by two different manufacturers. In one sample the largest size observable was 20 microns and it was 40 microns in the other sample.

[3] J. W. Andersen and R. Friedman, Rev. Sci. Inst. **20**, 61 (1949).

The success of the stroboscopically illuminated particle method depends upon the ability of the particle to accurately indicate the filament velocity. A sample of particles from the larger size range mentioned above was added to the gas stream and a photograph of the non-ignited jet taken. It was found that the total flow measured from particle tracks agreed to within 1 percent of the metered value. Across the flat portion of the velocity profile (90 percent of the diameter for the 0.500-inch exit diameter nozzle) individual particle tracks were within 0.3 percent of the average value.

Results

Figure 3 illustrates the photographs obtained. The central portion of the flame front, indicated in Fig. 3 between the short lines ruled perpendicular to the flame front, is the zone over which the normal burning velocity can be accurately measured. This section is not subject to the pre-heating effect which occurs at the tip of the flame, or to the divergence of streamlines that occurs near the base of the cone. The divergence of the streamlines in the unburned gas is caused by the pressure drop across the flame and by the lower gas velocities near the edge of the nozzle.

The propane used in the following experiments was stated by the manufacturer to have a purity of 99 percent. Precautions were taken to keep the water in the fuel-air mixture below 0.07 percent.

The use of the nozzle simplifies the measurement of the angle of the flame front because a straight-sided

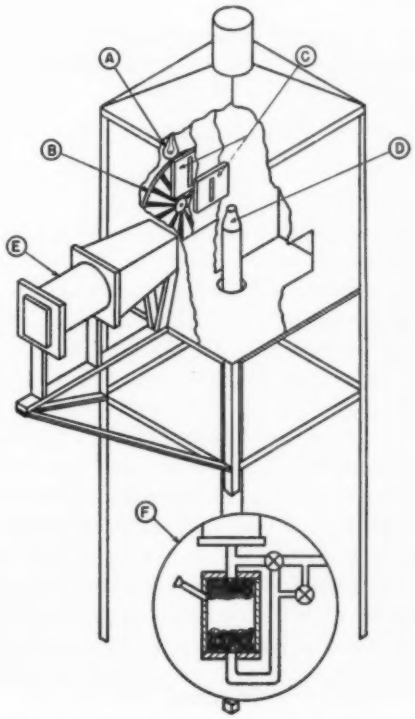

FIG. 2. Burner housing. *A*, Flash bulb; *B*, Stroboscopic disk; *C*, Slits; *D*, Nozzle; *E*, Camera; *F*, Particle feeder.

TABLE I.

Film number	Flow conditions	Filament velocity	Angle	Normal burning velocity
54	Nozzle	147 cm/sec	17° 30′	45.1 cm/sec
57e	Nozzle	92.0	22° 0′	44.6
58e	Nozzle	100.5	28° 30′	43.9
59a	Nozzle	159	16° 40′	45.6
61b	Straight tube	247	10° 40′	45.7
61b	Straight tube	289	9° 30′	45.0
			Average:	45.0 cm/sec

Bunsen cone is formed. The normal burning velocities that were measured are presented in Fig. 4.

The values of u_{n1} for a 4.12 percent propane-air mixture, obtained with the nozzle and a straight tube of the same exit diameter, are given in Table I and illustrate the agreement under the two different flow conditions.

Filament velocities were calculated from the measured lengths of particle tracks and the time of the light cycle. Nozzle flame angles were measured in the zone previously described. For the straight tube flames, the best tangent to the flame front (as indicated by the luminous zone) at the intersection of the filament whose velocity was measured, determined the flame angle. The spread in the data presented represents the maximum deviation which has been observed.

The range of composition, for which the normal burning velocity has been determined, is limited by the size of the nozzle. Outside of this composition range, the flow rate required to maintain a flame on the nozzle is too low to produce a straight-sided cone.

PART II. FLAME TEMPERATURES FROM STROBOSCOPICALLY ILLUMINATED PARTICLE TRACKS

Introduction

The measurement of the temperature of laminar flames has generally been accomplished by the use of line-reversal techniques. These methods can be applied most readily to the zone outside the Bunsen cone. It is felt that much information may be gained by the determination of the temperature gradient in the cone itself. However, optical methods are not feasible in this study because of the relatively large area which must be observed. The insertion of wires for the application of thermoelectric techniques would disturb the flow lines.

The procedure presented here may be used for the study of temperature gradients in the Bunsen cone. With the aid of stroboscopic and streak photographs, the gas particle velocities on both sides of the flame front are determined. These velocity measurements are then combined with the equation of continuity and the equation of state to yield the flame temperature.

Method

Figure 5 illustrates the cross section of a stream tube through a Bunsen cone as indicated by particle tracks. In the case of laminar flow, the equation of continuity for a stream tube is given by

$$u_1\rho_1A_1=u_2\rho_2A_2, \tag{1}$$

where the velocities are perpendicular to the areas considered.

With a pair of dividers, it can be readily demonstrated from Fig. 6 that the distance between streamlines is constant when measured parallel to the flame front. That is to say:

$$b_1=b_2.$$

For ease of application, consider an infinitely thin stream tube, for which

$$db_1=db_2.$$

Since there is cylindrical symmetry, Eq. (1) may be written as follows:

$$u_{n1}\rho_1 2\pi r_1 db_1=u_{n2}\rho_2 2\pi r_2 db_2,$$

hence

$$u_{n1}\rho_1 r_1=u_{n2}\rho_2 r_2. \tag{2}$$

The density terms from the equation of state are:

$$\rho_1=\frac{M_1}{V_1}=\frac{(\Sigma n_iM_i)_1}{(\Sigma n_i)_1RT_1}P_1,$$

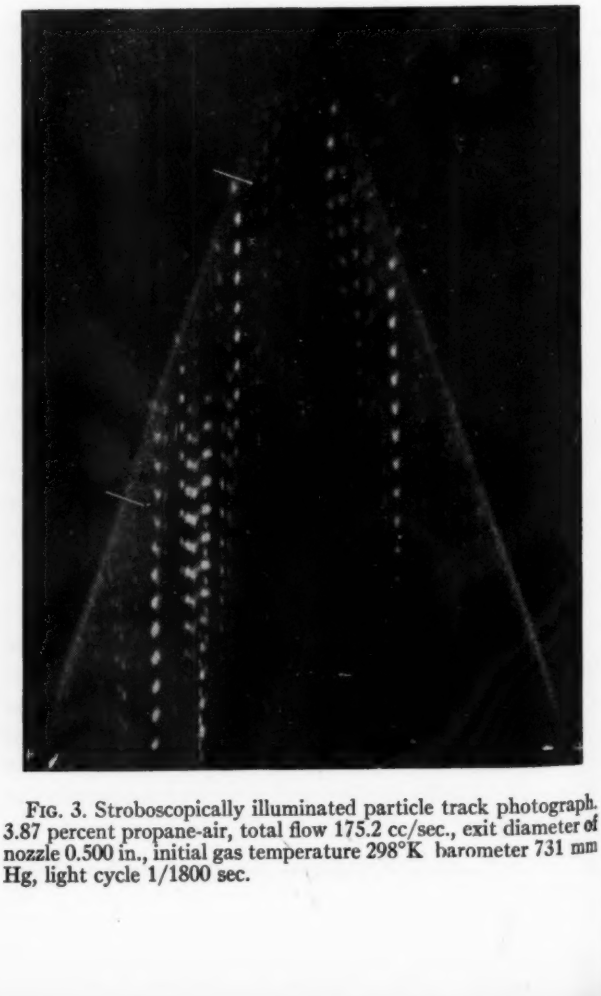

FIG. 3. Stroboscopically illuminated particle track photograph. 3.87 percent propane-air, total flow 175.2 cc/sec., exit diameter of nozzle 0.500 in., initial gas temperature 298°K barometer 731 mm Hg, light cycle 1/1800 sec.

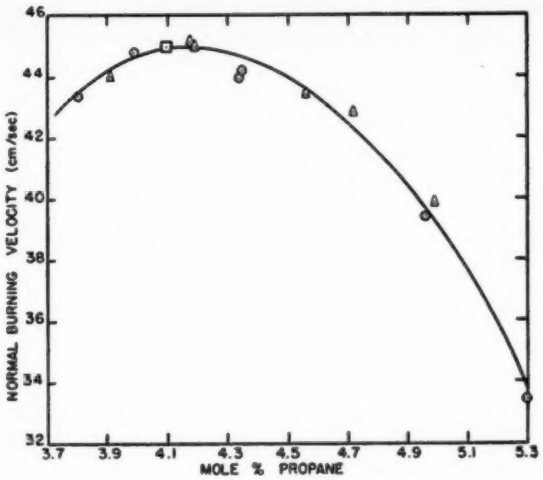

FIG. 4. Propane-air normal burning velocities. The different symbols represent data taken at various dates.

and

$$\rho_2=\frac{M_2}{V_2}=\frac{(\Sigma n_i M_i)_2}{(\Sigma n_i)_2 RT_2}P_2.$$

Since the pressure drop across the flame is very low, P_1 may be taken as equal to P_2. Substituting for the density in Eq. (2) and observing that $(\Sigma n_i M_i)_1=(\Sigma n_i M_i)_2$, the following relationship is obtained:

$$T_2=T_1\frac{(\Sigma n_i)_1}{(\Sigma n_i)_2}\frac{r_2}{r_1}\frac{u_{n2}}{u_{n1}}, \tag{3}$$

wherein $u_{n2}=u_r \sin\beta$, where u_r is the resultant exit velocity of the particle.

Experimental Procedure

To demonstrate the application of the above method, a 3.87 percent propane-air flame will be considered. This flame was established on a constant-velocity profile nozzle and particles were introduced into it by the method outlined in Part I. Stroboscopic photographs were taken of the particles for determination of emergent velocities (u_r) and streak photographs were taken for the determination of emergent angle β.

A study of Figs. 3 and 6 will reveal that some of the particles do not appear to follow the streamlines as well as others. Those particles which show this deviation are either too large or do not lie in the plane of the diameter. If the particles lie in this plane and are the same size, the paths of particles close together should be parallel. It is to be observed from the figures that those particles which appear to be small exhibit parallel paths. Also, they have the largest emergent angles, which indicates a more faithful representation of the streamline. Thus, correct results will be obtained if measurements are confined only to those tracks which appear to be from small particles. Unfortunately, these tracks are not the easiest to work with and need for an alternate method arises.

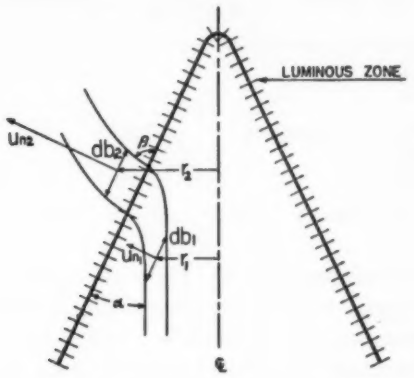

FIG. 5. Cross section of a stream tube through a Bunsen cone.

It will be observed from the photographs that many of the tracks of apparently larger particles become parallel to tracks of the smaller particles a short distance from the cone. These tracks may be extrapolated back to the luminous zone as indicated in Fig. 6, and are then equivalent to those made by the smaller particles.

To eliminate incidental errors, sines of the emergent angles and particle velocities are plotted against an arbitrary abscissa as indicated in Fig. 7. In this case, the abscissa chosen is the distance along the outside of

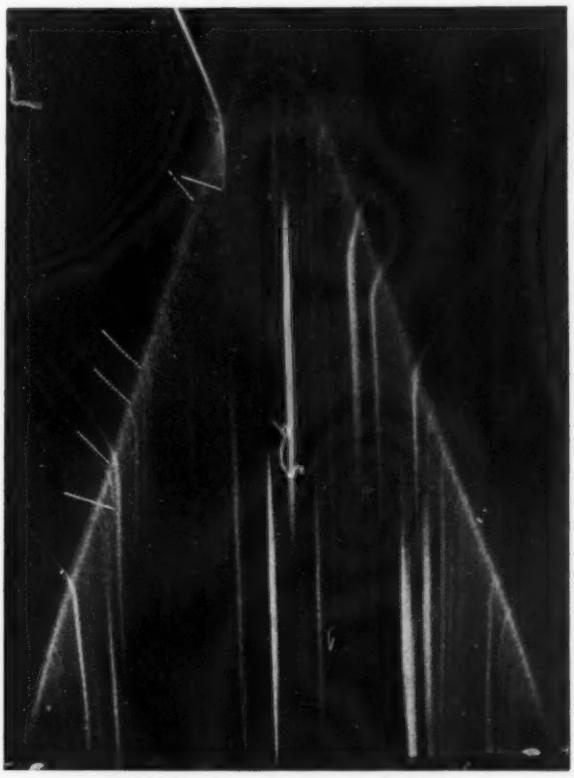

FIG. 6. Streak photograph. 3.87 percent propane-air, total flow 175.2 cc/sec., exit diameter of nozzle 0.500 in., initial gas temperature 298°K, barometer 731 mm Hg.

TABLE II.

Percent propane	Measured temperature	Theoretical temperature
4.03% (Stoichiometric)	2220°K	2280°K
3.87%	2240	2250
3.81%	2230	2240

the luminous zone from the point of intersection of the particle track to the reference point denoted by the white cross on Fig. 3 and Fig. 6. The above method makes possible the use of separate streak and stroboscopic particle photographs.

Since $u_{n2}(r_2/r_1)=u_r(r_2/r_1)\sin\beta$, consistent values for $u_{n2}(r_2/r_1)$ are obtained by multiplying the two ordinate values for a given abscissa in Fig. 7. If the best straight lines are drawn through the points, it is seen that $u_{n2}(r_2/r_1)$ is constant within 1 percent over the zone considered. The maximum deviation of any point from the straight line is $2\frac{1}{2}$ percent.

To determine the factor $(\Sigma n_i)_1/(\Sigma n_i)_2$, the necessary data for $(\Sigma n_i)_2$ was obtained from equilibrium considerations by the method described by Wenner[4] and $(\Sigma n_i)_1$ from the equation

$$C_3H_8+5.21\ O_2+19.6\ N_2 = 3\ CO_2+4\ H_2O+19.6\ N_2+0.21\ O_2.$$

This represents the combustion of one mole of propane in the 3.87 percent propane-air mixture. At the temperature 2250°K, the dissociation products of CO_2 and H_2O increase the total number of moles of reaction products from 26.8 to 27.0.

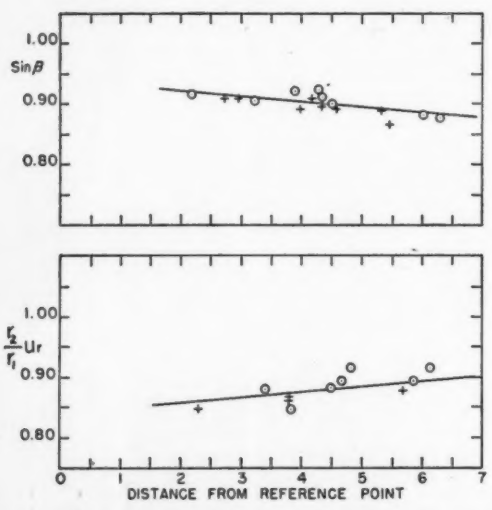

FIG. 7. Plot of $\sin\beta$ and $(r_2/r_1)u_r$ for determination of u_{n2}. Two runs are represented in this figure.

The following substitution may be made in Eq. (3) to obtain the flame temperature:

$$T_1=298°K,$$
$$(\Sigma n_i)_1/(\Sigma n_i)_2=25.8/27.0,$$
$$(r_2/r_1)u_{n2}=(r_2/r_1)u_r\sin\beta=0.795,$$
$$u_{n1}=u_f\sin\alpha=0.296\sin20.0°=0.1012.$$

Then $T_2=(298)(25.8/27.0)(0.795/0.1012)=2240°K$.

In this manner the data in Table II has been obtained.

It is worthwhile to note that Lewis and von Elbe[5] list a value of 2198°K for a 4.15 percent propane-air mixture. In the present work, flame temperatures were not determined for rich mixtures because of the difficult equilibrium calculation of the number of moles of burned gas.

Approximate Temperature Distribution in the Flame Front

After careful study of many photographs, several particle tracks were located which appeared to follow closely the very high acceleration which occurs in the flame zone. This was shown by an angle β, in the luminous zone, that agreed with the extrapolated values. By use of these tracks, it was possible to obtain the temperature gradient in the flame.

To determine the temperature gradient in the flame, it was necessary to assume the manner in which the velocity parallel to the flame front varies; the manner in which the change in number of moles occurs; and, of almost negligible consequence, that radial expansion through the flame front can be neglected. With no

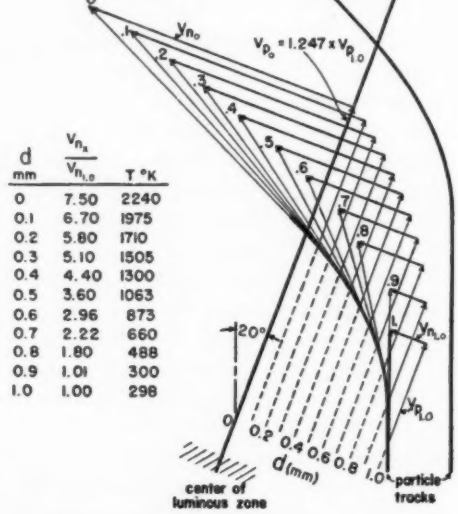

FIG. 8. Determination of temperature distribution in flame front.

[4] R. Wenner, *Thermochemical Calculations* (McGraw-Hill Book Company, Inc., New York, 1941), pp. 236–242.

[5] B. Lewis and G. von Elbe, *Combustion, Flames, and Explosions of Gases* (The Macmillan Company, New York, 1938), p. 399.

reliable information, the simplest assumption is that the change in moles and the change of velocity parallel to the flame front are linear with the distance normal to the flame front. The velocity assumption is most subject to criticism, but it should be pointed out that the increase in this component of velocity is only 25 percent.

The procedure in the determination of the temperature gradient in the flame front is shown in Fig. 8. The illustrated particle tracks are direct tracings of enlarged streak photographs. Actual distances are indicated: 1.0 mm is the point of first deflection of the streaks and 0.0 mm is the center of the visible zone. In brief, the analysis of these tracks is as follows:

a. The parallel velocity vector is drawn in as shown. This vector was assumed to vary in a linear manner as indicated previously. Its magnitude at the 0.0 mm distance was determined trigonometrically from the resultant velocity and emergent angle; and at 1.0 mm from the cone angle and filament velocity.

b. The tangent to the curve is drawn. This represents the direction of the resultant velocity.

c. The perpendicular to the flame front from the tip of the parallel vector is drawn. This is u_n and its length is determined by the intersection with the resultant vector.

d. Insertion of the values of u_n into Eq. (3) yields the temperature distribution in the flame front. The gradient is indicated in Fig. 9.

Discussion of Temperature Gradient

The thickness of the flame front determined here is approximately 10^{-1} cm. This may be compared with 10^{-3} to 10^{-4} cm for the decomposition of ozone obtained by Lewis and von Elbe[6] and 10^{-2} cm for carbon monoxide and 10^{-3} cm for hydrogen obtained by Tanford.[7]

It is of interest to calculate the temperature gradient of a hypothetical one-dimensional propane-air flame in which all of the heat release occurs at a plane. The steady-state heat transfer can be represented by:

$$(d^2T/dx^2)-(u_nc_p\rho/k)(dT/dx)=0, \qquad (4)$$

where $k/c_p\rho$ = thermal diffusivity. The solution of this equation is

$$\frac{T-T_1}{T_2-T_1}=\exp\left(-\frac{u_nc_p\rho}{k}x\right). \qquad (5)$$

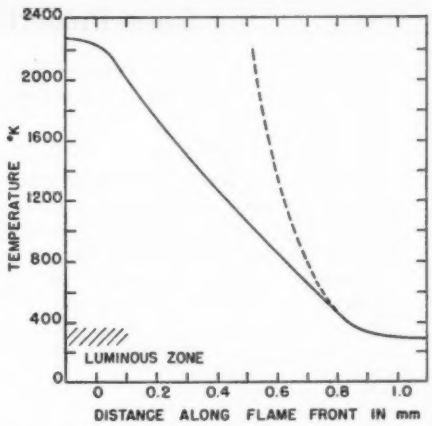

FIG. 9. Temperature gradient through a 3.87 percent propane-air flame.
——— Experimental curve.
- - - - Theoretical curve with heat release at a plane.

Since the propane has a negligible effect on the properties of the fuel-air mixture at the lower temperature, the physical properties of dry air[8] were averaged over 100°K intervals. These were substituted into Eq. (5) and the resulting temperature distribution is plotted in Fig. 9.

The temperature at which heat release becomes important is indicated by the place where the two curves of Fig. 9 begin to diverge. Evaluation of the rate of heat release through the flame would seem possible from the experimental curve, however, the errors involved in doing this graphically are too great to yield results.

ACKNOWLEDGMENT

The authors wish to thank Dr. J. O. Hirschfelder and Dr. H. Lowell Olsen for their helpful criticism of this work and the Navy Bureau of Ordnance for their financial support under Contract NOrd 9938.

[6] B. Lewis and G. von Elbe, J. Chem. Phys. **2**, 537 (1934).
[7] C. Tanford, J. Chem. Phys. **15**, 433 (1947).
[8] Thermal conductivity evaluated from viscosity data of Hirschfelder, Bird, and Spotz, J. Chem. Phys. **16**, 968 (1948) by the equation: $k=(\eta/28.966)(c_v+9/4)$.

Some Properties of van der Waals' Liquids

FREDERICK T. WALL AND WILLIAM R. KRIGBAUM
Noyes Chemical Laboratory, University of Illinois, Urbana, Illinois

(Received April 28, 1949)

A theoretical consideration of the volume of a van der Waals' liquid suggests some new rules, comparable to that of Trouton, relating coefficients of expansion and compressibility to heats of vaporization. According to the simplest and most reliable of these new relationships, the product of the coefficient of cubical expansion and the heat of vaporization, $\alpha\Delta H_v$, is the same for many liquids and equal to about 10 cal./deg. It is further shown that at a given temperature, $\Delta H_v^2\beta/V$ is also constant where β is the compressibility and V the volume of the liquid. Certain corollary rules are derived by combining the above two with each other and with Trouton's law. These new rules should prove of some value in estimating compressibilities and heats of vaporization from coefficients of expansion.

INTRODUCTION

IT has frequently been demonstrated that van der Waals' equation, although not quantitatively exact, can be used for the qualitative prediction of many phenomena exhibited by fluids. Although the equation has been most successfully applied to gases and vapors, it also appears to have considerable validity in describing the behavior of liquids. For example, it has been possible to derive from van der Waals' equation a vapor pressure relationship which has the correct functional form.[1] Moreover, it is possible to predict the orders of magnitude of the constants associated with certain empirical rules, such as those of Trouton or Guldberg and Guye. Numerous other conclusions can be drawn from van der Waals' equation; these have been summarized by van Laar,[2] who thoroughly investigated the equation.

The successful application of van der Waals' equation in deducing vapor pressure and related formulas leads one to suppose that still other relationships might be forthcoming, especially in connection with the liquid state. Thus from a consideration of the volume of a van der Waals' liquid, there can be derived some new general rules relating the coefficients of expansion and compressibility of liquids to their heats of vaporization or normal boiling points. The relationships are verified by comparison with published data, and are found to be about as reliable as Trouton's rule.

The conclusions of this paper do not constitute a verification of van der Waals' equation; instead they test the more general law of corresponding states. In fact, by using Pitzer's method for corresponding states, Guggenheim[2a] made certain deductions closely related to some of those set forth in the present article.

COEFFICIENT OF THERMAL EXPANSION

In the aforementioned theory of vapor pressures based on van der Waals' equation,[1] use was made of the molar volume of a van der Waals' liquid, the first approximation to which is

$$V=b+b^2RT/a, \tag{1}$$

where a and b are van der Waals' constants. Employing the above expression for volume in connection with some basic thermodynamics, there was derived the following equation for the vapor pressure of a liquid:

$$\ln p=\ln(a/b^2)-a/(bRT). \tag{2}$$

From Eq. (2) it is readily seen that the heat of vaporization is simply equal to a/b.

Further examination of the volume of a van der Waals' liquid suggests that a simple relationship should exist between the coefficient of thermal expansion and the heat of vaporization. If α is used to denote the coefficient of thermal expansion, then the first approximation to α will be given by

$$\alpha=(1/V)(\partial V/\partial T)_p=bR/a. \tag{3}$$

Higher terms would involve the temperature and pressure, but such terms will be small compared to bR/a as long as a/b (the heat of vaporization) is large compared to RT and the pressure is well below the critical pressure. Recognizing that according to theory $\Delta H_v=a/b$, we see from (3) that

$$\alpha\Delta H_v=R \text{ (a constant)}. \tag{4}$$

Equation (4) suggests that the coefficient of thermal expansion multiplied by the heat of vaporization should be a constant for all liquids. This prediction is a reasonable one, for it implies that a liquid which expands readily upon heating also requires little energy for evaporation.

From a consideration of Trouton's rule,

$$\Delta H_v/T_0=C, \tag{5}$$

where T_0 is the normal boiling point, it is apparent that the coefficient of thermal expansion should also be inversely proportional to the normal boiling temperature, or

$$\alpha T_0=R/C \text{ (a constant)}. \tag{6}$$

[1] F. T. Wall, J. Chem. Phys. **16**, 508 (1948).
[2] J. J. van Laar, *Die Zustandsgleichung von Gasen and Flüssigkeiten* (Leopold Voss, Leipzig, 1924); J. J. van Laar, Zeits. f. anorg. u. angew. Chemie **171**, 42 (1928).
[2a] K. S. Pitzer, J. Chem. Phys. **7**, 583 (1939). E. A. Guggenheim, J. Chem. Phys. **13**, 253 (1945).

To the best of our knowledge, Eqs. (4) and (6) have never been proposed as empirical relationships, so we have tested them by use of data contained in tables of physical constants. To provide a fair test of Eq. (4) it was felt desirable to utilize coefficients of thermal expansion and heats of vaporization for one temperature, say 25°C. Satisfactory data of this type, especially heats of vaporization which are usually given at the normal boiling point, are not generally available for all classes of compounds. Suitable data were found, however, for 37 hydrocarbons,[3,4,5] and these are summarized in Table I. The product of α and ΔH_v for the 37 hydrocarbons is found to be quite constant, the average value being 10.1 ± 0.4 cal./deg. Although the empirical constant is about five times larger than predicted ($R=2$ cal./deg.), the form of Eq. (4) is fully substantiated.

Equation (4) is further tested by use of data for 63 organic liquids[4,5,6] appearing in Table II. For these compounds the heats of vaporization correspond to the normal boiling points of the liquids and not to 25°C. For this set the average value of the product $\alpha\Delta H_v$ is 9.4 ± 0.9 cal./deg. The principal reason for the greater variation in values (10 percent) is that the heats of vaporization were not all taken at the same temperature. The lower value (9.4 instead of 10.1) is largely due to the inclusion of highly associated liquids, such as formic and acetic acids, which are of an abnormal nature. On the other hand, the products for butyric acid and higher members of this series are close to the average value. Strangely enough, methyl and ethyl alcohol also appear to be quite normal on the basis of this criterion.

When relationship (4) is tested for inorganic liquids[6] and for the elements in the liquid state[7] (Table III) the agreement is not nearly so good. Water is definitely abnormal and certain metals such as zinc and mercury also show low values for the product $\alpha\Delta H_v$. Copper, hydrogen, and magnesium, on the other hand, show abnormally high values. This behavior is not unexpected as such substances generally do not conform to other relationships of a similar nature.

It is interesting to test Eq. (6) directly, although we would expect it to hold by virtue of Trouton's rule whenever Eq. (4) is valid. Values of αT_0 for 37 hydrocarbons are listed in Table I and the average is found to be 0.464 ± 0.032. The quotient $\alpha\Delta H_v/\alpha T_0$, which should be Trouton's constant, is 22 or 20 cal./deg., depending on whether $\alpha\Delta H_v$ is taken as 10.1 or 9.4. This agreement with Trouton's constant is to be expected and does not in any way test the validity of (4) or (6). Values of αT_0 for 63 miscellaneous organic liquids are given in Table II, and the average value of the product is 0.434 ± 0.027.

TABLE I. Values of $\alpha\Delta H_v$ for 37 hydrocarbons at 25°C.

Paraffins	ΔH_v[a] cal.	$\alpha\cdot10^3$[b] per °K	$\alpha\Delta H_v$ cal/°K	T_0[c] °K	αT_0
n-propane	3605	3.240	11.68	231.1	0.749
n-butane	5035	2.304	11.60	273.1	0.629
2-methyl butane	4570	2.304	10.53	271.5	0.602
n-pentane	6316	1.54	9.73	309	0.476
iso-pentane	5878	1.546	9.08	302	0.467
n-hexane	7540	1.35	10.18	341.9	0.462
2-methyl pentane	7138	1.476	10.54	333.5	0.492
2,3-dimethyl butane	6617	1.406	9.30	331.2	0.466
n-heptane	8735	1.222	10.67	371.6	0.454
2-methyl hexane	8318	1.259	10.47	363.3	0.457
3-methyl hexane	8385	1.228	10.30	365.2	0.470
2,2-dimethyl pentane	6969	1.268	9.83	352.4	0.447
2,3-dimethyl pentane	6617	1.220	9.30	331.2	0.404
2,4-dimethyl pentane	7860	1.268	9.97	353.7	0.448
3,3-dimethyl pentane	7892	1.223	9.65	359.3	0.439
2,2,3-trimethyl butane	7657	1.215	9.39	354.1	0.430
3-ethyl pentane	8419	1.222	10.29	366.7	0.448
n-octane	9915	1.116	11.06	398.9	0.445
2,5-dimethyl hexane	9048	1.19	10.77	382.3	0.455
2,2,3-trimethyl pentane	8823	1.118	9.86	383.0	0.428
3,3-diethyl pentane	10360	1.044	10.82	418.8	0.437
Cycloparaffins					
cyclopentane	6810	1.32	8.99	322.5	0.436
methyl cyclopentane	7560	1.25	9.45	345	0.431
cyclohexane	7895	1.20	9.47	353.7	0.424
methyl cyclohexane	8451	1.18	9.97	374	0.441
Olefins					
butene-1	4870	2.052	9.99	266.9	0.548
butene-2	5220	2.037	10.63	274.1	0.558
2-methyl propene	4920	1.954	9.61	266.3	0.520
Aromatic					
benzene	8090	1.215	9.83	353.3	0.429
toluene	9080	1.06	9.62	383.8	0.407
o-xylene	10380	0.9181	9.53	417.6	0.383
m-xylene	10195	0.999	10.18	412.3	0.412
p-xylene	10128	1.02	10.33	411.6	0.420
ethyl benzene	10100	0.955	9.64	409.4	0.391
pseudo cumene	11457	0.95	10.88	442.5	0.420
mesitylene	11346	0.937	10.63	437.9	0.410
propyl benzene	11049	0.97	10.72	432.4	0.419
		Average	10.1 ± 0.4		0.464 ± 0.032

[a] See reference 3.
[b] See reference 4.
[c] See reference 5.

The coefficients of thermal expansion are plotted against $1/\Delta H_v$ in Fig. 1, using the data of Table I, and it is seen that the points are well reproduced by a straight line passing through the origin and having a slope equal to 10.1. In Fig. 2 coefficients of thermal expansion are plotted against $1/T_0$. The points in the graph represent all liquids appearing in Table I for which the normal boiling temperatures exceed 250°K. Liquids boiling below that temperature exhibit large deviations, presumably because of irregularities in their α-values, which at 20°C must have been measured under high pressures. To establish more fully the trend for low boiling liquids, all compounds appearing in Table II having boiling points in the range 250–330°K are also included in Fig. 2. The solid line is drawn to pass through the origin and has a slope equal to 0.437. It is seen, however, that a better representation is given by the broken line, not passing through the origin, for which the equation is

$$\alpha T_0=0.61-4.4\times10^{-4}T_0. \qquad (7)$$

Taking $\alpha\Delta H_v$ as 10.1, we can derive from (7) a modified

[3] *Selected Values of Properties of Hydrocarbons* (American Petroleum Institute Project 44, National Bureau of Standards, Washington, D. C., 1945).
[4] *Physical Constants of the Principal Hydrocarbons* (The Texas Company, New York, 1943), 4th edition.
[5] *Handbook of Chemistry and Physics* (Chemical Rubber Publishing Company, Cleveland, Ohio, 1947), 30th edition.
[6] N. A. Lange's Handbook (Handbook Publishers, Sandusky, 1946), 6th ed.
[7] *International Critical Tables* (McGraw-Hill Book Company, Inc., New York, 1926), Vol. 1, p. 102.

TABLE II. Values of $\alpha\Delta H_v$ for 63 organic liquids (ΔH_v at the normal boiling point).

A. Hydrocarbons	ΔH_v[a] cal.	$\alpha \cdot 10^{3a}$ per °K	$\alpha\Delta H_v$ cal/°K	T_0[b] °K	αT_0
Paraffins					
methane	2218	3.681	8.16	89.2	0.328
ethane	3515	3.750	13.18	101.2	0.380
decane	8878	1.06	9.41	447	0.473
undecane	9144	0.9678	8.85	469.0	0.454
dodecane	9351	0.9619	8.99	487.7	0.469
tridecane	9494	0.9166	8.70	507	0.465
tetradecane	9562	0.893	8.54	525.7	0.469
pentadecane	9537	0.8573	8.18	543.7	0.466
hexadecane	9487	0.8045	7.63	560.7	0.451
Bicyclic Aliphatic					
tetralin	10483	0.96	10.06	480.4	0.461
decalin (*cis*)	10575	(0.86)	9.09	(467.8)	(0.402)
decalin (*trans*)	10147		8.73		
(turpentine)	9330	0.973	9.08	429	0.417
Diolefins					
1,3-butadiene	5398	1.84	9.93	270	0.490
Aromatic					
o-cymene	8898	0.923	8.21	448	0.414
p-cymene	9073	0.96	8.71	449	0.431
methyl triisopropyl benzene	11355	0.975	11.07	527	0.514
ethyl triisopropyl benzene	11414	0.998	11.39	528	0.527
dimethyl triisopropyl benzene	11878	0.7855	9.33	548.8	0.431
1-phenyl-1-hexyl heptane	11980	0.885	10.60	551	0.488
tetraisopropyl toluene	11825	0.693	8.19	543	0.376
styrene	9050	0.849	7.68	419	0.356
Bicyclic Aromatic					
biphenyl	11472	0.935	10.73	527	0.492
1,2-diphenyl ethane	10662	0.85	9.06	557	0.473
Tricyclic Aromatic					
anthracene	13099	0.801	10.49	627	0.502
phenanthrene	12654	0.66	8.35	613.4	0.405

B. Other Organic Liquids	ΔH_v[c] cal.	$\alpha \cdot 10^{3c}$ per °K	$\alpha\Delta H_v$ cal/°K	T_0[b] °K	αT_0
Halogen Derivatives					
methyl iodide	6516	1.273	8.29	315.7	0.401
ethyl chloride	5949	1.706	10.15	285.4	0.487
ethyl bromide	6588	1.418	9.34	311.2	0.441
ethyl iodide	7113	1.179	8.39	345.4	0.407
amyl bromide	10498	1.102	11.57	402.1	0.443
amyl iodide	9428	0.986	9.30	429	0.423
ethylene chloride	8442	1.161	9.80	356.7	0.414
carbon tetrachloride	7138	1.218	7.80	349.9	0.426
chloroform	7044	1.236	8.82	334.5	0.413
chloral	7960	1.273	8.97	371	0.472
Ketones, Ethers					
acetone	7231	1.487	10.75	329.7	0.490
methyl ethyl ketone	7643	1.315	10.05	352.8	0.464
diethyl ketone	7821	1.233	9.64	375.9	0.463
ethyl ether	6220	1.656	10.30	307.8	0.509
Alcohols, Glycols					
methyl alcohol	8240	1.199	9.90	337.9	0.405
ethyl alcohol	9420	1.12	10.55	351.7	0.394
n-propyl alcohol	9885	0.956	9.42	370.4	0.354
isopropyl alcohol	9554	1.094	10.45	355.5	0.389
n-butyl alcohol	10451	0.950	9.93	390.9	0.371
i-butyl alcohol	9694	1.023	9.91	356.2	0.364
amyl alcohol	10596	0.902	9.56	404	0.364
allyl alcohol	9467	1.049	9.93	369	0.387
ethylene glycol	11855	0.6375	7.56	470	0.300
Acids, Esters					
formic acid	5524	1.025	5.66	374	0.383
acetic acid	5813	1.071	6.23	391.5	0.419
propionic acid	7319	1.102	8.07	412.5	0.455
n-butyric acid	10043	1.063	10.68	463.7	0.464
isobutyric acid	9852	1.068	10.50	427	0.456
n-valeric acid	10540	1.004	10.58	457.8	0.460
methyl formate	6360	1.563	9.92	304.5	0.476
ethyl formate	7110	1.417	10.10	326.5	0.463
methyl acetate	7310	1.427	10.43	330.3	0.471
ethyl acetate	8060	1.389	10.55	350.4	0.487
methyl propionate	7718	1.304	10.06	353.1	0.460
ethyl benzoate	9686	0.900	8.72	485.8	0.437
Miscellaneous					
carbon disulfide	6403	1.218	7.80	319.5	0.389
aniline	9657	0.858	8.29	457.6	0.393
		Average	9.4 ±0.9		0.434 ±0.027

[a] See reference 4.
[b] See reference 5.
[c] See reference 6.

form of Trouton's rule, namely

$$\Delta H_v/T_0 = 16.6 + 0.012T_0. \quad (8)$$

Equation (8) is in excellent agreement with Bingham's modification[8] of Trouton's rule, which is

$$\Delta H_v/T_0 = 17 + 0.011T_0. \quad (8a)$$

Since the same type of data was employed both for Bingham's calculations and our own, this agreement is also expected although it is not entirely trivial. It is significant that the modification involving a linear function of T_0 is not required for the $\alpha\Delta H_v$ relationship whereas it does improve both the rule for αT_0 and that of Trouton. This suggests that the constancy of $\alpha\Delta H_v$ is of greater reliability than Trouton's rule as ordinarily stated, although it is probably not as good as Hildebrand's modification.[9]

For practical purposes we suggest provisionally that the product $\alpha\Delta H_v$ be assumed equal to 9.4 cal./deg., using heats of vaporization at the normal boiling point. If the heat of vaporization is known at 25°C, then it would be better to use 10.1 cal./deg. for the constant. The rule should prove of some value, especially for hydrocarbons, for estimating heats of vaporization from coefficients of expansion.

COMPRESSIBILITIES OF LIQUIDS

As a first approximation, the volume of a van der Waals liquid depends upon the temperature but not upon the pressure, so such a liquid would be considered incompressible. Actually that is a reasonable prediction, for it is observed that the volume of a liquid is generally affected less by pressure than by temperature. To make any more detailed predictions concerning compressibilities, it is necessary to take recourse to higher approximations for the volume of a liquid. Unfortunately the higher approximations are of doubtful significance and the paucity of experimental data makes it difficult to rigorously test the predictions.

An effort in this direction has been made, however, by use of the second approximation[1] to the volume, namely:

$$V = b + \frac{b^2RT}{a} + \frac{2b^3R^2T^2}{a^2} - \frac{b^4RTp}{a^2}. \quad (9)$$

From Eq. (9) it can be shown that the first term for the compressibility will be

$$\beta = -(1/V)(\partial V/\partial p)_T = b^3RT/a^2. \quad (10)$$

From (10) it can further be shown (neglecting higher powers of bRT/a) that

$$\Delta H_v^2\beta/V = RT \text{ (a constant at a given } T). \quad (11)$$

Assuming Trouton's rule, Eq. (11) can be modified to

$$T_0^2\beta/V = RT/C^2 \text{ (a constant at a given } T). \quad (12)$$

[8] E. C. Bingham, J. Am. Chem. Soc. **28**, 723 (1906).
[9] J. H. Hildebrand, J. Am. Chem. Soc. **37**, 970 (1915).

The equations have been subjected to test using such data as are available. From the data of Table IV[5,10] it is found for a series of liquids that the expressions corresponding to (11) and (12) are fairly constant. In that table, β is the compressibility at 20°C measured over the pressure range 100–300 atmospheres. It is observed that $\Delta H_v^2\beta/V=53.6\pm3.2$ (cal.)^2/ml-atmos. and $T_0^2\beta/V=0.105\pm0.007$ (degrees)^2/ml-atmos. The square root of the quotient is 22.6 cal./deg., which is to be compared with Trouton's constant. These rules should be of some use in estimating compressibilities of normal liquids. Theoretically, $\Delta H_v^2\beta/VT$ (and $T_0^2\beta/VT$) should also be constant but the available data do not permit checking the effect of temperature and our rule is therefore restricted to 20°C.

By combining the rules expressed by Eqs. (4) and (11), the heat of vaporization can be eliminated and a relationship deduced between α and β, namely:

$$V\alpha^2/\beta=R/T \text{ (a constant at a given temperature).} \quad (13)$$

It will be recalled that the difference between the heat capacities at constant pressure and constant volume (C_p-C_v) is precisely $TV\alpha^2/\beta$, so from (13) it appears that this difference should be the same for all liquids. The predicted constant, R, is of course not numerically correct but the form of the law is approximately substantiated by the data of Table V, which includes all liquids appearing both in Tables I or II and in Table IV. (As indicated earlier, the lack of data restricts our test to one temperature, 20°C.)

It is found at 20°C that $V\alpha^2/\beta=1.65\pm0.20$ ml-atmos./deg^2. This rule should find some application in estimating compressibilities from coefficients of cubical expansion, although it appears to be less reliable than the relationships involving ΔH_v.

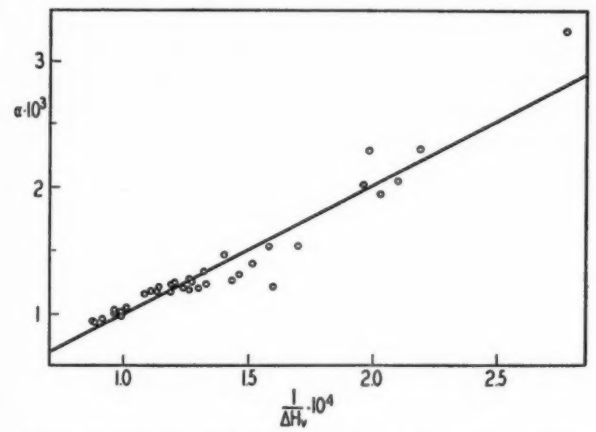

FIG. 1. Graph of coefficient of expansion (α) *vs.* reciprocal of heat of vaporization (ΔH_v). Solid line corresponds to Eq. $\alpha\Delta H_v=10.1$ cal./deg.

[10] *International Critical Tables* (McGraw-Hill Book Company, Inc., New York, 1928), Vol. 3, p. 35.

TABLE III. Values of $\alpha\Delta H_v$ for some inorganic liquids.

A. Inorganic Liquids	ΔH_v[a] cal.	$\alpha\cdot10^3$[a] per °K	$\alpha\Delta H_v$ cal/°K
phosphorus trichloride	7060	1.154	8.15
silicon tetrachloride	6133	1.430	8.77
stannic chloride	7894	1.178	9.30
sulfur monochloride	6684	0.968	6.47
water	9700	0.207	2.01
B. Elements in the Liquid State	ΔH_v[b] cal.	$\alpha\cdot10^3$[b] per°K	$\alpha\Delta H_v$ cal/°K
A	1505	4.5	6.77
Ag	59490	0.11	6.54
Al	53750	0.113	6.07
Bi	46100	0.122	5.62
Br_2	7168	1.100	7.88
Cd	26852	0.150	4.02
Cl_2	4778	1.500	7.17
Cs	17440	0.37	6.45
Cu	11560	0.190	21.2
F_2	(2867)?	3.00	(8.60)?
H_2	2150	13.0	28.0
Hg	14166	0.182	2.58
I_2	10512	0.800	8.41
K	20068	0.290	5.82
Li	40613	0.180	7.31
Mg	62600	0.380	23.7
N_2	1338	6.0	8.02
Na	25080	0.280	7.02
O_2	1632	4.10	6.69
O_3	3498	2.00	7.00
P_4	16108	0.52	8.36
Pb	46108	0.12	5.53
Rb	17680	0.340	6.01
S_8	17162	0.430	7.38
Sb	45390	0.100	4.54
Sn	77643	0.100	7.76
Tl	(61158 / 28670) (?)	(0.140)	(8.56 / 4.01)
Zn	23700	0.150	3.55

Average 8.10±2.07

[a] See reference 6.
[b] See reference 7.

REDUCED VOLUME OF A VAN DER WAALS' LIQUID

The expression for the volume of a van der Waals' liquid can readily be put into reduced form by use of appropriate formulas for the critical constants. Denoting the reduced volume, V/V_c, by ϕ, and the reduced

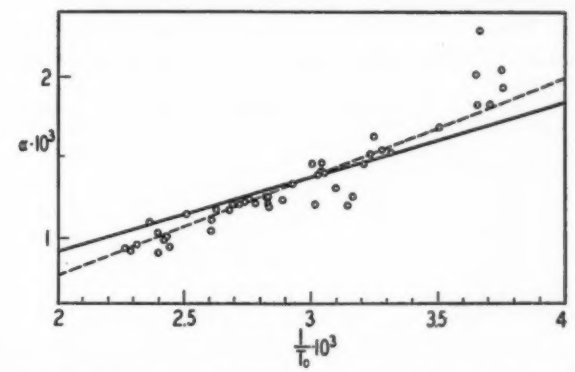

FIG. 2. Graph of coefficient of expansion (α) *vs.* reciprocal of normal boiling point (T_0). Solid line corresponds to Eq. $\alpha T_0=0.467$, and dotted line to Eq. (7) of text.

TABLE IV. Values of $\beta\Delta H_v^2/V$ and $\beta T_0^2/V$.

Hydrocarbons	V[a] ml.	$\beta\cdot10^6$[c] per atm.	ΔH_v[a] cal.	$\beta\Delta H_v^2/V$ (cal)^2/ ml. atm.	T_0[a] °K	$\beta T_0^2/V$ deg^2/ml. atm.
n-octane	162.35	97.5	9915	59.0	399.1	0.096
2,5-dimethyl hexane	163.54	105	9048	52.6	381.6	0.093
3,4-dimethyl hexane	158.43	94.5			389.8	0.091
2-methyl heptane	162.51	101			389	0.094
3-ethyl hexane	159.34	96			392.2	0.093
cyclohexane	108.02	93	7895	53.7	354.7	0.108
benzene	88.82	78	8090	57.5	353.4	0.110
toluene	106.39	74	9080	57.3	384.1	0.103
ethyl benzene	122.46	71	10100	59.1	409.4	0.097
n-propyl benzene	139.43	69.7	11049	61.0	432.7	0.094
isopropyl benzene	139.11	70.3			425	0.091
t-butyl benzene	154.80	68			442.0	0.086
mesitylene	139.21	67	11346	62.0	437.9	0.092
pseudocumene	137.20	64	11049	56.9	443.1	0.092
Ketones, Alcohols						
acetone	73.3	82	7231	58.4	331	0.123
diethyl ketone	105.56	84	7821	48.7	376	0.112
cyclohexanone	103.55	58			430	0.104
n-butyl alcohol	91.53	76.5	10451	91.3	391.1	0.128
t-butyl alcohol	93.98	89	9694	89.0	356.1	0.120
isoamyl alcohol	108.56	84	10560	86.3	403.8	0.126
ethylene glycol	55.64	34	11855	85.7	470.5	0.135
benzyl alcohol	102.98	43	12142	61.6	478.5	0.096
o-cresol	103.33	44			464.8	0.092
m-cresol	104.57	45.5	10878	51.4	476.1	0.103
p-cresol	104.50	44			475.8	0.095
Acids, Esters						
n-butyric acid	108.42	77	10043	71.6	460	0.150
n-propyl formate	97.82	87	7762	53.6	354.6	0.112
isobutyl formate	112.13	86	8017	49.3	380.1	0.111
isoamyl formate	133.36	80	8549	43.8	396.8	0.095
methyl acetate	79.7	87.5	7310	58.7	330	0.120
ethyl acetate	97.8	90	8060	59.8	350	0.112
isobutyl acetate	133.33	87	8573	48.0	389.8	0.099
ethyl propionate	115.45	87.5	8181	50.7	372.4	0.105
methyl butyrate	113.73	84	8078	48.3	375.6	0.104
methyl isobutyrate	114.62	89	7976	49.4	365.9	0.104
ethyl butyrate	132.15	85	8677	48.4	394.6	0.100
ethyl isobutyrate	133.62	90	8375	47.2	385	0.100
Miscellaneous						
carbon tetrachloride	96.4	88	7138	46.5	350	0.112
chloroform	79.8	83	7044	51.6	334	0.117
ethylene chloride	78.74	67.5	8442	61.1	356.8	0.109
o-toluidine	106.72	44			473.1	0.092
m-toluidine	108.34	45			476.6	0.094
			Average	53.6 ±3.2		0.105 ±0.007

[a] See reference 5.
[b] See reference 6.
[c] See reference 10.
[d] See reference 2.

temperature, T/T_c, by θ, it is easily seen that for the first approximation

$$\phi=\tfrac{1}{3}\{1+8\theta/27\}. \qquad (14)$$

The validity of Eq. (14) can be tested in part by comparison with the experimental results of Young[11] who investigated the volumes of 19 organic liquids all coexisting with their vapors at a reduced pressure

[11] S. Young, *Stoichiometry* (Longmans, Green and Company, London, 1908) p. 203.

TABLE V. Values of $V\alpha^2/\beta$ at 20°C.

Liquid	$\alpha\cdot10^3$[a] per deg.	V[b] ml.	$\beta\cdot10^6$[c] per atm.	$V\alpha^2/\beta$ ml. atm./ deg^2
n-octane	1.116	162.35	97.5	2.07
2,5-dimethyl hexane	1.19	163.54	105	2.21
cyclohexane	1.20	108.02	93	1.67
benzene	1.215	88.82	78	1.68
toluene	1.06	106.39	74	1.61
ethyl benzene	0.955	122.46	71	1.57
mesitylene	0.937	139.21	67	1.82
n-propyl benzene	0.97	139.43	69.7	1.88
pseudocumene	0.95	137.20	64	1.93
acetone	1.487	73.3	82	1.98
diethyl ketone	1.233	105.56	84	1.91
n-butyl alcohol	0.950	91.53	76.5	1.08
t-butyl alcohol	1.023	93.98	89	1.10
ethylene glycol	0.6375	55.64	34	0.67
n-butyric acid	1.063	108.42	77	1.59
methyl acetate	1.427	79.7	87.5	1.85
ethyl acetate	1.389	97.8	90	2.10
carbon tetrachloride	1.218	96.4	88	1.63
chloroform	1.236	79.8	83	1.47
ethylene chloride	1.161	78.74	88	1.21
			Average	1.65±0.20

[a] See reference 4.
[b] See reference 5.
[c] See reference 10.
[d] See reference 2.

($\pi=p/p_c$) equal to 0.08846. Under these circumstances the 19 liquid-vapor systems all had very nearly the same reduced temperature, the average value being 0.7459 with a maximum variation therefrom of a few percent. Setting $\theta=0.7459$ in Eq. (14) we calculate a reduced volume equal to 0.4069. This compares very favorably with the average value observed by Young, namely, $\phi=0.4030$. This agreement is better than we might reasonably expect, for most reduced relationships derived from van der Waals' equation are only qualitatively correct. For example, the reduced vapor pressure equation corresponding to (2) is not nearly so good as (14) appears to be. Our test of Eq. (9) is so limited that the agreement may be coincidental; nevertheless it does appear that the equation is reliable.

Although the higher approximations[1] to the volume of a van der Waals liquid are of doubtful significance, we record here for the sake of greater completeness, the third approximation to the reduced volume:

$$\phi=\tfrac{1}{3}+\tfrac{1}{3}(8\theta/27)+\tfrac{2}{3}(8\theta/27)^2-\tfrac{1}{3}(8\theta/27)(\pi/27)+5/3(8\theta/27)^3-2(8\theta/27)^2(\pi/27)+\tfrac{1}{3}(8\theta/27)(\pi/27)^2+\cdots. \qquad (15)$$

A Normal Coordinate Analysis of the Planar Vibrations of Substituted Ethylenes. I. CH Bending Modes

P. TORKINGTON
Physical Chemistry Laboratory, South Parks Road, Oxford, England

(Received April 29, 1949)

A normal coordinate analysis of the planar vibrations of some substituted ethylenes is carried out. Thirteen compounds are studied, including mono-substituted and 1:1- and *cis*- and *trans*-1:2-disubstituted ethylenes. Various solutions for the CH bending force constants are obtained and correlated. Some attempt is made to study the range of allowed solutions, and to examine the coupling of the different coordinates in the potential function.

I. INTRODUCTION

SATISFACTORY vibrational assignments are now available for a number of substituted ethylenes. In the present work, it is proposed to carry out a normal coordinate analysis of the planar vibrations, with the object of finding sets of force constants for the various coordinates occurring in the valence-force potential functions, having particular regard to the possibility of there being small variations in the value of a force constant going with any particular coordinate common to a series of related molecules as the substituents change. This type of analysis has been developed because of inconsistencies which have arisen through the carrying-over of force constants between related molecules, which suggest that some formal investigation should be made into the allowed variations in the force constants of a given molecule. A somewhat similar treatment of the non-planar vibrations of substituted ethylenes has already been carried out;[1] the balance of evidence is in favor of detectable variations in force constants, which can be correlated with the electro-negativities and powers of conjugation of the substituents. In the present investigation, use is made of recent developments in the theory of the secular equation,[2] which facilitate comparatively rapid handling of quite high order matrix equations.

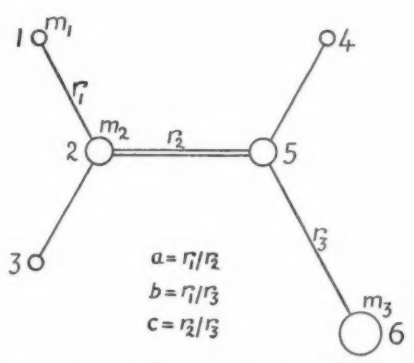

FIG. 1. Numbering of coordinates for mono-substituted ethylenes.

[1] P. Torkington, Proc. Roy. Soc. London (in press); Nature **163**, 96 (1949).
[2] P. Torkington, J. Chem. Phys. **17**, 1026 (1949); Nature **162**, 370, 607 (1948).

II. THE SECULAR EQUATIONS

The notation used in previous papers[2,3] is adopted here; for an nth-order symmetry-factor, the n valence-type symmetry coordinates Δ_1 to Δ_n are defined in terms of N Cartesian displacement coordinates z_1 to z_N:

$$\Delta_i=\sum_{j=1}^{N} a_{ij}z_j \tag{1}$$

and the secular equation is written in matrix form:

$$|\mathbf{dA}-\lambda\mathbf{I}|=0, \tag{2}$$

where the elements of $\mathbf{d}$ are the force constants in the potential function defined below:

$$2V=\sum_{i=1}^{n}\sum_{j=1}^{n} d_{ij}\Delta_i\Delta_j \tag{3}$$

and the elements of $\mathbf{A}$ (related to the inverse kinetic energy matrix $\mathbf{G}$ of Wilson),[4,5] are as follows:

$$A_{ij}=\sum_{k=1}^{N} a_{ik}a_{jk}(M/m_k) \tag{4}$$

where m_k is the mass of the atom whose Cartesian dis-

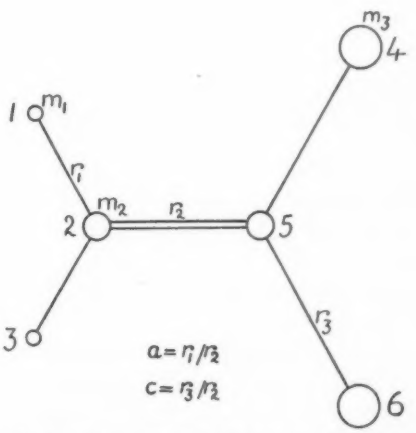

FIG. 2. Numbering of coordinates for 1:1-disubstituted ethylenes.

[3] P. Torkington, J. Chem. Phys. **17**, 357 (1949).
[4] E. B. Wilson, Jr., J. Chem. Phys. **7**, 1047 (1939).
[5] E. B. Wilson, Jr., J. Chem. Phys. **9**, 76 (1941).

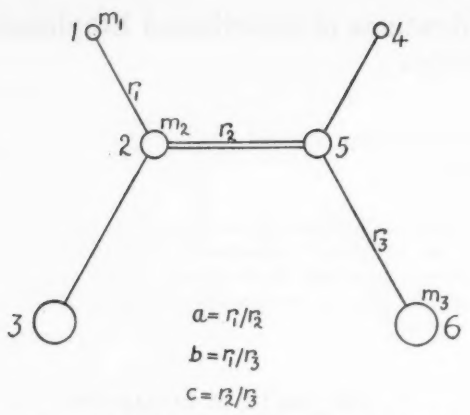

FIG. 3. Numbering of coordinates for *cis*-1:2-disubstituted ethylenes.

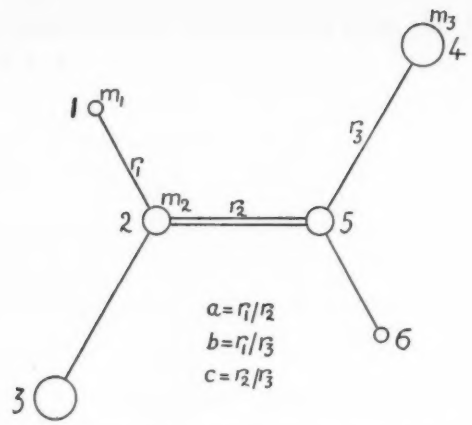

FIG. 4. Numbering of coordinates for *trans*-1:2-disubstituted ethylenes.

placement coordinate is z_k, and M is an arbitrary mass (conveniently chosen to be one of the m_k's), introduced in order that the A_{ij} shall be dimensionless quantities of convenient magnitude. Both **d** and **A** are symmetric; only half the matrix will be given whenever they are introduced explicitly. **I** is the unit matrix, and the quantity λ is defined as follows:

$$\lambda = 4\pi^2\sigma^2c^2M, \qquad (5)$$

σ being a fundamental vibration frequency in cm^{-1} and c the velocity of light in cm $sec.^{-1}$. In the numerical calculations, the force constants and related quantities are usually given to four significant figures, as this is sometimes necessary to illustrate small differences between various solutions for the same constant. No absolute significance is to be attached to the fourth figure.

The symmetry coordinates and the derived **A** matrices are given in Tables I to IV; for the coordinates z_j and other quantities, see Figs. 1 to 4. The same matrices are used for the unsaturated hydrocarbons dealt with, treating the methyl groups as single masses; it will be shown that this approximation does not affect the values of the force constants seriously. Angles of 120° are used throughout; the order of the corrections to be applied for variations from this angle will be estimated. The degree of the equations is in all cases reduced before solving for the constants by factoring out the C−H valence modes, using the method introduced by Wilson.[5] The small corrections to be applied may be assumed constant for force constants going with coordinates common to a series of molecules.

TABLE I. Symmetry coordinates for substituted ethylenes.

(a) *Mono-Substituted ethylenes*, $CH_2=CHX$[a]

$\Delta_1 = \Delta r_{12} - \Delta r_{23}$	$\Delta_6 = r_1(\Delta\theta_{46} - \Delta\theta_{24})$
$\Delta_2 = \Delta r_{45}$	$\Delta_7 = r_1(\Delta\theta_{15} - \Delta\theta_{35})$
$\Delta_3 = \Delta r_{12} + \Delta r_{23}$	$\Delta_8 = \Delta r_{56}$
$\Delta_4 = \Delta r_{35}$	$\Delta_9 = r_2\Delta\theta_{26}$
$\Delta_5 = r_1(\Delta\theta_{13} - \Delta\theta_{15} - \Delta\theta_{35})$	

(b) *1:1-disubstituted ethylenes*, $CH_2=CX_2$[b]

$\Delta_1 = \Delta r_{12} + \Delta r_{23}$	$\Delta_6 = \Delta r_{12} - \Delta r_{23}$
$\Delta_2 = \Delta r_{35}$	$\Delta_7 = r_1(\Delta\theta_{15} - \Delta\theta_{35})$
$\Delta_3 = r_1(\Delta\theta_{13} - \Delta\theta_{15} - \Delta\theta_{35})$	$\Delta_8 = \Delta r_{45} - \Delta r_{56}$
$\Delta_4 = \Delta r_{45} + \Delta r_{56}$	$\Delta_9 = r_2(\Delta\theta_{24} - \Delta\theta_{26})$
$\Delta_5 = r_2(\Delta\theta_{46} - \Delta\theta_{24} - \Delta\theta_{26})$	

(c) *Cis-1:2-disubstituted ethylenes*[c]

$\Delta_1 = \Delta r_{12} + \Delta r_{45}$	$\Delta_6 = \Delta r_{12} - \Delta r_{45}$
$\Delta_2 = \Delta r_{25}$	$\Delta_7 = r_1(\Delta\theta_{15} - \Delta\theta_{24} - \Delta\theta_{13} + \Delta\theta_{46})$
$\Delta_3 = r_1(\Delta\theta_{15} + \Delta\theta_{24} - \Delta\theta_{13} - \Delta\theta_{46})$	$\Delta_8 = \Delta r_{23} - \Delta r_{56}$
$\Delta_4 = \Delta r_{23} + \Delta r_{56}$	$\Delta_9 = r_2(\Delta\theta_{35} - \Delta\theta_{26})$
$\Delta_5 = r_2(\Delta\theta_{35} + \Delta\theta_{26})$	

(d) *Trans-1:2-disubstituted ethylenes*[d]

$\Delta_1 = \Delta r_{12} + \Delta r_{56}$	$\Delta_6 = \Delta r_{12} - \Delta r_{56}$
$\Delta_2 = \Delta r_{25}$	$\Delta_7 = r_1(\Delta\theta_{15} - \Delta\theta_{26} - \Delta\theta_{13} + \Delta\theta_{46})$
$\Delta_3 = r_1(\Delta\theta_{15} + \Delta\theta_{26} - \Delta\theta_{13} - \Delta\theta_{46})$	$\Delta_8 = \Delta r_{23} - \Delta r_{45}$
$\Delta_4 = \Delta r_{23} + \Delta r_{45}$	$\Delta_9 = r_2(\Delta\theta_{35} - \Delta\theta_{24})$
$\Delta_5 = r_2(\Delta\theta_{24} + \Delta\theta_{35})$	

[a] See Fig. 1.
[b] See Fig. 2.
[c] See Fig. 3.
[d] See Fig. 4.

III. THE VIBRATIONAL ASSIGNMENTS

For the four vinyl halides and for vinylidene fluoride and chloride the assignments of Thompson and Torkington[6] are used, with the following minor alterations. In vinyl fluoride, the infra-red absorption maxima at 1363 and 1393 cm^{-1} are now taken for the P and R branches of a parallel band, δCH_2[e] then having the value 1378 in place of 1393 cm^{-1}. In vinylidene chloride, the Raman line at 375 cm^{-1} previously assigned to (non-planar) B_1 rocking, is now taken for planar B_2 rocking. In vinylidene fluoride, for which Raman data are not available, 559 and 680 cm^{-1} are accepted for A_1 CF_2 deformation and B_2 CCF rocking respectively, though these values seem rather high; there are infra-red-Raman coincidences at 570 and 650 cm^{-1} in $CF_2=CCl_2$,[6] though the strong Raman line[7] at 435 cm^{-1} seems likely to be δCF_2[e].[(a)] For *cis*- and *trans*-1:2-dichloro-* and 1:2-dibromo-ethylenes

[6] H. W. Thompson and P. Torkington, Proc. Roy. Soc. London **A184**, 21 (1945); Trans. Faraday Soc. **41**, 236 (1945); J. Chem. Soc. 303 (1944).
[7] J. B. Hatcher and D. M. Yost, J. Chem. Phys. **5**, 992 (1937).
[a] But there is an A type band at 559 cm^{-1} in C_2F_4 (see reference 6) which could be assigned to B_{3u} CF_2 deformation.
* *Note added in proof.*—The infra-red spectra of *cis*- and *trans*-$C_2H_2Cl_2$, $C_2D_2Cl_2$, have recently been measured, (H. J. Bernstein and D. A. Ramsay, J. Chem. Phys. **17**, 556 (1949)); the suggested assignments for the H compounds are essentially the same as used here, except that B_1 CCCl bending is given as 571 $cm.^{-1}$, which is almost certainly too high for such a mode. It is of interest

TABLE II. The **A** matrix for mono-substituted ethylenes.*

$$\begin{bmatrix}
(3+2\mu_1) & 0 & 0 & 0 & 0 & -a\sqrt{3} & -\sqrt{3}(1+2a) & 0 & -\sqrt{3} \\
 & (1+\mu_1) & 0 & -(1/2) & 0 & \sqrt{3}(a-b)/2 & a\sqrt{3} & -(1/2) & \sqrt{3}(c+1)/2 \\
 & & (1+2\mu_1) & -1 & -2\sqrt{3} & 0 & 0 & 0 & 0 \\
 & & & 2 & 2\sqrt{3} & \sqrt{3}(b+2)/2 & 0 & -(1/2) & -c\sqrt{3}/2 \\
 & & & & 4(3+2\mu_1) & 0 & 0 & 0 & 0 \\
 & & & & & (P_1+4\mu_1+b^2\mu_2) & a(3+4a-b) & -\sqrt{3}(a+2)/2 & (P_4-bc\mu_3) \\
 & & & & & & (P_2+2\mu_1) & -a\sqrt{3} & (1+4a+b) \\
 & & & & & & & (1+\mu_3) & -\sqrt{3}/2 \\
 & & & & & & & & (P_3+c^2\mu_3)
\end{bmatrix}$$

$\cdots\nu_{CH_2}{}^a$
$\cdots\nu_{CH}$
$\cdots\nu_{CH_2}{}^s$
$\cdots\nu_{C=C}$
$\cdots\delta_{CH_2}{}^s$
$\cdots\delta_{CH}$
$\cdots\delta_{CH_2}$
$\cdots\nu_{C-X}$
$\cdots\delta_{CCX}$

* $\mu_1=(m_2/m_1)$ throughout $P_1=2(2+a+b+a^2)-b(a-b)$
$\mu_3=(m_2/m_3)$ $P_2=1+4a+8a^2$
$P_3=2+c+c^2$
$P_4=1+2a-c(1+b)$.

TABLE III. **A** matrices for 1:1-disubstituted ethylenes.

Class A_1

$$\begin{bmatrix}
(1+2\mu_1) & -1 & -2\sqrt{3} & 0 & 0 \\
 & 2 & 2\sqrt{3} & -1 & 2\sqrt{3} \\
 & & 4(3+2\mu_1) & 0 & 0 \\
 & & & (1+2\mu_3) & -2\sqrt{3} \\
 & & & & 4(3+2\mu_3)
\end{bmatrix}$$

$\cdots\nu_{CH_2}{}^s$
$\cdots\nu_{C=C}$
$\cdots\delta_{CH_2}{}^s$
$\cdots\nu_{CX_2}{}^s$
$\cdots\delta_{CX_2}{}^s$

Class B_2

$$\begin{bmatrix}
(3+2\mu_1) & -(2a+1)\sqrt{3} & 0 & 2c\sqrt{3} \\
 & (1+4a+8a^2+2\mu_1) & 2a\sqrt{3} & -2(a+c+4ac) \\
 & & (3+2\mu_3) & -(2c+1)\sqrt{3} \\
 & & & (1+4c+8c^2+2\mu_3)
\end{bmatrix}$$

$\cdots\nu_{CH_2}{}^a$
$\cdots\delta_{CH_2}$
$\cdots\nu_{CX_2}{}^a$
$\cdots\delta_{CCX}$

TABLE IV. **A** matrices for *cis*-1:2-disubstituted ethylenes.*

Class A_1

$$\begin{bmatrix}
2(1+\mu_1) & -1 & b\sqrt{3} & -1 & c\sqrt{3} \\
 & 2 & -(b+2)\sqrt{3} & -1 & -c\sqrt{3} \\
 & & (4A_{11}+a^2A_{55}+4b) & 2\sqrt{3} & (2c+aA_{55}) \\
 & & & 2(1+\mu_3) & 0 \\
 & & & & 2c^2(1+\mu_3)
\end{bmatrix}$$

$\cdots\nu_{CH}$
$\cdots\nu_{C=C}$
$\cdots\delta_{CH}$
$\cdots\nu_{C-X}$
$\cdots\delta_{CCX}$

Class B_1

$$\begin{bmatrix}
2(1+\mu_1) & -(2a-b)\sqrt{3} & -1 & (c+2)\sqrt{3} \\
 & \{A_{33}+4a(2+2a-b)\} & 2(1+a)\sqrt{3} & \{A_{35}-4(1+2a)\} \\
 & & 2(1+\mu_3) & -2\sqrt{3} \\
 & & & \{A_{55}+4(c+2)\}
\end{bmatrix}$$

$\cdots\nu_{CH}$
$\cdots\delta_{CH}$
$\cdots\nu_{C-X}$
$\cdots\delta_{CCX}$

* The subsidiary quantities A_{11}, A_{55} etc., are the elements of the class A_1 factor of **A**. The matrices for the *trans*-1:2-disubstituted ethylenes[a] are obtained from the above for the *cis*-compounds by striking out the second row and column from the class A_1 factor and inserting them to form the second row and column of the class B_1 factor; the residue of the former is then the class B_u factor of the *trans*-compound, and the latter has become the class A_g factor.

the assignments given in Wu[8] and Herzberg[9] are accepted, with the alteration that the strong depolarised Raman lines at 406 and 372 cm^{-1} in the *cis*-compounds are assigned to B_1 CCCl and CCBr bending respectively, instead of to the twisting modes. (See $CH_2=CHCl$ (395), $CH_2=CCl_2$ (375); $CH_2=CHBr$ (345), $CH_2=CBr_2$ (322).) The unobservable B_u skeletal bendings in the *trans*-compounds are predicted here by making the sum of the A_g and B_u bending constants the same as the sum of the A_1 and B_1 bending constants in the corresponding *cis*-compound. For vinylidene bromide, the infra-red data of Thompson and Torkington[6] and the Raman data of de Hemptinne, Velghe, and van Riet[10] are used; the latter have also measured the Raman spectra of the deuterated vinyl and vinylidene bromides. For propy-

that B_u CCCl bending is predicted from combination bands to be at 265 $cm.^{-1}$, in excellent agreement with the predicted value here.

[8] T. Y. Wu, *Vibrational Spectra and Structure of Polyatomic Molecules* (Edwards Brothers, Inc., Ann Arbor, 1946).

[9] G. Herzberg, *Infrared and Raman Spectra of Polyatomic Molecules* (D. van Nostrand Company, Inc., New York, 1945).

[10] M. de Hemptinne and C. Velghe, Bull. Class. Sci. Acad. Roy. Belgium **30**, 75 (1944); de Hemptinne, Velghe, and van Riet, Bull. Class. Sci. Acad. Roy. Belgium **30**, 40 (1944).

lene[b] and isobutene, the assignments given by Kilpatrick and Pitzer[11] are accepted, with the alteration that 1062 cm^{-1}, assigned by them to B_1 CH_3 rocking in the latter, is taken for planar CH_2 bending;[c] 1280 cm^{-1} is too high for this mode. Their assignments for the 2-butenes are not thought sufficiently certain to justify detailed calculations; thus, there is no infra-red band, (or only a very weak one), at 1267 cm^{-1} in the *cis*-compound, where there is a Raman line which they assign to A_1 CH wagging; it seems peculiar that this mode should be so weakly-active in the infra-red. And there is some confusion between methyl rocking and C—C stretching modes.

The assignments are summarized in Tables V to VIII.

IV. SOLUTIONS FOR THE FORCE CONSTANTS

In the substituted ethylenes, the fundamental modes of vibration can be conveniently grouped into four types, as follows:

(a) C—H stretching,
(b) C=C stretching,
(c) C—H bending,
(d) Skeletal stretching and bending other than (b).

Type (a) is factored off before solving for the constants for types (b), (c), and (d). For the latter, the procedure developed in a previous paper[2] is used. For each molecule, a standard solution for the force constants is obtained, (together with the matrix of components in the displacements and the percentage of potential energy in the principal square terms). This standard solution corresponds to the fundamental vibrations factoring off in the order in which the corresponding coordinates occur in the matrix **A** (see Tables II to IV). The standard force field can thus be regarded as subjecting the molecule to a graded rigidity; in passing from ν_1 to ν_n each fundamental mode involves one fewer coordinate. With the order adopted here, the C=C stretching coordinate takes no part in the displacements for modes other than $\nu_{C=C}$. It is reasonable to assume that the error introduced by this step in a constant going with any given coordinate will be the same for all members of a series of molecules for which this is a common coordinate. This means that a constant correction can be applied for, for example, $\Delta r_{C=C} \cdot \Delta\theta_{CCH}$ interaction. The standard force constant matrix $\mathbf{d}^0$ having been obtained, small off-diagonal elements are then removed as described previously;[2] the relevant quantities $(\partial\lambda_k/\partial d_{ij})$ are readily calculated from the matrix determining the components in the displacements. This removal of small interaction constants smooths off the step-like graded rigidity, since in the standard solution the interaction constants take such values that coordinates Δ_1 to Δ_{i-1} are prevented from taking part in ν_i. With $\mathbf{d}^0$ and the partially diagonalized matrix $\mathbf{d}'$ the coordinates Δ_{i+1} to Δ_n are represented in the displacement for ν_i; these solutions can be regarded as allowing a natural coupling, (determined by the off-diagonal elements of the matrix **A**), between the C—H bending modes and the lower-frequency skeletal vibrations (d). For comparison, the solution for the C—H bending constants in which all coordinates other than Δ_i remain rigid in ν_i is found. These constants,[12] which will be referred to as the Wilson-Pitzer constants, are given by the following formula:

$$d_{ii}'' = (|\mathbf{A}|_{ii}/|\mathbf{A}|)\lambda_i \qquad (6)$$

where $|\mathbf{A}|_{ii}$ is the minor of $|\mathbf{A}|$ obtained by striking out the ith row and column. Pitzer has developed a semi-rigid-molecule approximation for dealing with large symmetry factors.[13] In his method, the fundamentals are grouped into classes, (e.g., skeletal vibrations and vibrations of attached groups), and the matrix **A**, (or **G**), reduced to a series of matrices of lower order, one for each class, that for any given class being obtained by applying the conditions that all coordinates of other classes shall remain rigid. The method is an extension of Wilson's treatment of C—H stretching vibrations.[5] Each reduced matrix gives rise to a reduced secular equation, which can then be solved for vibrations of that class. It should be remembered that these reduced equations are not factors of the complete secular equation; constants which satisfy the reduced equation will not satisfy the complete symmetry factor from which it is derived, the error depending on the degree of coupling between coordinates allocated to different classes. The Wilson-Pitzer constants given here go with linear reduced equations; d_{ii}'' is identical with d_{ii}^0 when ν_i and ν_n are transposed. They are therefore associated with $(n-1)$ interaction constants, required to maintain the remaining coordinates rigid.

The following values, given in angstrom units, are used here for the bond lengths.

$r_{C-H}=1.071$,[14] $r_{C=C}=1.353$[14] throughout;
$r_{C-Cl}=1.69$,[15] $r_{C-Br}=1.83$,[d] $r_{C-I}=2.03$;[16]
$r_{C-F}=1.36$[d,17] in $CH_2=CHF$, 1.33[d] in $CH_2=CF_2$;
Effective $r_{C-C}=1.60_3$.[e]

[b] 1042 cm^{-1} is assigned to CH_2 wagging in the text; this is accepted in the present work. In their table it is assigned to CH_3 wagging, and CH_2 wagging given as 1172 cm^{-1}. The assignments for non-planar CH wagging and twisting also appear to have become transposed.

[11] J. E. Kilpatrick and K. S. Pitzer, J. Research Nat. Bur. of Stand. **38**, 191 (1947).

[c] The value given by Kilpatrick and Pitzer is 1066; the present value is taken from the Catalog of Infra-red Spectrograms, American Petroleum Institute Research Project 44.

[12] P. Torkington, Nature **164**, 113 (1949).

[13] W. J. Taylor and K. S. Pitzer, J. Research Nat. Bur. of Stand. **38**, 1 (1947).

[14] W. S. Gallaway and E. F. Barker, J. Chem. Phys. **10**, 88 (1942).

[15] Brockway, Beach, and Pauling, J. Am. Chem. Soc. **57**, 2693 (1935).

[16] Huggill, Coop, and Sutton, Trans. Faraday Soc. **34**, 1518 (1938).

[d] Estimated from comparison of data for C_2H_3Cl, CH_3Cl and CH_3F, CH_2F_2 (see reference 17).

[17] L. O. Brockway, J. Phys. Chem. **41**, 747 (1937).

[e] Assuming a mass (m_C+3m_H) at the center of gravity of the

TABLE V. Vibration frequencies of planar modes of $CH_2=CHX$, in cm^{-1}.

X	$\nu_{C=C}$	δ_{CH_2}[a]	δ_{CH}	δ_{CH_2}	ν_{C-X}	δ_{CCX}
CH_3	1649	1415	1297	1042	920	417
F[b]	1650	1378	1306	924	1153	500
Cl	1610	1370	1280	1030	724	395
Br	1605	1377	1262	1008	615	345
I	1593	1376	1242	990	550	309

[a] Numbering from the left, in vinyl fluoride $\nu_5>\nu_4$ and in vinylidene fluoride $\nu_8>\nu_9$; the order here is retained for consistency.

TABLE VI. Vibration frequencies of planar modes of $CH_2=CX_2$, in cm^{-1}.

	A_1				B_2		
X	$\nu_{C=C}$	δ_{CH_2}[a]	ν_{CX_2}[a]	δ_{CX_2}[a]	δ_{CH_2}	ν_{CX_2}[a]	δ_{CCX}
CH_3	1664	1390	800	378	1062	986	431
F[b]	1730	1386	921	559	945	1295	680
Cl	1620	1395	605	295	1094	794	375
Br	1593	1379	467	184	1085	696	322

[a] Numbering from the left, in vinyl fluoride $\nu_5>\nu_4$ and in vinylidene fluoride $\nu_8>\nu_9$; the order here is retained for consistency.

All ethylenic angles are assumed 120° throughout; deviations from this value will not affect the C−H bending constants; their effect on the skeletal constants will be estimated when these are dealt with.

The results for C−H bending modes are summarized in Tables IX to XI. Force constants are given in units of 10^5 dynes cm^{-1} and the energy fractions $V_{ii}^0(\nu_i)$, referring to the standard solutions, as percentages. The subscripts are ordered to go with the reduced matrices **A**, and with the assignments given in Tables V to VIII. Thus d_{22} in the vinyl compounds is here the constant going with the coordinate for CH_2 deformation, given as Δ_5 in Table I (a).

V. DISCUSSION OF THE RESULTS

We have obtained three solutions for each of the C−H bending constants occurring in the potential functions for substituted ethylenes. From the results summarized in Tables IX to XI it is seen that, with the coordinates used, the CH_2 deformation constant lies between 0.130 and 0.145, the C−H bending constant between 0.18 and 0.24, and the CH_2 rocking constant between 0.20 and 0.35, in units of 10^5 dynes cm^{-1}. In every case, the elimination of the small interaction constants from $\mathbf{d}^0$ produces negative increments in the CH bending constants, and the Wilson-Pitzer constant is greater than either of the other two*; i.e., $d_{ii}''>d_{ii}^0>d_{ii}'$. d_{ii}'' is associated with a pure vibration ν_i in which the potential energy is a function of only the one coordinate Δ_i, (i.e., $V_{ii}''(\nu_i)=1$, $V_{ij}''(\nu_i)=0$ for $i\neq j$). With d_{ii}^0, $V_{ii}(\nu_i)$ is greater than unity, there being negative contributions from the various cross-terms $d_{ij}\Delta_i\Delta_j$, $(j>i)$. With d_{ii}', $V_{ii}(\nu_i)$ is in general less than unity, and terms involving Δ_j, $(j<i)$, take non-zero values. (See Appendix II.) The range of values covered by the three solutions can be taken as representative of the range physically possible, the standard constants d_{ii}^0 being convenient mean values. Change of sign of all the small off-diagonal elements of $\mathbf{d}^0$ reduced to zero in $\mathbf{d}'$ would give a fourth solution $\mathbf{d}^m$ such that $(d_{ii}^0-d_{ii}')\approx(d_{ii}'-d_{ii}^m)$. $\mathbf{d}^m$ could be regarded as a conventional minimum solution, but since the small off-diagonal elements of $\mathbf{d}^0$ have no physical significance when their sign is changed, we will not go beyond $\mathbf{d}'$ here. The absolute values of the constants have still to be corrected for coupling with C=C stretching; as already stated, it is justifiable to assume that, for a given type of C−H bending, this interaction will remain constant throughout the series of substituted ethylenes. Variations deduced from the values in Tables IX to XI can therefore be taken as absolute.

Consider first the CH_2 deformation constant. For the vinyl halides, a value lying between 0.132 and 0.134 will fit all four compounds; for propylene, however, a value greater than 0.139 is required, which will not fit any of the other halides. In the vinylidene compounds, a value within the range 0.135 to 0.139 fits all four molecules. The analogous constants, $(d^0=d'')$, in ethylene, with $\nu_{A_g}=1342.4$, $\nu_{B_{3u}}=1443.5$,[9,14] have the following values: 0.1337(A_g), 0.1380(B_{3u}). The constant for the A_g mode is probably better chosen as a standard, since the B_{3u} mode does not interact with C=C stretching. Thus, the value 0.134–0.135 will fit all ethylenic molecules studied here, with the exception of propylene. This anomaly of propylene is rather obscure. In the series $CH_2=CHX$, $CH_2=CX_2$, δ_{CH_2}[a] is higher in the di-substituted than in the mono-substituted compounds in all cases except $X=CH_3$, which suggests that the observed frequency

TABLE VII. Vibration frequencies of planar modes of *cis*-CHX=CHX, in cm^{-1}.

	A_1				B_1		
X	$\nu_{C=C}$	δ_{CH}	ν_{CX}	δ_{CCX}	δ_{CH}	ν_{CX}	δ_{CCX}
Cl	1587	1179	711	173	1303	857	406
Br	1584	1150	580	109	1229	673	372

TABLE VIII. Vibration frequencies of planar modes of *trans*-CHX=CHX, in cm^{-1}.

	A_g				B_u		
X	$\nu_{C=C}$	δ_{CH}	ν_{CX}	δ_{CCX}	δ_{CH}	ν_{CX}	δ_{CCX}
Cl	1576	1270	844	349	1200	820	270(calc.)
Br	1578	1246	748	218	1145	746	247(calc.)

methyl group, taking r_{C-C} in propylene as 1.53, (allowing for a small degree of shortening from the value 1.57_3 found in ethane (see reference 9)) $r_{C-H}=1.093_6$, as in methane (see reference 9), and assuming tetrahedral angles.

* It can be shown that inclusion of Δ_j in the displacement for ν_i decreases or increases d_{ii} from the value d_{ii}'' for the pure mode, according as ν_i is greater than or less than ν_j; similarly, that d_{ii}^0 is always greater than d_{ii}'.

TABLE IX. Solutions for mono-substitutes ethylenes $CH_2=CHX$.

X	CH_3			F		
i	2	3	4	2	3	4
d_{ii}^0	0.1407	0.2290	0.2532	0.1338	0.2339	0.2077
d_{ii}'	0.1393	0.2183	0.2297	0.1317	0.2184	0.1718
d_{ii}''	0.1424	0.2333	0.2886	0.1355	0.2368	0.2252
j						
2	1			1		
3	−0.0393	1		−0.0409	1	
$\Delta_j^0(\nu_i)$ 4	−0.0009	0.0762	1	−0.0009	0.0744	1
5	0.0088	−0.0331	−0.0368	0.0088	−0.0326	−0.0369
6	0.0113	0.0276	0.1347	0.0135	0.0233	0.1387
$V_{ii}^0(\nu_i)$	100.496	102.231	104.868	100.748	103.178	109.472

X	Cl			Br		
i	2	3	4	2	3	4
d_{ii}^0	0.1320	0.2238	0.2470	0.1333	0.2177	0.2352
d_{ii}'	0.1305	0.2139	0.2249	0.1320	0.2087	0.2168
d_{ii}''	0.1343	0.2314	0.2887	0.1364	0.2275	0.2807
j						
2	1			1		
3	−0.0388	1		−0.0381	1	
$\Delta_j^0(\nu_i)$ 4	−0.0009	0.0770	1	−0.0009	0.0778	1
5	0.0088	−0.0334	−0.0367	0.0088	−0.0337	−0.0367
6	0.0107	0.0338	0.1330	0.0099	0.0369	0.1311
$V_{ii}^0(\nu_i)$	100.527	102.110	104.671	100.481	101.986	104.070

X	I		
i	2	3	4
d_{ii}^0	0.1330	0.2108	0.2258
d_{ii}'	0.1318	0.2026	0.2103
d_{ii}''	0.1363	0.2218	0.2734
j			
2	1		
3	−0.0373	1	
$\Delta_j^0(\nu_i)$ 4	−0.0009	0.0787	1
5	0.0088	−0.0339	−0.0366
6	0.0088	0.0387	0.1292
$V_{ii}^0(\nu_i)$	100.429	101.859	103.563

for propylene and/or isobutene is not the true one. The symmetrical methyl deformation lies close, at 1370 to 1380 cm^{-1}; it is possible that Fermi resonance between these two modes occurs, for which a correction should be applied.[f, 18] Resonance is also possible between $\nu_{C=C}$ and CH bending modes, but it seems reasonable to assume that for a given mode this would take place to the same extent for all related molecules.

The CH_2 bending constant varies much more in passing from **d′** to **d″** than does the symmetrical CH_2 deformation constant; the coupling with coordinates other than C=C stretching is of more importance. A value of 0.225 can satisfy all the vinyl halides; if we omit the fluoride, a range of 0.225 to 0.27 is allowed, nearly the whole being also available for propylene. Passing to the vinylidene compounds, the minimum allowed value becomes raised to 0.245, which is also the maximum for vinylidene fluoride. The value 0.245 could thus be a common solution for all the molecules studied, except vinyl fluoride. Since this compound falls outside the range, it seems probable that this is also the case for vinylidene fluoride. 0.245 is the value of the Wilson-Pitzer constant for $CH_2=CF_2$; it seems most unlikely that there should be less kinetic coupling in the fluoride, where ν_{C-X} and δ_{CCX} are higher, than in the other halides. The values of the comparable CH_2 rocking constants in ethylene, ($d^0=d''$), with $\nu_{B_{1g}}=1050$, $\nu_{B_{2u}}=995$ cm^{-1}[9, 14] and with accepted molecular dimensions,[14] are as follows: 0.1987(B_{1g}), 0.2833(B_{2u}); (mean: 0.2410).

The range of values for CH wagging constants is less than for CH_2 rocking constants, though rather more

[f] On the other hand, δCH_2^s in the allyl halides (see reference 18) lies at 1405 to 1410 cm^{-1}; any resonance would involve the saturated CH_2 deformation at 1440 to 1450 cm^{-1}, leading to a positive correction.

[18] H. W. Thompson and P. Torkington, Trans. Faraday Soc. 42, 432 (1946).

TABLE X. Solutions for 1:1-disubstituted ethylenes $CH_2=CX_2$.

X	CH_3		F		Cl		Br	
i	2	5	2	5	2	5	2	5
d_{ii}^0	0.1359	0.2671	0.1357	0.2369	0.1368	0.2788	0.1335	0.2718
d_{ii}'	0.1342	0.2274	0.1329	0.1546	0.1353	0.2443	0.1319	0.2443
d_{ii}''	0.1395	0.3119	0.1392	0.2455	0.1421	0.3407	0.1400	0.3421
j								
2	1		1		1		1	
3	0.0168		0.0168		0.0168		0.0168	
$\Delta_j^0(\nu_i)$ 4	−0.0581		−0.0581		−0.0581		−0.0581	
5		1		1		1		1
6		0.0850		0.0850		0.0850		0.0850
7		−0.3340		−0.2855		−0.3495		−0.3744
$V_{ii}^0(\nu_i)$	100.599	108.031	101.055	121.025	100.557	106.272	100.455	105.322

TABLE XI.* Solutions for *cis*- and *trans*-1:2-disubstituted ethylenes CHX=CHX.

	Cis-				*Trans*-			
X	Cl		Br		Cl		Br	
i	2	5	2	5	2	5	2	5
d_{ii}^0	0.2044	0.2192	0.1946	0.1938	0.2234	0.1952	0.2150	0.1786
d_{ii}'	0.2034	0.1942	0.1938	0.1752	0.2100	0.1860	0.2022	0.1700
d_{ii}''	0.2052	0.2358	0.1958	0.2160	0.2364	0.2092	0.2292	0.1924
j								
2	1		1		1		1	
3	0.0115		0.0120		0.0351		0.0355	
$\Delta_j^0(\nu_i)$ 4	−0.0017		−0.0037		−0.0940		−0.0958	
5		1		1		1		1
6		0.0529		0.0530		0.0328		0.0329
7		−0.0608		−0.0651		0.0272		0.0228
$V_{ii}^0(\nu_i)$	100.225	106.057	100.206	105.063	103.097	102.388	103.062	102.514

* The constants here are obtained from those going with the coordinates in Table I by multiplying by a factor of two, (this being equivalent to there being a normalizing factor of $(1/\sqrt{2})$ included in the coordinates), to be comparable with those in Table IX.

than for CH_2 deformation constants. A value of about 0.22 will satisfy all the vinyl compounds, including propylene. With the *cis*- and *trans*-di-substituted compounds it is likely that the constants comparable with the d_{33} of the vinyl compounds will be those for the symmetrical (A_1 and A_g) modes, (i.e., the d_{22} of Table XI) since the B_1 and B_u vibrations do not interact with $\nu_{C=C}$. These are rather lower than the corresponding constants in the vinyl compounds, except for the *trans*- Wilson-Pitzer constants. The value 0.22 can be fitted to both *trans*-compounds, but this has to be lowered to about 0.20 for the *cis*-isomers; and, in addition, there is for the latter no overlapping of the allowed ranges of values in the chloride and bromide. There is thus some evidence for the constant in the *trans*-compounds being greater than in the *cis*-isomers, and also for there being a variation in the CH bending constant with change in the substituent X. This latter is to be expected, since the coordinate used involves the angle HCX. (See Table I.) For the *cis*-compounds, the B_1 constants overlap with the A_1 constants, but for the *trans*-compounds there is no such overlap, the B_u constants taking the lower range of values. However, no absolute significance is to be attached to this difference, since the correction for coupling with C=C stretching is not known.[g]

Recapitulating, it has been shown that it is possible to use the same value for the CH_2 deformation constant as in ethylene for all the vinyl and vinylidene compounds studied here, with the possible exception of propylene. And that the ethylenic CH_2 wagging constant (taking the mean for B_{1g} and B_{2u} modes), can also be carried over except to the fluorides, for which a lower value must be used. For CH bending there is definite evidence that the constant varies with the substituent.

Reconsidering the CH_2 bending constant, it has been shown that this is the most strongly affected by kinetic coupling. (This fact is also very evident from ethylene itself; the difference between the (unnormalized) constants for B_{1g} and B_{2u} bending amounts to 17.5 percent of the mean constant, this being equivalent to constants +0.0417, −0.0417 for interaction between adjacent angles on the same side of C=C, and between alternate

[g] In such a case it is usual to assume the constants the same; this would enable the $\Delta r_{C=C} \cdot \Delta\theta_{CCH}$ interaction here to be determined. But such constants are not necessarily equal. (See the pairs of CH_2 rocking constants in ethylene: B_{1g}, B_{2u}, (see Appendix I), B_{1u}, B_{2g}, (see reference 1).)

TABLE XII.

	C_2H_4			C_2D_4		
	B_{1g}	B_{2u}	B_{3u}	B_{1g}	B_{2u}	B_{3u}
ν_1(obs.)	3075	3105.5	2989.5	2304	2345	2200.2
ν_2(obs.)	1050	995	1443.5	883	723.4	1077.9
d_{11}^c	1.237_8	1.270_5	1.271_3	1.229_1	1.300_8	1.318_9
d_{22}''	0.0993_3	0.1416_6	0.0689_8	0.1068_9	0.1454_7	0.0699_2
ν''(calc.)	3074.5	3105.4	2989.5	2304.5	2344.9	2200.8
ν_2''(calc.)	1046.6	994.7_4	1442.5	872.6_5	722.8_0	1075.2
d_{22}^c	0.1002_7	0.1417_9	0.0690_7	0.1091_0	0.1458_2	0.0701_0
ν_1^c(calc.)	3074.6	3105.4	2989.5	2305.2	2344.9	2200.8
ν_2^c(calc.)	1051.4_5	995.2_0	1443.4_5	881.4	723.6_6	1076.6
d_{11}	1.238_2	1.270_6	1.271_2	1.227_7	1.300_9	1.318_1
d_{22}	0.0999_9	0.1417_3	0.0690_7	0.1095_1	0.1457_6	0.0702_7
$V_{11}(\nu_1)$	99.255	99.942	99.820	97.188	99.816	99.338
$V_{11}(\nu_2)$	0.745	0.058	0.180	2.812	0.184	0.662

angles, respectively.) If the results for ethylene are interpreted as meaning that the CH_2 bending constant can vary over the range from the B_{1g} to the B_{2u} constant, then it can be said to be possible to carry over the ethylenic constant in every case studied here, though the significance of variations would be rather obscure. It seems best to take the mean constant, which occurs as the square-term constant in the expanded valence-force potential function for ethylene, as the significant value. Now this value occupies various positions in the ranges of allowed solutions. In the vinyl compounds, excluding the fluoride, $d_{44}=0.241$ is associated with decreasing coupling in passing from $X=CH_3$ to $X=I$; for the former, $d^0>0.241>d'$, and for the latter $d''>0.241>d^0$. This seems the likely direction for such variation in degree of coupling. In vinylidene chloride and bromide, $d'>0.241$, and unless a higher value of the constant is used, the coupling will be greater than in any of the vinyl compounds. This may be due to the presence of a higher degree of symmetry.[h]

The same decrease in coupling occurs when a constant CH bending constant is fitted into the range of values for the vinyl halides; in the fluoride, $d^0>0.22>d'$, and in the iodide $d''>0.22>d^0$, propylene lying roughly between fluoride and chloride. Common values for CH and CH_2 rocking constants could therefore be used for all the monosubstituted ethylenes here, with the exception of δCH_2 in the fluoride. However, it has been shown from the results for the disubstituted compounds that there is probably a real variation with X of the CH bending constant.

[h] The assignments for these two molecules may be incorrect. For each there is a close pair of A-type bands in the region of 1100 cm^{-1}. The lower frequency member was chosen in the chloride; any correction for Fermi resonance would raise the frequency. The higher frequency member was chosen for the bromide, because it led to a better frequency prediction for the deuterated compound, for which there is only a single Raman line. But there are different anharmonicity corrections for CH and CD bending modes, and it is possible that $\delta CH_2(B_2)$ is the band at 1056 cm^{-1}.

VI. CONCLUSION

The present analysis has given series of values for the force constants for planar CH bending modes in substituted ethylenes. The evidence for a given force constant varying with different substituents is not very definite, but it seems likely that, since there is positive evidence in some cases, there are real variations in the remainder; the effect is more noticeable with two substituents than with one. Variations in a group frequency may be due to any or all of three causes, (a) changes in the force constant going with the coordinate determining the group vibration, (b) changes in the overlapping coordinates, (c) changes in the interaction constants in cross-product terms involving the group coordinate. Some attempt has been made here to determine the relative probabilities of (a) and (b); as regards (c), the interaction constants are in general negligible with the exception of those for interaction with C=C stretching. The non-diagonal elements of $\mathbf{d}^0$ are a measure of the maximum allowed values of these interaction constants. It is readily shown that in most cases they would have to take improbably large values to produce the same effect as a given small increment in the square-term constant for the group vibration. (See Appendix III.)

It is hoped to treat the skeletal vibrations of substituted ethylenes in a second paper. The author wishes to express his gratitude to Courtaulds Limited for making the present program of work possible, and to Sir Cyril Hinshelwood for granting him facilities at the Physical Chemistry Laboratory. Also to Dr. H. W. Thompson, F. R. S., Dr. J. W. Linnett, and Professor C. A. Coulson, for helpful discussions.

APPENDIX I. ERRORS INTRODUCED THROUGH THE FACTORING OF THE C–H STRETCHING MODES

The following results were obtained with ethylene and ethylene-d_4; the coordinates used are unnormalized and analogous to those used for the substituted ethylenes

(see Table XII). The un-primed d_{11}, d_{22} are the constants obtained by solving explicitly,[3] assuming the interaction constants zero; the V_{11} are the energy-fractions, (given as percentages), going with this solution. d_{11}^e, d_{22}^e, are the constants obtained by applying a correction for kinetic coupling in place of factoring and d_{22}'' is the factored Wilson-Pitzer constant. ν_i'' and ν_i^e are the frequencies predicted using d_{22}'' and d_{22}^e respectively, d_{11}^e being used for both. The differences in the case of ethylene are seen to be very small; the constants d^e are the closer approximation. With ethylene-d_4, the error introduced by factoring off the C−D stretching modes is considerably larger; this would be expected from the potential energy distributions. In general, the correction for kinetic coupling again gives the better approximation. Comparing the corresponding results for the hydrogen and deuterium compounds, it is seen that, with the exception of the constant for B_{1g} stretching, the C−D constants are higher than the C−H constants. This can be attributed to the different anharmonicity corrections required for motions involving hydrogen and deuterium atoms. The difference is of the order of 10 percent for B_{1g} rocking, 3 percent for B_{2u} rocking and 1 percent for B_{3u} deformation. If the C−D stretching vibrations are factored, the following values are obtained for the A_1 and A_g C−D bending constants in *cis-* and *trans-*CDCl=CDCl respectively: *cis-*, $d^0=0.1055$, $d'=0.1039$; *trans-*, $d^0=0.1312$, $d'=0.1126$, $\times 10^5$ dynes/cm. These values are higher than those obtained with the hydrogen compounds by 3 percent for the *cis-* isomer and 7–15 percent for the *trans*, which differences are significantly comparable with those found in C_2H_4 and C_2D_4. Considerable difficulty has been experienced in finding the correct potential function for the ethylenes;[11] the data here suggest that it may be best to solve for the two molecules separately, choosing constants which give consistent anharmonicity increments.

If the partially-diagonalized matrix $\mathbf{d}'$ for $CH_2=CBr_2$ is used to predict the fundamental frequencies of $CD_2=CBr_2$, the following results are obtained:

	A_1				B_2			
ν(calc.)	1548	1003	455	180	947	642	291	$\}$ cm^{-1}.
ν(obs.)$_{10}$	1544	1019	453	183	932	625	283	

APPENDIX II. THE DISPLACEMENTS ASSOCIATED WITH d′ AND THE ACCURACY OF THE REDUCTION d⁰→d′

To illustrate the effect of partially diagonalizing the standard force constant matrix $\mathbf{d}^0$, the results for A_1 CH wagging in *cis*-$C_2H_2Cl_2$ are given below:

With $\mathbf{d}'$

$$\Delta_i[0.00255 \quad 1 \quad 0.01693 \quad -0.00556]$$

$$V_{ij}\begin{bmatrix} 0.065 & 0.554 & 0.040 & -0.005 \\ & 98.280 & 0 & 0 \\ & & 0.485 & -0.011 \\ & & & 0.012 \end{bmatrix}$$

With $\mathbf{d}^0$

$$\Delta_i[0 \quad 1 \quad 0.01155 \quad -0.00173]$$

$$V_{ij}\begin{bmatrix} 0 & 0 & 0 & 0 \\ & 100.225 & -0.227 & 0.001 \\ & & 0.229 & -0.002 \\ & & & 0.001 \end{bmatrix}$$

To illustrate the degree of accuracy of the reduction $\mathbf{d}^0\rightarrow\mathbf{d}'$, the roots of the equation $|\mathbf{d}'\mathbf{A}-\lambda\mathbf{I}|=0$ were found for the class A_1 factor for *cis*-$C_2H_2Cl_2$. The calculated fundamental frequencies are given below, together with the true values:

ν(calc.)	1588.1	1179.6	710.1	162.3	$\}$ cm^{-1}.
ν(obs.)	1587	1179	711	173	

The error for the three higher frequencies is of the order of only 0.1 percent.

APPENDIX III. THE RELATIVE EFFECTS OF A GIVEN INCREMENT TO A PRINCIPAL CONSTANT AND TO AN INTERACTION CONSTANT, FOR CH BENDING MODES IN SUBSTITUTED ETHYLENES

The derivatives $(\partial\lambda_k/\partial d_{ij})$ are readily obtained for the standard solution, as described in a previous paper.[2] These quantities are given here for vinyl chloride:

i \ k	2				
2	101.1	−3.917	−0.091	0.890	1.084
3		0.152	0.0035	−0.034	−0.042
4			0.0001	−0.0008	−0.0010
5				0.0078	0.0095
6					0.0116

i \ k	3			4		
3	52.85	4.070	−1.766	1.783		
4		0.313	−0.136	0.137	31.78	−1.167	4.227
5			0.059	−0.060		0.043	−0.155
6				0.060			0.562

The elements for the other vinyl compounds only differ slightly from the above. Inspection shows that a given increment in the interaction constant possessing the largest derivative has only 4 percent, 8 percent and 15 percent on the frequencies ν_2, ν_3 and ν_4 respectively as the same increment in the main constant. These constants, (d_{23}, d_{34} and d_{46}), have values 0.00775, −0.0142 and −0.0597 in the standard solution for vinyl chloride. The effect of reducing them separately to zero is to produce the following increments in the three vibration frequencies:

$$\Delta\nu_2=+3.14, \quad \Delta\nu_3=+6.37, \quad \Delta\nu_4=+34.11 \text{ cm}^{-1}.$$

The same effect would be produced by the following increments to the principal constants:

$$\Delta d_{22}=+0.00060, \quad \Delta d_{33}=+0.00219,$$
$$\Delta d_{44}=+0.01589\times 10^5 \text{ dynes/cm}.$$

The increment in the diagonal element A_{33} in passing from chloride to iodide is equivalent to a shift $\Delta\nu_3=-4.53$ cm^{-1}; for the other two modes, the diagonal

elements remain constant and no frequency-shift can arise from this source.

It is seen from the above results that, with the possible exception of the CH_2 bending mode, it is most unlikely that the observed frequency-shifts encountered on passing from chloride to iodide could be accounted for by variations in small interaction constants normally assumed zero. Since we are dealing here with closely-related structures, there seems no justification for postulating the existence of small interaction constants which undergo relatively large variations in passing along the series.

THE JOURNAL OF CHEMICAL PHYSICS VOLUME 17, NUMBER 12 DECEMBER, 1949

Physical Properties of Polonium. I. Melting Point, Electrical Resistance, Density, and Allotropy*

CHARLES R. MAXWELL**
Los Alamos Scientific Laboratory, Los Alamos, New Mexico
(Received May 2, 1949)

Measurements on the electrical resistance, thermal coefficient of electrical resistance, melting point and density of polonium are reported. An abrupt change in the electrical resistance near 100°C indicates that polonium exists in two allotropic forms. Observations which indicate that the temperature for crystal transformation is a function of the size and history of the specimen are reported.

SINCE its discovery in 1898, many investigations have been made into the chemical properties of polonium but the small quantities of the element available in the past made the determination of its ordinary physical properties impractical if not impossible. The larger, though still minute, amounts of polonium available today in the Manhattan Project have made possible the development of techniques by which rough measurements on some of the physical properties of polonium have been made.

The selection of a method and the accuracy of the method were influenced not only by the small amount of material available but by the radioactivity of the element: (1) The high specific activity of polonium makes it extremely toxic if absorbed into the body, hence any method employed must keep mechanical scattering and general contamination of the laboratory at a minimum; (2) Since polonium has a half-life of 138 days,[1] the lead content of a freshly prepared sample increases at the rate of one-half percent per day. Methods requiring a long time to attain equilibrium or requiring successive measurements over an appreciable period are impractical; (3) The heat produced by the radioactivity (0.12 calorie per microgram per hour)[1] maintains polonium and its immediate surroundings at a temperature higher than the ambient temperature. The magnitude of this temperature differential varies with the size of the sample and the heat transfer characteristics of its immediate environment. This phenomenon makes the determination or reproducibility of temperature difficult.

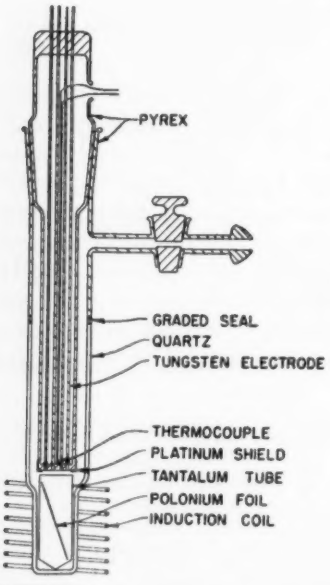

FIG. 1. Apparatus for measuring electrical resistance.

PREPARATION AND PURITY OF POLONIUM

Metallic polonium was prepared by electro-deposition on platinum foils from dilute nitric acid solution of polonium nitrate. Earlier work by other members of the laboratory had shown that metal prepared in this manner was very pure, except, of course, for lead which is formed in the metal after deposition. A further check of the purity was made by the spectrochemical analysis of a sample used for a melting point determination. The analysis showed only the expected amount of lead and small amounts of aluminum and calcium. It is believed that these latter impurities were introduced with the acid used to dissolve the sample in preparing it for spectrochemical analysis. In the chemical process used in the recovery of the material for subsequent experiments it is possible but unlikely that other impurities

* This paper is based on a portion of thesis presented in partial fulfillment of the requirements for the degree of Doctor of Philosophy at Iowa State College, Ames, Iowa.

** Present address, Laboratory of Physical Biology, National Institutes of Health, Bethesda 14, Maryland.

[1] W. H. Beamer and W. E. Easton, J. Chem. Phys. **17**, 1298 (1949).

were introduced, since the electro-deposition is in itself a purification.

ELECTRICAL RESISTIVITY

The specific resistivity and the thermal coefficient of resistivity were determined on thin distilled films of polonium in the apparatus shown in Fig. 1.

After the introduction of a freshly prepared polonium coated platinum foil, the apparatus was evacuated to a pressure of from 10^{-5} to 10^{-6} mm of Hg. The polonium was then distilled onto the end of the electrode assembly by heating the tantalum tube to a dull red heat by high frequency induction. The end of the glass electrode holder and the electrodes had been ground and polished so that they formed a smooth flat surface on which the polonium condensed as a thin film and shorted the electrodes.

The apparatus was filled with approximately one-third an atmosphere of helium and placed in a vertical tube furnace where the temperature was slowly raised. The temperature of the end of the electrode assembly was measured by the thermocouple which was in contact with the glass upon which the film was deposited.

The *IR* drop across that portion of the polonium between the center electrodes was measured with a potentiometer while a constant current, usually 10 ma, was being passed through the film between the outer electrodes.

The amount of polonium in the film was determined after the completion of the measurements by inserting the electrode assembly into a special alpha-counter. The dimensions of the film were assumed to be those of the rectangular opening in the platinum shield fastened across the end of the electrode assembly and the thickness of the film was calculated by further assuming uniform deposition.

The validity of the last assumption was checked by D. T. Vier, who took alpha-ray photographs of several films in a special evacuated pinhole camera. The density of the photographic image thus obtained was a measure of the thickness of the polonium since the deposit was so thin that there was no complete self-absorption of alpha-particles. Visual inspection of the photographic plates showed that the edges of the polonium film were quite sharp and the deposition apparently uniform. Densitometer traces taken from end to end of two such images showed a uniform taper in the thickness of the deposit amounting to 8 percent in one case and 20 percent in the other. The assumption of uniform thickness for a film with 20 percent taper introduces an error of only 3 percent to 4 percent in the calculated specific resistance.

Microscopic examination up to 200× showed a smooth uniform film with small grain size. However, the grain size and general character of the films were found to be dependent upon rate and temperature of distillation. The optimum rate of distillation was different for polonium and each of the metals (lead, zinc, and bismuth) used as stand-ins while developing the technique.

TABLE I. Electrical resistivity of polonium.

Determination	Heating rate °C/min.	Transition range °C	Specific resistivity, 0°C micro-ohm-cm $\alpha-P_0$	$\beta-P_0$	Thermal coefficient electrical resistivity* $\alpha-P_0$	$\beta-P_0$
VIA	8.0	— –86	43	47	0.0045	0.0058
VIB	0.4	65–85	39	42	0.0045	0.0066
VIIA	0.5	78–110	50	43	0.0046	0.0081
VIIB	0.5	70–105	47	46	0.0037	0.0071
VIII	0.8	100–130	33	36	0.0056	0.0071
Average			42±10	44±10	0.0046	0.0070

* $=(\Delta R)/(R_0\Delta t)$.

The results of several determinations made as described above are shown graphically in Fig. 2 and are also tabulated in Table I.

It will be noted in Fig. 2 that between 65°C and 130°C there is a definite discontinuity in each curve. This was interpreted as due to a change in the crystal structure of polonium. The low temperature phase has been designated α-polonium and the high temperature phase β-polonium. This interpretation of the discontinuity has since been proven correct by the x-ray diffraction studies.[2]

A polonium film was held at a temperature of −64°C for 12 hours. The resistance of the film was then measured as the apparatus was slowly heated to 50°C. There was no indication of a phase change in this region.

It is estimated that all of the polonium films used in obtaining these data contained between one-half and two percent lead which was formed by radioactive decay during the electro-deposition of the metal and the preparation of the film. This could not be reduced because it was necessary for the freshly prepared film, which was deposited as β-polonium on the uncooled electrode assembly, to stand for several hours in order to form α-polonium. It was thought inadvisable to subject the glass electrode assembly with its many glass-metal seals to the thermal shock of a refrigerant during the distillation in order to deposit the alpha-phase.

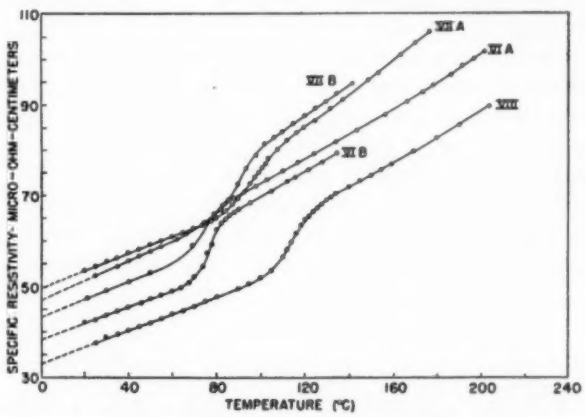

FIG. 2. Specific resistivity of polonium.

[2] W. H. Beamer and C. R. Maxwell, J. Chem. Phys. **17**, 1293 (1949).

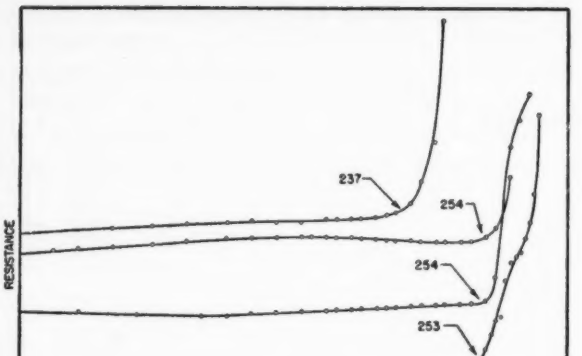

FIG. 3. Electrical resistance curves showing the melting point of polonium.

The average values of 42±10 micro-ohm-centimeters for R_0 of α-polonium and 44±10 micro-ohm-centimeters for R_0 of β-polonium are believed to be maximum values. All undetermined errors due to cracks, porosity or other physical defects in the polonium film add to make the specific resistivity secured with this technique larger than the true specific resistivity for massive metal. Furthermore, the presence of the unavoidable lead gives an alloy whose resistance is undoubtedly higher than that of pure polonium. It is thought that the effect of the lead is small since the resistance of a sample did not change with lapse of time and increasing lead content.

MELTING POINT

Films of polonium prepared in the same manner as described for the resistivity measurements were heated to temperatures around 250°C. Near this temperature the resistance of the films always showed a large, abrupt increase which was usually followed by the breaking of the film. Figure 3 shows the results of several melting point determinations. These curves have been displaced vertically to show clearly the change in slope. The point of abrupt change in slope was taken as the melting point.

Figure 4 is a photograph of the end of the electrical resistivity apparatus after a melting point determination. Globules of once molten metal have formed on the ends of the metal electrodes and a rectangular "fence" of tiny beads outline the edges of the film.

The melting points of several other elements (Baker's C.P. grade) were determined by J. B. Roberts using the same technique and apparatus with the following results:

Metal	Experimental	Literature
Bi	269°C	271°C
Cd	315	320.9
Zn	417	419.5.

A visual melting point was taken with a slight modification of the resistivity apparatus. Polonium was distilled from a tantalum tube with a small nozzle onto a glass surface at liquid air temperature. The sample was transferred from the distillation apparatus to a jacket containing a window through which the polonium deposit could be observed and photographed. Figure 5 shows the sample after it had warmed up to room temperature. Note the large shrinkage cracks produced in the metal when it was "heated" from −190°C to 25°C. This shrinkage corroborates the evidence of a negative coefficient of expansion for α-polonium indicated by x-ray patterns.

The apparatus was placed in a tube furnace and the temperature slowly raised. The temperature was measured by a thermocouple placed on the other side of the glass surface. The polonium deposit was viewed through a low power microscope during the heating period. At 246°C there was a distinct change in the surface of the deposit which was interpreted as due to the melting of the sample.

DENSITY

The density of polonium was determined by measuring the length of an "ingot" of polonium which had been centrifugally cast into the end of a small capillary of predetermined cross-sectional area. The amount of polonium in the ingot was determined calorimetrically by W. E. Easton.[1]

The polonium was distilled into the capillary and sealed from the distillation apparatus by a technique of successive vacuum distillations described in detail in a companion paper.[2] The capillary was placed in a special centrifuge cup and heated to 450°C, which is well above the melting point of polonium. While at this temperature the massive centrifuge cup and capillary were placed in a centrifuge and whirled until cool. In this manner the molten polonium was centrifugally cast into the calibrated end of the capillary. The length of the "ingot" was then measured with a comparator and microscope.

The density of polonium was calculated to be 9.4 ±0.5 g/cc.

The capillary and ingot were cooled overnight in an oil bath at a temperature of −50°C and then heated slowly until the ingot was observed to melt near 250°C. The measurements made of the length of the ingot over

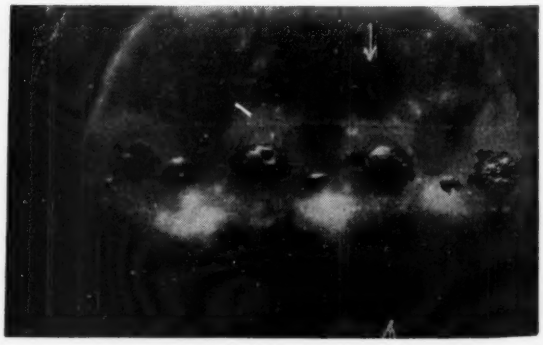

FIG. 4. End of specific resistivity apparatus after melting point determination.

this temperature range were not sufficiently accurate to detect the allotropic change in polonium or to give a measure of the thermal coefficient of expansion.

THE ALLOTROPY OF POLONIUM

No extensive investigation of the transformation of polonium has been made. The observations presented here were incidental to other investigations and the conclusions drawn are only suggestive.

Both the x-ray data, in an accompanying paper,[2] and the electrical resistivity data of this investigation show that alpha- and beta-polonium co-exist for long periods of time over a considerable range of temperature and that the temperature of the transformation of beta-polonium to alpha-polonium is considerably lower than the temperature of the transformation from alpha-polonium to beta-polonium. Furthermore, the range of temperature of the α- to β-transformation was found to vary with the thickness of the sample used for the determination.

For a given film of polonium the range of temperature over which the alpha- to beta-transformation is observed to occur is independent of the rate of heating. Data for curve VIA of Fig. 2 was obtained while the sample was being heated rapidly. The sample was heated from 50°C to 98°C in six minutes. The data for curve VIB was obtained several hours later by slowly heating the same sample. The transformation began at 65°C. Eight minutes later the temperature reached 68°C and was held constant at this temperature for ten minutes. There was no change in the resistance to indicate that the transformation had proceeded during this interval. The temperature was then slowly raised until the transformation was complete. The temperature range from 50° to 98°C was covered in 103 minutes. The curves show that in both cases the transformation was complete at essentially the same temperature.

When the samples used in obtaining Fig. 2 were slowly cooled to room temperature there were no indications of a β- to α-transition. The β- to α-transition usually required 10 to 15 hours for completion at room temperature although a decided drop in resistance could be observed in one or two hours. Two complete heating cycles for sample VI are recorded in Fig. 6. The numbers on the graph give the elapsed time in minutes from the start of the first cooling curve.

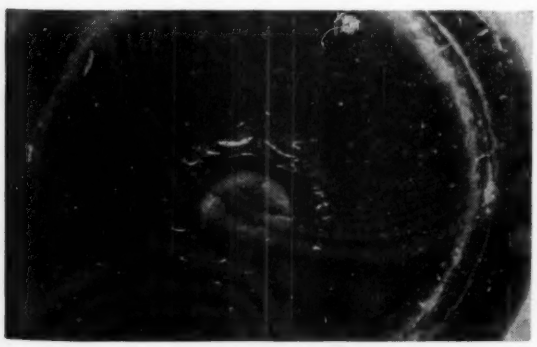

FIG. 5. Distilled polonium bead showing thermal cracks when heated from −190°C to 25°C.

The possibility that this hysteresis was solely the result of a slow reaction rate was investigated by holding the sample used in obtaining curve VIIB, Fig. 2 at 60°C for four hours. Although this was 15° below the beginning of the α- to β-transition observed on heating, only one hour earlier, there was no change in resistance to show that any β- to α-transformation had occurred.

The range of temperature over which the α- to β-transformation occurred was dependent upon the size of the sample used in the determination. Curve VIB of Fig. 2 obtained with a sample approximately 4000 atoms thick shows a transition range from 65° to 85°C. Curve VIII obtained with a film only 350 atoms thick shows a range from 100° to 130°C. Curves VIIA and VIIB obtained with an intermediate thickness of approximately 3000 atoms show an intermediate range of from 75° to 105°C. Other curves with films 10,000 atoms thick show a range of 65° to 85°C.

Apparently the dependence of the transition temperature upon the thickness of the polonium is real and not the result of a systematic temperature differential between the temperature of the polonium film and the temperature observed with the thermocouple inside the electrode assembly. The temperature of a polonium film several thousand atoms thick was found to be only 3° above room temperature by the use of a special electrode assembly constructed of soft glass with three platinum and one platinum-10 percent rhodium electrodes. The transition range and melting point were observed to be 68–86°C and 254°C with this sample. It is believed that the true temperature of the polonium is measured by the (platinum)-(platinum-rhodium) thermocouple formed by the two center electrodes when they are connected by the distilled film of polonium and the polonium sample is the "bead" of the thermocouple.

The difference in transformation temperature cannot be explained by a difference in lead content since resistivity curves run on the same sample with an elapse of time sufficient to double the lead content showed no appreciable change.

An unsuccessful attempt to extend these observations to higher lead contents and to obtain a liquidus curve for lead alloys was made by R. W. Senseman. The distilled films upon which the electrical resistivity was being measured were destroyed by oxidation when they stood for long periods of time. Because of the low melting point of polonium there was no obvious way to degas the apparatus and prevent this oxidation.

The dependence of crystal transformation temperature upon grain size and heat treatment of the sample has been observed in at least one other case by Edwards and Lipson[3] in their investigation on the transformation

[3] O. S. Edwards, and H. Lipson, J. Inst. Metals **69**, 177 (1943).

TABLE II. Comparison of the physical properties of polonium and other elements.

Element	Atomic No.	Group in periodic table	Specific resistivity micro-ohm-cm	Thermal coefficient of electrical resistivity $\alpha=\Delta R/\Delta t R_0$	Melting point °C	Density g/cc
S	16	VI	2×10^{23}	Large negative coefficient	113	2.07
Se	34	VIB	2×10^{11}	Large negative coefficient	220	4.80
Te	52	VIB	2×10^{5}	Large negative coefficient	452	6.24
Po	84	VIB	42 (α) 44 (β)	0.0046 (α) 0.0070 (β)	254	9.4
Bi	83	VB	115	0.0045	271	9.80
Pb	82	IVB	22	0.0043	327	11.34
Tl	81	IIIB	18	0.0040	303	11.85

of cobalt. The two cases are quite parallel. The β- to α-cobalt transformation and the α- to β-polonium transformation both occur over ranges of temperature, the length of the range increasing with decreasing size of specimen. The transformation begins at different temperatures for both metals and in each case the smaller specimen requires the greater thermal stress to make the reaction proceed. The reverse transformation in both metals occurs only after the specimen has been stressed considerably beyond the temperature at which the first transformation was observed to be.

According to Dehlinger[4] the change in surface energy for small grains may become comparable with the energy of the crystal transformation, if there is a volume change accompanying the transition. In such a case the temperature of transition for a specimen would depend upon the grain size of the specimen and if there were a range in grain sizes then there would be observed a range of transition temperatures. The magnitude of the temperature change would be a function of (1) the surface energy, (2) the volume change, (3) the heat of transformation for massive metal and (4) the angle at which the free energy-temperature curves of the two phases intersect.

Dehlinger calculated that in the case of thallium, which undergoes a h.c.p. to f.c.c. transition similar to cobalt, the change in surface energy accompanying crystal transformation would be of the order of the heat of transformation for grains with a diameter of 2×10^{-5} cm. This diameter is of the order of magnitude of the thickness of the polonium samples investigated.

[4] U. Dehlinger, Metallwritschaft. 11, 223 (1932).

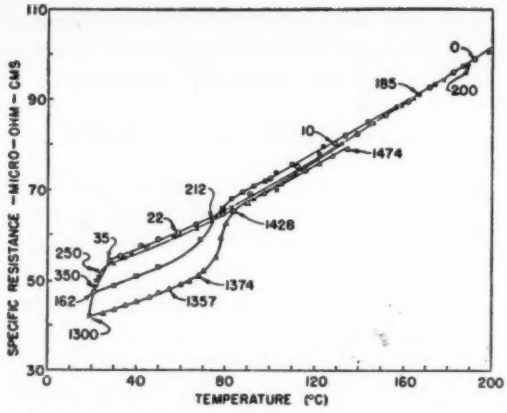

FIG. 6. The specific resistance of polonium as a function of temperature and heat treatment. ○—first cooling curve, □—first heating curve, ×—second cooling curve, △—second heating curve, 10, 1474, etc., elapsed time in minutes.

Dehlinger's theory seems to account for the anomalous observations on the polonium transition. There is a volume increase of 3 percent accompanying the α- to β-transition, the transition occurs over a range of temperatures and these temperatures increase with a decrease in the thickness of the samples used for the determination.

SUMMARY

Table II lists the properties of polonium as determined by this investigation and the properties of other elements as taken from the International Critical Tables.

It is apparent that polonium is quite metallic in character and resembles Tl, Pb and Bi in its physical properties more closely than it does Se and Te although these latter elements are in the same group in the periodic table.

ACKNOWLEDGMENTS

The author gratefully acknowledges his indebtedness to Dr. I. B. Johns, at whose suggestion the work was initiated, Dr. D. S. Martin and Dr. E. R. Jette for their many suggestions and helpful discussions. He also thanks Mr. Dave Durrill for the electro-deposition of most of the polonium used in the study.

This document is based on work performed at Los Alamos Scientific Laboratory of the University of California under Contract No. W-7405-eng-36 for the Manhattan Project and the information contained therein will appear in Division V of the Manhattan Project Technical Series as part of the contribution of the Los Alamos Laboratory.

Physical Properties of Polonium. II. X-Ray Studies and Crystal Structure*

WILLIAM H. BEAMER** AND CHARLES R. MAXWELL***
Los Alamos Scientific Laboratory, Los Alamos, New Mexico
(Received May 2, 1949)

Structures are proposed which account for the powder diffraction patterns obtained from samples of polonium containing various amounts of lead. Unusual temperature effects are recorded for α-polonium. It is suggested that the Pb and Po are present in interpenetrating primitive cubic lattices which are indistinguishable because the atomic numbers are nearly the same.

INTRODUCTION

A STUDY of polonium by x-ray diffraction powder photographs was undertaken to determine whether the abrupt change in electrical conductivity with temperature[1] is caused by a phase transformation. The existence of two forms of polonium has been confirmed and reported earlier.[2] The fact that only microgram quantities of polonium are available and the difficulties of handling a material of such great radioactive toxicity have not permitted the growth of single crystals for x-ray diffraction. Structures have been found which account for the data available from the powder diagrams.

EXPERIMENTAL

X-Ray Apparatus

Two cameras were used; one was a 7.5-cm radius Debye camera covering a range of $\sin^2\theta$-values from 0.003 to 0.97; the other was a back reflecting cylindrical type of radius 5 cm covering $\sin^2\theta$ from 0.018 to 0.985. Iron and copper radiations from General Electric CA-6 diffraction x-ray tubes were used with double-coated Blue Brand Eastman x-ray film. Direct tests on this film showed no appreciable film shrinkage under the conditions of the experiments.

The films were measured without magnification with a pointer attached to a slide and vernier. The smallest division which could be read on the vernier was 0.1 mm. The measurement of any one sharp line had a possible error of ± 0.1 mm; the diameter of any sharp ring had a possible error of ± 0.2 mm.

Preparation of Sample

Because of the characteristics of polonium discussed in the introduction only glass-enclosed powder samples were used. From 30 to 100 micrograms of polonium were put into the very end of a thin wall capillary with three successive vacuum distillations. The capillary was drawn from a low absorbing lithiaborosilicate glass (Corning No. 707) which can be sealed directly to Pyrex. A drawing of the apparatus used is shown in Fig. 1.

The procedure for the preparation of powder samples was as follows:

(1) The capillary and the end of the distillation apparatus up to the point (A) was thoroughly outgassed to get rid of oxygen, evacuating to a pressure of 10^{-6} mm of Hg for 15–20 hours while holding at a temperature of 400–425°C in a tube furnace.

(2) The polonium was electroplated on a 40-mil platinum wire. The wire was placed in a small closed-end platinum tube (B) which was in turn placed in a small close-fitting quartz tube (C).

(3) The distillation apparatus was filled with a positive pressure of helium and the quartz tube (C) was inserted at the end (E) while helium was flowing through the apparatus. The apparatus was again evacuated to a pressure of approximately 10^{-6} mm of Hg.

(4) The quartz tube was slid to the position (F) by tilting the apparatus on a ball joint. A high frequency induction coil was placed around the entire apparatus at (F) and the platinum tube heated rapidly to a red heat. This distilled the polonium from the platinum wire in from 5 to 10 seconds. The polonium condensed as a shiny metallic mirror on the walls of the apparatus near the capillary. The quartz tube served as insulation

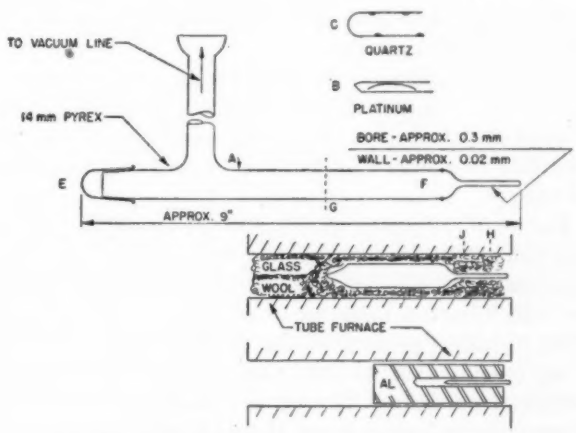

FIG. 1. Apparatus for preparation of x-ray sample.

*This paper is based on a portion of a thesis presented by C. R. Maxwell in partial fulfillment of the requirements for the degree of Doctor of Philosophy at Iowa State College, Ames, Iowa.

** Present address, Spectroscopy Laboratory, The Dow Chemical Company, Midland, Michigan.

*** Present address, Laboratory of Physical Biology, National Institutes of Health, Bethesda 14, Maryland.

[1] C. R. Maxwell, J. Chem. Phys. **17**, 1286 (1949).

[2] W. H. Beamer and C. R. Maxwell, J. Chem. Phys. **14**, 569 (1946).

TABLE I. Calculated and observed spacing and intensities for α-polonium. Simple cubic with $a=3.345$A.

$h^2+k^2+l^2$	Calculated $1/d^2$	Observed $1/d^2$	Calculated intensity	Observed intensity
1	0.0894	0.0896	100	100 VS
2	0.1787	0.1795	91	80 VS
3	0.2681	0.2692	38	40 MS
4	0.3575	0.3595	21	25 M
5	0.4469	0.4486	62	55 S
6	0.5362	0.5371	50	45 S
8	0.7150	0.7169	18	10 W
9	0.8045	0.8065	42	30 M
10	0.8937	0.8978	32	25 M
11	0.9831	0.9866	32	15 MW
12	1.0725	—	11	0 —
13	1.1619	1.1628	35	15 MW
14	1.2512	1.2526	75	30 M
16	1.4300	1.432	12	5 F
17	1.5193	1.5193*	132	20 W
18	1.6087	1.608*	144	15 VW

* Average of resolved α_1- and α_2-measurements.

and prevented the red hot platinum from breaking the glass tube.

The apparatus was open to the vacuum line during the distillation so that any permanent gases liberated from the platinum and quartz were continually removed. During the distillation the pressure of the permanent gases in the system did not exceed 10^{-4} mm.

(5) The quartz tube and platinum were returned to position (*E*) and the apparatus was sealed off at point (*G*). This tube was wrapped in glass wool and placed in a tube furnace so that the end of the capillary was exposed to the open air. The tube furnace was held at 400°C for two or three hours. Due to the temperature gradient in the apparatus the polonium migrated into the capillary but since the temperature gradient in the capillary was not sharp, the polonium was distributed over a considerable length (*H*) of the capillary.

(6) The capillary was sealed off from the main apparatus at the point (*J*), and placed in a close-fitting hole in an aluminum block which was held at 400°C for another few hours. The temperature gradient in the capillary was now sharp and the polonium migrated to the end of the capillary.

(7) The capillary was then mounted and photographed in the usual manner. By this procedure a small amount of polonium was concentrated into one spot in a capillary without exposure to air or danger of mechanical loss.

The capillaries used were 0.3 to 0.4 mm O.D. with a wall thickness of approximately 0.02 mm or less. The alpha-particles which are released by radioactive decay and which have a range in air of 5 cm at this altitude (7300 ft.) often penetrated the capillary walls (five cm of air is equivalent to 0.02 mm of glass). The alpha-particles from sample II used in obtaining films 27 and 28 reported in Tables I and II had a range of over two cm in air after penetrating the capillary walls.

Calibration of Cameras

The technique described for the preparation of polonium samples was developed with zinc as a stand-in for polonium. Zinc was selected because it has approximately the same vapor pressure as polonium. These samples were used to calibrate the cameras for the investigation. The zinc was obtained by electrodeposition from a solution of Baker's C.P. zinc sulfate. The constants for the crystal structure of zinc were taken from Barrett[3] and were: $a=2.6595$A; $c=4.9368$A. The values for the camera radius which were calculated from individual zinc lines did not vary with the diffraction angle as did the values calculated from the pattern of a nickel wire of comparable size photographed in the same mounting. This indicates very small absorption in small metal samples prepared by this technique.

Estimation of Intensities

Estimations of intensities were made visually. In addition to the usual method of reporting intensities from very strong (VS) to faint (F), a numerical value was assigned to each line.

An arbitrary high value in agreement with the value of the calculated intensity was assigned to the first line. The intensity of the second line was estimated in terms of the first line and a value assigned. The intensity of the third line was estimated in terms of the assigned value for the second line and so forth. The error in any estimation was thus carried through all subsequent estimations. Any non-linearity in the exposure characteristics of the film affects these numerical values.

The intensity estimations were made difficult by the presence of an over-all background from the gamma-radiation associated with the radioactive decay. An exposure of 100 hours to the gamma-radiation from one sample completely blackened the film. The average exposure for unfiltered copper radiation was 10–12 hours, while CuKα-radiation secured by filtering with one mil nickel foil required an exposure of 30 hours. The α-phase polonium patterns were exposed to gamma-radiation for several additional hours while the sample was cooled before x-ray exposure.

Temperature Measurement and Control

Only a rough estimate can be made of the temperature of the polonium samples when the diffraction patterns were photographed. The heat evolved in stopping the alpha-particles is 27.42 calories/curie/hour, so the sample is maintained at a temperature above that of its surroundings. The actual temperature of the sample depends upon the distribution of the polonium in the capillary, thickness of the capillary walls, and thermal contact with the surrounding air.

[3] C. S. Barrett, *Structure of Metals* (McGraw-Hill Book Company, Inc., 1943), p. 554.

The diffraction patterns photographed with freshly prepared samples at thermal equilibrium with static air always showed the high temperature, or β, phase only. The low temperature, or α, phase pattern was only obtained after prolonged cooling in a stream of refrigerated air. On returning the sample to thermal equilibrium with static air at room temperature, the diffraction pattern was predominantly that of β-polonium although the stronger α-polonium lines were always present. Thus it appears that the temperature of the polonium samples when in equilibrium with static air at room temperature was near the α- to β-transformation temperature. In view of the electrical resistivity measurements the temperature of the polonium sample under these conditions is estimated as 75 ± 15°C.

To obtain the α-phase alone the polonium samples were cooled by a stream of dry air which had been refrigerated by passing through a copper coil immersed in dry ice and trichloroethylene. A constant, brisk rate of flow was used to obtain as good heat transfer as possible and thus decrease the temperature differential between the metal and the air stream.

The temperature of the air stream was determined by exploring the air stream in the vicinity of the sample with a thermocouple made of 3-mil wire. This temperature was found to be approximately -10°C. The temperature of the polonium sample under this condition is estimated as 10 ± 10°C.

RESULTS

Crystal Structure of α-Polonium

The diffraction pattern of α-polonium can be interpreted as that arising from a simple cubic crystal with a parameter of 3.345 ± 0.002A.

Columns (3) and (6) of Table I list the spacings and intensities observed on the best α-Po film. Columns (2) and (5) list the corresponding values calculated for a simple cubic structure with $a=3.345$A.

The film from which the values in Table I were taken was photographed with Ni filtered CuKα-radiation. The film had a very high background since it was exposed to gamma-radiation for 55 hours while the sample was cooled and photographed. The spacing corresponding to $(h^2+k^2+l^2)$ equal to 12 was not observed on this film but has been observed on other films with less background. A freshly prepared sample was used so that the lead content (approx. 1.5 percent) would be as low as possible.

The agreement between observed and calculated values of $1/d^2$ is quite satisfactory. A variation of 0.002A in the parameter would cause the observed and calculated patterns to disagree by an amount larger than the experimental error in measuring this particular film. Hence, the precision with which the parameter may be determined is ±0.002A although the parameter change associated with the large uncertainty in temperature is much larger than this.

TABLE II. Calculated and observed spacings and intensities for β-polonium. Simple rhombohedron $a=3.359$A, $\alpha=98°\ 13'$.

Pseudo-cubic $h^2+k^2+l^2$	Rhombohedral indices	Calculated $1/d^2$	Observed $1/d^2$	Calculated intensity	Observed intensity
6	100	0.0931	0.0931	200	200 VS
10	$1\bar{1}0$	0.1552	0.1550	108	100 S
14	110	0.2173	0.2169	78	60 MS
16	$11\bar{1}$	0.2483	0.2486	65	50 M
24	111 200	0.3725	0.3733	13 40	50 M
26	$2\bar{1}0$	0.4035	0.4045	73	60 MS
30	$\bar{2}11$	0.4656	0.4669	30	15 MW
34	210 $21\bar{1}$	0.5277	0.5279	53 53	60 MS
40	$2\bar{2}0$	0.6203	0.6231	22	8 W
46	211 $2\bar{2}1$	0.7139	0.7153	19 38	15 W
54	$22\bar{1}$ 300 $3\bar{1}0$	0.8380	0.8393	17 17 34	30 MW
56	220 $\bar{3}11$	0.8691	0.8708	17 17	5 VW
64	$22\bar{2}$ $31\bar{1}$	0.9932	0.9941	16 32	10 W
66	310 $3\bar{2}0$	1.0243	1.0255*	32 32	10 W
70	221 $\bar{3}21$	1.0863	1.0868*	17 34	5 VW
74	$3\bar{2}1$	1.1484	1.151	35	3 F
80	311	1.2415	—	18	not obs.
86	$32\bar{1}$ $\bar{3}22$	1.3346	1.3344*	44 22	2 F
90	320 $3\bar{3}0$	1.3967	1.3947*	48 24	1 F
94	$32\bar{2}$ $4\bar{1}0$ $\bar{4}11$	1.4588	1.4586*	58 58 27	15 MW
96	222 $3\bar{3}1$ 400	1.4898	1.4902*	10 62 31	10 W
104	$4\bar{2}0$	1.6140	1.6126*	110	3 VW
106	321 $\bar{4}21$	1.6450	1.641	144 144	6 W

* Value is average of resolved α_1- and α_2-measurements.

The agreement between the calculated and observed intensities is excellent for the first six lines. The observed intensity values for the high angle lines were

TABLE III.

	Ratio	α-Po	β-Po
Goldschmidt	1.04	3.42	3.49
Westgren and Almin	1.123	3.69	3.77
Pauling		3.47	3.54
This work	1.07	3.52	3.60

considerably less than the calculated intensity values. There is a general weakening of the entire observed pattern with increasing diffraction angle and not an isolated weakening of a particular line. This trend in the intensities of the higher angle lines was observed with both α-Po and β-Po and in the calibration photographs taken with a zinc sample prepared in the same manner. Comparison should be made between adjacent or near adjacent lines. When the ratio between the observed intensity values of adjacent lines is compared with the ratio between the calculated values for the same lines, satisfactory agreement is obtained for the entire pattern.

The calculated density for this structure is 9.32 g/cc which is in the satisfactory agreement with the measured value of 9.4±0.5 g/cc.

The structure belongs to the space group O_h^1.

Crystal Structure of β-Polonium

The diffraction pattern of β-polonium can be interpreted as that arising from a simple rhombohedral crystal with a parameter of 3.359±0.002A and an angle of 98° 13′±3′.

Columns (4) and (6) of Table II list the spacings and intensities observed on the best β-Po film. Columns (3) and (5) list the corresponding spacings and intensities calculated for a rhombohedral cell with $a=3.359$ and $\alpha=98°\ 13'$. In Column (2) are listed the corresponding rhombohedral indices. The spacings of this pattern occur in the ratio of simple whole numbers, and cubic indices may be assigned to each line. Column (1) lists the $(h^2+k^2+l^2)$ values corresponding to the pseudo-cubic indices.

The agreement between observed and calculated spacings is completely satisfactory. When the ratio between the observed intensity values of adjacent lines is compared with the ratio between the calculated values for the same lines, satisfactory agreement is obtained for every line except line "94." The presence of a high background makes it impossible to say whether this apparent discrepancy is real or not. The line is very sharp, and for this reason may appear more intense.

Two or more indices are assigned to thirteen of the twenty-two spacings observed in β-Po. This accidental agreement in the spacings of different families of planes must be very close since the lines observed on the photographic film are quite sharp. Exact agreement for all such accidental superpositions is obtained when $\alpha=98°\ 12'\ 40''$. The exactness of this superposition is a function of α alone and does not depend upon the parameter a. The exactness of the superposition of planes 400 and 331 observed together as line "96" is the most susceptible to slight changes in α. A change of $\pm 3'$ would cause the spacing of these planes to be different by an observable amount. Similar consideration of planes 410 and 411 observed as line "94" sets a limit of $\pm 5'$. The distance between lines "94" and "96" is also very dependent upon α. A change of more than $\pm 3'$ would be easily detected.

Because of the pseudo-cubic nature of the β-Po pattern, many crystal lattices will give completely satisfactory agreement between the calculated and observed values of the spacings. A number of possible structures in the cubic, orthorhombic and hexagonal systems have been considered and ruled out on intensity calculations.

The patterns reported in Table I and II were obtained from the same sample. The β-polonium pattern was photographed immediately after the preparation of the sample. The lead content at this time was 0.5 percent.

The calculated density for this structure is 9.51 g/cc which is in satisfactory agreement with the measured value of 9.4±0.5 g/cc.

This structure belongs to space group D_{3d}^5.

The Po-Pb Alloy System

The effect of the growth of lead in the polonium on the x-ray pattern was studied by following a sample for one half-life, 138 days. No new lines were observed on any of the films taken over this period indicating that lead forms a solid solution with α-polonium to the extent of at least 50 atomic percent. The photographs taken the first few days showed only the pattern of β-polonium. The sample was cooled and the pattern of the α-phase was obtained when the sample contained 4 percent lead. All subsequent photographs taken with the sample in thermal equilibrium with static air showed some lines of α-Po. At first the pattern was predominantly that of β-Po with only the stronger α-Po lines appearing. With time the α-Po lines gained in intensity while the β-Po lines lost. The β-Po lines were not observed when the sample contained more than 25 atomic percent lead. This change in the relative amounts of the

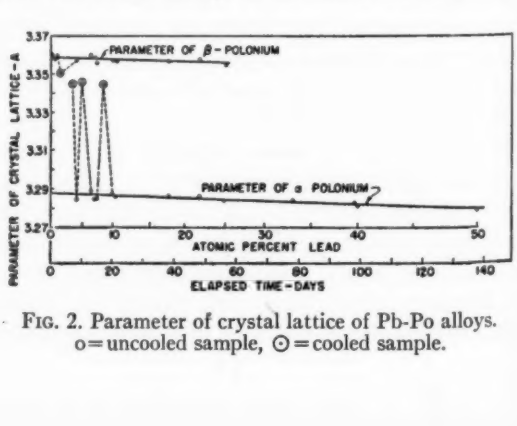

FIG. 2. Parameter of crystal lattice of Pb-Po alloys. o=uncooled sample, ⊙=cooled sample.

two phases present is probably a function of the lead content and of the temperature which is decreasing with the decay of the sample.

Figure 2 shows the parameters of the two phases as a function of time. The parameters plotted here are averages calculated from low angle, strong lines. These lines were selected because they appeared on all films and had no interferences. Since systematic errors in the camera affect the value of the parameter calculated from low angle lines the same lines were used to compare parameters from film to film. The values of the parameter of α-polonium designated by encircled points on Fig. 2 were calculated from films taken while the sample was cooled. The average parameter for the α-Po lines recorded on these films is 3.345A. The other points were taken while the sample was in equilibrium with static air at room temperature. The average parameter for α-Po recorded on these films is 3.286A. The difference is many times larger than the differences between the individual measurements which were averaged. We are not able to offer a suitable explanation for this temperature effect. If the structure of these alloys is in reality more complex than our data indicates, the parameter plotted in Fig. 2 may have no physical significance in the true structure. If, on the other hand, the plotted parameter represents a distance between primary lattice sites, a negative coefficient of thermal expansion is indicated. Based on the simple cubic structure and using the temperature estimates made earlier the value of this coefficient for alloys containing 4 percent to 9 percent lead is $-300\pm100\times10^{-6}$ cm/cm/°C. From diffraction patterns at 41 percent lead the coefficient is about -30×10^{-6} cm/cm/°C.

Only one film was made recording the β-phase at a temperature lower than normal. The parameter value from this film is indicated also by an encircled point on the β-polonium parameter plot of Fig. 2. The sample contained 1.5 percent lead when the film was made. The coefficient of expansion from this single parameter value is $+50\pm25\times10^{-6}$ cm/cm/°C.

Atomic Diameter of Polonium

Figure 2 shows that the parameter of α-polonium phase decreases slightly with time. Neglecting the temperature change of the sample and taking the extrapolated value of the atomic diameter of α-polonium at zero lead content as 3.288A the atomic diameter for lead was calculated to be 3.27A in a simple cube with a coordination number of six.

The atomic diameter of lead in a f.c.c. crystal with coordination number of twelve is observed to be 3.49A. The ratio between this value and the value calculated for a coordination number of six is 1.07. According to Goldschmidt[4] the expected ratio is 1.04. On the other hand Westgren and Almin[5] have, on the assumption of constant atomic volume, calculated the ratio to be 1.123. More recently Pauling[6] has developed an equation for the change of atomic diameter with coordination number based on the idea that metallic bonds are resonating covalent bonds. His equation predicts a value of 3.31A for lead with a coordination of six.

Possible values for the atomic diameter of polonium with a coordination number of twelve are listed below using the ratios of Goldschmidt, Westgren, and Almin, the Pauling formula, and the ratio obtained for lead in the above. These values are for polonium at a temperature where the two phases co-exist, probably near 75°C (Table III).

Hume-Rothery[7] has divided the periodic table into three classes according to the crystal structures of the elements.

Class I includes those elements which have the typical metallic structures, body-centered cube, face-centered cube and close-packed hexagonal.

Class III contains the elements of Groups IV, V, VI, and VII which crystallize so that each atom has (8-N) close neighbors, where N is the number of the group to which the element belongs. The structure of sulfur and selenium (Group VI) are such that the atoms are arranged in spiral chains so that each has two close neighbors in accordance with the "(8-N) rule."

The elements of Class II form a transition group in which the crystal structure is a distorted form of the typical metallic structures. Examples of this class are zinc, cadmium, and mercury. In considering the structures of other members of this class Hume-Rothery has pointed out that the interatomic distances of thallium and lead are much greater than that of the preceding univalent element gold and that the same is true for indium and white tin in relation to silver. In the first long period the interatomic distances do not change greatly in the whole series of elements. This can be explained by assuming that these four metals of Class III are incompletely ionized.

Polonium most closely resembles this sub-group of elements. The simple cubic structure has not been observed for any other element. It has the symmetrical properties associated with true metallic bonding but it represents a rather loosely packed structure. If polonium were a member of Class III and conformed to the (8-N) rule, one would expect its interatomic distance to be of the order of magnitude of 3.10A observed for bismuth. Instead the interatomic distance is observed to be around 3.60A when corrected for change in coordination number. With the same coordination number the interatomic distance of polonium is slightly larger than that of lead. Further the melting point, electrical resistance, density, and hardness are similar to those of lead and are characteristic of metallic bonding.

[4] V. M. Goldschmidt, Zeits. f. physik. Chemie **133**, 397 (1928).
[5] A. Westgren and A. Almin, Zeits. f. physik. Chemie, Abstract B 5, 14 (1929).
[6] L. Pauling, J. Am. Chem. Soc. **69**, 542 (1947).
[7] W. Hume-Rothery, *The Structure of Metals and Alloys* (Institute of Metals, London, 1936).

It has been suggested that the lead always present in polonium samples may exert a great effect on the structure. These samples contain from 1.0 percent to 50 percent lead. At the higher concentrations of lead the NaCl type structure is likely. The atomic number of lead and polonium are 82 and 84 respectively and so intensities of lines from Pb-containing planes and from Po-containing planes would be very nearly equal. At low lead concentrations the interpenetrating lattices of Pb and Po might be maintained with Po atoms occupying the sites not filled by Pb atoms. This explanation of the simple cubic and simple rhombohedral patterns would fit well with the observed solubility of lead in the polonium and with the fact that PbS, PbSe and PbTe all have the NaCl structure.

ACKNOWLEDGMENT

The encouragement and advice of Dr. E. R. Jette and Dr. Don Martin are gratefully acknowledged. In particular, the authors wish to thank Professor F. W. H. Zachariasen, University of Chicago, for suggesting the rhombohedral structure for β-polonium.

This document is based on work performed at Los Alamos Scientific Laboratory of the University of California under Contract No. W-7405-eng-36 for the Manhattan Project and the information contained therein will appear in Division V of the Manhattan Project Technical Series as part of the contribution of the Los Alamos Laboratory.

THE JOURNAL OF CHEMICAL PHYSICS VOLUME 17, NUMBER 12 DECEMBER, 1949

The Physical Properties of Polonium. III. The Half-Life of Polonium

WILLIAM H. BEAMER* AND WILLIAM E. EASTON**
University of California, Los Alamos Scientific Laboratory, Los Alamos, New Mexico
(Received May 2, 1949)

The half-life of polonium has been measured by a calorimetric method. The reproducibility and precision of the data is much greater than has been previously reported. The value is found to be 138.3±0.1 percent days.

INTRODUCTION

THE half-life of polonium has been measured many times and values in the literature vary from 126 to 148 days.[1] Counting, total ionization, and calorimetric methods have been used. Schweidler[2] measured the decrease of ionizing power of a sample of polonium mounted on a copper foil over 2200 days and found the half-life to be 136.5 days. This value was accepted for some time. M. Curie[3] found the half-life to be 140 days by electrical counting methods extending over 184 days. The polonium was deposited on quartz and covered with an aluminum foil 0.01 mm thick.

There are a number of errors inherent in the counting methods, such as coincidence corrections, change of counter characteristics, etc. Several of these tend to increase the apparent half-life, for example, incomplete separation from other radioactive substances such as radium D. However, most of the errors tend to decrease the half-life by effective decrease of the amount of polonium with time. (1) Atomic aggregates of polonium are known to be knocked off the sample by alphas leaving the material; (2) diffusion of polonium into the support material; (3) covering of the surface of the polonium by a layer of oxide or foreign material. These effects are all known to occur.

The calorimetric method, which measures the decrease of heat evolution with time of a sealed polonium sample, is affected only by these errors: (1) radioactive impurities, (2) heat evolved by secondary chemical or nuclear reactions produced by the alphas. Microcalorimetric determinations of half-life have been made by Sanielevici[4] (138.7±0.4 percent and 139.6±1 percent) and A. Dorablaska[5] (137.6±0.4 percent) but the measurements of the heat evolved were not consistent. The value of the heat evolved by a curie of polonium can be calculated from the energy of the alphas and of the recoil lead atoms. The accepted value for the energy of the alpha-particles is 5.303 Mev as measured by Rutherford, Wynn-Williams, Lewis, and Boden.[6] The alpha-spectrum for polonium has been investigated by Chang[7] and found to contain less than 0.1 percent of alphas different in energy from the 5.303-Mev value. Polonium gives off about seven quanta of gamma-rays per million alphas;[8] this can be neglected. The energy of the recoil atoms, disregarding relativity effects, is

* Present address: Spectroscopy Laboratory, The Dow Chemical Company, Midland, Michigan.

** Present address: 1550 Stone Road, Rochester, New York.

[1] St. Meyer and E. Von Schweidler, *Radioaktivitat* (B. G. Teubner, Leipzig, 1927), second edition.

[2] E. V. Schweidler, Verh. d. D. Phys. Ges. (2), **14**, 539 (1912).

[3] M. Curie, J. de phys. et rad. (6) **1**, 12 (1920).

[4] A. S. Sanielevici, J. de chimie phys. **33**, 779 (1936).

[5] A. Dorablaska, Rocznik Chem. (Poland) **11**, 475 (1931).

[6] Rutherford, Wynn-Williams, Lewis, and Boden, Proc. Roy. Soc. **A139**, 617 (1933).

[7] W. Y. Chang, Phys. Rev. **69**, 60 (1946).

[8] W. Bothe, Zeits. f. Physik **96**, 607 (1935).

$A(\alpha) \div A$ (recoil) or 4/206 of that of the alpha. Thus

$$-Q = \frac{(1+4/206)\ 5.303\ \text{Mev/alpha} \times 1.6020 \times 10^{-6}\ \text{erg/Mev} \times 2.208 \times 10^{12}\ \text{alpha/min./curie}}{10^{7}\ \text{erg/joule (abs.)}},$$

$-Q = 114.7$ joules (abs.)/curie/hour.

EXPERIMENTAL

Preparation and purity of samples.—In this investigation two samples were studied. The pure polonium was electroplated from a dilute nitric acid solution onto a platinum foil. This foil was placed inside a platinum capsule in a nitrogen atmosphere and then this was sealed off in a glass ampule after evacuation and filling with pure helium. By the use of a noble metal and a helium atmosphere the possibility of secondary reactions was minimized. The neutrons produced by the (α, n) reaction are an indication of the purity of the deposit. A count of the neutrons emitted by the samples was very low and showed no rise over the period of time the samples were measured, thus indicating that the samples were free of significant quantities of light elements. A count of the gammas from the samples agreed very well with the value of pure polonium thus indicating the absence of other gamma-emitters or of impurities giving off gammas in secondary reactions.

Apparatus.—The calorimeter used in these experiments was a modification of that described by Watson and Henderson[9] and Rutherford and Robinson.[10] This modification was developed by Dr. L. V. Coulter. It consists of two aluminum cylinders on each of which are wound the two opposite arms of a copper wire (No. 38 double silk) resistance bridge. The aluminum cylinders are mounted rigidly by wooden pegs in separate brass tubes which are immersed in a constant-level water bath which is held to a constant temperature at about 30°C ±0.001°C. The sample, centered in a cylindrical brass container, is placed in one of the aluminum tubes and the unbalance of the d.c. bridge is determined by a potentiometer when equilibrium is reached. At this point the heat evolved is equal to the heat leaking out to the bath and the temperature of the aluminum bobbin is constant. This heat effect is calibrated by passing a known current through a manganin heater of known resistance which replaces the sample in the sample tube. The other tube is used as a dummy and contains a dummy sample holder during the runs but stays at the constant temperature of the bath. The current which passes through the heater passes through shorted leads in the dummy to reproduce heat effects of the leads. The value of the temperature rise of the sample container and therefore the magnitude of the voltage across the bridge and the time elapsed in obtaining equilibrium depends upon the amount of heat generated by the sample and the heat leak away from the aluminum tube.

[9] Watson and Henderson, Proc. Roy. Soc. **A118**, 318 (1928).
[10] Rutherford and Robinson, Phil. Mag. **25**, 312 (1913).

Figure 1 gives the calorimeter bridge circuit. Figure 2 gives the heater circuit. A Wenner thermocouple potentiometer is used across the resistance bridge. The lowest dial of the lower of the two ranges reads in 0.1-microvolt increments. This potentiometer is also used across the standard resistance shown in Fig. 2 to set the bridge current at a constant value. The potentiometer for the energy circuit is a Leeds & Northrup Type K-1 and the current and voltage across the heater are measured to five significant figures.

A typical measurement of polonium sample for the half-life determination follows these steps:

(1) The bridge current is adjusted to its constant value and this adjustment is checked frequently during the whole series of operations.

(2) Since all the resistances of the bridge are not exactly the same, readings of the unbalance of the bridge are made with the empty sample holder in place. The bridge drop is always measured by taking readings until three or four values taken at five-minute intervals agree within 0.1 or 0.2 microvolt and no trend is observable. This reading is called the zero value of the bridge.

(3) The sample is placed in the sample holder and when equilibrium has been established the voltage across the bridge is read as before.

(4) The sample is replaced by the heater and a zero value obtained. This differs slightly from the zero without the heater.

(5) The current is passed through the heater to duplicate the voltage of the bridge obtained from the sample. The current through the heater and the IR drop across the heater are measured. Since it is often not possible to duplicate exactly the potential drop caused by the sample a straight line interpolation is made to find the value of the sample. This interpolation is taken

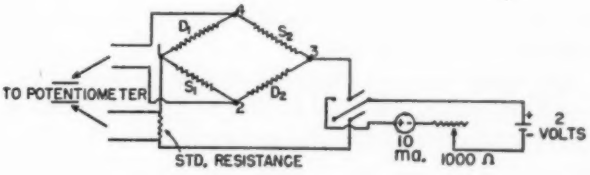

FIG. 1. Calorimeter circuit.

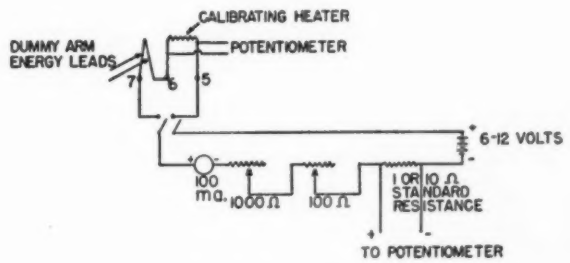

FIG. 2. Energy circuit.

TABLE I. Sample 1.

Point No.	Days	Value of sample in curies
1	0	1.093
2	7.03	1.051
3	9.03	1.043
4	10.01	1.036
5	15.01	1.009
6	21.00	0.9826
7	23.01	0.9674
8	26.95	0.9526
9	28.97	0.9424
10	31.03	0.9305
11	34.08	0.9191
12	35.94	0.9091
13	38.06	0.8986
14	40.98	0.8805
15	43.01	0.8761
16	47.96	0.8576
17	49.93	0.8490
18	51.97	0.8396
19	54.97	0.8272
20	57.03	0.8186
21	58.94	0.8132
22	61.96	0.7987
23	63.96	0.7890
24	65.97	0.7846
25	68.96	0.7706
26	73.52	0.7547
27	75.95	0.7460
28	77.92	0.7361
29	83.23	0.7174
30	85.00	0.7090
31	93.12	0.6905
32	97.00	0.6648

Least squares equations: $\log y = 0.03710 - 0.0021763 \times$ half-life $= 138.32$ days.

TABLE II. Sample 2.

Point No.	Days	Value of sample in curies
1	0	1.435
2	8.87	1.371
3	9.75	1.366
4	10.88	1.356
5	13.86	1.338
6	20.76	1.291
7	23.04	1.278
8	29.82	1.238
9	31.83	1.224
10	34.84	1.202
11	36.82	1.190
12	38.81	1.179
13	41.83	1.161
14	46.01	1.140
15	48.83	1.121
16	50.74	1.115
17	55.74	1.085
18	57.65	1.072
19	64.51	1.036
20	66.55	1.027
21	71.91	1.001
22	73.49	0.9922

Least squares equation: $\log y = 0.15644 - 0.0021773 \times$ half-life $= 138.26$ days.

from a calibration curve for the instrument and never has to be made over a range of more than one percent of the value of the sample. The calibration curve is a straight line over the range of heat input used. For very small samples a current is passed through shorted leads in both the dummy and sample holders when the sample is being measured to duplicate any heat effects produced when the heater is in place.

The water bath is maintained at a constant temperature near 30°C to within ±0.001°C by a mercury-in-glass thermoregulator which operates a thyratron relay circuit. The circular bath is about three feet in diameter, holds about 100 gallons of water and is stirred by a centrifugal pump which circulates 110 gallons of water a minute. The water is heated by three constant heat and three thermoregulator-controlled 250-watt knife heaters. The temperature of the room is maintained constant within ±1°F by special air-conditioning apparatus.

RESULTS

The results of the experiments are shown in Tables I and II for the two samples studied. Column 1 gives time in days; column 2 gives the value of the sample.

The half-life was obtained from the data by the least squares method. The probable error of the least squares constants was calculated by the standard procedure[11] and found to be about ±0.05 percent for both samples.

ACKNOWLEDGMENT

This document is based on work performed at Los Alamos Scientific Laboratory of the University of California under Government Contract W-7405-Eng-36 and the information contained therein will appear in the National Nuclear Energy Series as part of the contribution of the Los Alamos Scientific Laboratory.

[11] A. G. Worthing and J. Geffner, *Treatment of Experimental Data* (John Wiley and Sons, Inc., New York, 1943), p. 249.

THE JOURNAL OF CHEMICAL PHYSICS VOLUME 17, NUMBER 12 DECEMBER, 1949

The Dimensions of Chain Molecules Containing Branches and Rings

BRUNO H. ZIMM
Department of Chemistry, University of California, Berkeley, California
AND
WALTER H. STOCKMAYER
Department of Chemistry, Massachusetts Institute of Technology, Cambridge, Massachusetts
(Received May 2, 1949)

Formulas for the mean square radii of various branched and ringed polymer molecules are developed under the usual assumptions regarding the statistics of chain configuration. For branched molecules, the mean square radii vary less rapidly with molecular weight than for strictly linear molecules, while for systems containing only rings and unbranched chains the variation is more rapid than for the linear case. These results show that in principle the quantity of branches or of rings can be determined from light-scattering measurements.

I. INTRODUCTION

It is well known that no quantitative methods of determining the presence of branching in a high polymer chain molecule are now in use. Recently, however, it has been shown that the light-scattering phenomenon may be employed to measure the mean square radius of a molecule.[1–3]

The purpose of this paper is to calculate the mean square radii of molecules containing branches and rings in order to develop a method of demonstrating the presence or absence of such structures. It has been known for some time that the mean square of the distance between any two points on a flexible polymer chain is proportional to the number of segments between these points, as long as certain assumptions hold. It will be shown that as long as this proportionality exists, the calculation of the mean square radius of branched molecules is not a difficult matter.

The most significant and questionable assumption involved here is the neglect of what has been called the "volume effect," i.e., the prohibition of configurations of the chain in which two segments occupy the same position.

Fortunately there is at least one way out of the difficulty. Since the bonds in polymer chains are generally rather stiff, a collision of two segments of the same chain is only likely to occur if the loop between the segments is large compared to the segments. Consider now that around one of the segments a sphere is described, whose diameter is several times the diameter of the segment but much less than that of the loop. Unless there are attractive forces between the segments, the second segment will be less likely to lie inside the circumscribed sphere than it would in an equal volume outside, because of the volume excluded in the sphere by the first segment. But if there are attractive forces between the segments, over and above those normally existing between segments and solvent, the probability of the second segment lying in the sphere may be increased again. In fact, the probability may become equal to what it would be in an equal neighboring volume which does not include a segment initially. In this condition, therefore, the volume effect may properly be neglected.

It has also been shown[4] that when the probability of occupancy of a region by a segment is independent of the possible previous presence of another segment in the region, the "second virial coefficient" (A_2 below) in the power series expansion of the osmotic pressure of the solution vanishes. That is, when A_2 in the expression for the osmotic pressure, π, in terms of concentration, c,

$$\pi = A_1 c + A_2 c^2 + A_3 c^3 + \cdots,$$

is zero, the volume effect may be neglected in the calculation of the mean square radius of the molecules.[4a]

Of course, further investigation may show that the volume effect may also be negligible under other circumstances as well. In any case, it will be omitted in the following calculations.

II. PRELIMINARY OPERATIONS

Chain molecules may generally be divided, in a more or less arbitrary way, into small units which by repetition may be considered to generate the chain. Such units will be called *segments*. While most of these segments will be attached to only one or two others, certain ones may be attached to three or more. Such segments will be termed *branch units*. The number of segments attached to a branch unit will be called the *functionality* of the branch unit.

In a chain molecule we may select a certain segment for particular attention, referring to it as the *reference segment*. Let the vector to some other segment, e.g., the i'th segment, from the reference segment be $\mathbf{x}_i$, while the vector from the center of mass of the molecule to

[1] P. Debye, J. Phys. Coll. Chem. **51**, 18 (1947).
[2] Doty, Affens, and Zimm, Trans. Faraday Soc. **42B**, 66 (1946).
[3] B. H. Zimm, J. Chem. Phys. **16**, 1099 (1948).
[4] B. H. Zimm, Polymer Bull. **1**, 53 (1945); J. Chem. Phys. **14**, 164 (1946).
[4a] Since the above was written, an interesting discussion of the volume effect has been presented by P. J. Flory, J. Chem. Phys. **17**, 303 (1949). But the point that the volume effect becomes zero when A_2 is zero does not appear in his discussion, apparently because of the particular statistical method he used.

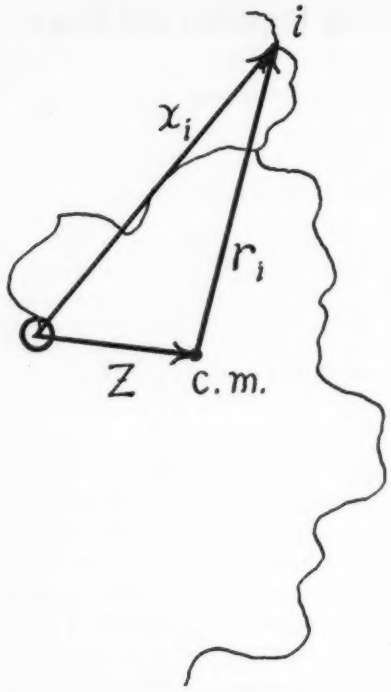

FIG. 1. Relations between the reference segment (circle), the center of mass (c.m.), and an arbitrary segment i of a chain molecule.

the i'th segment is $\mathbf{r}_i$. In particular, let the vector *from* the reference segment *to* the center of mass be $\mathbf{Z}$, so that

$$\mathbf{r}_i=\mathbf{x}_i-\mathbf{Z}. \tag{1}$$

These relations are indicated in Fig. 1.

We may now establish a useful lemma. The definition of the $\mathbf{r}_i$ as vectors to the center of mass requires that their sum be zero:

$$\sum\mathbf{r}_i=0, \tag{2a}$$

or alternatively this may be written,

$$\mathbf{Z}=(1/N)\sum\mathbf{x}_i \tag{2b}$$

$$Z^2=(1/N^2)\sum_i\sum_j\mathbf{x}_i\cdot\mathbf{x}_j, \tag{2c}$$

if N is the total number of segments in the molecule. Now from Eqs. (1) and (2a) the following relations succeed:

$$\begin{aligned}(1/N)\sum r_i^2&=(1/N)\sum(\mathbf{r}_i+\mathbf{Z})\cdot\mathbf{r}_i\\&=(1/N)\sum\mathbf{x}_i\cdot(\mathbf{x}_i-\mathbf{Z}).\end{aligned}$$

Combination with Eqs. (2b) and (2c) produces the desired lemma:

$$(1/N)\sum r_i^2=(1/N)\sum x_i^2-(1/N^2)\sum_i\sum_j\mathbf{x}_i\cdot\mathbf{x}_j. \tag{3a}$$

Again, since $\mathbf{x}_i\cdot\mathbf{x}_j=(x_{ij}^2-x_i^2-x_j^2)/2$, where $\mathbf{x}_{ij}=\mathbf{x}_i-\mathbf{x}_j$, it can be shown that

$$(1/N)\sum r_i^2=(1/2N^2)\sum_i\sum_j x_{ij}^2, \tag{3b}$$

an alternative form of the lemma.

If the chain is flexible, it may assume many configurations. Without considering further, for the moment, the nature of these, we shall assume that it is possible to average functions of the several defined vectors over the configurations, indicating the process by angular brackets with a subscript Av. In particular,

$$\langle\mathbf{A}\cdot\mathbf{x}_i\rangle_{Av}=\langle\mathbf{A}\cdot\mathbf{r}_i\rangle_{Av}=\langle\mathbf{A}\cdot\mathbf{Z}\rangle_{Av}=0,$$

where $\mathbf{A}$ is any constant vector (assumption of isotropy). Also we shall assume that the chain is so flexible that the average of the scalar product of two chain vectors which end in the same segment vanishes,

$$\langle(\mathbf{x}_i-\mathbf{x}_j)\cdot(\mathbf{x}_j-\mathbf{x}_k)\rangle_{Av}=0, \tag{4a}$$

provided that j lies on a chain connecting i and k, *and provided that* there are no other chains connecting i and k. As corollaries we obtain:

$$\langle\mathbf{x}_i\cdot(\mathbf{x}_i-\mathbf{x}_j)\rangle_{Av}=0, \tag{4b}$$

$$\langle\mathbf{x}_i\cdot\mathbf{x}_j\rangle_{Av}=\langle x_i^2\rangle_{Av}, \tag{4c}$$

if segment i lies on the chain connecting segment j and the reference segment, and

$$\langle\mathbf{x}_i\cdot\mathbf{x}_j\rangle_{Av}=0, \tag{4d}$$

if the reference segment lies on the chain connecting i and j.

We may now define R^2, the mean square radius of the molecule, as

$$R^2=(1/N)\sum_i\langle r_i^2\rangle_{Av}. \tag{5}$$

Likewise a quantity X^2 may be defined as

$$X^2=(1/N)\sum_i\langle x_i^2\rangle_{Av}. \tag{6}$$

Now returning to Eqs. (3a) and (3b), it is seen their averages may be written in terms of R^2 and X^2:

$$R^2=X^2-\langle Z^2\rangle_{Av} \tag{7a}$$

$$R^2=(1/2N^2)\sum_i\sum_j\langle x_{ij}^2\rangle_{Av}. \tag{7b}$$

In the first equation the mean square radius, R^2, is expressed as the mean square distance, X^2, of the rest of the chain from a reference segment, less the mean square distance, $\langle Z^2\rangle_{Av}$, of that segment from the center of mass. This form is particularly useful for branched molecules, where one of the branch units may be taken as the reference segment.

The latter Eq. (7b) is more useful in treating rings, in which $\langle Z^2\rangle_{Av}$ is not as simply evaluated.

We may further observe that if the reference segment is a branch unit, from which grow several branches of M_ν segments each (where ν is the distinguishing index of the branch), $\langle Z^2\rangle_{Av}$ and X^2 may be given as sums of parts, X_ν^2 and $\langle Z^2\rangle_{Av}$, one from each branch:

$$X^2=(1/N)\sum_\nu M_\nu X_\nu^2, \tag{8a}$$

$$\langle Z^2\rangle_{Av}=(1/N^2)\sum_\nu M_\nu^2\langle Z_\nu^2\rangle_{Av}. \tag{8b}$$

The latter relation follows particularly from Eq. (2c) combined with Eq. (4d).

Finally, if the chains are reasonably flexible, the usual proportionality will hold between $\langle x_i^2\rangle_{Av}$ and n_i, the number of segments between the reference segment and the i'th segment:

$$\langle x_i^2\rangle_{Av}=b^2n_i. \tag{9}$$

The quantity b is determined by the detailed structure of the chain, especially the length and flexibility of its bonds.[5]

III. CALCULATIONS FOR BRANCHED MOLECULES CONTAINING NO RINGS

III.1. Linear Chains

We first consider the[6,6a] case of linear chains, i.e., those with no branch units. This problem has been studied before but it is included here as an introduction to the more complicated cases.

Let the reference segment be one of the end segments of the chain. Using Eqs. (6) and (9), we obtain

$$X^2=(b^2/N)\sum_1^N{}_i n_i,$$

where $n_i=i$. Recognizing that

$$\sum_1^N i=N(N+1)/2,$$

the result is

$$X^2=b^2N/2. \tag{10}$$

Terms of order unity have been dropped.

Now using successively Eqs. (2c), (4c), and (9), we obtain

$$\langle Z^2\rangle_{Av}=(2b^2/N^2)\sum_1^N{}_i(N-n_i)n_i,$$

where $n_i=i$. Again recognizing that

$$\sum_1^N i^2=N(N+1)(2N+1)/6,$$

and dropping terms of order unity, the result is:

$$\langle Z^2\rangle_{Av}=b^2N/3. \tag{11}$$

Combination of these results according to Eq. (7a) yields R^2;

$$R^2=b^2N/6. \tag{12}$$

It may be noted that R^2 is just one-sixth of the mean square end-to-end length of the chain, b^2N.

[5] See Wm. J. Taylor, J. Chem. Phys. **15**, 412 (1947); **16**, 257 (1948). References to previous work are given in these papers.

[6] P. Debye, J. Chem. Phys. **14**, 636 (1946).

[6a] A closely related study has been made by H. A. Kramers, J. Chem. Phys. **14**, 415 (1946).

III.2. Chains of One Branch Unit

We will let the functionality of the branch unit, i.e., the number of branches that grow from it, be f. The number of segments in the ν'th chain growing from it will be N_ν, with ν an index running from one to f, and

$$\sum_1^f{}_\nu N_\nu=N.$$

By Eqs. (10) and (8a), the value of X^2 is

$$X^2=(b^2/2N)\textstyle\sum_\nu N_\nu^2. \tag{13}$$

Likewise, by Eqs. (11) and (8b), the value of $\langle Z^2\rangle_{Av}$ is

$$\langle Z^2\rangle_{Av}=(b^2/3N^2)\textstyle\sum_\nu N_\nu^3. \tag{14}$$

Finally by Eq. (7a), R^2 is found:

$$R^2=(b^2/N)\textstyle\sum_\nu[(N_\nu^2/2)-(N_\nu^3/3N)]. \tag{15}$$

For convenience, we symbolize by g the ratio of R^2 of the branched molecule to that for a linear molecule, $b^2N/6$. Thus:

$$g=\textstyle\sum_\nu[(3N_\nu^2/N^2)-(2N_\nu^3/N^3)]. \tag{15a}$$

III.3. Chains of Two Branch Units

Before attacking the main problem, it is necessary to find X^2 and Z^2 for a chain of one branch unit, when the unattached terminal segment of one of the chains is chosen as the reference segment.

Let the molecule be described otherwise as above, but with the reference segment at the outer end of chain one, of length N_1; assign the segments of chain one numbers in increasing order from the reference segment toward the branch unit, and assign those of the other chains numbers, i, in order outward from the branch unit. Let M be the total number of segments. Then by Eq. (9),

$$\begin{aligned}\langle x_{i\nu}^2\rangle_{Av}&=b^2(N_1+i_\nu) \quad (\nu\neq 1)\\ &=b^2i_1 \qquad\qquad (\nu=1).\end{aligned}$$

$$\begin{aligned}X^2&=\frac{1}{M}\sum_1^f{}_\nu\sum_1^{N_\nu}{}_{i_\nu}\langle x_{i\nu}^2\rangle_{Av}\\ &=\frac{b^2}{M}\left[\sum_1^f{}_\nu\frac{N_\nu^2}{2}+N_1\Big(\sum_2^f{}_\nu N_\nu\Big)\right].\end{aligned} \tag{16}$$

Since R^2 has already been shown to be given by Eq. (15), $\langle Z^2\rangle_{Av}=X^2-R^2$ can be found:

$$\langle Z^2\rangle_{Av}=\frac{b^2}{M}\left[\sum_1^f{}_\nu\frac{N_\nu^3}{3M}+N_1\Big(\sum_2^f{}_\nu N_\nu\Big)\right]. \tag{17}$$

It is now possible to proceed to the case of two branch units. Here we will designate the two branch units by

a and b, and their functionalities by f_a and f_b. The indices of the linear branches growing from a will be ν_a, and those from b, ν_b; the index of the chain connecting the two units will be ab.

Let us consider branch unit a as the reference segment. There will be f_a-1 linear branches, whose X^2 and $\langle Z^2\rangle_{Av}$ are given by Eqs. (10) and (11), and one ramified branch, which includes unit b, and whose X^2 and $\langle Z^2\rangle_{Av}$ are given by Eqs. (16) and (17). These may all be combined by Eqs. (8a) and (8b), yielding the following:

$$g=\frac{6R^2}{b^2N}=6\Bigg[\sum_{\text{all chains}}\left(\frac{N_\nu^2}{2}-\frac{N_\nu^3}{3N}\right)+6\left(1-\frac{N_{ab}+\sum_{\nu b}N_{\nu b}}{N}\right)N_{ab}\left(\sum_{\nu b}N_{\nu b}\right)\Bigg]$$

$$=6\Bigg[\sum_{\text{all chains}}\left(\frac{N_\nu^2}{2}-\frac{N_\nu^3}{3N}\right)+6\frac{N_{ab}}{N}\Big(\sum_{1}^{f_a-1}N_{\nu a}\Big)\Big(\sum_{1}^{f_b-1}N_{\nu b}\Big)\Bigg]. \quad (18)$$

III.4. Chains of Three Branch Units

In any molecule of three branch units and containing no rings, one of the three units must be unique in that it is connected to both the other two. We will designate this unit as unit a, the others as b and c. The chains connecting a with b and c will be designated ab and ac; the remaining symbols will be obvious extensions of the preceding ones.

If the reference segment is taken as branch unit a, the present case differs from the preceding one only in that there are two ramified branches and f_a-2 linear branches on the reference segment.

As a result, the ratio, g, is immediately found to be

$$g=\frac{6R^2}{b^2N}=6\Bigg[\sum_{\text{all chains}}\left[\left(\frac{N_\nu^2}{2}\right)-\left(\frac{N_\nu^3}{3N}\right)\right]+N_{ab}\left(1-\frac{N_{ab}+\sum_{\nu b}N_{\nu b}}{N}\right)\left(\sum_{\nu b}N_{\nu b}\right)+N_{ac}\left(1-\frac{N_{ac}+\sum_{\nu c}N_{\nu c}}{N}\right)\left(\sum_{\nu c}N_{\nu c}\right)\Bigg],$$

$$=6\Bigg[\sum_{\text{all chains}}\left[\left(\frac{N_\nu^2}{2}\right)-\left(\frac{N_\nu^3}{3N}\right)\right]+\frac{N_{ab}}{N}\Big(\sum_{1}^{f_a-2}N_{\nu a}+\sum_{1}^{f_c-1}N_{\nu c}+N_{ac}\Big)\Big(\sum_{1}^{f_b-1}N_{\nu b}\Big)+\frac{N_{ac}}{N}\Big(\sum_{1}^{f_a-2}N_{\nu a}+\sum_{1}^{f_b-1}N_{\nu b}+N_{ab}\Big)\Big(\sum_{1}^{f_c-1}N_{\nu c}\Big)\Bigg]. \quad (19)$$

This kind of process could be extended stepwise to more and more complicated molecules. It does not seem desirable to carry it further here, since the general formulas become excessively unwieldy. Specific cases of four and five branch units will be treated below.

However, before proceeding we should recognize that pure samples of molecules all with the same definite chain lengths seldom occur in practice. To apply these formulas to actual materials, therefore, it is required that averages be made over the varying chain lengths. We are thus led to consider the following topic.

III.5. Materials With Branch Units Distributed at Random

Any real polymeric material will have a characteristic distribution of chain lengths, number of branch units per molecule, distribution of branch units in the molecule, and so on, which will usually depend on the chemical process that creates the material. For many materials these distributions are still a matter of surmise, although in some special cases they have been studied.[7,8] It would be premature in any case to calculate the average R^2 of materials of all the possibly important distributions. Therefore we study only an idealized example, which may, however, not be so different from actuality as to be useless.

For the beginning it will be assumed that the material is of uniform molecular weight, with a given number, p, of branch units per molecule, but that all possible arrangements of chains of varying lengths occur with equal frequency. More specifically, if it is assumed that each chain of the molecule is labeled, and the "arrangement" of the molecule is defined by the number of segments in each chain, all arrangements with the correct total number of segments are considered to be equally probable.

The process of averaging the expressions for R^2 over the different arrangements then consists of summing the values of R^2 of all the possible arrangements and dividing by the total number of arrangements. When integration is substituted for summation, the general formula for the average of R^2 becomes:

$$\langle R^2\rangle_{Av}=\frac{\displaystyle\int_0^N dn_{\Omega-1}\int_0^{N-n_{\Omega-1}}dn_{\Omega-2}\cdots\int_0^{N-\Sigma_2^{\Omega-1}n_\nu}R^2dn_1}{\displaystyle\int_0^N dn_{\Omega-1}\cdots\int_0^{N-\Sigma_2^{\Omega-1}n_\nu}dn_1}. \quad (20)$$

Ω is the total number of chains in the molecule.

[7] P. J. Flory, Chem. Rev. **39**, 137 (1946); for experiments relating to the problem of this paper, see J. R. Schaefgen and P. J. Flory, J. Am. Chem. Soc. **70**, 2709 (1948).

[8] W. H. Stockmayer, J. Chem. Phys. **11**, 45 (1943).

By elementary integrations it is found that for molecules of N segments in Ω chains,

$$\langle N_\nu^x\rangle_{Av}=\frac{x!(\Omega-1)!}{(\Omega+x-1)!}N^x \tag{21a}$$

$$\langle N_\mu^x N_\nu^y\rangle_{Av}=\frac{x!y!(\Omega-1)!}{(\Omega+x+y-1)!}N^{x+y} \tag{21b}$$

$$\langle N_\lambda^x N_\mu^y N_\nu^z\rangle_{Av}=\frac{x!y!z!(\Omega-1)!}{(\Omega+x+y+z-1)!}N^{x+y+z}. \tag{21c}$$

For molecules of one branch unit of functionality f, use of these equations on the previous result, Eq. (15), gives:

$$g=\frac{6\langle R^2\rangle_{Av}}{b^2N}=\frac{6f}{(f+1)(f+2)}. \tag{22}$$

Likewise, if we consider molecules containing two branch units, each of functionality f, the result from Eq. (18) is

$$g=\frac{6\langle R^2\rangle_{Av}}{b^2N}=\frac{3(5f^2-6f+2)}{f(4f^2-1)}. \tag{23}$$

If there are three branch units the result from Eq. (19) is

$$g=\frac{6\langle R^2\rangle_{Av}}{b^2N}=\frac{2(13f^2-20f+8)}{f(9f^2-9f+2)}. \tag{24}$$

As a partial check on the work, we observe that all three formulas reduce to the value unity for the linear molecule when $f=1$ or 2.

III.6. Molecules with Four and Five Tri-Functional Branch Units

The preceding may be extended without much trouble to molecules containing four or five branch units. Considering that the results will be of interest principally when the units are tri-functional, the discussion will be restricted to these with some gain in simplicity.

It is first necessary to find X^2 and $\langle Z^2\rangle_{Av}$ for a form with two branch units, when one terminal segment is considered as the reference segment. Let the form be represented as in Fig. 2*a*, with the individual chains indexed as shown. Then the individual $\langle x_{i\nu}^2\rangle_{Av}$, where i is the index of a segment and ν is the index of the chain, will be given by the following:

$$\begin{aligned}\langle x_{i\nu}^2\rangle_{Av}&=b^2(N_1+N_3+i_\nu); && \nu=4,5,\\ &=b^2(N_1+i_\nu); && \nu=2,3,\\ &=b^2 i_1; && \nu=1.\end{aligned} \tag{25}$$

Then X^2, which is equal to $\sum_1^5{}_\nu \sum_1^{N\nu}{}_{i\nu}\langle x_{i\nu}^2\rangle_{Av}/M$ where M is the total number of segments, will be given by the expression:

$$\langle X^2\rangle_{Av}=\frac{b^2}{M}\left[\sum_{\text{all chains}}\frac{N_\nu^2}{2}+N_1(N_2+N_3)+(N_1+N_3)(N_4+N_5)\right]. \tag{26}$$

Since R^2 is already known, Eq. (18), $\langle Z^2\rangle_{Av}$ is soon found from $\langle Z^2\rangle_{Av}=X^2-R^2$;

$$\langle Z^2\rangle_{Av}=\frac{b^2}{M^2}\left[\sum_{\text{all chains}}\frac{N_\nu^3}{3}+MN_1(M-N_1)+MN_3(N_4+N_5)-N_3(N_1+N_2)(N_4+N_5)\right]. \tag{27}$$

From consideration of the averages given by Eqs. (21a, 21b, 21c), and by means of Eqs. (7a), (26), and (27), it may be seen that in any molecule of Ω chains each doubly ramified (d.r.) branch will contribute

$$b^2N\left[\frac{6\Omega-26-(\Omega-5/\Omega-3)}{\Omega(\Omega+1)(\Omega+2)}\right] \tag{28}$$

to $\langle R^2\rangle_{Av}$, over and above what its five chains contribute individually, Eq. (30).

Likewise, each singly ramified (s.r.) branch will contribute

$$b^2N\left[\frac{2\Omega-6}{\Omega(\Omega+1)(\Omega+3)}\right], \tag{29}$$

by virtue of Eqs. (21) applied to Eqs. (16) and (17).

In addition every chain wherever located in the molecule contributes the quantity:

$$b^2N/(\Omega+1)(\Omega+2). \tag{30}$$

Linear branches contribute nothing further.

It now follows that $\langle R^2\rangle_{Av}$ can be found by adding the above contributions for any molecule that can be analyzed into one branch unit bearing linear, singly ramified, or doubly ramified branches, if all the branch units are trifunctional. All molecules of four and five trifunctional branch units may be analyzed in this way.

Two types of molecules containing four branch units exist, a "normal" form and an "iso" form, as illustrated in Figs. 2*b* and 2*c*. The "normal" form may be thought of as a branch unit bearing one d.r., one s.r., and one linear branch. There are nine chains ($\Omega=9$). Adding Eqs. (28), (29), and nine times Eq. (30) yields $\langle g\rangle_{Av}$:

$$g=\frac{6\langle R^2\rangle_{Av}}{b^2N}=\frac{361}{495}. \tag{31}$$

The second kind of molecule of four branch units, the "iso"-form, consists of a branch unit bearing three s.r. branches. Again Ω is nine. Adding three times Eq.

(29) and nine times Eq. (30), we find,

$$g=\frac{6\langle R^2\rangle_{Nw}}{b^2N}=\frac{117}{165}, \tag{32}$$

somewhat smaller than for the "normal" form.

The ratio of abundance of the normal- and iso-forms of the molecule of four branch units in any material will depend on the nature of the polymerization reactions. If all molecules of four branch units are formed by the irreversible addition of single branch units to chain-ends of molecules of three units, the normal form should be just four times as abundant as the iso-form. If the reaction is reversible, or if molecules of four branch units can also form by combination of two molecules of two units each, a somewhat different ratio of isomers[7,8] obtains. This latter case is discussed fully in the next section. A chain transfer reaction acting on the middle of the chains of a previously formed three-unit molecule would also favor the normal form, though by a still different ratio.

In molecules with five trifunctional branch units, there also exist two structural isomers, as illustrated in Figs. 2d and 2e. Again, the proportions of these isomers will depend on the polymerization mechanism. The "normal" form of the five-unit molecule may be analyzed as a branch unit bearing two d.r. branches and a linear branch. The number of chains, Ω, is 11; g may be found as described above.

$$g=399/572. \tag{33}$$

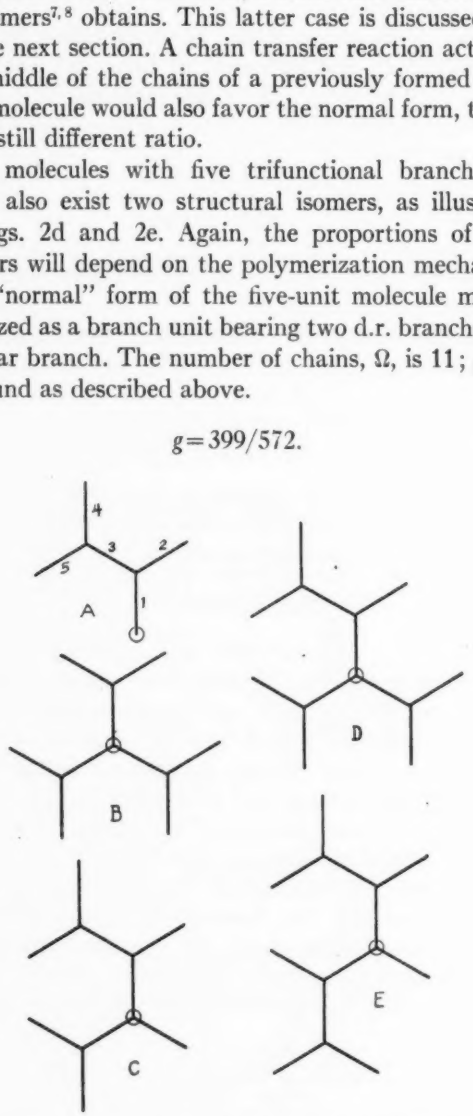

FIG. 2. Types of branched molecules: *A*, doubly ramified (d.r.) branch; *B*, "iso"-form and *C*, "normal" form of molecule of four branch units; *D*, "iso"-form and *E*, "normal" form of molecule of five branch units. Reference segment circled in each case.

The "iso"-form of the five-unit molecule contains two s.r. branches and a d.r. branch, with $\Omega=11$:

$$g=766/1144. \tag{34}$$

III.7. Highly Branched Molecules: Heterogeneous Systems

For treating still more highly branched molecules and heterogeneous polymeric mixtures, the method of the preceding sections becomes unwieldy. An alternative approach, based on a theorem of Kramers,[6a] is more powerful in dealing with such cases, some of which are considered below.

The Kramers theorem may be stated as follows: Consider a polymeric molecule containing any number of branches but no rings, and consisting in all of N segments. Imagine cutting the molecule at one segment into two fragments of N_1 and $N_2(=N-N_1)$ segments respectively. Then the mean square radius of the molecule is given by

$$R^2/b^2=\langle N_1N_2\rangle_{Nw}/N \tag{35}$$

where the average in the second member is taken over all possibilities of cutting.* In other words, the contribution of any segment to $\sum\langle r_i^2\rangle_{Nw}$ is given by the quantity $b^2N_1N_2/(N_1+N_2)$ for that segment. For heterogeneous systems, the average is taken over all segments, yielding *weight-* or *z-average* values of R^2.[8a] In general, we have

$$\langle g\rangle_w=\langle R^2\rangle_w/\langle R^2\rangle_w{}^0=6\langle N_1N_2/N\rangle_w/\langle N\rangle_w \tag{36a}$$

and

$$\langle g\rangle_z=\langle R^2\rangle_z/\langle R^2\rangle_z{}^0=6\langle N_1N_2\rangle_w/\langle N^2\rangle_w. \tag{36b}$$

* The derivation of this theorem is briefly as follows: For any molecule, Σr_i^2 may be expressed as a quadratic form $b^2\Sigma_j\Sigma_k\lambda_{jk}(\boldsymbol{\sigma}_j\cdot\boldsymbol{\sigma}_k)$, where $\boldsymbol{\sigma}_j$ is a unit vector along the jth bond and the λ_{jk} are numerical coefficients. Closely related is the relative kinetic energy with respect to the center of mass, given by $m\Sigma\dot{r}_i^2/2=mb^2\Sigma_j\Sigma_k\lambda_{jk}(\dot{\boldsymbol{\sigma}}_j\cdot\dot{\boldsymbol{\sigma}}_k)/2$ where m is the mass per chain atom. Consider now a special instantaneous phase of the molecular motion such that the relative kinetic energy happens to be simply $(mb^2/2)\lambda_{jj}(\dot{\sigma}_j)^2$; this would be the case if only the jth link were rotating, all others performing translations only. But then the relative kinetic energy is equal to that of a rotating diatomic molecule with masses mN_1 and mN_2 connected by a rod of fixed length b, and this equality gives $\lambda_{jj}=N_1N_2/N$. Now if the molecule contains no rings, $\langle\boldsymbol{\sigma}_j\cdot\boldsymbol{\sigma}_k\rangle_{Nw}=\delta_{jk}$ for flexible chains, and hence $R^2/b^2=\Sigma_j\lambda_{jj}/N=\langle N_1N_2\rangle_{Nw}/N$. Kramers used similar arguments to determine λ_{jk} which is needed for the treatment of rings (see Section V) by this method.

[8a] This usage implies an extension of the common definition of weight average. If ν_N is the number of molecules of N segments in the system, and y is a quantity whose average is to be taken, then the weight average of y is defined as

$$\langle y\rangle_w=\Sigma\nu_NNy/\Sigma\nu_NN.$$

However, since $\Sigma\nu_NN$ is the total number of segments in the system, $\langle y\rangle_w$ may also be written

$$\langle y\rangle_w=\Sigma_{\text{all segments}}\,y/\Sigma\nu_NN,$$

provided that y may be considered as a property of the individual segments. Likewise, the "z-average," $\langle y\rangle_z$, may be written

$$\langle y\rangle_z=\Sigma\nu_NN^2y/\Sigma\nu_NN^2,$$

or alternatively

$$\langle y\rangle_z=\Sigma_{\text{all segments}}\,Ny/\Sigma\nu_NN^2.$$

Where the subscripts w denote weight averages (i.e., over all segments), and the subscripts z denote z-averages. The second of these quantities is pertinent for values of $\langle R^2\rangle_{Aw}$ derived from measurements of light scattering. However, this implies that the z-average molecular weight of the sample is known independently, and such is rarely the case. Probably a more common situation would restrict the measurements to $\langle R^2\rangle_z$ and $\langle N\rangle_w$ for a given polymer sample. In this case, the quantity obtainable from the experiments would be

$$6\langle R^2\rangle_z/b^2\langle N\rangle_w=\langle g\rangle_z\langle N^2\rangle_w/\langle N\rangle_w{}^2=\langle g\rangle_z\langle N\rangle_z/\langle N\rangle_w. \quad (36c)$$

Of course, if fractions of a single molecular weight are involved, the distinction between these various g's becomes unimportant.

In this section, Eqs. (36) will be applied to randomly branched polymers containing branch units of any single functionality f, with the aid of distribution theory previously given.[7,8] By specializing to the case of uniform molecular weight and a uniform number of branches per molecule, we obtain an expression reducing to Eqs. (22)–(24) for molecules of one, two, and three branch units, and corresponding to special proportions of the structural isomers for more highly branched species.

To calculate $\langle N_1N_2/N\rangle_{Aw}$, we require the probability that a randomly chosen segment is connected to N_1 segments at one end and to N_2 at the other. But since this probability depends on the frequency of branching, we must first find the chance P_i that one end of the segment is connected to a network of i branch units. For random distribution of branches and chain lengths, it is found in Appendix B that

$$P_i=(1-\alpha)\beta^i\frac{(fi-i)!}{i!(fi-2i+1)!}, \quad (37)$$

where α is Flory's branching probability[7] and $\beta=\alpha(1-\alpha)^{f-2}$.

Now this network of i branch units consists of $\Omega=fi-i+1$ chains. If it contains N_1 segments, these can be distributed among the chains in $\binom{N_1-1}{\Omega-1}$ ways. For long chains, $\Omega\ll N_1$ and approximately $\binom{N_1-1}{\Omega-1}\cong N_1{}^{fi-i}/(fi-i)!$. Also, for chains randomly distributed in length, the chance that the νth chain has x_ν segments is $(1-q)q^{x_\nu-1}$, where q is the probability of continuation of the chain. Hence, the chance that one end of a chosen segment is connected to a network of $N_1(=\sum x_\nu)$ segments carrying i branch units is

$$P_i\frac{N_1{}^{fi-i}}{(fi-i)!}q^{N_1}[(1-q)/q]^{fi-i+1}.$$

Then the chance that simultaneously the other end of the chosen segment is connected to a network of N_2 segments and j branch units is

$$Q(N_1,N_2,i,j)=P_iP_j\frac{N_1{}^{fi-i}N_2{}^{fj-j}q^{N_1+N_2}[(1-q)/q]^{fi+fj-i-j+2}}{(fi-i)!(fj-j)!}. \quad (38)$$

On substituting for P_i and P_j from Eq. (37), this becomes

$$Q(N_1,N_2,i,j)=(1-\alpha)^2\times\frac{\beta^{i+j}N_1{}^{fi-i}N_2{}^{fj-j}q^{N_1+N_2}[(1-q)/q]^{fi+fj-i-j+2}}{i!j!(fi-2i+1)!(fj-2j+1)!}. \quad (39)$$

This equation gives the required distribution over which the quantities $N_1N_2/(N_1+N_2)$ and $N=N_1+N_2$ must be averaged. For unfractionated systems, the sums run over all positive values of i, j, N_1 and N_2. For fractions of a given molecular weight N and a given number of branches n, the sums must be restricted to such values that $i+j=n$ and $N_1+N_2=N$. This latter case is considered first, in order to compare with the earlier results. For such fractions,

$$g_f(n)=\frac{6}{N}\frac{\sum_{i=0}^{n}\sum_{N_1=0}^{N}\left[\frac{N_1(N-N_1)}{N}\right]Q(N_1,N-N_1,i,n-i)}{\sum_{i=0}^{n}\sum_{N_1=0}^{N}Q(N_1,N-N_1,i,n-i)}$$

$$=\frac{3}{(f-1)n+3}\left[1+\sum_{j=1}^{n}(f-1)^j\prod_{i=0}^{j}\frac{n-i}{(f-1)n+2-i}\right], \quad (40)$$

details of summation being given in Appendix B. The sum in the last member appears irreducible. Specialization to $n=1$, 2, and 3 yields Eqs. (22)–(24). For higher values of n, as earlier stated, g_f corresponds to the special proportions of structural isomers subsisting in random polymers.

In Appendix B it is shown that at large values of n an asymptotic relation may be found for $g_f(n)$, of the form:

$$g_f(n)\doteq 3\left(\frac{\pi}{2(f-1)(f-2)n}\right)^{\frac{1}{2}}-\frac{2(6-f)}{(f-1)(f-2)n}. \quad (40a)$$

For f equal to three and four the following modifications represent $g_f(n)$ within the stated limits for n greater than five:

$$g_3(n)\doteq\tfrac{3}{2}(\pi/n)^{\frac{1}{2}}-5/2n \quad \text{(error}<3\text{ percent)} \quad (40b)$$

$$g_4(n)\doteq\tfrac{1}{2}(3\pi/n)^{\frac{1}{2}}-2/3n \quad \text{(error}<5\text{ percent)} \quad (40c)$$

We may note that, at large values of n, $g_f(n)$ tends to decrease as the reciprocal of the square root of n.

TABLE I. Mean square radii of branched molecules.

Number of branch units	Functionality of branch units	$g=6\langle R^2\rangle_{Nv}/b^2N$ Fixed equal chain lengths	Random distribution of chain lengths
0	(1 or 2)	1	1
1	3	0.778	0.900
	4	0.625	0.800
	8	0.344	0.533
2	3	0.712	0.829
	4	0.525	0.690
3	3	0.668	0.774
	4	0.496	0.618
4	3*n**		0.729
	3*i*		0.709
	3*e*		0.728
	4*e*		0.567
5	3*n*		0.698
	3*i*		0.672
	3*e*		0.693
	4*e*		0.525
6	3*e*		0.663
	4*e*		0.493
7	3*e*		0.637
15	3*e*		0.504
	4*e*		0.345
50	3*e*		0 318

* *n* = "normal" form
i = "iso"-form
e = equilibrium mixture, Eq. (40).

For unfractionated polymers, we obtain, by similar methods

$$\langle g_f\rangle_w=\frac{6\sum_{i=0}^{\infty}\sum_{j=0}^{\infty}\sum_{N_1=0}^{\infty}\sum_{N_2=0}^{\infty}\frac{N_1N_2}{N_1+N_2}Q(N_1,N_2,i,j)}{\sum_{i=0}^{\infty}\sum_{j=0}^{\infty}\sum_{N_1=0}^{\infty}\sum_{N_2=0}^{\infty}(N_1+N_2)Q(N_1,N_2,i,j)}=\frac{3(1-\alpha)^2[1-(f-1)\alpha]G_f(\alpha)}{(f-1)\beta^{3/(f-1)}},\tag{41}$$

where

$$G_f(\alpha)=\int_0^{\alpha}\frac{z^{(4-f)/(f-1)}dz}{[1-(f-1)z][1-z]^{3/(f-1)}}.$$

For arbitrary functionality, this result is intractable, but for the cases of major interest ($f=3$ or 4) the integrations are elementary. For these cases, Eq. (41) becomes

$$\langle g_3\rangle_w=\frac{3(1-2\alpha)}{\alpha}\left[\frac{1}{2}\left(\frac{1-\alpha}{\alpha}\right)^{\frac{1}{2}}\times\ln\left(\frac{(1-\alpha)^{\frac{1}{2}}+(\alpha)^{\frac{1}{2}}}{(1-\alpha)^{\frac{1}{2}}-(\alpha)^{\frac{1}{2}}}\right)-1\right],\tag{42}$$

and

$$\langle g_4\rangle_w=[(1-3\alpha)/2\alpha]\ln(1-\alpha/1-3\alpha),\tag{43}$$

These results are more conveniently expressed in terms of n_w, the weight-average number of branch units per molecule. With the relation[8] $\alpha=n_w/[2+(f-1)n_w]$, they become

$$\langle g_3\rangle_w=\frac{6}{n_w}\left[\frac{1}{2}\left(\frac{2+n_w}{n_w}\right)^{\frac{1}{2}}\ln\left(\frac{(2+n_w)^{\frac{1}{2}}+(n_w)^{\frac{1}{2}}}{(2+n_w)^{\frac{1}{2}}-(n_w)^{\frac{1}{2}}}\right)-1\right],\tag{44}$$

and

$$\langle g_4\rangle_w=(1/n_w)\ln(1+n_w),\tag{45}$$

the last equation being particularly simple in form.

These formulas are restricted in application to properties which depend directly on $\langle R^2\rangle_w$, such as intrinsic viscosity in the absence of the shielding effect (see Sect. IV.3.).

In other cases we may be interested in $\langle g_f\rangle_z$, the z-average value of g. Here we find

$$\langle g_f\rangle_z=\frac{6\sum_{i=0}^{\infty}\sum_{j=0}^{\infty}\sum_{N_1=0}^{\infty}\sum_{N_2=0}^{\infty}N_1N_2Q(i,j,N_1,N_2)}{\sum_{i=0}^{\infty}\sum_{j=0}^{\infty}\sum_{N_1=0}^{\infty}\sum_{N_2=0}^{\infty}(N_1+N_2)^2Q(i,j,N_1,N_2)}=\frac{1-(f-1)\alpha}{1+[(f-1)(f-5)/3]\alpha}.\tag{41a}$$

In terms of n_w, this gives

$$\langle g_f\rangle_z=\frac{1}{1+(f-1)(f-2)n_w/6}$$

$$\langle g_3\rangle_z=1/(1+n_w/3)\tag{44a}$$

$$\langle g_4\rangle_z=1/(1+n_w).\tag{45a}$$

Also, we may note the equation,

$$\langle g_f\rangle_z\langle N\rangle_z/\langle N\rangle_w=\tfrac{3}{2}(1-\alpha)^2.\tag{41b}$$

IV. FINAL RESULTS FOR BRANCHED MOLECULES

In Table I are collected numerical results for several types of molecules, expressed in terms of the ratio $g=\langle R^2\rangle_{Nv}/\langle R^2\rangle_{Nv}{}^0$. As would be expected, the value of g decreases regularly as the number of branch units increases. Fortunately, the various structural isomers (for molecules with four or more branch units) have almost the same radii, so that even extreme assumptions concerning the proportions of these isomers would scarcely affect the results.

It is noteworthy that as many as five branch units introduced at random decrease $\langle R^2\rangle_{Nv}$ by only thirty percent, an effect which would also be achieved by reducing the weight of a linear molecule by the same

amount. One might infer that branching would have to be very extensive before such properties of the material as tensile strength would be significantly affected.

IV.1. Variation of R^2 in a Series of Homologous Fractions

A situation of interest arises when a material of heterogeneous molecular weight containing a proportion of randomly distributed branch units is fractionated. Let us suppose that the fractionation divides the material into a series of samples, each of a different but homogeneous molecular weight, but that the branch units are still randomly distributed.

The distribution of trifunctional branch units is known for fractions derived from polymers of the type considered in Section III.7. If the chains are long, the fraction w_n of molecules in the sample carrying n trifunctional branch units is given by

$$w_n=\frac{1}{I_2(y)}\frac{(y/2)^{2n+2}}{n!(n+2)!}, \tag{46}$$

with

$$y=2N\beta^{\frac{1}{2}}/(1-q).$$

In this equation, the symbols N, β, and q are those employed previously, and $I_k(y)=i^kJ_k(iy)$, a familiar type of Bessel function. The average number, m, of branch units per molecule is found to be

$$m=\sum nw_n=yI_3(y)/2I_2(y). \tag{47}$$

In the range of interest ($m<5$), m varies more rapidly than N, but less rapidly than N^2. To find $\langle g_3\rangle_{Av}$ for fractions obeying Eq. (46), the sum $\sum g_3(n)w_n$ is required, where $g_3(n)$ is given by Eq. (40). Finding no closed sum formula, we have made numerical calculations in the range of interest. The results, among others, are included in Table II.

For highly branched samples (y and m large), m becomes asymptotically proportional to N, and the distribution function w_n resembles the simple Poisson formula $m^ne^{-m}/n!$ In order to investigate the dependence of $\langle g_3\rangle_{Av}$ on the detailed form of w_n, calculations were also made on the assumption that the Poisson distribution obtains for *all* values of m. It is gratifying that at $m=1$ the Poisson distribution yields a value of $\langle g_3\rangle_{Av}$ only 0.001 higher than that based on Eq. (46); and for $m\geq 2$ the agreement is exact in the third place. Thus, the values of $\langle g_3\rangle_{Av}$ for fractions are not highly sensitive to the form of the distribution of branch units. Moreover, these values are only slightly different from those of $g_3(n)$ calculated from Eq. (40) with $n=m$, as is seen by comparison of Tables I and II. The latter circumstance is of course due to the approximate symmetry of w_n about its maximum. Similar results are found for the case of tetrafunctional branch units, with the use of the Poisson distribution.

In Table II, the calculations for fractions are summarized, values of $\langle g_3\rangle_{Av}$ and $\langle g_4\rangle_{Av}$ being shown in the third column. For convenience in plotting, the degree of polymerization is expressed in units of $N'=N/m$, the average number of segments in a sample whose molecules contain just one branch unit on the average. Thus, the fourth column gives $m\langle g\rangle_{Av}=6\langle R^2\rangle_{Av}/b^2N'$, a convenient magnitude proportional to $\langle R^2\rangle_{Av}$. Log-log and semi-log plots of the resulting curves are shown in Figs. 3 and 4. In the former, the straight line of unit slope, to which all curves approach as m becomes small, is the plot for strictly linear molecules.

TABLE II. Mean square radius as function of average frequency of branch units with random branching.

Average number, m, of branch units per molecule	$\log_{10}m$	$\langle g\rangle_{Av}$	$m\langle g\rangle_{Av}$	$\log_{10}m\langle g\rangle_{Av}$ $=\log\langle R^2\rangle_{Av}+$const.
	A. Trifunctional branch units			
0.250	−0.602	0.976	0.244	−0.612
0.500	−0.301	0.953	0.477	−0.322
1.000	0.000	0.912	0.912	−0.040
2.000	0.301	0.840	1.680	+0.225
3.000	0.477	0.784	2.352	0.371
4.00	0.602	0.73	2.92	0.465
5.00	0.699	0.69	3.45	0.538
10.00	1.000	0.58	5.8	0.764
15.00	1.176	0.50	7.5	0.875
50.00	1.699	0.32	16.0	1.204
	B. Tetrafunctional branch units			
0.125	−0.903	0.976	0.122	−0.913
0.250	−0.602	0.953	0.238	−0.623
0.500	−0.301	0.910	0.455	−0.342
1.000	0.000	0.835	0.835	−0.078
2.00	0.301	0.70	1.40	+0.146
3.00	0.477	0.62	1.86	0.270
6.00	0.778	0.49	2.94	0.468
15.00	1.176	0.35	5.25	0.720

It has also been found that these results may be represented, with a maximum error of less than two percent, by the relations

$$\langle g_3(m)\rangle_{Av}=[(1+m/7)^{\frac{1}{2}}+4m/9\pi]^{-\frac{1}{2}} \tag{47a}$$

$$\langle g_4(m)\rangle_{Av}=[(1+m/6)^{\frac{1}{2}}+4m/3\pi]^{-\frac{1}{2}}. \tag{47b}$$

These formulas have the correct asymptotic behavior at large m, in accordance with Eqs. (40b) and (40c).

IV.2. A Method of Detecting Branching

The curves of Figs. 3 and 4 suggest an experimental method of detecting the presence of branching in a material. The material could be fractionated, on the basis of molecular weight, into a series of samples, and the relative degree of polymerization and mean square radius, $\langle R^2\rangle_{Av}$, of each fraction measured by light scattering. Fitting of the logarithms of these numbers to the curves of Figs. 3 and 4 would reveal the presence or absence of branching and allow an estimate of its frequency.

It is interesting to note that, when branching occurs, $\langle R^2\rangle_{Av}$ increases linearly with N at small values of N but only as $N^{\frac{1}{2}}$ at large values.

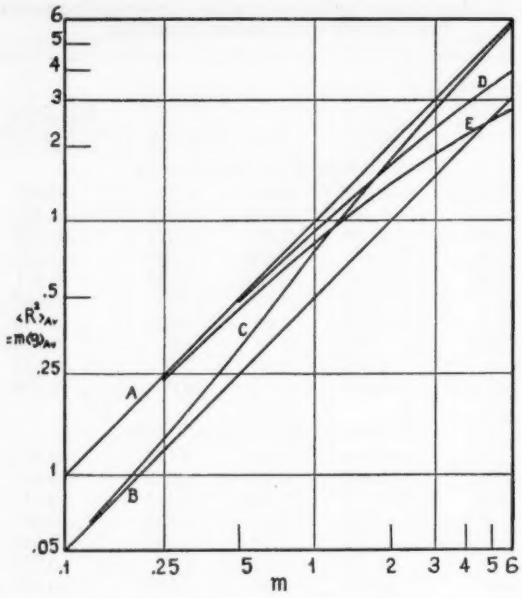

FIG. 3. Mean square radius as function of relative degree of polymerization: *A*, linear chains; *B*, rings; *C*, ring closure incomplete; *D*, trifunctional branch units distributed at random; *E*, tetrafunctional branch units distributed at random.

Since it has been observed[9] that branching alters the solubility of polymers, it is unlikely that an experimental fractionation will be governed only by molecular weight. Nevertheless, it has been seen that the calculated values of $\langle R^2\rangle_{Av}$ given in Table II are quite insensitive to the fine details of the distribution of branch units. Consequently, the proposed method may be considered at least semi-quantitatively useful. The most serious difficulty is due to the "volume effect" discussed in the introduction. It should also be remarked that measurements of high precision are required.

IV.3. Applications to Intrinsic Viscosity

The intrinsic viscosity, $[\eta]$, unlike angular dissymmetry of light-scattering, in general does not permit the direct evaluation of $\langle R^2\rangle_{Av}$, because of the "shielding" effect.[10,11] Thus, although $[\eta]$ is proportional to $\langle R^2\rangle_{Av}$ for the extreme case of no shielding,[6,6a] corresponding to low molecular weights and to Standinger's rule, it becomes proportional to $\langle R^3\rangle_{Av}$ for complete shielding at very high molecular weights. However, it is a simple matter to compare a branched polymer fraction with a chemically similar unbranched fraction of the same molecular weight, using the Debye-Bueche formulas. Denoting the unbranched sample by a subscript zero, we find

$$[\eta]/[\eta]_0 = g^{\frac{1}{2}}\phi(\sigma)/\phi(\sigma_0) = g^{2-\epsilon_0}, \tag{48}$$

where $\phi(\sigma)$ is the shielding function and ϵ_0 is the exponent in the semi-empirical law $[\eta]=KN^{\epsilon_0}$ for the *linear* polymers. For a series of the *branched* polymer fractions, the viscosity exponent is predicted to be

$$\epsilon = \epsilon_0 + (2-\epsilon_0)\, d\ \mathrm{lng}/d\ \ln N. \tag{49}$$

Since $d\ \mathrm{lng}/d\ \ln N$ is always negative, according to Table II and Fig. 4, branching is seen to lower the value of the exponent.

Returning to Eq. (48), we note that branching is predicted to decrease the intrinsic viscosity according to the factor $g^{2-\epsilon_0}$; that is, shielding amplifies the effect of branching. However, the experiments of Schaefgen and Flory[7] and of Weil[12] show considerably smaller decreases (roughly by half) than those calculated from Eq. (48), even if ϵ_0 is taken as unity. The indication is therefore strong that the "volume effect" restricts g to larger values than those calculated herein, in the systems thus far studied. Clearly it is still hazardous to draw inferences about branching from empirical viscosity-molecular weight relationships, and the method of Section IV.2, based on evaluations of $\langle R^2\rangle_{Av}$ from light scattering, is much to be preferred.

V. MOLECULES CONTAINING RINGS

The average radius of chain molecules in which the chain closes on itself to form a continuous ring may also be treated by similar methods. Their consideration has been deferred to the last because such molecules are less familiar than those containing branch units. Presumably they are of rarer occurrence.

V.1. $\langle R^2\rangle_{Av}$ of Ring Molecules

A molecule consisting of N segments in a simple ring, with no branches, will now be studied. For such a molecule it is necessary to find a new expression for $\langle x_{ij}^2\rangle_{Av}$.

Let $W_r(x_{ij})$ be the function that gives the probability density of x_{ij} for a ring molecule. Two chains emanate in opposite directions from any segment, i. These two chains will be designated a and b. The density of probability that chain a will arrive at x_{ij} after n_a segments will be $W_a(x_{ij})$; likewise there will be a function $W_b(x_{ij})$ for chain b. The density of the probability that both will arrive at x_{ij} is the product of these two functions, but this is also $W_r(x_{ij})$, since when both a and b arrive at x_{ij} a ring is formed.

It is well known[13] that

$$W_a(x_{ij}) = C\exp\left(-\frac{3x^2{}_{ij}}{2b^2n_a}\right),$$

$$W_b(x_{ij}) = C\exp\left(-\frac{3x^2{}_{ij}}{2b^2n_b}\right),$$

[9] W. O. Baker, J. Am. Chem. Soc. **69**, 1125 (1947).
[10] P. Debye and A. M. Bueche, J. Chem. Phys. **16**, 573 (1948).
[11] J. G. Kirkwood and J. Riseman, J. Chem. Phys. **16**, 565 (1948).
[12] L. L. Weil, Doctoral Dissertation (Columbia University, 1945).
[13] W. Kuhn, Kolloid Zeits. **68**, 2 (1934). E. Guth and H. Mark, Monatsh. **65**, 63 (1934).

where C is a constant, so that

$$W_r(x_{ij})=C' \exp\left(-\frac{3Nx_{ij}^2}{2b^2n_an_b}\right), \tag{50}$$

since $n_a+n_b=N$. Given the density function, $\langle x_{ij}^2\rangle_{Av}$ is found by elementary operations:

$$\langle x_{ij}^2\rangle_{Av}=b^2(|j-i|)(N-|j-i|)/N. \tag{51}$$

Here $|j-i|$ and $N-|j-i|$ have been substituted for n_a and n_b, respectively.

From Eqs. (7b), (6), and (7a) R^2, X^2, and $\langle Z^2\rangle_{Av}$ may be found in order.

$$R^2=\frac{\sum_i\sum_j\langle x_{ij}^2\rangle_{Av}}{2N^2}=\frac{b^2N}{12}, \tag{52a}$$

$$X^2=\frac{\sum_j\langle x_{ij}^2\rangle_{Av}}{N}=\frac{b^2N}{6}, \tag{52b}$$

$$\langle Z^2\rangle_{Av}=X^2-R^2=\frac{b^2N}{12}\cdot \tag{52c}$$

The reference segment in Eqs. (52b) and (52c) may, of course, be any of the segments of the ring, since all are equivalent.

The difference between the mean square radius of a ring and of a linear chain is striking; the former is just half the latter.** The mean square radius of a ring is almost as small as the average for molecules of the same weight containing ninefold branch units, Eq. (22).

The small values of X^2 and $\langle Z^2\rangle_{Av}$, compared to those of the linear chain, Eqs. (10) and (11), show that rings also would contribute relatively little to the mean square radius of a branched molecule containing rings as well as linear chains.

V.2. The Dependence of $\langle R^2\rangle_{Av}$ of Samples Containing Ring Molecules on the Degree of Polymerization

If the heterogeneous mixture of chain molecules produced by a polymerization reaction be divided into fractions on the basis of the molecular weight, it would be expected that most of the ring molecules, if any are present, would occur in the fractions of smaller N. This statement is based on the premise that a short chain is more likely to close to a ring than a long one.

In addition polymers, rings may be formed if both ends of a growing chain molecule can react with each other, e.g., if both are free radicals resulting simultaneously from a diradical initiator. In condensation polymers, rings are readily formed by intra-molecular esterification, ester interchange, and similar reactions.[14]

** This result was obtained by Kramers (reference 6a).

[14] A complete treatment of ring formation in condensation polymers, based on the same physical ideas discussed here, has been given by H. Jacobson, Doctoral Dissertation, Columbia University (1948).

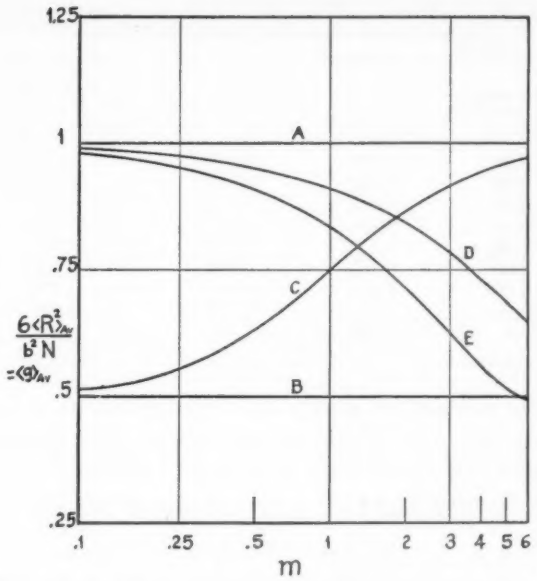

FIG. 4. Ratio of mean square radius to mean square radius of linear molecule of same weight as function of relative degree of polymerization. For curve labels, see Fig. 3.

As a plausible, though perhaps over-simple, assumption it might be postulated that the *a priori* probability of ring closure would be proportional to the probability of the two chain ends lying close to each other. This probability is proportional to L^{-3}, where L^2 is the mean square end-to-end distance of the chain. If, as in polyesters, rings and chains are in chemical equilibrium, the probability of ring closure is further reduced by a factor proportional to N^{-1}, since the ring may be reopened at any one of the inter-monomer linkages.[14] If the reaction is unidirectional, as would probably be the case for combining diradical chains under ordinary polymerization conditions, this factor is omitted. On the other hand, the probabilities of chain growth and of intermolecular termination would be constant, independent of L. Also, we recall that $L^2=b^2N$.

From these considerations, it follows for the case of irreversible ring formation that the fraction, $\rho(N)$, of molecules of N units in ring form, and the corresponding fraction, $\lambda(N)$, of N-unit molecules in linear form, are related thus:

$$\rho(N)=\frac{A/b^3N^{\frac{3}{2}}}{1+A/b^3N^{\frac{3}{2}}}; \tag{53a}$$

$$\lambda(N)=\frac{1}{1+A/b^3N^{\frac{3}{2}}}; \tag{53b}$$

with A a constant. The fraction of rings, $\rho(N)$, decreases from nearly unity to nearly zero as N increases. For ring-chain equilibrium, the exponent of N in Eqs. (38) becomes 5/2, but the relations are otherwise unaffected. It might be added that in this case the constant A is inversely proportional to the concentration, and can be explicitly formulated.[14]

TABLE III. Variation of $6\langle R^2\rangle_{Av}/b^2N$ with degree of polymerization in samples in which ring closure may occur.

Relative degree of polymerization, m	Fraction of rings, $\rho(m)$	$\frac{1+2m^{\frac{1}{2}}}{2+2m^{\frac{1}{2}}}=\frac{6\langle R^2\rangle_{Av}}{b^2N}$	$\log\frac{m}{2}\left(\frac{1+2m^{\frac{1}{2}}}{1+m^{\frac{1}{2}}}\right)$ $=\log\langle R^2\rangle_{Av}+\text{const.}$
0.00	1.000	0.500	—
0.10	0.969	0.515	−1.288
0.25	0.888	0.555	−0.857
0.50	0.739	0.631	−0.501
1.00	0.500	0.750	−0.125
2.00	0.261	0.869	+0.240
4.00	0.111	0.944	0.577
10.00	0.031	0.985	0.994
∞	0.000	1.000	—

The average of R^2 for the mixture of rings and chains can now be found by adding the properly weighted values of R^2 for each type of molecule:

$$\langle R^2\rangle_{Av}=\rho(N)(b^2N/12)+\lambda(N)(b^2N/6),$$
$$=\frac{b^2N}{12}\left(\frac{A+2b^3N^{\frac{1}{2}}}{A+b^3N^{\frac{1}{2}}}\right),$$
$$=\frac{b^2N}{12}\left(\frac{1+2m^{\frac{1}{2}}}{1+m^{\frac{1}{2}}}\right). \tag{54}$$

In the last equation a convenient new variable, m, has been introduced as a measure of molecular weight; it is the ratio of N to the number of segments per molecule in the sample of half rings and half chains.

Calculations of $\langle R^2\rangle_{Av}$ from Eq. (54) are given in Table III. When this formula is valid, the samples change from nearly pure rings to nearly pure chains in two decades of N, and altering the exponent of m from 3/2 to 5/2 in Eq. (54) would make the change even sharper.

Eq. (54) is plotted, on a semi-logarithmic scale, in Fig. 3 and on a double logarithmic scale in Fig. 4. Its rising sigmoid curve contrasts with the gentle downward curvature characteristic of branched molecules and the unit slope of the line for linear chains. Thus, while Eq. (54) may not be exactly correct, it is manifest that effects of rings and branches are quite different. Obviously, these curves offer in principle a means of detecting rings, as well as branches, from observable quantities. Estimates of the constant A in Eq. (53) indicate that the crucial range of molecular weights lies far below that required to give angular dissymmetry of light scattering, but intrinsic viscosities have been used to study ring-chain equilibria.[14]

APPENDIX A

The Relation of the Mean Square Radius, R^2, to Light Scattering

A short derivation of the relation between R^2 and light scattering, which offers the principal means of measurement of R^2, may not be out of place.

The intensity of light, $I(s)$, scattered by an isolated polymer molecule may be calculated as a function of angle of scattering by the following well-known formula:

$$I(s)=F\sum_1^N{}_i\sum_1^N{}_j\int_0^\infty\frac{\sin ksx_{ij}}{ksx_{ij}}W(x_{ij})\,x_{ij}^2dx_{ij} \tag{A1}$$

F is a simple function of the polarization of the incident light, $k=2\pi/\lambda$, where λ is the wave-length, $s=2\sin(\vartheta/2)$, where ϑ is the angle of scattering, and the other symbols are those used previously in this paper.

If $\sin ksx_{ij}$ is expanded in power series, and use is made of the normalization of $W(x_{ij})$, and of the formula defining $\langle x_{ij}^2\rangle_{Av}$, i.e.

$$\int_0^\infty W(x_{ij})x_{ij}^2dx_{ij}=1,$$
$$\int_0^\infty x_{ij}^2W(x_{ij})x_{ij}^2dx_{ij}=\langle x_{ij}^2\rangle_{Av},$$

Eq. (A1) becomes:

$$I(s)=F\Sigma_i\Sigma_j\left[1-\frac{\langle x_{ij}^2\rangle_{Av}k^2s^2}{6}+\cdots\right]. \tag{A2}$$

However, Eq. (7b) may now be used and the summation over the unity be performed:

$$I(s)=N^2F[1-(R^2k^2s^2/3)+0(k^4s^4)] \tag{A3}$$

where $0(k^4s^4)$ represents terms of order four and higher in ks.

R^2 may thus be found by obtaining the initial slope of $I(s)$ against s^2 with light of known wave-length. If many molecules of the same number of segments, N, are present at once, $\langle R^2\rangle_{Av}$ will be the quantity measured. However, if molecules of different size are present, the average of R^2 measured will be a "z-average," not a weight average (see reference 3).

APPENDIX B

We first deduce Eq. (37), giving the probability, P_i, that one end of a chain is connected to a network of i branch units of functionality f. For brevity, it is convenient to start from the probability, W_n, that a chain is part of a molecule bearing n branch units. If the chains are long, W_n is given (reference 8, Eq. (41)) by

$$W_n=2(1-\alpha)^2\frac{(fn-n+1)!\beta^n}{n!(fn-2n+2)!} \tag{B1}$$

with $\beta=\alpha(1-\alpha)^{f-2}$, where α is[7] the probability that one end of a chosen chain ends in a branch unit. From the definitions of P_i and W_n, it is clear that

$$W_n=\sum_{i=0}^{n}P_iP_{n-i} \tag{B2}$$

Now, we define a function

$$\phi(\xi)=\sum_{i=0}^{\infty}P_i\xi^i, \tag{B3}$$

and recognize that

$$[\phi(\xi)]^2=\sum_{i=0}^{\infty}\sum_{j=0}^{\infty}P_iP_j\xi^{i+j}=\sum_{n=0}^{\infty}\xi^n\sum_{i=0}^{n}P_iP_{n-i}=\sum_{n=0}^{\infty}W_n\xi^n. \tag{B4}$$

The last member of Eq. (B4) presents a sum that can be evaluated from formulas previously given:[8]

$$\sum_{n=0}^{\infty}(\beta\xi)^n\frac{(fn-n+1)!}{n!(fn-2n+2)!}=\frac{1}{2(1-z)^2}, \tag{B5}$$

with

$$\beta\xi=z(1-z)^{f-2}.$$

Use of this result gives

$$\phi(\xi)=(1-\alpha)/(1-z). \tag{B6}$$

Now, Eq. (B3) shows that P_i is the coefficient of ξ^i in the series defining $\phi(\xi)$. Hence, by Cauchy s theorem,

$$2\pi(-1)^{\frac{1}{2}}P_i=\oint\frac{\phi(\xi)d\xi}{\xi^{i+1}}. \tag{B7}$$

Expressing $\phi(\xi)$ and $d\xi$ by Eqs. (B5) and (B6), we have

$$2\pi(-1)^{\frac{1}{2}}P_i=(1-\alpha)\beta^i\oint\frac{[1-(f-1)z]dz}{z^{i+1}(1-z)^{fi-2i+2}}. \tag{B8}$$

On binomial expansion of the power of $(1-z)$, this becomes

$$2\pi(-1)^{\frac{1}{2}}P_i=(1-\alpha)\beta^i\sum_{\nu=0}^{\infty}\binom{fi-2i+1+\nu}{\nu}\oint z^{\nu-i-1}[1-(f-1)z]dz. \tag{B9}$$

The only terms contributing to the sum are those for which $\nu=i$ and $\nu=-i-1$. Evaluating these, we obtain the expression for P_i stated as Eq. (37) of the text.

We must now perform the summations indicated in Eqs. (40) and (41), leading to the expressions there given for $g_f(n)$ and $\langle g_f\rangle_{Nv}$. In each case, the procedure is to replace the summations over N_1 and N_2 by integrations, consistent with the assumption of long chains, and then to evaluate the sums over i and j by making use of Eq. (B5) and other sums already given.[8]

Writing $N_1=Nu$, and using Eq. (39) for Q in Eq. (40), we obtain

$$\begin{aligned}g_f(n)&=\frac{6\sum_{i+j=n}\dfrac{P_iP_j}{(fi-i)!(fj-j)!}\int_0^1u^{fi-i+1}(1-u)^{fj-j+1}du}{\sum_{i+j=n}\dfrac{P_iP_j}{(fi-i)!(fj-j)!}\int_0^1u^{fi-i}(1-u)^{fj-j}du}\\&=\frac{6\sum_{i+j=n}P_iP_j(fi-i+1)(fj-j+1)/(fn-n+3)!}{\sum_{i+j=n}P_iP_j/(fn-n+1)!}\end{aligned} \tag{B10}$$

The sum in the denominator is seen to be that for W_n in Eq. (B2). Thus, with the aid of Eqs. (B1) and (37), the equation becomes

$$g_f(n)=\frac{3(n!)/(fn-2n+2)!}{(fn-n+3)!}\sum_{i+j=n}\frac{(fi-i+1)!(fj-j+1)!}{i!j!(fi-2i+1)!(fj-2j+1)!}. \tag{B11}$$

The remaining sum is transformed to its more convenient final form as follows. In Eq. (B5), define a new variable y by the relation $\beta\xi=y^{f-2}$, and differentiate Eq. (B5) with respect to y. Expressing the result in terms of z, one finds

$$\sum_{n=0}^{\infty}\frac{(fn-n+1)!(\beta\xi)^n}{n!(fn-2n+1)!}=\frac{1}{(1-z)[1-(f-1)z]}, \tag{B12}$$

a result also useful later. Taking the square of this expression, we have

$$\sum_{i=0}^{\infty}\sum_{j=0}^{\infty}\frac{(fi-i+1)!(fj-j+1)!(\beta\xi)^{i+j}}{i!j!(fi-2i+1)!(fj-2j+1)!}=\frac{1}{(1-z)^2[1-(f-1)z]^2}, \tag{B13}$$

and it is clear that the sum of Eq. (B11) is just the coefficient, C, of $(\beta\xi)^n$ in this double sum. Hence, by Cauchy's theorem,

$$\begin{aligned}2\pi(-1)^{\frac{1}{2}}C&=\oint\frac{d(\beta\xi)}{(1-z)^2[1-(f-1)z]^2(\beta\xi)^{n+1}}=\oint\frac{dz}{[1-(f-1)z]z^{n+1}(1-z)^{fn-2n+2}}\\&=\sum_{\nu=0}^{\infty}\sum_{\mu=0}^{\infty}\binom{fn-2n+2+\nu}{\nu}(f-1)^{\mu}\oint z^{\nu+\mu-n-1}dz\end{aligned} \tag{B14}$$

Only terms with $\mu=n-\nu$ contribute, and thus, on returning to Eq. (B11), the result is obtained:

$$g_f(n)=\frac{3(n!)(fn-2n+2)!}{(fn-n+3)!}\sum_{\nu=0}^{n}\binom{fn-2n+2+\nu}{\nu}(f-1)^{n-\nu}. \tag{B15}$$

This may be rearranged into Eq. (40), in which the magnitudes of the terms of the sum decrease in order.

An asymptotic form, Eq. (40a), may be found for $g_f(n)$ at large n as follows. Eq. (40) may be written:

$$\begin{aligned}g_f(n)&=\frac{3}{(f-1)n+3}\sum_{j=0}^{n}T_j,\\T^0&=1\\T_j&=\left(1+\frac{2}{(f-1)n}\right)^{-j}\prod_{i=0}^{j-1}\left(1-\frac{i}{n}\right)\left(1-\frac{i}{(f-1)n+2}\right)^{-1},\quad j\neq0.\end{aligned} \tag{B16}$$

However, if x_i are a set of numbers less than unity, the following relation is approximately true:

$$\begin{aligned}\Pi(1-x_i)&=\Pi e^{-x_i}\Pi(1-x_i)e^{x_i}\\&\doteq e^{-\Sigma x_i}[1-\Sigma(x_i^2/2)].\end{aligned} \tag{B17}$$

Expression of T_j in this manner, with the neglect of some minor terms, leads to the form:

$$T_j \doteq 1-\frac{f(f-2)j^3}{6(f-1)^2n^2}\exp\left[-\frac{(f-2)j^2-(f-6)j}{2(f-1)n}\right]. \tag{B18}$$

But by the Euler-MacLaurin summation formula $g_f(n)$ may be represented,

$$g_f(n) \doteq \frac{3}{(f-1)n+3}\left(\int_0^n T_j dj+\tfrac{1}{2}T_0\right). \tag{B19}$$

Substitution of (B18) into (B19) and the resolute suppression of all terms of order n^{-1} or less leads to Eq. (40a).

For the unfractionated systems, Eq. (41) can be written

$$\langle g_f\rangle_w = \frac{6\sum_{i=0}^{\infty}\sum_{j=0}^{\infty}[P_iP_j/(fi-i)!(fj-j)!](1-q/q)^{(f-1)(i+j)+2}\int_0^{\infty}N^{(f-1)(i+j)+2}q^N dN\int_0^1 u^{fi-i+1}(1-u)^{fj-j+1}du}{\sum_{i=0}^{\infty}\sum_{j=0}^{\infty}[P_iP_j/(fi-i)!(fj-j)!](1-q/q)^{(f-1)(i+j)+2}\int_0^{\infty}N^{(f-1)(i+j)+2}q^N dN\int_0^1 u^{fi-i}(1-u)^{fj-i}du}, \tag{B20}$$

by the same procedure used for Eq. (B10). Since long chains are assumed, $(1-q)\ll 1$, and $\ln q \cong (q-1)$. To this approximation, the parameter q cancels and Eq. (B20) simplifies to

$$\langle g_f\rangle_w = \frac{6\sum_{i=0}^{\infty}\sum_{j=0}^{\infty}P_iP_j[(fi-i+1)(fj-j+1)/(fi+fj-i-j+3)]}{\sum_{i=0}^{\infty}\sum_{j=0}^{\infty}P_iP_j(fi+fj-i-j+2)}. \tag{B21}$$

On substituting for P_iP_j, the double sum in the numerator becomes

$$\sum_{i=0}^{\infty}\sum_{j=0}^{\infty}\binom{fi-i+1}{i}\binom{fj-j+1}{j}\frac{\beta^{i+j}}{(fi+fj-i-j+3)},$$

which is closely related to that of Eq. (B13). With a change of variable, $\beta\xi=v^{f-1}$, and after multiplication by v^2, Eq. (B13) gives

$$\sum_{i=0}^{\infty}\sum_{j=0}^{\infty}\binom{fi-i+1}{i}\binom{fj-j+1}{j}v^{fi+fj-i-j+2}=\frac{(\beta\xi)^{2/(f-1)}}{(1-z)^2[1-(f-1)z]^2}. \tag{B22}$$

This equation is now multiplied by dv and integrated, $\beta\xi$ and dv being expressed in terms of z in the second member. Choosing the lower limit at $v=0$ and the upper limit at $v=\beta^{1/(f-1)}$, corresponding to $\xi=1$ or $z=\alpha$, we obtain

$$\sum_{i=0}^{\infty}\sum_{j=0}^{\infty}\binom{fi-i+1}{i}\binom{fj-j+1}{j}\frac{\beta^{i+j}}{(fi+fj-i-j+3)}=\frac{1}{(f-1)\beta^{3/(f-1)}}\int_0^{\alpha}\frac{z^{(4-f)/(f-1)}dz}{[1-(f-1)z][1-z]^{3/(f-1)}}. \tag{B23}$$

A similar procedure serves to evaluate the sum in the denominator of Eq. (B21). From Eqs. (B4) and (B6), after substituting for P_i, we may write

$$\sum_{i=0}^{\infty}\sum_{j=0}^{\infty}\frac{(fi-i)!(fj-j)!(\beta\xi)^{i+j}}{i!j!(fi-2i+1)!(fj-2j+1)!}=\frac{1}{(1-z)^2}. \tag{B24}$$

With the auxiliary variable v, this relation can be put in the form

$$\sum_{i=0}^{\infty}\sum_{j=0}^{\infty}\frac{(fi-i)!(fj-j)!v^{fi+fj-i-j+2}}{i!j!(fi-2i+1)!(fj-2j+1)!}=\frac{v^2}{(1-z)^2}. \tag{B25}$$

Differentiating with respect to v, dividing by v, and then setting $v=\beta^{1/(f-1)}$, $\xi=1$, and $z=\alpha$ as before, we get

$$\sum_{i=0}^{\infty}\sum_{j=0}^{\infty}\frac{(fi-i)!(fj-j)!(fi+fj-i-j+2)\beta^{i+j}}{i!j!(fi-2i+1)!(fj-2j+1)!}=\frac{2}{(1-\alpha)^2[1-(f-1)\alpha]^2}, \tag{B26}$$

which is the desired sum. On substituting this result and that of Eq. (B23) into Eq. (B21), the final expression for $\langle g_f\rangle_w$, as given by Eq. (41), is obtained.

For $\langle g_f\rangle_z$, the equations required run parallel to Eqs. (B20–B23). Thus,

$$\langle g_f\rangle_z = \frac{6\sum_{i=0}^{\infty}\sum_{j=0}^{\infty}[P_iP_j/(fi-i)!(fj-j)!](1-q/q)^{(f-1)(i+j)+2}\int_0^{\infty}N^{(f-1)(i+j)+3}q^N dN\int_0^1 a^{fi-i+1}(1-a)^{fi-i+1}da}{\sum_{i=0}^{\infty}\sum_{j=0}^{\infty}[P_iP_j/(fi-i)!(fj-j)!](1-q/q)^{(f-1)(i+j)+2}\int N^{(f-1)(i+j)+3}q^N dN\int a^{fi-i}(1-a)^{fi-i}da} \tag{B27}$$

$$=\frac{6\sum_{i=0}^{\infty}\sum_{j=0}^{\infty}P_iP_j(fi-i+1)(fj-j+1)}{\sum_{i=0}^{\infty}\sum_{j=0}^{\infty}P_iP_j(fi+fj-i-j+3)(fi+fj-i-j+2)}. \tag{B28}$$

The sum in the numerator has already been given, Eq. (B13), and that of the denominator is easy. Instead of (B25), we need only write

$$\sum_{i=0}^{\infty}\sum_{j=0}^{\infty}\frac{(fi-i)!(fj-j)!v^{fi+fj-i-j+3}}{i!j!(fi-2i+1)!(fj-2j+1)!}=\frac{v^3}{(1-z)^2} \tag{B29}$$

and differentiate *twice* with respect to v. The sum (for arbitrary ξ and z) becomes:

$$\frac{6+2(f-1)(f-5)z}{(1-z)^2[1-(f-1)z]^3}. \tag{B30}$$

When this is used with Eq. (B13), putting $z=\alpha$, the stated result, Eq. (41a), appears.

THE JOURNAL OF CHEMICAL PHYSICS VOLUME 17, NUMBER 12 DECEMBER, 1949

Complete Sets and Redundancies among Small Vibrational Coordinates*

J. C. DECIUS**
Metcalf Chemical Laboratories, Brown University, Providence, Rhode Island
(Received May 6, 1949)

A simple prescription is given for defining internal coordinates of the bond stretching, bending, out-of-plane bending, and torsional types which yields a kinematically complete set of vibrational coordinates with no redundancies in acyclic molecules and with 6μ redundancies in cyclic molecules, where μ is the number of bonds which must be deleted to render the molecule acyclic.

I. INTRODUCTION

THERE are four types of internal coordinates which have been used most extensively in the mathematical formulation of the small vibration problem for polyatomic molecules. All are defined with reference to the valence bonding system assumed for the molecule. They may be described as follows:

(i) Bond stretching: to be designated in general by the symbol r, this coordinate represents the difference of the distance between two directly bonded atoms in a distorted configuration and the distance at equilibrium.

(ii) Bond angle: this class of coordinates is given the general symbol, ϕ, and represents the difference between the angle formed by two adjacent bonds in a distorted configuration and the corresponding angle at equilibrium. In the case of a linear molecule, or of a linear part of a larger molecule (such as the four carbons of dimethyl acetylene) *two* ϕ's can be defined at each internal atom, taking the motion to occur in perpendicular planes whose line of intersection is along the molecule. Whenever this case occurs, the second set of angles will be designated by ϕ'.

(iii) Out-of-plane bending: coordinates of this class can be defined at any atom where three or more coplanar bonds are coincident (e.g. formaldehyde, carbonate ion, ethylene). Such a coordinate, for which the class symbol is γ, can be taken as the angle of one bond relative to the plane of any two other bonds.

(iv) Bond torsion: a coordinate of this last class, designated by τ, can be defined wherever the atoms at each end of a bond (or of a linear part of a molecule comprising any number of colinear bonds) each are also bonded to additional atoms by bonds not colinear with the bonds connecting the two atoms in question. These latter two terminal bonds taken respectively with the connecting bond (or bonds) define two planes, and the torsional angle may be defined as the change in the dihedral angle between the two planes. Examples are very common, such as torsion about the carbon-carbon bond in ethane, about a carbon-carbon bond in a benzene or cyclohexane ring, etc.

Once these coordinates have been defined, two rather interesting questions arise. The first is whether coordinates of these four classes are in every case sufficient to describe all vibrational degrees of freedom, i.e., whether sets of them can be chosen so as to be "complete." The second question is concerned with the problem of redundancy, i.e., linear dependency between some of the coordinates chosen when, for reasons of exploiting the symmetry[1] of the molecule, more than the required number of coordinates are selected. It should be remarked at this point that the redundancies may most conveniently be discovered in some cases after passing to symmetry coordinates.[2]

In the remainder of this paper, it will be shown how to choose coordinates of only the four types described above in such a way as to obtain an exactly complete set for acyclic molecules (no redundancies), or a set which contains redundancies of a purely cyclic nature for cyclic molecules. In other words, we shall show how to distinguish between the only two possible types of redundancies which can occur with our four fundamental coordinate classes, namely *local* and *cyclic* redundancies.

II. CONNECTIVITY OF THE MOLECULE

In our analysis, we shall make use of some of the simplest concepts of *analysis situs*[3] in reference to the aggregation of atoms and bonds which constitute the molecule. It will be assumed that all molecules are connected, which means, loosely, that all atoms in the molecule are bonded either directly or indirectly. Put somewhat differently, it is possible to trace a path from any point of the molecule (either an atom or a point along a bond) to any other point, without leaving the bonds or atoms. If the molecule is acyclic, it is not hard to see that

$$a-b=1 \qquad (1)$$

where a is the number of atoms and b is the number of

* This work was supported by the Office of Naval Research under Contract N6ori-88, Task Order No. 1.
** Present address: Department of Chemistry, Oregon State College, Corvallis, Oregon.

[1] E. B. Wilson, Jr., J. Chem. Phys. **9**, 76 (1941).
[2] C. E. Sun, R. G. Parr, and B. L. Crawford, Jr., J. Chem. Phys. **17**, 840 (1949).
[3] The following correspondence exists between the notation in this paper and that employed by O. Veblen, "Analysis Situs" (American Mathematical Society, New York, 1931):

Present paper	Veblen
μ	μ
a	α_0
b	α_1

bonds.[4] For cyclic molecules, the quantity, μ, defined by

$$\mu = b - a + 1 \tag{2}$$

is greater than zero, and is, in fact, equal to the number of bonds which must be deleted in order to render the molecule acyclic. As an example, napthalene has 19 bonds and 18 atoms, hence $\mu = 2$.

It will prove useful to classify atoms in terms of their *multiplicity*, that is the number of bonds which meet at the atom in question. If the number of atoms of multiplicity m be designated by the symbol a_m, then it is obvious that

$$a = \sum_{m \geq 1} a_m \tag{3}$$

moreover

$$b = \tfrac{1}{2} \sum_{m \geq 1} m a_m \tag{4}$$

since $\sum m a_m$ counts every bond twice.

III. LINEAR MOLECULES

Although the case of the linear molecule is very simple, it is carried through by way of introduction. The number of vibrational degrees of freedom is

$$f = 3a - 5. \tag{5}$$

Obviously there are $n_r = b = a - 1$ independent stretching coordinates. Moreover, the numbers of bending coordinates are clearly $n_\phi = a - 2$ and $n_{\phi'} = a - 2$. Thus there are in all

$$n_r + n_\phi + n_{\phi'} = (a-1) + 2(a-2) = 3a - 5 \tag{6}$$

independent internal coordinates, which is precisely the required number.

IV. PLANAR MOLECULES

Here the in-plane and out-of-plane degrees of freedom can be distinguished, with

$$f_i = 2a - 3, \tag{7}$$

$$f_o = a - 3 \tag{8}$$

respectively. The numbers of coordinates of the four basic types may therefore be considered separately for the two types of motions.

In-plane modes. Only two of the types can contribute to the description of in-plane motions, namely r and ϕ. For the first type, the maximum number of coordinates which can be defined is clearly

$$n_r = b.$$

On the other hand, it is possible to define a maximum of $m(m-1)/2$ ϕ's at each atom of multiplicity m, but this would lead to certain *local* redundancies which we prefer to eliminate at the outset. From elementary geometry it is apparent that the number of locally independent angles at an atom of multiplicity m is $m-1$. Therefore, this number of angles will be taken at each such atom, giving rise to the following total number of ϕ:

$$\begin{aligned} n_\phi &= a_2 + 2a_3 + 3a_4 + \cdots \\ &= \sum (m-1) a_m \\ &= 2b - a \end{aligned} \tag{9}$$

where the final form makes use of (3) and (4). Therefore, the sum of the stretching and bending coordinates is

$$\begin{aligned} n_r + n_\phi &= 3b - a \\ &= f_i + 3\mu \end{aligned} \tag{10}$$

using the definition of μ given in (2). We conclude that the above prescription of the choice of coordinates leads to at least 3μ redundancies. But it is proved in an Appendix that the coordinates left after deleting μ-bonds (so as to make the molecule acyclic) are linearly independent (the proof is conveniently given for linear, planar, or general molecules, simultaneously), hence the sets of internal coordinates prescribed are complete.

Out-of-plane modes. To simplify the discussion, it will be assumed initially that the molecule contains no linear submolecule, that is, no set of two or more adjacent colinear bonds. Later it will be shown how to modify the result when such submolecules do occur.

The prescription of coordinates is as follows:

(i) Choose one τ to correspond to each non-terminal bond (e.g., one for each of the six C−C bonds in benzene, but none for the C−H bonds).

(ii) Choose $m-2$ γ's at each atom of multiplicity m. The numbers of out-of-plane coordinates are then:

$$n_\gamma = \sum_{m \geq 2} (m-2) a_m = 2(b-a) + a_1 \tag{11}$$

and

$$n_\tau = b - a_1 \tag{12}$$

so that the sum is:

$$n_\gamma + n_\tau = 3b - 2a = f_o + 3\mu. \tag{13}$$

This result makes it clear that if the molecule has been rendered acyclic by deleting μ-bonds, the number of coordinates defined will be exactly the number required. An examination of the elementary geometry of any one of the polygons constituting a cycle shows that the redundancies consist of exactly three relations per polygon between the τ's only. In the symmetrical case, one relation is the simple sum of the τ's (in a given polygon), while the other two relations are slightly more complicated, appearing as a degenerate pair amongst the symmetry coordinates.

It must next be shown how to modify the prescription if there are linear submolecules. It is not hard to see that each linear submolecule of length l (bonds), $l > 1$, reduces the total number of γ and τ by $l-1$, but introduces exactly $l-1$ coordinates of type ϕ'. Thus the net count

[4] It should be clear that in the present analysis the chemical nature of the bond is irrelevant, i.e., the carbon-carbon bond counts as one bond only, whether in ethane, ethylene, or acetylene.

is unaffected. It should be noted that in some cases it will be necessary to include a torsion around the whole length of colinear bonds.

V. GENERAL MOLECULES

The number of vibrational degrees of freedom is

$$f=3a-6. \tag{14}$$

Initially it will be assumed that the molecule contains neither linear submolecules, nor atoms for which $m>2$ at which all the incident bonds are coplanar. Under these conditions, the prescription of coordinates will take the following form.

(i) Let a bond stretch be defined for each bond; then

$$n_r=b. \tag{15}$$

(ii) A maximum of $m(m-1)/2$ coordinates of type ϕ can be defined at each atom of multiplicity m. However, it can be shown** that only $2m-3$ such angles are independent locally. If this number of angles be chosen† at each such atom, then the total number will be:

$$n_\phi=\sum_{m\geq 2}(2m-3)a_m=4b-3a+a_1. \tag{16}$$

(iii) As previously in the planar case, the number of torsions will be taken to correspond with the number of non-terminal bonds, which is

$$n_\tau=b-a_1. \tag{17}$$

Thus the following sum of coordinates is obtained:

$$\begin{aligned} n_r+n_\phi+n_\tau&=b+(4b-3a+a_1)+(b-a_1)\\ &=f+6\mu. \end{aligned} \tag{18}$$

Thus, in the general case, our prescription leads to 6μ redundancies, or no redundancies in the acyclic case. The proof that the f coordinates remaining in any case after the deletion of μ-bonds are independent is given, as noted above, in the Appendix.

It is now possible to eliminate the previous restriction which excluded cases in which the molecule contained linear submolecules, or atoms of multiplicity greater than two with all bonds coplanar. For each case of the first kind, when the linear submolecule is of length l bonds, the loss in definable τ's is $l-1$, but this is exactly compensated by the addition of $l-1$ coordinates of type ϕ'. Here again, if the linear submolecule is not terminal, there will be one torsion which can still be defined extending across the entire linear submolecule.

When the second situation occurs, the $2m-3$ ϕ's defined at the atom in question are no longer independent. However, it is merely necessary to substitute $m-2$ γ's for ϕ's (leaving $m-1$ ϕ's) at each such atom so that there is no net loss of coordinates. Thus the general prescription becomes: choose as many r's as there are bonds; as many τ's as there are non-terminal bonds, replacing as many τ's as necessary by ϕ''s in the event of linear submolecules; finally, choose $2m-3$ ϕ's at each atom of multiplicity m, but at each atom with $m>2$ at which all bonds are coplanar, replace $m-2$ ϕ's by γ's. The resulting set of coordinates will consist of $f+6\mu$ coordinates in all, of which f are linearly independent.

VI. SOME EXAMPLES AND CONCLUSIONS

First, a few examples will be given to illustrate the count of redundancies and definition of complete sets of coordinates.

1. Sulfur hexafluoride:

$$\begin{aligned} &a=7,\quad b=6,\quad \mu=0,\quad f=15,\\ &n_r=6,\quad n_\phi=9,\\ &n_r+n_\phi=15=f. \end{aligned}$$

The nine ϕ's may be chosen, for example, by taking all bond angles which are 90° at equilibrium except those bordering one octant.

2. Benzene:

$$\begin{aligned} &a=12,\qquad b=12,\\ &f_1=21,\quad f_o=9;\quad \mu=1. \end{aligned}$$

In-plane modes:

$$\begin{aligned} &n_r=12,\quad n_\phi=12,\\ &n_r+n_\phi=24=f_i+3\mu=21+3. \end{aligned}$$

Out-of-plane modes:

$$\begin{aligned} &n_\gamma=6,\quad n_\tau=6,\\ &n_\gamma+n_\tau=12=f_o+3\mu=9+3. \end{aligned}$$

3. P_4O_6:

Consider this molecule to be of tetrahedral form, with the phosphorus atoms at the vertices, the oxygen atoms midway along the edges.

$$\begin{aligned} &a=10,\quad b=12;\quad f=24,\quad \mu=3,\\ &n_r=12,\quad n_\phi=18,\quad n_\tau=6,\quad n_{\phi'}=6. \end{aligned}$$

In this example, three O−P−O ϕ's are taken at each vertex and one P−O−P is taken as a ϕ at each O. The six torsions are about the six P−O−P bond sequences (each edge). The set ϕ' consists of six additional P−O−P bendings at the oxygens. The sum of the coordinates is:

$$n_r+n_\phi+n_\tau+n_{\phi'}=42=f+6\mu=24+18.$$

** This can be done by spherical trigonometry or by consideration of a molecule consisting of the atom in question plus m radially bonded atoms. The m bond stretches are independent of one another and of any ϕ's which can be described in such a system (see Appendix). Since $3a-6$ is here $3(m+1)-6=3m-3$, it follows that $(3m-3)-m=2m-3$ angles are independent.

† It is to be noted that not every choice of $2m-3$ angles is correct. For $m=5$, seven ϕ's might be chosen in such a way that all pairs for four of the bonds were used, giving 6ϕ's, the seventh being chosen so as to include the fifth bond. Since this choice would be incorrect for the methane-like submolecule, it would also be incorrect for the larger molecule. In general, a choice which is shown in the Appendix to be independent can be made as follows: select three bonds which are not coplanar and define a ϕ between each pair; then in a stepwise fashion, define two additional non-coplanar ϕ's for each additional bond, in each step using only the bonds which have been tied together at the end of the previous step.

If the oxygen atoms are displaced from the lines between the various pairs of phosphorus atoms, $n_\tau=12$, $n_{\phi'}=0$.

In conclusion, two points should be emphasized. The first is, that for reasons of symmetry, numerous additional redundancies may be introduced *locally:*†† the present analysis makes it possible to distinguish these redundancies from the cyclic ones. The second point to be made is, that although the sets of coordinates prescribed in this paper have been shown to be complete, there are molecular examples in which simpler, more symmetrical prescriptions can be shown to be complete. The P_4 molecule, with atoms as vertices and bonds as edges of a tetrahedron is of this type, since the set of the six bond stretches alone is a complete set.

APPENDIX

It is desired to prove that the f coordinates remaining in any molecule after deletion of $\mu=b-a+1$ bonds are linearly independent.

If the t-th such coordinate be designated by S_t, then the set of coordinates will be linearly independent if and only if the only set of constants, c_t, which satisfy

$$\sum_{t=1}^{f} c_t S_t=0 \tag{19}$$

are

$$c_t=0, \quad t=1, 2, \cdots f. \tag{20}$$

Using concepts introduced by Wilson,[1] the internal coordinates may be expressed in terms of independent displacement vectors, $\varrho_1, \varrho_2 \cdots \varrho_a$ of the several atoms in the form

$$S_t=\sum_{\sigma=1}^{a} \mathbf{s}_{t\sigma}\cdot\varrho_\sigma. \tag{21}$$

where $\mathbf{s}_{t\sigma}$ is a vector which indicates the direction in which the displacement of the σ-th atom makes the maximum contribution to S_t. The condition for linear independence can then be formulated as follows: Combining (19) and (21)

$$\sum_{t=1}^{f} c_t \sum_{\sigma=1}^{a} \mathbf{s}_{t\sigma}\cdot\varrho_\sigma=\sum_{\sigma=1}^{a}\sum_{t=1}^{f} c_t\mathbf{s}_{t\sigma}\cdot\varrho_\sigma=0. \tag{22}$$

But, owing to the independence of the ϱ_σ, (22) holds if and only if

$$\sum_{t=1}^{f} c_t\mathbf{s}_{t\sigma}=0, \quad \sigma=1, 2, \cdots a. \tag{23}$$

Therefore, linear independence of the f coordinates requires that the only solution of the a equations of (23) be that in which all c_t vanish.

The proof will be given by mathematical induction. It will be shown that:

(i) The prescribed set of coordinates for the case, $a=2$, is linearly independent;

(ii) If the set of coordinates prescribed for the case $a=n$ is *assumed* linearly independent, then the prescribed set for $a=n+1$ is necessarily linearly independent.

The proof of (i) is trivial: the prescribed set for the diatomic molecule consists solely of the single bond stretching coordinate, which, as is well known, represents the single vibrational degree of freedom in such a case.

In order to prove (ii), first consider every possible way by which the addition of one atom to a set of n atoms augments the prescribed set of coordinates. Note that only acyclic molecules need be considered. Depending upon the multiplicity of the atom to which the additional atom is attached, and also upon the possibility that the new bond may be colinear or coplanar with bonds in the original molecule, the new coordinates must constitute a set of one of the following five types:‡

(1) r, ϕ, τ,
(2) r, ϕ, ϕ',
(3) r, ϕ, ϕ,
(4) r, ϕ, γ,
(5) r, ϕ.

A detailed examination of the $\mathbf{s}_{t\sigma'}$ vectors for the new atom ($\sigma'=n+1$), shows that for each of the above five sets, the vectors are linearly independent. For example, for the first set $\mathbf{s}_{r\sigma'}$ is along the new bond, $\mathbf{s}_{\phi\sigma'}$ is perpendicular to the new bond and in the plane defined by the new bond and a (terminal) bond of the original molecule, $\mathbf{s}_{\tau\sigma'}$ is perpendicular to both $\mathbf{s}_{r\sigma'}$ and $\mathbf{s}_{\phi\sigma'}$. Case (3), on the other hand, gives rise to an $\mathbf{s}_{r\sigma'}$ which is along the new bond, and to $\mathbf{s}_{\phi_1\sigma'}$ and $\mathbf{s}_{\phi_2\sigma'}$ which are perpendicular to the new bond but not themselves colinear.

Case (5) holds for the transition from a linear to a planar molecule.

It is now evident that (23) can only hold in the augmented molecule at the new atom if the c_t corresponding to the new coordinates are all zero. Therefore, any linear dependence for the augmented molecule must involve only the original coordinates, which by hypothesis, are linearly independent. This shows that the set of coordinates prescribed for the augmented molecule is linearly independent if that for the original molecule was. This completes the proof of the independence of the coordinates prescribed for any acyclic molecule.

†† Local redundancies in this sense must be taken to include those introduced, for example, in ethane by taking more than one τ about the carbon-carbon bond.

‡ This statement holds even when the addition of an atom changes the molecule from linear to planar, or from planar to nonplanar, with one exception, namely the case where the new atom is bonded to a planar molecule at an atom of multiplicity m greater than two in such a way as to produce a non-planar molecule. For this special case, the strict use of the coordinate prescription yields one new r, m new ϕ's, and results in a loss of $m-2$ γ's. This difficulty may be eliminated by the observation that any final acyclic configuration may be reached from the diatomic molecule by steps of addition of one atom in which the special step just described is not required. Thus, for any atom which is ultimately to have m bonds not coplanar, we may imagine the atoms added in such an order that the first three are bonded to the central one by noncoplanar bonds, subsequently adding as many as desired in a given plane.

The Microwave Spectrum of Chloroacetylene and Deuterochloroacetylene*

A. A. WESTENBERG, J. H. GOLDSTEIN,** AND E. BRIGHT WILSON, JR.
Mallinckrodt Chemical Laboratory, Harvard University, Cambridge, Massachusetts

(Received May 12, 1949)

The $J=1\rightarrow2$ pure rotational transitions in the linear molecules $HCCCl^{35}$, $HCCCl^{37}$, $DCCCl^{35}$, and $DCCCl^{37}$ have been observed using a Stark modulation microwave spectrograph. The expected quadrupole hyperfine structure has been observed and analyzed in the usual manner, yielding values for the nuclear quadrupole coupling constants of -79.67, -62.75, -79.66, and -63.12 (mc) respectively. The observed Stark effect is in good agreement with that calculated for a linear molecule with a single quadrupolar nucleus using the previously reported value of 0.44 Delsye unit for the dipole moment. The dipole moment calculated from the Stark Effect data is 0.44 ± 0.01 D. Bond distances calculated are $H-C=1.052\pm0.001$A, $C\equiv C=1.211\pm0.001$A, and $C-Cl=1.632\pm0.001$A.

I. INTRODUCTION

THIS work was undertaken with the primary purpose of determining accurately the three structural parameters in the linear molecule chloroacetylene, special interest being centered in the value for the carbon-chlorine distance. According to present theory,[1] such a C—Cl bond adjacent to a triple bond should be appreciably shorter than one adjacent to a single bond because of the contribution of the resonating structure $H-\overset{-}{C}=C=\overset{+}{Cl}$, which thus imparts partial double bond character to the C—Cl bond and consequent shortening. Electron diffraction results on chloroacetylene bear out this prediction.[2] However, because the recent work on the microwave spectrum of vinyl chloride[3] has aroused interest in this laboratory in the general problem of the C—Cl bond in such unsaturated molecules, it was felt that a microwave study of chloroacetylene would be desirable. The bond shortening would be expected to be greater in this molecule than in vinyl chloride because of the enhanced effect of the triple bond over the double bond. It was also desired to obtain a value for the quadrupole coupling constant in chloroacetylene, for comparison with the values reported for other molecules containing chlorine.

II. PREPARATION

Chloroacetylene was prepared essentially as described previously.[4] $Hg(C\equiv CCl)_2$ was prepared by adding 10 cc of sym-dichloroethylene (*cis*) to a solution of 5 g of $Hg(CN)_2$ and 2.3 g of KOH in 20 cc of water. It was purified by extraction from hot chloroform (Soxhlet). 0.4 g of the $Hg(C\equiv CCl)_2$ was reacted with a solution of 1.3 g of KCN and 0.3 g of KOH in 4.5 cc of water. The reaction was carried out in an all-glass flow system using a stream of N_2 which was freed of any oxygen by passage through a pyrogallol-KOH bubbler. The $H-C\equiv C-Cl$ was condensed in liquid nitrogen. Purification was accomplished by several evaporations and condensations in a good vacuum system, and finally, high boiling impurities were trapped out in a dry ice-acetone bath at -80°C.

$D-C\equiv C-Cl$ was prepared in exactly the same way except that the $Hg(C\equiv CCl)_2$ was reacted with a solution of KCN and KOD in D_2O. The $KOD-D_2O$ solution was prepared by a method analogous to that described for making metal-ammonia solutions.[5]

It should be mentioned that since chloroacetylene is spontaneously combustible it is necessary that all oxygen be excluded and that, if possible, the preparation be carried out with only very small amounts of materials as described here. It is especially important to evacuate the $H-C\equiv C-Cl$ receiver with a good vacuum system while it is immersed in liquid nitrogen *before* making the first evaporation to room temperature. Despite the current of N_2, some O_2 diffuses back from the air and condenses with the $H-C\equiv C-Cl$. The writers observed one explosion when the receiver was evacuated with just a mechanical pump and the contents allowed to evaporate. A diffusion pump should be included in the vacuum line to remove the last traces of O_2.

III. APPARATUS

The Stark modulation microwave spectrograph previously described[6] was used. The modulation source was a 0–1000 v square wave generator. All frequencies were measured with a crystal-controlled frequency standard and an associated radio receiver calibrated against Station WWV. The frequencies reported herein should be accurate to at least 0.1 mc/sec.

IV. DESCRIPTION OF SPECTRA

We have observed the $J=1\rightarrow2$ pure rotational transitions for the four isotopic species $H-C\equiv C-Cl^{35}$, $H-C\equiv C-Cl^{37}$, $D-C\equiv C-Cl^{35}$, and $D-C\equiv C-Cl^{37}$.

* The research reported in this document was made possible through support extended Harvard University by the Navy Department (Office of Naval Research) under Office of Naval Research contract N5ori-76, T. O. V.

** National Research Council Predoctoral Fellow.

[1] L. Pauling, *The Nature of the Chemical Bond* (Cornell University Press, Ithaca, 1939).

[2] L. O. Brockway and I. E. Coop, Trans. Faraday Soc. **34**, 1429 (1938).

[3] J. H. Goldstein and J. K. Bragg (to be published).

[4] Bashford, Emeleus, and Briscoe, J. Chem. Soc., 1358 (1938).

[5] Kraus, J. Am. Chem. Soc. **30**, 1197 (1908).

[6] Hughes and Wilson, Phys. Rev. **71**, 562 (1947).

TABLE I. $J=1\rightarrow2$ transition for chloroacetylene. Comparison of observed and predicted hyperfine structure.

F	$H-C\equiv C-Cl^{35}$ Obs.	$H-C\equiv C-Cl^{35}$ Calc.	$H-C\equiv C-Cl^{37}$ Obs.	$H-C\equiv C-Cl^{37}$ Calc.	$D-C\equiv C-Cl^{35}$ Obs.	$D-C\equiv C-Cl^{35}$ Calc.	$D-C\equiv C-Cl^{37}$ Obs.	$D-C\equiv C-Cl^{37}$ Calc.
5/2→7/2								
3/2→5/2	22738.6$_8$ mc	22738.6$_8$	22290.8$_5$	22290.8$_5$	20749.7$_6$	20749.7$_6$	20338.2$_9$	20338.2$_9$
5/2→5/2	22718.8$_0$	22718.7$_6$	22275.1$_0$	22275.1$_7$	20729.7$_9$	20729.8$_4$	20322.5$_0$	20322.5$_1$
5/2→3/2	22732.9$_0$	22732.9$_9$	—	—	20744.0$_0$	20744.0$_7$	—	—
3/2→3/2	22752.9$_5$	22752.9$_0$	22302.1$_0$	22302.0$_6$	20763.9$_6$	20763.9$_8$	20349.4$_8$	20349.5$_0$
3/2→1/2	22772.8$_2$	22772.8$_2$	—	—	20783.8$_0$	20783.9$_0$	—	—
1/2→3/2	22717.0$_7$	22717.0$_5$	22273.9$_0$	22273.8$_2$	20728.0$_3$	20728.1$_3$	20321.1$_2$	20321.1$_6$
1/2→1/2	22737.0$_0$	22736.9$_7$	22289.5$_5$	22289.5$_1$	20748.0$_2$	20748.0$_5$	20336.8$_4$	20336.9$_4$

According to the well-known theory[7] of the quadrupole splitting for a linear molecule containing one quadrupolar nucleus, there should be eight lines in the pattern for a $J=1\rightarrow2$ transition with the nucleus (chlorine) having a spin of 3/2. Two of these will coincide ($F=5/2\rightarrow7/2$ and $3/2\rightarrow5/2$). All eight lines have been detected in the naturally more abundant species containing Cl^{35} and all but the two weakest ($\Delta F=-1$) in the Cl^{37} species. The observed frequencies are listed in Table I.

From a least-squares fit to the observed data for each molecule, values were obtained for the quadrupole coupling constants eqQ. The frequencies for the $J=1\rightarrow2$ transitions were then corrected to zero quadrupole effect from these coupling constants and the observed frequency of the main line of each multiplet ($F=5/2\rightarrow7/2$, $3/2\rightarrow5/2$). The coupling constants, corrected frequencies, and rotational constants appear in Table II. The calculated frequencies of Table I were obtained from the coupling constants and the corrected frequencies in the usual way.

The ratios of the quadrupole moments for the two chlorine isotopes Cl^{35}/Cl^{37} obtained from the coupling constants for the two pairs $H-C\equiv C-Cl^{35}/H-C\equiv C-Cl^{37}$ and $D-C\equiv C-Cl^{35}/D-C\equiv C-Cl^{37}$ are 1.270 and 1.262 respectively. The coupling constants in methyl chloride[8] are −75.13 and −59.3 mc for Cl^{35} and Cl^{37} giving a ratio of 1.267, and in cyanogen chloride[9] they are −83.4 and −65.3 with a ratio of 1.277.

It must be reported that our samples of $H-C\equiv C-Cl$ and $D-C\equiv C-Cl$ gave four or five extra lines in a range of about 100 mc on the high frequency side of the main patterns of both Cl^{35} molecules. It seems unlikely that they are due to impurities since attempts at purification by means of condensing at various temperatures, effusion methods, and preferential adsorption did not reduce the relative intensity of these lines. The relative intensity did decrease appreciably at dry ice temperature, however. In view of these facts, it is probable that the lines are due to excited vibrational states.

[7] See, for example, J. Bardeen and C. H. Townes, Phys. Rev. **73**, 97 (1948).
[8] Gordy, Simmons, and Smith, Phys. Rev. **74**, 243 (1948).
[9] Townes, Holden, and Merritt, Phys. Rev. **74**, 1113 (1948).

V. BOND DISTANCES

In calculating the moments of inertia we have used the following values: $h=6.6242\times10^{-27}$ erg-sec., H = 1.00813 a.m.u., D = 2.01471 a.m.u., C = 12.00386 a.m.u., Cl^{35} = 34.98107 a.m.u., and Cl^{37} = 36.97829 a.m.u. Solving simultaneously for the three bond distances from the moments of inertia for $H-C\equiv C-Cl^{35}$, $H-C\equiv C-Cl^{37}$, and $D-C\equiv C-Cl^{35}$ the values are H−C = 1.0525A, C≡C = 1.2095A, and C−Cl = 1.6333A. From $H-C\equiv C-Cl^{35}$, $D-C\equiv C-Cl^{35}$, and $D-C\equiv C-Cl^{37}$ the values are (in the same order) 1.0518, 1.2115, and 1.6318A. The distances given in Table III represent averages of these pairs. The electron diffraction result for the (C−Cl) distances in chloroacetylene[2] are 1.68±0.04A for the C−Cl bond and 1.21±0.04 for the C≡C bond.

VI. STARK EFFECT

The matrix for the complete Hamiltonian in an electric field, $H=H_0+H_q+H_e$, was set up in the JIM_JM_I representation and then subjected to a transformation e^{-iS} defined by the relation[10]

$$i[S, H_e]=-H_e$$

leading to the transformed Hamiltonian

$$H'=H_0+H_q+\frac{i}{2}[S, H_e]$$

with the property that the off-diagonal Stark effect terms can now be ignored if a result correct to the second order in the electric field is desired. The quadrupole term, H_q, then introduces off-diagonal elements which require the solution of small secular equations. The results are equally valid for weak, intermediate, or strong fields, although in general for the field strengths employed, only the intermediate field case was realized. A more general and detailed account of the above procedure will be given elsewhere.[11]

[10] R. Karplus and A. Harry Sharbaugh, Phys. Rev. **75**, 889 (1949).
[11] J. H. Goldstein and J. K. Bragg, to be published.

TABLE II. Corrected frequencies for $J=1\rightarrow2$ transition. Rotational constants and quadrupole coupling constants.

	H−C≡C−Cl[35]	H−C≡C−Cl[37]	D−C≡C−Cl[35]	D−C≡C−Cl[37]
Frequency (mc)	22736.9$_7$	22289.5$_1$	20748.0$_8$	20336.9$_4$
B_0 (mc)	5684.2$_4$	5572.3$_8$	5187.0$_1$	5084.2$_4$
eqQ (mc)	−79.6$_7$	−62.7$_5$	−79.6$_8$	−63.1$_2$

TABLE III. Bond distances (rigid rotor approximation).

H−C (A)	C≡C	C−Cl
1.052±0.001	1.211±0.001	1.632±0.001

Eight Stark components in the multiplet were studied at field strengths up to 15 e.s.u./cm. The observed frequency shifts agreed quite well with the theoretical values except in a very few cases at low field strength where the Stark component was not clearly resolved from a set of closely spaced zero-field lines. Table IV gives the results for the three Stark components of the strongest $(5/2\rightarrow7/2)$ line of the multiplet. The theoretical shifts were calculated using the value of 0.44 D for the dipole moment.[2]

The mean deviation between the experimental and predicted values for all Stark components examined is about 0.09 Mc, excluding a very few doubtful points at low field strength as mentioned above. The dipole moment of ClC≡CH calculated from the Stark effect is 0.44±0.01 D, which is identical with the previously reported value.

VII. CHARACTER OF C−Cl BOND

According to current ideas, both the bond distance[7] and the quadrupole coupling constant are directly related to the bond type. Any contribution of $C=Cl^+$ should cause a shortening of the C−Cl distance and a decrease in the absolute value of the quadrupole coupling constant. The bond length does decrease from CH_3Cl to vinyl chloride to chloroacetylene but the quadrupole constant does not show this simple behavior. Thus the constant decreases in the order ClCN, ClCCH, CH_3Cl, vinyl chloride. This is presumably strong evidence for the importance of other structures and indicates that caution is desirable in attempting to account for changes in one or two molecular properties by postulating a small number of resonating structures.

TABLE IV. Comparison of theoretical and observed Stark effect for $5/2\rightarrow7/2$ line of the $J=1\rightarrow2$ transition for $HCCCl^{35}$.

	Δν, Mc					
	$M=5/2$		$M=3/2$		$M=1/2$	
E e.s.u./cm	Expt.	Theor.	Expt.	Theor.	Expt.	Theor.
5	+0.90	+0.91	−0.62	−0.09	—	—
7.5	2.03	2.06	0.61	0.51	—	−0.44
10	3.82	3.71	1.48	1.60	—	+0.05
12.5	5.94	5.87	3.67	3.74	+1.60	1.56
15	8.61	8.59	7.22	7.09	4.17	4.24

VIII. ACKNOWLEDGMENTS

We are indebted to Dr. Robert M. Fristrom for calling our attention to the method of preparing the $KOD-D_2O$ solution and for aiding in this and the effusion experiments; to Mr. Bruce Worcester for helping with some of the calculations; and to Mr. Langdon C. Hedrick for his work on the electronic equipment.

The Hydrolysis of Ferric Ion

A. R. Olson and T. R. Simonson
Department of Chemistry, University of California, Berkeley, California
(Received May 17, 1949)

The first hydrolysis of ferric ion in the presence of various perchlorate salts has been studied spectrophotometrically. At a given concentration of perchloric acid, the equilibrium has been shown to depend on the concentration of perchlorate ion.

In a recent brief communication,[1] we stated that the equilibrium $Fe^{+++}+H_2O=FeOH^{++}+H^+$ in the presence of perchlorate ion depended upon the concentration of the perchlorate ion. We present here the experimental details upon which the statement was based.

PREPARATION OF MATERIALS

A stock solution of ferric perchlorate was prepared by oxidizing G. F. Smith ferrous perchlorate with an excess of Merck "Superoxol" preservative-free hydrogen peroxide in the presence of sufficient perchloric acid so that the final solution after dilution was about $0.1M$ (moles per liter) in ferric perchlorate and $0.1M$ in perchloric acid. The excess of peroxide was destroyed by boiling the solution. The solution was analyzed for iron by titration with potassium dichromate using barium diphenylamine sulfonate indicator after reducing the iron with stannous chloride. Since the reduction of ferric ion by stannous ion in the absence of chloride ion is extremely slow, hydrochloric acid was added to the aliquots removed for analysis. Analysis for acid was made by the method of Schumb and Sweetser.[2]

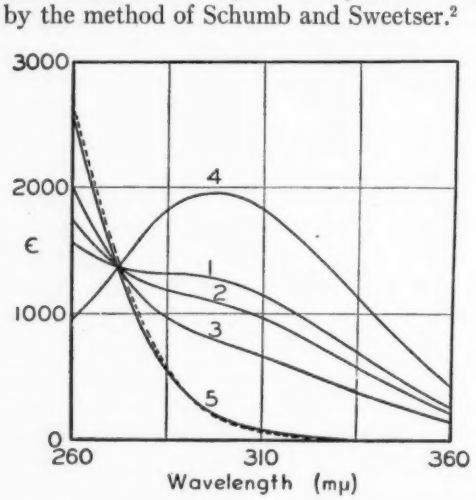

FIG. 1. Absorption spectra of $4.70\times10^{-4}M$ ferric perchlorate solutions at constant perchlorate ion concentration ($0.046M$). (1): $(HClO_4)=1.485\times10^{-3}M$; (2): $(HClO_4)=2.473\times10^{-3}M$; (3): $(HClO_4)=5.454\times10^{-3}M$; (4): Calculated curve for $FeOH^{++}$; (5): Solid curve is calculated for Fe^{+++}, dotted curve is measure at $(HClO_4)=3.7M$. Ordinates are apparent molar extinction coefficients.

A sodium perchlorate solution was made by the neutralization of standardized perchloric acid with analytical reagent grade sodium carbonate to a pH of about four, using an outside indicator. After boiling off the carbon dioxide, neutralization was completed to a pH of about 6.5 with sodium hydroxide solution, checking the pH by testing small portions, using a Beckman pH meter with microelectrodes.

A barium perchlorate solution was prepared from G. F. Smith barium perchlorate. It was analyzed gravimetrically by precipitation of barium sulfate with sulfuric acid. After ignition, the precipitates were moistened with more sulfuric acid which was fumed off under a heat lamp, and were again ignited. Three analyses had a maximum deviation of 0.1 percent. The pH of this solution was 6.2.

A lanthanum perchlorate solution was prepared by the reaction of a known amount of standardized $1M$ perchloric acid with an excess of lanthanum oxide. The lanthanum oxide was strongly ignited in platinum and weighed, added to the perchloric acid, and the resulting solution stirred for three hours. The excess oxide was filtered off, ignited, and weighed as a rough check on the amount which had gone into solution. The final concentration was calculated from the total acid used. This agreed within less than one percent with the calculation from oxide used. The pH of the solution was 7.0.

SPECTRAL MEASUREMENTS

Absorption spectra were measured with a Beckman quartz spectrophotometer arranged for constant temperature measurements. The cell compartment was replaced with one that permitted water to be circulated around the one-cm absorption cells, leaving only about five mm of the top of the cells out of the thermostating liquid. The compartment was provided with fused silica windows. The temperature for a single set of measurements was constant to about 0.1°C.

NATURE OF THE EQUILIBRIUM

The absorption spectra of ferric ion and its first hydrolysis product are appreciably different. Rabinowitch and Stockmayer[3] have analyzed these in the visible and in the ultraviolet region from about 320 to

[1] A. R. Olson and T. R. Simonson, J. Chem. Phys. **17**, 348 (1949).
[2] W. C. Schumb and S. B. Sweetser, J. Am. Chem. Soc. **57**, 871 (1935).
[3] E. Rabinowitch and W. H. Stockmayer, J. Am. Chem. Soc. **64**, 335 (1942).

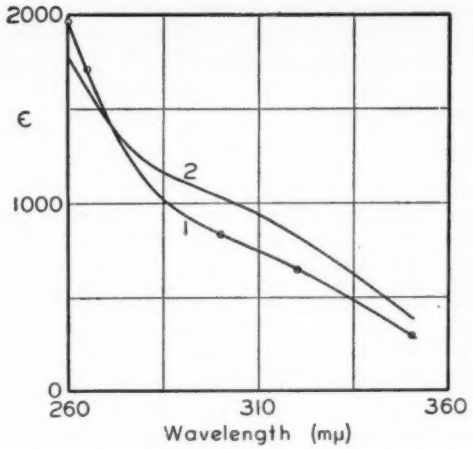

FIG. 2. Absorption spectra of a $4.70\times10^{-4}M$ solution of ferric perchlorate. $(HClO_4)=2.47\times10^{-3}M$. $(NaClO_4)=0.6M$. (1): 25.0°C. (2): 35.0°C. The two curves are drawn smoothly through the observed points. The circles represent measurements at 25.0° after cooling the solution again to this temperature. Ordinates are apparent molar extinction coefficients.

350 mμ, using solutions acidified with perchloric acid. The present investigation makes use of solutions that are much more dilute in iron and in perchloric acid than the ones used by the above investigators.

Figure 1 shows three absorption spectra of $4.70\times10^{-4}M$ ferric perchlorate solutions at various concentrations of perchloric acid. In each case, sufficient sodium perchlorate was added to make the total concentration of perchlorate ion $0.046M$. The reason for maintaining a constant perchlorate ion concentration will be evident later. An interesting feature of these curves is the fact that they all have a point in common at about 272 mμ. This is a strong indication that the iron is present in only two forms, both of which absorb strongly in this region. Any third component must be present to only a very small concentration. Designating the two iron species that are present as α and β, we obtain

$$E=(\alpha)\epsilon_\alpha+(\beta)\epsilon_\beta, \qquad (1)$$

where E is the measured extinction (optical density) of a solution in a one-cm cell, and the ϵ's are molar extinction coefficients. Subject to the condition that $(\alpha)+(\beta)=\Sigma(\mathrm{Fe})$, the concentration equilibrium quotient for the hydrolysis may be written

$$[(\beta)(H^+)]/(\alpha)=K. \qquad (2)$$

Solving (2) for (α) and (β) in terms of K and the total iron concentration and substituting in (1) gives

$$[(H^+)+K]E=(H^+)\Sigma(\mathrm{Fe})\epsilon_\alpha+K\Sigma(\mathrm{Fe})\epsilon_\beta. \qquad (3)$$

Since there are three absorption curves at different acidities, three equations like (3) may be written. Eliminating the ϵ's with their $\Sigma(\mathrm{Fe})$ constant multipliers, and for brevity, writing h for (H^+), we get

$$(h_2-h_1)(h_3+K)E_3-(h_3-h_1)(h_2+K)E_2+(h_3-h_2)(h_1+K)E_1=0$$

as the relation between the observed extinctions at a given wave-length. This equation is linear in the E's, and so the numerical values for the observations may be summed for all wave-lengths to give a single equation which may be solved for an average K by a series of successive approximations. This method gives 2.8×10^{-3} for an equilibrium quotient from the data of Fig. 1.[4] Substituting this value in (3) for each wave-length permits the calculation of the two molar extinction coefficients. Since the curve representing the molar extinction coefficient for α differs only slightly from that obtained by the direct measurement of the absorption spectrum of ferric perchlorate at the same concentration in $3.7M$ perchloric acid, it seems reasonable to us to identify α with ferric ion. These slight changes might be expected from the drastically changed nature of the solvent. The directly measured absorption also is shown in Fig. 1. The general shape of the curve for β, i.e., $FeOH^{++}$, and the great difference between this curve and that for the ferric ion show that the spectrum of a mixture should be sensitive to small changes in the equilibrium $Fe^{+++}+H_2O=FeOH^{++}+H^+$.

REVERSIBILITY

Small effects of other possible equilibria (as, for example, the second hydrolysis) superimposed on the principal one just discussed are not important for our present purpose. If suffices, for the present, to show that there is rapid, reversible, equilibrium among the various possible species in solution. Figure 2 shows the effect of a ten degree temperature change. The curve for 25° was

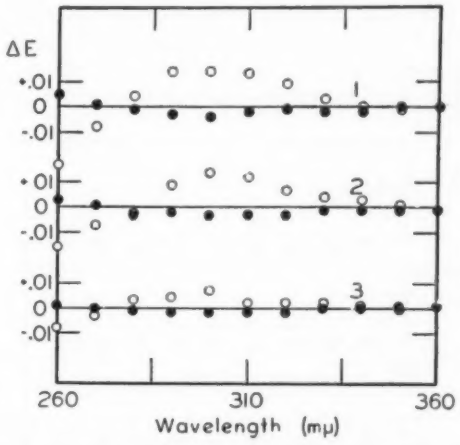

FIG. 3. Comparison of absorption spectra of ferric perchlorate solutions to which sodium perchlorate or lanthanum perchlorate has been added. $[Fe(ClO_4)_3]=4.70\times10^{-4}M$. $(HClO_4)=1.485\times10^{-3}M$. Ordinates are $(E_{La}-E_{Na})$, where E is optical density. Filled circles are comparisons at equal normalities of added salt. Open circles compare equal ionic strength contributions of added salt. Normalities or ionic strength contributions are (1): 0.040, (2): 0.020, (3): 0.0040.

[4] This value may be compared with the calculated results of W. C. Bray and A. V. Hershey, J. Am. Chem. Soc. **56**, 1889 (1934), which gave 2.98×10^{-3} and 2.46×10^{-3} at ionic strengths of 0.04 and 0.09, respectively.

TABLE I. Effect of various perchlorates on the absorption spectrum of ferric perchlorate.

$[Fe(ClO_4)_3] = 4.70 \times 10^{-4} M$				$[HClO_4] = 1.485 \times 10^{-3} M$								One-cm absorption cell						$T = 25.0°C$		
							$10^3 \times$(optical density)													
	Na	Ba	La	Na	Ba	La	Na	Ba	La	Na	Ba	La	Na	Ba	La	Na	Ba	La	Na	Ba	La
Salt cation	$N^a = 0.004$			$\mu^b = 0.004$			$N^a = 0.02$			$\mu^b = 0.02$			$N^a = 0.04$			$\mu^b = 0.04$					
Wave-length (mμ)																				
360	128	128	129	128	128	129	125	124	124	125	125	124	121	119	121	121	120	121		
350	201	201	202	199	199	199	195	193	194	196	196	197	192	190	192	192	191	191		
340	293	293	293	292	292	293	283	281	282	284	284	287	277	275	275	278	278	278		
330	394	395	394	395	396	397	378	375	377	380	382	384	368	365	366	370	371	373		
320	497	498	495	499	501	501	475	473	472	477	481	484	456	453	455	457	461	466		
310	590	590	588	593	593	595	557	555	554	560	567	572	536	532	534	538	544	551		
300	648	649	646	656	659	663	614	611	611	616	623	630	592	588	588	593	601	607		
290	664	665	662	667	668	671	635	634	633	636	641	645	615	612	612	616	622	630		
280	644	645	643	644	645	647	632	630	629	640	641	642	622	620	621	622	623	626		
270	630	632	630	633	630	630	640	640	641	641	638	634	647	647	648	647	642	639		
260	669	672	670	672	667	664	710	712	713	702	692	686	731	732	736	730	715	707		

[a] Normality of added salt.
[b] Ionic strength contribution from added salt.

run first; then the temperature was raised to 35° and another series of measurements was made. The temperature was again dropped to 25° and additional observations made. The last set of readings at 25° agreed with those of the first set well within the experimental error of a few units in the third decimal place of optical density.

The work of Lamb and Jacques[5] indicates that these solutions may be unstable with respect to the slow precipitation of $Fe(OH)_3$. In none of the experiments reported here did more than one hour elapse between dilution of the concentrated stock solution and completion of the measurement of the absorption spectra. A small change in absorption with time was found to occur over a period of days, but its effect in one hour was negligible. Usually this was verified by checking a few of the first measurements of a spectrum at the conclusion of a run. In no case was there a significant change during the course of the observations. This fact, together with the observation of reversibility with temperature change, indicates clearly that we are studying an equilibrium phenomenon.

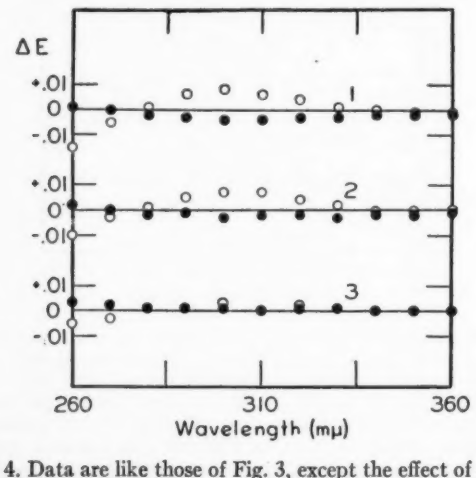

FIG. 4. Data are like those of Fig. 3, except the effect of sodium and barium perchlorates are compared. Normalities or ionic strength contributions from added salt: (1): 0.040, (2): 0.020, (3): 0.0040.

[5] A. B. Lamb and A. G. Jacques, J. Am. Chem. Soc. **60**, 967, 1215 (1938).

EFFECT OF ADDED PERCHLORATES

The principal experiments consisted of determining spectra of solutions of ferric perchlorate and perchloric acid to which various perchlorates were added. In these runs the concentration of ferric perchlorate was $4.70 \times 10^{-4} M$ and that of perchloric acid was $1.485 \times 10^{-3} M$. Four one-cm cells were used in the instrument at one time. All four were filled with water, and three of the cells were calibrated against the fourth which was used throughout as a reference cell. The working cells were then repeatedly rinsed with the solutions to be measured without removing them from the instrument. This was done by aspirating the contents between fillings, thus eliminating the errors caused by changes in cell positions. In one series of experiments we measured the extinction of iron solutions containing sodium, barium, or lanthanum perchlorate, all at the same perchlorate ion concentration. This was done at three different concentrations. In another series of experiments we measured the extinction of the same iron solutions to which these salts had been added in such amounts as to produce the same ionic strength. These results are shown in Table I. In Fig. 3 we have plotted the difference between the measured extinctions for the solutions containing the sodium perchlorate and those for the solutions containing the corresponding amounts of lanthanum perchlorate. The filled circles refer to solutions that have the same perchlorate ion concentration, the open circles to solutions having the same ionic strength. Figure 4 shows a similar comparison for sodium perchlorate and barium perchlorate.

The two diagrams make strikingly clear the close correlation between equilibrium concentrations of iron species and the concentration of perchlorate ion. When

solutions of equal ionic strength are compared, the one with less perchlorate ion is appreciably more hydrolyzed. Rabinowitch and Stockmayer[3] observed that some specific effect of perchlorate ion on this equilibrium must occur at constant ionic strength, and pointed out that Brønsted's principle of specific interaction of ions[6] predicted deviations of this nature. The results of the present experiments, however, indicate that at a given perchloric acid concentration the concentration of perchlorate ions is the major factor concerned with the equilibrium.

The equilibrium $Fe^{+++}+H_2O \underset{r_2}{\overset{r_1}{\rightleftarrows}} FeOH^{++}+H^+$ is the result of the equality of two opposing rates, neither of which formally involves a negative ion. The effect of adding perchlorate ion might be explained by assuming that such addition produces a greater decrease in the forward rate, r_1, than in r_2. This could come about if ferric ion formed a complex of sufficient stability and in sufficient magnitude to account for the shift in equilibrium. If this were the case, we might have expected to find a marked difference between the two absorption spectra for ferric ion shown in Fig. 1. Of course, it is possible that the perchlorate complex has almost the same absorption as ferric ion throughout the whole range. An alternative explanation could be based on the kinetic experiments,[7] in which it was shown that the large increase in the rate of a reaction between ions of the same sign depends almost entirely on the concentration and character of ions of opposite sign, and the further observation that the rate of the reaction between an ion and a neutral molecule shows only a small salt effect. Until reliable experimental evidence for the existence of a sufficient amount of a complex between ferric ion and perchlorate ion in dilute aqueous solution is presented, we incline to the belief that the shift in the equilibrium studied here is due almost entirely to the increase in r_2 caused by the specific effect of the negative ion.

[6] J. N. Brønsted, J. Am. Chem. Soc. 44, 877 (1922).

[7] A. R. Olson and T. R. Simonson, J. Chem. Phys. 17, 1167 (1949).

THE JOURNAL OF CHEMICAL PHYSICS VOLUME 17, NUMBER 12 DECEMBER, 1949

The Mercury Photo-Sensitized Hydrogenation of the Butenes and the Photolysis of Di-*n*-butylmercury

WALTER J. MOORE AND LEO A. WALL
Department of Chemistry of the Catholic University of America and the National Bureau of Standards, Washington, D. C.

(Received May 23, 1949)

The $Hg-{}^3P_1$ photo-sensitized hydrogenations of isobutene, butene-1, and butene-2 have been studied from 24 to 300°C at an $H_2:C_4H_8$ ratio of 10:1. Mass spectrometer analyses of the products have led to the following conclusions: (1) When a H atom adds to isobutene, the tertiary butyl radical is formed. Any isobutyls decompose immediately into methyl and propene. (2) Addition of a H atom to butene-2 produces little *sec.*-butyl, mostly methyl plus propene. (3) Addition of a H atom to butene-1 produces considerable *sec.*-butyl. Any *n*-butyls decompose into ethyl and ethene. (4) The isomeric constitution of the octanes suggests that radicals add to olefinic double bonds at the carbon atom with highest electron density. Products from the photolysis of di-*n*-butylmercury at $\lambda = 2537$A indicate that $n\text{-}C_4H_9 = C_2H_5 + C_2H_4$ has an activation energy of around 35 kcal.

THIS investigation was designed to study some of the elementary reactions of butyl radicals. It is an extension of earlier work with propylene.[1] Hydrogen atoms from the reaction of $Hg-{}^3P_1$ with H_2 might be expected to add to the butenes as follows:

$$H+(CH_3)_2C{:}CH_2=(CH_3)_3C. \quad \textit{tert.}\text{-butyl} \qquad (1a)$$

$$H+(CH_3)_2C{:}CH_2=(CH_3)_2CHCH_2. \quad \text{isobutyl} \qquad (1b)$$

$$H+CH_3CH{:}CHCH_3 = CH_3(C_2H_5)CH. \quad \textit{sec.}\text{-butyl} \qquad (2)$$

$$H+CH_2{:}CHCH_2CH_3 = CH_3(C_2H_5)CH. \quad \textit{sec.}\text{-butyl} \qquad (3a)$$

$$H+CH_2{:}CHCH_2CH_3 = CH_3CH_2CH_2CH_2. \quad \textit{n}\text{-butyl} \qquad (3b)$$

Butyl radicals so produced might react by (a) combination, (b) disproportionation, (c) hydrogenation with H or H_2, (d) decomposition, (e) addition to butene (polymerization). Analysis of the final products should provide some information about the relative probabilities of these diverse reactions. The photolysis of di-*n*-butylmercury was also studied, to obtain further data on the products from *n*-butyl.

EXPERIMENTAL

The reaction vessel, a quartz tube 40 mm in diameter by 40 cm long, was mounted in a furnace provided with quartz windows. A Hanovia SC-2537 arc was used for the photo-sensitization experiments and a Hanovia type-L arc for the photolyses. The general experimental procedure has been described previously.[1,2]

[1] W. J. Moore, J. Chem. Phys. 16, 916 (1948).

[2] W. J. Moore and H. S. Taylor, J. Chem. Phys. 8, 396 (1940).

TABLE I. Products from isobutene hydrogenation.

	23°C	300°C
2,2,3,3-tetramethylbutane	12.2	11.0
2,4,4-trimethylpentene-1	—	1.3
neopentane	11.7	5.5
isobutane	52.2	73.5
propane	2.2	—
propene	5.5	—
ethane	0.6	—
ethene	0.8	—
methane	15.2	9.0

TABLE II. Products from butene-2 hydrogenation.

	23°C	300°C
3,4-dimethylhexane	0.8	1.7
2,3-dimethylpentane	—	4.8
2,2-dimethylpentane	—	1.2
n-hexane	—	1.2
hexene	—	1.0
2,3-dimethylbutane	—	2.7
pentane (*n*-?)	4.7	7.0
pentene	—	2.3
n-butane	48.7	23.5
propane	2.1	6.0
propene	13.7	11.3
ethane	4.5	5.8
ethene	4.9	—
methane	18.8	31.4

The hydrocarbons used were Phillips Research Grade, and mass spectrometer analyses confirmed their purity as 98.5 percent or better. The dibutylmercury was Eastman (white label), redistilled in vacuum. The hydrogen was deoxygenated by passage through palladized asbestos, anhydrous calcium sulfate, and a silica gel trap at −195°C.

The hydrogenation runs were made with an olefine pressure of 20 to 30 mm and an 8 to 10 fold excess of hydrogen. A few runs with 20 to 30 fold excess of hydrogen showed little change in the product distribution. Assuming the quantum yield of the ethylene hydrogenation to be unity at 23°C, the light input to the reaction vessel could be calculated roughly to be of the order of 5×10^{-8} einsteins/sec. A few runs were made with about 10 times this intensity.

At the end of a run, gas non-condensible at −195°C was pumped off; the hydrogen was burned on cupric oxide and the residual gas recorded as methane. A second fraction was taken at −68°, and a third at room temperature. These were separately analyzed with a Consolidated mass spectrometer. For these analyses we are indebted to the Mass Spectrometer Section of the National Bureau of Standards.

RESULTS

A. Isobutene Hydrogenation

The products from runs at 23° and 300°C are shown in Table I. Except for a trace of 3,4-dimethylhexane the only C_8 product is 2,2,3,3-tetramethylbutane, the dimer of the tertiary butyl radical. The sole product of the addition of a hydrogen atom to isobutene appears to be tertiary butyl. Either the isobutyl radical is not formed at all owing to a higher activation energy of reaction (1b) compared with (1a) or it decomposes before reacting,

$$(CH_3)_2CHCH_2=CH_3+CH_3CH:CH_2. \qquad (4)$$

The considerable amounts of methane, propene, and neopentane (methyl+*tert*-butyl) are consistent with reaction (4). Reactions (1a) to (3b) are exothermic by 36 to 44 kcal./mole[3] so that the radicals formed by binary collisions are "hot" to this extent. It is likely, therefore, that the activation energy of reaction (4) is less than 40 kcal. whereas that for decomposition of *tert*-butyl is considerably greater than 40 kcal.

In addition to the volatile products there is considerable polymer.

B. Butene-2 Hydrogenation

The products are shown in Table II. Only the *sec.*-butyl radical can be formed in this instance. Like the isobutyl, this can split without rearrangement into methyl and propene. Thus methane, propene, 2,3-dimethylpentane (isopropyl+*sec.*-butyl) are found in the products. There is only a small amount of the dimer of *sec.*-butyl, 3,4-dimethylhexane, but there is a large amount of unidentified higher polymer. The expected pentane would be isopentane (methyl+*sec.*-butyl), but the analyses suggest *n*-pentane.

C. Butene-1 Hydrogenation

The products are given in Table III. Because of the complexity of the product distribution an analysis in terms of the exact isomers present was not always possible. The much higher percent of 3,4-dimethylhexane from butene-1 as compared with butene-2 is noteworthy, inasmuch as this octane is presumed to arise from the *sec.*-butyl radical in both cases. This difference may arise from a distinction in the hydrogen atom addition:

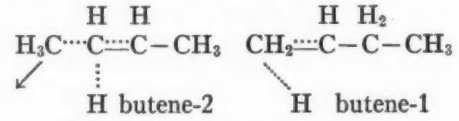

When a H atom attacks butene-2, a CH_3 radical can be driven off by a simple replacement reaction on the C atom attacked. When a H atom adds to butene-1, however, the *sec.*-butyl radical formed is less likely to decompose since the methyl broken off must come from the other end of the molecule.

[3] J. S. Roberts and H. A. Skinner, Trans. Faraday Soc. **40**, 339 (1949).

TABLE III. Products from butene-1 hydrogenation.

	24°	24° ($I \times 10$)	220°	300°
n-octane	0.4	0.4	0.2	—
3,4-dimethylhexane	30.0	16.6	9.6	1.5
2,2,3-trimethylpentane	—	—	—	1.0
octene-1	3.0	0.9	2.2	—
heptane+heptene	1.4	0.4	1.2	1.6
hexane+hexene	1.6	3.4	8.3	2.9
pentane+pentene	3.0	4.3	4.3	4.7
n-butane	45.7	53.5	38.3	16.9
propane	2.7	2.4	4.5	16.6
propene	5.4	6.9	11.2	14.8
ethane	1.9	4.0	2.9	14.1
ethene	4.3	—	6.2	2.1
methane	0.5	6.7	10.2	21.7

TABLE IV. Products from di-*n*-butylmercury photolysis.

	140°	220°	320°
n-octane	4.5	2.9	3.6
3,4-dimethylhexane	1.6	0.1	0.4
n-hexane	8.9	16.8	14.1
n-pentane	4.0	0.9	2.3
butene-1	—	4.2	1.9
n-butane	54.4	42.2	32.4
propane	—	1.6	4.1
propene	—	2.0	4.4
ethane	7.7	6.4	9.2
ethene	15.0	9.4	12.9
acetylene	0.4	1.0	2.3
methane	1.8	4.7	5.4
hydrogen	3.8	7.0	4.9

D. Di-*n*-Butyl Mercury Photolysis

The mercury dibutyl photolyses were run with a constant amount of alkyl, sufficient to yield a pressure of 20 mm in the reaction vessel at 120°C. The pressures were therefore greater in the high temperature runs but the vapor densities were about the same. The product analyses are given in Table IV.

The strength of the Hg−C bond has been estimated to be around 16 kcal.[4] Hence butyl radicals formed by $HgBu_2+h\nu(2537)=Hg+2Bu$ would be "hot" to the extent of about 27 kcal. each (on the average). These butyls are therefore somewhat comparable with those from the atomic hydrogenation. The results in Table IV indicate that the preferred mode of decomposition of the radical is $C_4H_9=C_2H_5+C_2H_4$.

The occurrence of 2,3-dimethylbutane as the sole hexane product from propene was interpreted as the result of a preferential addition of the H atom to yield the *sec.*-propyl radical.[1] It is also possible that, like *n*-butyl, *n*-propyl is so unstable that it immediately breaks into methyl and ethylene,[5] but the small amounts of ethane and butane found in the propene hydrogenation lend some support to the view that little *n*-propyl is formed in the H atom addition.

The ΔH_{298} for the decomposition of the radicals can be estimated by combining the bond energies of Roberts and Skinner[3] with the National Bureau of Standards heats of formation of hydrocarbons.[6]

$$n\text{-}C_4H_9=C_2H_5+C_2H_4-28 \text{ kcal.}$$
$$sec.\text{-}C_4H_9=CH_3+C_3H_6-31 \text{ kcal.}$$
$$n\text{-}C_3H_7=CH_3+C_2H_4-26 \text{ kcal.}$$

Since the reverse reactions probably have low activation energies,[7] the activation energies for decomposition of these radicals into an olefin and a smaller radical would all appear to be around 35 kcal. Such values are in accord with the results of the present experiments.

E. Polymerization Reactions

In all of the above reactions a considerable fraction of the final product was a polymer of undetermined composition. The extent of polymerization varied from 45 to 65 percent of the total olefin consumption. In previous work with propene, about 40 percent of the olefin went to polymer. In contrast with these results is the slight polymerization of ethylene reported by LeRoy and Kahn[8] under similar reaction conditions.

If any appreciable fraction of the octanes formed from the butene hydrogenations arises from chain breaking steps in a polymerization,

$$C_4H_9+C_4H_8=C_8H_{17}$$
$$C_8H_{17}+H=C_8H_{18}$$
$$2C_8H_{17}=C_8H_{18}+C_8H_{16},$$

one must conclude that butyl radicals add to olefins at the position of highest electron density. The radical acts like an electron-deficient compound. The predominant radical addition is at the opposite end of the double bond from the predominant hydrogen atom addition.

ACKNOWLEDGMENT

A grant-in-aid of research from the Penrose Fund of the American Philosophical Society provided some of the equipment used in this investigation. We are indebted to Mr. Robert Reese, Miss Dorothy Thompson, and Miss Laura Williamson for the hydrocarbon analyses.

[4] N. V. Sidgwick and H. D. Springall, Nature **156**, 599 (1945).
[5] See Rabinowitch, Davis, Winkler, Can. J. Research **B21**, 251 (1943).
[6] Nat. Bur. of Stand. Circular No. C-461 (U. S. Government Printing Office, Washington, D. C., November, 1947).
[7] E. W. R. Steacie, *Atomic and Free Radical Reactions* (Reinhold Publishing Corporation, New York, 1946).
[8] D. J. LeRoy and A. Kahn, J. Chem. Phys. **15**, 816 (1947).

Hexacovalent Bond Orbitals I

GEORGE H. DUFFEY
Chemistry Department, South Dakota State College, Brookings, South Dakota
(Received May 23, 1949)

A set of six equivalent orthogonal bond orbitals of type $s^n p^{1+2m} d^{5-n-2m}$ are considered. The fact that these are of trigonal prism symmetry is pointed out. Calculations were made of the bond strengths and angles at various values of m with n set equal to one and at various values of n with m set equal to zero.

THE method of directed valence bonds has been employed[1-3] in discussing hexacovalent structures possessing equivalent cylindrical bonds. Two structures were found, the octahedral structure and the trigonal prism structure. However, the trigonal prism structure is observed when $1s$, $1p$, and $4d$ orbitals are readily available for bond formation. The structure discussed by Hultgren employed $17/18s$, $7/3p$, and $49/18d$ orbitals. It seems of interest to consider more general hexacovalent orbitals.

In this paper some calculations are reported on a set of orbitals which yields the trigonal prism configuration. The set is formed by spd hybridization.

Differences in the radial parts of the s, p, and d wave functions are neglected. Then the angular parts, normalized to 4π, are given by the equations

$$s=1, \tag{1}$$

$$p_x=\sqrt{3}\sin\theta\cos\varphi, \tag{2}$$

$$p_y=\sqrt{3}\sin\theta\sin\varphi, \tag{3}$$

$$p_z=\sqrt{3}\cos\theta, \tag{4}$$

$$d_z=[(5)^{\frac{1}{2}}/2](3\cos^2\theta-1), \tag{5}$$

$$d_{xy}=[(15)^{\frac{1}{2}}/2]\sin^2\theta\cos 2\varphi, \tag{6}$$

$$d_{x+y}=[(15)^{\frac{1}{2}}/2]\sin^2\theta\sin 2\varphi, \tag{7}$$

$$d_{x+z}=(15)^{\frac{1}{2}}\sin\theta\cos\theta\cos\varphi, \tag{8}$$

and

$$d_{y+z}=(15)^{\frac{1}{2}}\sin\theta\cos\theta\sin\varphi, \tag{9}$$

where θ and φ are the angles used in polar coordinates. The following functions are formed:

$$\psi_1=\{[1/(6)^{\frac{1}{2}}]\cos\alpha\}s+[1/(6)^{\frac{1}{2}}]p_z+[(1/\sqrt{3})\cos\beta]p_x+\{[1/(6)^{\frac{1}{2}}]\sin\alpha\}d_z+[(1/\sqrt{3})\sin\beta]d_{xy}+(1/\sqrt{3})d_{x+z}, \tag{10}$$

$$\psi_2=\{[1/(6)^{\frac{1}{2}}]\cos\alpha\}s+[1/(6)^{\frac{1}{2}}]p_z-[(1/2\sqrt{3})\cos\beta]p_x+[(1/2)\cos\beta]p_y+\{[1/(6)^{\frac{1}{2}}]\sin\alpha\}d_z$$
$$-[(1/2\sqrt{3})\sin\beta]d_{xy}-[(1/2)\sin\beta]d_{x+y}-(1/2\sqrt{3})d_{x+z}+(1/2)d_{y+z}, \tag{11}$$

$$\psi_3=\{[1/(6)^{\frac{1}{2}}]\cos\alpha\}s+[1/(6)^{\frac{1}{2}}]p_z-[(1/2\sqrt{3})\cos\beta]p_x-[(1/2)\cos\beta]p_y+\{[1/(6)^{\frac{1}{2}}]\sin\alpha\}d_z$$
$$-[(1/2\sqrt{3})\sin\beta]d_{xy}+[(1/2)\sin\beta]d_{x+y}-(1/2\sqrt{3})d_{x+z}-(1/2)d_{y+z}, \tag{12}$$

$$\psi_4=\{[1/(6)^{\frac{1}{2}}]\cos\alpha\}s-[1/(6)^{\frac{1}{2}}]p_z+[(1/\sqrt{3})\cos\beta]p_x+\{[1/(6)^{\frac{1}{2}}]\sin\alpha\}d_z+[(1/\sqrt{3})\sin\beta]d_{xy}-(1/\sqrt{3})d_{x+z}, \tag{13}$$

$$\psi_5=\{[1/(6)^{\frac{1}{2}}]\cos\alpha\}s-[1/(6)^{\frac{1}{2}}]p_z-[(1/2\sqrt{3})\cos\beta]p_x+[(1/2)\cos\beta]p_y+\{[1/(6)^{\frac{1}{2}}]\sin\alpha\}d_z$$
$$-[(1/2\sqrt{3})\sin\beta]d_{xy}-[(1/2)\sin\beta]d_{x+y}+(1/2\sqrt{3})d_{x+z}-(1/2)d_{y+z}, \tag{14}$$

$$\psi_6=\{[1/(6)^{\frac{1}{2}}]\cos\alpha\}s-[1/(6)^{\frac{1}{2}}]p_z-[(1/2\sqrt{3})\cos\beta]p_x-[(1/2)\cos\beta]p_y+\{[1/(6)^{\frac{1}{2}}]\sin\alpha\}d_z$$
$$-[(1/2\sqrt{3})\sin\beta]d_{xy}+[(1/2)\sin\beta]d_{x+y}+(1/2\sqrt{3})d_{x+z}+(1/2)d_{y+z}. \tag{15}$$

These functions represent six equivalent orthogonal bond orbitals of type $s^n p^{1+2m} d^{5-n-2m}$ where

$$n=\cos^2\alpha \tag{16}$$

and

$$m=\cos^2\beta. \tag{17}$$

the functions reduce to the functions given by Hultgren[3] for equivalent, cylindrical, regular[4] trigonal prism orbitals when $\cos\alpha=(34)^{\frac{1}{2}}/6$ and $\cos\beta=\sqrt{2}/\sqrt{3}$. Changing α and β from the values obtained from these equations makes the bonds non-cylindrical but it does not destroy the trigonal prism symmetry.

In each case the axis of the regular trigonal prism coincides with the Z axis. Let the numbering of the bonds be the same as the numbering of the ψ_i. Thus bond one is described by ψ_1. Bonds one, two, and three lead to atoms in one base of the regular trigonal prism. Bonds four, five, and six lead to the corresponding atoms in the other base.

Three orbital functions orthogonal to $\psi_1, \psi_2, \cdots\psi_6$ can be set up as follows:

$$\psi_7=(\sin\alpha)s-(\cos\alpha)d_z, \tag{18}$$

$$\psi_8=(\sin\beta)p_x-(\cos\beta)d_{xy}, \tag{19}$$

$$\psi_9=(\sin\beta)p_y+(\cos\beta)d_{x+y}. \tag{20}$$

[1] L. Pauling, *The Nature of the Chemical Bond* (Cornell University Press, Ithaca, New York, 1940).
[2] L. Pauling, J. Am. Chem. Soc. **53**, 1367 (1931).
[3] R. Hultgren, Phys. Rev. **40**, 891 (1932).
[4] A regular trigonal prism is a right prism whose bases are equilateral triangles.

TABLE I. Results of calculations on trigonal prism orbitals of type $sp^{1+2m}d^{4-2m}$.

m	S, Strength of a bond	θ_1, Angle between axis and bond 1
1.0000	2.737	47° 5′
0.9800	2.817	48° 36′
0.9000	2.898	50° 17′
0.8000	2.944	51° 23′
0.5575	2.979	52° 50′
0.3000	2.943	53° 29′
0.2000	2.904	53° 30′
0.1000	2.838	53° 18′
0.0200	2.727	52° 40′
0.0000	2.623	51° 52′

TABLE II. Results of calculations on trigonal prism orbitals of type $s^n pd^{5-n}$.

n	S, Strength of a bond	θ_1, Angle between axis and bond 1
1.0000	2.623	51° 52′
0.9800	2.631	49° 47′
0.9600	2.634	48° 54′
0.9000	2.640	47° 7′
0.8000	2.644	45° 4′
0.7094	2.645	43° 37′
0.3000	2.620	38° 55′
0.2000	2.601	38° 1′
0.1000	2.569	37° 12′
0.0000	2.462	36° 25′

In the calculations reported in Table I n was set equal to one. A value was assigned to m. Then θ_1, the angle between the axis and bond one, was determined by finding the position of the maximum in ψ_1. The corresponding value of ψ_1 gave the strength of the bond, S. In the calculations reported in Table II m was set equal to zero. Then θ_1 and S were determined as before.

The strongest bonds when n equals one occur when m equals 0.5575. These bonds have a strength equal to 2.979. This is only slightly smaller than the value 2.982 reported by Hultgren[3] for cylindrical trigonal prism orbitals. The strongest bonds when m equals zero occur when n equals 0.7094. These bonds have a strength equal to 2.645.

It is evident that the bond angles change somewhat as the composition of the bonds is altered. Thus one may obtain some information about the composition of the bonds from the observed bond angles.

As an example consider the MoS_2 crystal. The sulfur atoms are arranged in the form of trigonal prisms[1,5] about the molybdenum atoms. If the unshared pair outside the core of a molybdenum atom is put into a d orbital, then $1s$, $1p$, and $4d$ orbitals are available for bond formation. Hence one might expect the trigonal prism structure to be assumed with the angle between bond one and the axis equal to 51° 52′. However, stronger bonds may be formed if m does not equal zero (more of the unstable p orbitals used for shared pairs) and if n does not equal one. The unshared pair may go into the orbital described by ψ_7. The actual composition used may be estimated following the method of Kuhn.[6] That such bonds are formed is indicated by the fact that the observed[1,5] angle between bond one and the axis is 49°.

[5] R. G. Dickinson and L. Pauling, J. Am. Chem. Soc. **45**, 1466 (1923).
[6] H. Kuhn, J. Chem. Phys. **16**, 727 (1948).

The Ionization of Polymeric Electrolytes*

FREDERICK T. WALL AND EDWARD H. DEBUTTS, JR.[1]
Noyes Chemical Laboratory, University of Illinois, Urbana, Illinois
(Received May 24, 1949)

A theory is developed for the ionization of polymeric acids and bases. Using the theory it is possible to calculate the *pH* and equivalent conductances of aqueous polymeric electrolyte solutions as functions of concentration. A general formula is derived for ionization constants of acids and bases of any basicity. A graphical comparison of calculated and measured equivalent conductances confirms the essential features of the theory. It is also shown indirectly that the conductance of a polymeric acid is due almost entirely to the hydrogen ions.

THE ionization of a simple electrolyte, such as an ordinary acid, base or salt, is fairly well understood from a thermodynamic point of view. Moreover the equilibria involved in the ionization of many weak electrolytes have been investigated quite thoroughly, During recent years, however, there has been an in. creasing interest in polymeric substances of all varieties, so it is natural to examine the electrolytic properties of such substances. The work here reported is concerned with the behavior of certain "weak" polymeric electrolytes both theoretically and experimentally. Fuoss and Strauss[2] have recently investigated a number of polymeric electrolytes which would be "strong" electrolytes for very low degrees of polymerization.

There are a number of long chain polymeric acids and bases available for study. One of the simplest of these is polyacrylic acid which can be considered a long chain paraffin hydrocarbon with carboxyl substituents on alternate carbon atoms. Another polymeric acid, which can be readily made, is the hydrolyzed copolymer of maleic anhydride and styrene. This polymer is substantially a long chain made up of alternating maleic acid and styrene units. Recently Reynolds and Kenyon[3] prepared a polymeric base, namely, polyvinyl amine, which is structurally like polyacrylic acid except that amino groups take the places of the carboxyls.

There will be developed below a statistical theory for the ionization of polymeric electrolytes which should be valid for either acids or bases, but not for mixed types. The model is essentially that assumed by Cohn and Edsall,[4] but the method by which the theory is derived has certain unique features. This theory will be compared with experimental results reported by Kern[5] on polyacrylic acid and on electrical conductance measurements which we have carried out on the hydrolyzed copolymer of maleic anhydride and styrene. Although the data available up to the present time are not very extensive, they appear to justify the essential features of the theory.

THEORY

The model which we shall assume for making our calculations is as follows. The polymeric electrolyte (assumed to be an acid for convenience) is supposed to be of uniform basicity, containing s carboxyl groups per molecule. Although the different carboxyl groups in a given molecule are distinguishable from each other, they will be considered equivalent from an energetic point of view. In other words, the ionization tendency of a given carboxyl group in a certain molecule will be assumed to depend only upon the net charge on the molecule and not upon the particular location of the carboxyl group under consideration. This assumption has only a limited validity and further refinements in the theory will have to take account of this limitation.

Suppose that an aqueous solution of this s basic acid contains N molecules. Let there be n_i ions with i unionized hydrogens, and hence possessing $s-i$ negative charges. Furthermore, let there be B unionized carboxyl groups in all, thus implying the presence of $Ns-B$ hydrogen ions in solution. Let us further denote the energy associated with each of the n_i ions in the specified class as ϵ_i. Then evidently

$$N=\sum_i n_i, \tag{1}$$

$$B=\sum_i i n_i \tag{2}$$

and

$$E=\sum_i n_i \epsilon_i \tag{3}$$

where E is the energy of the system under consideration. Our statistical problem now involves the calculation of the entropy of the protons in the system. In effect we have N large boxes, each made up of s sub-boxes, among which we can distribute B protons subject to the condition that no sub-box can contain more than one proton. Assuming the protons to be indistinguishable, but the polymer molecules distinguishable, the number of ways

* This work was carried out in part under sponsorship of the Office of Rubber Reserve, Reconstruction Finance Corporation, in connection with the Government Synthetic Rubber Program (first reported in October, 1947).

[1] Present address: Department of Chemistry, Harvard University, Cambridge 38, Massachusetts.

[2] R. M. Fuoss and U. P. Strauss, J. Polymer Sci. **3**, 246, 602 (1948).

[3] D. D. Reynolds and W. D. Kenyon, J. Am. Chem. Soc. **69**, 911 (1947).

[4] E. J. Cohn and J. T. Edsall, *Proteins, Amino Acids and Peptides* (Reinhold Publishing Corporation, New York, 1943).

[5] W. Kern, Zeits. f. physik. Chemie **A181**, 249, 283 (1935–36).

a given statistical state can be realized is given by

$$W=\left\{\frac{N!}{\prod_i n_i!}\right\}\left\{\prod_i\left[\frac{s!}{(s-i)!i!}\right]^{n_i}\right\}. \quad (4)$$

The first factor above is the number of ways we can choose our polymer molecules, specifying how many protons are present in each molecule but not specifying the manner in which the protons are distributed in a given molecule. The second factor is the product of terms each indicating the number of ways i protons can be distributed among the s sub-boxes of a given molecule.

The most probable distribution can be determined by setting the variation of $\ln W$ equal to zero, subject to the conditions of constraint expressed by Eqs. (1), (2), and (3). Making use of Stirling's approximation for the logarithm of a factorial quantity and taking the variation of $\ln W$, considering all of the n_i's as capable of undergoing variations, we find that

$$\delta \ln W=\sum_i\left\{-\ln n_i+\ln\frac{s!}{(s-i)!i!}\right\}\delta n_i=0. \quad (5)$$

Also

$$\delta N=\sum_i \delta n_i=0, \quad (6)$$

$$\delta B=\sum_i i\delta n_i=0, \quad (7)$$

$$\delta E=\sum \epsilon_i\delta n_i=0. \quad (8)$$

Introducing Lagrangian multipliers λ, μ, and ν in conjunction with Eqs. (6), (7), and (8) respectively, then combining the equations, and setting the coefficient of each of the variations, δn_i, equal to zero, we obtain the following:

$$-\ln n_i+\ln\frac{s!}{(s-i)!i!}-\lambda-i\nu-\mu\epsilon_i=0 \quad (9)$$

or

$$n_i=\frac{s!}{(s-i)!i!}\exp(-\lambda-i\nu-\mu\epsilon_i). \quad (10)$$

Evidently μ is equal to $1/kT$ and λ can be eliminated by dividing n_i by N and making use of Eq. (1). There remains, however, the problem of determining the significance of ν, which can be done as follows. Letting the entropy, S, equal $k \ln W_{\max}$, we have

$$S=k\ln W_{\max}=k\ln N!+k\sum_i n_i(\lambda+i\nu+\mu\epsilon_i+1)$$

$$=k\ln N!+Nk\lambda+k\nu B+k\mu E+Nk. \quad (11)$$

It is apparent that the term, $k \ln N!$, occurs because we assumed distinguishability of polymer molecules. Its presence is immaterial in our problem, however, since we are concerned only with the entropy of protons and not with that of the polymer molecules. Taking the differential of S, keeping N constant, we obtain

$$dS=Nkd\lambda+kBd\nu+kEd\mu+k\nu dB+k\mu dE. \quad (12)$$

But from Eqs. (1) and (10) we find that

$$dN=-Nd\lambda-Bd\nu-Ed\mu=0. \quad (13)$$

Hence, combining (13) with (12) it is seen that

$$dS=k\nu dB+k\mu dE. \quad (14)$$

Equation (14) verifies our previous surmise that $\mu=1/kT$ since $(\partial S/\partial E)_{N,B}=1/T$. The new fact which we establish is that

$$k\nu=(\partial S/\partial B)_{N,E}. \quad (15)$$

But from thermodynamics, we know that the chemical potential of the protons, μ_H, is given by

$$\mu_H=-T(\partial S/\partial B)_{N,E} \quad (16)$$

since B is the number of unionized protons distributed in our system. Hence

$$\nu=-(\mu_H/kT). \quad (17)$$

But at ionization equilibrium, the chemical potential of the protons associated with the polymer in unionized form must equal the chemical potential of the protons in the solution, so

$$\mu_H=\mu_H{}^0+kT\ln[H^+]=-kT\nu \quad (18)$$

where $\mu_H{}^0$ is a standard chemical potential. Therefore,

$$\nu=-(\mu_H{}^0/kT)-\ln[H^+] \quad (19)$$

or

$$\exp(-\nu)=C_1[H^+]$$

where (20)

$$C_1=\exp(\mu_H{}^0/kT).$$

Obviously ν is a linear function of the pH of the solution.

Before proceeding further it is necessary to say something about the energies (ϵ_i) associated with the different ions. Consider the s possible ionization steps, each supposed to involve a characteristic energy of ionization as follows:

$$\begin{aligned} H_sA&=H^++H_{s-1}A^-; \quad \Delta E_1,\\ H_{s-1}A^-&=H^++H_{s-2}A^{=}; \quad \Delta E_2,\\ &\vdots\\ HA^{(s-1)-}&=H^++A^{s-}; \quad \Delta E_s. \end{aligned} \quad (21)$$

Let us now assume that each ionization energy is the sum of two terms: first, an energy term associated with the removal of a proton from a carboxyl group, irrespective of its environment; and second, an energy term proportional to the charge resulting from previous

TABLE I.

Equivalent concentration c	Specific conductance $K\times10^4$	Equivalent conductance	pH calculated from conductance	pH measured by meter
9.021×10^{-2}	4.803	53.24	2.86	2.75
3.609×10^{-2}	2.624	72.71	3.12	3.06
1.443×10^{-2}	1.390	96.3	3.40	3.37
5.774×10^{-3}	0.7167	124.1	3.69	3.69
2.309×10^{-3}	0.3588	155.4	3.99	4.00
9.238×10^{-4}	0.1719	186.1	4.31	4.31
3.695×10^{-4}	0.0775	209.7	4.65	4.65
1.487×10^{-4}	0.0322	217	5.03	5.01

ionizations. On this basis we can write

$$\begin{aligned}\Delta E_1&=a,\\ \Delta E_2&=a+b,\\ \Delta E_3&=a+2b,\\ &\cdot\\ &\cdot\\ &\cdot\\ \Delta E_i&=a+(i-1)b,\\ &\cdot\\ &\cdot\\ &\cdot\\ \Delta E_s&=a+(s-1)b,\end{aligned}\tag{22}$$

where a is the inherent ionization energy of a carboxyl group and b is the energy necessary to pull the proton away from a singly charged ion. It is with respect to the second ionization term, b, that the theory takes on an approximate form. If the polymer molecules and ions can be considered coiled into spheres of fixed radius, then the term $(i-1)b$ in ΔE_i would be quite accurate, at least statistically. However, if the shape of the molecule depends upon the charge—and that is most likely the case—then expressions (22) can be considered a first approximation only. Kuhn, Künzle, and Katchalsky[6] recently investigated the effect of charge on ion size.

Let us now examine the relationship between the ionization energies and the energies of the ions. Looking at (21) it follows that

$$\Delta E_i=\epsilon_{s-i}-\epsilon_{s-i+1}+\epsilon_H\tag{23}$$

where ϵ_H is the energy of the hydrogen ion in solution, ϵ_{s-i+1} is the energy of an ion with $s-i+1$ protons attached, and ϵ_{s-i} that of an ion with $s-i$ protons. Then from (22) and (23)

$$\begin{aligned}\sum_{i=1}^{k}\Delta E_i&=\epsilon_{s-k}-\epsilon_s+k\epsilon_H\\ &=ka+((k-1)k/2)b.\end{aligned}\tag{24}$$

Therefore

$$\epsilon_{s-k}=ka+((k-1)k/2)b+\epsilon_s-k\epsilon_H.\tag{25}$$

Before introducing the above expression for ϵ_{s-k} into Eq. (10), it is convenient to define some new quantities, the use of which will simplify the final expressions. These new quantities and their definitions are

$$X=\exp(\nu-a/kT+\epsilon_H/kT)\tag{26}$$

and

$$Y=\exp(-b/kT).\tag{27}$$

Combining Eqs. (26) and (19) we obtain

$$X=K_0/[H^+]\tag{28}$$

where

$$kT\ln K_0=-\mu_H{}^0-a+\epsilon_H.\tag{29}$$

For reasons which will appear later, we shall call K_0 the "inherent ionization constant" of the polymer acid.

Rewriting Eq. (10), replacing i with $s-i$, and then combining Eq. (10) with Eqs. (25), (26), and (27), we find that

$$n_{s-i}=C_2\frac{s!}{(s-i)!i!}X^iY^{i(i-1)/2}\tag{30}$$

where C_2 is determined by use of Eq. (1).

The i'th ionization constant of the acid can now be readily calculated. Evidently

$$\begin{aligned}K_i&=\frac{[H^+]n_{s-i}}{n_{s-i+1}}\\ &=\frac{[H^+](s-i+1)}{i}Y^{i-1}X\\ &=\frac{s-i+1}{i}Y^{i-1}K_0.\end{aligned}\tag{31}$$

If $s=1$ (indicating a monobasic acid) then the ionization constant of that acid is just K_0. In general $K_1=sK_0$, the factor s appearing because of the s different hydrogens that can be initially ionized. From probability considerations alone, Maxwell and Partington[7] derived Eq. (31) without the factor Y^{i-1}. That factor appears here because of the different energies of ionization that

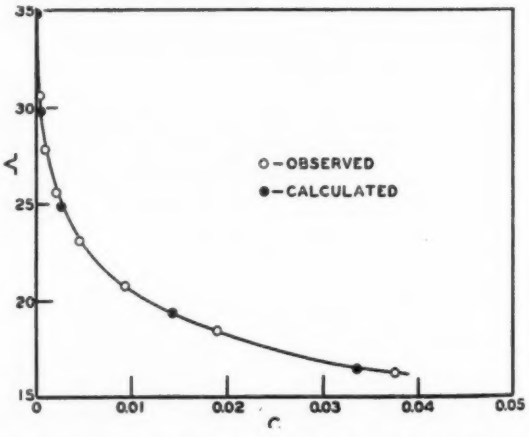

FIG. 1. Equivalent conductance *vs.* concentration for hydrolyzed copolymer of maleic anhydride and styrene.

[6] Kuhn, Künzle, and Katchalsky, Helv. Chim. Acta **31**, 1994 (1948).

[7] W. R. Maxwell and J. R. Partington, Trans. Faraday Soc. **31**, 922 (1935).

are involved. Bjerrum[8] considered the different energies for dibasic and tribasic acids, but he did not derive a general expression for acids of higher basicity. Cohn and Edsall[4] derived an expression for K_i substantially equivalent to that reported here. However, our theory can be readily modified to allow the calculation of the dissociation constants of acids whose groups are not energetically equivalent.

If c is the concentration of the acid in equivalents per liter, it is seen that the over-all degree of dissociation, α, is given by

$$\alpha=\frac{[H^+]}{c}=\frac{Ns-B}{Ns}=\frac{\sum in_{s-i}}{Ns}. \tag{32}$$

Making use of Eq. (30) it appears that

$$\frac{[H^+]}{c}=\frac{X+(s-1)X^2Y+\dfrac{(s-1)(s-2)}{2!}X^3Y^3+\cdots}{1+sX+\dfrac{s(s-1)}{2!}X^2Y+\dfrac{s(s-1)(s-2)}{3!}X^3Y^3+\cdots}. \tag{33}$$

Solving for c and noting that $X=K_0/[H^+]$, it follows that

$$c=K_0\left\{\frac{1+sX+\dfrac{s(s-1)}{2!}X^2Y+\cdots}{X^2+(s-1)X^3Y+\dfrac{(s-1)(s-2)}{2!}X^4Y^3+\cdots}\right\}. \tag{34}$$

Equation (34) is useful for computational purposes, since it enables one to calculate the value of c which would correspond to a specified hydrogen ion concentration, assuming that s, K_0, and Y are known. From a table or graph of such values, the hydrogen ion concentration corresponding to a given equivalent concentration of the acid can then be found by interpolation.

The expression for α given by Eq. (33) can be readily put into a closed form. Upon examination of the sum of the ratios n_i/n_s it is seen that

$$\sum\frac{n_i}{n_s}=1+sX+\frac{s(s-1)}{2!}X^2Y+\cdots. \tag{35}$$

This sum is the denominator of Eq. (33). It will further be noted by algebraic manipulation that

$$\alpha=\frac{X}{s}\frac{\partial\ln\sum\dfrac{n_i}{n_s}}{\partial X}=-\frac{X}{s}\frac{\partial\ln n_s}{\partial X}. \tag{36}$$

Equation (36) can evidently be written

$$\alpha=\frac{-1}{2.303s}\frac{\partial\ln n_s}{\partial pH}. \tag{37}$$

[8] N. Bjerrum, Zeits. f. physik. Chemie **106**, 219 (1923).

It is interesting to note what happens if $Y=1$, under which circumstances the electrostatic contribution to the ionization energy would be zero. In this instance it can be seen that

$$\frac{[H^+]^2}{c-[H^+]}=K_0 \tag{38}$$

which is precisely the same as the equation describing the ionization of a monobasic acid of concentration c. In other words, if $Y=1$, the ionization equilibria would be independent of intramolecular energy effects, and the system would act as if all the carboxyls were in separate molecules. It is for this reason that K_0 is given the name "inherent ionization constant."

EXPERIMENTAL

Experimental measurements were made in this laboratory on the hydrolyzed copolymer of maleic anhydride and styrene. This co-polymer was prepared by dissolving equimolar quantities of maleic anhydride and styrene in a 2 percent solution of benzoyl peroxide in xylene and allowing the mixture to react at 45°C. After the reaction was complete, the co-polymer was multiply extracted with xylene to remove low molecular weight materials and then dried under vacuum. The co-polymer was hydrolyzed by keeping it in contact with conductivity water at 80°C for about five hours.

Conductance data were obtained on aqueous solutions of the co-polymer using an alternating current wheatstone bridge of the type built and analyzed by Jones and Josephs.[9] A student-type conductance cell was used, its constant being 1.065 ± 0.001 cm^{-1}. The pH measurements were also made on the solutions using a Beckman pH meter. Results of the measurements together with a discussion appear in the next section.

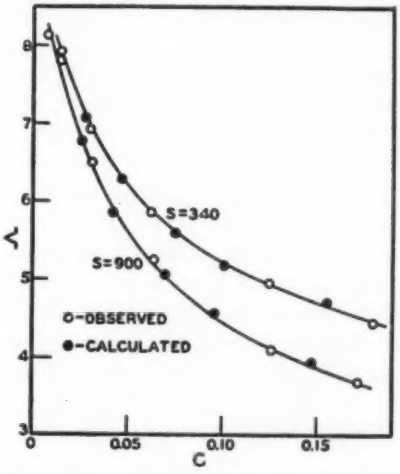

FIG. 2. Equivalent conductance *vs.* concentration for polyacrylic acid (Kern, reference 5).

[9] G. Jones and R. C. Josephs, J. Am. Chem. Soc. **50**, 1049 (1928).

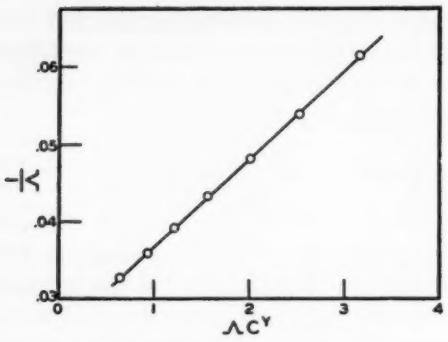

FIG. 3. Plot of $1/\Lambda$ *vs.* Λc^Y for hydrolyzed copolymer of maleic anhydride and styrene.

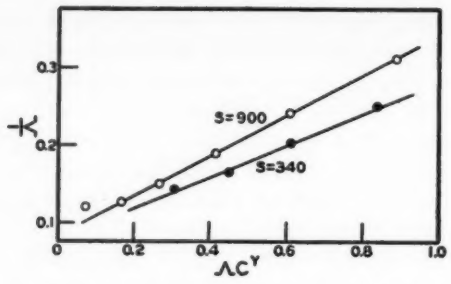

FIG. 4. Plot of $1/\Lambda$ *vs.* Λc^Y for polyacrylic acid (Kern[5]).

RESULTS AND DISCUSSION

Equivalent conductance values for aqueous polymer solutions are readily calculated from the measured specific conductances (corrected for solvent). As a first approximation, the degree of dissociation, α, is given by the ratio of the equivalent conductance, Λ, to the equivalent conductance at infinite dilution, Λ_0. Because a polymeric acid is exceedingly weak as far as over-all ionization is concerned, Λ_0 cannot be obtained by extrapolation of measured values. However, it is reasonable to assume that most of the conductance is due to the hydrogen ions, since the mobility of a polymeric anion should be very small.† Hence we will suppose that Λ_0 is equal to the limiting equivalent conductance of hydrogen ions.

It follows from the preceeding arguments and assumptions that a conductance measurement on a polymeric acid is substantially equivalent to a measurement of the hydrogen ion concentration, since the hydrogen ion concentration can readily be calculated by use of the equation

$$[H^+]=(1000K/\Lambda_0) \qquad (39)$$

where K is the specific conductance. This hydrogen ion concentration can then be compared with that measured directly by a *pH* meter.

The experimental results on the maleic acid-styrene co-polymer appear in Table I. In calculating *pH* values from the measured conductances, it was further assumed that the concentrations equal the activities.

It will be observed that except for the two most concentrated solutions, the agreement between the calculated and observed *pH* values is excellent. Actually the agreement is better than might be expected considering the approximations involved in the calculations. However, the results do support the assumption that the conductance of a polymeric acid is due almost entirely to the ionized hydrogens alone and that the anion contribution is negligible.

COMPARISON OF EXPERIMENT WITH THEORY

Assuming that conductance measurements do measure hydrogen ion concentrations according to Eq. (39), it should be possible to test the statistical theory outlined earlier. The basicity, s, of the acid used was taken to be 100, a value not unreasonable in light of other measurements made in this laboratory. Actually as long as s is sufficiently large, the results are not very sensitive to moderate variations in its value.

K_0 and Y were determined by a method of trial and error involving successive approximations. Graphical methods were found particularly useful in this connection. When the plot of Λ *vs.* c calculated from theory was found to agree with that obtained from experiment, it was supposed that the correct pair of values for K_0 and Y had been obtained.

For the copolymeric acid referred to above, it was found that K_0, the inherent ionization constant, equals 1.6×10^{-3} and Y equals 0.5. Decreasing the value of K_0 and increasing Y would not seriously affect the agreement with experiment, so it is quite possible that K_0 is really smaller and Y larger than indicated above. A plot of Λ *vs.* c showing experimental and theoretical points is given in Fig. 1. Although the agreement appears to be excellent, it must be remembered that three parameters were involved, namely: s, K_0, and Y, although s was not adjusted as arbitrarily as the other two.

Similar calculations were made on data furnished by Kern on two samples of polyacrylic acid. Kern reported results on acids for which $s=340$ and $s=900$. Using his values for the basicity and assuming further that K_0 is the same for both acids, calculations of K_0 and the two Y values were made with results indicated in Fig. 2. K_0 was found to be 5.32×10^{-5}, Y for the smaller acid was 0.76, and Y for the larger was 0.92. The relative order of values for Y is to be expected, since the term b in Eq. (27) should diminish with increasing anion radius, thus giving a larger Y value for the larger molecule.

An empirical relationship of some interest was also found for Λ as a function of c. Plotting $1/\Lambda$ *vs.* Λc^Y gave straight lines valid at all but the lowest concentrations. There is no simple theoretical explanation for this; in fact, the theory departs markedly from the empirical relationship for very dilute solutions. Accordingly, linear plots of $1/\Lambda$ *vs.* Λc^Y should not be used for extrapolations to infinite dilution to obtain Λ_0 values since no theoretical coherence could be obtained by such a procedure. Figures 3 and 4 show graphs of this type.

† Other experiments in this laboratory have confirmed this assumption.

Letters to the Editor

THIS section will accept reports of new work, provided these are terse and contain few figures, and especially few half-tone cuts. The Editorial Board will not hold itself responsible for opinions expressed by the correspondents. Contributions to this section should not exceed 600 words in length and must reach the office of the Managing Editor not later than the 15th of the month preceding that of the issue in which the letter is to appear. No proof will be sent to the authors. The usual publication charge ($4.00 per page) will not be made and no reprints will be furnished free.

Thermodynamic Properties of the Surface of Magnesium Oxide

GEORGE JURA
Department of Chemistry, University of California, Berkeley, California
October 18, 1949

PARKS and Kelley[1] measured the heat capacity of large crystals of magnesium oxide, while Giauque and Archibald[2] measured what is apparently a very fine crystalline form of the same solid. Giauque believes that their solid was so fine as to be colloidal.[3] From a comparison of these two results it is possible to obtain an approximate idea of all of the surface thermodynamic properties (free surface energy, entropy, and total surface energy) from 0°K to room temperature. Unfortunately the sample of the oxide used by Giauque and Archibald is no longer available. Thus it is impossible to give exact values for these surface thermodynamic properties. However, even with the uncertainty introduced by the lack of an area for the solid under consideration, a better idea of the thermodynamic properties of the surfaces of solids is obtainable than heretofore possible.

The entropy of the surface approaches zero as the temperature approaches 0°K.[3] Thus at any temperature the entropy per unit area, s, is

$$s=\frac{1}{\Sigma}\int_0^T \frac{1}{T}\Delta C_p aT,$$

where Σ is the area of the fine solid under consideration and ΔC_p is the difference in heat capacities of the fine and coarse powder. The heat content of the surface, h, at a temperature T_1 is

$$h_2=h_1+\int_{T_1}^{T_2}\Delta C_p dT,$$

where h_1 is the value of the heat content at T_1°K, etc. h_1 can be obtained from the difference in the heats of solution of the fine and coarse powders.

For this sample of magnesium oxide the difference is 888 cal. mole^{-1}.[3] If the surface energy of 1360 ergs cm^{-2} for the 100 plane of MgO computed by Lennard-Jones and Taylor[4] is correct, and it is assumed that the crystals used in the experiments of Giauque and Archibald exhibit only the 100 face, the area the oxide used by these workers is approximately 67 m^2 g^{-1}. This area figure is in accord with the reported areas of magnesium oxide which range from 10 to somewhat over 100 m^2 g^{-1}. Because of the uncertainty in the area of the sample of oxide used by Giauque and Archibald, the computed values for the surface properties are uncertain. The value actually used for these computations is 50 m^2 g^{-1}. The resulting values of the total and free surface energy are exhibited in Fig. 1.

The features of interest are the increase in both free and total surface energy. The above show that there is a feasible experimental method for the determination of the free surface energy or the surface tension of a solid. Also, there is experimental evidence

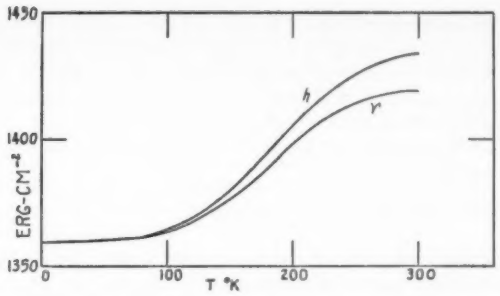

FIG. 1. The free surface energy, γ, and total surface energy, of magnesium oxide. The values are based on a computed value at 0°K of 1360 ergs cm^{-2} and an area of 50 m^2 g^{-1} for the sample of the oxide used by Giauque and Archibald.

that the computed surface energies of ionic solids at 0°K are not in any way comparable with the measured values of the liquids at high temperatures since there is an increase in the surface energy of the solid with increase in temperature. This increase is due to the fact that the presence of the surface increases the "characteristic temperature" of the solid. The above follows from a consideration of the vibration frequencies. Rodebush[5] has discussed this point on the application of an Einstein model to a supposed lattice structure of liquids.

[1] G. S. Parks and K. K. Kelley, J. Phys. Chem. **30**, 47 (1926).
[2] W. F. Giauque and R. C. Archibald, J. Am. Chem. Soc. **59**, 561 (1937).
[3] W. F. Giauque, J. Am. Chem. Soc. **71**, 3192 (1945).
[4] J. E. Lennard-Jones and P. A. Taylor, Proc. Roy. Soc. **109**, 476 (1925).
[5] W. H. Rodebush, J. Chem. Phys. **9**, 284 (1941).

On the Quasi-Chemical Theory of Order

YIN-YUAN LI
Department of Physics, University of Illinois, Urbana, Illinois
October 13, 1949

BELOW Eq. (8) of my paper "Quasi-chemical theory of order for the copper gold alloy system,"[1] the statement "$\mu_{\lambda i}=\mu$ for all λ and i, when $\theta_1=\theta_2=\cdots=\theta$" is true for the cases mostly used in practical calculations but *not* in general. By investigating Eqs. (4) and (5) of reference 1 we can only draw the conclusion that the paramenters of *geometrically equivalent* sites are equal when $\theta_\lambda=\theta$. For the sake of simplicity in calculating work the group is usually chosen in such a manner that most sites in the group are geometrically equivalent. For example, in the tetrahedron group taken in reference 1 all the four sites are equivalent and therefore $\mu_i=\mu$ ($i=1, \cdots, 4$) when $\theta_\lambda=\theta$. A different example is the group taken from a body-centered cubic alloy and containing a central site with its eight nearest neighbors and six

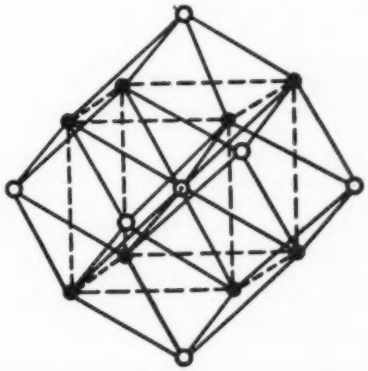

FIG. 1. A local group taken from a body-centered lattice containing a center site, denoted by ⊙ in the figure, its first shell sites, ●'s, and 6 sites, ○'s, from the second shell. Solid lines stand for the nearest interactions and dotted lines for the lattice frame.

from the next nearest ones.[2] It has not only one but three sets of equivalent sites; hence even in disordered states we must take care of three parameters for the 15 sites, i.e., μ_1 for the central site, μ_2 for each of its first shell sites and μ_3 for each of the six sites taken from second shell (see Fig. 1.)

It is still quite easy to prove that the disordered distribution is always a solution of

$$\sum_{\lambda} c_{\lambda} \sum_{(h)} \ln\mu_{\lambda i} - r_h(D \ln(\theta_h/1-\theta_h) - C) = 0.$$

We see that when $\theta_h = \theta$ the parameter of the ith site has the same value no matter to which sublattice it belongs, i.e., $\mu_{\lambda i} = \mu_i$ $(\lambda = 1, \cdots, l)$. It follows that

$$\sum_{\lambda} c_{\lambda} \sum_{(h)} \ln\mu_{\lambda i} = \sum_{\lambda} c_{\lambda} \sum_{(h)} \ln\mu_i = r_h \sum_{i} \ln\mu_i,$$

when $\theta_h = \theta$. Therefore the m equations of the above set reduce to the equation

$$\sum_{i} \ln\mu_i - D \ln(\theta/1-\theta) + C = 0.$$

The latter can always be satisfied because of the arbitrariness of C.

[1] Y-Y Li, J. Chem. Phys. **17**, 447 (1949).
[2] Some results of an approximation using this group have been published in the article by Y-Y Li, Phys. Rev. **76**, 972 (1949).

Spectral Changes of Dyes in Colloidal Solutions of Hydrous Oxides

BENJAMIN CARROLL AND ARTHUR W. THOMAS
Newark Colleges of Rutgers University and Columbia University, Newark, New Jersey
October 10, 1949

RECENT publications have shown that dyes which do not follow Beer's law will exhibit spectral changes when mixed with colloidal solutions. This effect is attributable to the existence of an equilibrium between two or more forms of the dye, one of which is preferentially adsorbed by the micelles.[1,2] It appears to be generally accepted that dyes that follow Beer's law exhibit only slight spectral change in colloidal solutions although it has been shown that native albumin forms complexes with simple dye anions.[3]

We have obtained some results with dyes that follow Beer's law which indicate that single dye ions that are bound by hydrous oxides show a spectral absorption curve distinctly different from that of the free ion. The addition of salts causes the displacement of the bound dye and the absorption spectrum is shifted back toward that of the free dye ion.

The spectral change of Orange I caused by colloidal hydrous alumina is shown in Fig. 1. The molar extinction coefficient at 475 mμ shows a decrease of about 40 percent in the presence of the hydrous oxide and the absorption maximum is shifted some 30 mμ toward the violet. The displacing ability and hence the affinity for competing anions to form complexes with the hydrous alumina may be measured by the extent of the reversal of the absorption spectrum towards that for the free dye. In the case of sulphate ions, complete displacement of the dye was observed when the total concentration of sulphate was comparable to that for dye.

When dye and sol are mixed, the greater part of the spectral change takes place within a few minutes. This rapid process is followed by a slow uptake of the dye by the colloidal particle suggesting penetration of the micelles by the dye ions. About ten to twenty hours were required to reach the equilibrium values given in the figure.

That the sorbed dye ions on the surface are in mobile equilibrium with the ions in the bulk of the solution is shown by the rapid response of the colloidal solution to temperature changes. An increase of a few degrees caused an increase of several percent in the optical density, indicating a desorption process. Bringing the colloidal solution back to its original temperature brought the optical density back to its former value within a few minutes.

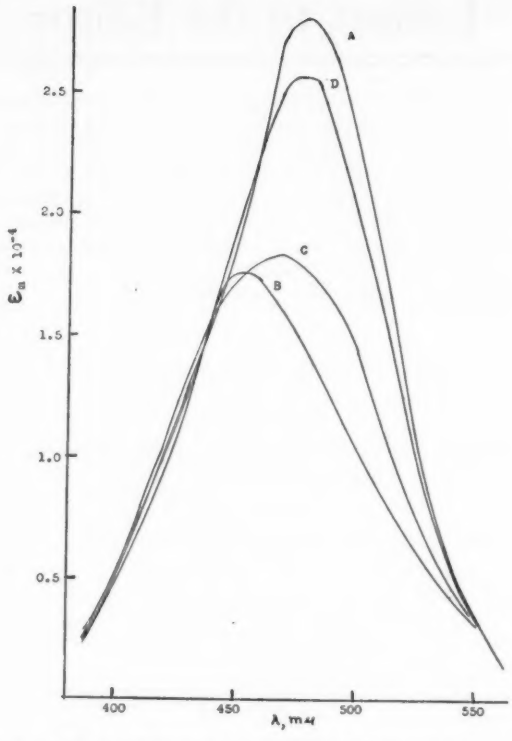

FIG. 1. Molar Extinction Coefficient of 2.0×10^{-5}M Orange I. (A) Dye and acetate buffer at pH 4.0. (B) Dye and colloidal solution of hydrous alumina peptized by HCl. pH 3.9; Al_2O_3 content 0.880 g/liter. (C) Same as (B) in presence of 0.01M KCl. (D) Same as (B) in presence of 0.01M KAc. Addition of 0.01M K_2SO_4 to (B) gave curve identical with (A).

In the case of dyes which do not follow Beer's law, the gradual changes in the intensity, position and shape of absorption bands generally indicate an increase in the proportions of the polymeric form of the dye. This is brought on by the colloidal particles combining with the polymeric dye molecules as a result of electrostatic and van der Waals forces. The spectral changes which we have observed with simple dye anions in the presence of hydrous oxides, however, is consistent with the postulate of chemical bonding as suggested previously by one of us.[4]

The use of suitable dye ions to study changes in colloidal solutions of hydrous oxides offers several advantages over the usual procedure employing e.m.f. measurements. It should be noted that a "suitable dye ion" is one whose spectral characteristics are not altered by the salt and pH changes involved in a particular investigation. Some of these advantages are the following:

1. Increase in sensitivity of detecting changes. For example, the colloidal solution whose effect on Orange I is given in Fig. 1, showed a change of about a 0.1 of a pH unit upon the addition of the salts, whereas, the optical density of the system was altered considerably.

2. It should be possible to investigate readily those systems whose dispersed particles are not quite large enough to be considered micellar, and yet are outside the crystalloidal range.

3. Several methods are available for determining the extinction coefficient for the sorbed dye ions, thus making it possible to express quantitatively the exchange processes that occur in colloidal solutions in terms of number of molecules.

[1] Merrill and Spencer, J. Am. Chem. Soc. **70**, 3683 (1948).
[2] Michaelis and Granick, J. Am. Chem. Soc. **67**, 1212 (1945); also see S. E. Sheppard and A. L. Geddes, J. Chem. Phys. **13**, 63 (1945).
[3] Klotz, Triwush, and Walker, J. Am. Chem. Soc. **70**, 2935 (1948).
[4] A. W. S. Thomas, *Colloid Chemistry* (McGraw-Hill Book Company, Inc., New York, 1934).

The Mechanism of Oxidation of Ferrous Sulfate by γ-Rays in Aerated Water

F. H. KRENZ AND H. A. DEWHURST
National Research Council, Chalk River, Ontario, Canada
October 3, 1949

WE have studied the oxidation of ferrous ions by γ-rays absorbed in dilute aqueous solutions of ferrous ammonium sulfate saturated with air and in solutions from which the air was removed by exhaustive pumping. We have been particularly interested in establishing the role of oxygen in the mechanism of this oxidation.

The most feasible primary process in both aerated and air-free solutions appears to be

$$H_2O \xrightarrow{\gamma\text{-rays}} HO + H, \qquad (1a)$$

followed in aerated solutions by

$$H + O_2 \rightarrow HO_2. \qquad (1b)$$

The oxidation of ferrous ions in solution then proceeds according to reactions originally proposed to account for the ferrous ion catalyzed decomposition of aqueous hydrogen peroxide.[1]

$$Fe^{++} + HO \rightarrow HO^- + Fe^{+++}, \qquad (2)$$

$$Fe^{++} + HO_2 \rightleftharpoons HO_2 + Fe^{+++}, \qquad (3a)$$

$$H^+ + HO_2^- \rightleftharpoons H_2O_2, \qquad (3b)$$

$$Fe^{++} + H_2O_2 \rightarrow HO + HO^- + Fe^{+++}. \qquad (4)$$

Reactions (3a), (3b), and (4) combine to oxidize ferrous ions quantitatively in strongly acid solutions. We have found that in solutions 0.1 N or higher in sulfuric acid ferrous ions are oxidized quantitatively by sufficiently large doses of γ-radiation. In these studies we have made our solutions 0.8 N in sulfuric acid to conform to earlier work.[2-4] The solutions were irradiated with the γ-rays from a 2-curie radium source.

Our experimental results are summarized in Fig. 1. The yield of the oxidation is expressed in terms of the number of ferrous ions oxidized per 100 ev of γ-ray energy absorbed by the solution. Since the ferrous sulfate system has been accurately established by Miller[3b] as a dosimeter for x- and γ-radiation, it was possible to estimate the energy absorbed in our samples merely by determining the number of ferrous ions oxidized in a sample of suitable concentration.

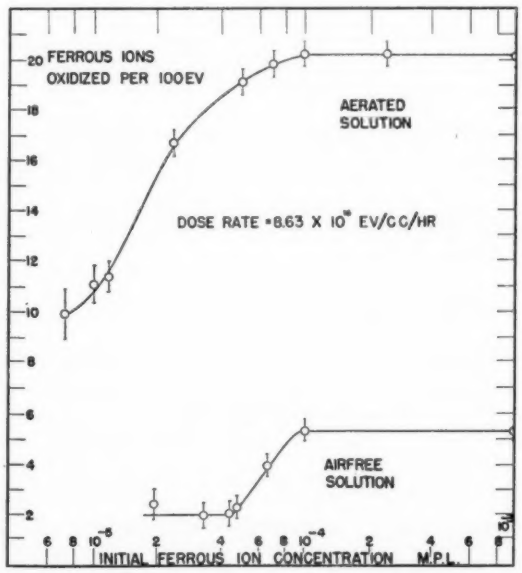
20 FERROUS IONS OXIDIZED PER 100 EV
AERATED SOLUTION
DOSE RATE = 8.63 X 10^16 EV/CC/HR
AIRFREE SOLUTION
INITIAL FERROUS ION CONCENTRATION M.P.L.

FIG. 1. The yield of ferrous ions oxidized per 100 ev of γ-ray energy absorbed in aqueous solutions 0.8 N in H_2SO_4 as a function of the initial ferrous ion concentration in (a) aerated solutions and (b) solutions from which the air had been removed by exhaustive pumping.

The yields were determined by plotting the amount of oxidation as a function of the energy absorbed in the solution and taking the tangent to this curve at the origin. Each point on Fig. 1 represents the average of a number of experiments.

Above a starting concentration of 10^{-4} m.p.l. the yield of oxidation was independent of the ferrous ion concentration as has been well established.[2-4] Below this concentration the yield falls off with concentration presumably because of the recombination of HO and HO_2. The kinetic consequences of recombination have been studied and will be reported elsewhere.

We wish to point out here that the reduction of the yield above 10^{-4} m.p.l. by a factor of approximately 4 when the oxidation is performed in air-free water can be predicted from Eqs. (1)–(4). Inspection of these equations will show that for every free radical pair formed in aerated solution 4 ferrous ions are oxidized. In air-free water no HO_2 could be formed by (1b) and the oxidation should be described by reaction (2). Only one ferrous ion would then be oxidized per free radical pair formed.

A summary by Miller[3a] of previous work on this subject shows that attempts to remove oxygen from ferrous sulfate solutions have reduced the oxidation yield by no more than a factor of 2.6. We attribute this to incomplete removal of oxygen. We have found great difficulty in removing oxygen from these solutions, and have noticed that the difficulty appears to increase with increasing ferrous ion concentration.

A detailed account of this work will be submitted to the Canadian Journal of Research. We are very much indebted to Dr. Miller for discussions and for access to his unpublished results.

[1] F. Haber and J. Weiss, Proc. Roy. Soc. **A147**, 332 (1930).
[2] H. Fricke and S. Morse, (a) Am. J. Roentgenology and Radium Therapy **18**, 430 (1927); (b) Phil. Mag. **7**, 129 (1929).
[3] N. Miller, (a) Nature **162**, 448 (1948); (b) J. Chem. Phys. (to be published).
[4] N. A. Shishacow, Phil. Mag. **14**, 198 (1932).

Surface Tension of Small Droplets from Volmer and Flood's Nucleation Data

V. K. LAMER
Chemistry Department, Columbia University, New York, New York
AND
G. M. POUND
Metals Research Laboratory, Carnegie Institute of Technology, Pittsburgh, Pennsylvania
October 28, 1949

CURRENT theoretical work on the effect of droplet size on surface tension predicts that the surface tension of a droplet smaller than about 200A in diameter should be appreciably different from the value obtained by measurements on the bulk phase. Using a quasi-thermodynamic approach, Tolman[1] predicted a decrease in surface tension at small droplet sizes, and this result is supported by a statistical mechanical treatment due to Kirkwood and Buff.[2] Martynov,[3] on the other hand, takes the view that surface tension should increase with droplet curvature.

As yet, there seems to be no direct experimental method for confirmation of these theoretical results, but the authors suggest that insight into this problem might be gained by a consideration of nucleation phenomena. Volmer and Flood[4] have measured the critical supersaturation pressure necessary for spontaneous production of fog at a given temperature for a series of vapors by an adiabatic expansion method. Their data are well described in terms of directly measured properties of the substance by means of the kinetic treatment of Becker and Döring.[5,6] According to their treatment, the critical size for a stable droplet is about 20A in diameter. This means that an embryo droplet that has attained this size through a series of statistical fluctuations will, in general, grow to become a macroscopic drop of liquid. Further, the exponential function expressing nucleation rate is such that critical pressure necessary for spontaneous nucleation of droplets from

TABLE I.

Vapor	Number of molecules in stable nucleus	Nucleus radius r in angstroms	σ^* $=\frac{\sigma}{\sigma_0}$	P/P_∞ calculated using σ	P/P_∞ calculated using σ_0	P/P_∞ measured
Water, 275.2°K	80.0	8.9	0.82	2.9	4.2	4.2±0.1
Water, 261.0°K	72.0	8.0	0.80	3.2	5.0	5.0
Methanol, 270.0°K	32.0	7.9	0.80	1.5	1.8	3.0
Ethanol, 273.0°K	128.0	14.2	0.88	2.0	2.3	2.3
n-propanol, 270.0°K	115.0	15.0	0.88	2.6	3.2	3.0
Isopropyl alcohol, 265.0°K	119.0	15.2	0.88	2.4	2.9	2.8
n-butyl alcohol, 270.0°K	72.0	13.6	0.88	3.5	4.5	4.6
Nitromethane, 252.0°K	66.0	11.0	0.85	4.2	6.2	6.0
Ethyl acetate, 242.0°K	40.0	11.4	0.85	6.4	10.4	8.6 to 12.3**

* Ratio of surface tension predicted from Tolman's results to the surface tension measured in the bulk liquid phase.
** The higher value is assumed to be more nearly correct.

supersaturated vapor is strongly dependent on the surface tension. This is illustrated by Fig. 1 where calculated values of the ratio of critical supersaturation pressure to equilibrium vapor pressure of the bulk liquid phase, P/P_∞, are plotted as a function of assumed values of surface tension, σ, for the case of condensing water vapor at 275.2°K. The surface tension values are assumed for the purpose of calculating P/P_∞ as a function of σ by means of the Becker and Döring[5] treatment. It is seen that a value of surface tension very close to that measured for the bulk liquid phase is required if calculated and experimental values of P/P_∞ are to agree.

The present authors have computed the critical droplet size for a number of vapors by the Becker and Döring[5] method, using the measured critical supersaturation ratio and the value for surface tension measured on the bulk liquid phase. Then, using Tolman's[1] theoretical results for decrease in surface tension with droplet radius, a value for surface tension at the critical droplet size was obtained. This new value of σ was used to calculate P/P_∞ for comparison with the experimental quantity. The results are summarized in Table I. It is seen that in most of the cases fair agreement is obtained between measured values of P/P_∞ and values calculated using the surface tension σ_0 as measured on the bulk liquid phase. On the other hand, values of P/P_∞ calculated using the surface tension σ, as predicted from Tolman's results, are in poor agreement with the data. The inconsistency between the work on nucleation and the current theoretical studies on surface tension of droplets is evident. It may be that some revision of the present theoretical approach is in order.

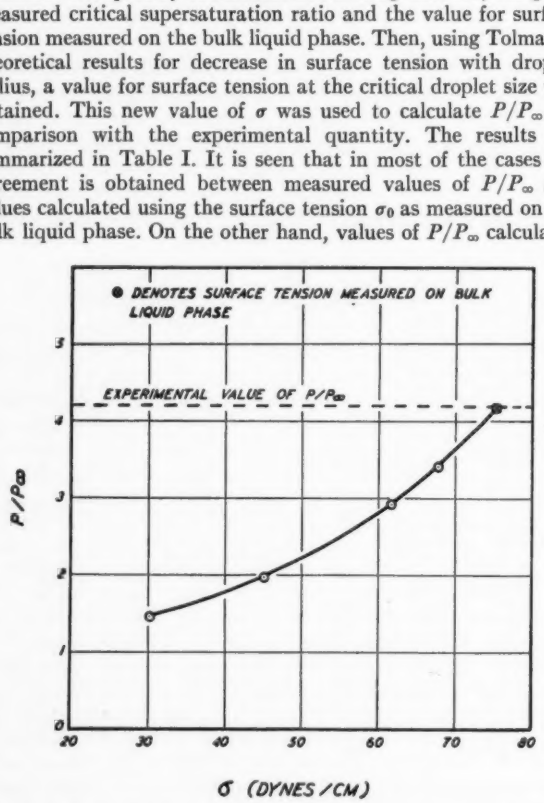

FIG. 1. Calculated values of critical supersaturation pressure ratio *versus* assumed values of surface tension for the case of condensing water vapor at 275.2°K.

It is interesting to note that in the two anomalous cases, methanol and ethyl acetate, the number of molecules per stable nucleus is considerably smaller than in the other cases. Further, these anomalies could be resolved by employing a value for surface tension somewhat higher than that measured on the bulk liquid phase.

[1] R. C. Tolman, J. Chem. Phys. **17**, 333 (1949).
[2] J. G. Kirkwood and F. P. Buff, J. Chem. Phys. **17**, 338 (1949).
[3] V. Martynov, Zhur. Fiz. Khim. **23**, 278–80 (1949).
[4] M. Volmer and H. Flood, Zeits. f. physik. Chemie (A) **170**, 273 (1934).
[5] R. Becker and W. Döring, Ann. d. Physik **24**, 719 (1935).
[6] M. Volmer, *Kinetik der Phasenbildung* (Edwards Brothers, Inc., Ann Arbor, Michigan, 1945), Chapter 4.

A Theoretical Calculation of the Parameters α and β Used in the Molecular Orbital Method

J. VAN DRANEN AND J. A. A. KETELAAR
Laboratory for General and Inorganic Chemistry, University of Amsterdam, Netherlands
October 31, 1949

THE molecular orbital method in the usual L.C.A.O. approximation enables us to express the energy of the π-electrons in two parameters: the Coulomb integral

$$\alpha \equiv \int \varphi_1 H \varphi_1 d\tau$$

and the exchange integral

$$\beta_{12}' \equiv \int \varphi_1 H \varphi_2 d\tau - S_{12}\alpha', \quad S_{12} = \int \varphi_1 \varphi_2 d\tau.$$

φ_1 and φ_2 are the P_z-orbitals of adjacent C atoms.

Hitherto β_{12}' (and α) were empirical parameters. There is, however, a large discrepancy between the values calculated for β_{12}' from resonance energies and from electronic-transition processes. We have therefore tried to calculate α and β_{12}' theoretically to get some insight into the nature of this discrepancy.

For benzene we put for the Hamilton operator:

$$H = -\frac{h^2}{8\pi^2 m}\nabla^2 + \sum_k H_k + V_\pi.$$

For the part

$$-\frac{h^2}{8\pi^2 m}\nabla^2 + \sum_k H_k,$$

we refer to Goeppert-Mayer and Sklar;[2] V_π is the potential energy of one π-electron (ν) in the field of the other five π-electrons (μ) which are supposed to be distributed among the six P_z-orbitals of the C atoms. The electron is also supposed to be equally distributed, which is numerically equivalent to a localization on one carbon atom. This gives

$$V_\pi = \tfrac{5}{6}e^2 \sum_\mu \frac{1}{r_{\nu\mu}} \quad \text{and} \quad \int \varphi_1(\nu) V_\pi \varphi_2(\nu) d\tau = V_\pi \cdot S_{12}.$$

For this calculation of α and β_{12}' we further need integrals as

$$\int \varphi_i(\nu)\varphi_j(\nu) H_k(\nu) d\tau$$

and

$$\int \varphi_i(\nu)\varphi_j(\nu)\frac{e^2}{r_{\nu\mu}}\varphi_k^2(\nu) d\tau.$$

They are reduced to known integrals by substituting

$$S_{ij}\int \varphi_m^2(\nu)\cdots \quad \text{for} \quad \int \varphi_i(\nu)\varphi_j(\nu)\cdots.$$

$\varphi_m(\nu)$ is a virtual P_z function located midway between the original i and j functions.[3,4]

With this approximation and using the values of Parr and Crawford,[5] we obtain as a value for $\alpha - 4.20$ ev and for $\beta_{12}' - 2.42$ ev.

The only experimental data we have used are the effective nuclear charge for a C atom $Z = 3.18$[6] and the C–C distance 1.39A in benzene.[7] In the calculation of α we used for $W2p$, the energy of a $2p$-electron in the unexcited carbon atom, instead of the experimental ionization potential of -11.24 ev, a value of -10.82 ev calculated theoretically with the effective nuclear charge of 3.18; β_{12}' is independent of $W2p$.

From these and analogous calculations we conclude:

(1) β_{12}' is with good approximation, independent of the potential field of the r-electrons (the term $V_r \cdot S_{12}$ cancels).

(2) For a definite C–C bond β_{12}' is proportional to S_{12}. This was already known from empirical data.[8]

(3) β_{12}' is strongly dependent on the environment of the bond in the molecule (e.g., for naphthalene $\beta_{12}' = -1.93$ ev and $\beta_{910}' = -2.26$ ev).

(4) The quantitative results of the molecular orbital method are improved if we consider as a second approximation also the exchange and lack of orthogonality integrals between non-adjacent atoms. Following our method with a, for this correction reasonable approximation, we obtain for benzene

$$\beta_{13}' = \frac{S_{13}}{S_{12}}\beta_{12}'; \quad \beta_{14}' = \frac{S_{14}}{S_{12}}\beta_{12}',$$

$$(S_{12} = 0.26; \quad S_{13} = 0.04; \quad S_{14} = 0.02).$$

In this second approximation we compute for the resonance energy (R-E.) of benzene, $0.76\beta_{12}'$ (zero-approximation R.E. $2\beta_{12}$, first-approximation R.E. $1.06\beta_{12}'$[1]). With the experimental value for the R.E. (39 kcal.[9]), we compute for $\beta_{12}' = -2.23$ ev. The calculated R.E. with our theoretical value for β_{12}' is 42 kcal.

For the energy difference ΔE between the ground state and the first excited state we evaluate in second approximation $2.14\beta_{12}'$, which gives 2410A with our theoretical value of -2.42 ev as compared with the experimental value of 2550A.

For the quantity ΔE/R.E., which is independent of β_{12}', we obtain experimentally, 2.86; calculated, 2.82. Thus the well-known discrepancy between the spectroscopical and the thermochemical value is eliminated in our second approximation.

For ethene we find with the same method $(S_{12} = 0.287)\beta_{12}' = -2.95$ ev, in agreement with the experimental spectroscopical value $\beta_{12}' = -3.0$ ev[10] (They are, however, not strictly comparable.) The theoretical value for α is 8.0 ev.

For naphthalene, we compute in second approximation, R.E. is $1.22\beta_{12}'$; for anthracene, $1.61\beta_{12}'$. We have taken into account β_{13}', S_{13}' etc., but β_{12}', contrary to our third conclusion, was not varied with the environment in the molecule.

For the ultraviolet spectrum, we obtain with the calculated values of ΔE/R.E. with the experimental values of R.E.:[9]

	0° approx.	1° approx.	2° approx.	obs.
benzene	7143A	3630A	2600A	2550A
naphthalene	11,430A	5461A	3524A	2750A
anthracene	17,212A	8236A	5037A	3800A.

A further improvement might be obtained from a variation of β_{12}'.

If this method leads to reasonable results it will, in the future, be possible to calculate β_{12}' for an arbitrary bond in a molecule by a simple addition if we know the internuclear distances of that molecule, and to expand this method, e.g., to heterocyclic molecules.

[1] G. W. Wheland, J. Am. Chem. Soc. **63**, 2025 (1941).
[2] M. Goeppert-Mayer and A. L. Sklar, J. Chem. Phys. **6**, 645 (1938).
[3] A. L. Sklar, J. Chem. Phys. **7**, 984 (1939).
[4] A. London, J. Chem. Phys. **13**, 396 (1945).
[5] R. G. Parr and B. L. Crawford, J. Chem. Phys. **16**, 1049 (1948).
[6] C. Zener, Phys. Rev. **36**, 51 (1930).
[7] V. Schomaker and L. Pauling, J. Am. Chem. Soc. **61**, 1769 (1939).
[8] Mulliken, Rieke, and Brown, J. Am. Chem. Soc. **63**, 41 (1941).
[9] L. C. Pauling, *Nature of the Chemical Bond* (Cornell University Press, Ithaca, New York, 1945).
[10] C. C. J. Roothaan and R. S. Mulliken, J. Chem. Phys. **16**, 1049 (1948).

Infra-Red Absorption Spectra at Low Temperatures*

D. H. Rank and D. W. E. Axford
Spectroscopy Laboratory, The Pennsylvania State College, State College, Pennsylvania
October 17, 1949

A VERY and Ellis[1] and Avery and Morrison[2] have shown that for certain hydrocarbons many of the infra-red absorption bands are very considerably narrowed when the temperature is reduced. The above authors give conclusive evidence that Bjerrum's formula is valid even in the liquid and solid state for the particular cases which they have investigated.

Walsh and Willis[3] have recently questioned the phenomenon of temperature narrowing of infra-red bands in a single phase (liquid or solid) attributing the effect to change in phase. Study of the papers of Avery and Ellis[1] and Avery and Morrison[2] does not support the contention of Walsh and Willis.[3] Comparison of the low temperature spectrum of Avery and Ellis with A.P.I. Spectrogram No. 245 for liquid 2, 2 dimethylbutane is completely unjustified since comparison of line breadth is impossible due to widely different instrumental factors entering into the two above mentioned spectra.

We have recently investigated[4] the infra-red absorption spectra of a number of hydrocarbons at different temperatures through much of the liquid and solid range. Our investigation was concerned chiefly with the occurrence of rotational isomers and not in a discussion of band breadth. However, in the case of all the spectra which we have investigated, one of the most prominent features was the distinct sharpening of the bands as the temperature was reduced.

Reduction of band width with decreasing temperature in the liquid phase was immediately apparent since in many cases double bands were merely resolved as shoulders at room temperature while at low temperature clean resolution of these doublets was achieved. In addition, the narrowing of the bands was considerably greater than mere appearance of the curves would indicate. (Since the cell thickness is sensibly constant and the density of the liquid increases with decrease of temperature, more molecules are in the absorbing beam at low temperature than at high temperatures. The effect of increased absorbing path would be to decrease the transmission and make the bands appear wider from this cause alone. For quantitative measurements it is of course necessary to compare band widths at the same percentage transmission as Avery and Ellis[1] have done.)

The curves shown in our paper,[4] Figs. 1 to 5, for *n*-pentane, *n*-hexane, *n*-heptane, 2 methylbutane and 2:3 dimethylbutane are reproduced on too small a scale to show clearly the large effect of temperature on narrowing of these absorption bands.

We wish to point out further that the narrowing of Raman lines at low temperatures in liquids can be easily and unequivocally observed for a number of the hydrocarbons. Microphotometer curves of the Raman spectrum of liquid *n*-butane at 300°K and 147°K obtained by one of us[5] clearly show the effect of temperature in narrowing these bands.

We are not aware of any incontrovertible evidence in the literature where distinct rotational fine structure has been found in the infra-red absorption spectrum of a liquid. The situation with respect to solids is similar.[6] In spite of the lack of direct spectroscopic evidence for the existence of discrete rotational and rotational vibrational states in a liquid, the breadth and temperature behavior of many infra-red bands yields indirect spectroscopic evidence for rotation. It seems plausible that discrete rotational structure is not to be expected in a liquid since the pressure broadening of the lines would be extremely large.

The observation of Avery and his co-workers[1,2] that quantitatively certain infra-red bands in liquids and solids follow Bjerrum's formula with regard to their breadth as a function of temperature can only be considered to be fortuitous in its strict quantitative aspect. It is certain that at the present time our

knowledge of the liquid state is insufficient to give a strictly quantitative theoretical treatment to this problem, but it should be expected that the behavior of gases should furnish a first crude approximation.

Finally we wish to emphasize the point that many of the infrared absorption bands in a liquid (for small hydrocarbon molecules) sharpen very markedly as the temperature is decreased. A similar phenomenon can also be observed with regard to some Raman lines of certain liquids.

* This research was carried out on Contract N6onr-269, Task V, of the ONR.
[1] W. H. Avery and C. F. Ellis, J. Chem. Phys. **10**, 10 (1942).
[2] W. H. Avery and J. R. Morrison, J. App. Phys. **18**, 960 (1947).
[3] A. Walsh and J. B. Willis, J. Chem. Phys. **17**, 838 (1949).
[4] D. W. E. Axford and D. H. Rank, J. Chem. Phys. (to be published).
[5] Szasz, Sheppard, and Rank, J. Chem. Phys. **16**, 704 (1948).
[6] L. F. H. Bovey and G. B. B. M. Sutherland, J. Chem. Phys. **17**, 843 (1949).

Carrier-Free Radioisotopes from Cyclotron Targets. III. Preparation and Isolation of $Sb^{122, 124}$ from Tin*

ROY D. MAXWELL,** HERMAN R. HAYMOND, WARREN M. GARRISON, AND JOSEPH G. HAMILTON

Crocker Laboratory, Radiation Laboratory and Divisions of Medical Physics, Experimental Medicine, and Radiology, University of California, Berkeley and San Francisco, California

October 3, 1949

DEUTERON bombardment of tin produces[1] $Sb^{122, 124}$ by the nuclear reactions $Sn^{122}(d, 2n)Sb^{122}$, $Sn^{124}(d, 2n)Sb^{124}$. The present paper reports a carrier-free method of isolating these activities from the target element and from the radioisotopes of indium (n, p) and cadmium (n, α) which are formed concurrently by secondary neutrons produced by the 19 Mev deuteron beam of the 60-inch medical cyclotron at Crocker Laboratory. Other possible[2] shorter-lived radioisotopes of antimony were allowed to decay out prior to the chemical separation.

The target was a block of C.P. tin, soft soldered to a water-cooled copper plate. It was bombarded with 19 Mev deuterons for a total of 83.1 μa-hr. in the 60-inch cyclotron at Crocker Laboratory. The bombarded surface was removed by milling.

0.5 gram of turnings were dissolved in a minimum volume of aqua regia. 12 N HCl was added to destroy excess HNO_3 and the solution was diluted to approximately 25 ml of 0.1 N HCl. 10 mg of cadmium were added and precipitated with H_2S after addition of 1 g of oxalic acid to prevent[3] precipitation of tin sulfide. The antimony activity carried quantitatively. The CdS was dissolved in HCl plus oxalic acid, reprecipitated with H_2S, dissolved in a minimum volume of 12 N HCl and transferred to an all-glass distilling flask.[4] 16 ml of 60 percent $HClO_4$ were added and traces of tin were distilled[3] at 200°C during the gradual addition of 10 ml of 12 N HCl. Approximately 98 percent of the carrier-free antimony remained in the residue. The antimony activity was then distilled with the gradual addition of 10 ml of 40 percent HBr. The distillate contained 95 percent of the $Sb^{122, 124}$. Indium and cadmium were retained in the residue.

To obtain carrier-free radio-antimony in isotonic saline for subsequent biological investigation, the distillate was treated with aqua regia to destroy HBr and evaporated to dryness on 40 mg of NaCl. The activity dissolved quantitatively with the addition of 5 ml of distilled water.

The decay curve was followed for 300 days and showed two periods: 2.8-day Sb^{122} and 60-day Sb^{124}. One month after bombardment, the activity contained only 60-day Sb^{124}; mass absorption measurements in Pb showed the 1.7 Mev gamma-ray previously reported.[3] A tracer amount of carrier-free antimony was added to a solution containing milligram amounts of tin, antimony and indium; the antimony fraction was separated chemically[5] and contained 98 percent of the activity.

We wish to thank Professor G. T. Seaborg for many helpful suggestions, the 60-inch cyclotron crew for bombardments and Mrs. Alberta Mozley and Mrs. Helen Haydon for technical assistance.

* This document is based on work performed under auspices of the Atomic Energy Commission.
** Lieutenant Colonel, U. S. Army, now stationed at Walter Reed Hospital, Washington, D. C.
[1] J. J. Livingood and G. T. Seaborg, Phys. Rev. **55**, 667 (1939).
[2] G. T. Seaborg and I. Perlman, Rev. Mod. Phys. **20**, 585 (1948).
[3] W. Rall and R. G. Wilkinson, Phys. Rev. **71**, 321 (1947).
[4] J. A. Scherrer, J. Research Nat. Bur. Stand. **21**, 95 (1938).
[5] F. P. Treadwell and W. T. Hall, *Analytical Chemistry* (John Wiley & Sons, Inc., New York, 1942), Vol. II.

Carrier-Free Radioisotopes from Cyclotron Targets. IV. Preparation and Isolation of Mn^{54} and $Co^{56, 57, 58}$*

ROY D. MAXWELL,† JEANNE D. GILE, WARREN M. GARRISON, AND JOSEPH G. HAMILTON

Crocker Laboratory, Radiation Laboratory, and Divisions of Medical Physics, Experimental Medicine, and Radiology, University of California, Berkeley and San Francisco, California

October 21, 1949

CARRIER-FREE radioisotopes of manganese and cobalt of useful half-life may be obtained only by cyclotron bombardment. The present paper describes chemical methods of isolating Mn^{54} and $Co^{56, 57, 58}$ from an iron target bombarded with 19-Mev deuterons in the 60-in. cyclotron at the Crocker Laboratory. At this energy, Mn^{54} and $Co^{56, 57, 58}$ are produced in a thick target by the nuclear reactions:[1] $Fe^{56}(d, \alpha)Mn^{54}$, $Fe^{56}(d, 2n)Co^{56}$, $Fe^{56}(d, n)Co^{57}$, $Fe^{57}(d, 2n)Co^{57}$, $Fe^{57}(d, n)Co^{58}$. Other possible shorter-lived radioisotopes of manganese and cobalt were allowed to decay out prior to the separation.

The iron[2] target was silver-soldered to a water-cooled copper probe and bombarded for 2000 μa-hr. at an average beam intensity of approximately 50 μa. The bombarded surface was dissolved off in 6*N* HCl.

All but approximately 10 mg of the target iron was extracted with ether. The aqueous phase was neutralized with NH_4OH, a few drops of bromine were added, and $Fe(OH)_3$ was precipitated with 15*N* NH_4OH in excess. Under these conditions carrier-free radio-manganese was quantitatively carried, presumably in the quadrivalent state. Over 98 percent of the radio-cobalt remained in the supernatant.[3] The $Fe(OH)_3$ plus radio-manganese was reprecipitated twice with Br_2—NH_4OH in the presence of 1 mg of cobalt hold-back carrier. Three additional precipitations removed traces of carrier cobalt. The $Fe(OH)_3$ was washed, dissolved in 6*N* HCl and iron was extracted with ether. The solution of carrier-free radio-manganese in 6*N* HCl was evaporated to dryness after the addition of 5 ml of isotonic saline solution. Addition of 5 ml of distilled water gave an isotonic solution of carrier-free Mn^{54} for subsequent biological experiments.

The activity was identified by the 310-day half-life and by the 0.85-Mev gamma-ray reported[4] for Mn^{54}. As further identification, a small amount of activity added to a solution containing carrier amounts of Mn, Fe, and Co was quantitatively recovered in the Mn fraction from a chemical separation.[5]

The supernatant from the first $Fe(OH)_3$ precipitation containing carrier-free radio-cobalt, NH_4Cl, and NH_4OH was evaporated to dryness and treated with 16*N* HNO_3 to destroy ammonium salts. 12*N* HCl was added to remove HNO_3 and the solution was evaporated to dryness on 40 mg of NaCl. The activity dissolved quantitatively in 5 ml of water.

The radio-cobalt showed the 72-day half-life of $Co^{56, 58}$; after 200 days the longer period of Co^{57} was apparent. In addition, chemical separation with added Mn, Fe, and Co carriers identified the activity as cobalt. Mass absorption measurements showed the 1.2-Mev beta-reported[6] for Co^{56}. The combined gamma-radiation had a half-thickness of approximately 10 g/cm^2 in lead.

We are grateful to Professor G. T. Seaborg for reading this manuscript, to the staff of the 60-in. cyclotron for bombardments, and to Mrs. Alberta Mozley and Mrs. Helen Haydon for technical assistance.

* This document is based on work performed under the auspices of the AEC.

† Lieutenant Colonel, U. S. Army, now stationed at Walter Reed Hospital, Washington, D. C.

[1] G. T. Seaborg and I. Perlman, Rev. Mod. Phys. **20**, 585 (1948).

[2] The iron was obtained from Johnson Mathey & Company. Manganese and cobalt were not detected by spectrographic analysis.

[3] E. G. Ardagh and G. R. Bongard, J. Ind. Eng. Chem. **16**, 297 (1924).

[4] J. J. Livingood and G. T. Seaborg, Phys. Rev. **54**, 391 (1938).

[5] F. P. Treadwell and W. T. Hall, *Analytical Chemistry* (John Wiley and Sons, Inc., New York, 1942), Vol. I.

[6] J. J. Livingood and G. T. Seaborg, Phys. Rev. **60**, 913 (1941).

Decrease of an Electrical Discharge by External Radiation: Joshi-Effect

K. S. VISVANATHAN
Chemistry Department, College of Science, Benares Hindu University, Benares, India
October 17, 1949

THE letter entitled "Decrease of an Electrical Discharge by External Radiation" by R. Parshad and S. Karim[1] in a recent issue of the Journal implies the claim that some new phenomenon has been observed by the authors. But there can be no doubt that what they have observed is the now well-known negative Joshi-Effect predicted and discovered by Professor Joshi, Benares, as early as 1938.[1a] The Effect consists in an instantaneous and reversible photo-variation, usually diminution, of the discharge current when a number of gases and their mixtures, e.g., Cl_2, H_2, O_2, air etc. as well as metallic vapors, e.g., Hg, K, Se etc. and organic substances are subjected to electrical discharge and irradiated by visible, ultraviolet or x-rays. The Effect has been observed in full and semi-ozonizers as well as in Geissler tubes fitted with internal[2] or sleeve electrodes.[3] This phenomenon has been the subject of extensive investigation in these laboratories and elsewhere since 1938 and the literature on the subject is already considerable. It is of interest to recall that R. Parshad himself has contributed two notes on the subject,[4] wherein he has attempted to formulate a theory explaining the origin of the Effect. It may, however, be added that results obtained in these laboratories are not in accord with Parshad's theory.

Attention may be drawn to K. R. Dixit's letter[5] wherein he has critically examined the problem of the Joshi-Effect and offered suggestions for further experimental work. Working at Professor Joshi's suggestion, Ramana Rao[2] has studied the Joshi-Effect in air and chlorine subjected to Geissler discharge and observed the transition from negative Joshi-Effect at low applied potentials to positive Effect at high potentials. Again, Joshi-Effect of large magnitude, *viz.*, 90–100 percent current suppression by external radiation by visible light has been observed in chlorine,[6] and in air,[7] especially with the ozonizer walls coated with KCl. It is hence incomprehensible that Parshad and Karim should make no reference to the Joshi-Effect and to the spectral observations of P. G. Deo[8] on the emission spectrum of Cl_2, of K. V. Rao[9] and of Venkateswarlu[10] on the absorption spectrum of iodine vapor and mercury vapor respectively, under conditions when all the systems under excitation showed large Joshi-Effect, and especially to the general conclusion that an "adsorption-like electrode layer" represents the seat of the phenomenon.

[1] R. Parshad and S. Karim, J. Chem. Phys. **17**, 667 (1949).

[1a] Joshi, Presidential Address, Chem. Sec., Indian Sci. Cong. (1943), Proc. Ind. Acad. Sci. **22**, 389 (1945).

[2] D. V. Ramana Rao, Proc. Ind. Sci. Cong., Phys. Sec., Abst. **32**, *ibid.*, Chem. Sec., Abst. 35.

[3] D. P. Jatar, Proc. Ind. Sci. Cong. (1949), Phys. Sec., Abst. 20, 21.

[4] R. Parshad, Nature **155**, 362 (1945); J. Sci. Ind. Research **68** (Nov. 1946).

[5] K. R. Dixit, J. Chem. Phys. **16**, 742 (1948).

[6] P. G. Deo, Nature **153**, 434 (1944).

[7] K. S. Visvanathan and B. L. Rao, Proc. Ind. Acad. Sci. **29**, 117 (1949).

[8] P. G. Deo, Phil. Mag. **39**, 978 (1948).

[9] K. V. Rao, Proc. Ind. Acad. Sci. **29**, 211 (1949).

[10] V. Venkateswarlu, Proc. Ind. Sci. Cong. (1949), Phys. Sec., Abst. 35.

Diamagnetic Anisotropy of *p*-Polyphenyls

R. MCWEENY
University of Durham, King's College, England
October 28, 1949

IN a note published some time ago in this Journal,[1] Brooks has shown how London's calculations[2] of the diamagnetic anisotropy of various unsaturated aromatic molecules may be modified in order to allow for non-orthogonality between the atomic $(2p)$-orbitals on adjacent atoms. Although the modification of London's results is quite small for most of the molecules considered, diphenyl appears to provide a remarkable exception to the rule, the implication being that any agreements between experiment and theory are largely fortuitous. In an application of London's method to the *p*-polyphenyls $C_{6n}H_{4n+2}$, $n=2, 3, 4, \cdots$, it was necessary to check previous calculations, with the following results.

(i) The energy level $x=0.070,5$ quoted from London's paper by Brooks, is too small by a factor of 10 (printer's error). On using the correct value the anomaly mentioned above no longer exists.

(ii) A numerical error in London's calculations (contribution to the susceptibility from electrons in the level $x-=1.317,4$) completely invalidates his final result.

(iii) In terms of $\Delta\chi_{\text{benzene}}$ the following corrected results have been obtained

$$\Delta\chi_{\text{diphenyl}}=1.869,5\Delta\chi_{\text{benzene}} \text{ (without overlap)},$$
$$\Delta\chi_{\text{diphenyl}}=1.966,7\Delta\chi_{\text{benzene}} \text{ (with overlap integral } S=0.25).$$

These figures may be compared with London's result,

$$\Delta\chi_{\text{diphenyl}}=2.21\Delta\chi_{\text{benzene}} \text{ (without overlap)}.$$

Whereas London's calculations suggest that conjugation across the connecting link in diphenyl would raise the susceptibility normal to the plane, our results indicate an exactly opposite effect, the fusion of two benzene rings in this manner leading to a decrease in their net susceptibility.

This result is not significantly altered if one makes allowance for the change in ring size due to conjugation: Moreover, calculations which will be fully reported in due course predict the maintenance of this trend in higher members of the series, the diamagnetic anisotropy of the n rings in a *p*-polyphenyl continuing to fall below that of n independent (coplanar) rings.

Although a quantitative agreement with experimental data cannot be anticipated, one might expect to find experimental evidence for a trend of this kind. In fact, the very limited data available[3] does not appear to support our conclusions. In view, however, of the indirect nature of the experimental determinations, and in particular of the uncertainty in $\Delta\chi_{\text{benzene}}$, the disagreement should not, we feel, be regarded as conclusive.

[1] H. Brooks, J. Chem. Phys. **9**, 463 (1941).

[2] F. London, J. de phys. et. rad. **8**, 397 (1937).

[3] Lonsdale, Proc. Roy. Soc. **A159**, 149.

Carbon Isotope Effect on Reaction Rates

KENNETH S. PITZER
U. S. Atomic Energy Commission, Washington, D. C.
October 10, 1949

RECENT experiments[1–3] have shown surprisingly large effects on reaction rates with the substitution of carbon 13 or 14. Bigelseisen[4] has discussed these results in terms of statistical rate theory. While his fundamental theory and formulas are sound, the writer believes his choice of simplified model for one of the molecules can be improved. The possible interpretation will also be discussed for cases where agreement with simple statistical rate theory cannot be obtained.

TABLE I.

$\omega(C^{12})$	$\omega(C^{14})$	$\Delta\omega$	$G(u)$	$G(u)\Delta u$
		Normal acid molecule		
1800	1713	87	0.343	0.107
837	834	3	0.219	0.002
493	490	3	0.140	0.002
1423	1346	77	0.301	0.083
483	481	2	0.138	0.001
700	659	41	0.180	0.029
				0.222
		Activated complex		
1711	1633	78	0.332	0.093
1088	1053	35	0.260	0.032
				0.125

For the decarboxylation reaction of malonic and bromomalonic acids, investigated by Yankwich and Calvin,[3] we take a model:

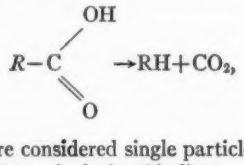

where R and OH are considered single particles. Experience with many normal vibration calculations[5] indicates that for the stretching vibrations with zig-zag chains the distant heavy atoms have little effect. Thus we take effective masses of 16 for both OH and R. Although one might have preferred 17 for OH and 14 or 15 for R, the complication to the calculation seemed not worth while. The distant heavy atoms do effect bending vibrations, but inspection of the details of the rate calculations indicates that the net effect of these vibrations is much smaller than that of the stretching motions.

Taking force constants yielding approximately the observed frequencies of carboxylic acids, one then substitutes the mass 14 instead of 12 for the carboxyl carbon and calculates[6] the frequencies of the "heavy" molecule. Selection of all details of the activated complex is less certain but it seems very likely that the C=O bond remains about normal. Since the R—C bond is being broken, its force constant is set to zero. Presumably the C—O bond has not yet become a double bond so it is given the same force constant as in the unreacted acid. Undoubtedly, the rigidity of bond angles is reduced in the activated state. Since the isotope effect on low frequencies is small anyway, all bending constants were set to zero. Thus there are just the C=O and the C—O vibrations in the activated complex model. All frequencies of the real molecule which the model omits are assumed to be unchanged by the isotopic substitution.

The calculated frequencies are given in Table I and apply equally to malonic or bromomalonic acid.

Bigeleisen has shown the ratio of rates for processes differing only isotopically to be

$$\frac{k}{k'}=\left(\frac{\mu'}{\mu}\right)^{\frac{1}{2}}\left[1+\sum_{i}^{3N-6}G(u_i)\Delta u_i-\sum_{j}^{3N-7}G(u_j^{\ddagger})\Delta u_j^{\ddagger}\right],$$

where $G(u)$ is the function defined by Bigeleisen and Mayer[7] and $u=hc\omega/kt$. The reaction coordinate reduced mass, μ, is taken as the reduced mass, $m_1m_2/(m_1+m_2)$, associated with the atoms forming the bond being broken. The symbol ‡ refers to the activated complex. Table I shows the items in this calculation for the malonic acid reaction at 400°K.

The resulting calculated ratio of rates of breaking $C^{12}-C^{12}$ to $C^{12}-C^{14}$ bonds is 1.14 as compared to the experimental 1.12±0.03 for malonic acid and 1.4±0.1 for bromomalonic acid. Bigeleisen's calculation yielded 1.04. Thus the present model accounts for the malonic acid results satisfactorily. The bromomalonic acid value comes from a single measurement internally less consistent than the others. If it should be confirmed, it will require a more drastic explanation.

The statistical rate theory[8] makes the assumption that a full equilibrium concentration of activated complexes is maintained (remembering that these complexes have only positive velocities in the reaction coordinate). In a malonic acid with one C^{14} carboxyl group the $C^{12}-C^{12}$ bond can break at a lower activation free energy than that required to break the $C^{12}-C^{14}$ bond. Now, if in the process of activation to the $C^{12}-C^{14}$ break, the molecule has a chance to react by the $C^{12}-C^{12}$ break then this will tend to deplete the concentration of $C^{12}-C^{14}$ reacting complexes below the equilibrium value. This process would yield exceptionally high ratios of reaction rates.

The present model and standard statistical rate theory yield the same rate of $C^{12}-C^{12}$ bond rupture in a C^{14} containing malonic acid as in the normal (all C^{12}) molecule. However, if as postulated above, the rate of activation is not sufficient to maintain full equilibrium concentrations of activated complexes, then the double possibility of $C^{12}-C^{12}$ bond rupture might deplete this concentration more in the normal molecule than the single possibility of $C^{12}-C^{12}$ rupture does in the isotopic molecule. This point has not been checked experimentally in the malonic acid case but seems to arise in the behavior of the $C_3H_8^+$ ion in the mass spectrometer.[1] Beeck and co-workers report that the $C^{12}-C^{12}$ break is 7 percent more probable in a molecule with one C^{13} than in the normal molecule. The $C^{13}-C^{12}$ break is 12 percent less probable than the normal $C^{12}-C^{12}$ reaction.

Since the effective temperature of the propane ion in a mass spectrometer source is uncertain, no attempt will be made to carry analysis of that experiment further. The data[2] on the thermal cracking of propane-1-C^{13} at about 800°K show a higher ratio of rates than seems likely on a simple rate theory. However, details of the exact mechanism of this chain reaction are sufficiently uncertain to preclude further conclusions here.

[1] Beeck, Otvos, Stevenson, and Wagner, J. Chem. Phys. **16**, 255 (1949).
[2] Stevenson, Wagner, Beeck and Otvos, *ibid.* **16**, 993 (1948).
[3] P. E. Yankwich and M. Calvin, *ibid.* **17**, 109 (1949).
[4] J. Bigeleisen, *ibid.* **17**, 344, 425 (1949).
[5] For example note the frequencies near 1000 cm^{-1} in Fig. 2, J. Chem. Phys. **8**, 714 (1940).
[6] G. Herzberg, *Infrared and Raman Spectra* (D. Van Nostrand & Company, Inc., New York, 1945), pp. 179–180 and p. 174.
[7] J. Bigeleisen and M. G. Mayer, J. Chem. Phys. **15**, 261 (1947).
[8] See Glasstone, Laidler, and Eyring, *The Theory of Rate Processes* (McGraw-Hill Book Company, Inc., New York, 1941).

A New Method of Calculating Resonance Energies

RALPH G. PEARSON
Northwestern University, Evanston, Illinois
October 17, 1949

THE purpose of this note is to introduce a simple method for the approximate calculation of energies in molecules for which several reasonable electronic structures exist. The method is essentially a molecular orbital one in that the wave function for the system is written as the product of one-electron wave functions. Each such one-electron wave function is a molecular orbital (approximated as an *LCAO*) which has the characteristic of being *centered* on a single nucleus but which may be extended to include all nuclei *adjacent* to the central one.

To construct the *MO*'s first write down all of the structures, *I*, *II*, *III*$\cdots$, assumed to contribute to the ground state of the molecule. Each electron, or pair of electrons, in each structure is represented by a localized *MO* of the form $\psi=(1/\sqrt{2})(\psi_A+\psi_B)$ for an electron in a bond between nuclei A and B and $\psi=\psi_A$ for an electron on a single nucleus. (ψ_A and ψ_B are suitable, normalized atomic orbitals.) The complete *MO* centered on nucleus A is now obtained by taking a linear sum of all of the localized *MO*'s involving nucleus A. This is done with due regard for the contribution of each structure to the ground state.

$$\psi(A)=a\psi_I(A)+b\psi_{II}(A)+c\psi_{III}(A)\cdots. \quad (1)$$

Each complete *MO* so constructed holds on the average zero, one, or two electrons, the number being uniquely determined by the structures used. (A pair of electrons in a bond can be considered as one electron on each nucleus or two electrons on one nucleus and none on the other. However, if any of the structures used show a nucleus with no electrons, or one or two unpaired electrons, then the *MO* constructed on that nucleus must have the same electron population in all structures.)

The coefficients a, b, $c\cdots$ above can be found by solving the secular equation

$$\begin{vmatrix} H_{II}-W & H_{I\,II}-\Delta_{I\,II}W\cdots \\ H_{I\,II}-\Delta_{I\,II}W & \cdots\cdots \\ \cdot & \\ \cdot & \\ \cdot & \end{vmatrix}=0, \qquad (2)$$

where since the total electronic energy is to be a minimum, H_{II} is the sum of the electronic energies in structure I, each calculated in terms of Coulombic integral q and exchange integral β by the usual simplified *MO* method. $H_{I\,II}$ is the sum of the electronic energies calculated, for example, for an electron in the *MO* centered on nucleus A:

$$H'_{I\,II}=\int \psi_I(A)H'\psi_{II}(A)d\gamma \qquad (3)$$

where H' is a single electron Hamiltonian. $\Delta_{I\,II}$ is the average value of the overlap integral $\Delta'_{I\,II}$

$$\Delta'_{I\,II}=\int \psi_I(A)\psi_{II}(A)d\gamma \qquad (4)$$

for each *MO* weighted according to its population. The lowest root of (2) then gives the values of a, b, $c\cdots$ which make the total energy of the system a minimum.

This method in general gives excellent agreement with ground state energies calculated by either the usual *MO* method or the valence bond method and is frequently simpler to use. It has the advantage for chemists of emphasizing conventional bond structures while retaining the simplicity of *MO* calculations.

As an example, calculate the energy of the six π-electrons of benzene considering only the two Kekulé structures. (For simplicity but not by necessity the usual assumptions as to orthogonality and exchange integrals between non-adjacent atoms will be made.) The secular equation calculated by the rules given above is

$$\begin{vmatrix} 6q+6\beta-W & 3q+6\beta-\frac{W}{2} \\ 3q+6\beta-\frac{W}{2} & 6q+6\beta-W \end{vmatrix}=0 \qquad (5)$$

which has the lowest root $W=6q+8\beta$. The six complete molecular orbitals centered on each carbon nucleus are all equivalent and of the form $\psi(B)=1/(6)^{\frac{1}{2}}(2\psi_B+\psi_A+\psi_C)$, etc. Each has an average population of one electron with an energy of $q+4/3\beta$. It is of interest to note that the inclusion of the Dewar structures of benzene does not improve the energy; in fact, they make no contribution in this method of calculation.

A One-Dimensional Treatment of the Hydrogen Molecule Ion

MAC WALSH AND F. A. MATSEN
Departments of Physics and Chemistry, The University of Texas, Austin, Texas
October 8, 1949

THE Pauling treatment[1] of the H_2^+ leads to the energy expression

$$E=W_H+e^2/R_{ab}+(J+K)/(1+\Delta),$$

where

$$J=\int \frac{U_{1a}U_{1a}d\tau}{r_b},$$

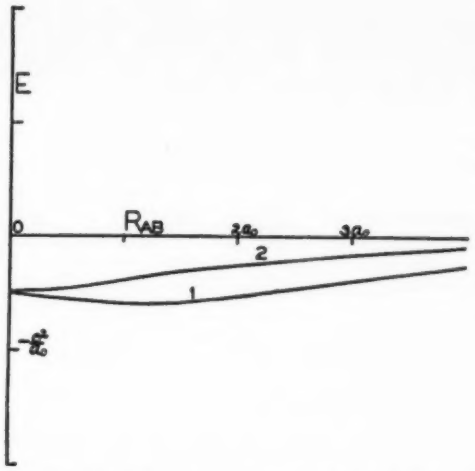

FIG. 1. $K/1+\Delta$. (1) for the one-dimensional model, (2) for the three-dimensional model.

$$K=\int \frac{U_{1a}U_{1b}d\tau}{r_b},$$

$$\Delta=\int U_{1a}U_{1b}d\tau.$$

This treatment yields a binding energy for H_2^+ of $0.384e^2/a_0$ compared with the experimental $0.603e^2/a_0$.

One of the reasons for the low result is the lack of polarization in the atomic wave functions. It was of interest, therefore, to ascertain the effect of 100 percent polarization, i.e., the restriction of the motion of the electron along the axis of the molecule. The exchange integral $K/1+\Delta$ can be evaluated for this model although the Coulomb integral $J/1+\Delta$ cannot.

The one-dimensional hydrogen atom Schroedinger equation[2] is

$$d^2\psi/dx^2+(8\pi^2M)/h^2(W+e^2/|x|)\psi=0$$

with solution $\psi=(2/a_0^{\frac{1}{2}})|x|\exp-|x|/a_0$ corresponding to the ground state energy, $W_H=0.5e^2/a_0$. The expression for $K/(1+\Delta)$ in units of e^2/a_0 becomes

$$\frac{-(R^2+R+1)e^{-R}}{1+(R^2/3+R+1)e^{-R}},$$

where $R=(R_{ab})/a_0$. As is expected, the value of $K/1+\Delta$ is larger for the one-dimensional (100 percent polarized) model than for the three-dimensional model (see Fig. 1). Combining the former with the three-dimensional $J/1+\Delta$ the binding energy is 37 percent greater than the exact value.

[1] L. Pauling, Chem. Rev. 5, 173 (1928); L. Pauling and E. B. Wilson, *Introduction to Quantum Mechanics* (McGraw-Hill Book Company, Inc., New York, 1935), p. 327.
[2] V. R. Vrkljan, Zeits. f. Physik. 52, 735 (1927).

The Transport Properties for Non-Polar Gases

J. O. HIRSCHFELDER, R. B. BIRD, AND E. L. SPOTZ
Department of Chemistry, University of Wisconsin, Madison, Wisconsin
October 17, 1949

OUR attention has just been called to the work of T. Kihara and M. Kotani on the determination of intermolecular forces from transport phenomena in gases.[1]

In this article Kihara and Kotani performed essentially the same integrations as we did[2] to obtain the Chapman and Coeling collision integrals for non-polar gases using the Lennard-Jones potential, with an inverse twelfth power energy of repulsion and an inverse sixth power energy of attraction.

The F_n^m tabulated by Kihara and Kotani are very simply related to the $W^{(m)}(n)$ which we presented in our publication: $W^{(m)}(n) = (2\epsilon/kT)^{1/6} F_n^m$. Table I exhibits typical numerical agreement in the values of the collision integrals.

TABLE I.

	$kT/\epsilon = 1$		$kT/\epsilon = 20$	
	Kihara and Kotani	Hirschfelder, Bird, and Spotz	Kihara and Kotani	Hirschfelder, Bird, and Spotz
$W^{(1)}(1)$	0.7199	0.7197	0.3320	0.3320
$W^{(1)}(2)$	1.806	1.806	0.9442	0.9439
$W^{(1)}(3)$	6.455	6.456	3.631	3.629
$W^{(2)}(2)$	1.590	1.587	0.7437	0.7432
$W^{(2)}(3)$	5.550	5.550	2.866	2.864
$W^{(2)}(4)$	25.15	25.16	13.92	13.90

This excellent agreement obtained by the two independent groups greatly increases our confidence in the accuracy of our respective tables. We are sorry that we were previously unaware of this Japanese publication.

A few values of these integrals were calculated by J. deBoer and J. Van Kranendonk,[3] and excellent agreement was obtained with their results. A few other numerical calculations were made by Rowlinson.[4]

[1] T. Kihara and M. Kotani, Proc. Phys.-Math. Soc. (Japan) **24**, 76 (1942); **25**, 602 (1943).
[2] Hirschfelder, Bird, and Spotz, J. Chem. Phys. **16**, 968 (1948).
[3] J. deBoer and J. Van Kranendonk, Physica **14**, 442 (1948).
[4] J. S. Rowlinson, J. Chem. Phys. **17**, 101 (1949).

Hydrocarbon Flame Spectra*

ROBERT C. HERMAN AND GEORGE A. HORNBECK
Applied Physics Laboratory, The Johns Hopkins University, Silver Spring, Maryland
October 3, 1949

THE combustion of hydrocarbons has been studied intensively for many years because of its theoretical and practical interest. The spectra of hydrocarbon flames were first investigated in detail under low dispersion by Vaidya.[1] He described the appearance of a system of bands called the hydrocarbon (or ethylene) flame bands which are degraded to the red and lie between 2500 and 4100A. These bands were arranged in a vibrational scheme and it was suggested that the emitter of this system was the HCO radical. Since that time many investigations with explosion and various types of stationary hydrocarbon flames have been conducted with the result that the hydrocarbon flame bands have been reported in practically all cases of hydrocarbons burning with air, oxygen or atomic oxygen.[2]

Since most of these flame spectra were investigated with rather low dispersion instruments we have been studying the stationary flames of methane and ethylene under a variety of conditions. A 2-meter Baird grating spectrograph was employed with dispersion 4A/mm and 8A/mm in the regions 3000–4000A and 7000–9000A, respectively.

In a recent note[3] we reported the appearance of the $^1\Pi_g - {}^1\Pi_u$ Deslandres-D'Azambuja band system of the C_2 molecule in the spectra of the low pressure stationary flames of ethylene and methane burning with oxygen at stoichiometric proportions. Further studies of these flames reveal, in the region 3000–4000A, bands of the $^3\Sigma_u^- - {}^3\Sigma_g^-$ Schumann-Runge system of the O_2 molecule in addition to the C_2 bands mentioned above, as well as various OH and CH bands, e.g., the (0,1) OH band at 3428A and the (1,0) CH band at 3628A. The O_2 bands are stronger the higher the relative concentration of oxygen. These results are similar to those reported by one of us[4] in the $CO+O_2$ explosion flame.

At this point in our investigations we suggest the possibility that the overlapping of the various bands of the diatomic species OH, CH, C_2 and O_2 may produce, in the region 3000–4000A, what has the appearance of a system of bands heretofore ascribed to the HCO radical. Whether or not the above mentioned diatomic species account for all the band structure in this spectral region requires more detailed study.

We have also observed in emission from hydrocarbon flames the heads of the (0,0) and (1,1) bands of the $^1\Sigma_g^+ - {}^3\Sigma_g^-$ atmospheric absorption system of O_2 which lie at 7594 and 7685A respectively. In addition we find the (2,0) band at 8751A of the recently discovered $^1\Pi_u - {}^1\Sigma_g$ Phillips' system[5] of the C_2 molecule. Since the Phillips' bands involve the lower states of the $^1\Pi_g - {}^1\Pi_u$ Deslandres-D'Azambuja and the $^1\Sigma_u^+ - {}^1\Sigma_g^+$ Mulliken systems, one would expect both the Deslandres-D'Azambuja and Phillips' bands to be found together in the flame spectrum. The Mulliken bands of C_2 as well as the Fourth Positive bands of CO appear in flames of ethylene and oxygen. These bands have been observed by Gaydon[2] in the oxyacetylene flame Thus, all the known band systems of the C_2 molecule have been observed in hydrocarbon flames except the $^3\Pi_g - {}^3\Pi_u$ Fox-Herzberg bands and we are now searching for the latter system which may account for some of the structure in the region 3000–4000A.

We hope in the near future to report the detailed results of these investigations as well as further studies of the hydrocarbon flame spectrum between 2500–3000A.

We wish to thank Dr. G. Herzberg and Dr. J. G. Phillips for their interest and many profitable discussions.

* The work described herein was supported by the Bureau of Ordnance, U. S. Navy under Contract NOrd-7386.
[1] W. M. Vaidya, Proc. Roy. Soc. **A147**, 513 (1934).
[2] A. G. Gaydon, *Spectroscopy and Combustion Theory* (Chapman and Hall Ltd., London, 1948).
[3] G. A. Hornbeck and R. C. Herman, J. Chem. Phys. (to be published).
[4] G. A. Hornbeck, J. Chem. Phys. **16**, 845, 1005 (1948).
[5] J. G. Phillips, Ap. J. **107**, 389 (1948).

Chemical Oxidation States of Cl and N Formed by the $S^{34}(p, n)Cl^{34}$ and $O^{16}(p, \alpha)N^{13}$ Reactions in Crystals

DALE J. MEIER AND CLIFFORD S. GARNER
Department of Chemistry, University of California, Los Angeles, California
October 20, 1949

ALTHOUGH many studies have been made of the fate of atoms after radiative neutron capture (Szilard-Chalmers reaction), little has been done in determining the chemical fate of transmuted atoms arising from bombardment with high energy ions, especially in inorganic crystals. Libby[1] has discussed the expected fate of hot transmuted atoms in crystal lattices, and a few investigations of such processes have been made.[2]

We are extending this work of determining chemical states after bombardment of inorganic crystals with high energy ions, and wish to report our work on the chemical state of Cl and N produced by the $S^{34}(p, n)Cl^{34}$ and $O^{16}(p, \alpha)N^{13}$ reactions.

Chlorine was chosen because of the many oxidation states possibly present after bombardment: -1 (Cl^-), 0 (Cl_2), $+1$ (ClO^-), $+3$ (ClO_2^-), $+4$ (ClO_2), $+5$ (ClO_3^-), and $+7$ (ClO_4^-). Production of the higher oxidation states would presumably be favored by bombardment of crystals rich in oxygen,[3] so sulfates and peroxydisulfates were chosen as targets. Powdered anhydrous C.P. Na_2SO_4 and $K_2S_2O_8$ samples were wrapped in thin aluminum foils and bombarded with 14-Mev protons in the circulating beam of the U.C.L.A. 37-in. frequency-modulated cyclotron[4] for 30-min. periods (current ~ 1 μa). The targets showed activities with half-

lives of 10, 33, and 112 min. after the shorter-lived activities decayed out. The 33- and 112-min. activities were shown to be associated with the expected Cl^{34} and $F^{18}(O^{18}(p, n)F^{18})$; the source of the 10-min. activity was puzzling until chemical and absorption tests showed it to be the previously known[5] N^{13}. The only conceivable reaction which would lead to this activity in the targets used is $O^{16}(p, \alpha)N^{13}$. This reaction, as well as the $S^{34}(p, n)Cl^{34}$ reaction, seems not to have been reported before.

Following a bombardment the target crystals were dissolved in water, Cl^-, ClO_3^-, and ClO_4^- carriers were added, as well as F^- hold-back carrier, and a Cl^- fraction precipitated with excess Ag^+. The filtrate was treated with SO_2 or NO_2^- to reduce higher valent states, excepting ClO_4^-, to Cl^-, and a second AgCl precipitate removed. Finally, the ClO_4^- was precipitated with methylene blue.[6] All precipitates were filtered onto paper disks, dried, and mounted for counting[7] in a reproducible geometry under a Geiger-Müeller counter and scale-of-64, the 2.5- and 5.1-Mev positrons[5] being used for the detection. Typical results are shown in Table I.

TABLE I. Corrected activities of Cl fractions from $S^{34}(p, n)Cl^{34}$ reaction.

Fraction	Net activity, c/m[a] Na_2SO_4	$K_2S_2O_8$
Cl^-	13743 ± 115	1047 ± 24
ClO^-	22 ± 3	0 ± 2
ClO_4^-	40 ± 3	9 ± 2

[a] Error includes only standard counting error.

These experiments indicate that essentially all of the Cl^{34} activity appears as Cl^- or in a form rapidly exchangeable with Cl^-; thermal exchange between Cl^- and ClO_2, ClO_3^-, and ClO_4^- under the given conditions has been shown[8-10] to be slow, whereas Cl^- and Cl_2 are known[11] to undergo rapid exchange. It is indeterminate whether the Cl^- exists in the crystal lattace as such or arises as a result of dissolving the crystals. The hot chlorine atom may be ejected as a neutral atom or positive ion and take up electrons before it can react with the oxygen in the crystal. Similar results have been reported[8] for the Szilard-Chalmers reaction on ClO_4^-.

An attempt was made to determine the chemical state of the N^{13}, but no quantitative results can be given. The addition of NH_4^+ carrier to the solution (chemically freed from Cl^{34} and F^{18} activities), followed by its precipitation with Nessler's reagent, carried down a moderately large, but unreproducible, fraction of the N^{13} activity. A Kjeldahl reaction experiment indicated higher oxidation states were present. The N^{13} does not exist appreciably in any volatile form in the solution inasmuch as little activity was lost when the aqueous solution was evaporated to dryness. Since it was important to know whether exchange would take place between certain oxidation states in the time required for the experiments, the exchange of NH_4^+ and NO_2^- was investigated briefly. In solutions $0.23f$ in both NH_4^+ and NO_2^-, and $0.012f$ in H^+, 3.3±2.6 percent exchange was found after 92 min. at room temperature, separation being achieved by the use of Nessler's reagent.

[1] W. F. Libby, J. Am. Chem. Soc. **69**, 2523 (1947).
[2] See, for example, A. H. W. Aten, Jr., Phys. Rev. **71**, 641 (1947); Sherr, Muether, and White, Phys. Rev. **75**, 282 (1949).
[3] Aten (see reference 2) found that the radiophosphorus produced by (n, p) or (n, α) reactions with radium-beryllium neutrons on inorganic crystals containing sulfur or chlorine tends to form phosphates in oxygen-rich crystals.
[4] We wish to thank Professor J. R. Richardson and the cyclotron crew for their co-operation in arranging the bombardments.
[5] G. T. Seaborg and I. Perlman, Rev. Mod. Phys. **20**, 585 (1948).
[6] F. J. Welcher, *Organic Analytical Reagents* (D. Van Nostrand Company, Inc., New York, 1948), Vol. IV.
[7] Background, decay, and coincidence corrections were applied. Activities in the precipitates were shown to be due only to 33-min. Cl^{34} by decay measurements. Final filtrates were counted with a dipping counter and no residual Cl^{34} activity was found.
[8] W. F. Libby, J. Am. Chem. Soc. **62**, 1930 (1940).
[9] H. Dodgen and H. Taube, J. Am. Chem. Soc. **71**, 2501 (1949).
[10] We confirmed that the exchange between Cl^- and ClO_3^- and between Cl^- and ClO_4^- is very slow for our experimental conditions.
[11] F. A. Long and A. R. Olson, J. Am. Chem. Soc. **58**, 2214 (1936).

Photo-Chemical Reduction of Water by Europium (*II*) Ion, and the Magnetic Susceptibilities of Europium (*II*) and (*III*) Ions

DAVID L. DOUGLAS AND DON M. YOST
*Gates and Crellin Laboratories of Chemistry, California Institute of Technology, Pasadena, California**
October 14, 1949

THE slow reaction of europium (*II*) ion with hydrogen ion or water to produce hydrogen and europium (*III*) ion has been previously reported.[1-4] Prior to an investigation of the aqueous chemistry of europium (*II*) ion, the study of this reaction was undertaken. It was decided to follow the course of the reaction by observing the change in magnetic susceptibility of the reaction mixture, using a Gouy balance. This method was suggested by the aforementioned work of R. A. Cooley.[4] Preliminary experiments showed that solutions 0.25 m in europium (*II*) chloride and about 0.3 m in hydrochloric acid were stable over periods of weeks when kept in the dark, but evolved hydrogen and changed susceptibility rapidly when exposed to bright light (either sunlight or a tungsten lamp). One other such system has been reported in the literature. Poterill, Walker, and Weiss investigated the photo-chemical reduction of water by iron (*II*) ion.[5]

A systematic investigation of this reaction, including the thermal reaction, has been in progress for some time. The apparatus will be described in detail in a future report. It permits the sidewise irradiation, with the 3660A line group of a 20-cm mercury arc, of a Gouy tube containing the reaction mixture and an identical tube containing a uranyl oxalate actinometer. Experiments so far have been confined to solutions 0.50 m in HCl, 0.15 m in $EuCl_2$ and 0.05 m, 1.05 m or 2.05 m in KCl, the ionic strength in these cases being 1.0, 2.0 and 3.0 respectively. Table I contains a summary of some of the results obtained thus far. It is considered that insufficient data are available to elucidate completely the mechanism and so a discussion of this will be deferred.

TABLE I. Quantum yields of photo-chemical reduction of water by europium (*II*) ion.*

(HCl) = 0.50 m		(EuCl₂) = 0.15 m		Volume = Ca 12 ml	
(1)	(2)	(3)	(4)	(5)	(6)
Expt. No.	Ionic strength of solution	Change in conc. of Eu (*II*)	Molecules Eu (*II*) oxidized	Quanta absorbed	Quantum yield = column (4) / column (5)
14-*b*	1.0	0.0072	5.2×10^{19}	3.1×10^{19}	1.7 ± 0.2
14-*c*	1.0	0.0071	5.1×10^{19}	2.8×10^{19}	1.8 ± 0.2
16-*b*	2.0	0.0071	5.1×10^{19}	2.5×10^{19}	2.0 ± 0.2
17-*b*	3.0	0.0082	6.2×10^{19}	2.7×10^{19}	2.3 ± 0.2

* Activated by the 3660A radiation, of which Eu (*II*) is the only absorber in these solutions.

With regard to the analytical method, the literature contains many values of the magnetic susceptibility of europium (*III*) ion. Yost, Russell, and Garner present a summary of these.[6] We have determined the molar susceptibility of europium (*III*) ion in aqueous solution at 25.0°C to be 4.50×10^3 c.g.s. units; this value is independent of the ionic strength of the solution. The magnetic susceptibilities of a number of compounds of europium (*II*) is reported[7,8] but no value for the ion in solution appears in the literature. By working in an atmosphere of carbon dioxide when preparing the solutions, and when carrying out analyses, by the method recommended by H. N. McCoy,[9] we have measured the susceptibility of europium (*II*) ion in aqueous solution, over the concentration range 0.3 m to 0.1 m, with the following result: $\chi_M = 26.2_6 \pm 0.1\times10^3$ c.g.s./g ion. The ionic diamagnetic susceptibilities listed by L. F. Bates[10] were used throughout. This value of χ_M is in good agreement with Van Vleck's[11] theoretical value of 26.1×10^3 c.g.s./g ion for the isoelectronic gadolinium

(*III*) ion. In calculating the amounts of europium present in the two oxidation states the validity of Wiedemann's additivity law was assumed.

The europium used in these researches was a gift of the late Dr. H. N. McCoy and was of greater than 99.9 percent purity as regards other rare earths. Our supply was augmented by a loan of more of the same material by Mrs. Ethel Terry McCoy, for which we are exceedingly grateful.

We wish to thank Professor N. Davidson and Dr. O. Wulf for many helpful discussions and suggestions. We are also very grateful to the Research Corporation for a grant which aided, in part, the work reported here. The junior author (David L. Douglas) is indebted to the Atomic Energy Commission for financial a[illegible]e in the form of a fellowship for the year 1948–49.

* Contribution No. 1345.

[1] Yost, Russell, and Garner, *The Rare Earth Elements and Their Compounds* (John Wiley and Sons, Inc., New York, 1947), page 66.
[2] Jantsch, Grubitsch, and Lischka, Zeits. f. Electrochemie **43**, 293 (1937).
[3] F. D. S. Butement, Trans. Faraday Soc. **XLIV**, 617 (1948).
[4] R. A. Cooley, Ph.D. Thesis, California Institute of Technology, 1941.
[5] Poterill, Walker, and Weiss, Proc. Roy Soc. **A156**, 561 (1936).
[6] See reference 1, page 14.
[7] P. W. Selwood, J. Am. Chem. Soc. **55**, 4869 (1933).
[8] W. Klemm and W. Döll, Zeits. f. anorg. unt allg. Chem. **241**, 233 (1939).
[9] H. N. McCoy, J. Am. Chem. Soc. **61**, 2455 (1939).
[10] L. F. Bates, *Modern Magnetism* (Cambridge University Press, London 1947), page 132.
[11] J. H. Van Vleck, *Electric and Magnetic Susceptibilities* (Oxford University Press, Cambridge, 1932), page 243.

Spectra of Disordered Crystals

D. F. Hornig
Metcalf Research Laboratory, Brown University, Providence, Rhode Island
October 3, 1949

THE spectra of crystals, both electronic and vibrational, have been discussed by a number of authors.[1–5] All of these discussions have been based on the premise that a crystal is a perfectly ordered system with a clearly defined structure about all interior points. Elementary statistical considerations make it apparent that if alternative structures which do not differ too much in their free energy are possible, and if they are accessible in the sense that the activation energy for the transition to the alternative structure is not too high, a finite fraction of the domains of the crystal will exist with alternative structures at any temperature other than absolute zero. That is, disorder must be very common in crystals at finite temperatures. It is the purpose of this note to point out (a) that the selection rules and character of the spectra cannot be simply obtained from the crystallographic symmetry in such cases and (b) that spectra may be expected to be sensitive to short-range or local order and are therefore a useful complement to x-ray methods which are most sensitive to long-range order.

Disorder has been extensively investigated in alloy structures.[6] Evidence is also available for disorder in many molecular and ionic crystals, a particularly common type being that in which molecules or ions are located at essentially fixed lattice points but in which the equilibrium *orientation* of each molecule is not specified. Free rotation would be a particular case of such disorder although it is questionable whether free rotation in a crystal has been definitely demonstrated in even a single case. Examples of such disorder might include crystalline carbon monoxide, the cubic modifications of many nitrates and a variety of crystals involving symmetric molecules or ions. A common feature of disordered phases of this kind is that the crystal symmetry is higher than in the ordered (or less disordered) phase existing at lower temperatures. Several authors have accordingly considered that the effective symmetry for vibrational spectra is also higher, implying more stringent selection rules, absence of splitting of degeneracies, etc. In fact, the symmetry of the Hamiltonian is always reduced in passing to a less ordered phase and we may rather expect that selection rules will be relaxed and degeneracies split; in some cases the spectrum may approach that of a liquid.

Since the spectra of molecules and ions in a crystal differ only very slightly from the spectra of the corresponding gases, they must be only very slightly perturbed by the crystalline environment. In this case the Hamiltonian of the crystal may be written

$$H=\sum_i H_i^0+H',$$

where H_i^0 is the internal Hamiltonian of the ith molecule and H' is the small perturbation due to the crystal. If H' is expanded in terms of nearest neighbor interactions, next nearest neighbor interactions, etc., the successive terms decrease rapidly in magnitude since all of the interactions fall off at least as rapidly as the inverse square of the distance and proposition (b) follows immediately, that most of the observed effects are due to local structures. Since in a disordered state a variety of local structures coexist, the symmetry effects may be expected to vanish to a degree depending on the nature of the local structures. In general, one may expect that in a disordered structure the sharp line spectra expected in ordered structures[4,5] should be broadened.

Such effects appear to have been observed in studies of the vibrational spectra of ammonium and deutero-ammonium halides above (disordered) and beneath (ordered) the λ-point.[7] It is hoped that the spectra of crystals may provide a generally useful tool in studying order-disorder transitions of transparent substances and further experimental studies are now in progress.

[1] H. Bethe, Ann. d. Physik **3**, 133 (1929).
[2] S. Bhagavantam and T. Venkatarayudu, Proc. Ind. Acad. Sci. **A9**, 224 (1939).
[3] R. S. Halford, J. Chem. Phys. **14**, 8 (1946); H. Winston and R. S. Halford, *ibid.* **17**, 607 (1949).
[4] D. F. Hornig, J. Chem. Phys. **16**, 1063 (1948).
[5] A. S. Davydov, J. Exp. Theor. Phys. (U.S.S.R.) **18**, 210 (1948).
[6] F. C. Nix and W. Shockley, Rev. Mod. Phys. **10**, 1 (1938).
[7] E. L. Wagner and D. F. Hornig, J. Chem. Phys. (to be published); see Phys. Rev. **75**, 1282 (1949).

Solubility of Water in Hydrocarbons

J. H. Hildebrand
Department of Chemistry, University of California, Berkeley, California
October 3, 1949

A VALUABLE paper bearing this title was published recently by Black, Joris, and Taylor.[1] They reported the solubility of water in 15 hydrocarbons and discussed the results in connection with the usual equation for regular solutions, and also with an equation of the Flory-Huggins type designed to take account of discrepancy in molal volumes.

In view of the general importance of being able to predict the solubility of water in any hydrocarbon, I believe that the following method of analyzing and correlating these results will prove useful to many.

The equations for the heat of mixing and the entropy of mixing may be combined to give[2]

$$RT\ln(a_2/\varphi_2)=\mathrm{v}_2\varphi_1^2(\delta_1-\delta_2)^2+RT\varphi_1(1-\mathrm{v}_2/\mathrm{v}_1), \qquad (1)$$

where a denotes activity, v molal volume, φ volume fraction, and δ the "solubility parameter," which is the square root of the energy of vaporization per cc. We shall let subscript 2 stand for water and 1 for the hydrocarbon. The first term on the right is intended to account for the heat, the second the entropy of mixing. The latter should be unusually significant in these solutions because of the relatively small molal volume of water.

One would hardly be surprised if a value of δ_2 derived from the heat of vaporization of water would fail to fit these solutions since hydrogen bonds contribute so largely to the cohesion of liquid water but not to the attraction between water and hydrocarbon molecules. It seemed possible, nevertheless, that a uniform even if somewhat artificial solubility parameter for water might serve to

correlate the data, and to test this I substituted them in Eq. (2) and calculated the values of $\delta_2-\delta_1$ and then δ_2 with the results shown in Table I. The necessary δ_1-values are those given in the third edition of *Solubility of Non-electrolytes.*

TABLE I. Solubility of water in hydrocarbons, mole fraction, x_2 at 20°C.

	10^4x_2	v_1	$\delta_2-\delta_1$	δ_1	δ_2
Normal paraffins					
n-C_4H_{10}	2.1	101.4	17.4	6.7	24.1
n-C_5H_{12}	3.6	116.1	17.0	7.05	24.1
n-C_6H_{14}	5.3	131.6	16.7	7.3	24.0
n-C_7H_{16}	7.3	147.5	16.5	7.45	24.0
n-C_8H_{18}	9.0	163.5	16.4	7.55	24.0
Branched paraffins					
i-C_4H_{10}	2.4	101	17.0	6.25	23.3
i-C_5H_{12}	3.6	117	17.0	6.75	23.8
Cyclic					
cycl. C_6H_{12}	4.65	109	16.6	8.2	24.8
C_6H_6	19.0	89	15.1	9.15	24.2
$C_6H_5CH_3$	22.0	107	15.1	8.9	24.0
				Mean	24.0
Olefins					
1,C_4H_8	12.4	95	15.6	6.7	22.3
2,C_4H_8	14.0	91	15.8	7.0	22.8
1,C_7H_{14}	57.0	141	14.3	7.7	22.0
Diolefins					
C_4H_6	19.0	86	15.1	7.6	22.7
1,5,C_6H_{10}	46.0	119	14.4	8.2	22.6
				Mean	22.5

The table reveals that the δ_2-values are close to 24.0 for all but the olefins and are close to 22.5 for these. One may expect therefore to calculate the solubility of water in another hydrocarbon with good approximation by using one or the other of these two values, as appropriate.

The smaller value for the olefins corresponds to greater solubility and accords with the attraction between olefin bonds and water revealed by the well-known structures of layers of fatty acids adsorbed on water.

The astonishing feature of this analysis is that the δ-value 24.0, obtained from the solubility data, turns out to be practically identical with the value derived from the energy of vaporization of water, 23.8. This may well be the result of a fortuitous cancellation of various factors.

[1] Black, Joris, and Taylor, J. Chem. Phys. **16**, 537 (1948).
[2] Compare J. H. Hildebrand, Chem. Rev. **44**, 37 (1949).

Statistical Mechanics of Dilute Polymer Solutions

PAUL J. FLORY
Department of Chemistry, Cornell University, Ithaca, New York
October 3, 1949

THE recently published theory[1] of intramolecular interactions in isolated polymer molecules may be extended, as described below, to the calculation of the partition function for a pair of polymer molecules in a dilute solution. The methods of the theory of real gases may then be employed for the calculation of the coefficients B' and C' in the virial expansion

$$\pi/c=(RT/M)[1+(B'/M)c+(C'/M^2)c^2+\cdots], \qquad (1)$$

where π represents the osmotic pressure, M is the molecular weight and c the concentration in g per unit volume. The present treatment represents a refinement of one presented several years ago,[2] in that the molecule is treated as a Gaussian distribution of segments about the center of gravity rather than as a uniform distribution within a sphere; further, the energy of mixing term, previously neglected, is here included.

Consider a volume element δv near two identical polymer molecules i and j the centers of gravity of which are separated by a distance a. Let ρ_i and ρ_j represent the densities, within δv, of "lattice segments" belonging to the respective molecules. The spatial distributions of segments are assumed to be Gaussian, e.g.,

$$\rho_i=x(\beta'/\pi^{\frac{1}{2}})^3\exp(-\beta'^2s_i^2), \qquad (2)$$

where x is the number of lattice segments per molecule, s_i is the distance of the volume element from the center of gravity of molecule i, and $\beta'=3/\alpha lZ^{\frac{1}{2}}$; Z represents the number of segments of length l in the "equivalent chain," and α (which assumes an important role in the intrinsic viscosity expression)[1] expresses the linear expansion of the molecule owing to intramolecular interactions of the segments. The probability that the segments of molecule j in the volume δv do not interfere with those of i is

$$p^{\delta v}=(1-\rho_iV)^{\rho_j\delta v}\cong\exp(-\rho_i\rho_jV\delta v), \qquad (3)$$

where V is the volume of one segment. The quantity $k\ln p^{\delta v}$ may be looked upon as the entropy change on combining the $\rho_j\delta v$ segments of polymer j with the $\rho_i\delta v$ segments of polymer i within the same volume element δv, the respective sets of segments occupying initially separate volume elements of the same size. If the presence of the solvent molecules of molar volume x_sV is approximately taken into account,[1] Eq. (3) is to be replaced by

$$p^{\delta v}=\exp(-\rho_i\rho_jV\delta v/x_s). \qquad (3')$$

The heat change accompanying the above superposition process may be written

$$\delta H=\rho_i\rho_jV(\gamma-2)(-2\Delta\epsilon)\delta v=-2kT\rho_i\rho_j\kappa_1V\delta v/x_s, \qquad (4)$$

where γ is the lattice coordination number and $\Delta\epsilon$ is the difference in interaction energy between a solvent-polymer pair of near neighbor segments and the mean of the interactions for solvent-solvent and for polymer-polymer. The quantity κ_1, which is defined by the second equality in Eq. (4), replaces the previous μ_1, which has fallen into widespread misuse.

The factor contributed by the interactions in the volume element δv to the partition function $f(a)$ for a pair of molecules at a distance a apart is given according to Eqs. (3') and (4) by

$$f^{\delta v}=\exp[-\rho_i\rho_j(V/x_s)(1-2\kappa_1)\delta v]$$

and

$$f(a)=\Pi f^{\delta v}=\exp\left[\int-\rho_i\rho_j(V/x_s)(1-2\kappa_1)dv\right].$$

Substituting the Gaussian functions for ρ_i and ρ_j and integrating over-all space

$$f(a)=\exp\{-[(\beta'^2/2\pi)^{\frac{1}{2}}x^2(V/x_s)(1-2\kappa_1)]\exp(-\beta'^2a^2/2)\} \qquad (5)$$

$f(a)$ represents the relative probability (per unit volume) that the center of molecule j occurs within a volume element at a distance a from molecule i. The volume effectively excluded by a molecule as reckoned for binary encounters is given by

$$\int_0^\infty[1-f(a)]4\pi a^2da. \qquad (6)$$

The second virial coefficient of Eq. (1) is half of this quantity per mole, or substituting Eq. (5) in (6)

$$B'=(2^{5/2}\pi N/\beta'^3)\int_0^\infty\{1-\exp[-K\exp(-y^2)]\}y^2dy \qquad (7)$$

where N is Avogadro's number, $y=\beta'a/2^{\frac{1}{2}}$, and

$$K=(\beta'^2/2\pi)^{\frac{1}{2}}x^2(V/x_s)(1-2\kappa_1). \qquad (8)$$

Substituting the expression for β' given above

$$K=(9/2^{\frac{1}{2}}\pi^{\frac{1}{2}})(1-2\kappa_1)C_1Z^{\frac{1}{2}}/\alpha^3$$

where $C_1=(3/\pi)Vx^2/Z^2l^2x_s$ is formally equivalent to the C_1 introduced in the intramolecular configuration theory.[1] Expanding the lower exponential in Eq. (7) and integrating

$$B'=(2^{\frac{1}{2}}\pi^{\frac{1}{2}}/\beta'^3)NK(1-K/2!\cdot2^{\frac{1}{2}}+K^2/3!\cdot3^{\frac{1}{2}}-\cdots) \qquad (9)$$

or

$$B'=(x^2NV/2x_s)(1-2\kappa_1)(1-K/2!\cdot2^{\frac{1}{2}}+K^2/3!\cdot3^{\frac{1}{2}}-\cdots). \qquad (9')$$

The partition function for a cluster of more than two molecules may be expressed as the product of the $f(a_{ij})$ for each pair in the

cluster, provided that the volume fraction of polymer segments is everywhere small.[4] Higher virial coefficients may, in principle, be calculated from the phase integral over the product of factors $[1-f(a_{ij})]$.[5] Straightforward evaluation of these integrals would be hopelessly laborious, but approximate evaluation in the "equivalent sphere" approximation gives[6]

$$C'=(5/8)(B')^2. \tag{10}$$

The parameters C_1 and κ_1 (which is inversely proportional to temperature) are indicative of the magnitudes of the entropy and heat of mixing of polymer segments with solvent. Their evaluation from B' (and C') and its temperature coefficient is complicated by the occurrence of the intramolecular expansion factor α in β' and K. This factor also is dependent on temperature.[1,7] It would appear that the elucidation of the fundamental parameters governing polymer-solvent interaction in dilute solutions may best be achieved through a combination of osmotic and viscosity measurements (or some other measure of molecular dimensions, e.g., angular dissymmetry of scattered light) on the same system at different temperatures. Contrary to the usual assumptions, π/c should not vary linearly with c in dilute solutions and the limiting slope is not independent of M. The same conclusions were reached previously.[2]

As $\kappa_1\rightarrow\frac{1}{2}$, Eq. (9′) simplifies through virtual disappearance of higher terms in the series. At $\kappa_1=\frac{1}{2}$, which corresponds to incipient limited miscibility for infinite molecular weight, the excluded volume becomes zero, the second and higher virial coefficients vanish, and Eq. (1) reduces to Van't Hoff's law, as has been found experimentally for polyisobutylene in benzene one degree above the critical temperature for total miscibility.[8] The disappearance of the resistance to overlapping of the molecules as κ_1 approaches $\frac{1}{2}$ provides an explanation for the enhanced dependence of η_{sp}/c on concentration in poor solvents.

[1] P. J. Flory, J. Chem. Phys. **17**, 303 (1949).
[2] P. J. Flory, J. Chem. Phys. **13**, 453 (1945).
[3] The notation follows closely that used in reference (1), except for the replacement of μ_1 by κ_1.
[4] Otherwise, approximations used in deriving Eq. (3) no longer are valid.
[5] See J. G. Kirkwood, J. Chem. Phys. **3**, 300 (1935).
[6] L. Boltzmann, *Vorlesungen uber Gastheorie* (Verlag Abschnitt, Leipzig, 1898), Vol. II, p. 138.
[7] T. G. Fox, Jr., and P. J. Flory, J. Phys. Coll. Chem. **53**, 197 (1949).
[8] P. J. Flory, J. Am. Chem. Soc. **65**, 372 (1943).

Microwave Investigations of Chloroform*

WILLIAM V. SMITH AND ROBERT R. UNTERBERGER
Department of Physics, Duke University, Durham, North Carolina
October 3, 1949

THE $J=2$ to 3 and $J=3$ to 4 rotational transitions of $CHCl_3^{35}$ have been observed by the techniques of Stark modulation[1] using a coiled cell of twenty-four foot equivalent length, and a four kilocycle modulation frequency. Since each chlorine nucleus gives rise to a quadrupole splitting of the energy levels,[2] the resolved structure is rather complex, and the individual lines weak. At pressures near one millimeter of mercury however, the strongest lines of $CHCl_3^{35}$ integrate to form a single absorption peak about 28 megacycles wide centering at 26,417 megacycles for the $J=3$ to 4 transition. The corresponding moment of inertia I_B is 254.1 $\times10^{-40}$ g cm^2.

For $CHCl_3$, 96 percent of I_B is contributed by the chlorine atoms, and about two percent each by the carbon and hydrogen. The structure thus is insensitive to isotope variation, although information from $CDCl_3$, which we are endeavoring to obtain, would be useful. This insensitivity of structure to isotope however allows rather accurate determination of the C—Cl and, especially, the Cl—Cl distances from a single moment of inertia. If the C—H distance is assumed to be 1.11A (equal to the value for CH_3Cl),[3] a value of the H—C—Cl angle of 106°±3° (consistent with electron diffraction data)[4] gives a Cl—Cl distance of 2.91∓0.01A, and a C—Cl distance of 1.75±0.02A. These values, while within the limits of electron diffraction data, are somewhat shorter than the average values. The C—Cl bond is shorter than the value of 1.779 found for methyl chloride,[3] a trend similar to that observed with CHF_3 and CH_3F.[5]

* This research reported in this document has been made possible through support and sponsorship extended by the Geophysical Research Directorate of the Air Force Cambridge Research Laboratories under Contract No. W19-122-ac-35. It is published for technical information only and does not represent recommendations or conclusions of the sponsoring agency.
[1] R. H. Hughes and E. B. Wilson, Jr., Phys. Rev. **71**, 562 (1947).
[2] Townes, Holden, Hardeen, and Merritt, Phys. Rev. **71**, 644 (1947).
[3] Gordy, Simmons, and Smith, Phys. Rev. **74**, 243 (1948).
[4] Louis R. Maxwell, J. Opt. Soc. Am. **30**, 374 (1940).
[5] Gilliam, Edwards, and Gordy, Phys. Rev. **75**, 1014 (1949).

On the Catalyst Surface Structure

SHOU-CHU LIANG
National Research Council, Ottawa, Canada
October 24, 1949

IN a recent article, Sips[1] advanced a mathematical formulation claiming to have established a method using which the heterogeneity of a catalyst surface can be calculated rigorously from an experimental isotherm. A close examination of his formulation reveals that it is unsatisfactory and in fact it cannot be of much use. While we have not been able to establish a new and useful formulation, we feel that it is important to point out his erroneous approach.

Before going into detail, the notation used by Sips must be corrected. In order to fulfill his condition $\int_{-\infty}^{+\infty}N(q)dq=1$ $N(q)$ should represent the *fraction* of the number of sites having heat of adsorption q instead of the number itself as designated by Sips. His errors may be summarized as follows:

(1) His Eq. (2) may be rewritten as

$$\theta=\sum_{q=-\infty}^{+\infty}\frac{N(q)}{1+(a/p)\exp(-q/RT)}. \tag{a}$$

After he gets the formulation of $N(q)$ by using the Freundlich isotherm, he is unable to obtain the original isotherm because the integral is "intractable". Without carrying out the integration, we can see from Eq. (a) that the resultant isotherm must be the Langmuir and not the Freundlich type. His treatment therefore fails to give a consistent result.

(2) It is to be noted that no matter what analytical form $N(q)$ may take, Eq. (a) will only yield a Langmuir isotherm. The sigmoidal isotherm which is commonly obtained cannot be possibly described by Sips' isotherm thus indicating the invalidity of the formulation. In fact, if one uses the *BET* isotherm equation in the uncondensed form to evaluate the heterogeneity distribution function, one finds that $N(q)=0$ for all values of q except for $q=-\infty$. This contradicts the original postulates from which $N(q)$ is derived and proves further the treatment lacking of consistency.

(3) Sips claims that the lack of knowledge of the form of the function of an experimental isotherm being "no obstacle, because the experimental values may always be represented as exactly as we like by using analytical expressions." This is fundamentally wrong. The function we need to calculate the distribution function $N(q)$ must not only describe the experimental isotherm well; but also represent the true mechanism, about which we have very little knowledge. Assigning an arbitrary form to the adsorption isotherm equation is equivalent to assigning an arbitrary form to $N(q)$. This will be discussed more fully elsewhere.

(4) Repeatedly, Sips is troubled by the non-convergence of $\int_{-\infty}^{+\infty}N(q)dq$. When working with the Freundlich isotherm, he attributes the reason to the form of the isotherm equation which goes to infinity when $p=\infty$. This is incorrect. The $N(q)$ evaluated by Sips' method should be valid for all the region where the isotherm equation is valid. Plainly, when the integration is carried

out from $q=-\infty$ to $+\infty$, the pressure can still remain low, fulfilling the condition under which the Freundlich isotherm is valid; and $\int_{-\infty}^{+\infty} N(q)dq$ would therefore remain finite if Sips' reasoning were sound. The non-convergence character of $\int_{-\infty}^{+\infty} N(q)dq$ is actually a consequence of Sips' use of Eq. (1) in which he contends that those sites where $q=-\infty$ are not counted. Therefore the lower integration limit of $\int N(q)dq$ should be some finite value instead of being $-\infty$ in order to make the operation consistent. Such a change in limit makes the integral convergent at all pressures where the isotherm equation holds.

In conclusion, Sips' treatment can only be useful if (a) the Langmuir isotherm is valid and (b) the isotherm equation representing the true adsorption mechanism (and not merely an analytical expression giving all the approximately correct *numerical* values) is known. These conditions practically deprive his formulation of all its significance, because the first condition is not always met and the second cannot yet even be approximated. Even if both conditions can be met, the function $N(q)$ obtained does not necessarily satisfy the equation $\int_{-\infty}^{+\infty} N(q)dq=1$.

[1] R. Sips, J. Chem. Phys. **16**, 490 (1948).

The Triple-Dipole Interaction between Atoms and Cohesion in Crystals of the Rare Gases

B. M. Axilrod
George Washington University, Washington, D. C.
October 3, 1949

THE application of third-order perturbation theory to the interaction of neutral atoms was reported[1] to result in an interaction between triplets of atoms. The term in the third-order interaction energy which depends on triplets of atoms is

$$W_0'''=\sum_{j\neq 0}\sum_{\substack{k\neq 0\\ k\neq j}}\frac{H_{0j}H_{jk}H_{k0}}{(W_j-W_0)(W_k-W_0)}, \tag{1}$$

where W_j, W_k, and W_0 are the unperturbed energies of the intermediate states j and k, and the ground state, respectively. H_{0j} etc. are the matrix elements of the perturbation. If the perturbing potential is limited to the dipole-dipole term, the following approximate expression, called the triple-dipole interaction, is obtained for W_0'''.

$$W_0'''\cong\frac{3}{2}\frac{(V_1+V_2+V_3)V_1V_2V_3\alpha_1\alpha_2\alpha_3(3\cos\gamma_1\cos\gamma_2\cos\gamma_3+1)}{(V_1+V_2)(V_2+V_3)(V_1+V_3)R_{12}^3R_{23}^3R_{13}^3}. \tag{2}$$

V_1, V_2, and V_3 are the ionization potentials and α_1, α_2, and α_3 the polarizabilities of the three atoms; R_{12}, R_{23}, and R_{13} are the sides and γ_1, γ_2, and γ_3 the angles of the triangle formed by the nuclei of the atoms. For like atoms (2) becomes:[2]

$$W_0'''\cong\frac{9}{16}\frac{V\alpha^3(3\cos\gamma_1\cos\gamma_2\cos\gamma_3+1)}{R_{12}^3R_{23}^3R_{13}^3}. \tag{2a}$$

The triple-dipole interaction W_0''' is positive, i.e., repulsive, for all acute triangles and negative for most obtuse triangles.

It can be shown that W_0''' for three rare gas atoms is about one percent of the dipole-dipole interaction energy of the London type.[3] Since W_0''' is relatively small, it does not appear likely to contribute much to the cohesive energy even for molecular crystals. The dependence of W_0''' on the configuration of three atoms, however, suggested that the structure of the rare gas solids might be explained by the triple-dipole interaction. Argon, neon, krypton, and xenon crystallize in the face-centered-cubic lattice, one of the two closest-packed structures,[4] the other being the hexagonal-closest-packed lattice. London[5] showed that, assuming pairwise additivity, the dipole-dipole interaction accounted largely for the cohesion of molecular crystals. However, the lattice sums of the dipole-dipole interaction for the f.c.c.[6] and h.c.p.[7] lattices do not differ by more than 0.01 percent. This is also true if the dipole-quadrupole or higher pole interactions are similarly summed, so the stability of the f.c.c. compared to the h.c.p. structure cannot be explained by differences in these interactions.

The triple-dipole interaction, W_0''', was directly summed in both the f.c.c. and h.c.p. lattices for a cylindrical region whose radius and semi-altitude were about three times the nearest-neighbor distance. These calculations were made on IBM punched-card machines.[8]

For the above region the sum of W_0'''/K, where K equals $\frac{9}{16}V\alpha^3/r_0^9$, is 56.686 for the f.c.c. and 56.727 for the h.c.p. lattice. From an examination of partial sums it seems that: (a) W_0'''/K converges to a value close to 57 and (b) the sum of W_0'''/K is roughly 0.04 greater for the h.c.p. compared to the f.c.c. lattice.

The triple-dipole interaction was computed for crystals of the rare gases using accepted values of V, r_0, and α, and 56.69 for the sum of W_0'''/K. From the results of Table I it is noted that the triple-dipole interaction amounts to two to nine percent of the cohesive energy for most rare gas solids.

TABLE I. Triple-dipole interaction for crystals of rare gases.

Element	Lattice sum of W_0''' (repulsion) kcal./mole	Heat of sublimation kcal./mole
Neon	0.0090	0.51
Argon	0.093	1.86
Krypton	0.229	2.57
Xenon	0.335	3.59

It seems unlikely that the difference in the triple-dipole interaction for the f.c.c. compared to the h.c.p. lattice, a difference less than a ten-thousandth of the cohesive energy, can explain the stability of the f.c.c. lattice for the rare gas elements. Details of this work will be published later.

[1] B. M. Axilrod and E. Teller, J. Chem. Phys. **11**, 299 (1943).
[2] The equation for W_0''' in reference 1 was incomplete in that the factor $\frac{9}{16}$ had not been determined. In March, 1948, a letter was received from Mr. Yosio Muto of Japan who had also worked out the triple-dipole interaction. Mr. Muto's result for W_0''' appeared to be in agreement with (2a).
[3] The dipole-dipole interaction energy is approximately $-\frac{3}{2}(V\alpha^2/R^6)$ for like atoms.
[4] *Handbook of Chemistry and Physics* (1945).
[5] F. London, Trans. Faraday Soc., **32**, 8 (1937).
[6] Lennard-Jones, Proc. Roy. Soc., **A107**, 636 (1935).
[7] M. Goeppert-Mayer and G. Kane, J. Chem. Phys. **8**, 642 (1940).
[8] These calculations were made by the Computation Laboratory of the National Bureau of Standards, New York City, under sponsorship of the ONR.

The Sodium (^2P) Photo-Sensitized Decomposition of Ethane*

G. L. Lee† and D. J. LeRoy
Department of Chemistry, University of Toronto, Toronto, Canada
October 19, 1949

THE excitation energy of the sodium (^2P) states is approximately 48.3 kcal.; the heat of formation of gaseous sodium hydride from the atoms is in the range 47[1] to 51.6[2] kcal. It might be expected, therefore, that, provided sodium hydride were formed, Na(^2P) atoms could sensitize the decomposition of hydrocarbons having C—H bond strengths not exceeding 95.3 to 99.9 kcal. The analogous reaction is known to occur with Cd($^3P_1$) atoms,[3] for which the excitation energy is 82.9 kcal. and the heat of formation of the hydride is 15.6 kcal.; in this case cadmium hydride bands were detected by resonance fluorescence.[4] Jungers and Taylor[5] made an unsuccessful attempt to sensitize the polymerization of ethylene with Na(^2P) atoms, but it seemed reasonable to assume that their negative result was, by analogy with the data on

$Cd(^3P_1)$ and the lower olefins,[6] due to the dissipation of the electronic energy of the excited atoms in the double bond.

We now wish to report that a sensitized decomposition of ethane cannot be accomplished with $Na(^2P)$ atoms. A total of seventeen experiments were performed at temperatures ranging from 228° to 292° and with ethane pressures from 18 to 118 mm. The sodium was distilled into the cell under high vacuum conditions in order to remove as much hydrogen as possible. From the data of Norrish and Smith[7] the quenching efficiency of hydrogen is approximately 117 times that of ethane. Purified ethane was admitted at the required pressure, frozen with liquid air, and the cell sealed off. In this way the whole of the cell volume could be kept at the temperature of the furnace to avoid distillation of the sodium to a cold zone with a consequent decrease in its partial pressure. In some experiments the sodium Lab Arc was placed outside the furnace and the light was admitted through a window; in other experiments the emitting portion of the lamp was inserted into the furnace where it entered a Dewar-shaped cell to take full advantage of the light intensity. The *D* lines were sufficiently narrow to be almost completely absorbed by the sodium vapor in the cell. The duration of illumination varied from three to 120 hours, after which the cell was sealed to the analysis apparatus and the gas removed through a break-off valve.

In most of the experiments the hydrogen recovered amounted to about 1.5 percent or less. The only other product consisted of less than one percent of a fraction having a vapor pressure of 0.1 mm at −32°C, but the same material was found without illumination, both in the presence and in the absence of sodium. It can be concluded, therefore, that no photo-sensitized decomposition occurred.

The values quoted for the C−H bond strength in ethane range from 96.8 to 98 kcal.[8] If the larger value for the heat of formation of sodium hydride is correct the reaction would be exothermic; for the smaller value it might be endothermic by as much as 2.7 kcal. scarcely enough to preclude reaction at the temperatures used. It can probably be concluded that a quenching process resulting in the formation of sodium hydride would involve a considerable activation energy.

Although, energetically, the dissociation of hydrogen by $Na(^2P)$ atoms is less favorable than that of ethane, a number of experiments were performed with hydrogen-ethane mixtures. If atomic hydrogen had been produced, products such as methane would undoubtedly be formed. However, the results were again negative.

* This research was supported by a grant from the Advisory Committee on Scientific Research, University of Toronto.

† Present address: Department of Chemistry, University of Colorado, Boulder City, Colorado.

[1] A. G. Gaydon, *Dissociation Energies* (Chapman and Hall, Ltd., London, 1947).
[2] F. R. Bichowsky and F. D. Rossini, *Thermochemistry of Chemical Substances* (Reinhold Publishing Corporation, New York, 1936).
[3] E. W. R. Steacie and R. Potvin, J. Chem. Phys. **7**, 782 (1939).
[4] E. W. R. Steacie and D. J. LeRoy, J. Chem. Phys. **12**, 34 (1944).
[5] J. C. Jungers and H. S. Taylor, J. Chem. Phys. **4**, 94 (1936).
[6] D. J. LeRoy and E. W. R. Steacie, J. Chem. Phys. **10**, 683 (1942).
[7] R. G. W. Norrish and W. MacF. Smith, Proc. Roy. Soc. (London) **A176**, 295 (1940).
[8] E. W. R. Steacie, *Atomic and Free Radical Reactions* (Reinhold Publishing Corporation, New York, 1946).

The Kinetics of the Pyrolysis of Allyl Bromide

ALLAN MACCOLL
Sir William Ramsay and Ralph Forster Laboratories, University College, London, England

July 20, 1949

THERE are three main processes by which the pyrolysis of organic bromides may occur. First, a direct unimolecular split into HBr and an olefin as observed by Kistiakowsky and Stauffer[1] in the case of *tert.*—butyl bromide. Second, a breaking of the C−Br bond, leading to a bromine atom, which may further interact with the system leading to HBr and an olefin by a non-chain, radical mechanism. This behavior has been postulated by Daniels[2–5] and his co-workers in the case of ethyl bromide. Third, the bromine atom may participate in the propagation of long chains. The behavior of methyl bromide, investigated by Meissner and Schumacher[6] is suggestive of such a mechanism. The case of allyl bromide is of particular interest, since the stability due to resonance of the allyl radical should facilitate the breaking of the C−Br bond.

Investigation has shown that essentially all the HBr is eliminated from allyl bromide and that the ratio of the final to initial pressure is about 1.5. The reaction is homogeneous and first-order rate constants calculated from both analytical and pressure results are in good agreement. However, it is found that as the initial pressure of allyl bromide is reduced below about 300 mm, the constants fall. Oxygen, nitrogen, and propylene have no influence on the rate, but hydrogen is capable of restoring the low pressure rate to its high pressure value.

In view of these observations it would appear that the pyrolysis of allyl bromide takes place by the initial step

$$C_3H_5Br \rightarrow CH_2-\widehat{CH}-CH_2+Br$$

and by a Lindemann mechanism. The rate constant in the range 320–380°C can be represented by the expression

$$k=2.11\times10^{12}e^{-45,500/RT}\ \text{sec.}^{-1}.$$

The Anhenius plot is shown in Fig. 1. Each point represents the

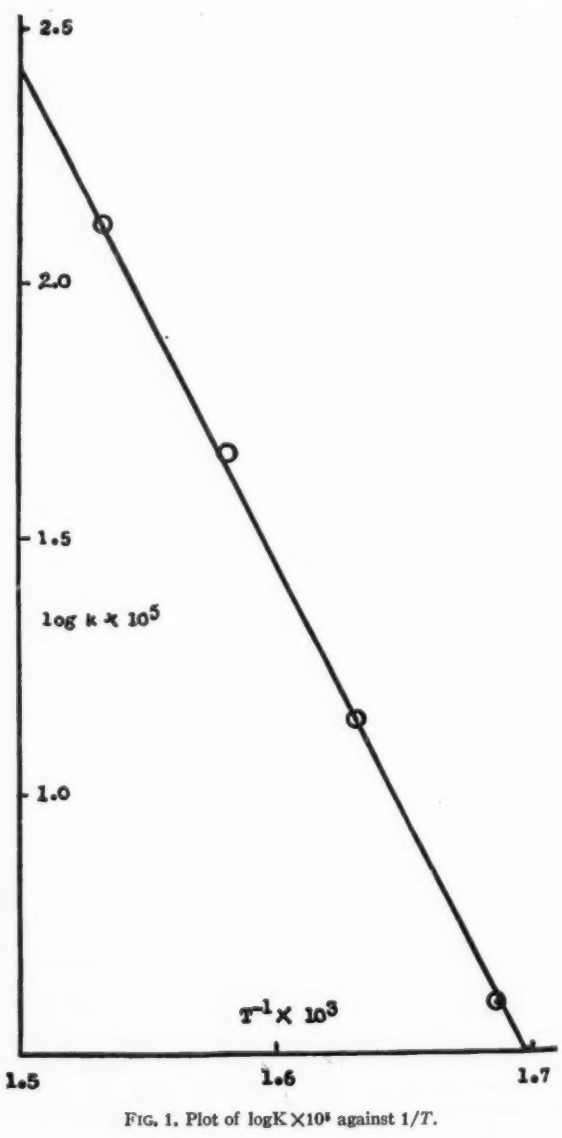

FIG. 1. Plot of $\log K\times10^5$ against $1/T$.

mean of about six runs. The activation energy of the reaction, is in excellent agreement with the bond dissociation energy of C—Br in allyl bromide suggested by Roberts and Skinner.[7] This value is derived from a measurement of the heat of formation of allyl bromide, together with the heat of formation of the allyl radical as determined by Szwarc[8] from the pyrolysis of propylene.

Using the Bichowsky and Rossini[9] data for the heat of formation of CH_3Br and that of Kistiakowsky *et al.* for the C—H bond dissociation energy in CH_4, the value 67.3 kcal. may be arrived at for the C—Br bond dissociation energy in methyl bromide. The difference between the value for methyl bromide and that for allyl bromide is not directly comparable with the quantum-mechanical calculation of the resonance energy of the allyl radical, because of the neglect of the difference in the energies of reorganization of the two radicals.

A fuller account of this work will shortly be presented elsewhere.

[1] Kistiakowsky and Stauffer, J. Am. Chem. Soc. **59**, 165 (1937).
[2] Lessig, J. Phys. Chem. **36**, 2225 (1932).
[3] Vernon and Daniels, J. Am. Chem. Soc. **55**, 922 (1933).
[4] Fugani and Daniels, J. Am. Chem. Soc. **60**, 771 (1938).
[5] Daniels and Veltman, J. Chem. Phys. **7**, 756 (1939).
[6] Meissner and Schumacher, Zeits. f. physik. Chemie **185**, 435 (1940).
[7] Roberts and Skinner, Trans. Faraday Soc. **45**, 339 (1949).
[8] Szwarc, J. Chem. Phys. **17**, 284 (1949).
[9] Bichowsky and Rossini, *The Thermochemistry of Chemical Substances* (Reinhold Publishing Corporation, New York, 1936).

The Vibrational Spectra and Structure of the Aluminum Hydride Ion

ELLIS R. LIPPINCOTT
Department of Chemistry, University of Connecticut, Storrs, Connecticut, and Spectroscopy Laboratory, Massachusetts Institute of Technology, Cambridge, Massachusetts
October 28, 1949

THE chemical and physical properties of lithium borohydride ($LiBH_4$) and lithium aluminum hydride ($LiAlH_4$) suggest the presence of the BH_4^- and AlH_4^- ions in their respective crystals.[1-3] In order to determine if the AlH_4^- ion exists in solution, the infra-red and Raman spectra of a 1.28 M solution of $LiAlH_4$ in diethyl ether have been studied. The sample of $LiAlH_4$ used in this work was obtained from the Metal Hydrides Corporation and had a purity of 96 percent. The transparent ether solution was prepared by refluxing the solid with anhydrous ether for several hours followed by decantation after the undissolved solid material had settled to the bottom of the container. Samples were pipetted under anhydrous conditions into Raman tubes and sealed before hydrolysis by atmospheric water vapor occurred. A similar procedure was used in filling the infra-red absorption cells.

The infra-red spectrum of the solution was obtained on a Beckman IR-2 infra-red spectrometer in the region 3μ to 15μ. The absorption peaks of the solute were obtained by subtracting the peaks due to the ether from those of the solution. By this procedure the infra-red spectrum was found to consist of two intense bands, with peaks at 764 and 1740 cm^{-1}. Both bands were broad. No weaker bands were observed although it is conceivable that some could be hidden under ether absorptions. The band at 1740 cm^{-1} has some asymmetry.

The Raman spectrum was obtained using a three-prism Zeiss instrument with a camera lens of aperture number 4.5. The plate factor at 4500A was 30A/mm. The excitation unit has been described elsewhere.[4] Its main features are six AH2 General Electric lamps, six elliptical reflectors, and a filter cell at the center of which is located a 5 ml Raman tube. The 4358A mercury line was used for excitation. The 4047A mercury line was removed using a filter solution of saturated sodium nitrite. Solutions of rhodamine 5D GN extra (0.01 g/l) and praseodymium chloride ($\frac{1}{10}$ saturated) were used through a thickness of 1 cm to cut down the continuum above 4358A. Several Raman spectra were taken on various samples before one sufficiently free of a continuum was obtained. On the best two plates exposure times of two hours were used. The Raman shifts of the solute were obtained by subtracting those due to ether from those of the solutions. The results are summarized in Table I. The reality of the 769-cm^{-1} line may be

TABLE I. Raman and infra-red data and assignments for the aluminum hydride ion.

Raman	I	Infra-red	I	Assignment	Symmetry
769	(1)	764	(5)	ν_4	F_2
799	(2)			ν_2	E
1741	(2)	1740	(5)	ν_3	F_2
1790	(3)			ν_1	A_1

questioned because of its intensity and the continuum on the plate, but its coincidence with the broad infra-red band at 764 cm^{-1} suggests that it is real.

Although rigorous selection rules derived for gases do not necessarily hold for substances in solution, the four Raman and two infra-red bands observed and the coincidence of the infra-red bands with two Raman bands are consistent with a tetrahedral model for the AlH_4^- ion in solution. The broadness of the infra-red bands is probably due to the partial splitting of the triply degenerate modes of vibration by liquid forces.

Force constants for the stretching and bending vibrations of the AlH_4^- ion have been calculated using a simple valence force model.[5] The values calculated for k and $k\delta/e^2$ are, respectively, 1.89 and $0.126 \cdot 10^5$ dynes/cm. Since the valence force model involves two force constants, there are two independent relations between the four frequencies which may be used as checks on the model. Table II gives calculated and observed values for $\lambda_3^2+\lambda_4^2$

TABLE II. Calculated and observed values for $\lambda_3+\lambda_4$ and $\nu_3\nu_4/\nu_1\nu_2$ assuming a simple valence force potential.

	Observed	Calculated
$\lambda_3+\lambda_4$	$2.14 \cdot 10^5$ dynes/cm	$2.26 \cdot 10^5$ dynes/cm
$\frac{\nu_3\nu_4}{\nu_1\nu_2}$	0.93	0.88

and $\nu_3\nu_4/\nu_1\nu_2$. The agreement is good for a simple valence force model, the percentage error being less than the corresponding error for a number of other tetrahedral molecules and ions.[5]

[1] Schlesinger and Brown, J. Am. Chem. Soc. **62**, 3429 (1940).
[2] Fenholt, Bond, and Schlesinger, J. Am. Chem. Soc. **69**, 1199 (1947).
[3] Smith, Sci. Progress **35**, No. 139, 515 (1947).
[4] Harrison, Lord, and Loofbourow, *Practical Spectroscopy* (Prentice-Hall, Inc., New York, 1948).
[5] G. Herzberg, *Infrared and Raman Spectra of Polyatomic Molecules* (D. Van Nostrand Company, Inc., New York, 1945), p. 182.

A Note on Temperature and the Recombination Coefficient

N. C. GERSON
Air Force Cambridge Research Laboratories, Cambridge, Massachusetts
November 12, 1949

EQUATIONS of the type

$$\alpha = AT^r,$$

where α = recombination coefficient (cm/sec.),[1] T = temperature (°K), and A = dimensional constant have been postulated on many occasions. In early studies on air, carbon dioxide and hydrogen, Erikson[2,3] obtained values which indicate that the exponent $-2.5 \leqslant r \leqslant -2.2$ when T varies from 90°K to 450°K. However, in Erikson's results, $A \neq$ constant. At about the same period Phillips experimentally found $r = -2.2$ for air at constant pressure in the temperature range from about 80°K to 500°K. At low pressures Thomson and Thomson[4] theoretically indicate that $r = -3$. On the

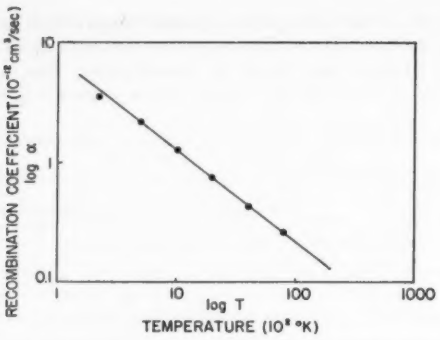

FIG. 1. Plot of α *versus* T. Amount of oxidation for various concentrations.

basis of statistical equilibrium, Milne[5] showed that $r=-\frac{1}{2}$ when $T=Te$, the electron temperature. Similar results were obtained by Tukada,[6] by Yamonauchi and Kotani[7] and by Hulbert.[8] Bates and Massey[9] indicate that $r=-\frac{3}{2}$ under ionospheric conditions. Thomson found that $r=-5/2$ at low pressures and $r=-\frac{3}{2}$ at high pressures. Loeb[9] indicates that for ionospheric work, $r=+\frac{1}{2}$.

Amidst the confusion of the above results, it is interesting to note a new value of r which may be obtained from the accompanying figure. Employing data recently computed by Bates and collaborators, a graph of α *versus* T was plotted. It is readily apparent that in the temperature range 250°K to 8000°K, the value $r=-\frac{3}{4}$ applies. The complete expression obtained from the figure is $\alpha=2.43\times10^{-10}T^{-0.738}$.

[1] Phillips, Proc. Roy. Soc. **A133**, 246 (1910).
[2] Erikson, Phil. Mag. **18**, 328 (1909).
[3] Erikson, Phil. Mag. **23**, 747 (1912).
[4] J. J. Thomson and G. P. Thomson, *Conduction of Electricity Through Gases* (Cambridge University Press, London, 1928), p. 50.
[5] E. A. Milne, Phil. Mag. **47**, 209 (1924).
[6] T. Tukada, Rept. Radio. Res. Japan **7**, 121 (1937).
[7] T. Yamonouchi and M. Kotani, Proc. Phys. Math. Soc. Japan **22**, 61 (1940).
[8] E. O. Hulbert, *Terrestrial Magnetism and Electricity* (McGraw-Hill Book Company, Inc., New York, 1939), Vol. 8, p. 519.
[9] D. R. Bates and H. S. W. Massey, Proc. Roy. Soc. **A187**, 261 (1946).
[10] J. J. Thomson, Phil. Mag. **47**, 337 (1924).
[11] L. B. Loeb, *Fundamental Processes of Electrical Discharges Through Gases* (John Wiley and Sons, Inc., New York, 1939).
[12] Bates, Buckingham, Massey, and Unwin, Proc. Roy. Soc. **A170**, 322 (1939).

The Entropy and Configuration of Methylhydrazine

G. J. JANZ AND K. E. RUSSELL
The School of Chemistry and Physics, Pennsylvania State College, State College, Pennsylvania
October 3, 1949

THE theoretical treatment of Penney and Sutherland[1] indicates that the most stable form of hydrazine should be a skew form as opposed to the symmetrical *trans* configuration. The recent entropy study on this compound by Scott, Oliver, Gross, Hubbard, and Huffman[2] is in accord with this. The present communication concerns methylhydrazine which is theoretically capable of existing in a *trans* form and two skew forms as shown in Fig. 1. It is possible to investigate the number of forms present by a comparison of experimental and calculated entropies of the ideal gas. The results of such an investigation[3] together with evidence from dipole moment data are reported in this letter. A summary of the experimental results is given in Table I.

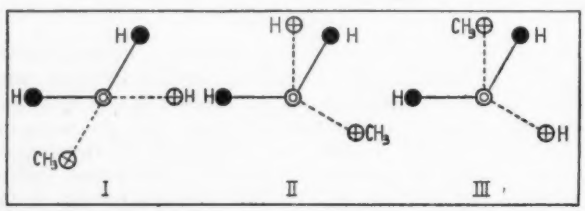

FIG. 1. End-on view of methylhydrazine. I—*Trans*-form. II—"Outer" skew form. III—"Inner" skew form.

TABLE I.

	E.U./Mole
0–15°K Debye function ($\theta=193$, six degrees of freedom)	0.073
15–220.79°K (graphical)	18.780
Fusion (2490.5/220.79)	11.279
220.79–298.16°K (graphical)	9.530
Entropy of liquid at 298.16°K	39.662 ±0.07
Vaporization (9650.3/298.16)	32.366 ±0.11
Entropy of real gas at 298.16°K/49.6 mm.	72.028 ±0.18
Entropy of ideal gas	72.036 ±0.18
Compression $R\ln(49.6/760)$	−5.423 ±0.02
Entropy of ideal gas at 298.16°K/760 mm.	66.61 ±0.20

Possible residual entropy at absolute zero has been neglected.[2] The results of calculations of the entropy from molecular structure and spectroscopic data are given in Table II for an equimolal mixture of the two optical isomers of the "outer" skew form.

TABLE II.

S^0 translational	37.393
S^0 ext. rot.	22.094
S^0 vibrational	1.418
S^0 int. rot. (CH_3 and NH_2)	3.751
S^0 mixing (2 o. isomers)	1.379
Total entropy (ideal gas, 298.16°K/760 mm.)	66.04 e.u.

The vibrational entropy contribution was calculated using an assignment made on the basis of work done by Kahovec and Kohlrausch[4] and of infra-red and Raman studies in this college. The entropy contributions for restricted internal rotation were taken from the tables of Pitzer and Gwinn,[5] barriers of 3200 cal./mole for the methyl group (CH_3 *vs.* $NHNH_2$) and 3000 cal./mole for the amino group (NH_2 *vs.* $NHCH_3$) being taken as best values. The symmetry of the potential energy barrier of the NH_2 group is assumed very nearly a symmetrical threefold cosine-type.[1,2] While from stereochemical considerations one would expect the "outer" form to be more stable than the "inner," one would expect a certain percentage of each of the two optical isomers of the "inner" form in the equilibrium mixture. In keeping with this, the experimental and calculated entropies reported above are brought into agreement if methylhydrazine be assumed to consist only of a mixture of 92 mole percent and 8 mole percent of the "outer" and "inner" forms respectively (entropy of mixing, 0.57 e.u.). This result gives a value of E_0 between the "outer" and "inner" forms as calculated from the relationship:

$$E_0=-RT\ln\frac{N\text{ (inner)}}{N\text{ (outer)}}\text{ of about 1450 cal./mole.}$$

It is evident that the above conclusions are dependent on the barriers hindering the internal rotation of the methyl and amino groups. Only if the barriers are chosen as 2700 cal./mole and 2050 cal./mole for the methyl and amino hindered rotation respectively (and these are reasonable minimum values corresponding to S^0 int. rot., 4.32 e.u.) does the entropy calculated for the "outer" isomers alone correspond to the calorimetric entropy (i.e., the "inner" and *trans* structures are not allowed). Again if the barriers are 3500 and 3400 cal./mole respectively for the methyl and amino groups (which are probably maximum values, giving S^0 int. rot. as 3.41 e.u.) the calculated entropy is in agreement with the experimental value if methylhydrazine vapor consists of a mixture of 84 mole percent of the "outer" form and 16 mole percent of the "inner" form (entropy of mixing, 0.91 e.u.), the E_0 between these being then about 1000 cal./mole.

The dipole moments were calculated assuming the net moment may be compounded vectorially from the bond moments. The results are summarized below:

"Inner" configuration	"Outer" configuration	Observed moment[6]
$\mu=1.13D.$	$\mu=1.91D.$	$\mu=1.68\pm0.14D.$

The dipole moment calculated for the *trans*-configuration is even less than that for the "inner" skew configuration. These results are therefore in accord with the entropy study, namely that methylhydrazine exists predominantly in the skew "outer" form with its methyl group farthest from the hydrogens of the NH_2 group.

This is a preliminary report of part of the program being carried out on Contract N6onr 269, Task Order III of the ONR under the direction of Professor J. G. Aston whose advice we have frequently sought in these calculations.

[1] Penney and Sutherland, Trans. Faraday Soc. **30**, 902 (1934); J. Chem. Phys. **2**, 492 (1934).
[2] Scott, Oliver, Gross, Hubbard, and Huffman, J. Am. Chem. Soc. **71**, 2203 (1949). (These authors kindly supplied us with a copy of their manuscript prior to publication.)
[3] Aston, Fink, Janz, and Russell (to be published).
[4] Kahovec and Kohlrausch, Zeits. f. physik. Chemie **B38**, 96 (1938).
[5] Pitzer and Gwinn, J. Chem. Phys. **10**, 428 (1942).
[6] Ulich, Peisker, and Audrieth, Ber. d. d. chem. Ges. **B68**, 1677 (1935).

The Potential Energy in Conjugated Polyenes and the Effective Nuclear Charge of the Carbon Atom

NOEL S. BAYLISS
Department of Chemistry, University of Western Australia, Nedlands, West Australia
July 18, 1949

IT has been shown recently by the author[1] and others[2,3] that a one-dimensional free electron model for the π-electrons can account for the positions and intensities of absorption bands in polyenes and polymethines. Retaining the one-dimensional approximation, the model can be refined by considering the actual potential energy along the axis of a polyene molecule (Fig. 1(a)). At points "outside" the molecule, the π-electron is in the field of the unit charge $+e$ of the rest of the molecule, and its potential energy is $-e^2/r$, where r is its distance from the center of the molecule. At points "inside" the molecule, the π-electron is in the field of the nuclei shielded by the electrons of the inner K shells and the σ bonds, and also by the other π-electrons. If the hydrogens are neglected and an effective nuclear charge $Z'e$ is assigned to each carbon, the potential energy at a point inside the molecule is $\Sigma_i(-Z'e^2/r_i)$ where r_i is the distance to the ith carbon. The inside curve must be joined smoothly to the outside portions at points beyond the end carbons at a distance we have rather arbitrarily assumed to be about 0.5A. (See Fig. 1(b).)

A numerical solution of the Schroedinger equation for a potential curve expressed graphically as in Fig. 1(b) can be obtained by Southwell's relaxation method[4] and leads to values for both the position of the main absorption band ν and the ionization energy I (Fig. 1(b)). Mr. J. C. Riviere of this department has carried out the calculations for butadiene, and after some trial and error found that the experimental ν and I data[5] require that $Z'=1.2$.

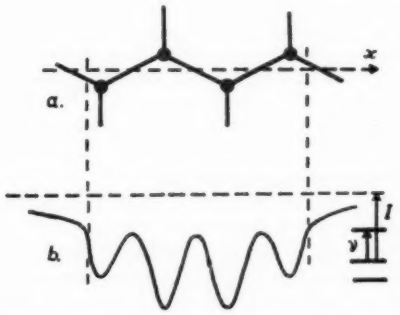

FIG. 1. Model and potential function with ionization potential I and main absorption band.

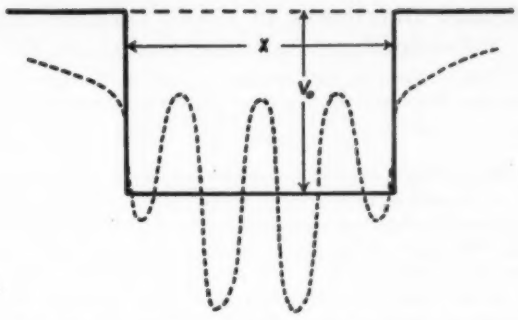

FIG. 2. Rectangular potential compared to that of Ib.

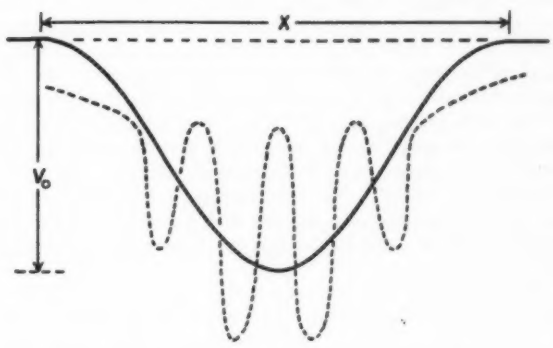

FIG. 3. Sine curve potential compared to that of Ib.

Figures 2 and 3 show two simpler approximations to the potential energy, 2 being a rectangular potential well of width X and depth V_0, and 3 has the form $V=-V_0\sin^2(\pi x/X)$. The first can be solved by the potential staircase method, and the second in terms of Mathieu's equation. In each case the experimental ν and I data determine X and V_0 uniquely. Figures 2 and 3 show to scale the comparison in each case with the calculated Fig. 1(b) curve for butadiene. We have made similar comparisons between the three types of curve for hexatriene and octatetraene (but without carrying out the relaxation calculations) using the ν and I data quoted by Price and Walsh[5] and in each case the value $Z'\approx1$ is required to secure reasonable matching.

The Zener-Slater value[6] of $Z'=3.2$ for a carbon atom is based on the equivalence of the $2s$ and $2p$ electrons. In a double-bonded or conjugated compound, the σ- and π-electrons are not equivalent. If one assumes the π, σ and K electrons in butadiene to be in successive shells, and if Slater's[7] shielding constant of 0.35 is adopted for electrons in the same shell, and 0.85 and 1.00 for successive inner shells, the total shielding towards one π-electron in butadiene is $(3\times0.35)+(12\times0.85)+(8\times1.00)=19.25$, leaving an effective charge of 4.75 for four nuclei, or $Z'=1.19$ per nucleus. This good agreement with the value obtained above may be fortuitous, and may not be retained if it were possible to carry out a proper three-dimensional potential energy calculation. It does however suggest the need to re-examine the proper value of Z' to be used in calculations on the π-electrons in double-bonded compounds.

[1] N. S. Bayliss, J. Chem. Phys. **16**, 287 (1948).
[2] H. Kuhn, J. Chem. Phys. **16**, 840 (1948); Helv. Chim. Acta, **31**, 1441 (1948).
[3] W. T. Simpson, J. Chem. Phys. **16**, 1124 (1948).
[4] R. V. Southwell, *Relaxation Methods in Theoretical Physics* (Oxford University Press, New York, 1946).
[5] W. C. Price and A. D. Walsh, Proc. Roy. Soc. **A185**, 182 (1946).
[6] C. Zener, Phys. Rev. **36**, 54 (1930); J. C. Slater, Phys. Rev. **36**, 58 (1930).
[7] J. C. Slater and N. H. Frank, *Introduction to Theoretical Physics* (McGraw-Hill, Book Company, Inc., New York, 1933), p. 432.

Energy Differences in Liquid Dichloro- and Dibromoethane Rotational Isomerism VI*

D. H. RANK, R. E. KAGARISE, AND D. W. E. AXFORD
Spectroscopy Laboratory, Physics Department, Pennsylvania State College, State College, Pennsylvania
October 3, 1949

RECENTLY a number of papers have appeared on the subject of rotational isomerism in dichloro- and dibromoethane.[1-3] Previously Gerding and Meerman[4] had made measurements on the energy difference of the rotational isomers in the liquid state by means of the Raman effect. The above authors[4] have found that $\Delta H \sim 0$ for liquid dichloroethane. Bernstein[2] working with the infra-red spectrum of the gas has shown that $\Delta H = 1325 \pm 50$ cal. per mole. Mizushima *et al.*[3] have reported results which agree with those of Bernstein[2] on gaseous dichloroethane. The above authors[3] also obtain a result of similar magnitude for gaseous dibromoethane, which result surprisingly agrees with the value of ΔH found by Gerding and Meerman[4] for liquid dibromoethane. The results obtained by the above mentioned authors[1,3] yield a value of ΔH for both gaseous dichloro- and dibromoethane which is substantially the same, and in agreement with the value obtained from dielectric constant measurements of the gas.

As stated previously, the value Gerding and Meerman obtained for liquid dichloroethane was $\Delta H \sim 0$. Mizushima *et al.*[3] report a small but definite value for ΔH from their measurements on liquid dichloroethane.

The surprising situation exists that these two very similar molecules behave so differently with regard to variation of relative intensity of line pairs with temperature in the liquid state, while in the gaseous state the behavior of the two molecules is identical.

Making use of direct photoelectric measurement of intensities, we have repeated the measurements on the Raman spectra of liquid dichloro- and dibromoethane. From a large amount of previous work in this laboratory it is well known that the precision of intensity measurements on Raman lines is very much greater with the photoelectric spectrograph than can be obtained by the methods of photographic photometry used by authors given in references 3 and 4.

Dichloroethane. We have made measurements on the relative intensity of the line pair $\Delta\nu = 653$ and 753 cm^{-1}, which is the same line pair as used in both previous investigations[3,4] on dichloroethane. Measurements were made at 278° and 369°K. At 278°K we obtain $[I(653)/I(753)] = 0.813$ with a mean deviation over ten determinations of ± 0.004 and a maximum deviation of 0.013. At 369°K we have obtained the above mentioned intensity ratio, the mean of ten determinations to be 0.780 with a mean deviation of ± 0.007 and a maximum deviation of 0.012. To all intents and purposes these measurements seem to show no variation of intensity ratio of this line pair with temperature, in agreement both qualitatively and quantitatively with the result obtained by Gerding and Meerman.[4] (The mean value obtained by Gerding and Meerman was 0.78. Mizushima *et al.*[3] have quoted the intensity ratio of this line pair at 298°K to be 0.56 and at 423°K to be 0.50. These last mentioned results do not agree with our results or those of Gerding and Meerman and also do not agree with the general frequency and intensity Table I of reference 3.)

The result of our measurements is to show, in agreement with Gerding and Meerman, that ΔH in the liquid for dichloroethane ~ 0.

Dibromoethane. In the case of this molecule the line pair used by Gerding and Meerman[4] ($\Delta\nu = 552$ and 660 cm^{-1}) is less favorable for photographic photometry than the previous case of the dichloro compound, as $[I(552)/I(660)] \sim 0.10$. We have obtained as the mean of ten determinations at 293°K, $[I(552)/I(660)] = 0.128$ with a mean deviation of ± 0.001 and maximum deviation of 0.003. At 371°K we have found the intensity ratio of this line pair to be 0.167 as the mean result of ten determinations with a mean deviation of ± 0.002 and a maximum deviation of 0.005. Making use of the mean deviation, we obtain $\Delta H = 740 \pm 80$ cal. per mole. If we use the maximum deviation the error will be ± 120 cal. per mole. In any event, it is impossible to reconcile our value with the value of 1385 cal. per mole obtained by Gerding and Meerman[4] which was in substantial agreement with the values obtained by Mizushima *et al.*[3] from infra-red measurements made on the vapor.

Dilution of the dibromoethane with a solvent would be expected to bring its behavior closer to that of the gas. However, in dealing with the Raman effect the manageable degree of dilution obtainable consistent with accurate intensity measurement would be small. We have repeated our intensity measurements on the line pair mentioned above with a solution of one part by volume dibromoethane in 3 parts of CCl_4. The result of this experiment was that the ΔH obtained was 580 ± 100 cal. per mole which is in substantial agreement with the value we have obtained for the pure material. It seems that this degree of dilution is insufficient to bring about a marked difference in behavior from that of the pure liquid.

It should be noted that extremely high accuracy in determining ΔH by the above mentioned method is not easy since the intensity ratio of the line pair used is approximately 10 to 1. However, it seems beyond the realm of doubt that our experiments with both liquid dibromoethane and dichloroethane show that behavior in the liquid state does not furnish a reliable measure of the energy difference of the rotational isomers. The influence of change of state of aggregation on the value obtained for ΔH for dibromoethane while not as great as for the dichloro compound, is different only in magnitude and not in kind.

In addition, it should be remarked that in the dilute solution $[I(552)/I(660)]$ at 288°K was measured to be 0.085, while in the pure material this quantity had a value of 0.128. The reason for the apparent change in population of the rotational isomers in solution must await further investigations concerning the influence of solvent solute interaction on the molecular polarizabilities.

Our experiments on diluted dibromoethane largely were the outcome of private discussion (Axford) with Dr. H. J. Bernstein who has recently carried out extensive investigations in the infra-red on the influence of dilution on energy differences between rotational isomers.

* This research was carried out on Contract N6onr-269, Task V of the ONR.
[1] H. J. Bernstein, J. Chem. Phys. **17**, 258 (1949).
[2] H. J. Bernstein, J. Chem. Phys. **17**, 262 (1949).
[3] Mizushima, Morino, Watanabe, Simanouti, and Yamaguchi, J. Chem. Phys. **17**, 591 and 663 (1949).
[4] H. Gerding and P. G. Meerman, Rec. Trav. Chim. **61**, 523 (1942).

Vibration Potential Function and Structure of NH_3 and AsH_3 Molecules

JULES DUCHESNE AND IVAN OTTELET
Department of Chemical Physics, Institute of Astrophysics, University of Liège, Belgium
October 24, 1949

IN a recent letter to the Editor of this Journal, one of us with A. Monfils[1] has suggested that the length-length cross term is always negative when the bonds to which it refers are adjacent and contain at least one hydrogen atom. Essentially the same idea has just been put forward by Linnett and Hoare.[2] The purpose of this note is, in particular, to carry further in a more precise form our previous suggestions taking into account the results of the study of appropriate molecules (NH_3 and AsH_3).

The vibration spectra of the NH_3 and AsH_3 molecules and of their fully deuterated derivatives have been completely analysed recently.[3] Not only is the assignment of the fundamental frequencies well known, but it has also been possible to determine the zeroth-order frequencies. These data provide the possibility of computing the most general potential function describing the molecular movements. We have chosen a force field the expression

of which is given in terms of valency-deformation and interaction forces. If l_i and θ_i are the bond lengths and angles, it may be written

$$2U = f_1 \Sigma \langle \Delta l_i^2 \rangle_{Av} + f_2 \Sigma \Delta l_i \Delta l_j + g_3 l^2 \Sigma \langle \Delta \theta_{ij}^2 \rangle_{Av} + g_4 l^2 \Sigma \Delta\theta_{ij}\Delta\theta_{ik} + g_5 l \Sigma \Delta l_i \Delta\theta_{jk} + g_6 l \Sigma [\Delta\theta_{ij} + \Delta\theta_{ik}]\Delta l_i.$$

Δl_i and $\Delta\theta_{ij}$ are respectively the changes of the NH and AsH bond lengths and of the H−N−H and H−As−H angles from their equilibrium position. The determinantal equation corresponding to that potential gives relations which have been computed by de Hemptinne and Delfosse.[4] On the assumption that the potential is the same in the hydrogenated and deuterated compounds, the force constants in the potential can be calculated with the harmonic frequencies. From these, if we use for the dimensions of the molecules the values given by Dennison[3] and McConaghie and Nielsen,[3] we obtain $f_1 = 7.171$; $f_2 = 0.074$; $g_2 = 0.612$; $g_4 = -0.087$; $g_5 = 0.291$; $g_6 = 0.436$ for NH_3 and $f_1 = 2.878$; $f_2 = -0.032$; $g_2 = 0.301$; $g_4 = -0.018$; $g_5 = -0.276$; $g_6 = 0.305$ for AsH_3. Every constant is expressed in units 10 dynes/cm.

Both series of figures show some striking features. The magnitude of the cross terms is not at all negligible as compared with valency forces, in spite of the fact that we are dealing with hydrogenated bonds. Among these forces, however, the length-length cross term f_2 is small, whereas the length-angle cross term g_6 is rather large. It may be worth while noticing that the relative smallness of f_2 seems a general property of hydrogenated bonds (CH_4, C_2H_4, H_2O, NH_3, AsH_3). As the cross terms measure the influence on one bond of a change in another bond or angle, they certainly arise from the hydrogen-hydrogen interactions and from the changes of hybridization at the central atom.[5] One of the main points is concerned with the change of the sign of f_2 in NH_3(+) and AsH_3(−). This fact presumably depends upon the influence of hybridization which plays a greater part in the former than in the latter. So the positive contribution of hybridization to f_2 would offset the negative contribution due to the H−H interactions in NH_3. Moreover, we have new evidence that the repulsive atom-atom interaction, which is the main factor in AsH_3, gives rise to a negative sign. Consequently, for molecules without resonance[5] and especially in case of hydrogenated bonds, the length-length cross term is expected to be negative (H_2O, H_2S, HCN, C_2H_2, AsH_3). It may however occur that the cross term becomes positive either by an offsetting due to hybridization of the central atom in favorable conditions (NH_3) or because the representative point of the atom-atom interaction is at the bottom of the atom-atom potential curve. The type of potential recently proposed by Duchesne and Monfils[1] is strongly supported by these results. A full account of this work will appear elsewhere.

[1] J. Duchesne and A. Monfils, J. Chem. Phys. **17**, 586 (1949).
[2] J. W. Linnett and F. M. Hoare, Trans. Faraday Soc. **45**, 844 (1949).
[3] D. M. Dennison, Rev. Mod. Phys. **12**, 175 (1940); V. M. McConaghie and H. H. Nielsen, Phys. Rev. **75**, 633 (1949).
[4] M. de Hemptinne and J. M. Delfosse, Ann. Soc. Sci. Brux. **56**, 373 (1936).
[5] Coulson, Duchesne, and Manneback, V. Henri Mém. Vol., Desoer, Liège (1948).

Molecular Structure of Methylbromosilanes

KAZUO YAMASAKI, AKIRA KOTERA, MASATOKI YOKOI, AND MACHIO IWASAKI
Chemical Laboratory, Science Faculty, University of Nagoya, Chikusa, Nagoya, Japan
October 3, 1949

MONOMETHYLTRIBROMOSILANE and dimethyldibromosilane were prepared by passing methyl bromide over heated silicon containing copper at 350°C.[1] Trimethylmonobromosilane was prepared by passing a mixture of methyl bromide and dimethyldibromosilane over heated aluminum at 350°C.[2]

The molecular structures of these compounds revealed by electron diffraction experiments at 20–30°C are summarized in Table I. Assumptions made at the calculation are (1) C−H distance 1.09A, (2) angle HCSi 109° 28′ and (3) staggered relative position of Br and H in CH_3.

TABLE I.*

Compound	Number of rings observed	Si−Br	Si−C	BrSiBr	CSiBr
$SiBr_4$[a]	—	2.15±0.02A	—	109° 28′	—
CH_3SiBr_3	12	2.17±0.02	x	109° 28′	x
$(CH_3)_2SiBr_2$	11	2.21±0.03	1.92±0.06A	109° 28′	x
$(CH_3)_2SiBr$	9	2.21±0.03	1.86±0.05	—	105° ±4°

* x means undetermined.
[a] Spitzer, Howell, and Schomaker, J. Am. Chem. Soc. **64**, 62 (1942).

The Si−Br distance is shorter than the sum of the covalent radii of Si and Br, that is 2.31A.[3] The observed Si−Br distance increases with the substitution of Br by CH_3 and this means the decrease of double bond character of Si−Br bond. The same phenomena were observed in the case of silicon tetrachloride and methylchlorosilanes where the following Si−Cl distances were observed: $SiCl_4$[4] 2.01±0.02A, CH_3SiCl_3[5] 2.01±0.02A, $(CH_3)_2SiCl_2$[5] 1.99±0.03A, $(CH_3)_3SiCl$[6] 2.09±0.03A.

[1] F. G. Rochow, J. Am. Chem. Soc. **67**, 963 (1945).
[2] D. T. Hurd, J. Am. Chem. Soc. **67**, 1545 (1945).
[3] L. Pauling, *Nature of the Chemical Bond* (Cornell University Press, Ithaca, New York, 1940), p. 164.
[4] Yamasaki, Kotera, Tatematsu, and Yokoi, J. Chem. Soc. (Japan) **69**, 104 (1948).
[5] L. O. Brockway and R. L. Livingston, J. Am. Chem. Soc. **66**, 94 (1944).
[6] R. L. Livingston and L. O. Brockway, J. Am. Chem. Soc. **68**, 719 (1946).

The Effect of an Electric Field on the Thermal Conductivity of Glass

CLIFFORD E. BERRY
Consolidated Engineering Corporation, Pasadena, California
October 3, 1949

WE have recently observed a phenomenon which is apparently little known and which may be of both theoretical and experimental interest. The effect observed is an increase in the thermal conductivity of glass when a high potential gradient is applied across it.

The experimental setup was made as follows: A pyrex insulator ring $\frac{3}{16}''$ long, $\frac{3}{4}''$ O.D., and with $\frac{1}{16}''$ wall thickness was clamped between two blocks of metal. The ends of the ring were highly polished as were the mating metal surfaces. One block of metal was maintained approximately at room temperature, while the other was heated to approximately 250°C by a tungsten heater. The assembly was operated in a vacuum of about 10^{-6} mm Hg. Roughly $\frac{3}{4}$ of the heat supplied to the heated block was conducted through the glass ring, the remainder being lost by radiation and by conduction through the electrical leads. The temperature of the heated block was measured with a thermocouple.

With constant heater power, the following effects were observed:

(1) Application of 3000 volts d.c. between the two blocks, with the heated block positive, caused a reduction in temperature of about 10°C, corresponding to a 4 percent increase in thermal conductivity.

(2) With reversed polarity, i.e., the heated block negative, no effect was observed.

(3) Using fused quartz in place of Pyrex, no effect was observed.

(4) Using Vycor, about half the effect noted with Pyrex was observed.

(5) Using a Pyrex ring with one face relieved a few thousandths of an inch except for three small projections, no effect was observed when the projections were in contact with the heated block; however, the effect was not reduced when the projections were in contact with the cold block.

In all cases, the leakage current was of the order of one microampere. It is possible that if more sensitive measuring apparatus had been employed some correlation of the effect with the leakage current would have been noticed.

The fact that the effect is polarity sensitive and that it depends on the contact area on the heated side suggests perhaps that it is related to the electrolytic action known to take place in glass. Since our efforts were aimed primarily at eliminating the effect in an existing piece of apparatus, rather than studying the effect *per se*, it is probable that more refined experiments would shed more light on the matter.

The Infra-Red Spectra of Liquid and Solid Methane*

ROBERT B. HOLDEN, WILLIAM J. TAYLOR, AND HERRICK L. JOHNSTON
The Cryogenic Laboratory and the Department of Chemistry, The Ohio State University, Columbus, Ohio
October 3, 1949

THE infra-red absorption spectra of liquid and solid methane in the rock salt region have been obtained recently in this laboratory using the Perkin-Elmer Model 12-B infra-red spectrometer. The purpose of this note is to describe these spectra briefly and to point out some of their more interesting features.

These spectra have been obtained at sample thicknesses of 12, 4, 0.4, and 0.1 mm in both the liquid and the solid. At the thickest of these sample layers the spectrum of the liquid consists simply of two regions which are completely absorbing, one from 1190 to 1825 cm^{-1}, and one from 2520 to 3340 cm^{-1}. By using progressively thinner sample layers, these regions are resolved into relatively broad peaks at 2600, 2820 and 3015 cm^{-1}, and an even broader peak at 1300 cm^{-1}, this last peak having a small shoulder at 1500 cm^{-1}. The spectrum of the solid presents absorption maxima at the same positions as those observed in the liquid, but the small shoulder appearing on the 1500 cm^{-1} band seems to be somewhat diminished. However, it is difficult to obtain quantitative information in this region due to the interference of the atmospheric water vapor spectrum. These spectra were obtained at various temperatures ranging from 77°K to 100°K. All these frequencies may be correlated with absorption frequencies previously observed in the gas.

Of particular interest is the shoulder at 1500 cm^{-1}, which apparently corresponds to the "optically inactive" fundamental ν_2 which has only very recently been observed in the infra-red spectrum of the gas.[1] The weak activity of this mode in the infra-red absorption spectrum of the gas is due to a Coriolis interaction of ν_2 with the optically active fundamental ν_4. This mechanism may also be partially operative in the condensed phases, but the transition may also be allowed, particularly in the liquid, as a result of the disturbance of the strict tetrahedral symmetry of the molecule by neighboring molecules.

These spectra were obtained with a variable-thickness transmission-type infra-red absorption cell and cryostat designed and constructed as a part of the low temperature spectroscopy program of this laboratory. Detailed descriptions of this apparatus and of the above reported spectra will be presented at a later date.

* This work was supported in part by ONR under contract with the Ohio State University Research Foundation.
[1] John S. Burgess, Phys. Rev. **76**, 302 (1949).

The Kinetics of Heterogeneous Atom and Radical Reactions. II. The Recombination of Hydroxyl Radicals

K. E. SHULER*
Applied Physics Laboratory, The Johns Hopkins University, Silver Spring, Maryland
AND
K. J. LAIDLER
Department of Chemistry, The Catholic University of America, Washington, D. C.
November 7, 1949

IN a recent paper (Part I)[1] we have applied the theory of absolute reaction rates to the calculation of surface recombination coefficients, and have arrived at probable mechanisms for the combination of hydrogen atoms on various types of surfaces and under different temperature conditions. It is the purpose of the present note to extend this treatment to the recombination of hydroxyl radicals.

It was found by Taylor and Lavin[2] that on a surface poisoned by water vapor the concentration of hydroxyl radicals decreases more rapidly than that of hydrogen atoms; assuming the disappearance to be on the surface, this would imply that the recombination coefficient for the OH radical, γ_{OH}, is greater than γ_H. Smith[3] made a more quantitative study, using glass and oxide surfaces poisoned by water vapor. At 453°K he found that γ was apparently 2.1×10^{-3}, which is less than for hydrogen atoms on clean glass by a factor of only about 10. However, the activation energy for the OH recombination was found by Smith to be ~9 kcal., as compared with ~1 kcal. for the hydrogen atom reaction. These facts would indicate a much higher frequency factor for the hydroxyl radical reactions, a result that is inconsistent with the fact that there is a loss of rotational and vibrational freedom in forming the activated complex.

This inconsistency becomes more apparent when quantitative calculations are made. Postulating the recombination mechanism to be either

$$S-OH+OH\rightarrow S+H_2O_2$$

or

$$S-OH+OH\rightarrow S-O+H_2O$$
$$S-O+H\rightarrow S-OH$$

(by analogy with the mechanism of hydrogen atom recombination) the recombination coefficient is

$$\gamma=\frac{c_a h^2}{2\pi mkTb_g}\exp(-E/RT) \qquad (1)$$

(cf. Eq. (10), reference 1) where b_g, if the vibrational contribution is neglected, is equal to $8\pi^2IkT/h^2$. Numerical evaluation for OH radicals using $c_a=10^{15}$ gives $\gamma=(48.5/T^2)\exp(-E/RT)$; at 453°K and with $E=9$ kcal., one obtains $\gamma=1.9\times10^{-7}$. This is less by a factor of 10^4 than the experimental figure, and agreement could only be obtained if in the calculation a zero activation energy were assumed. It may be noted that no heterogeneous mechanism will give a higher value of γ than the one above, as long as the activation energy of 9 kcal. is used.

In view of the good agreement found for hydrogen atom recombination, this discrepancy makes it extremely likely that the reaction investigated by Smith was not predominantly heterogeneous but occurred largely in the gas phase. Owing to experimental difficulties, Smith could not establish directly whether a surface or gas-phase reaction was more important; he considered the alternatives of surface recombination and homogeneous three-body reaction, and assumed the greater importance of the former because of the low pressure at which he worked. However hydroxyl radicals may also disappear by second-order gas-phase reactions, and a very probable one in this connection is

$$OH+H_2\rightarrow H_2O+H.$$

This has an activation energy of ~7 kcal.,[4] which is close to Smith's value; moreover, the equilibrium is well over to the right, accounting for Taylor and Lavin's result that hydroxyl radicals disappear more rapidly than hydrogen atoms.

Our conclusions are therefore that the experimental investigations have given information as to the rate of the gas-phase removal of hydroxyl radicals, and that the surface reaction is very much slower. To complete the argument it is necessary to show that the rate measured is consistent with the assumption of homogeneous reaction. The γ calculated above was $\sim 2\times 10^{-7}$ at 453°K, and since $\gamma = 2kr/v$ (Eq. (4) of Part I), and with $r = 0.55$ cm³ the first-order rate constant is $\sim 2\times 10^{-2}$ sec.$^{-1}$. If the reaction is really a second-order gas reaction involving molecular hydrogen at a concentration of $^{c}H_2$, the second-order rate constant is $\sim 2\times 10^{-2}/{}^{c}H_2$ liter mole^{-1} sec.$^{-1}$. With a frequency factor of 10^{12} sec.$^{-1}$ and an activation energy 7 kcal., the calculated second-order rate constant is $\sim 3\times 10^{8}$ liter mole^{-1} sec.$^{-1}$. The homogeneous and heterogeneous reactions then have about the same rates if the hydrogen pressure is $\sim 10^{-4}$ mm, and the homogeneous will predominate at higher pressures. The actual hydrogen pressure in the system is not known, but the water vapor pressure was 5×10^{-2} mm. Taking a lower limit of about 20 percent for the degree of dissociation in the discharge, there is certainly enough molecular hydrogen to account for the experimental rate of disappearance of OH radicals by the reaction proposed.

The true value of γ for the surface recombination therefore remains unknown, but it can be bracketed: at 453°K it must be less than the apparent figure of $\sim 2\times 10^{-3}$ and is probably greater the previously calculated value of $\sim 2\times 10^{-7}$, since the activation energy for the surface recombination is probably less than the 9 kcal. quoted by Smith and used in our calculations.

Some recently published results of Byrne[5] are also consistent with our conclusions.

* AEC Postdoctoral Fellow.

[1] K. E. Shuler and K. J. Laidler, J. Chem. Phys. (to be published); cf. also, K. J. Laidler, Bull. soc. chim. **16**, D171 (1949); J. Phys. Colloid Chem. **53**, 712 (1949).
[2] H. S. Taylor and G. I. Lavin, J. Am. Chem. Soc. **52**, 1910 (1930).
[3] W. V. Smith, J. Chem. Phys. **11**, 110 (1943); thesis, Harvard University (1941).
[4] K. H. Geib, Ergeb. d. exakt. Naturwiss. **15**, 44 (1936).
[5] J. F. Byrne, *Third Symposium on Combustion and Flame and Explosion Phenomena* (Williams and Wilkins, Baltimore), p. 481.

A New Method of Estimating the Surface Area of Powder

MASATAKA MIZUSHIMA
Physics Department, Faculty of Science, Tokyo University, Tokyo, Japan
October 7, 1949

THERE are three methods now to estimate the surface area of powder: Methods of Brunauer-Emmett-Teller[1] and Harkins-Jura,[2] using adsorption isotherm, and the thermal measurements of the latter.[3] In this note a new method will be suggested.

Let us consider the following thermodynamic process (Fig. 1):

(1) vaporize the ample amount of pure liquid (n molecules) at its saturation pressure p_s,
(2) then decrease the pressure of the vapor to p_0, at which the first molecule of the vapor is adsorbed on the powder,
(3) put the powder into the room,
(4) increase the pressure, following up the adsorption isotherm, until the pressure of the vapor attains again its saturation value p_s.

In these processes, we assume that the adsorption is reversible and the amount of liquid is ample enough. All of the processes must be under isothermal condition.

The change in Gibbs' free energy in each step is easily calculated. In (1) $\Delta G = 0$, (2) $nkT \ln(p_s/p_0)$, (3) 0, (4) $kT\int_1^n \ln(p_0/p(\nu))d\nu$; thus the total change is $\Delta G = kT\int_1^n \ln(p_s/p(\nu))d\nu$, where ν is the number of molecules adsorbed on the powder, and $p(\nu) = p$ is the adsorption isotherm.

This ΔG can be expressed in another way. The initial and the final states of the above process differ only in the point that the surface of the powder is clean or covered with liquid. From this point of view, we may put $\Delta G = a(\sigma_{SA} - \sigma_{LS})$, where a is the area of the powder, and σ_{SA}, σ_{LS} are the surface tensions (surface Gibbs' free energy) of the interface between powder and air, and between powder and liquid, respectively.

From these two formulas we obtain,

$$kT\int_1^n \ln\frac{p_s}{p(\nu)}\,d\nu = a(\sigma_{SA} - \sigma_{LS}), \tag{1}$$

or, introducing the contact angle θ between the powder and the liquid, by the Dupre's relation[3] $\sigma_{AL}\cos\theta = \sigma_{SA} - \sigma_{LS}$, σ_{AL}: surface tension of the liquid. (1) becomes

$$a = kT\int_1^n \ln\frac{p_s}{p(\nu)}d\nu/\sigma_{AL}\cos\theta. \tag{2}$$

If we obtain the adsorption isotherm with some suitable liquid and the powder whose area we want to know, then, measuring the contact angle, we can calculate the required area by (2).

There are no suitable data to test (2), except that of Carver's old one.[4] He obtained the adsorption isotherm with toluene and glass, whose surface area he measured directly. With his result we obtain

$$kT\int \ln\frac{p_s}{p(\nu)}d\nu/a = 44 \text{ erg/cm}^2. \tag{3}$$

The contact angle between glass and toluene is measured by Bertell,[5] from whose result

$$\sigma_{LA}\cos\theta = 46.5 \text{ erg/cm}^2. \tag{4}$$

(3) and (4) agree within 5 percent, confirming our prediction (2).

[1] Brunauer, Emmett, and Teller, J. Am. Chem. Soc. **60**, 316 (1938).
[2] W. D. Harkins and G. Jura, J. Chem. Phys. **11**, 430, 431 (1943).
[3] Dupre, *Théorie Mecanique de la Chaleur* (1869), p. 369.
[4] Carver, J. Am. Chem. Soc. **45**, 63 (1923).
[5] Bartell and Merrill, J. Phys. Chem. **36**, 1178 (1932).

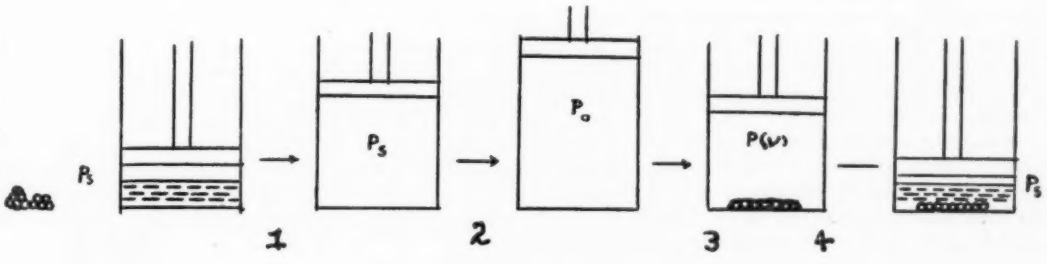

FIG. 1. A process diagram.

Energy Levels of Aromatic Hydrocarbons

D. P. CRAIG
Sir William Ramsay and Ralph Forster Laboratories, University College, London, England
July 20, 1949

SOME current theories of the π-electron energy levels of aromatic molecules[1-3] start from a scheme of one-electron molecular orbitals and work from the supposition that the lower absorption bands record transitions, by one electron, from one molecular orbital to another. According to this view a molecular state can be described by a single "configuration," or assignment of electrons to molecular orbitals, the latter being either made up from atomic orbitals[1,2] or chosen in some other way[3] to fit a potential having the symmetry of the molecule. Evidently, it is essential for a theory built up in this way that there should be no large interaction terms between different configurations; this has usually been taken for granted, perhaps from the fact that in atomic theory "configuration interaction" can often be neglected.

There are indications however that configuration interaction in molecular theory does not play the same minor role as it does in atomic theory, and that calculations neglecting it may go seriously wrong. The subject has been explored in benzene[4] by setting up a number of wave functions, corresponding to different configurations but of the same symmetry, and using them as a basis for a variation calculation with electron repulsion as the perturbing potential. The procedure is an extension of the method of Goeppert-Mayer and Sklar[1] in benzene and follows it closely in technique: Goeppert-Mayer and Sklar calculated the effect of electron repulsion on single configurations, and the extension is to work out as well the degree to which electron repulsion causes the mixing of different configurations. A measure of the importance of this mixing is the depression in the energy, measured relative to the most stable single configuration, caused by other configurations.

Symmetry	Lowest configuration energy	Energy including config. interaction	Depression relative to lowest configuration
A_{1g}	0	0	2.0 ev
B_{2u}	3.7 ev	1.2 ev	4.5 ev
B_{1u}	4.2 ev	3.3 ev	2.9 ev
E_{2g}	6.1 ev	3.0 ev	5.1 ev

Interactions are considered between configurations whose energies fall within 10 ev of the lowest of any one symmetry type. The effect varies strongly between symmetries, and to put the magnitudes in their proper perspective it may be noted that the depressions are comparable with spectral intervals.

The calculations are being published in detail.[4] As is to be expected in any non-empirical theory, good agreement with experiment will have to await inclusion of many-center integrals and perhaps some more subtle refinements. The chief interest of the work at this stage is to suggest that a basis of single configurations in one-electron molecular orbitals is not likely to prove well suited to the discussion, even qualitatively, of excited states and spectral bands of aromatic molecules. Physically it must be the case that the electron motions depart considerably from the uncorrelated motions implicit in any theory of single configurations, and therefore have to be described as a linear combination of configurations. It follows that a satisfactory theory will need either to include configuration interaction within a basis of several configurations, or to start from a different basis altogether, such as electron-pair wave functions or some elaboration of them.

There is one spectral assignment in benzene, previously made on the basis of Goeppert-Mayer and Sklar's work, which these calculations call seriously in question. It is the assignment $A_{1g}-B_{1u}$ for the 2000A band. Under configuration interaction, an E_{2g} state is depressed very strongly relative to the B_{1u}, suggesting that some attention should be paid to the alternative assignment $A_{1g}-E_{1g}$ which was mentioned as a possibility some years ago by Nordheim, Sponer, and Teller.[5] It is a significant, and perhaps hopeful, sign that this assignment agrees with valence-bond theory including polar structures,[4] and an experimental decision would greatly assist in sifting the claims of present theories.

[1] M. Goeppert-Mayer and A. L. Sklar, J. Chem. Phys. **6**, 645 (1938).
[2] Coulson, Proc. Phys. Soc. **60**, 257 (1948).
[3] John R. Platt, J. Chem. Phys. **17**, 484 (1949).
[4] D. P. Craig, to be published.
[5] Nordheim, Sponer, and Teller, J. Chem. Phys. **8**, 455 (1940).

Mass Spectra of *cis*- and *trans*-Decahydronaphthalene

FRED L. MOHLER, LAURA WILLIAMSON, EDMUND J. WELLS, JR., AND HELEN M. DEAN
National Bureau of Standards, Washington, D. C.
October 3, 1949

MASS spectra of many *cis*- and *trans*-isomers of hydrocarbons have been measured and, in general, there is very little difference between the two isomers.[1] A notable exception is the *cis*- and *trans*-forms of decahydronaphthalene. Recently, pure NBS standard samples of these two isomers have become available and we have measured the spectra for publication in the API Catalog.[1] Spectra were measured with a Consolidated mass spectrometer following standard procedures except that pressure in the reservoir was measured by a micromanometer to obtain the sensitivity (current per unit pressure) at the maximum peaks.

Table I lists some of the larger and more distinctive peaks obtained with 70 volts ionizing voltage. The most conspicuous difference between the spectra occurs on the 68^+ and 67^+ peaks but there are large differences on all the larger peaks heavier than 68, while on all the lighter peaks differences are small. It is rather surprising that the most probable ionization processes give ions with five carbon atoms for three C—C bonds must be broken to give C_5 ions while only two bonds need to be broken to give other ions.

TABLE I. Mass spectra of *cis*- and *trans*-decahydronaphthalene.

m/e	Formula	Relative intensities *cis*	*trans*
138	$C_{10}H_{18}$	71.8	85.5
123	C_9H_{15}	0.90	0.93
110	C_8H_{14}	7.3	6.9
109	C_8H_{13}	30.8	16.7
97	C_7H_{13}	9.7	8.0
96	C_7H_{12}	88.4	62.9
95	C_7H_{11}	52.1	63.7
83	C_6H_{11}	11.2	14.1
82	C_6H_{10}	64.2	68.2
81	C_6H_9	88.6	57.0
69	C_5H_9	22.5	49.7
68	C_5H_8	42.3	100.0
67	C_5H_7	100.0	96.3
55	C_4H_7	47.6	43.7
54	C_4H_6	29.2	23.9
41	C_3H_5	85.1	86.9
39	C_3H_3	46.8	46.5
29	C_2H_5	30.1	29.6
28	C_2H_4	12.9	11.9
27	C_2H_3	44.4	42.9
Sensitivity relative to *n*-butane		0.432	0.555

[1] Catalog of Mass Spectral Data. API Research Project 44, Nat. Bur. of Standards.

$A_{1g}-E_{2g}$
ordheim,
eful, sign
including
l greatly

(1938).

, JR.,

ocarbons
ery little
s the *cis*-
re NBS
able and
Catalog.[1]
rometer
reservoir
nsitivity

eaks ob-

ene.

	ans
.5	
.93	
.9	
.7	
.0	
.9	
.7	
.1	
.2	
.0	
.7	
.0	
.3	
.7	
.9	
.9	
.5	
.6	
.9	
.9	
.555	

differ-
ks but
han 68,
rather
ve ions
oken to
e other

Bur. of

Physics Lib.

THE JOURNAL OF CHEMICAL PHYSICS

VOLUME 17 NUMBER 12

DECEMBER, 1949

Published by the

AMERICAN INSTITUTE OF PHYSICS

Incorporated

LANCASTER, PA., AND NEW YORK, N. Y.

THE JOURNAL OF CHEMICAL PHYSICS

BOARD OF EDITORS

JOSEPH E. MAYER, *Editor*

Associate Editors

Term ending December 31, 1949	*Term ending December 31, 1950*	*Term ending December 31, 1951*
K. J. MCCALLUM	J. G. ASTON	PAUL DOTY
A. L. PATTERSON	TERRELL L. HILL	PAUL EMMET
HERTHA SPONER	GILBERT W. KING	C. A. HUTCHISON
GEORGE UHLENBECK	F. LONDON	J. G. KIRKWOOD
BRUNO H. ZIMM	GLENN T. SEABORG	R. S. MULLIKEN
	NATHAN SUGARMAN	

THE JOURNAL OF CHEMICAL PHYSICS is published monthly by the American Institute of Physics. Its purpose is to bridge a gap between journals of physics and journals of chemistry. The artificial boundary between physics and chemistry has now been in actual fact completely eliminated, and a large and active group is engaged in research which is as much the one as the other. It is to this group that the Journal is rendering its principal service and makes its greatest appeal, both as a prompt and efficient medium for publication of research and as a convenient and carefully edited assemblage of pertinent information.

Suggestions for Contributors

Send **manuscripts** to Joseph E. Mayer, Kent Chemical Laboratory, University of Chicago, Chicago 37, Illinois. Textual material (abstract, body of the paper, tabular material, references, and figure captions) must be in English, typewritten (except mathematical expressions) double opaced with wide margins on a durable, white paper, preferably letter size. The original copy, not the carbon, should be submitted. For general style, spellings, abbreviations, and form, consult recent issues of this journal. The authors' institutions are requested to pay a **publication charge** of $4.00 per page which, if honored, entitles them to 100 free reprints. Instructions will be sent with galley proofs.

An **abstract** must accompany each article. It should be adequate as an index and as a summary.

All but the simplest **mathematical expressions** should be carefully printed in by hand. Be sure to distinguish between capital and small letters. Indicate clearly superscripts and subscripts by inverted carets and carets, respectively. Avoid complicated superscripts and subscripts. Avoid repetition of a complicated expression by representing it by a symbol. Identify in the margin Greek letters and unusual symbols. Use fractional exponents instead of root signs. Use the solidus (/) for fractions wherever its use will save vertical space.

References should appear as footnotes, numbered consecutively.

Tables may be typewritten on sheets separate from the running text. Each table must have a caption which will make the data in the table intelligible without reference to the text. Avoid complicated column headings.

Wherever possible **figures** should be planned for the width of a column (3 in.). A convenient reduction ratio is about 2:1 or 3:1. Lettering should be large enough on the original that when reduced it shall not be less than about $\frac{1}{16}$ in. (~1.5 mm). Line drawings must be in *india ink* on white paper or tracing cloth. Coordinate paper is not desirable but if used must be blue lined and the coordinate lines which are to show must be inked over. Photographs should have maximum black and white contrast. Identify each original drawing or photograph on the back with the author's name and the figure number. Figures should be numbered consecutively. Captions should be typed on a separate sheet of paper.

A limited number of **alterations** in proof are unavoidable, but the cost of making extensive alterations after the article has been set in type will be charged to the author.

Proof and all **correspondence** concerning papers in the process of publication should be addressed to the Publication Manager, American Institute of Physics, 57 East 55 Street, New York 22, New York.

Subscription Price

	U. S. and Canada	Elsewhere
To members and associate members of the American Institute of Physics	$12.00	$13.00
To all others	15.00	16.00

Back Number Prices

Yearly rate when complete year is available: $13.00.
Single copies: $1.25 each.

Subscriptions and orders for single copies should be addressed to Prince and Lemon Streets, Lancaster, Pennsylvania, or to the American Institute of Physics, 57 East 55 Street, New York 22, New York.

Changes of address should be sent to the Business Manager, American Institute of Physics.

The Journal of Chemical Physics is published monthly at Prince and Lemon Streets, Lancaster, Pennsylvania.

Entered as second-class matter December 30, 1932, at the Post Office at Lancaster, Pa., under the Act of August 24, 1912. Acceptance for mailing at special rate of postage, provided for in the Act of February 28, 1925, embodied in paragraph 4, Section 538, P. L. & R.: authorized February 5, 1933.